20030205084

DTIC FILE COPY

Elastomers and Rubber Technology

Edited by Robert H. Snyder and Catherine A. Bynum

AD-A180 207

SAGAMORE ARMY
MATERIALS RESEARCH
CONFERENCE PROCEEDINGS
May 22-26, 1985 Lake Luzerne, NY

32

DTIC
ELECTE
MAY 11 1987
S D
A

87 5 6 215

UNCLASSIFIED

SECURITY CLASSIFICATION OF THIS PAGE (When Data Entered)

REPORT DOCUMENTATION PAGE	READ INSTRUCTIONS BEFORE COMPLETING FORM
1. REPORT NUMBER	2. GOVT ACCESSION NO. A180 207 / 3. RECIPIENT'S CATALOG NUMBER
4. TITLE (and Subtitle) ELASTOMERS AND RUBBER TECHNOLOGY Proceedings of the 32nd Sagamore Conference, held July 22-26, 1985, Lake Luzerne, New York	5. TYPE OF REPORT & PERIOD COVERED Final Report 6. PERFORMING ORG. REPORT NUMBER
7. ~~AUTHOR(s)~~ Edited by Robert E. Singler and Catherine A. Byrne	8. CONTRACT OR GRANT NUMBER(s)
9. PERFORMING ORGANIZATION NAME AND ADDRESS U.S. Army Materials Technology Watertown, Massachusetts 02172-0001 SLCMT-CM	10. PROGRAM ELEMENT, PROJECT, TASK AREA & WORK UNIT NUMBERS
11. CONTROLLING OFFICE NAME AND ADDRESS U.S. Army Laboratory Command 2800 Powder Mill Road Adelphi, Maryland 20783-1145	12. REPORT DATE 13. NUMBER OF PAGES 586
14. MONITORING AGENCY NAME & ADDRESS(if different from Controlling Office)	15. SECURITY CLASS. (of this report) Unclassified 15a. DECLASSIFICATION/DOWNGRADING SCHEDULE

16. DISTRIBUTION STATEMENT (of this Report)

Approved for public release; distribution unlimited.

17. DISTRIBUTION STATEMENT (of the abstract entered in Block 20, if different from Report)

18. SUPPLEMENTARY NOTES

For sale by the Superintendent of Documents, U.S. Government Printing Office, Washington, D.C. 20402 - S/N 008-000-00465-0, until supply is exhausted.

Library of Congress No. 86-600600 $28.00

19. KEY WORDS (Continue on reverse side if necessary and identify by block number)

Elastomers
Rubber technology
Tanks
Track rubber
Material characterization

20. ABSTRACT (Continue on reverse side if necessary and identify by block number)

(SEE REVERSE SIDE)

DD FORM 1 JAN 73 1473 EDITION OF 1 NOV 65 IS OBSOLETE

UNCLASSIFIED

SECURITY CLASSIFICATION OF THIS PAGE (When Data Entered)

Block No. 20

ABSTRACT

The U.S. Army Materials Technology Laboratory has been conducting the annual Sagamore Army Materials Research Conferences since 1954. The specific purpose of these conferences has been to bring together scientists and engineers from academic institutions, industry, and the Government to explore in depth a subject of importance to the Department of Defense, the Army, and the scientific community.

The 32nd Sagamore Conference, titled "Elastomers and Rubber Technology," has attempted to focus on major Army requirements for elastomers, including improved tank track rubber durability and chemical defense applications. Exploratory polymer synthesis, characterization, elastomeric networks, polymer blends, new commercial developments, tearing and fracture of rubber, dynamic mechanical properties, mathematical modeling, laboratory and field degradation studies, were discussed at the meeting. This volume provides an important summary for researchers and technologists interested in fundamental aspects of elastomer science, and in elastomers for military applications.

PARTIAL LIST OF CONTENTS

Synthesis and Characterization of Novel Polyurethanes • NMR Studies of Elastomers in Solution and the Solid State • Application of NMR Spectroscopy to Sulfur Vulcanized Natural Rubber • Characterization of Elastomers by Thermal Analysis • Phosphazene Elastomers • Statistical Design Applied to Elastomer Compound Development • Bimodal Networks and Networks Reinforced by In-Situ Precipitation of Silica • Interfacial Adhesion in Polymer Blends • Failure Processes in Elastomers • Applications of the J-Integral to Fracture of Nonelastic Rubber • The Influence of Cavitation on the Mechanical Behavior of Filled Elastomers and Heat Build-up in Nonhysteretic Elastomers • Computer Modeling of Tank Track Elastomers • Mechanisms of Elastomer Degradation and Wear • Thermal Mechanical Degradation of Elastomers • Scanning Auger Analysis • Poly-(dichlorophosphazene) • Analysis of Filled Elastomers by FT-IR • Dark Field Microscopy • Mass Spectrometry of Elastomer Systems • Relationship between Chemical Composition and Hysteresis in Polyurethanes • Chemical Screening Studies of Rubber for Chemical Defense Applications • Vapor Interactions with a Phase Segregated Polyurethane • Enhancement of Rubber Properties Via Short Aramid Fibers • Stretching in an Elastomer Cylinder During an Axial Probe Penetration • High Performance Polyurethanes • Santoweb Fiber Reinforcement • Fatigue of a Rubber Tank Track Compound Under Tensile Loading • Rubber Processing and Compounding Studies for Tank Track Pads • Reinforcement with Fibrillated Kevlar Fiber.

(2)

Elastomers and Rubber Technology

Proceedings of the 32nd Sagamore Conference, held July 22–26, 1985, Lake Luzerne, New York.

As of October 1, 1985, the Army Materiel Command (AMC) consolidated several independent laboratories under the new Laboratory Command (LABCOM) in order to better focus the work of these laboratories within AMC. With this reorganization, the Army Materials and Mechanics Research Center (AMMRC) was renamed the U.S. Army Materials Technology Laboratory (MTL). The mission of MTL remains essentially the same as before: materials research and development for AMC and the Department of the Army.

U.S. Government Printing Office/Washington: 1987

For sale by the superintendent of documents, U.S. Government Printing Office
Washington, D.C. 20402
S/N 008–000–00465–0

$28.00

DTIC
ELECTE
MAY 11 1987
A

SAGAMORE ARMY MATERIALS
RESEARCH CONFERENCE PROCEEDINGS

Recent volumes in the series:

21st: Advances in Deformation Processing
Edited by John J. Burke and Volker Weiss

22nd: Application of Fracture Mechanics to Design
Edited by John J. Burke and Volker Weiss

23rd: Nondestructive Evaluation of Materials
Edited by John J. Burke and Volker Weiss

24th: Risk and Failure Analysis for Improved Performance and Reliability
Edited by John J. Burke and Volker Weiss

25th: Advances in Metal Processing
Edited by John J. Burke, Robert Mehrabian, and Volker Weiss

26th: Surface Treatments for Improved Performance and Properties
Edited by John J. Burke and Volker Weiss

27th: Fatigue: Environment and Temperature Effects
Edited by John J. Burke and Volker Weiss

28th: Residual Stress and Stress Relaxation
Edited by Eric Kula and Volker Weiss

29th: Material Behavior Under High Stress and Ultrahigh Loading Rates
Edited by John Mescall and Volker Weiss

30th: Innovations in Materials Processing
Edited by Gordon Bruggeman and Volker Weiss

31st: Materials Characterization for Systems Performance and Reliability
Edited by James W. McCauley and Volker Weiss

32nd: Elastomers and Rubber Technology
Edited by Robert E. Singler and Catherine A. Byrne

Price: $28.00

Elastomers and Rubber Technology

Edited by

Robert E. Singler

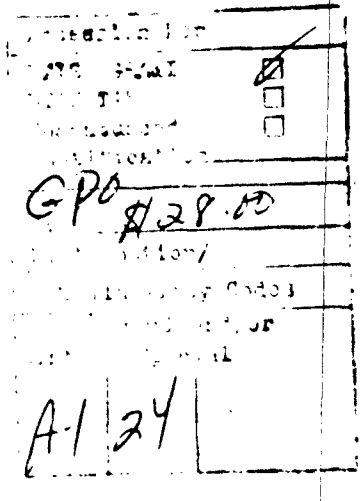
Army Materials and Mechanics Research Center
Watertown, Massachusetts

and

Catherine A. Byrne

Army Materials and Mechanics Research Center
Watertown, Massachusetts





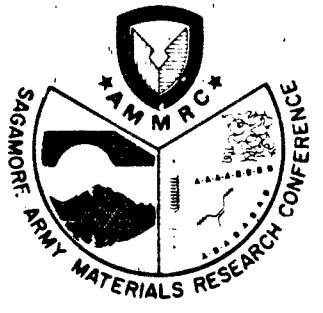
Library of Congress Cataloging in Publication Data

Sagamore Army Materials Research Conference (32nd: 1985: Lake Luzerne, N.Y.)
Elastomers and rubber technology.

(Sagamore Army Materials Research Conference proceedings; 32nd)

Includes index.

Library of Congress Catalog Card Number: 86-600600



Proceedings of the 32nd Sagamore Conference, titled Elastomers and Rubber Technology, held July 22-26, 1985, at Lake Luzerne, New York

32nd SAGAMORE CONFERENCE COMMITTEE

Chairman

WENZEL E. DAVIDSOHN
Army Materials and Mechanics Research Center

Co-Chairman

ROBERT E. SINGLER
Army Materials and Mechanics Research Center

Conference Coordinator

KAREN A. KALOOSTIAN
Army Materials and Mechanics Research Center

Program Committee

ROBERT E. SINGLER
Army Materials and Mechanics Research Center

CATHERINE A. BYRNE
Army Materials and Mechanics Research Center

ROBERT E. SACHER
Army Materials and Mechanics Research Center

DOMENIC P. MACAIONE
Army Materials and Mechanics Research Center

Poster Coordinator

ROBERT E. SACHER
Army Materials and Mechanics Research Center

Conference Administration

BATTELLE COLUMBUS DIVISION
505 King Avenue
Columbus, OH 43201

The findings in this report are not to be construed as an official Department of the Army position, unless so designated by other authorized documents.

Mention of any trade names or manufacturers in this report shall not be construed as advertising nor as an official indorsement or approval of such products or companies by the United States Government.

PREFACE

The Army Materials Technology Laboratory (formerly the Army Materials and Mechanics Research Center) has been conducting the Annual Sagamore Army Materials Research Conferences since 1954. The specific purpose of these conferences has been to bring together scientists and engineers from academic institutions, industry, and government to explore in-depth a subject of importance to the Department of Defense, the Army, and the scientific community.

The 32nd Sagamore Conference, titled "Elastomers and Rubber Technology", has attempted to focus on a major Army requirement for elastomers, namely improved tank track rubber durability. Opening remarks by Dr. Wenzel E. Davidsohn, Conference Chairman, and Dr. Robert W. Lewis, Director of Science & Technology at Natick R&D Center, highlighted the importance of rubber to the Army's mission. Presentations and posters ranged from highly theoretical to the practical engineering requirements for improving track rubber performance in field service. Exploratory polymer synthesis, characterization, elastomeric networks, polymer blends, new commercial developments, tearing and fracture of rubber, dynamic mechanical properties, mathematical modeling, laboratory and field degradation studies, were also topics at the meeting.

Other Army concerns were discussed, such as the need for improved elastomers in chemical defense applications. The banquet presentation reminded all of us that the largest single use of rubber is for automobile tires, both in the United States and abroad. Not only the Army, but modern society relies on rubber products in so many ways.

We wish to acknowledge the assistance of Ms. Karen Kaloostian of the Army Materials Technology Laboratory for all the many arrangements provided before and during the conference. Timely suggestions from Roger Beatty and the encouragement from last year's Conference Chairman

Dr. James McCauley were sincerely appreciated. We also wish to acknowledge the technical and logistical assistance of the Metals and Ceramics Information Center operated by Battelle Columbus Division, and the efforts of Aaron Friedman and Donna Blackburn of the Army MTL, Mrs. Joan Purvis of Synergic Communication Services, Inc., and Ms. Nancy Hill McClary of Battelle Columbus Division, all for assistance during the conference and in assembling these proceedings for publication.

Robert E. Singler and
Catherine A. Byrne

Watertown, MA
August, 1986

CONTENTS

PAGE

SESSION I: SYNTHESIS--Robert E. Singler

SYNTHESIS AND CHARACTERIZATION OF NOVEL POLY-ETHERURETHANEUREAS: "CHAIN EXTENSION" WITH TERTIARY ALCOHOLS 1
B. LEE, J. E. McGRATH, and G. L. WILKES
Virginia Polytechnic Institute and State University
D. TYAGI
Eastman Kodak Co.

SYNTHESIS OF BLOCK COPOLYMERS BY GROUP TRANSFER POLYMERIZATION 29
W. R. HERTLER, O. W. WEBSTER, D. Y. SOGAH, and T. V. RAJANBABU
E.I. du Pont de Nemours and Company, Inc.

SESSION II: CHARACTERIZATION--Robert E. Sacher

APPLICATION OF SOLID STATE ^{13}C NMR SPECTROSCOPY TO SULFUR VULCANIZED NATURAL RUBBER 31
JACK L. KOENIG and DWIGHT J. PATTERSON
Case Western Reserve University

^{13}C NMR STUDIES OF ELASTOMERS IN SOLUTION AND THE SOLID STATE 55
RICHARD A. KOMOROSKI, J. P. SHOCKCOR, and J. L. SAVOCA
The BFGoodrich Research and Development Center

PROGRESS IN CHARACTERIZATION OF ELASTOMERS BY THERMAL ANALYSIS 73
ANIL K. SIRCAR
University of Dayton Research Institute

THE CHROMATOGRAPHIC ANALYSIS OF ELASTOMERS 117
D. McINTYRE
University of Akron

SESSION III: SPECIAL TOPICS--Wenzel E. Davidsohn

POLY(FLUOROALKOXYPHOSPHAZENE) ELASTOMERS--PERFORMANCE PROFILE 119
JEFFREY T. BOOKS
Ethyl Corporation

PAGE

A RATIONAL APPROACH TO ELASTOMER COMPOUND DEVELOPMENT 129
GEORGE C. DERRINGER
Battelle Columbus Division

BIMODEL NETWORKS AND NETWORKS REINFORCED BY THE IN-SITU PRECIPITATION OF SILICA 141
JAMES E. MARK
University of Cincinnati

SESSION IV: ADHESION AND FRACTURE--ROBERT F. LANDEL

INTERFACIAL ADHESION IN POLYMER BLENDS 155
A. J. TINKER
Malaysian Rubber Producers' Research Association

FAILURE PROCESSES IN ELASTOMERS 169
A. N. GENT
University of Akron

APPLICATIONS OF THE J-INTEGRAL TO FRACTURE OF NON-ELASTIC RUBBER 175
J. A. DONOVAN, D. J. LEE, and R. F. LEE
University of Massachusetts

PROSPECTS FOR THE APPLICATION OF NONLINEAR FRACTURE MECHANICS TO ELASTOMERS 191
C. F. SHIH, R. D. JAMES, M. ORTIZ, S. SURESH, and J. DUFFY
Brown University

SESSION V: HEAT BUILD-UP CONSIDERATIONS--Avrom I. Medalia

EFFECT OF CARBON BLACK ON DYNAMIC MECHANICAL PROPERTIES OF RUBBER 193
A. I. MEDALIA
Consultant

COMPRESSIVE FATIGUE OF ELASTOMERS 195
D. DWIGHT, N. LAWRENCE, and L. C. LOPEZ
Virginia Polytechnic Institute and State University
JACOB PATT
U. S. Army Tank Automotive Command

PAGE

THE INFLUENCE OF CAVITATION ON THE MECHANICAL BEHAVIOR OF FILLED POLYMERS AND HEAT BUILD UP IN NONHYSTERETIC ELASTOMERS 197
RICHARD J. FARRIS and R. FALABELLA
University of Massachusetts

SESSION VI: TRACK RUBBER--JACOB PATT

COMPUTER MODELING OF TANK TRACK ELASTOMERS 211
DONALD R. LESUER and ALFRED GOLDBERG
Lawrence Livermore National Laboratory
JACOB PATT
U. S. Army Tank Automotive Command

MECHANISMS OF ELASTOMER DEGRADATION & WEAR 229
DAVID W. DWIGHT
Virginia Polytechnic Institute and State University
H. R. NICK LAWRENCE
FMC Corporation
JACOB PATT
U. S. Army Tank Automotive Command

THERMOMECHANICAL DEGRADATION OF ELASTOMERS 251
J. L. MEAD, S. SINGH, and D. K. ROYLANCE
Massachusetts Institute of Technology
J. PATT
U. S. Army Tank Automotive Command

NATURAL RUBBER FROM GUAYULE 269
RICHARD WHEATON
U. S. Department of Agriculture

POSTER SESSION

MICROSCOPIC CHARACTERIZATION OF CARBON BLACK DISPERSION IN RUBBER 271
ABRAM O. KING
U. S. Army Materials and Mechanics Research Center

THERMAL AND DYNAMIC MECHANICAL PROPERTIES OF ELASTOMERS 273
JOEY L. MEAD and ELIAS R. PATTIE
U. S. Army Materials and Mechanics Research Center

PAGE

SCANNING AUGER IMAGES OF ADDITIVE DISPERSION IN RUBBER 281
SIN-SHONG LIN
U. S. Army Materials and Mechanics Research Center

ASPECTS OF THE SYNTHESIS OF POLY(DICHLOROPHOSPHAZENE) 297
MICHAEL S. SENNETT
U. S. Army Materials and Mechanics Research Center

APPLICATIONS OF HIGH PERFORMANCE LIQUID CHROMATOGRAPHY FOR RUBBER ANALYSIS 305
DAVID A. DUNN
U. S. Army Materials and Mechanics Research Center

ANALYSIS OF CARBON BLACK FILLED ELASTOMERS BY FT-IR 307
JAMES M. SLOAN, HARRY HART, and
MICHAEL J. MAGLIOCHETTI
U. S. Army Materials and Mechanics Research Center

CHARACTERIZATION OF ELASTOMERS FOR ARMY APPLICATIONS BY THERMAL ANALYSIS 317
DOMENIC P. MACAIONE, ROBERT E. SACHER,
ROBERT E. SINGLER, and WALTER X. ZUKAS
U. S. Army Materials and Mechanics Research Center

FAST ATOM BOMBARDMENT--MASS SPECTROMETRY OF ELASTOMER ADDITIVES 333
ALFRED J. DEOME and PETER J. KANE
U. S. Army Materials and Mechanics Research Center

RUBBER DISPERSION USING DARK FIELD MICROSCOPY 345
GUMERSINDO RODRIGUEZ
U. S. Army Belvoir Research, Development,
and Engineering Center

MASS SPECTROMETRY OF ELASTOMER SYSTEMS 353
ALFRED J. DEOME, DAVID A. BULPETT, and
CHRISTOPHER J. KULIG
U. S. Army Materials and Mechanics Research Center

PAGE

CHARACTERIZATION OF ELASTOMERS USING NEUTRON ACTIVATION AND HIGH RESOLUTION GAMMA RAY SPECTROSCOPY 365
FORREST C. BURNS
U. S. Army Materials and Mechanics Research Center

DEFORMATION OF MICROPHASE STRUCTURES IN POLYURETHANES 367
C. R. DESPER, N. S. SCHNEIDER, and J. P. JASINSKI
U. S. Army Materials and Mechanics Research Center
J. S. LIN
Oak Ridge National Laboratory

RELATIONSHIP BETWEEN CHEMICAL COMPOSITION AND HYSTERESIS IN POLYURETHANE ELASTOMERS 369
CATHERINE A. BYRNE
U. S. Army Materials and Mechanics Research Center

CHEMICAL SCREENING STUDIES OF RUBBER 379
ANTHONY F. WILDE, GEORGE W. BATTLE, and
CARYN F. MEE
U. S. Army Materials and Mechanics Research Center

PROPERTIES OF ELASTOMER BLENDS 403
EMILY A. McHUGH
U. S. Army Materials and Mechanics Research Center
EUGENE WILUSZ
U. S. Army Natick Research and Development Center

VAPOR INTERACTIONS WITH A PHASE SEGREGATED POLYURETHANE 405
CARYN F. MEE, ROSEMARY GOYDAN, and
NATHANIEL S. SCHNEIDER
U. S. Army Materials and Mechanics Research Center

REINFORCEMENT OF TRACK PAD ELASTOMERS FOR GREATER MILEAGE 415
ANTHONY ALESI
U. S. Army Materials and Mechanics Research Center
PAUL TOUCHET
U. S. Army Belvoir Research, Development and Engineering Center
JACOB PATT
U. S. Army Tank Automotive Command

PAGE

ARYLOXYPOLYPHOSPHAZENE APPLICATIONS: NON-HALOGENATED FIRE RETARDANT SPECIALTY POLYMERS 421
WARREN B. MUELLER
Ethyl Corporation

ENHANCEMENT OF RUBBER PROPERTIES VIA SHORT ARAMID FIBERS 427
ANDREW P. FOLDI
C & C Consultants

OLIGOMERIC DIAMINOBENZOATES--A UNIQUE CLASS OF LONG-CHAIN REACTIVE AMINES 445
D. J. FINOCCHIO and E. L. McINNIS
Polaroid Corporation

STRETCHING IN AN ELASTOMER CYLINDER DURING AN AXIAL PROBE PENETRATION 451
A. R. JOHNSON and C. J. QUIGLEY
U. S. Army Materials and Mechanics Research Center
I. FRIED
Boston University

TRACK PAD MATERIALS STUDY 473
CAROLYN DEARDOFF
FMC Corporation

HIGH PERFORMANCE POLYURETHANE ELASTOMERS 483
ANTHONY J. CASTRO
Akzo Chemie America
WALTER BRODOWSKI
Akzo Corporate Research
EJAZ SYED
Akzo Chemie Deventer

SANTOWEB® FIBER REINFORCEMENT OF RUBBER COMPOUNDS 485
LLOYD A. WALKER and W. W. PARIS
Monsanto Polymer Products Company
JOHN B. HARBER
Brad Ragan Rubber Company

DEVELOPMENT OF A 3500-POUND PIPE HANGER MOUNT FOR SHIPBOARD APPLICATION 523
MARSHALL L. SHERMAN
David Taylor Naval Ship R&D Center

PAGE

FATIGUE OF A RUBBER TANK TRACK COMPOUND UNDER TENSILE LOADING 525
G. B. McKENNA, G. W. BULLMAN, and K. M. FLYNN
National Bureau of Standards
J. PATT
U. S. Army Tank Automotive Command

RUBBER PROCESSING AND COMPOUNDING STUDIES FOR TANK TRACK PADS 535
PAUL TOUCHET
U. S. Army Belvoir Research, Development, and Engineering Center

ELASTOMERS REINFORCED WITH FIBRILLATED KEVLAR FIBER 547
J. A. CROSSMAN, D. C. EDWARDS, and J. WALKER
Polysar

TACOM TRACK RUBBER PROGRAM 555
G. C. SZAKACS, M. KING, and J. PATT
U. S. Army Tank Automotive Command

WORKSHOP PANEL DISCUSSION ON TRACK RUBBER--PRESENT REQUIREMENTS AND FUTURE PROSPECTS 557
CHAIRMAN: ROBERT E. SINGLER--U. S. Army Materials and Mechanics Research Center
PANEL MEMBERS: A. ALESI--AMMRC; D. LESUER--Lawrence Livermore Labs; J. McGRATH--Virginia Polytechnic Institute and State University; A. MEDALIA--Retired, Cabot Corporation; J. PATT--U. S. Army Tank Automotive Command; G. SZAKACS--U. S. Army Tank Automotive Command; P. TOUCHET--U. S. Army Belvoir Research, Development, and Engineering Center

BANQUET PRESENTATION 565
ERNEST H. ZIELASKO and ROBERT E. GLEASON
Rubber & Plastics News

PARTICIPANTS AND STAFF 575

INDEX 581

SYNTHESIS AND CHARACTERIZATION OF NOVEL POLYETHER-URETHANEUREAS: "CHAIN EXTENSION" WITH TERTIARY ALCOHOLS

BIN LEE[1], JAMES E. McGRATH*[1], GARTH L. WILKES[2] AND DINESH TYAGI[3]
(1) Department of Chemistry, (2) Department of Chemical Engineering, Polymer Materials and Interfaces Laboratory, Virginia Polytechnic Institute and State University, Blacksburg, Virginia 24061; (3) Electrophotography Div., Research Labs, Eastman Kodak Co., Rochester, NY 14650.

INTRODUCTION

Conventional urethane elastomers are well-known to have a number of desirable properties, but are not considered high temperature polymers (1a). Continuous service applications at temperatures above 100°C are not usually recommended. Softening and even thermal dissociation of high temperatures is an inherent characteristic of the urethane linkage. However, it has been recognized that the incorporation of urea linkages in the polyurethane hard segment has a profound effect on the phase separation and domain structure of polyurethaneureas. This is largely due to the high polarity difference between hard and soft segments and possibly to the development of a three-dimensional hydrogen-bonding network.

The hard segments, in the polyurethaneurea elastomers, are often composed of an aromatic diisocyanate reacted with a diamine chain extender, while the soft segments are a low molecular weight hydroxy-terminated polyether or polyester. Due to the rapid diisocyanate reaction with diamine, solution polymerization is usually essential in the synthesis of polyurethaneurea elastomers. A relatively low polymerization temperature is necessary to prevent significant side reactions. However, the solution polymerization suffers from the difficulty of obtaining a good common solvent for both soft and hard (sometimes crystalline) segments which have a large difference in solubility parameter. Clearly, the choice of solvent affects the degree of polymerization due to premature precipitation of the polymer. A mechanically weak polymer would be obtained if the molecular weight of the segmented copolymer is low. Diamines having a substituent on the benzene ring, ortho to the amine group, such as 3,3'-dichloro-4,4'-diaminodiphenylmethane (MOCA), provide an acceptable lowered diamine reactivity in the bulk preparation of polyurethaneurea elastomers. These chain extenders, as well as derivatives of

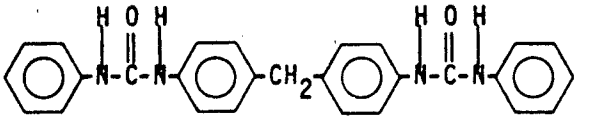
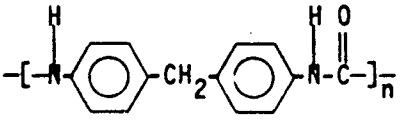
*To whom correspondence should be addressed

4,4'-diaminodiphenylmethane should be avoided since they present well-known carcinogenic hazards.

From the literature it is obvious that a variety of polyurethaneurea copolymers have been prepared and studied (1-16). Among the chain extenders studied, the 4,4'-diaminodiphenylmethane (DAM) chain extended polyurethaneureas (1,4,9,10,11) have been of great interest. A symmetric MDI/DAM hard segment would have better packing efficiency than a TDI/DAM hard segment. As a result, much stronger hard segment domains would be obtained with the former and the segmented copolymers would be expected to display a stronger mechanical response. Moreover, the "thermomechanical" stability of MDI/DAM type hard segment domains is expected to be higher than a hard domain constructed by MDI/ED (ethylene diamine). Due to the all aromatic structure in the MDI/DAM hard segment, a reasonable estimate of its transition temperature is in the range of 300°C to 375°C as shown in Table 1.

TABLE 1

CHARACTERISTICS OF SHORT AND LONG CHAIN MDI/DAM UREAS

STRUCTURE	T_m (°C) experimental	Reference
	330	18
	375	10,19

This thermal characteristic of MDI/DAM hard segment should provide better thermomechanical and heat resistance properties to polyurethane elastomer systems.

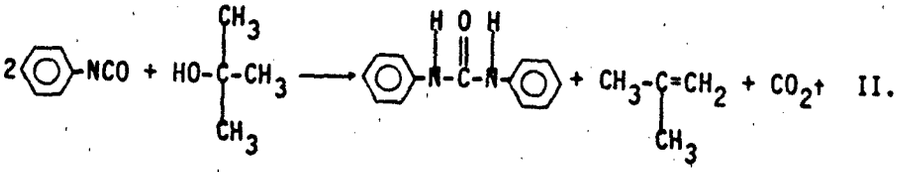
Chain extension of the isocyanate terminated prepolymer with water could also lead to polyurethaneureas with hard segment structure similar to the MDI/DAM system. The model

reaction scheme is illustrated below in Eq. I.

$$RNCO + H_2O \longrightarrow [RNHCOOH] \longrightarrow RNH_2 + CO_2\uparrow \xrightarrow{RNCO} RNHCONHR \qquad I.$$

Water extended polyurethane systems have been investigated for many years. However, one major problem with the addition of water directly into the system is its extremely low solubility in the reacting medium. Thus, a wide variation in reactivity occurs, which is no doubt related to the nature of the heterogeneous system (e.g. hard segment sequence distribution).

It is the purpose of this paper to further describe a new method for preparing urea-urethane block copolymers via a process we term carbamate-isocyanate interactions. This method allows us to synthesize high molecular weight polyurethaneureas (PEUU) with MDI/DAM type hard segment by using a bulk polymerization technique. Unusual tertiary alcohol "chain extenders" have been investigated in our laboratory recently. It was observed earlier that carbanilide and the corresponding olefin are formed by heating tertiary alcohols with phenyl isocyanate (20,21) as shown in Eq. II.

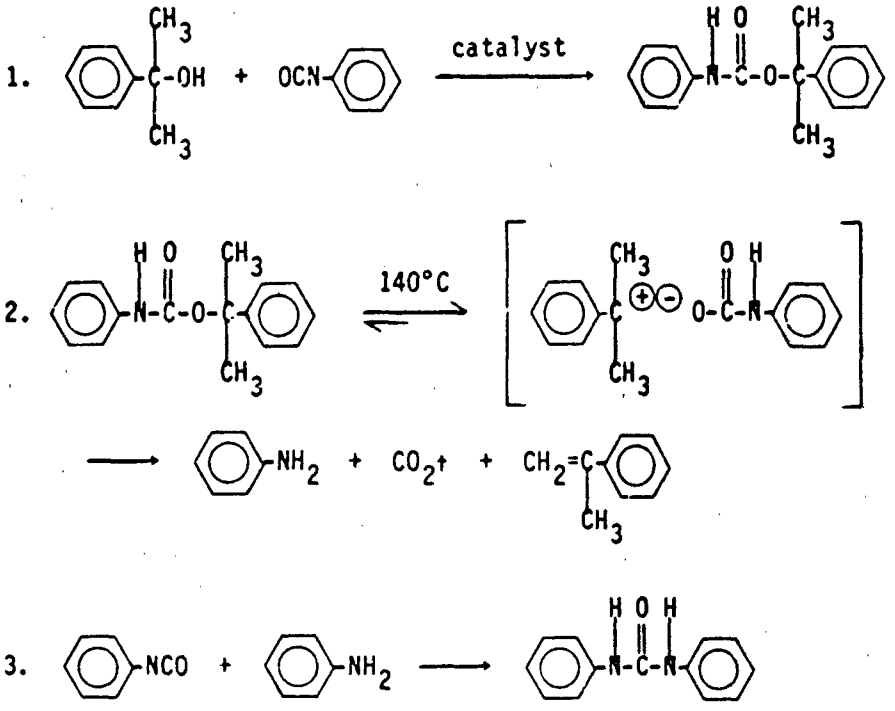


Although no mechanism was proposed, it was postulated that a tertiary alcohol would produce water at a sufficiently high temperature. If this is the case, such characteristics of tertiary alcohol can be utilized synthetically to introduce "molecularly dispersed" water in the preparation of water chain extended polyurethaneurea elastomers without immiscibility problems. Water presumably first reacts with the isocyanate to form a thermally unstable carbamic acid intermediate, which is then converted to the corresponding amine.

A series of model reactions have been conducted to further clarify the urea formation mechanism and are discussed in separate paper (22). We proposed that the carbamate-isocyanate interaction (Scheme 1) is likely to be responsible for the urea formation, based on those model reaction studies, in the tertiary alcohol "chain extended" polyurethanes.

SCHEME 1

PROPOSED UREA FORMATION MECHANISM



We have demonstrated that these interesting characteristics of tertiary alcohols (either mono- or di-functional) can be utilized synthetically to produce polyureas in the presence of dissocyanates. Thus far, we have investigated the effects of phenyl substituted tertiary alcohols and have defined preliminary conditions for the preparation of high molecular weight thermoplastic polyurethaneurea elastomers. The thermal and physical properties of MDI based elastomers as well as thermomechanical stability, have been achieved. The reader is referred to references 26 and 27 for more detailed morphological studies of these novel polyurethaneureas.

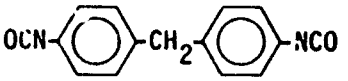
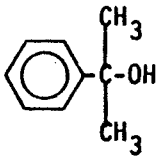
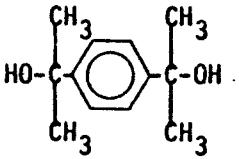
EXPERIMENTAL

SYNTHESIS

The materials used in this study are listed in Table 2. Hydroxy-terminated polytetramethylene glycols (PTMO, DuPont)

TABLE 2

MATERIALS USED IN POLYURETHANEUREA FORMULATIONS

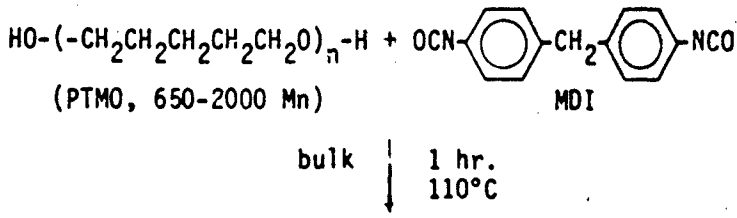
Material	Designation	Chemical Formula	Molar Mass	Supplier
Polyetherdiols: Polytetramethylene Oxide	PTMO-2000	$HO-[-(CH_2)_4-O-]_{27.5}-H$	2000	DuPont
	PTMO-1000	$HO-[-(CH_2)_4-O-]_{13.6}-H$	1000	DuPont
	PMTO- 650	$HO-[-(CH_2)_4-O-]_{8.8}-H$	650	DuPont
Diisocyanate: 4,4'-Methylene diphenylisocyanate	MDI		250	Mobay
"Chain Extenders": Cumyl Alcohol (2-phenyl-2-propanol)	CA		136	Aldrich
Dicumuyl Alcohol	DCA		194	Goodyear

were dehydrated at 70°C under vacuum for 24 hours before use. Cumyl alcohol (CA, Aldrich) was purified by vacuum distillation. Dicumyl alcohol (DCA, Goodyear) was used as received. MDI (Mobay) was vacuum distilled and stored in a desiccator at 0°C before use.

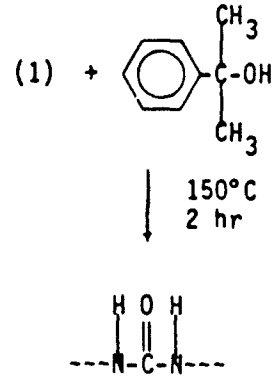
SYNTHESIS OF POLYURETHANEUREAS. The segmented polyurethaneurea elastomers were synthesized by a step-growth reaction (Scheme 2). MDI was charged into a N_2-filled resin kettle equipped with a high torque mechanical stirrer at room

SCHEME 2. Reaction Scheme for the Synthesis of PUR's Via 3° Alcohol "Chain Extenders".

I. CAPPING



II. CHAIN EXTENSION WITH CA



temperature. PTMO was then slowly syringed into the reactor at 110°C over a period of 20 minutes. After reacting the prepolymer/MDI mixture at 110°C for 1 hour, CA or DCA was added

and the temperature was increased to 150°C. At 150°C, the bulk viscosity gradually increases and the mechanical stirrer was stopped within 30 minutes due to the high viscosity. Essentially, a solid polymer had been formed at this stage. The reaction was continued for two additional hours at 150°C in order to have complete reaction. In fact, the synthesis can be accelerated by adding a suitable catalyst, and high molecular weight polymer can be obtained in a very short time. The copolymers synthesized in this fashion was extracted with hot THF for 24 hours to remove any soluble by-products such as α-methylstyrene and were dried in a vacuum oven at 70°C for 36 hours.

The molar ratio of MDI and PTMO and soft segment PTMO molecular weight were altered in different experiments to produce samples with systematically varied hard segment content and block length. By using this approach, tertiary alcohols are not directly involved in the chain extension step. Thus, the hard segment in the copolymers will be totally derived from the diisocyanates. The theoretical hard segment content is equivalent to the weight percent of the diisocyanate charged. The theoretical percentage of urea content can be calculated by using the following relationship (note that possible side reactions are not considered):

$$\% \text{ urea content} = \frac{\text{urea linkages}}{\text{urea linkages} + \text{urethane linkages}}$$

$$= \frac{\#\text{moles of } NH_2}{\#\text{moles of } NH_2 + \#\text{moles of OH}}$$

$$= \frac{(\#\text{ moles of MDI} - \#\text{ moles of PTMO})/2}{(\#\text{moles of MDI} - \#\text{moles of PTMO})/2 + \#\text{moles of PTMO}}$$

$$= \frac{\#\text{moles of MDI} - \#\text{moles of PTMO}}{\#\text{moles of MDI} + \#\text{moles of PTMO}}$$

The characteristics of the various polyurethaneureas synthesized are listed in Table 3.

TABLE 3

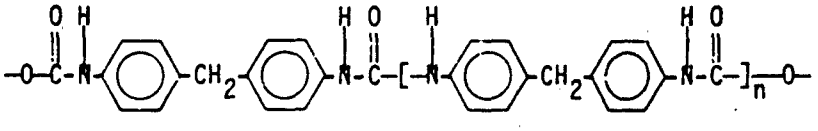
CHARACTERISTICS OF VARIOUS POLYURETHANEUREAS SYNTHESIZED

SAMPLE	Mole Ratio MDI/PTMO/CA OR DCA	% urea Content
PTMO-2000-MDI-23-CA	2.5/1/1.5	43
PTMO-2000-MDI-31-CA	3.7/1/2.7	57
PTMO-2000-MDI-41-CA	5.6/1/4.6	70
PTMO-2000-MDI-31-DCA	3.7/1/1.35	57
PTMO-1000-MDI-31-DCA	1.8/1/0.4	29
PTMO- 650-MDI-31-DCA	1.2/1/0.1	9

A system obtained with 2000 molecular weight PTMO, MDI and CA is referred to as PTMO-2000-MDI-X-CA, where X represents the weight percent of the hard segments and CA indicates the type of the chain extender. A similar nomenclature is employed for all other samples.

A clear polymer was obtained by dissolving the extracted copolymers in DMF at 100°C. This indicates that an essentially linear polymer was obtained. Films for physical testing were prepared by compression molding at 210°C.

SYNTHESIS OF MODEL POLYUREAS. The idealized chemical structure of the hard segment of the above urethaneurea copolymers is shown below:

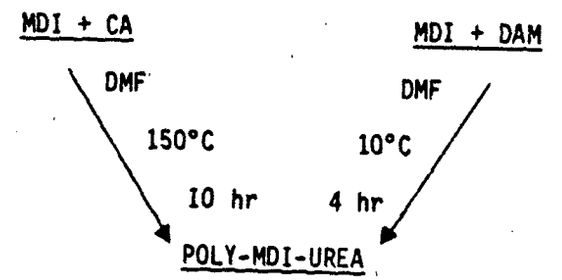


For the purpose of clarifying the structure and the thermal characteristics of the hard segment of polyurethaneurea elastomers, it was important to prepare a model polyurea with a structure similar to the designed hard segment.

Model polyureas were prepared by using two different approaches. First, CA and MDI were reacted in vacuum distilled DMF at 150°C for 10 hours (Scheme 3). It would, of course, be impossible to prepare a "polymer" via a conventional alcohol-isocyanate reaction since one of the reagents would be, nominally at least, monofunctional. However, moderate molecular weight polymer was in fact obtained and a sharp melting peak at around 375°C was observed from differential scanning calorimetry (DSC) measurements. Similar DSC results were obtained on a polymer which was synthesized more conventionally with MDI and DAM in DMF at 10°C for about 4 hours.

SCHEME 3

SYNTHESIS OF MODEL POLY-MDI-UREA



CHARACTERIZATION

SPECTROSCOPIC ANALYSIS: Structural characterization of the segmented copolymers was obtained with a Nicolet MX-1 FT-IR Spectrometer linked to a Nicolet Data Station. IR spectra were taken on polymer films and the polymerization extracts.

THERMAL ANALYSIS. DSC thermograms were recorded by using a Perkin-Elmer DSC II over the temperature range of -100 to 300°C. A constant flow of helium gas was used to purge the system and a heating rate of 10°C/min was employed throughout the measurements. The data were derived from second cycles in order to provide a constant thermal history. Thermal mechanical analysis (TMA) on polymer films was performed on a Perkin-Elmer Thermal Mechanical Analyzer over the temperature range -100 to 300°C. The experiments were carried out at a heating rate of 10°C/min under a constant load of 10 gm. Thermal gravimetric analysis (TGA) is used for the thermal degradation studies which began at 50°C to where the polymers degrade completely.

DYNAMIC MECHANICAL ANALYSIS. The dynamic mechanical data were recorded using Rheovibron DDV-IIC Viscoelastomer (Toyo Measuring Instruments) at a frequency of 110 Hz. The samples were rapidly cooled down to -100°C and the measurements were made with a heating rate of 3°C/min up to 300°C.

TENSILE TESTING. Uniaxial stress-strain experiments were performed on dog-bone specimens using an Instron Tensile Tester (Model 1122) at room temperature. These experiments were carried out at a strain rate of 200% per minute based on the initial sample length.

A butanediol chain extended segmented polyurethane, Estane™, with 31% hard segment content was also studied as a control for our novel PEUU's. This polymer was kindly supplied by BF Goodrich Chemical Company.

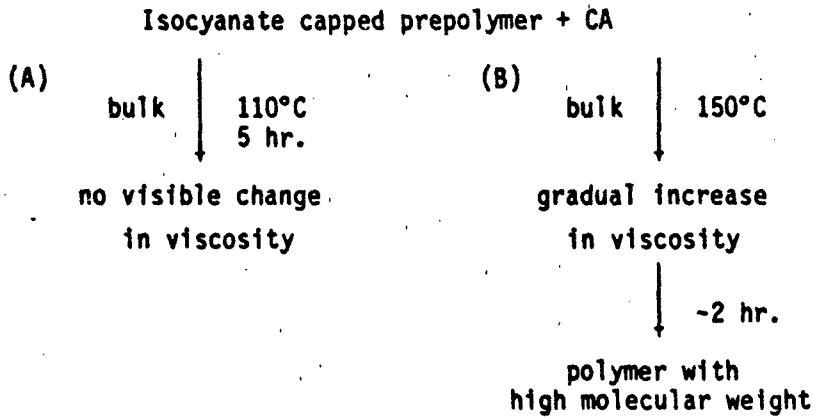
RESULTS AND DISCUSSION

In this approach to polyurethaneureas, phenyl-substituted tertiary alcohols have been selected as a chain extender. It has been reported in the literature (23) that, on heating to over 200°C, carbamates derived from phenyl isocyanate and t-butyl alcohol yields the corresponding amine, carbon dioxide and alkene. Both the high temperature requirement and volatility could cause some problems during the reactions. This immediately eliminated the use of t-butyl alcohol in our preliminary studies. As described in Scheme 1, the phenyl group on the tertiary carbon could stabilize the possibly resulting tertiary carbonium ion. Thus, a relatively lower dissociation temperature is expected for such a carbamate derived from cumyl alcohol and phenyl isocyanate. The typical reaction temperature was observed to be about 140-150°C (in the absence of catalyst) for most of the polymerizations.

As shown in Scheme 4, if the reaction was conducted at 110°C without catalyst, no increase in viscosity was observed. However, at higher temperatures, e.g., 150°C, an immediate increase in viscosity was observed which indicated an increase in polymer molecular weight. The high reaction temperature necessary is not surprising due to the effect of steric hindrance of phenyl substituted tertiary alcohols. In fact, the synthesis can be accelerated by adding catalyst and high molecular weight polymer was formed in a very short period of time (22).

SCHEME 4

TEMPERATURE EFFECTS ON THE CHAIN EXTENSION REACTION



INFRARED STUDIES. In order to characterize the reaction mechanism and to confirm the formation of urea linkages, the infrared spectra were obtained from the thin compression molded polymer films. Figure 1 is the FT-IR spectra for DCA chain extended polymers prepared by two different fashion-bulk (PTMO-2000-MDI-23-DCA) and solution (PTMO-2000-MDI-DCA-31-S). The presence of an absorption peak at 1640 cm^{-1} in the IR spectrum has confirmed the incorporation of urea linkages in an sample prepared by using bulk polymerization at 150°C. This intense peak is attributed to the hydrogen bonded urea carbonyl. The MDI based polyurethaneureas prepared by using this approach gave a very similar IR spectra with the MDI/DAM based PEUU prepared by Ishihara et al. (1). No absorption peak corresponding to the 1640 cm^{-1} was observed for the solution polymerized DCA chain extended polyurethane, PTMO-2000-MDI-DCA-31-S. This polymer is prepared in vacuum distilled DMF at 50°C in the presence of catalyst. Under such conditions, DCA is expected to react with MDI terminated prepolymer through a conventional alcohol-isocyanate mechanism. The resulting urethane linkages are expected to have reasonable thermal stability at 50°C. Model reactions have been conducted, and this has proved to be the case (22). The IR absorptions appearing at 1730 and 1703 cm^{-1} correspond to the nonhydrogen bonded and hydrogen bonded C=O stretching mode of urethane groups, respectively.

As mentioned earlier in the introduction, the carbamates derived from tertiary alcohols and phenyl isocyanate are thermally unstable. On heating such a carbamate with the

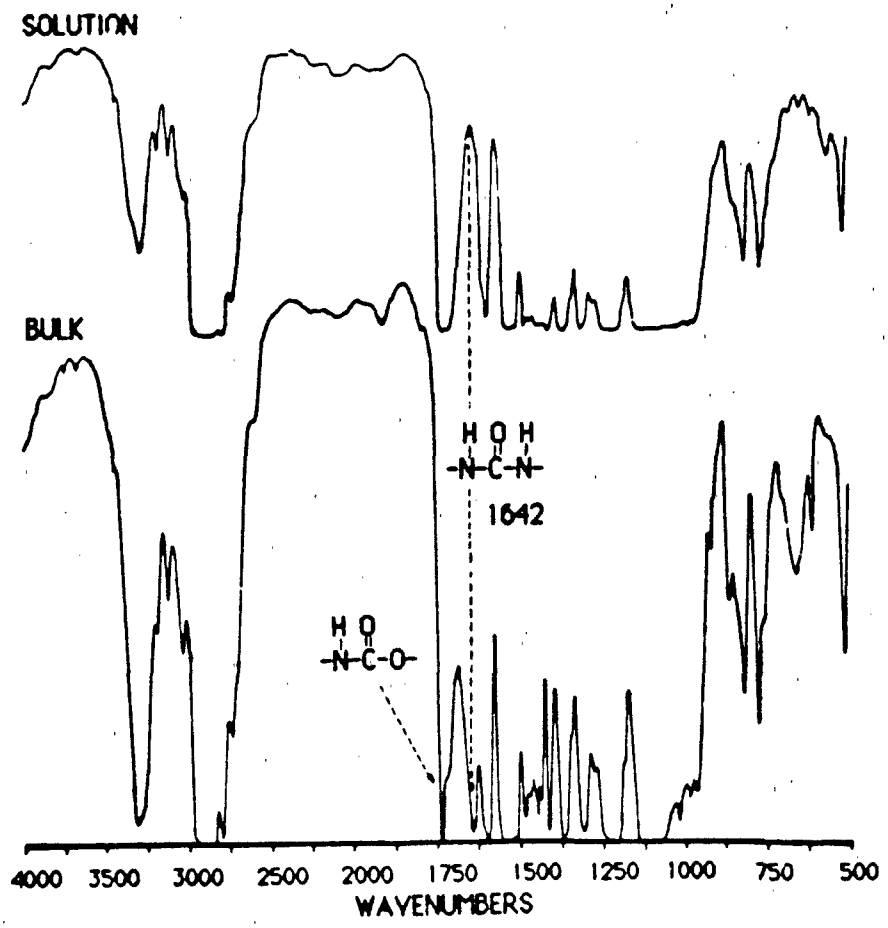


FIGURE 1. FT-IR Spectra of bulk and solution synthesized DCA chain-extended PUR's.

present isocyanate to 150°C, a thermally more stable urea linkage can be obtained. In other words, the tertiary alcohols in the polyurea synthesis are not directly incorporated into the polymer backbone. It is more likely that they convert the isocyanates to corresponding amines via carbamate-isocyanate interaction which then react with isocyanates to give polyurea. As a consequence, the basic structure of the polyureas should be independent of the type of the tertiary alcohol used (either mono- or di- functional) while the other starting materials are the same. The FT-IR spectra of both CA (monofunctional) and DCA (difunctional) chain extended polymers are shown in Figure 2. Basically, there is no difference between the polymer in

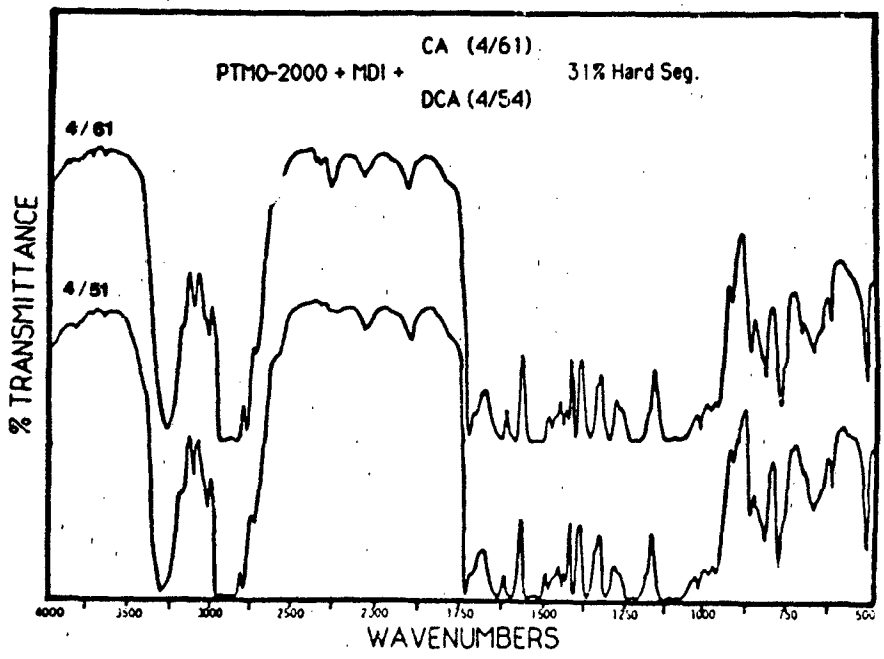


FIGURE 2. FT-IR of mono- and di- cumyl alcohol chain extended PEUU's.

terms of IR absorptions. Both polymers show a very intense absorption at 1640 cm^{-1} which is due to the hydrogen bonded urea carbonyl. Moreover, it would of course be impossible to prepare a "polymer" via a conventional alcohol-isocyanate reaction if one of the reagents is monofunctional material.

The reaction by-products resulting from the carbamate-isocyanate interaction will be carbon dioxide and olefin. We have observed the gas evolution during the polymerization that we believe to be carbon dioxide. More substantially, the evidence of the formation of olefin (α-MS, in the case of CA chain extended systems) is given in Figure 3. Three IR spectra were taken on CA and α-MS control and the reaction by-products. The liquid by-products were collected from the inside wall of the reaction kettle during the reaction. Due to the volatility of CA and α-MS at 150°C, the collected liquid is actually a mixture of α-MS and CA as demonstrated by IR (bottom spectrum of Figure 3). Fortunately, even though most of the absorption peaks overlapped with the olefin, absorptions are able to be differentiated from the background. The absorption peaks appearing at 1640 cm^{-1} and 850 cm^{-1} correspond to the C=C

stretching and $=CH_2$ wagging respectively and compare well with an authentic IR spectrum for α-methylstyrene.

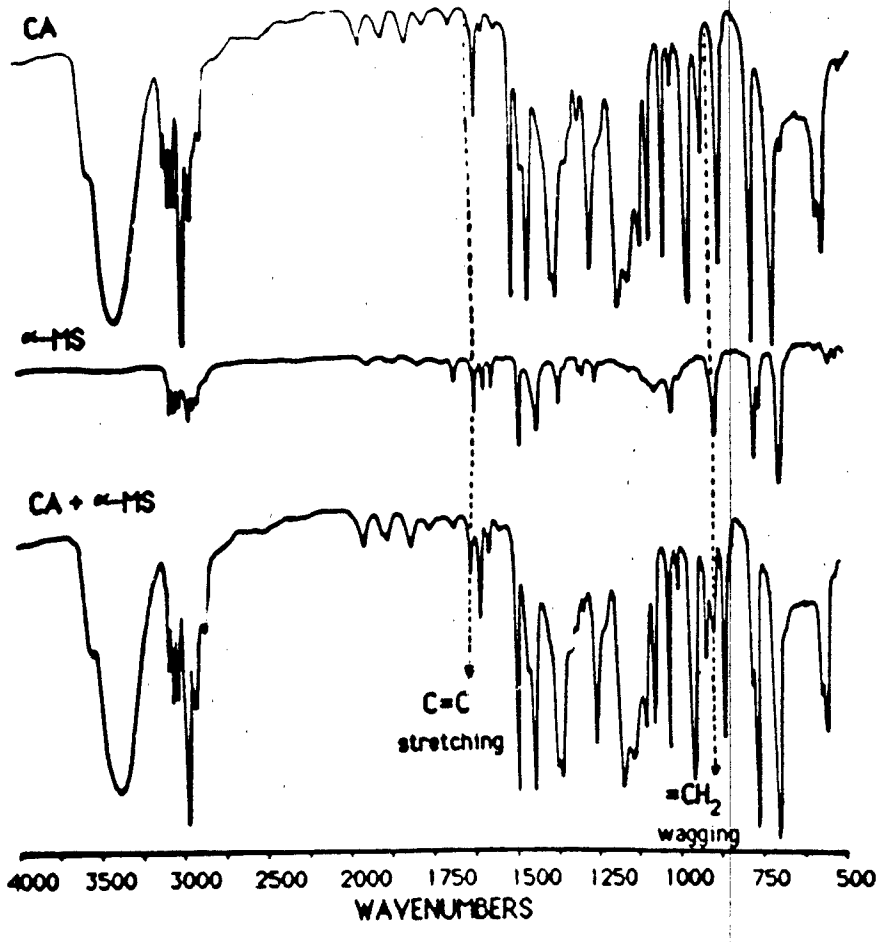


FIGURE 3. Olefin formation demonstrated by FT-IR.

DIFFERENTIAL SCANNING CALORIMETRY. As mentioned earlier in the introduction, the phase separation in the polyurethane elastomers can be promoted by the incorporation of urea linkages. Both mechanical and thermal properties of the polyurethanes could be affected dramatically by phase mixing. Interaction between soft and hard segments can increase the glass transition temperature (T_g) of the soft segment and

decrease the T_g of the hard segment. The degree of phase mixing is indicated by this shift of transition temperatures toward intermediate values. Both qualitative and quantitative evaluation of the degree of phase separation can be obtained by differential scanning calorimetry (DSC) (11,24). Table 4 presents a summary of the low temperature DSC results for the segmented PEUU copolymers.

TABLE 4

LOW TEMPERATURE BEHAVIOR OF POLYETHER-URETHANEUREAS

SAMPLE DESCRIPTION	T_g from	T_g to	T_g °C	T_c °C	T_m °C
PTMO-2000-MDI-23-CA	-83	-61	-75.2	-43.1	2.5
PTMO-2000-MDI-31-CA	-86	-62	-74.7	-34.1	3.5
PTMO-2000-MDI-41-CA	-84	-54	-72.0	-35.1	11.7
PTMO-2000-MDI-31-DCA	-89	-57	-73.7	-35.7	8.8
PTMO-1000-MDI-31-DCA	-59	-29	-47.9	---	---
PTMO- 650-MDI-31-DCA	-58	-19	-38.3	---	---
PTMO-2000	---	---	-78.0	---	24[a],27[b]
PTMO-1000	---	---	-82.0	---	*28,37
PTMO- 650	---	---	-84.0	---	23,36
PTMO-2000-MDI-BD-31 (ESTANE™)	-64	-29	-49.0	---	---

* a. metastable melting point
b. equilibrium melting point

The low temperature thermograms contain the transitions associated with the soft segments are presented in Figures 4 and 5. The thermograms in Figure 4 show the low temperature transitions indicated by various copolymers with different PTMO

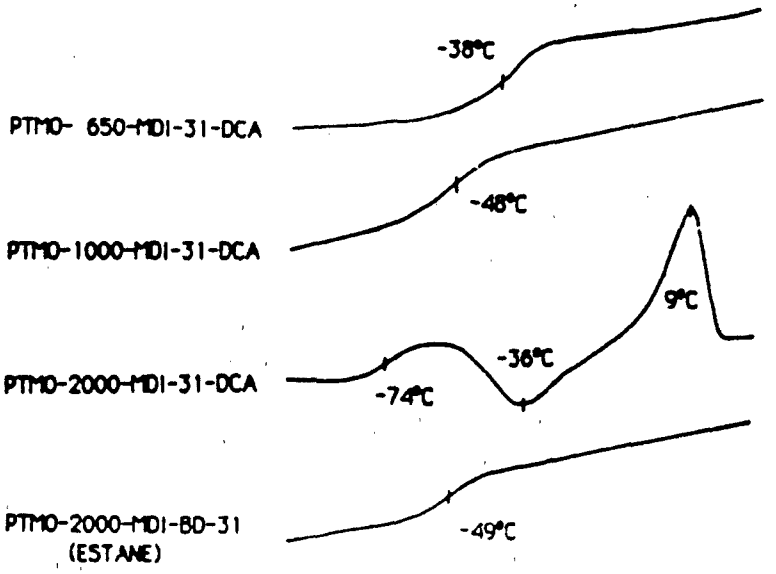


FIGURE 4. Low-temperature DSC curves of the PEUU's with different soft segment lengths.

molecular weight but the same hard segment content. For PTMO-2000 based PEUU, the soft segment glass transition occurs at -75°C and is followed by an in situ crystallization exotherm near -40°C and melting endotherm at about 10°C. Crystallization and melting transitions were not observed for the lower soft segment molecular weight based materials. For PEUU samples with 650 and 1000 molecular weight PTMO, the T_g was observed at -38 and -48°C respectively. These T_g's are substantially higher than the glass temperatures reported in Table 4 for pure PTMO oligomers (-84 and -82°C respectively). This indicates either a significant amount of interfacial mixing or an existence of mixed hard segments in the soft segment matrix of these materials, the extent of which is likely determined by the amount and length of both segments. In addition, the anchoring of soft segments at the phase boundaries of a domain structure would also raise the T_g due to the restrictions imposed by the coupling at the interface. The width of the glass transition zone is also longer for low soft segment molecular weight based copolymer suggesting a higher degree of segment mixing. All low temperature DSC thermograms on copolymers with 2000 molecular weight PTMO (see Figure 5) indicate the presence of crystallization and melting transitions, following the glass transition. The presence of a melting endotherm is observed as expected by virtue of the

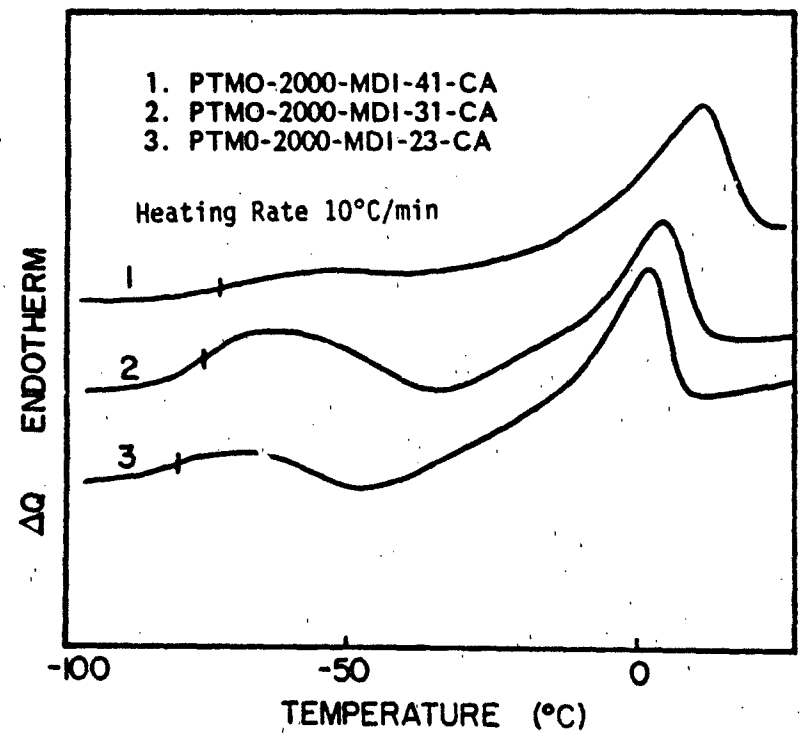


FIGURE 5. DSC Thermograms for various samples with different hard segment content.

greater molecular weight of soft segment involved and that the hard segments solubilization in the soft segment matrix is minimal. The crystallization exotherm is thus due to the soft segment. At room temperature, these segments are just above their melting point so that rapid cooling below room temperature is effectively a melt quench to an amorphous glassy state below T_g. When reheated, the soft segments crystallize above their glass transition temperature.

From Figure 5 and Table 4, the melting endotherms in these copolymers are observed to be shifted to lower temperatures as the hard segment content is decreased. This could imply that the amount of hard segments present in the soft segment matrix decreases as the hard segment content is increased. It is important to note that the hard segment sequence length increases with hard segment content under the synthesis conditions utilized.

DYNAMIC MECHANICAL PROPERTIES. To investigate the compositional dependence of the local scale motion as well as cooperative segmental motion which may exist in these segmented polyurethaneurea copolymers, dynamic mechanical spectra were obtained. It was also of interest to determine the mechanical and thermal properties in light of the role played by the variety of hydrogen bonding possibilities in these materials. Figures 6 and 7 show the overall dynamic behavior in terms of storage modulus (E') and loss modulus (E") as a function of temperature. The transitions observed by dynamic mechanical testing are in good agreement with DSC results. Figure 6 demonstrates the effect of hard segment content for PTMO-2000 based polyurethaneureas. A rubbery plateau, from the E' curves, is observed to be composition dependent and extends to 200°C for 23.5% hard segment content material and over 250°C for the sample with 41% hard segment content. The plateau modulus also increased upon increasing the hard segment content in the sample. An increase in the order of hard domains or in hard segment content results in the formation of a stiffer material which is reflected in the E' behavior. Interestingly, the plateau modulus in these polyurethaneureas is nearly one order of magnitude higher than the reported for a MDI/ED based PEUU with a similar hard segment content (2).

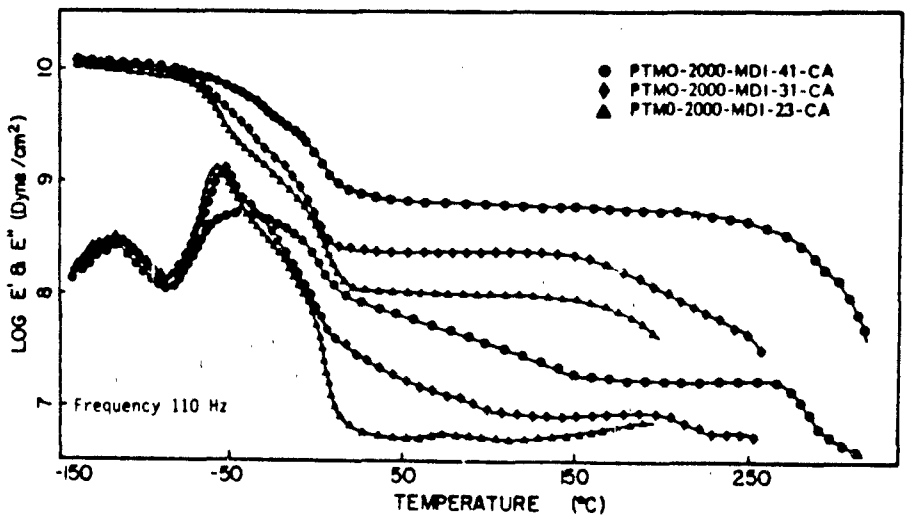


FIGURE 6. Dynamic mechanical spectra. Frequency 110 Hz.

The secondary loss peak near -120°C is designated as the γ relaxation. This peak has been ascribed to the short chain motion of methylene sequences in PTMO soft segment (2). The γ relaxation temperatures observed in these copolymers are in excellent agreement with the reported value (-120°) at the same frequency for polyolefin systems. This indirectly suggests that the degree of phase separation achieved in these copolymers may be very high. This is expected because of the highly polar nature of the aromatic urea linkages that form the hard segments in these copolymers.

The primary relaxation observed near -55°C in the dynamic mechanical spectra at 110 Hz for these copolymers is designated as the α_a relaxation and has been assigned to the glass transition temperature of the soft segment (2). On the high temperature side of the α_a peak, a mechanical dispersion is indicated as a shoulder near 0°C. This transition is designated as α_c and is related to the melting of crystalline for the PTMO soft segments.

The existence of δ relaxations in dynamic mechanical behavior has been observed for conventional MDI/BD based polyurethanes, and shown to be associated with the hard segments of the copolymer (25). The high temperature relaxation near 200°C in the dynamic mechanical spectra has been attributed to the melting of the hard segment microcrystallites with urea linkages and this dispersion is designated as δ. An endotherm at these temperatures was also observed by DSC. The melting point of the poly-MDI-urea control is about 375°C as described in the experimental section, although we are not certain that this represents the value associated with very high molecular weight components.

Figure 7 shows the dynamic mechanical behavior of segmented PEUU's as a function of the PTMO molecular weight. The results indicate that the α_a transition shifts to a lower temperature as the molecular weight of the PTMO soft segments is increased. This shift can be explained on the basis of a longer, more ordered and well defined domain structure which results when the molecular weight of the PTMO is increased at constant hard segment content. PTMO-650 and PTMO-1000 based PEUU, the α_c relaxation was not observed. The higher hard/soft segment mixing present is these systems may prevent the crystallization of the soft segments. The γ relaxations appear to be molecular weight dependent as they shift to low temperatures for high molecular weight PTMO based PEUU's of the same hard segment content. This may indicate a higher degree of phase mixing as the molecular weight of the PTMO soft segment is lowered for the same hard segment content.

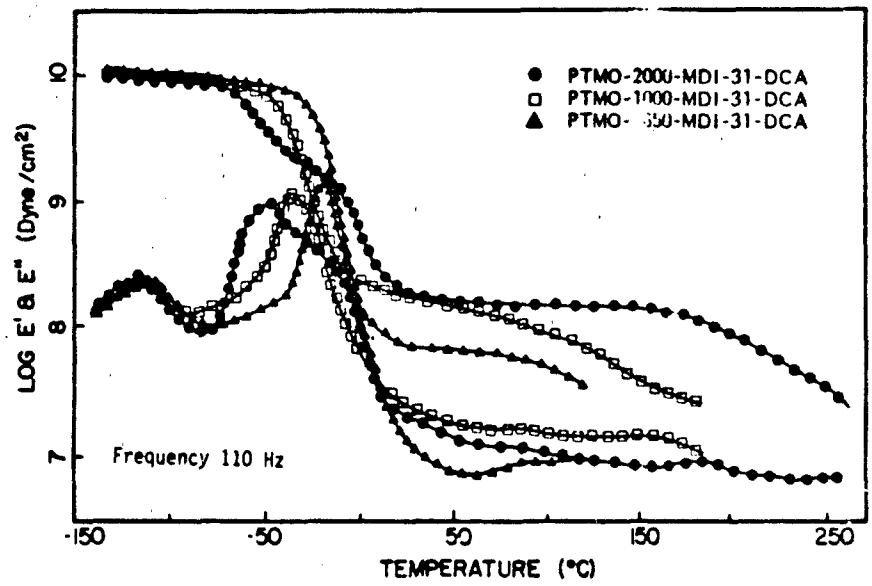


FIGURE 7. Dynamic mechanical spectra. Frequency 110 Hz.

The length and extent of the rubbery plateau is also shown to depend on the molecular weight of the PTMO soft segment. The plateau modulus is higher for samples where PTMO-2000 is utilized as compared to samples where the soft segment molecular weight is lower. For PTMO-2000 based copolymers, better phase separation is obtained and enhanced physical cross-linking and/or filler effects dominate the properties. Additionally, for samples with the same hard segment content, the concentration of urea groups is higher for samples with higher PTMO molecular weight as shown in Table 3. This higher concentration of urea groups, provides strong hydrogen bonding which improves interdomain cohesion.

TENSILE PROPERTIES. The engineering stress-strain curves for segmented MDI based PEUU's are shown in Figure 8 and Figure 9. All curves are shown up to the fracture stress of the sample. The Young's modulus, ultimate tensile strength, and ultimate elongation were determined from these results and are listed in Table 5 for each sample.

In Figure 8, the stress-strain behavior for materials with different soft segment molecular weight but the same hard segment content are shown. The results indicate that the Young's modulus and the tensile strength in these samples

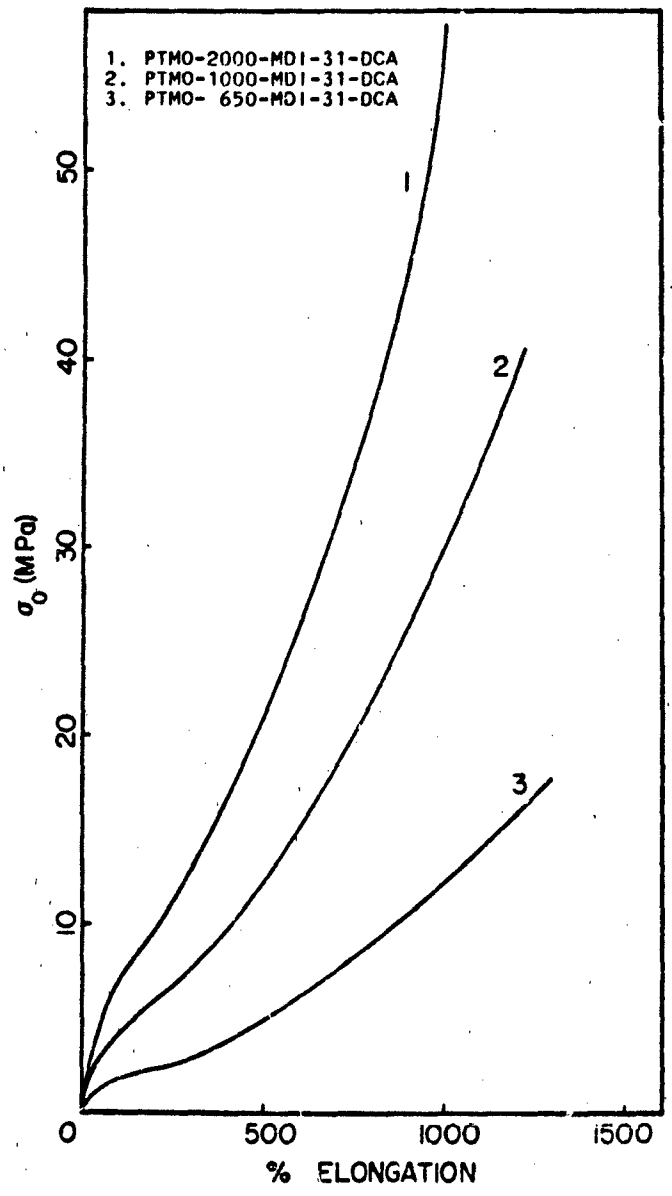


FIGURE 8. Stress-strain curves for various samples indicating the dependence on the soft segment molecular weight.

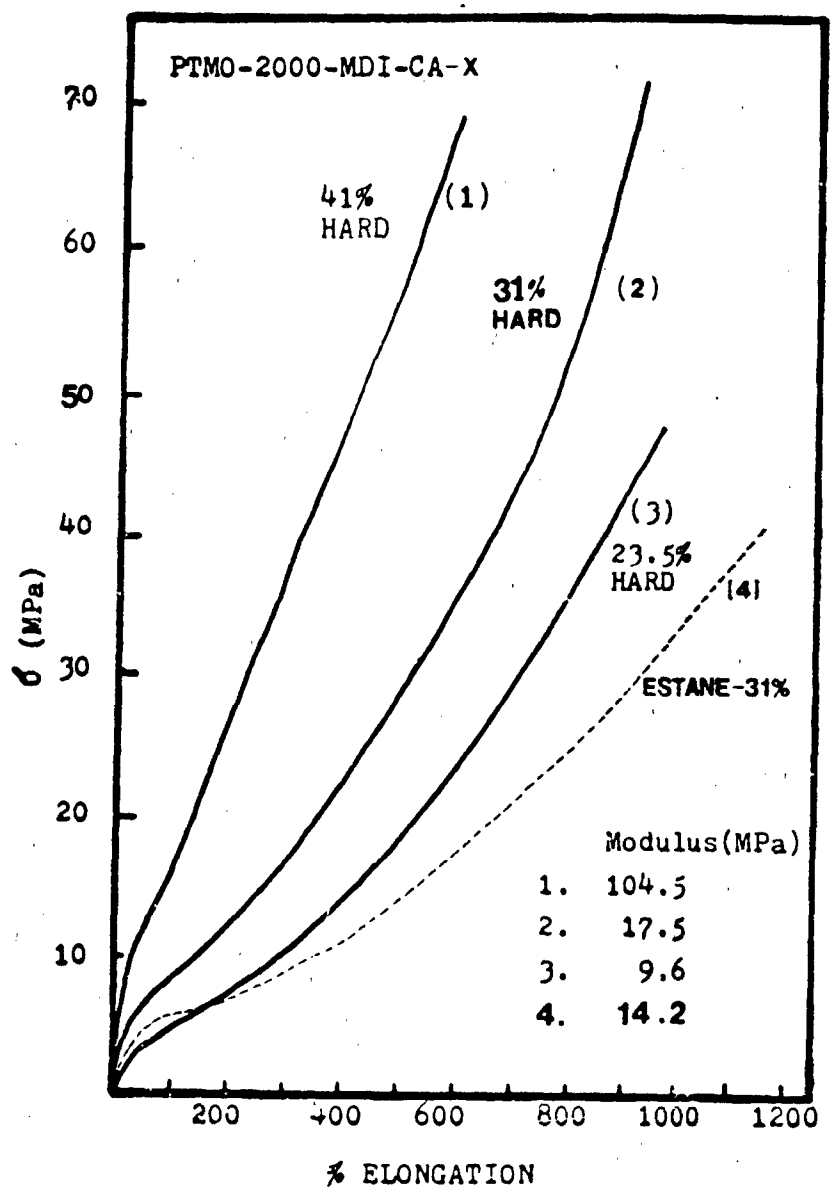


FIGURE 9: Effect of the hard segment contents on the stress-strain behavior of the PEUU's.

TABLE 5

MECHANICAL PROPERTIES OF SEGMENTED POLYURETHANEUREAS

SAMPLE	Ultimate Tensile Strength, MPa	Modulus MPa	Elongation %
PTMO-2000-MDI-23-CA	49.0	15.1	1000
PTMO-2000-MDI-31-CA	67.5	17.6	900
PTMO-2000-MDI-41-CA	59.0	104.5	600
PTMO-2000-MDI-31-DCA	59.0	11.4	1000
PTMO-1000-MDI-31-DCA	40.5	9.3	1100
PTMO- 650-MDI-31-DCA	17.5	6.8	1300
PTMO-2000-MDI-BD-31	41.0	13.2	1000

increase as the hard segment length is increased. This can be explained on the basis of the increase in the hard segment length necessary to maintain the same hard segment content with increasing molecular weight of the soft segments. Increasing the block length not only increases the aspect ratio of the dispersed hard domains but also leads to a higher degree of order in the hard domain since this results in more urea linkages per hard segment unit. Although the sample PTMO-650-MDI-31-DCA has a higher density of the hard segment units, the pseudo multifunctional cross-links formed by the hard domains are shorter and likely weaker. As a consequence of these poorly defined hard domains, the sample PTMO-650-MDI-31-DCA exhibits lower mechanical strength.

The stress-stain behavior for PEUU's based on PTMO-2000 with varying the hard segment contents is shown in Figure 9. It is indicated that the mechanical response of these materials is strongly affected when hard segment content is raised from 23.5% to 41% by weight. The observed behavior can be explained on the basis of the introduction of a higher volume fraction of hard segments as well as a higher degree of order in the hard segment domains. The higher modulus and tensile strength with increasing hard segment content in these samples is also consistent with their greater urea content which results in more cohesive hard domains. The dotted lines in Figure 9 depict the Estane control (PTMO-2000-MDI-BD-31) which has no urea linkages in the polymer backbone. This sample shows the lowest ultimate tensile strength. Clearly, the weaker interdomain secondary binding forces result

in less cohesive hard domains, poor hard/soft phase separation and may limit the development of a three dimensional hydrogen bonding network.

THERMOMECHANICAL ANALYSIS. The penetrometer mode of thermomechanical (TMA) spectrum was obtained for these PEUU's to observe the transitions associated with the hard and soft segments. Figure 10 compare the TMA measurements of three representative copolymers with different hard segment content. The primary transition near -70°C is ascribed to the soft segment glass transition. The hard segment transition is indicated to be composition dependent and varies from 200 to 250°C as the hard segment content is increased from 23.5 to 41% by weight. These results are consistent with the dynamic mechanical data as shown before. One significant feature of conventional polyurethane materials (e.g. Estane) is that they soften at relatively low temperatures, about 100°C, as expected. By contrast, both the strength and the service temperatures have been dramatically improved in these PEUU's.

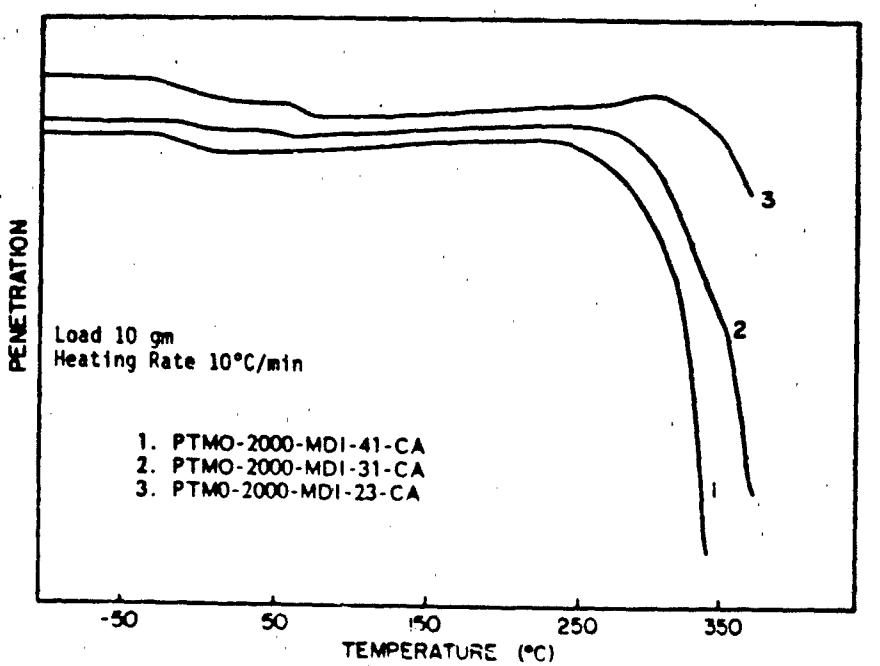


FIGURE 10. Thermomechanical penetration curves for various samples with different hard segment content.

The TMA response is also affected when the molecular weight of soft segment is varied for constant hard segment (see Figure 11). The PTMO-2000 based copolymer shows the highest softening temperature while PTMO-650 is the lowest.

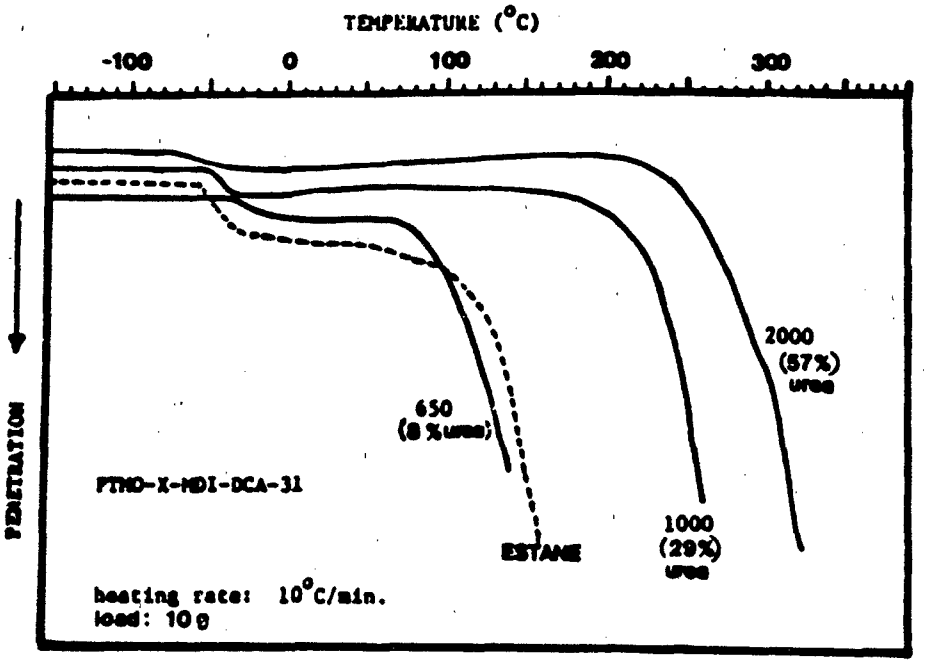


FIGURE 11. TMA penetration curves of the PEUU's with different soft segment lengths.

THERMOGRAVIMETRIC ANALYSIS. The TGA experiments were also conducted in order to investigate whether PEUU basically has a higher thermal stability than the polyurethanes. The results shown in Figure 12 demonstrate that PEUU is perhaps about 30-40°C more thermally stable than polyurethane at the same soft segment molecular weight and hard segment content as judged by TGA. Since the other components are identical, we believe this must reflect differences between the butandiol carbamates and the phenylurea hard segment systems.

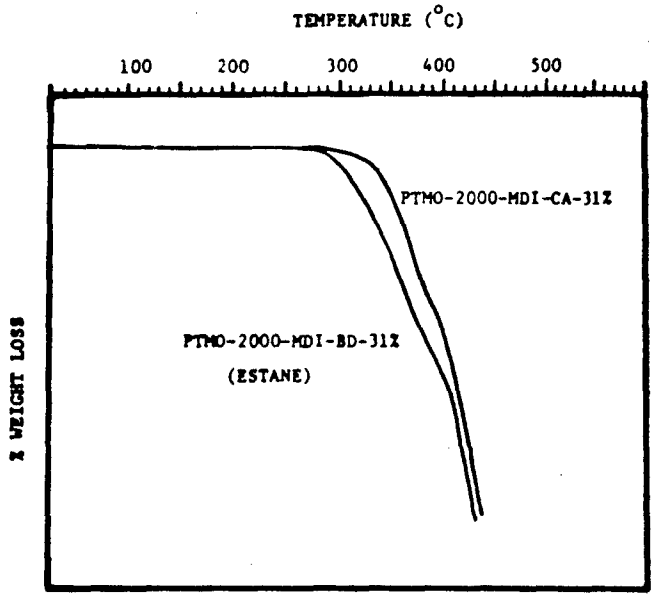


FIGURE 12. TGA curves for the polyether-urethane-urea and Estane.

CONCLUSIONS

A new route to urea linked polyurethane systems has been investigated. It has been shown that it is possible to synthesize novel polyurethane ureas by utilizing the rearrangement characteristics of carbamate-isocyanate interactions at a sufficiently high temperature. FT-IR spectra show the urea linkages have been efficiently incorporated into the polymer backbone. From the spectroscopy point of view, there is basically no difference in structure between mono- and difunctional tertiary alcohol chain extended PEUU's. Thus, it strongly suggests that these tertiary alcohols are not directly involved in the chain extension step. They rather form carbamates with isocyanates which tend to dissociate at high temperatures to give the corresponding amines. The phenyl substituted carbamates significantly reduce this temperature, probably by stabilizing the intermediate carbocation. By using this approach, the hard segment in the copolymer will be totally derived from the diisocyanates.

Good agreement with dynamic mechanical measurements was observed for DSC results as well. The PEUU's based on PTMO-

2000 exhibited a much higher upper temperature relaxation than the PEUU's based on PTMO-1000 and PTMO-650 or the control polyurethane. This is also reflected by a much lower soft segment T_g in the PEUU-2000 series. This has no doubt reflected some significant differences in phase separation as well as possible sequence length effect in the hard segment.

The mechanical properties were observed to depend primarily on the degree of order in the hard domains. It was shown that this order can be improved by increasing either the hard segment content at constant molecular weight of the soft segment or soft segment molecular weight at the same hard segment content. Both approaches increase the concentration of urea linkages in the PEUU's and hence the tensile properties. At comparable hard segment content, all materials indicated superior mechanical strength over polyether-urethane controls chain extended with butanediol.

ACKNOWLEDGEMENTS

The authors would like to thank TACOM for supporting this research under research contract no. DAAE-07-82-C-4094. JEM also thanks the Exxon Foundation for their generous support.

REFERENCES

1. Ishihara, H., Kimura, I., Saito, K., and Ono, H. (1974): J. Macromol. Sci., Phys. Ed., B10(4):591.
1a. Hepburn, K. (1982): Polyurethane Elastomers, Halstead Press.
2. Wang, C. B., and Cooper, S. L. (1983): Marcomolecules, 16:775.
3. Nakayama, K., Ino, T., and Matsubara, I. (1969): J. Macromol. Sci., Chem., Ae(5):1005.
4. Suzuki, H., and Ono, H. (1970): Bull. Chem. Soc., Japan, 43:682.
5. Khransovskii, V. A. (1980): Polym. Sci. U.S.S.R., 22(6):1516.
6. Paik Sung, C. S., Smith, T. W., and Wu, C. S. (1980): Marcomolecules, 13:117.
7. Paik Sung, C. S., Wu, C. B., and Wu, C. S. (1980): Macromolecules, 13:111.
8. Paik Sung, C. S., and Wu, C. B. (1981): Macromolecules, 14:212.
9. Kimura, I., Ishihara, H., Ono, H., Yoshihara, N., Nomura, S., and Kawai, H. (1974): Macromolecules, 7:355.

10. Ishihara, H., Kimura, I., Saito, K., and Ono, H. (1983): J. Macromol. Sci., Phys., B22:713.
11. Hu, C. B., Ward, Jr., R. S., and Schneider, N. S. (1982): J. Applied Polym. Sci., 27:2167.
12. Lyon, R. E., Wang, D. X., Farris, R. J., and Mackinght, W. J. (1984): J. Applied Polym. Sci., 29:2857.
13. Takahara, A., Tashita, J. I., Kajiyama, T., and Macknight, W. J. (1985): Polymer, 26:978.
14. Takahara, A., Tashita, J. I., Kajiyama, T., and Macknight, W. J. (1985): Polymer, 26:987.
15. Bauart, R., Morbitzer, L., and Rinke, H. (1970): Kolloid-Z. Z. Polym., 240:807.
16. Khranovskii, V. A., and Gul'ko, L. P. (1983): J. Macromol. Sci., Phys., B22(4):497.
17. Khranovskii, V. A., and Gul'ko, L. P. (1983): J. Macromol. Sci., Polym. Sci. U.S.S.R., 25(1):123.
18. Skuches, G. S., and Carleton, P. S. (1984): J. Applied Polym. Sci., 29:3431.
19. Lee, B., Tyagi, D., Wilkes, G. L., and McGrath, J. E.: ACS Rubber Div. Meeting, Los Angeles, April 23, 1985.
20. Saunders, J. H., and Slocombe, R. J. (1948): Chem. Revs., 43:203.
21. Bailey, W. J., and Cesare, F.: ACS Meeting, April, 1956.
22. Lee, B., Tyagi, D., Wilkes, G. L., and McGrath, J. E. (1986): ACS Polymer Preprints, 27(1) (in press).
23. Wicks, Jr., Z. W. (1975): Progress in Org. Coating, 3:73.
24. Camberlin, Y., and Pascault, J. P. (1983): J. Polym. Sci., Chem. Ed., 21:415.
25. Ng, H. N., Allegrezza, A. E., Seymour, R. W., and Cooper, S. L. (1973): Polymer, 24:255.
26. Tyagi, D., Armistead, J. P., Lee, B., Wilkes, G. L., and McGrath, J. E. (1985): ACS Polymer Preprints, 26(2):12.
27. Tyagi, D., Lee, B., Wilkes, G. L., and McGrath, J. E. (1986): Advances in Elastomers and Rubber Elasticity, edited by J. Lal and J. E. Mark, ACS Symposium Series, in press (1986).

SYNTHESIS OF BLOCK COPOLYMERS BY GROUP TRANSFER POLYMERIZATION

W.R. HERTLER, O.W. WEBSTER, D.Y. SOGAH, T.V. RAJANBABU
Central Research and Development Department, E.I. du Pont de Nemours and Company, Inc., Experimental Station, Wilmington, Delaware 19331

Group transfer polymerization (GTP) is a powerful method for controlled polymerization of acrylic monomers to form living polymers using organosilicon initiators, typically ketene silyl acetals such as $(Me)_2C = C(OMe)(OSiMe_3)$. Polymers with predetermined molecular weights as high as 100,000 and with narrow dispersivity have been obtained by adjusting the monomer/initiator ratio. Because GPT gives living polymers, block copolymers with controlled block size can be made by simply changing the monomer feed. Thus, GTP provides the means for controlled design of block copolymers for evaluation as elastomers, compatibilizers, adhesives, and as components of high performance finishes.

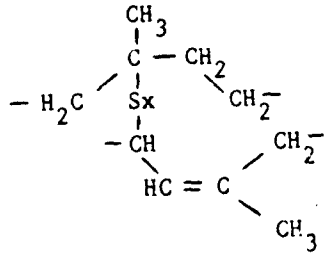
APPLICATION OF SOLID STATE ^{13}C NMR SPECTROSCOPY TO SULFUR VULCANIZED NATURAL RUBBER

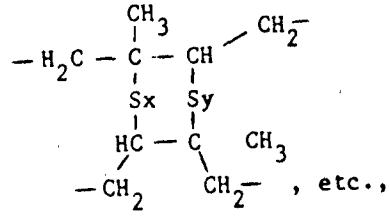
JACK L. KOENIG AND DWIGHT J. PATTERSON
Department of Macromolecular Science, Case Western Reserve University, Cleveland, Ohio 44106

INTRODUCTION

Over 140 years have passed since the initial discovery of sulfur vulcanization of natural rubber (NR) by Charles Goodyear and Thomas Hancock. Because of the many end uses of rubber vulcanizates, the components in the curing mixture have changed to produce finished products with good physical and mechanical properties with much shorter cure times than the original inefficient recipe containing only sulfur and NR.

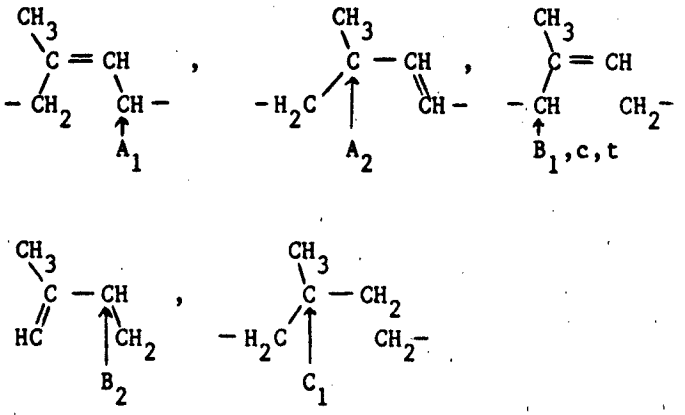
The vast range of properties that can be produced with cured NR is due to the structural variations of the crosslinked network arising from the variety of chemical reactions that can occur during the curing process. These reactions produce a variety of alkyl-alkenyl type of structures, such as:





, etc.,

(polysulfide, disulfide, monosulfide, cyclic sulfide, pendent sulfide, and conjugated diene and trienes). The alkenyl groups (and alkyl) are designated as follows:



(↑ indicates the point of attachment of sulfur) (1-4). The researchers at the MRPRA (formally NRPRA) have used model olefin compounds to elucidate the products and reaction pathways involved in sulfur vulcanization. These results suggested that at least two different mechanisms are responsible for unaccelerated and accelerated sulfur vulcanization of natural rubber a free radical mechanism (1,5,6) and a polar mechanism (1,7). Additional complexities in the structure are introduced by the desulfurization reactions (conversion of polysulfides to lower sulfides) (5,6,8).

The use of sulfur to cure NR is an inefficient (requiring 45-55 sulfur atoms per cross-link) curing process (9) and tends to produce a large portion of cyclic and polysulfides structures. To overcome this problem, conventional, semiefficient and efficient cure recipes were developed that produce a higher ratio of mono- and disulfidic cross-linked structures (4).

Even though these systems make more efficient use of sulfur, they can suffer similar maturing reactions as found with sulfur cured NR. It has been observed in some instances, that the modulus and the cross-link density goes through a maximum and continues to decrease with additional cure times (the loss of network structure by non-oxidative thermal aging). This process, which can occur in addition to the maturing reactions, is known as reversion (1,10,11). Reversion occurs when the desulfurization reactions are faster than the crosslinking reactions (12,13). The researchers at the MRPRA have divided these sulfur maturing reactions into two categories, see Figure 1. The left side is the desulfurization of

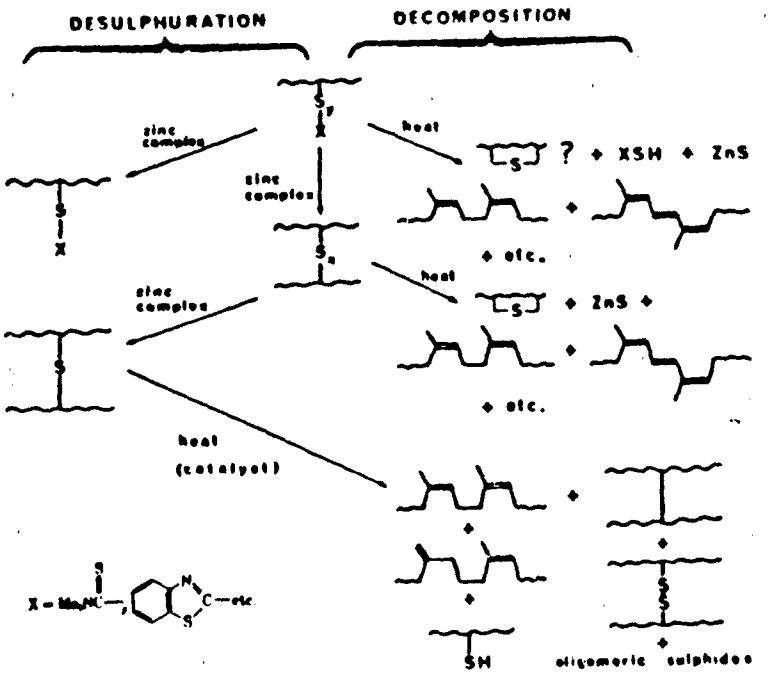


FIGURE 1. The cross-linking and cross-link decomposition scheme for natural rubber vulcanizations.

polysulfides to di- and monosulfidic cross-links. This pathway has been shown to be affected by the Zn-accelerator complex (found in accelerated sulfur vulcanizations mixes). The other routes are characterized as thermal decomposition, where the cross-links and the sulfuration species decompose into conjugated species, cyclic sulfides, shorter sulfur cross-links and main chain modification (14). Chen et al., (15) have shown that for certain accelerated sulfur cured systems, the reversion process is accompanied by the formation of a trans butadiene-like structure, in addition to formation of trienes and cyclic sulfides. In this paper, we have studied by solid state ^{13}C NMR, a series of sulfur cured NR (accelerated and unaccelerated) in search of the structural changes that occur during curing and in the desulfurization reactions.

EXPERIMENTAL

Sample Origin and Preparation. The natural rubber used had a technical classification of SMR-5. The compounded natural rubber samples were prepared by mixing the different ingredients in a Brabender mixing head. The temperature was controlled at 80°C and the mixing blades at 40 RPM for 15 minutes with virgin rubber and an additional 10 minutes with the ingredients, see Table 1. The same compounding conditions were

Table 1

COMPOSITION OF THE NATURAL RUBBER MIXES

Parts weight (phr)	A	B	C	D	E
Natural rubber (SMR-5)	100	100	100	100	100
Sulfur (insoluble)	10	-	-	2	4
TMTD	-	10	10	-	-
MOR	-	-	-	0.8	0.8
Zinc Oxide	-	-	10	2.5	2.5
Steric Acid	-	-	-	2.5	2.5

phr = parts per hundred

used for all mixings. After mixing, the samples were stored in screwcap bottles and placed in a refrigerator until needed. Two different accelerators were chosen because of their practical importance in the rubber industry, Tetramethylthiuriam disulfide, (TMTD) an ultrafast curing agent, and 9-oxydiethylene-2-benzothiol sulfenamide, (MOR) a delayed reaction accelerator. Both were obtained from Monsanto Industrial Chemical Company and used as received. Stearic acid was obtained from Aldrich Chemical Company and used as supplied.

The samples were cured in a template that gave specimens of 0.010 inch thickness. The template and samples were placed in a platen press at a pressure of 20,000 lbs/in^2 and heated for varying times (5, 10, 15, 30, 45, 60, 90 minutes) and temperatures (120, 130, 140, and 150°C).

For the equilibrium swelling measurements, 0.1 gm of rubber vulcanizate was placed in a stoppered glass vial containing benzene for 48 hours. The samples were removed, blotted dry with a paper towel, placed in clean stoppered vials and weighed. The samples were air dried for 72 hours and then reweighed to obtain the weight of the network gel and the amount of swelling solvent uptake.

Calculation of the Degree of Cross-linking. The modified Flory-Rehner equilibrium swelling equation (16) was used to determine the network chain density following the method of Shelton and McDonald (17) and Adams and Johnson (18):

$$\nu = \frac{1}{M_c} = \frac{-[\ln(1-V_r)+V_r+\chi V_r^2]}{\rho_r V_0 [V_r^{1/3} - V_r/2]}$$

ν = network chain density per gram of rubber
Mc = molecular weight between crosslinks
Vr = volume fraction rubber in the swollen vulcanizate
χ = Huggins interaction constant
ρ_r = density of rubber
Vo = molar volume of the solvent
ρ_s = density of the solvent

The volume fractions, Vr, was calculated from the reciprocal of the degree of swelling:

$$Vr = 1/[1+Q]$$

$$\text{where } Q = \frac{[\text{wt. of sol. in network}]}{[\text{wt. of network}]} \frac{\rho r}{\rho s}$$

The weight of the network was corrected for the sol component. The values of the constants used in the above calculation were: $\rho r = 0.915$ gm/cc (NR) $\rho s = 0.879$ gm/cc (benzene) $V_o = 89.40$ cc/mole $\chi = 0.42$ (NR) (19-22).

Fourier Transform ^{13}C Solid State NMR. The ^{13}C spectra were recorded on a Nicolet Technology NT-150 spectrometer operating at 38 MHz equipped with a cross polarization (CP) accessory for sensitivity enhancement (23). Radio-frequency amplifiers were adjusted to satisfy the Hartmann-Hahn conditions between 53-67 kHz rf (24). The high power proton decoupling fields were the same as the spin lock fields. Contact times between 1-1.5 msec. and a delay between pulses of 2 seconds were used. In the CP experiment 5-6K transients were accumulated. The vulcanized samples were packed into hollow Beams-Andrews rotors (24, 26) which were spun at speeds between 2.1-3.5 KHz. The rotors were machined out of polyoxymethylene and/or poly(chlorotrifluroethylene). The magic angle was set by maximizing the intensity of the carbonyl resonance of glycine. All FID's were zero filled to 8K data points. Two different one pulse Bloch decay experiments were used to probe the mobile network domains. Both experiments utilized gated decoupling (off during the delay period). One experiment utilized scalar decoupling (SD) with a 5 second delay between aquisitions and the other dipolar decoupling (DD) with 5-10 seconds delay. 500-5000 transients were accumulated in the MAS/SD experiment and 2-18K transients in the MAS/DD experiment. All experiments utilized quadrature detection and spin temperature alternation (27).

RESULTS AND DISCUSSION

In order to monitor the structural changes that had occured with the decomposition and desulfuration reactions, solid state ^{13}C NMR spectra were obtained for the samples cured at 150 degrees C. The spectra obtained by the MAS/SD experiment for the 10% sulfur cured samples are shown in Figure 2. Some of the expected structural

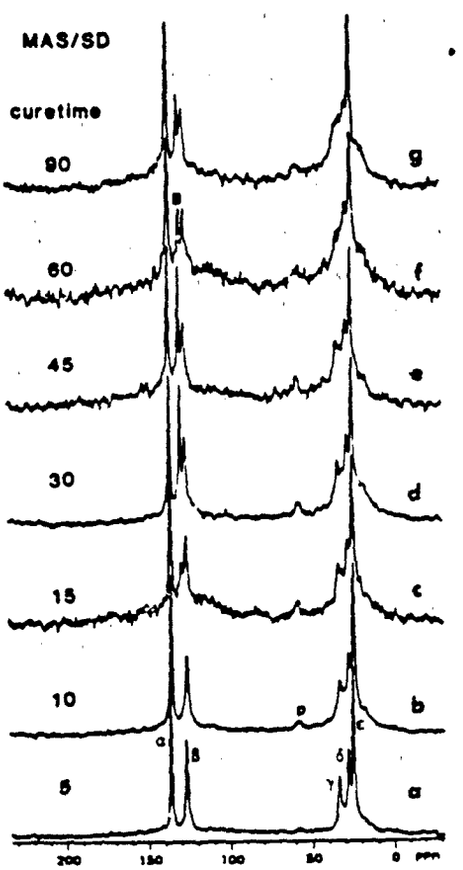


FIGURE 2. Stack plots of 10% sulfur cured natural rubber, different times of cure. b=butadiene-like species, p=polysulfidic cross-links cured at 150°C.

features (28) are shown in Figure 3. The assignments of the resonances in the cross-linked NR were made in accordance with the previous published work based on model compounds and semi-empirical chemical calculations [29-34]. Figure 4 lists the shielding effects of sulfur cross-links in natural rubber [31]. The samples with a low degree of cure (A and B) showed five major signals at 135.4 (C_α), 126.4 (C_β), 33.3 (C_γ), 27.7 (C_δ), and 24.7 ppm (C_ε), corresponding to the carbon atoms in the cis-1,4 isoprene unit as shown below:

$$[-CH_2-C(\overset{\varepsilon}{C}H_3)=CH-CH_2]$$
$$\gamma \quad \alpha \qquad \beta \quad \delta$$

Spectrum B shows an additional resonance signal at 57.6 ppm, which is assigned to polysulfidic and vicinal cross-links. Some of the intensity of this peak may arise from the polypeptides found in

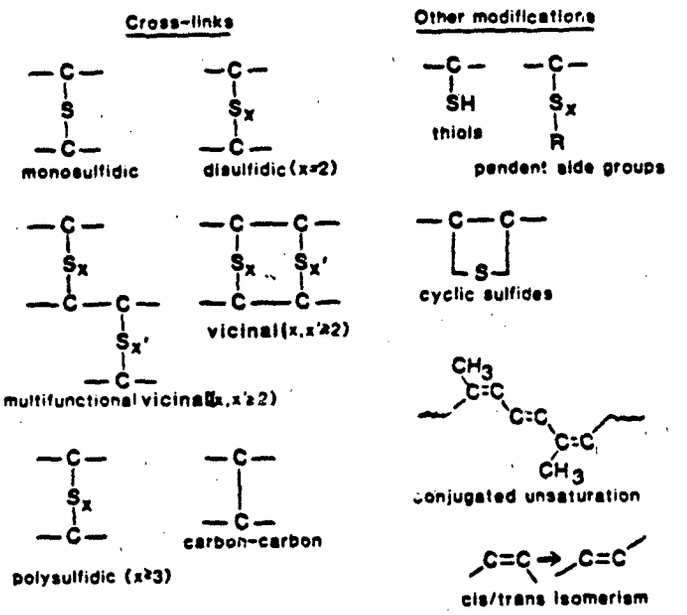


FIGURE 3. Schematic representation of different types of sulfur cross-links.

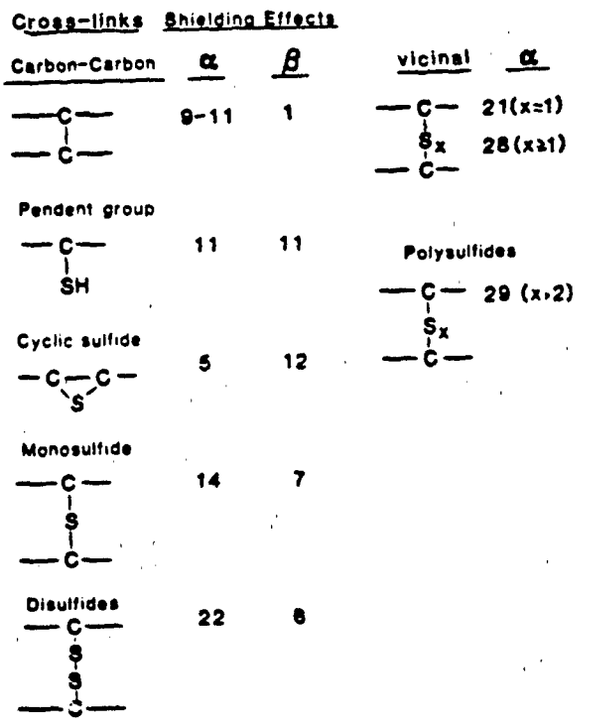
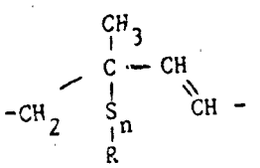


FIGURE 4. The listing of the cross-link types and their shielding effect on the carbon of attachment.

NR (36,37). A shoulder is observed on the high field (21-18 ppm) side of the NR methyl resonance at 24 ppm perhaps due to additional methyl groups at cross-link junctions and chain ends caused by chain scission. In the olefinic region of spectra (c-g) a new signal is observed to occur at 129.0 ppm, which is assigned to the olefinic methine carbons of a trans polybutadiene-like structure which is formed as a part of the reversion, see below:



Chen *et al.*[15] observed an FTIR band at 965 cm^{-1} which they assigned to *trans*-methine in the above structure. The trans butadiene-like resonance intensity reaches a maximum and then decreases with further cure time, see spectra F and G. This ultimate decrease indicates attack at the butadiene-like olefinic double bonds and hence loss of unsaturation. With the appearance of the olefinic butadiene-like structure, the aliphatic region begins to lose spectral resolution due to the increase in chemical shift dispersion and line broadening due to changes in molecular motion. The chemical shift dispersion is a result of the generation of new carbon species due to cross-link formation, desulfuration and thermal decomposition of polyfunctional sulfide units. The shoulders on the C_γ NR resonance (33 ppm) contain resonances due to monosulfidic (47 ppm) and cyclic mono- and disulfides (30-33 ppm) that occur upon network decomposition (28). The shoulders on the high field side of the C_δ carbon (24 ppm) assigned to methyl groups, are observed to increase in spectra c to g. These methyl groups are formed by the attack of the sulfurating species at the quaternary olefinic carbon and produced upon main chain scission.

By using the MAS/SD NMR data with the swelling data (Figure 5), the changes in the swelling curves can be related to the structural modifications observed by NMR. The increase in the swell data (150 °C swelling curve) is shown to occur with the appearance of the resonance line at 130 ppm. This is further depicted in Table 2 where network chain density and molecular weight between cross-links, obtained by the Flory-Rehner equilibrium swelling equation are listed. The molecular weights between cross-links decrease by an order of magnitude in curing from 5 minutes to 90 minutes at 120°C and likewise in going from 120 to 150°C at 5 minutes.

It is very tempting to try to measure the fractions of each of the network structures by quantitatively measuring the relative areas of the well resolved resonances present in the MAS/SD spectra . One must be cautious in this endeavor for Ford *et al.* (38, 39) have shown that cross-

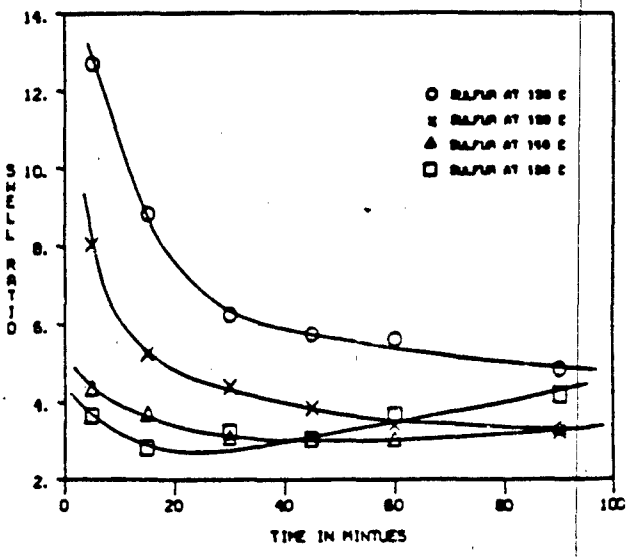


FIGURE 5. Plot of swell ratio versus time of cure.

linked polymers are heterogeneous and all carbons are not observed even with the additional motional freedom imparted by solvent swelling of the gel. Koenig et al. (35,36) have shown that not all of the carbons of a benzene swollen, peroxide-cured NR are observed by a MAS/SD experiment which only detects mobile species. With this in mind we obtained the CP/MAS/DD spectra of the sulfur cured samples since the CP /MAS/DD experiment is sensitive to rigid species in the network.

Typical spectra obtained by the CP/MAS/DD experiments are shown in Figure 6. The spectra indicate that there is an abundance of rigid network species that experience strong dipolar coupling and hence short cross relaxation times. Because we have strongly coupled species we are able to observe CP spectra. A weak broad resonance is observed between 160-170 ppm. This resonance is due to carbonyl groups of acid and aldehyde species. These species were formed by oxidation during the vulcanization process. It is observed that these resonances do not appear in the MAS/SD spectra. The carbon resonance at 135.9 ppm is

TABLE 2

THE CALCULATED NETWORK DENSITY AND MOLECULAR WEIGHT BETWEEN CROSS-LINKS

Time	Sulfur 120°C		Sulfur 130°C		Sulfur 140°C		Sulfur 150°C	
	$\nu X10^{-4}$ mole/gm	M_c g/mole	$\nu X10^{-4}$ mole/gm	M_c g/mole	$\nu X10^{-4}$ mole/gm	M_c g/mole	$\nu X10^{-4}$ mole/gm	M_c g/mole
5 min	.16	60,000	.39	25,000	1.24	8,000	1.74	5,700
15 min	.32	30,000	.87	11,400	1.67	5,900	2.82	3,500
30 min	.62	15,900	1.22	8,100	2.37	4,200	2.21	4,500
45 min	.73	13,500	1.58	6,300	2.42	4,100	2.47	4,000
60 min	.77	12,900	1.99	5,000	2.44	4,100	1.72	5,800
90 min	1.02	9,800	2.21	4,500	2.06	4,800	1.35	7,400

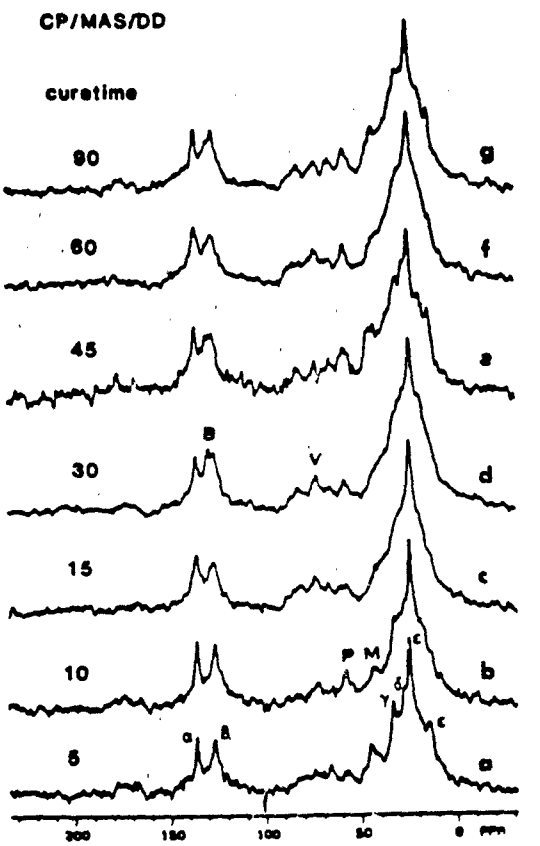
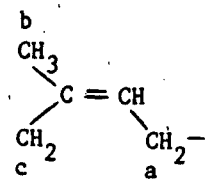


FIGURE 6. Stack plot of CP/MAS/DD spectra of 10% sulfur cured 150°C p=polysulfidic, v=vicinal, m=monosulfides, other species can contribute to these resonance, see text.

assigned to the olefinic quaternary carbon and the 126.3 ppm resonance is assigned to the olefinic methine carbon. The appearance of the resonance due to the trans butadiene-like species at 129.6 ppm is observed in the CP/MAS/DD experiment, see spectra c-g. The shoulder on the major olefinic carbon resonance (136 ppm) indicates the presence of other types of olefinic carbons.

Unlike the MAS/SD spectra where only one resonance (57.6 ppm) was observed between 90-50 ppm, the CP/MAS/DD spectra show at least four resonances in the same region. The observed chemical shifts for these resonances are 82.7, 76.3, 67.8, and 57.9 ppm. The three lowest field resonances would normally be assigned to peroxides-hydroperoxides, alcohols and epoxy groups, which are formed during oxidation (40). Other possibilities need to be considered, for we calculate chemical shifts between 55 to 73 ppm for polysulfidic, disulfidic, and vicinal cross-linked species, using the shielding effects given in Figure 4. This distribution in chemical shifts comes about because of the five isomeric alkenyl species available for attack in the polyisoprene molecule, see below:



The positions are the three α-carbon atoms allylic to the double bond. Their isoallylic counterparts are shown in the A_2 and B_2 alkenyl groups. We calculated chemical shifts for the allylic and the isoallylic carbon atoms bearing the series of cross-linked functionalities shown in figure 3. The specific shielding effect was added to the observed chemical shift of the carbon in virgin NR and the chemical shift of the alkyl function was calculated according to MacDonald (33). From this we found that isoallylic pendant thiol groups, allylic disulfides (position c), allylic polysulfides (position a), and vicinal cross-links ($x \geq 1$) were calculated to resonate at 56 $\pm$ 2 ppm. We had assigned the resonance at 57.8 ppm to poly and vicinal sulfides with the possibility of other species contributing due to its broad line shape. It has been shown lately by Zaper *et al.* (42), that raising the temperature of the sample to 80°C in a variable temperature probe, that the resonance at 57 ppm splits into three peaks. In order to make a more definitive assignment, model

compounds of the rubber analogs with the various sulfidic crosslinks are needed. The resonance at 68 ppm can be assigned to isoallylic vicinal (x>2) and isoallylic polysulfides. Of the structural combinations considered, no species produced a chemical shift in the 82 ppm range. Therefore the resonance lines in the 58 to 82 ppm region are postulated as due to oxygenated and sulfidic cross-linked species.

The resonance between 40-45 ppm is assigned to allylic and isoallylic monosulfides, allylic thiol groups, and methylene carbons β to the sulfur cross-link carbon. The methyl resonance at 14 ppm is assigned to methyl groups at cross-link junctions and end groups formed by chain scission. As we go from spectrum a to g the resonance at 30-33 ppm grows due to the formation of cyclic species. The resonance at 30.7 ppm can have contributions from γ-methylenes in the cis-trans isomerized species.

In Figure 7, the resolution enhanced spectra

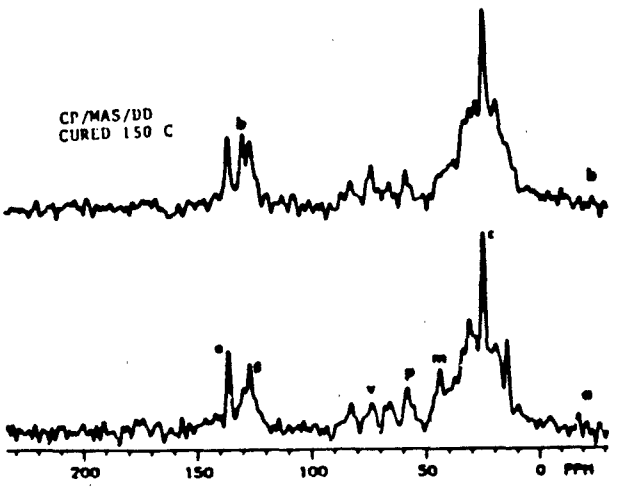


FIGURE 7. Resolution (CP/MAS/DD) enhanced spectra of 10% cured NR. A, cured 90 minutes, B, cured 30 minutes, B=butadiene-like species, v=vicinal, p=polysulfides, m=monosulfides.

of samples cured at 150°C for 30 and 90 minutes are plotted. The different spectral features shown by the two spectra are (1) the loss in intensity of the trans polybutadiene-like resonance at 129 ppm, (2)the increase in the combination band due to monosulfides and cyclic sulfides (45 ppm), and (3) the increase in the intensity of the methyl end groups (20-15 ppm). The structural complexity found for unaccelerated sulfur cured NR is consistent with the formation of polysulfidic cross-links which later desulfurate to monosulfidic links and the thermal decomposition of the allylic sulfides to cyclic sulfides and conjugated trienes.

In Figure 8 the spectra are shown of the NR samples cured 90 minutes with 10% sulfur, obtained by CP/MAS/DD (curve B) and CP-dipolar dephasing (curve A). The CP-dipolar dephasing experiment isolates the quaternary carbons which do not decay through the proton dipolar dephasng process since they have no bonded protons.. The dipolar dephasing delay was 100 seconds. In spectrum A the olefinic quaternary carbon resonance remains at 136 ppm. No resonances due to quaternary carbon-carbon crosslinks (43 ppm) are observed in the 10% sulfur cured sample. The four resonances present between 50-90 ppm are assigned to quaternary cross-links of the various sulfur functions.

A 10% TMTD cured system was also studied that is reported to cure by a free radical mechanism, see Table 3. In Figure 9, the aliphatic region of the NR sample cured with 10% TMTD at 140°C for 60 minutes is plotted. The resonance at 72 ppm is due to the rotor. The truncated resonances are due to the methylenes and methyl carbons of cis NR. The resonance at 68 ppm is assigned to isoallylic disulfides, isoallylic vicinal (x=1) cross-links.

The resonance at 58 ppm for the 10% TMTD cured system is assigned to polysulfides and vicinal groups. This may seem to be inconsistent with the fact that TMTD forms primarily mainly monosulfidic and disulfidic crosslinks in NR. However, Ccleman (43) has shown that the thermal decomposition of

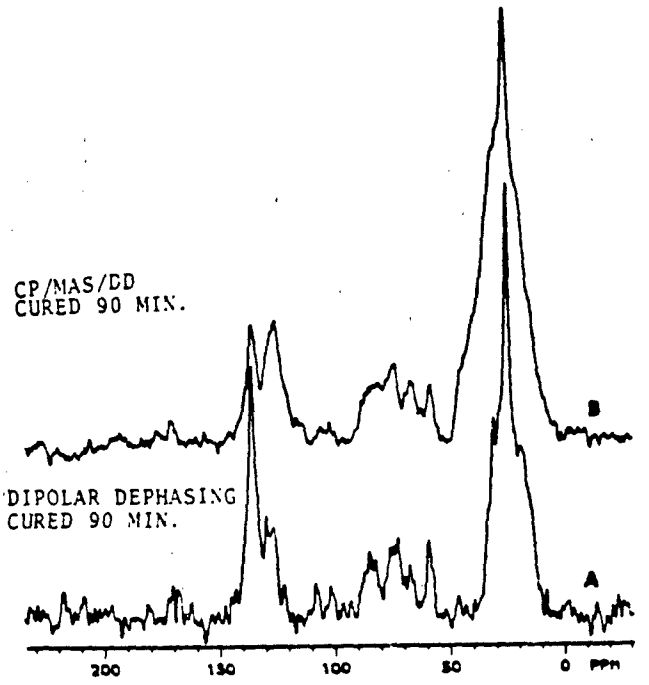


FIGURE 8. CP/MAS/DD spectra of 10% sulfur cured NR. Spectrum B, obtained by normal CP exp., Spectrum A, dipolar dephasing experiment tau delay 100 micro s. Resonances assigned to quaternary carbons with attached polyfunction cross-links.

TABLE 3

PROBABLE MECHANISM FOR NATURAL RUBBER VULCANIZATION

System	Comment
Unaccelerated sulfur	Mixed, polar and free radical
TMTD	Free Radical
TMTD-ZnO	Predominantly polar
Accelerated sulfur	Mixed, polar and free radical

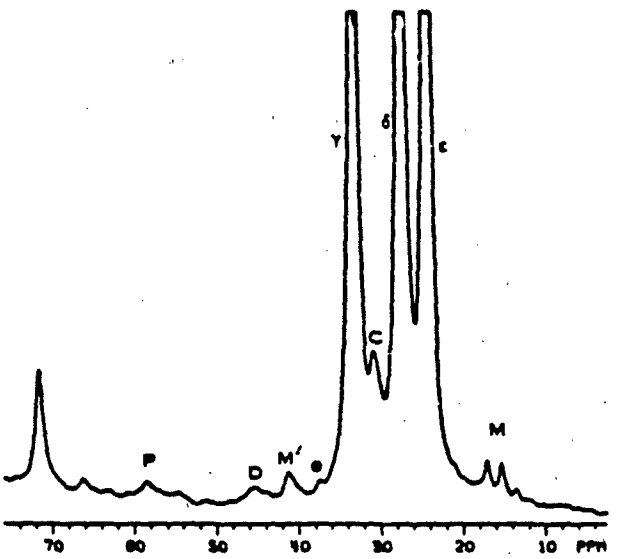


FIGURE 9. The MAS/DD spectrum of 10% cured TMTD in NR at 150°C for 1 hour. m=methyls, c=cis-trans junctions and cyclics, m=monosulfides, d=disulfides, p=polysulfides, e=trans-cis junction.

TMTD can form polysulfidic species. Therefore, it is reasonable to expect some polysulfidic cross-links to form in our system. The resonances at 52 ppm and 45 ppm have been assigned to di- and monosulfidic cross-links respectfully. The resonances at 41 and 17 ppm are due to trans NR, formed by cis-trans rearrangement. Two other resonances at 38 (trans) and 31 (cis) ppm are due to the methylene carbons at the junction of the trans and cis isomers. The two methyl resonances at 15 and 13 ppm are assigned as before. A weak resonance at 21 ppm is assigned to methyl groups attached to quaternary carbons.

Figure 10 is the truncated spectrum of 10% TMTD and 10% ZnO in Nʀ that has been cured for 90 minutes at 150°C. This formulation is reported to cure NR by a polar mechanism. The only additional resonances that we observe are at 17 and 41 ppm and are due to trans species.

The spectrum of a conventional mix of NR and additives cured for one hour at 150°C (formulation E, Table 1) is shown in Figure 11. The cross-linked resonances observed have been detected in the samples above (sulfur and TMTD cured) although the relative intensities are different. The resonances at 58 and 45 ppm are assigned to poly, vicinal, and monosulfides, respectfully. The resonance at 41 ppm has a shoulder with a low field peak assigned to allylic (A type) monosulfides and the high field resonance at 41 ppm to trans methylene carbons. The resonances at 31 ppm have been shown to be composed of two components when a line broadening

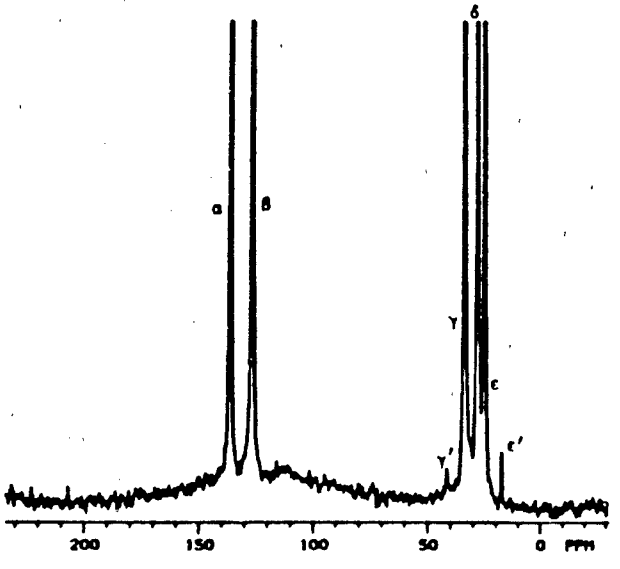


FIGURE 10. The MAS/DD spectrum of 10% TMTD + 10% ZnO cured Nr. Cured 150° hrs, , trans species.

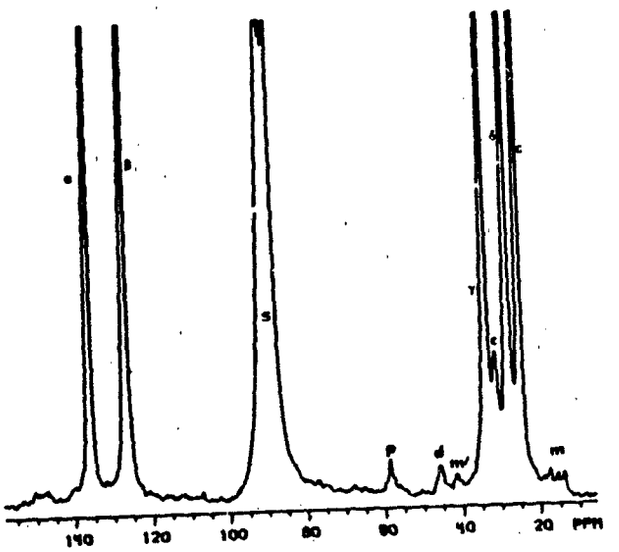


FIGURE 11. Conventional cured natural rubber (formulation E) cured 1 hr at 150°C. P=polysulfides, d=disulfides, m=monosulfides, c=cyclics plus cis-trans, m=methyl.

of 10 Hz was used. The shoulder at 30 ppm is due to cis methylene carbons at cis-trans junctions and the 31 ppm resonance to cyclic species. Four methyl resonances are observed above 20 ppm. At 130 ppm a weak signal is observed and assigned to the trans-butadiene-like species. From a preliminary CP/MAS/DD spectrum (5 msec contact time), a resonance due to cyclic sulfides was detected at 34 ppm. This resonance is masked in the MAS/SD spectrum by the methylene resonance at 33 ppm. In addition a new olefinic resonance was detected at 123 ppm.

SUMMARY

Sulfur cured NR shows a complex spectrum by solid state ^{13}C NMR. Polyfunctional sulfur cross-links are predominant. The *trans* polybutadiene-like resonance at 129 ppm forms with reversion. This resonance subsequently decreases in intensity with further cure due to attack of the olefinic carbons. The conventional cured sulfur system showed poly and monosulfidic cross-links. Cis-trans rearrangement was observed to occur in conventional, TMTD, and TMTD/ZnO cured systems. Chain scissions are observed in all cured formulations. Quantitative measurements of the structural components of these networks must await further developments in technique.

REFERENCES

1. Bateman, L. (1965): *The Chemistry and Physics of Rubber-Like Substances*. MacLaren and Sons, London
2. Porter, M. (1968): The Chemistry of Sulfur Vulcanization of Natural Rubber, in *The Chemistry of Sulfides*, edited by A. Tabolsky, Interscience, New York.
3. Coleman, M.M., Shelton, J.R., and Koenig, J.L. (1974): Ink. Eng. Chem., Prod. Res. Develop., 13:155.
4. Elliott, D.J. and Tidd, B.K. (1973/1974): Prog. Rubber Tech., 37:83.
5. Bloomfield, G.F. (1946): J. Polym. Sci., 1:312.
6. Farmer, E.H. and Shipley, F.W. (1946): J. Polym. Sci., 1:293.
7. Bateman, L., Moore, C.G. and Porter, M. (1958): J. Chem. Soc., 21:2866.
8. Maurer, J.J. (1981): Elastomers. In: *Thermal Characterization of Polymeric Materials*, edited by E.A. Turi, Acadamic Press, New York.
9. Moore, C.G., Mullins, L. and Swift, P.McL. (1961): J. Appl. Polym. Sci., 5:293.
10. Campbell, D.S., (1970): J. Appl. Polym. Sci., 14:1409.

11. Moore, C.G. and Porter. M. (1967): J. Appl. Polym. Sci., 11:2227.
12. Hofmann, W. (1967): Vulcanization and Vulcanizing Agents, MacLaren, London.
13. Blokh, G.A. (1968): Organic Accelerators In: The Vulcanization of Rubbers, Israel Program for Scientific Translation Ltd.
14. Morrison, N.J. and Porter, M. (1984): Rubb. Chem. Technol., 56:63.
15. Chen. C.H., Koenig. J.L., Shelton, J.R. and Collins, E.a. (1981): Rubb. Chem. Tech., 54:734.
16. Flory, P.J. (1953): Principles of Polymer Chemistry. Cornell Press, New York, 576 pp.
17. Shelton, J.R. and McDonel. E.T. (1959): Proc. Inter. Rubber Conf., 596.
18. Adams, E.H. and Johnson, B.L. (1953): Ind. Eng. Chem., 45:1539.
19. Hummel, K. and Kaiser, G. (1965): Rubber Chem. Tech., 38:581.
20. Thomas, D.K. (1962): J. Appl. Polym. Sci., 6:613.
21. Brandrup, J. and Immergut, E.H. (1975): Polymer Handbook. John Wiley, New York.
22. Saltman, W.M. (1977): The Stereo Rubber. Interscience, New York.
23. Pines, A., Gibby, M.G. and Waugh, J.S. (1973): J. Chem. Phys., 59:569.
24. Hartmann, S.R. and Hahn, E.L. (1962): Phys. Rev., 128:2042.
25. Beams, J.W. (1930): Rev. Sci. Instrum.,1:667.
26. Andrews, E.r. (1972): Prog. Nuc. Magn. Reson. Spectro., 8:1.
27. Scheafer, J. and Stejskal, E.O. (1975): J. Magn. Reson., 18:560.
28. Saville, B. and Watson. A.A (1967): Rubb. Chem. Technol., 40:100.
29. Duch, M.W. and Grant, D.M. (1970): Macromolecules, 3:165.
30. Scheafer, J. (1973): Macromolecules, 6:882.
31. Koenig, J.L. and Liu, N. unpublished results.
32. Stothers, J.B. (1972): Carbon-13 NMR Spectroscopy. Academic Press, New York.
33. MacDonald, J.C. (1979): J. Magn. Resonan.
34. Barbarella, G., Dembech, P. Garbesi, A. and Fave, A. (1976): Org. Magn. Reson., 8:108.
35. Komoroski, R.A. Personal communication.

36. Patterson, D.J., Koenig, J.L. and Shelton, J.R. (1983): Rubb. Chem. Technol., 56:971.
37. Patterson, D.J. and Koenig, J.L. (1984): In: Characteriztion of Highly Cross-linked Polymers, edited by S.S. Labana and R.A. Dickie, ACS Sym. Series, 203:205.
38. Ford, W.T. and Balakrishnan, T. (1981): Macromolecules, 14:284.
39. Ford, W.T. and Balakrishnan, T. (1983): Polymer Characterization: Spectroscopic, Chromatographic, and Physical Instrumental Methods, edited by C.D. Carver, Advances in Chem. Series, ACS 203:475.
40. Golyub, M.A., Hus, M.S., Wilson, L.A. (1975): Rubb. Chem. Technol., 48:953.
41. Zaper, A.M. and Koenig, J.L., to be published.
42. Morrison, N.J. and Porter, M. (1982): PRI, Annual National Conference, p104.
43. Coleman, M.M. (1973): Ph.D. Dissertation, CWRU, Cleveland, Ohio.

ACKNOWLEDGMENTS

The authors wish to acknowledge the financial support of the U.S. Tank Automotive Command under Contract #DAAE07-83-K-R010.

^{13}C NMR STUDIES OF ELASTOMERS IN SOLUTION AND THE SOLID STATE

R. A. KOMOROSKI*, J. P. SHOCKCOR, and J. L. SAVOCA
BFGoodrich Research and Development Center
9921 Brecksville Road
Brecksville, OH 44141

INTRODUCTION

High resolution NMR has undergone a revolution in the last ten years or so. The ability to manipulate spin systems to a high degree in the pulse FT NMR experiment, coupled with advances in NMR computing systems, has led to the design of many multipulse and two-dimensional (2-D) NMR experiments which can provide considerably more information than a standard spectrum.[1] In addition, experiments to obtain high resolution NMR spectra of solid materials have opened a whole area of chemistry to NMR.[2] The new interpretive techniques for spectra obtained in solution have been applied to synthetic polymers or polymer chemicals only recently. However, the solid state methods already have seen wide application in the polymer area.[3] In this report we describe some work from our laboratory employing some of these advanced methods in both solution and the solid state. This is not meant to serve as a detailed discussion of the techniques employed, but rather as an introduction to potential applications in the rubber and polymer industries.

MATERIALS AND METHODS

All spectra were obtained at 50.3 MHz on a Bruker WH-200 FTNMR spectrometer equipped with an Aspect 2000 RTC retrofit and fast-switching decoupler. This includes standard, APT,[4] and DEPT[5,6] spectra. For the spectra obtained on solutions, 10 mm o.d. tubes were used. The 90° rf pulse width was about 20 μs. Composite pulse decoupling (MLEV-16)[7] was used in most cases. The sulfur-cured sample was obtained by curing 100 parts natural rubber with 8 parts sulfur and 5 parts ZnO for 6 hrs at 280°F. For the vulcanized rubbers, a sheet of rubber was wound into cylindrical shape and inserted into a 20 mm o.d. NMR tube. The center was then filled with small chunks of the same rubber. The spectrum was obtained at about 90°C with no lock solvent. No significant broadening of the spectral lines from magnetic field drift occurred during an overnight run. Typical conditions for the bulk rubbers were: pulse repetition rate, 1s; spectral width, 13,513 Hz; artificial line broadening, 5 Hz; 90° rf pulse, 34-36 μs, using a probe designed for 20 mm tubes.

RESULTS AND DISCUSSION

Application of Spectral-Editing Techniques to Polymers

The interpretation of the ^{13}C spectra of organic compounds is greatly aided by techniques to determine the number of hydrogens attached to a given carbon atom. In the past, single frequency off resonance decoupling,[3] noise off resonance decoupling,[3] and APT (Attached Proton Test)[4] have been used with good success. The effects of tacticity and comonomer sequences can produce complex ^{13}C spectra for polymers with much of the critical information unresolved. Any technique which can improve the spectral resolution to aid in peak assignments or quantitative characterization is welcome. In the past it was often necessary to synthesize copolymers from isotopically enriched monomers to assign complex spectra. In some cases, spectral-editing techniques can provide spectral simplification.

The APT technique[4] relies on the variation of the amplitude and phase of signals in spin-echo ^{13}C spectra due to CH coupling when the decoupler is off. The pulse sequence is shown in Figure 1A. The technique introduces a 180° phase shift between CH and CH_3 carbons on the one hand, and CH_2 and C_q carbons on the other. Hence, in the FTNMR spectrum one group will appear inverted relative to the other group.

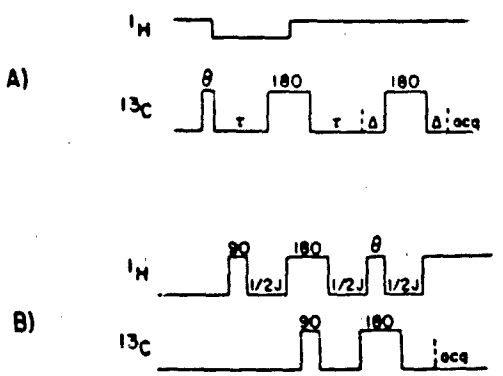


Figure 1. Two NMR multipulse sequences. A) APT; B) DEPT.

A good illustration of the use of APT is provided by the ^{13}C spectra in Figure 2. At the top is the spectrum of a low molecular weight, carboxyl-terminated butadiene-acrylonitrile copolymer (CTBN). The extensive peak multiplicity is due to geometrical isomerism of the butadiene units (cis, trans, and vinyl) coupled with copolymer sequences containing acryloni-

trile, and end group peaks. At the bottom is the APT spectrum. Based on the APT results, a number of resonances from the $HO_2C(CH_2)_2C(CN)(CH_3)$- end groups are assigned in the spectrum in Figure 2. The arrows indicate peaks which would be difficult to assign without the assistance of spectral editing. However, in these same cases there is some overlap, with cancellation of intensity that could prevent the observation of small, hidden peaks. Hence, although APT is good for detecting certain interfering combinations (such as CH with CH_2), it suffers from unreliable intensities because of cancellation and is not of general utility for separation of all carbon types.

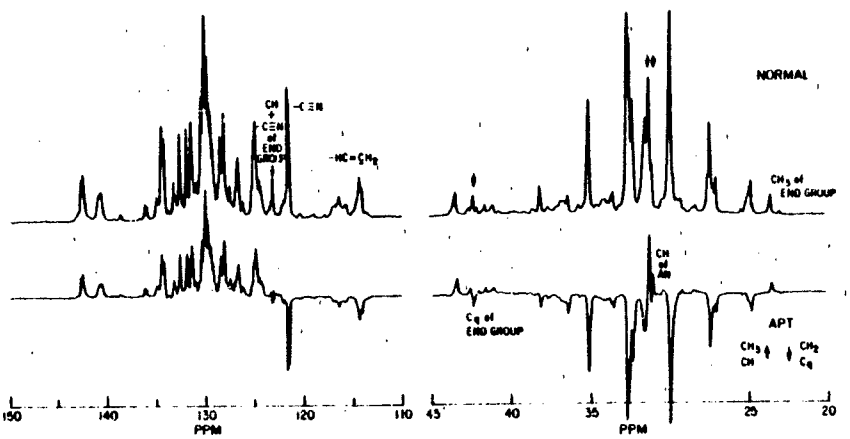


Figure 2. Normal ^{13}C (top) and APT (bottom) spectra of a low-molecular weight carboxyl-terminated butadiene-acrylonitrile copolymer (CTBN).

For example, in a study of a series of vinyl chloride-vinylidene chloride (VC-VDC) copolymers, we used partially relaxed and APT spectra to confirm the presence of several CH_2 peaks in a predominantly CHCl carbon region.[10] Tentative assignments were made. Unfortunately, that effort was of limited success because the overlap was so extensive that peak cancellation obscured resonance positions and intensities.

A spectral-editing sequence that provides unambiguous determination of carbon multiplicities is the Distortionless Enhancement by Polarization Transfer (DEPT) sequence.[5,6] We have implemented DEPT in our laboratory to aid in interpreting spectra of complex organic compounds. The value of the DEPT sequence lies in its ability to provide relatively clean subspectra, each of which is due only to one type (CH_3, CH_2, CH) of carbon.

The method, which is a variation of the INEPT sequence[11] for sensitivity enhancement, relies on the existence of a resolvable spin-spin coupling between two nuclei, one of which serves as the polarization source for the other. The polarization source is usually the proton while ^{13}C or ^{15}N is the insensitive nucleus being enhanced. The DEPT pulse sequence for the J-coupled, heteronuclear system of ^{13}C and ^{1}H is shown in Figure 1B. The behavior of the ^{1}H and ^{13}C spin systems during the DEPT sequence is complicated, and will not be explained here. Suffice it to say that the different multiplets (CH, CH_2, CH_3) behave differently during the sequence, allowing them to be separated from each other by proper pulse combinations. The pulse θ is set to 45, 90, or 135° to give three spectra which, when combined properly, give the three protonated carbon subspectra. Any carbons unaccounted for by these spectra are nonprotonated. The DEPT sequence has several advantages. It allows for complete editing; it is insensitive to J; and it is less sensitive to rf-pulse inhomogeneity than INEPT. These conditions produce more reliable intensities than INEPT. The DEPT sequence is more difficult to use than previous editing techniques in that three spectra must be acquired and co-added to produce the final result. Usually some slight admixture of the subspectra is seen when the above procedure is used. In practice it is necessary to determine additional linear combinations to produce clean subspectra. The method also requires careful calibration of the proton pulse widths.

DEPT can also be used purely for resolution enhancement by separating intensity from totally overlapping resonances for different carbon types, at least in the ideal case.[12,13] The DEPT technique has recently been applied to polymers. Barron et al[12] applied the method to copolymers of styrene with maleic anhydride or acrylonitrile. The information obtained allowed them to elucidate more fully the copolymerization mechanism. These authors also considered the use of DEPT for quantitative analysis. They concluded that quantitative comparisons of peak intensities within a single subspectrum were reliable, but that comparisons among different subspectra could be in error for several reasons, which they discussed. Newmark[13] examined eight commercial copolymers to ascertain the general utility of the technique, as well as the effect of spin-spin relaxation (T_2) behavior on the quality of the DEPT spectra.

We have applied DEPT to a number of polymers of interest in our laboratory. One example is styrene-butadiene rubber (SBR). Although the ^{13}C spectrum of SBR is complex, many peak assignments have been made, particularly at low field.[14] However, many of the resonances are closely spaced, even at 50.3 MHz, preventing unambiguous assignments in some cases. For example, in the aliphatic region of the ^{13}C spectrum of a

high-styrene SBR (52% styrene) shown in Figure 3, it is difficult to pick out the peaks due to styrene blocks. The expected positions based on the spectrum of polystyrene are shown in Figure 3. It is important to know the amount of

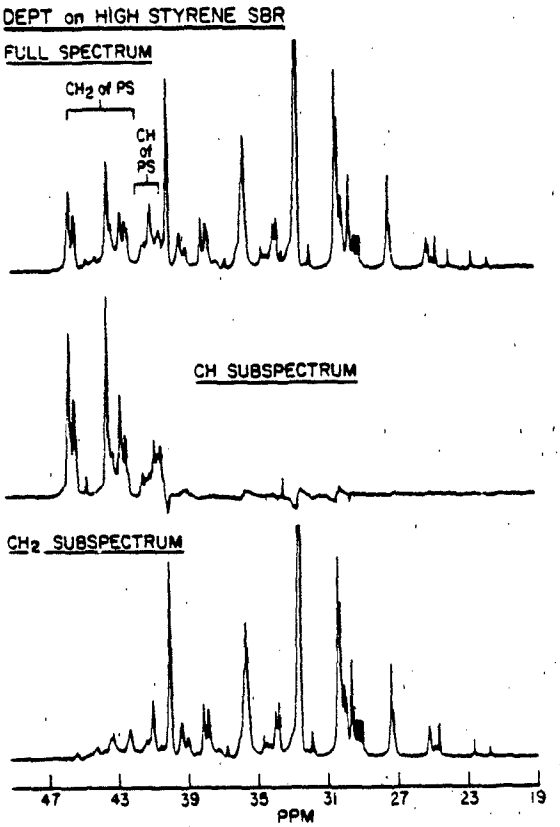


Figure 3. Full and DEPT spectra of a high-styrene SBR.

blocked styrene since this parameter will affect rubber properties. The DEPT subspectra provide separation of these resonances in the 39 to 43 ppm region, allowing identification of both the CH and CH_2 peaks due to block styrene. Both of these are obscured in the full spectrum by resonances due to other sequences. The CH subspectrum now clearly shows the block styrene CH at 40.5 to 41.5 ppm along with other CH resonances arising from vinyl or isolated styrene sequences at 42 to 46 ppm. The CH_2 subspectrum shows the block styrene CH_2 resonances split by tactic effects from 41 to 45 ppm.

We have also applied DEPT to the VC-VDC copolymer series examined previously.[10] Figure 4 shows the DEPT spectra for a

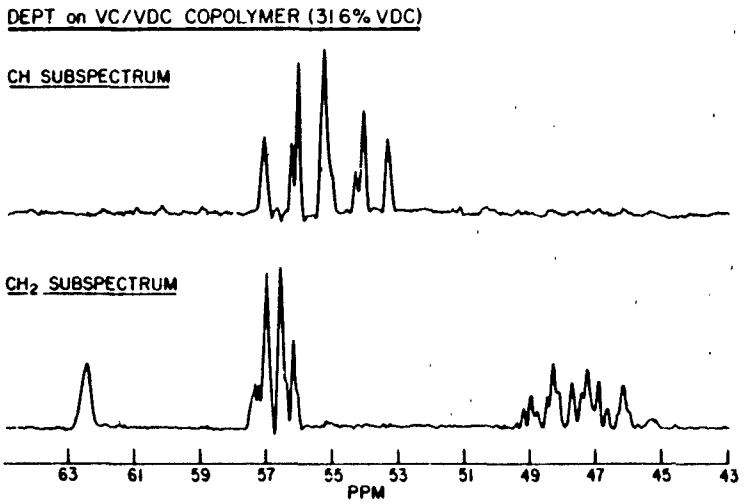


Figure 4. DEPT spectra of a vinyl chloride-vinylidene chloride copolymer with 31.6 mol% vinylidene chloride.

VC-VDC copolymer with about 32% VDC. These spectra should be compared to the corresponding unresolved spectrum in Figure 2 of reference 10. Obviously, in some cases there was total overlap of CH and CH_2 carbon intensity. It is now possible to see the unresolved CH_2 resonances quite clearly in the CH_2 subspectrum along with a greatly simplified CHCl region in the CH subspectrum. The high degree of separation is indicated by the low residual intensities of the CH_2 peaks in the CH subspectrum, and vice versa. Figure 5 shows the subspectra of CH_2 resonances for the entire series of copolymers with some peak assignments. Obviously the DEPT technique has provided a great improvement in our ability to extract information from the ^{13}C NMR spectra of these polymers. Some of the above assignments are still tentative, but this brief study has shown that DEPT will play a major role in any further work on this system. It remains to expand the utility of DEPT into quantitative analysis of polymers.

Solid State NMR of Elastomers

The development of NMR techniques to obtain high resolution ^{13}C spectra of rigid solids has understandably led to much activity on glassy and crystalline systems in recent years.[2,3] However, it is possible to obtain standard high resolution ^{13}C spectra of solid polymers well above their

glass transition temperatures. This area has been revieved recently.[13]

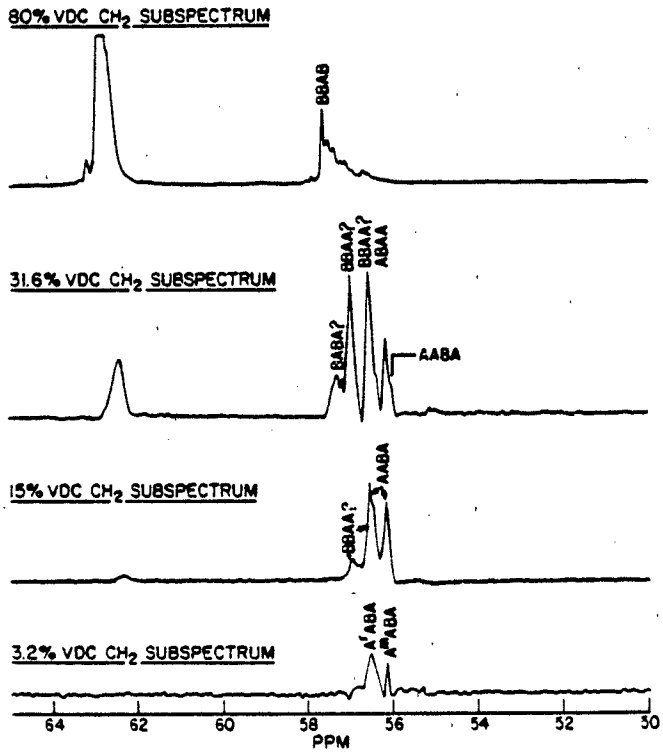


Figure 5. DEPT CH_2 subspectra for a series of vinyl chloride-vinylidene chloride copolymers.

High resolution ^{13}C spectra of solid polymers can be obtained in two ways - from a normal single-pulse free induction decay (FID) of the carbon magnetization as in FTNMR of liquids or from a ^{13}C signal derived by cross polarization with neighboring hydrogen atoms. In both cases, magic angle spinning (MAS) and high power decoupling can be used. For crystalline and glassy materials, the use of single-pulse FID's is inefficient due to the long carbon spin-lattice relaxation times (T_1's), which prevent short pulse repetition times. Cross polarization (CP) gives a signal up to four times larger than this and circumvents the problem of long ^{13}C T_1's. For cross-polarized spectra, the usually much shorter proton T_1's control the repetition rate, and hence faster pulsing is allowed.

Elastomeric systems behave differently. Because of their much greater chain mobility relative to glassy polymers, elastomers have short ^{13}C T_1's, making it easier to acquire satisfactory FID's. Cross polarization, although possible, is inefficient for elastomers because the static dipolar interaction, which is necessary for efficient cross polarization, is greatly reduced or eliminated. Figure 6 compares the spectra

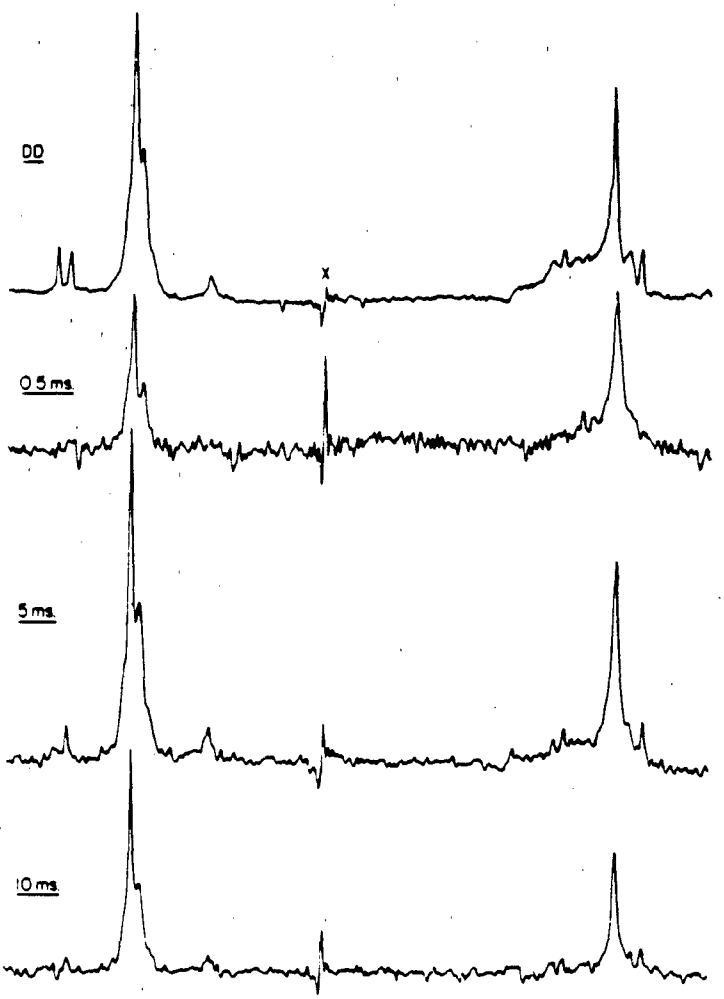


Figure 6. Solid state ^{13}C NMR spectra of an emulsion SBR. The top spectrum was obtained from the FID using dipolar decoupling (DD) and MAS. The others were obtained with cross polarization with contact time indicated. (Reprinted from reference 16 with permission. Copyright 1983, Rubber Division, ACS.)

of an emulsion SBR obtained with CP at three typical contact times to that obtained from the single pulse FID.[16] Although a cross polarized spectrum can be obtained for SBR at ambient temperature, the FID yielded a much better spectrum with regard to signal-to-noise ratio and reliability of resonance intensities. Relative peak intensities were found to be unreliable for cross-polarized ^{13}C spectra of SBR as well as various filled, vulcanized elastomeric blends.[13]

No systematic study has been performed to determine the point, relative to the glass transition temperature, at which cross polarization is more efficient than standard FTNMR. Work so far indicates that as long as the temperature of observation is about 70°C or so above T_g, FTNMR will be preferred.[15] Hence for elastomers cured to typical low levels, which do not significantly affect T_g, acquisition of the normal FTNMR spectrum is the method of choice. With increasing crosslink density, a point will eventually be reached[17] where cross polarization will be the more efficient approach.

The presence of filler can broaden the lines in a high resolution NMR spectrum of an elastomer beyond those seen for the pure polymer. This broadening can arise from a number of sources such as magnetic susceptibility differences or incomplete motional narrowing due to restriction of polymer chain mobility by the filler. Resolution can be enhanced significantly by employing MAS in the standard scalar decoupled (SD) or dipolar decoupled (DD) single pulse experiment.[16] The improvement is sufficient for the identification and quantification of the elastomeric components in simple, filled vulcanizates. Figure 7 shows the spectra at 22.6 MHz of three tire tread compounds containing different amounts of natural rubber (NR), cis-polybutadiene (BR), and emulsion SBR.[16] Although the spectra are not of the quality of the corresponding solubilized or pyrolyzed materials, many peaks are resolved. This permits easy identification of most elastomers in filled, vulcanized diblends or triblends. Moreover, quantitative analysis should be straightforward.

Although the quality of the results in Figure 7 is sufficient for many purposes, there are a number of problems. The 22.6 MHz spectra in Figure 7 each took about 6 hours or more to obtain, and because of certain peak overlaps at the low static magnetic field, a correction procedure was necessary to obtain complete quantitative data. In addition, the resolution of the small peaks due to SBR in the 35-45 ppm region is nonexistent or poor. This is even true for pure SBR's, as illustrated in Figure 8. Resolution of these peaks is necessary to distinguish different types of SBR's, such as solution and emulsion SBR's.[14,18]

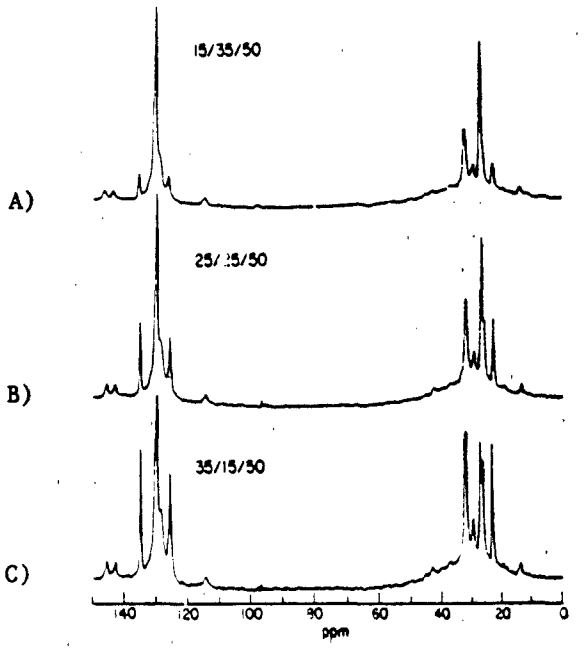


Figure 7. Solid state ^{13}C NMR spectra of three filled, vulcanized NR/cis-BR/SBR triblends. A) 15/35/50 NR/BR/SBR; B) 25/25/50 NR/BR/SBR; C) 35/15/50 NR/BR/SBR. (Reprinted with permission from reference 16. Copyright 1983, Rubber Division, ACS.)

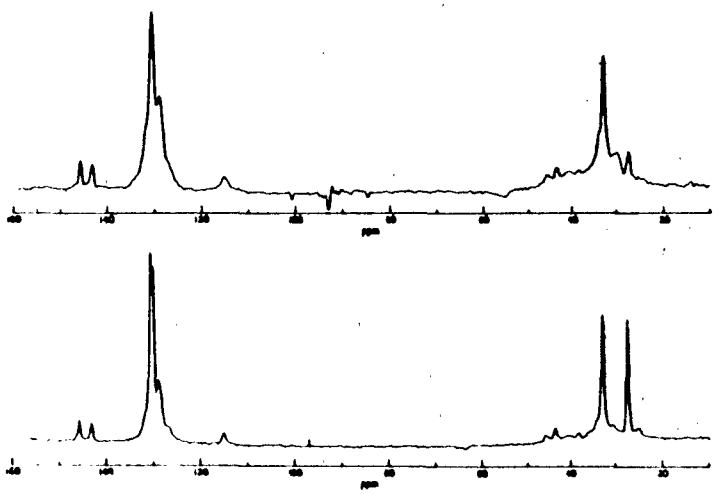


Figure 8. MAS ^{13}C NMR spectra of bulk, unfilled SBR's. Top: emulsion SBR; Bottom: solution SBR. (Reprinted with permission from reference 16. Copyright 1983, Rubber Division, ACS.)

Instrumental improvements should alleviate the above problems. In particular, MAS at higher magnetic field appears to offer substantial improvement in both resolution and sensitivity. Conventional wisdom in solid state NMR says that higher magnetic fields will not improve the spectral resolution in CPMAS NMR to a significant degree, because the lines will broaden concomitantly. However, this assumes that the line broadening is due to an isotropic distribution of chemical shifts, which is field dependent and not averaged by MAS. Although this is probably true for glassy polymers, it is not true to a large extent for rubbery polymers, where this distribution is averaged by substantial chain mobility. Hence, MAS and high fields should improve spectral resolution for elastomers.[15,19] This has been demonstrated for SBR (see spectra 55b and c of reference 19). Improved spectral resolution will allow ready identification of components in more complicated filled vulcanizates and make quantitative analysis easier.

Of course, operating at higher magnetic field will also improve the sensitivity of the experiment. Coupling this with improved MAS probes capable of handling large samples[20], analysis time should be reduced to an hour or less.

Sulfur Vulcanization of Natural Rubber

Our goal is to study the sulfur vulcanization of natural rubber (NR) by examining the cured rubber itself and determining directly the structures and concentrations of the various crosslinks formed. We are interested in both the number of sulfur atoms in a crosslink (sulfur rank) and the point of attachment to the polymer chain. Instrumental advances such as more sensitive probes, larger sample tubes, and higher magnetic fields have brought the sensitivity of ^{13}C NMR into the range where crosslinks at levels typical of vulcanized rubbers may be observable.

For the initial work reported here on sulfur-vulcanized natural rubber, FID acquisition should be the preferred method of signal acquisition, since T_2 has not been raised significantly. Ideally we would like to employ MAS to obtain as much line narrowing as possible. Unfortunately, we do not have MAS capability, high magnetic field, and large sample tubes on a single instrument. To compensate somewhat for not having MAS, we perform the standard FTNMR experiment on unfilled vulcanizates at elevated temperature to provide some line narrowing.[21]

Our knowledge of the chemistry of unaccelerated sulfur vulcanization is far from complete. Much of what is known comes from vulcanization studies on low-molecular-weight model alkenes.[22,23] However, it is not clear how well the models

actually mimic natural rubber as far as vulcanization is concerned.

Before attempting to determine the distribution and structures of the various crosslinks in typical vulcanizates, it is proper to assess how useful ^{13}C NMR can be under ideal circumstances. To do this we first examine model compounds to determine where the chemical shifts of the crosslink sites will occur, and how well different crosslink structures may be resolved. Table 1 gives the ^{13}C chemical shifts of selected carbons for a number of model compounds for crosslink sites in

TABLE 1

SELECTED ^{13}C NMR CHEMICAL SHIFTS OF SOME ORGANOSULFUR COMPOUNDS[a]

Compound	Carbon[b] 1	2	3
$(CH_3)_2S$	17.9		
$(CH_3)_2SS$	22.1		
$(CH_3)_2SSS$	22.5		
$(C_3H_7)_2S$[c]	33.9	22.7	13.0
$(C_3H_7)_2SS$[c]	41.2	22.5	13.0
$(C_3H_7)_2SSS$[c]	40.8	22.0	13.0
$(C_{12}H_{25})_2S$[c]	32.3	32.0	
$(C_{12}H_{25})_2SS$[c]	39.3	32.0	
$(C_{12}H_{25})_2SSS$[c]	38.9	32.0	
$[(CH_3)_3C]_2S$	45.6	33.2	
$[(CH_3)_3C]_2SS$	45.6	30.5	
$[(CH_3)_3C]_2SSS$	48.4	29.8	

[a] Chemical shifts are in ppm from TMS. They are taken from a variety of sources via the INKA (Information System Karlsruhe) ^{13}C NMR data base, except as noted.

[b] Starting at the carbon bonded to sulfur.

[c] This work.

sulfur vulcanization. For a number of aliphatic groups a direct comparison can be made among the chemical shifts for monosulfidic, disulfidic, and trisulfidic structures. For the most part, the chemical shift of the α-carbon in a disulfide

is about 7 ppm downfield of that due to the corresponding monosulfide. Hence one could expect to resolve monosulfidic and disulfidic crosslinks of the same chemical type, assuming there are no other interferences. Exceptions to this are the di-tert-butyl compounds, where the monosulfidic and disulfidic compounds have essentially the same chemical shift for the α-carbon. Apparently the high degree of branching in these compounds results in this exceptional behavior.

There is usually little difference between the α-carbon chemical shift in a trisulfide and the corresponding disulfide. Typically the difference is about one ppm. This is not surprising given the normal effect of substituents on ^{13}C chemical shifts. The largest difference is expected between the mono- and disulfidic linkages. Given the line widths usually seen in standard ^{13}C spectra of cured rubbers at elevated temperatures (and without MAS), it may be difficult to resolve tri- and polysulfidic from disulfidic crosslinks.

In addition to the number of sulfur atoms in a crosslink, it is essential to determine exactly where on the chain the crosslink occurs. For pure sulfur vulcanization, it appears from model studies that there are a number of possible crosslink structures, depending on the mechanism of vulcanization. Figure 9 shows some of the more likely structures, without specifying the number of sulfur atoms in the crosslink. Other possibilities arising from double bond shifts, cyclic structures, or multiple substitution can be envisioned, but are not considered here.

Using ^{13}C chemical shift substituent effects, we have calculated the approximate chemical shifts for carbons in the structures in Figure 9, where the calculated values are shown. The calculated values were obtained by taking the chemical shift of the appropriate carbon in the "starting compound", ie cis-polyisoprene[24] or an ethylene-propylene copolymer segment[23] and adding to it the appropriate value for the substituent effect (see Table 2). The substituent-effect values used are taken from reference 26, but are modified somewhat based on the model compounds in Table 2. Since the β and γ substituent effects are approximately the same for all the linkages, only the different α-carbon possibilities are listed in Figure 9. Many of the chemically shifted lines due to crosslink sites will not be resolved from the main cis-polyisoprene resonances given the typical line widths observed for vulcanizates. However, many of those given in Figure 9 will be resolvable. It remains to be determined experimentally how many of these can be resolved and identified. It should be emphasized that the calculated values are only approximate, since substituent effects are a function of other factors such as branching and the presence of other interacting groups.

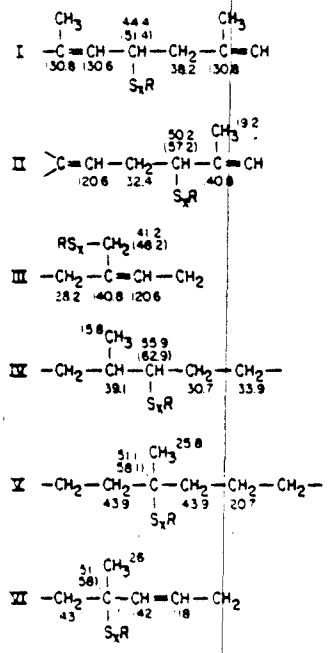


Figure 9. Predicted chemical shifts for some structures expected in the sulfur vulcanization of natural rubber. The chemical shifts are derived from the models and α-, β-, and γ-substituent effects for monosulfidic crosslinks (see Table 2). Values in parentheses are for disulfidic and polysulfidic crosslinks for the α-carbons. Disulfidic and polysulfidic β- and γ-effects are assumed to be the same as monosulfidic.

TABLE 2

SUBSTITUENT PARAMETERS FOR S_xR

	x=1	x>1
α	18	25
β	6	6
γ	-4	-4

Figure 10 shows the ^{13}C spectrum of natural rubber cured with sulfur alone for six hours at 280°F. A sulfur-only cure

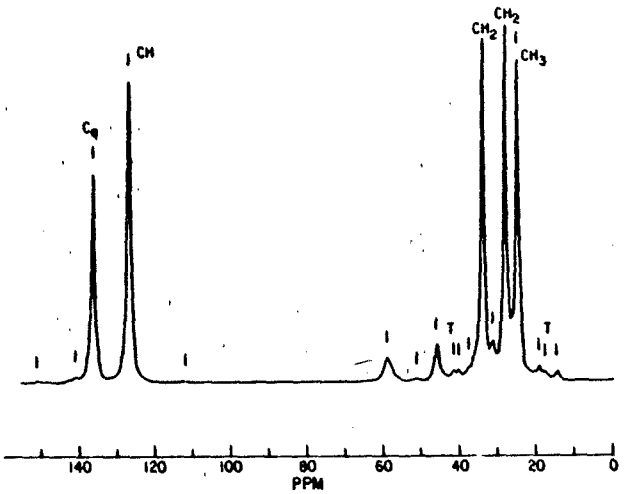


Figure 10. Standard ^{13}C spectrum of a sulfur-cured natural rubber (6 hrs at 280°F) at 90°C. The label "T" indicates peaks from trans-polyisoprene units.

was examined first since peaks due to remaining accelerator (TMTD) molecules (or fragments) can interfere with observation of peaks from the actual crosslink sites.[27] A number of new peaks are seen in the spectrum of Figure 10. Two of these can be assigned to trans-polyisoprene units (T) in the predominantly cis-polyisoprene chain. The level is on the order of 5%. This confirms that some isomerization of the double bond does occur in the sulfur vulcanization of NR. The other new resonances are due to the sulfur crosslink sites themselves. It is not yet known if the increased linewidths (relative to polyisoprene) of the crosslink peaks, particularly those at 46, 51 and 59 ppm, are due to restricted mobility or to overlap of two or more unresolved resonances. Given the calculated shifts in Figure 9, there is clearly the possibility of substantial overlap among the various resonances due to the crosslink sites. Additional discrimination is necessary. One way to achieve partial discrimination is to employ the DEPT technique described above.

Figure 11 shows the DEPT spectra of natural rubber cured with sulfur alone. There is reasonably good separation among the subspectra. Some "crosstalk" is observed for the major peaks, particularly for the residual methyl resonance in the CH subspectrum. Comparison of the DEPT spectra to the standard spectrum in Figure 10 shows that the signal-to-noise ratio in the DEPT spectra is reduced, probably because of the short T_2's encountered for this bulk polymer.[12,13] From these spectra we can further discriminate among the types of crosslinks

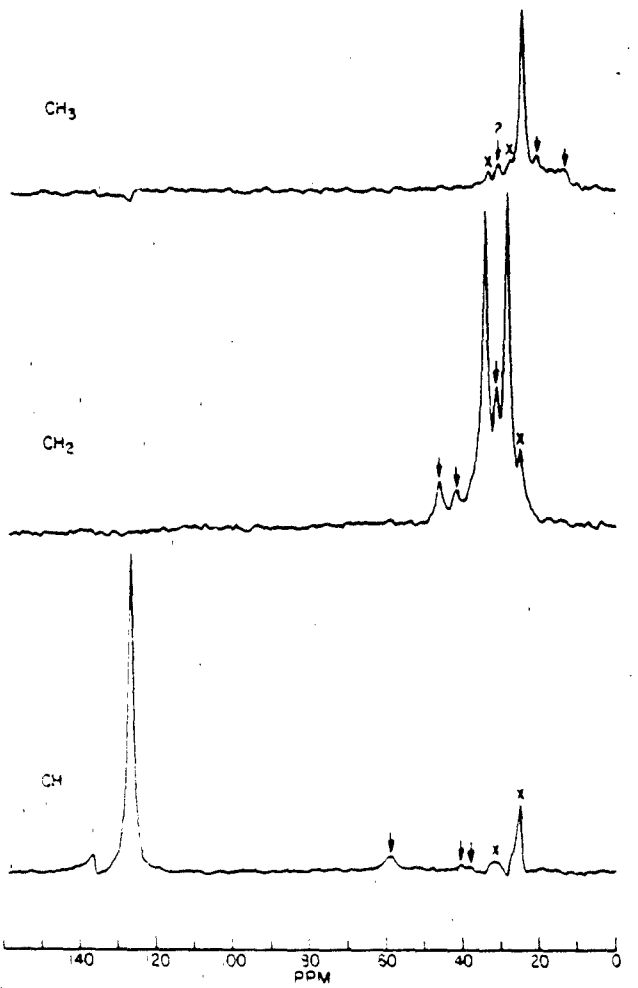


Figure 11. DEFT spectra of the sulfur-cured natural rubber of Figure 10. "X" marks residual peaks from other subspectra. Arrows indicate peaks due only to crosslink sites.

possible. For example, the peak at 59 ppm appears to be exclusively CH, suggesting di- or polysulfidic crosslinks of structure II, or possibly structure IV. Structure IV is also consistent with the methyl at about 15 ppm. The peak at 46 ppm for this sample is a CH_2 carbon, suggesting di- or polysulfidic crosslinks of structure III, although in this case structures V and VI are also possibilities. Confirmation of the presence of any particular type of crosslink ideally should rely on the observation of more than one resonance. Much additional work is necessary to totally sort out the

types and amounts of crosslinks which occur. The cure conditions for the current sample probably yield a mixture of mono-, di-, and polysulfidic crosslinks. Samples cured under conditions designed to give exclusively monosulfidic or polysulfidic crosslinks must be examined. Conditions of cure or spectrum acquisition must be found to improve the signal-to-noise ratio of the DEPT experiment, probably by lengthening T_2 for the crosslink carbons. Also, an independent determination of the positions of any quaternary carbons, possibly using a specific pulse sequence for this purpose, is necessary. However, the results obtained so far are promising.

REFERENCES

1. A. Bax, "Two-Dimensional Nuclear Magnetic Resonance in Liquids," Delft/Reidel, Dordrecht, 1982.
2. C. A. Fyfe, "Solid State NMR For Chemists," C. F. C. Press, Guelph, 1984.
3. R. A. Komoroski, Ed., "High Resolution NMR of Synthetic Polymers in Bulk," VCH Publishers, Inc., Deerfield Beach, 1985.
4. S. L. Patt and J. N. Shoolery, J. Magn. Reson. 46, 535(1982).
5. M. R. Bendall, D. M. Doddrell, D. T. Pegg, J. Am. Chem. Soc. 103, 4603(1981).
6. D. Doddrell, D. T. Pegg, and M. R. Bendall, J. Magn. Reson. 48, 323(1982).
7. M. H. Levitt, R. Freeman, and T. Frenkiel, J. Magn. Reson. 43, 502(1981).
8. F. J. Weigert, M. Jautelat, and J. D. Roberts, Proc. Nat. Acad. Sci. USA 60, 1152(1968).
9. E. Wenkert, A. O. Clouse, D. W. Cochran, and D. Doddrell, J. Am. Chem. Soc. 91, 6879(1969).
10. R. A. Komoroski, and J. P. Shockcor, Macromolecules 16, 1539(1983).
11. G. A. Morris and R. Freeman, J. Am. Chem. Soc. 101, 760(1979).
12. P. F. Barron, D. J. T. Hill, J. H. O'Donnell, and P. W. O'Sullivan, Macromolecules 17, 1967(1984).
13. R. A. Newmark, Applied Spectrosc. 39, 507(1985).
14. D. D. Werstler, Rubber Chem. Technol. 53, 1191(1980).
15. R. A. Komoroski, in "High Resolution NMR of Synthetic Polymers in Bulk," R. A. Komoroski, Ed., VCH Publishers, Deerfield Beach, 1985, Ch. 4.
16. R. A. Komoroski, Rubber Chem. Technol. 56, 959(1983).
17. D. J. Patterson, J. L. Koenig, and J. R. Shelton, Rubber Chem. Technol. 56, 971(1983).
18. C. J. Carman and K. C. Baranwal, Rubber Chem. Technol. 48, 705(1975).
19. "High Resolution NMR in Solids", Vol. 4, 1984. Product literature, Bruker Instruments, Inc., Billerica, MA.

20. Product literature, Doty Scientific, Inc., Columbia, SC, 1985.
21. C. J. Carman, ACS Symp. Ser. 103, 97(1979).
22. M. Porter in "Organic Chemistry of Sulfur," S. Oae, Ed., Ch. 3, p. 71, Plenum, New York, 1977.
23. A. Y. Coran in "Science and Technology of Rubber," Ch. 7, p. 291, Academic, New York, 1978.
24. Y. Tanaka and H. Sato, Polymer 17, 113(1976).
25. G. J. Ray, P. E. Johnson, and J. R. Knox, Macromolecules 10, 773(1977).
26. F. W. Wehrli and T. Wirthlin, "Interpretation of Carbon-13 NMR Spectra," Heyden, London, 1978.
27. R. A. Komoroski, J. P. Shockcor, E. C. Gregg, and J. L. Savoca, Rubber Chem. Technol., submitted for publication.

*Figures 1, 2, 3, and 10 from R.A. Komoroski, (1983) Rubber Chemistry and Technology, Vol. 56, pg. 959.

PROGRESS IN CHARACTERIZATION OF ELASTOMERS BY THERMAL ANALYSIS

ANIL K. SIRCAR
University of Dayton Research Institute, Dayton, OH 45469

INTRODUCTION

The present flourishing use of "thermal analysis" in polymers started around 1961 when an instrument with adequate resolution for polymer studies became commercially available. By 1972, at least 30 manufacturers were manufacturing thermal analyzers. The number of publications related to thermal analysis in basic chemical journals had been increasing at an exponential rate and numbered more than 5000 annually in 1972; 20% of which are estimated to be associated with polymers (1-3). Two journals, Thermochimica Acta (4) and Journal of Thermal Analysis (5), are now devoted to thermal analysis exclusively. Even thermal analysis abstracts (6) are becoming available. The Japanese journal, Calorimetry and Thermal Analysis (7), also covers a wide range of articles and reviews. An ASTM committee has also been formed with responsibility to formulate methods based on thermal analysis. Also, International Confederation of Thermal Analysis (ICTA) was formed in 1965 with affiliation in many countries. By far the largest affiliate is the North American Thermal Analysis Society (NATAS) with a 1985 membership of around 700.

Based on a presentation at the "Rubber-80" international conference in India (8), and a talk at the Cleveland meeting of the Rubber Division (9), the author published a review article, "Characterization of Elastomers by Thermal Analysis" (10). The present article is an updated version of the same publication and includes the work during the last 5 years (1981-1985). Also, a chapter on, "Miscellaneous Novel Applications", has been added, in order to cover significant contributions not included in the scope of the earlier presentation.*

* When the manuscript was first prepared, earlier work was included. However, at the request of the editors, the present manuscript has been reduced in size, omitting much of the earlier work. The only exception to the revised manuscript is that the references remain as in the original manuscript (Ref. 1 through 221).

TRANSITION IN ELASTOMERS

Tables 1 and 2 are provided to summarize the various thermoanalytical techniques and to explain how some of these methods perform elastomer characterizations.

Figure 1 shows a schematic DSC curve of an elastomer in oxygen (A) and nitrogen (B), which illustrates the sequence of thermal characteristics as they appear in DSC curve. As mentioned before, this sequence will be followed in the present review. Some of these transitions are physical and therefore are reversible on a heating and cooling cycle. These physical transitions are: glass transition (T_g), melting, crystallization, etc. Permanent chemical changes take place in others, e.g., oxidation, oxidative and thermal degradation, vulcanization. They are therefore, irreversible. Unlike

TABLE 1

COMMON THERMOANALYTICAL TECHNIQUES

Abbreviation	Technique	Response Measured
DTA	Differential Thermal Analysis	Temperature Difference
DSC	Differential Scanning Calorimetry	Energy (heat) Difference
TG	Thermogravimetry	Weight Change
DTG	Differential Thermogravimetry	Rate of Weight Change
TMA	Thermomechanical Analysis	Dimensional Changes
DTMA	Differential Thermomechanical Analysis	Rate of Change of Dimensions
DMA	Dynamic Mechanical Analysis	Modulus, Loss Tangent
AUDREY	Dielectric Analysis	Dielectric Loss
EGD	Effluent Gas Detection	Total Volatiles Evolved
EGA	Effluent Gas Analysis	Individual Volatiles Evolved
TOA	Thermooptical Analysis	Birefringence Change
TDA	Thermodepolarization Analysis	Birefringence Change
ETA	Electrothermal Analysis	Resistivity Change
ARC	Accelerating Rate Calorimetry	Adiabetic Temperature Rise

TABLE 2

CHARACTERIZATION OF ELASTOMERS BY THERMAL ANALYSIS

DSC Measure Heat Flow	TG and DTG Measure Weight Changes	TMA and DTMA Measure Dimensional Changes
Thermal Capacity	% Volatile, Water, Solvent	Thermal Expansion
Melting Point, T_g	% Plasticizer, Oil, Extender	Softening Point
% Crystallinity	% Polymer	Heat Deflection Temperature
Curing Profile	% Carbon Black	Modulus, Creep
Blend, Copolymer Analysis	% Carbonate	Mold Shrinkage
Additive Analysis	Degradation Profile	
Thermal Degradation	Thermal Stability	
Oxidative Degradation	Oxidative Stability	
Elastomer Identification	Elastomer Identification	
	Plasticizer Identification	

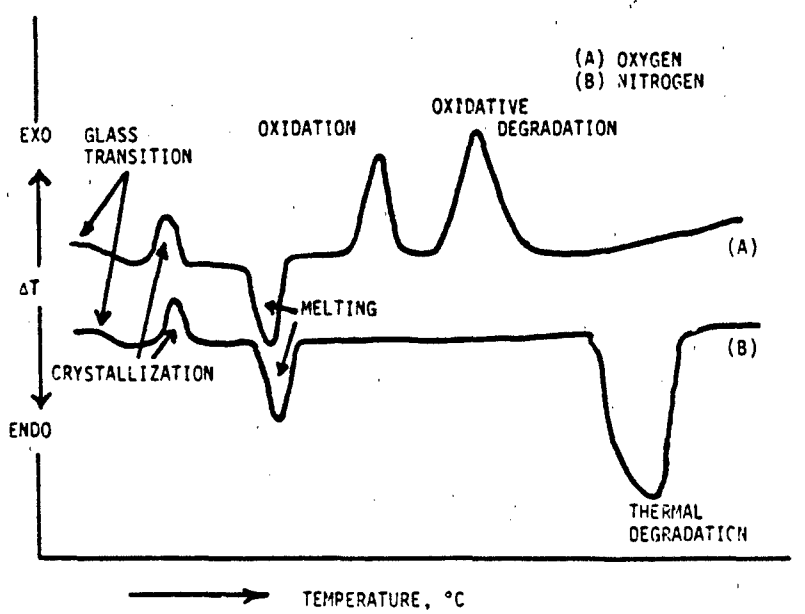


FIGURE 1. Schematic DSC Curve (104).

chemical transitions, the physical transitions are not affected by the environment. Also, no weight change accompanies such processes and therefore TG curves will not record the physical transitions. Chemical reactions, on the other hand, are usually accompanied by a change of weight and will be recorded in the TG-DTG curve. It is apparent that TMA works only for physical transitions and would show different rate of expansion at Tg and also a transition with penetration and extension probes. A softening point before crystalline melting is often observed in TMA for semicrystalline thermoplastic polymers.

These physical transitions are very susceptible to various morphological factors as well as pre-history of the sample. It is, therefore, very important to destroy the pre-history of the sample by annealing at a temperature higher than the melting point or T_g of the elastomer.

Intensity of the physical transitions are reduced by vulcanization. For example, BR crystallization endotherm often vanishes with vulcanization. This may serve as an indication of the extent of crosslinking of the sample.

In the following paragraphs, different uses of T_g in elastomers will be outlined. These are:

1. Identification of Elastomers
2. Estimation of Dry Rubber in Latices
3. Copolymer Microstructure
4. Compatibility Determination
5. Carbon Black Transfer
6. Level of Resin Plasticizer
7. Solubility of Plasticizer
8. Degree of Epoxidation of NR

Of these, (2), (6), (7), and (8) have been published after the last review and will be discussed in this revised report (10).

Estimation of Dry Rubber in Latices. Burfield (46) at the University of Malaya, proposed an extension of the T_g identification of dry rubber to that in latices. DSC analysis of NR latex concentrate shows T_g corresponding to NR-dry rubber and an endotherm for the heat of fusion (ΔH_f) of the serum. The Tg of NR sampled as latex is effectively indistinguishable from that of dry rubber isolated from the same latex (Figure 2A). The magnitude of the heat capacity change (C_p) (Figure 2B) associated with the glass transition shows a linear relationship with dry rubber content (DRC), thus permitting

monitoring of DRC at the same time. The DRC may also be monitored with respect to ΔH_f (Figure 2C) which decreases almost linearly with increasing rubber content.

Level of Resin Plasticizer. Brazier and Nickel (35) described a procedure for assessing the correct level of a resin plasticizer by TMA. The method uses an indentation probe. For normalized sample thickness, the depth of indentation prior to expansion varied predominantly with the level of a given plasticizer and a correlation with sample hardness was established.

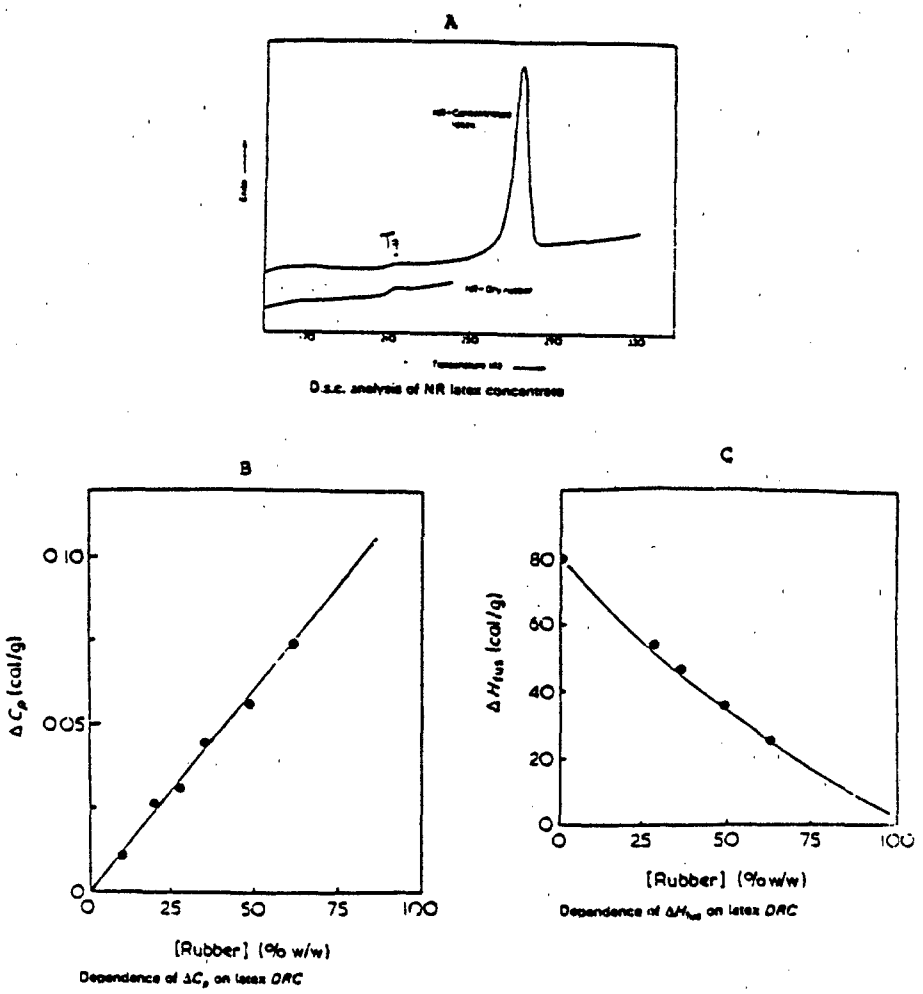


FIGURE 2. DSC Analysis of NR Latex (46).

Solubility of Plasticizer. G. Ceccoruli, et al. (58) studied the depression of T_g of PVC with ester plasticizers. With partially soluble esters, T_g decreases with increasing ester content up to a critical concentration corresponding to the solubility limit. At higher concentrations, the T_g remains constant.

Degree of Epoxidation of NR. Recently, there has been a growing interest in the modification of NR latex by epoxidation with peracids. The modified material shows certain outstanding properties vis-a-vis the unmodified rubber (59-63). Burfield et al., (62) observed that T_g values of epoxidized NR can be correlated with the level of epoxidation (Figures 3A and 3B), as measured by the primary methods (elemental analysis, ^{13}C NMR, HBr titration). T_g values are also directly related to density (Figure 3B). DSC analysis also permits the detection and estimation of blends of NR and ENR, since such mixtures are characterized by two distinct T_g values (62). Such an estimation could not readily by achieved by the primary methods.

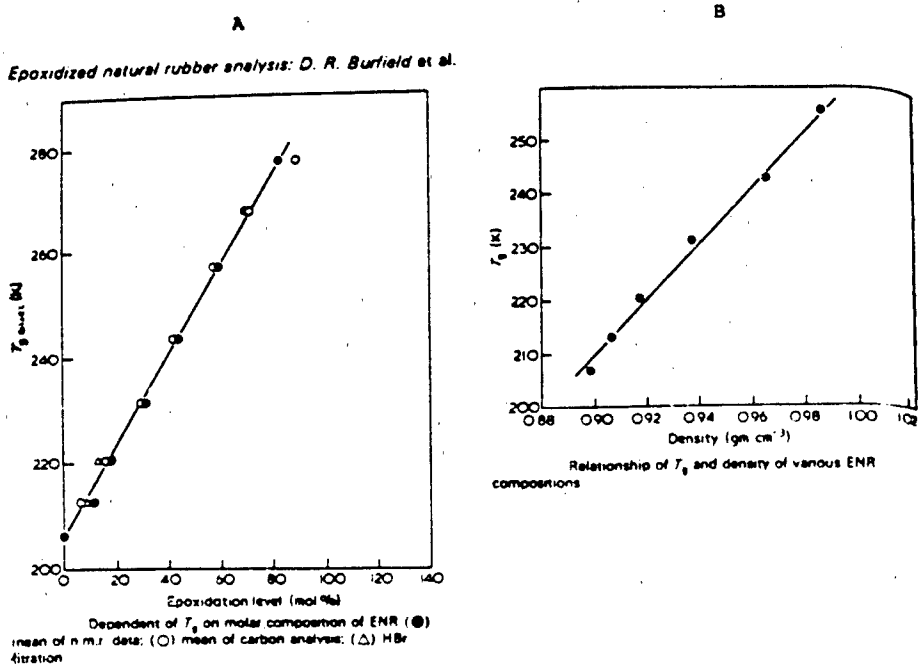


FIGURE 3. Glass Transition as a Measure of Exposition in NR (62).

Melting and Crystallization. DSC applications of melting and crystallization are as follows:

1. Characterization of Random vs. Block Copolymer
2. Compatibility of Binary Blends
3. Carbon Black Transfer
4. Degree of Dispersion of Elastomer Blends
5. Analysis of Plasticizer Levels
6. Solubility of Plasticizers
7. Estimation of Sulfur in Masterbatches
8. Purity of Accelerators

The last four will be described in detail.

Analysis of Plasticizer Level. Maurer (45) used the magnitude of the melting endotherm of different plasticizers to determine the amount of plasticizers present in butyl compounds for low temperature use. It was suggested that this method could be used as a rapid quality control test to assure correct plasticizer levels. DTA was favored in these determinations over DSC because it allows a larger sample size.

Solubility of Plasticizers. An interesting modification of Maurer's (45) method was due to G. Ceccoruli, et al. (58) in Italy. These workers evaluated the heat of fusion of the ester plasticizers in PVC, exceeding the solubility limit. A plot of heat of melting, per unit weight (Q/W) vs. the diluent weight fraction gives a straight line. The slope corresponds to the heat of fusion of the ester, while the intercept with the composition axis (Figure 4) indicates the critical concentration W_o for the PVC ester system.

Estimation of Sulfur in Masterbatches. In rubber compounding, it is a common practice to predisperse sulfur and/or accelerater in a masterbatch of the elastomer. Predispersion of sulfur improves accuracy and facilitates its incorporation into the formulation. Maurer and Brazier (14) suggested the use of the enthalpy for sulfur melting to monitor the amount of sulfur in such masterbatches. An unannealed DSC scan of such a dispersion (Figure 5A) reveals a complex melting endotherm due to the polymorphic nature of sulfur. Quenching and rerunning reveals only a single peak (Figure 5B). The enthalpy associated with this process correlates closely with sulfur content up to about 50% sulfur (Figure 5C).

Purity of Accelerators. Brazier and Nickel (76) used DSC melting endotherms of commercial accelerators to characterize the accelerators and to determine their purity. The purified accelerator, obtained by recrystallization from cyclohexane was used as the control. This is illustrated in Figure 6. For

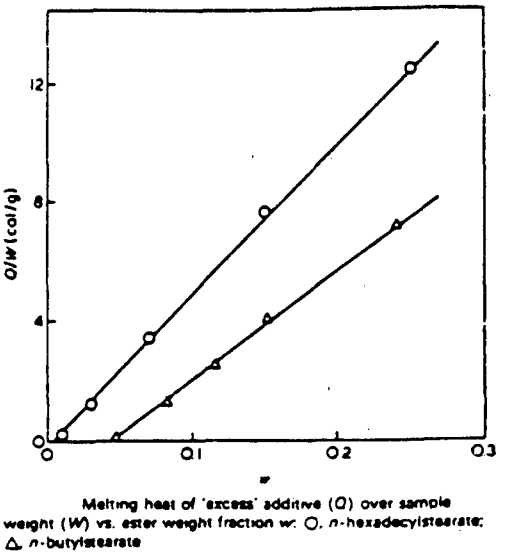


FIGURE 4. Solubility of Ester Plasticizers by Heat of Fusion (58).

MBTS, Brazier (15) reports that the purity of the commercial accelerators, determined by this method, are no better than 95%.

Chemical Transitions

Unlike the physical transitions, the chemical transitions occurring at higher temperaures are affected by the environment. The different transitions in nitrogen and oxygen atmosphere will therefore be treated separately.

By far the largest amount of work on thermal analysis of elastomers has been carried out in nitrogen which shows purely "thermal" or "thermo-chemical" effect, in contrast to the combined effect of heat and oxidation, "thermooxidative", effect in oxygen.

The transitions in nitrogen may again be categorized according to the temperature scale of the reaction. Enthalpy for room temperature vulcanization of silicone rubber was utilized for quality assurance of thermal protection system of fuel tanks for space vehicles (77). At around 150°-250°C, the exotherm for the unvulcanized compound is due to vulcanization; at higher temperature (350°-550°C) thermal degradation, either crosslinking or depolymerization takes place.

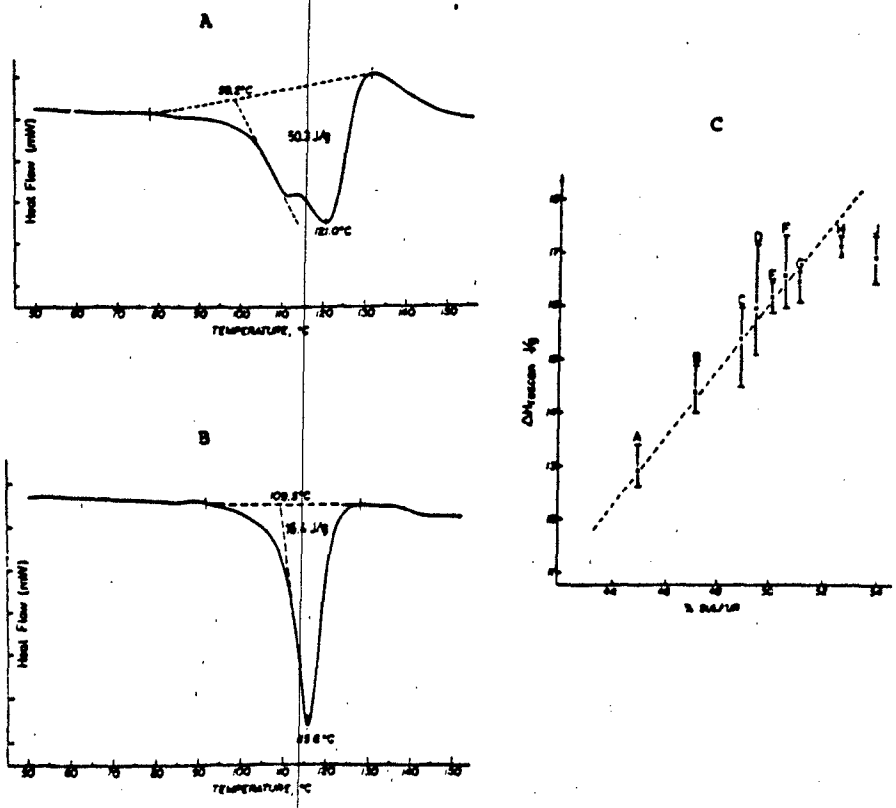


FIGURE 5. DSC Analysis of Sulfur: A - DSC curve of Sulfur Melting in Sulfur/Accelerated Masterbatch. Sulfur Content 52.7% Added as Oiled Crystex to Polyisoprene Containing MBTS Accelerator (D.W. Brazier and N.V. Schwartz unpublished data) (76); B - DSC Curve of Sulfur/Accelerator Masterbatch After Melting and Quenching. (D.W. Brazier and N.V. Schwartz, unpublished data) (76); C - Typical Calibration Data for the Analysis of Sulfur Masterbatches Over the Range 44 to 54% Sulfur by Weight. Enthalpy of Melt (H) After Melting and Quenching (76).

Thermal or Thermochemical Transitions

Thermal reactions between 150-350° and beyond 350°C are discussed separately. Following are the uses for thermal reactions between 150-350°C:

1. Enthalpy of vulcanization
2. Analysis of sponge formulation

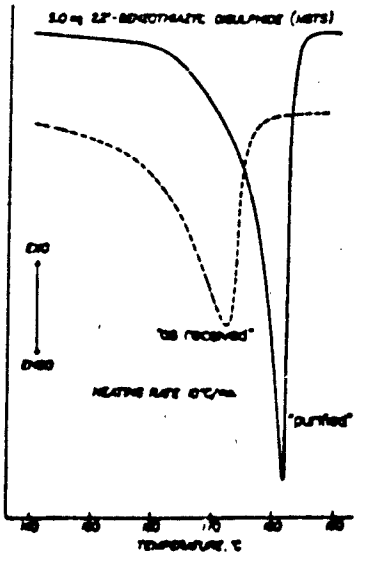


FIGURE 6. Purity of Accelerator by DSC: Purity of 2,2'-benzothiazyl Disulphide (MBTS) by DSC. Commercial Sample Purified by one Recrystallization from Cyclohexane (76).

3. Estimation of oil in oil-extended elastomer
4. Identification of oils and plasticizers.

Only (3) will be discussed, since others have been described in the earlier review (10).

Estimation of Oil in Oil-Extended Elastomers. Maurer (14) described the usefulness of the TG-DTG method in analyzing the amount of oil in oil-extended SBR (76) and EPDM (95) (Figure 7). SBR 1778, which contains 37.5 phr of a naphthenic oil, begins to lose oil $\sim$175°C and exhibits a maximum rate of oil loss $\sim$285°C. In contrast, SBR 1712, which contains 37.5 phr of a less volatile aromatic oil, exhibits a broad oil volatilization curve which overlaps the SBR degradation region. The use of lower heating rates to complete oil volatilization and/or reduced pressure has been suggested to remedy this situation. In contrast to SBR, oil-extended EPDM (84) shows no overlap of the weight losses due to oil and polymer. This is due to the higher thermal stability of EPDM.

Swaring and Wims (95) suggested three methods to calculate the oil content in cases of overlapping oil and polymer TG traces. These are: (a) overlaying a polymer decomposition curve on the curve of the oil-extended polymer, (b) construction of an intersection point, and (c) identification of the

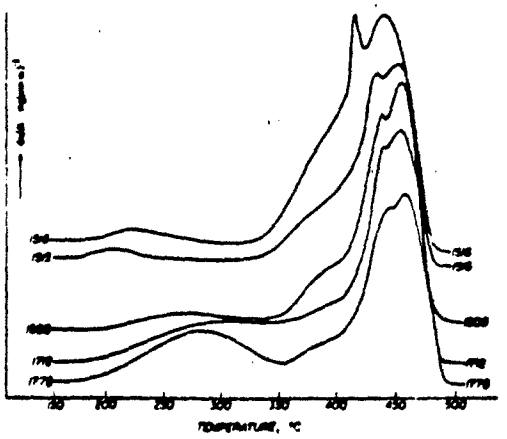


FIGURE 7. Estimation of Oil in Oil-Extended Elastomers (76): DTG Profiles of Commercial Raw SBR Elastomers. Heating Rate 10°C/min - Compositions: 1500, 23.5% styrene; 1515, 28% styrene; 1516, 40% styrene; 1712, 23.5% styrene, 37.5% aromatic oil; 1778, 23.5% styrene, 37.5% naphthenic oil (14).

oil-polymer region via the derivative TG curve. Calculation procedure (a) and (c) gave good results for EPDM, whereas method (b) gave a low oil/high polymer result. Because of its ease of application, the DTG method (c) is preferred by many (14), including the present author.

High Temperature Degradation

Very useful information can be obtained from thermographs of the high temperature degradation of elastomers. Unlike the physical transitions, as well as vulcanization, considerable weight loss generally accompany these transitions. Therefore, simultaneous TG-DTG along with DSC thermographs are very useful in the study of thermal degradation. For obvious reasons, TMA is seldom used in this range. The TG-DTG and DSC thermographs of thermal degradation of elastomers have been used for the following applications:

a. Thermal stability of elastomers.

b. Identification of elastomers.

c. Identification of blends.

d. Proportion of elastomers in blends.

e. Analysis of vulcanizates.

All of these have been discussed in the earlier review and thus will not be discussed in this report.

Thermooxidative Transitions

The effect of atmosphere on high temperature degradation of elastomers is quite dramatic. In general, elastomers will stand much higher temperature in nitrogen without significant deterioration than in air or oxygen. The relative stability of the elastmoers in oxygen depends on the polymer structure--dienes (NR, BR, NBR, SBR) are much more affected than the olefins (butyl, EPDM). Since oxidation accounts for the chemical or high temperature transition in oxygen, they are all exothermic. Uses of the DSC exotherms or TG curves in air or oxygen are as follows:

1. Identification of Elastomers

2. Antioxidant Evaluation

3. Carbon Black Identification

4. Predicting Service Life

A considerable amount of work on antioxidant evaluation has been published and thus the topic will be discussed in detail.

Antioxidant Evaluation. Thermoanalytical techniques have recently been used to study rubber oxidation (139-149). There are five main approaches to this study. They all use DTA or DSC and depend on the determination of the following:

a. Enthalpy

b. Energy of Activation

c. Onset Temperature

d. Isothermal Induction Time

e. Oxidation Peak Temperature

Antioxidant Evaluation by Enthalpy Determination. Smith and Stephens (142) used DSC to evaluate the effectiveness of the antioxidants in SBR and BR rubbers. The effectiveness of the antioxidants was correlated to the amount of heat change (enthalpy) during degradation. The smaller the heat change, the more effective is the antioxidant. In more recent work (143) with guayule rubber, small cast samples were used. This gave 5-10 times the value of ΔH as for larger samples. This indicates a diffusion controlled reaction and a more complete oxidation for the small size samples.

Antioxidant Evaluation by Energy of Activation. Goh (144) found that the energy of activation, evaluated from the thermoanalytical studies, provided a reasonable estimation of the effectiveness of the antioxidant. Goh and Pang (145) later estimated the effects of several metallic ions on the oxidation of NR, by comparing the apparent activation energies obtained from Kissinger's Plots. Thermal oxidation of guayule and NR have also been studied using the energy of activation (E_a) method (116). The suitability of different methods for evaluating E_a from DSC thermographs have also been discussed by these authors. Kotoyori (150) considered the activation energy, frequency factor, and specific reaction rate as a measure of stability. Lye, et al., (151) calculated the apparent activation energy of oxidation by both Kissinger (152) and Doyle-Ozawa equation (153-156). They concluded that E_a as evaluated by Kissinger and the estimated time relatinship devised by Doyle (154) and adapted for the DSC, appear to be valid for the oxidative stability in NR, subject to certain limitations. These are (1) oxidation mechanism remain unchanged at the temperature range studied, (2) Arrhenius equation holds, (3) no decomposition or volatilization of antioxidants, (4) no thermal lag and other thermal reactions--e.g., thermal degradation. Importance of small, cast samples are again emphasized in this investigation. Antioxidants should increase the degradation temperature and Ea.

Antioxidant Evaluation by Onset Temperature. Horvath, et al., (149) used the initial oxidation temperature (onset temperature) to determine the stability of NBR elastomers containing conventional antioxidants and bound antioxidants, introduced during polymerization. Extraction with methanol had no effect on bound antioxidant system; whereas, a decrease of onset temperature by 50°C was observed for others. The decrease of onset temperature shows the susceptibility of these samples to oxidation.

Gonzalez (143) determined the relative efficiencies of seven antioxidants in guayule rubber, based on the ability of the antioxidant to shift the oxidation exotherm to higher temperature.

Antioxidant Evaluation by Isothermal Induction Time. Isothermal DTA technique was also used for the evaluation of antioxidant (146,147). In this case, the sample is brought to the preselected temperature, preferrably in nitrogen, the atmosphere changed to oxygen and the delay before the oxidation exotherm begins or the induction period of oxidation then serve as an indication of the effectiveness of the antioxidant. The logarithm of the induction time is, in most cases, a linear function of the reciprocal of the test temperature. This isothermal approach has also been reported for plastics (148). Soviet workers (157) studied the effectiveness of antioxidants on butadiene rubber by combining DTA and TG. Some eighteen antioxidants were ranked in order of their effectiveness. In recent years, the isothermal induction method has gained in popularity (148,158-162). A small sample size, slow heating rate, and a solution cast sample is emphasized by several workers. In the wire and cable industry, an isothermal DTA/DSC test is now widely used to check the oxidative stability of polyolefin based materials. It has the advantage of speed, simplicity, and small sample size over the standard oxygen absorption method. It can be applied in varius ways: e.g., to the raw mix, to check that there is sufficient antioxidant to prevent degradation during processing, or to actual wire samples after extrusion, either to assess the effect of altering process conditions or as a routine quality control check of the finished product (163).

The oxidation Peak Temperature. The activities of antioxidants in SBR were studied by May, et al., (139,141) using DTA. A correlation was found between the DTA peak temperature versus the tensile strength and ultimate elongation of oxygen bomb-aged rubber vulcanizates. In a series of papers, Goh (115,138 158-162) used DSC to study the oxidation of NR, the catalytic effect of metal ions on the oxidation of NR, the inhibition of metal-ion catalyzed oxidation of NR by macrocyclic ligands and the oxidation of NR/IR blends. He used all the other parameters (a-d), as well as the peak oxidation temperature. He then tried to establish a correlation between activation energy of oxidation, E_a, isothermal induction time, t, and oxidation peak temperature, T_p. A typical plot with a 127 data set (159), at a 2°C/min heating rate is shown in Figure Similar plots were also obtained between E_a vs $1/T_p$ and log t vs E_a. In each case, correlation coefficient of the linear plot improved at a lower heating rate. Since all the

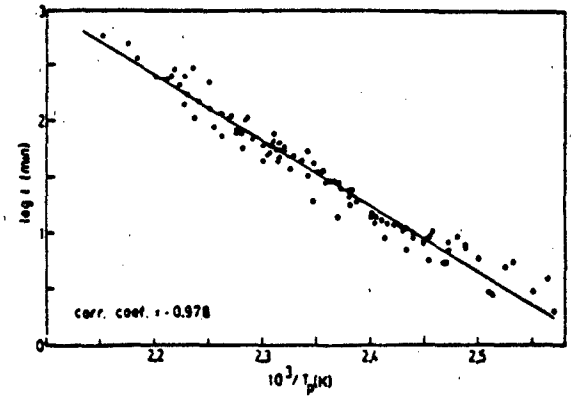


FIGURE 8. Induction Time vs. Reciprocal Peak Temperature: log t vs. $1/T_p$ (T_p based on a heating rate of 2K min^{-1}) (159a).

three parameters are interrelated, they all can be used to evaluate the oxidative stability of rubbers and the effectiveness of antioxidants. However, the use of induction time has the disadvantage that a long test time is needed for a sample of good stability. The evaluation of lthe activation energy by the Kissinger method (152) requires several scans at various heating rates. The use of the oxidation peak temperature based on a single scan is recommended as the most convenient method. However, as discussed earlier, values based on a slower heating rate, which require longer time, provide a better result. An optimum of 10-20°C/min, commonly used in DSC/DTA tests, provides a fast and yet reasonably good result.

In more recent publications (160,161) Goh proposed that for NR (160) and BR (161), stabilized by various antioxidants, the Arrhenius plots could be superimposed to form a single plot, using a shift factor dependent on the oxidation peak temperature obtained from a dynamic DSC test. The superimposed plot provides a rapid means for predicting the oxidation induction time from the more rapid dynamic DSC test. Plots of logarithms of induction time against the reciprocal of the absolute temperature for BR containing various antioxidants is shown in Figure 9. The oxidation peak temperature is shown in Table 3. Since log t and $1/T_p$ are linearly related, the order of effectiveness of the antioxidants are the same in both cases. The various Arrhenius plots in Figure 9 can be shifted horizontally using a shift factor, A, where A = T (reference) - T_p (sample). The superimposed plots of log t against $1/(T+A)$ are shown in Figures 10A and 10B. Here also the lower the heating rate, the better

the correlation coefficient. Straight line equations obtained from the linear plot allow the prediction of the induction time using the T_p values obtained from a dynamic DSC test. However, separate equations are needed for different rubber systems. Up to now, the method has been tested only for raw NR and BR. Work on extension of the method to vulcanized systems has not yet been published.

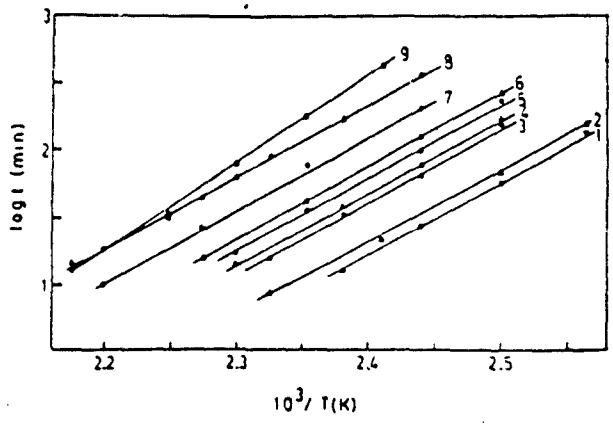


FIGURE 9. Oxidation Induction vs. Reciprocal Peak Temperature of BR. (1) Purified Butadiene Rubber; (2) Butadiene Rubber (BR) and Copper Naphthenate; (3) BR; (4) Purified BR and Antioxidant A; (5) BR and Antioxidant A; (6) BR and Antioxidant B; (7) BR and Antioxidant C; (8) BR and Antioxidant D, ▲ , BR, and Antioxidant E; (9) BR and Antioxidant F (161).

MISCELLANEOUS NOVEL APPLICATIONS

There are some applications of thermal analysis which do not record a transition and so cannot be included in the sections discussed in the preceeding chapters. Again, there are others, which, although concerns a transition, do not fall under the limited scope of this review, but are novel enough to deserve a mention. A number of such applications were compiled by Maurer and Brazier (14) in their review, "Applications of Thermal Analysis in the Rubber Industry" and will be mentioned here.

TABLE 3

EFFECT OF HEATING RATE ON THE OXIDATION PEAK TEMPERATURE T_p OF VARIOUS SAMPLES (161)

Effect of heating rate on the oxidation peak temperature (T_p) of various samples

	T_p(K)			
	2 K min^{-1}	8 K min^{-1}	16 K min^{-1}	64 K min^{-1}
Butadiene rubber (BR)	444	466	476	506
BR + copper naphthenate	436	457	468	497
BR + A	451	473	485	513
BR + B	453	475	486	517
BR + C	463	484	491	521
BR + D	469	492	504	534
BR + E	470	492	506	539
BR + F	470	491	502	531
BR (purified)	433	453	466	496
BR (purified) + A	447	468	480	312

In recent years, there have been some work which used DSC with some modification. This allows measurement of properties not obtainable directly from DSC, e.g., thermal conductivity, electrical resistivity. Two examples of these in the author's laboratory will also be included.

Crosslink Density of Elastomers via Thermogravimetry

The crosslink density of elastomers is a very basic parameter of the elastomer systems. Most of the important properties of the elastomer, e.g., modulus, tensile stress, elongation, and hardness, depend on the nature and level of the crosslinks. The classical method for evaluating crosslink density (CLD) is to determine volume swell and use the Flory-Rhener equation to determine CLD. The volume swell experiment is, however, very time consuming and takes 24 hours or more to reach equilibrium. Prime (191) suggested the use of TG with a hang-down type balance (Perkin-Elmer). The primary features of this experiment are the use of a thin sample and the use of a wick to aid in maintaining an equilibrium solvent vapor concentration above the solvent, thus facilitating the amount of solvent pick up by the sample. The method was tested for polydimethyl siloxane vulcanizates and is potentially useful for other types. The thin sample, suspended from the hook of a Perkin-Elmer TG balance is immersed in the solvent in a beaker and is then withdrawn from it by lowering the solvent reservoir. A closed equilibrium atmosphere of the solvent is maintained inside the balance. Equilibrium swell of

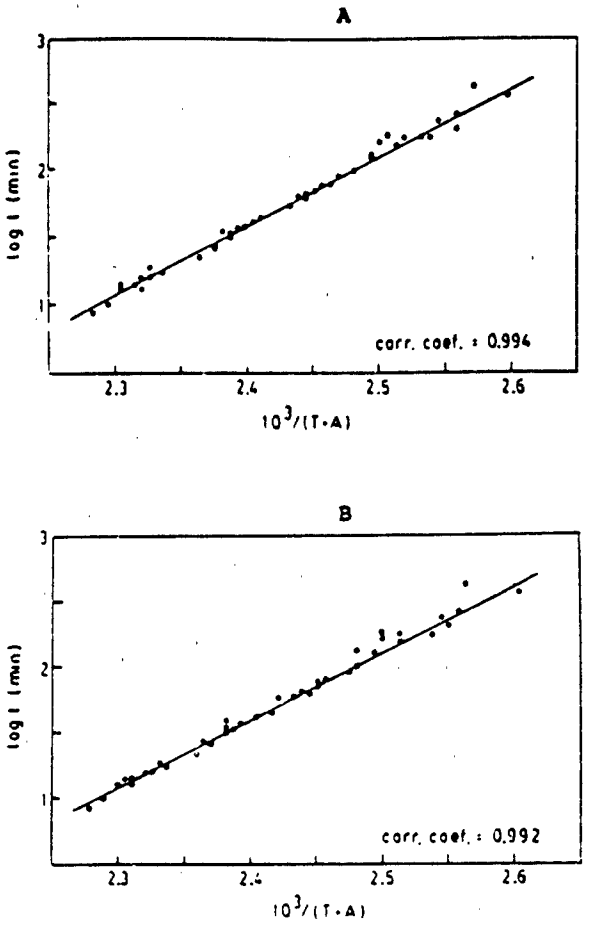


FIGURE 10. Superimposed Plot of log t vs. 1/(T+A): A - Using a Shift Factor Based on the T_p Value Obtained at a Heating Rate of 2K min^{-1} (■) BR and Antioxidant F; B - Using a Shift Factor Based on the T_p Value Obtained at a Heating Rate of 8K min^{-1} (■) BR and Antioxidant F (161)

polydimethyl siloxane samples is established in ten minutes, as is evident in Figure 11. Figure 12 shows the correlation of volume swell ratio with Young's modulus, which also relates to crosslink density. Prime notes that this method should, in principle, be applicable to other vulcanizate systems. It

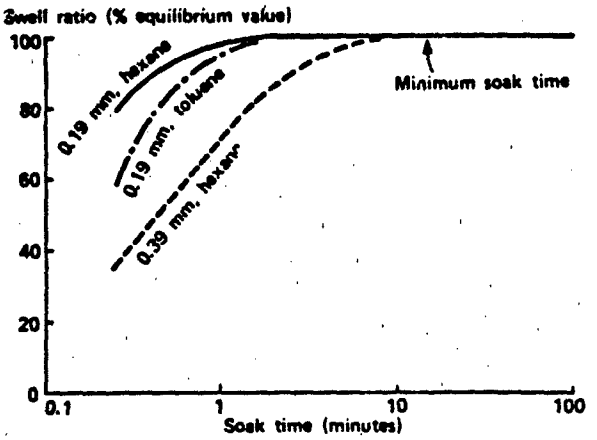


FIGURE 11. Time to Equilibrium Swelling as a Function of Sample Thickness and Solvent (191).

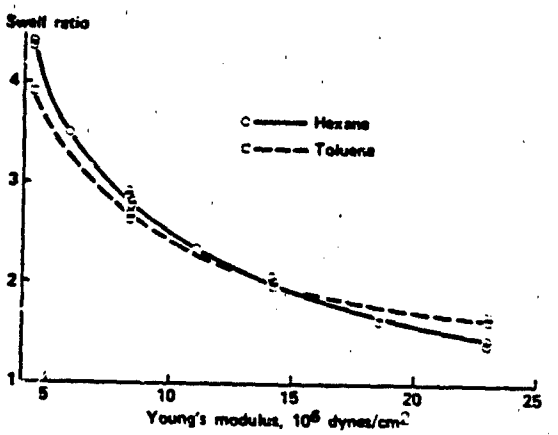


FIGURE 12. Direct Correlation Between Equilibrium Swell Ratio and Young's Modulus (191).

would, therefore, appear to offer a route to the evaluation of cure behavior of vulcanizates, and for studying polymer-filler interaction, etc.

Elastic Modulus via TMA

An alternative method of evaluating crosslink density is by measuring elastic modulus. Barral and coworkers (192,193) calculated elastic modulus (Em) from TMA (penetrometer) measurements following the equation developed by Gent (194)

$$Em = \left(\frac{f}{p^{1/2}}\right)\left(\frac{9}{16\, r^{1/2}}\right)$$

where F = load, p = penetration, and r = probe radius. Em is correlated to ν_e (effective crosslink/cm^3) by the relationship

$$\nu_e = \frac{Em}{3RT}$$

where T = 293K and R = 8,314.10^7 ergs/mole/K

The utilization of these techniques to study cure behavior and network formation in poly(dimethylsiloxane) polymers is described by Barrall and coworkers.

Another incident which led to utilization of this technique was described by Ellerstein (195). During August of 1971 the polymer characterization laboratory at Thiokol's Trenton facility was inundated by a flood. All the instruments that had been previously utilized for modulus determination were damaged. Led by this urgency, Ellerstein (195) determined Youngs moduli of fluorocarbon elastomers from the equation, E = (F/K), $L^{-3/2}$, where E = modulus, F = force, L = penetration, and K = empirical constant, which may be calibrated by using a reference material of known modulus E. The equation should be quite valid at temperatures above the glass transition region, and where the deformatin is small compared to the dimension of the sample. When these restrictions are not met, some deviation from the actual value of the modulus will occur. It is noted that for the case of a spherical indentor, this has been treated by Finkin (196) and verified by Hwo and Johnson (197).

While either a temperature programmed or an isothermal method may be used with a stable network rubber, only the latter method gives reliable results when time dependent effects are present. On the other hand, the former method provides a rapid tool for qualitative screening, since it shows where marked softening occurs.

The use of penetration and recovery furnishes viscoelastic information, and may be used to supplant or supplement creep experiments. It may often be used for a rapid estimate of compression set.

Care must be used with these methods, since a sample may not be homogeneous, and the surface region may be different than the interior. This may be especially true where long post cure treatments are required.

Volume Swell by TMA

Many rubber products are required to operate in a fluid environment in which swelling may occur. Isothermal TMA offers a convenient and accurate method for measuring dimensional changes accompanying solvent swelling. Brazier and Nickel (35) conducted limited studies of the phenomenon in plastics, but only limited information on rubbers has yet been noticed (15). The TMA furnace is replaced by the solvent reservoir for swelling measurements and the dimensional changes recorded as a function of time. As in the case of the TG method, equilibrium swell is reached in 10-15 minutes for thin samples. The sample is held between two porous glass fritters to allow intimate contact of the solvent and the sample. Anisotropic swelling of compression molded NR was observed by Brazier and Nickel (35). The TMA swell measurements were 3-5% lower than those determined by the solvent swell method.

Low Temperature Properties via TMA

ASTM D1053 describes a method for measuring low temperature stiffening of rubber and rubber-like material. Indication of low temperature stiffening is generally obtained by Gehman temperature (G_T). This is the temperature at which the rigidity modulus reaches 1000 kgm/cm^2 per radian. For a series of low temperature hose compounds, Brazier and Nickel (35) observed a linear relationship between G_T and the glass transition temperature determined by TMA expansion both by the extrapolation method (Tg_e) as well as by the derivative method (Tg_d). Tg_d shows a maximum at the maximum rate of dimensional change at the glass transition region and helps in identifying Tg. The TMA experiment requires 20 minutes as compared to around half a day for G_T.

Shrinkage in Molded Vulcanizate by TMA

Fogiel, et al., (198) utilized coefficient of expansion by TMA to study the shrinkage and expansion of fluoroelastomers, measured in all three directions. Their investigation il-

lustrates the use of TMA to measure anisotropy of shrinkage in molded vulcanizates.

A key aspect of this study was the use of vulcanized elastomer (FKM) standards, whose expansion coefficient was established by dilatometry, to calibrate the TMA instrument. These standards have the same level of expansion coefficient as the vulcanizate, in contrast to the customary metal standards (lead or aluminum), where a coefficient of expansion, too small for reliable calibration, is observed. For the press cured FKM, at 177°C, the predicted and experimental values of shrinkage were found to be in good agreement. The predicted values were calculated from the coefficient of expansion as follows:

$$s = (\alpha_c - \alpha_m)\,(t-25)/[1 + \alpha_c\,(t-25)],$$

where α_c and α_m refer to the expansion coefficient of the compound and the mold, respectively, at the pressure temperature, t. It was also shown that the average shrinkage values of the filled vulcanizates after pressure can be predicted from gum stock values, α_r. The following equation was used to calculate α_c of the filled stock.

$$\alpha_c = V_r\,\alpha_r + (1-V_r)\,\alpha_f$$

where V is the volume fraction of the rubber in the filled stock, and α_r and α_f refer to the linear isotropic expansion coefficients of the unfilled rubber and filler, respectively.

Beatty (199) measured shrinkage of a large number of rubber compositions with a micrometer and cathetometer. He came to the conclusion that the mold shrinkage of elastomer compositions depends upon the elastomer employed, the volume percent of the elastomer plus all other organic materials, and the kind and amount of pigment present. Pigments inhibit the shrinkage of rubber.

In calculating the shrinkage of a composition from its recipe, the follwoing formula was suggested by Beatty, when loading pigments are not present

$$S = \Delta T\,(C_1 - C_2)R$$

where S is shrinkage in cm/cm, ΔT is the temperature difference in °C between the curing temperature and room temperature. C_1 is the coefficient of thermal expansion of the gum stock

(cm/cm/°C), C_2 is the coefficient of thermal expansion of the mold material[2] (11.5×10^{-6} cm/cm/°C for steel, and R is the percentage by volume of rubber, sulfur, and all organic materials combined.

When a loading pigment or a combination of a loading pigment is present, the above formula must be modified by substracting the correction for shrinkage inhibition due to the pigments.

TMA, when properly calibrated, offers a relatively simple and precise method for the determination of isotropic linear expansion and hence the volumetric expansion of rubbers and the compounding ingredients. From the information generated, mold shrinkage can be predicted from the formulas that can be worked out.

TMA vs VICAT Softening Temperature

One of the tests performed on polymers is the VICAT softening test as described in ASTM method D-1525. This involves measuring the temperature at which a circular probe of 1.0 mm^2 cross section under a load of 1.0 kg penetrates 1.0 mm into a sample 12.7 mm thick. Yanai and coworkers (200) at the Rohm and Hass Company have used the standard DuPont TMA system to obtain data equivalent to the VICAT test by using a load of 10g and a penetration probe. TMA and comparable VICAT data are shown for a polyurethane elastomer in Figure 13.

Molecular Weight via TMA

A rough indication of molecular weight of natural rubber was obtained by Soviet workers (201) by TMA penetration method. The temperature corresponding to complete penetration (T_k) was found to be related to molecular weight determined by solution viscosity. Thus, thermomechanical curves can be used to study the effectiveness of milling of rubber.

Thermal Conductivity of Elastomer Vulcanizate

The rate at which heat can get into and out of rubber, i.e., its thermal conductivity, controls, many applications. It affects the design of processing machinery and controls the speed of many mixing, extruding, and molding operations. Although various methods for thermal conductivity measurements are well documented in the literature (202-206), including the widely accepted ASTM procedure (207), there remains a demand for rapid, versatile techniques for routine scouting research where requirement for sample preparation, temperature equilib-

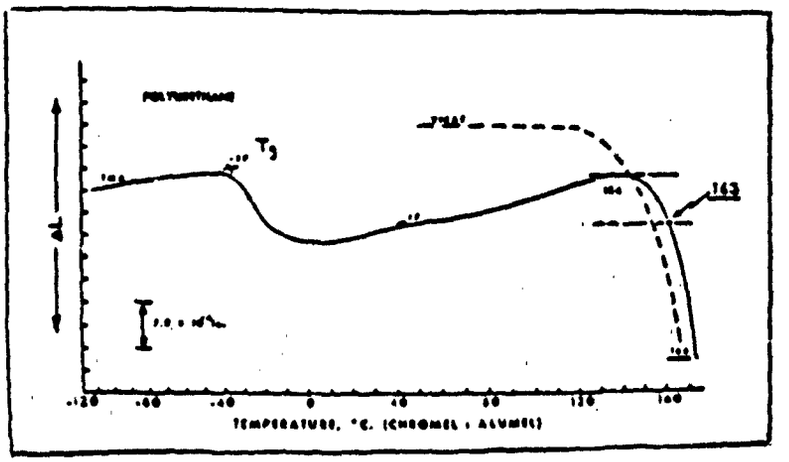
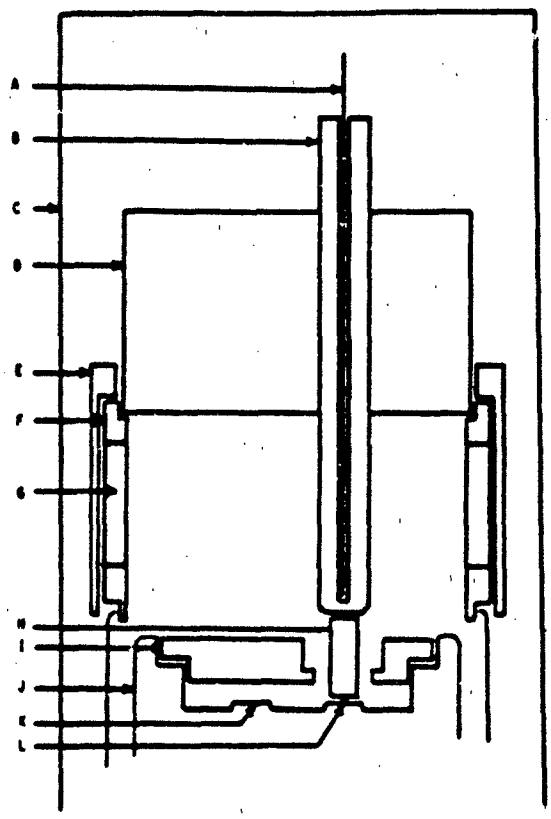


FIGURE 13. TMA vs. VICAT Test on Polyurethane Elastomer (200).

ration, and instrument operation are less stringent. Based on some earlier attempts to utilize differential scanning calorimetry (208-211), Sircar et al., (212) described a simple attachment to the DuPont Differential Scanning Calorimeter (DSC) cell for such measurements, without altering the base equipment. In contrast to the ASTM procedures, which require large samples and hours or days for a determination, the DSC procedure requires a relatively small amount of sample and takes only a few minutes for each determination of thermal conductivity. A further advantage of the DSC method is that the specific heat can be readily determined by the same unit, and if the specific gravity is known, the thermal diffusivity, α can be obtained from the relationship $\alpha = \lambda / \rho C_p$, where λ = thermal conductivity, ρ = specific gravity, C_p = specific heat at constant pressure. Because of the required retention of size and shape of the sample, the method is not suitable for unvulcanized compounds.

The thermal conductivity assembly and the method are shown in Figures 14 and 15. A finite quantity of heat flux, dependent on the temperature of measurement, I_1, is generated by the DSC unit. This flux travels through the sample H (Figure 14) to the copper conducter, B, which at the top is surrounded by the aluminum heat sink, D. Temperature at the top of the sample is measured with an iron-constant thermocouple reaching through a 1/8 inch hole in the copper conductor. The thermal conductivity of a cylindrical specimen is determined with respect to a standard, by using the following equation:



Thermal conductivity assembly. A, thermocouple; B, copper conductor; C, convection shield; D, aluminum heat sink; E, steel cover; F, steel spacer; G, window; H, sample; I, transite cover; J, DSC cell; K, reference platform; L, sample platform.

FIGURE 14. Thermal Conductivity Assembly (a) Thermocouple; (b) Copper Conductor; (c) Convection Shield; (d) Aluminum Heat Sink; (e) Steep Cover; (f) Steel Spacer; (g) Window; (h) Sample; (i) Transite Cover; (j) DSC Cell; (k) Reference Platform; (l) Sample Platform (212).

$$\lambda_s = \lambda_r \times \frac{hs}{h_r} \times \frac{Ss}{S_r} \times \frac{Ls}{L_r} \times \frac{Dr^2}{Ds^2} \times \frac{\Delta Tr}{\Delta Ts}$$

where s and r represent the sample and the reference standard (NR gum) respectively; λ = thermal conductivity, W/mk; h = chart deflection (measured distance between recorder zero and

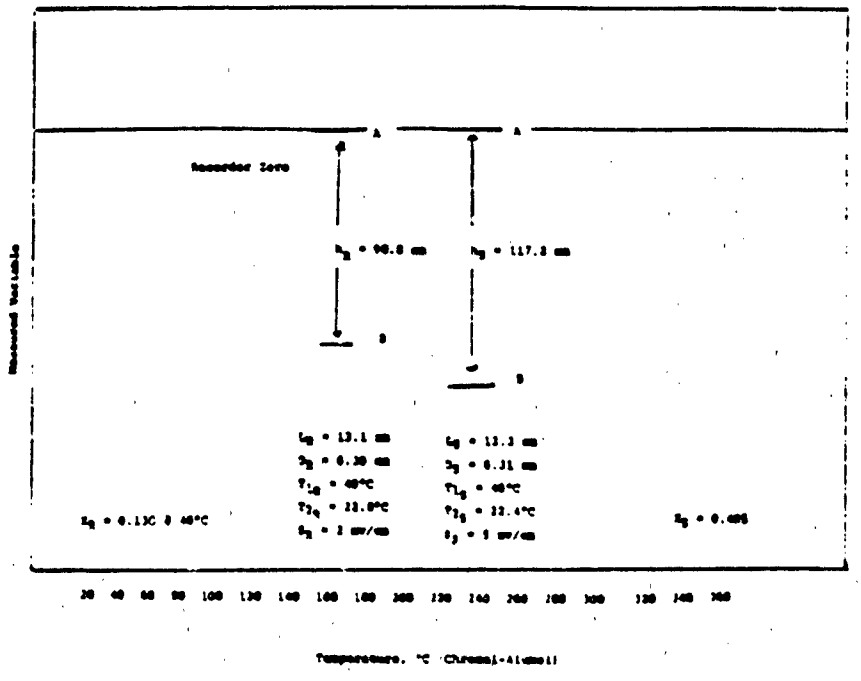


FIGURE 15. DSC Conductivity Method (212).

signal curve), mm; S = y axis sensitivity, mv/cm; L = specimen length, mm; A = specimen cross-sectional area = 0.7850^2; D = diameter of the specimen, mm; T = temperature differential (T_1-T_2); T_1 = temperature at the bottom of the specimen, °C, and T_2 = temperature at the top of the specimen, °C. Figure 16 shows the effect of black loading on thermal conductivity of a bladder compound, the thermal conductivity data as determined by this method, of some known materials compares favorably with those in the literature. Improved results are obtained when λ of the standard is not too far apart from that of the sample. The method is recommended to polymer and rubber processors.

Electrothermal Analysis

The determination of electrical properties of polymers as a function of temperature generally involves discrete electrical readings on samples heated in an oven. Such tests are tedious, time consuming, and require fairly large polymer samples. Following the lead of Chiu (213), Sircar and coworkers modified a DuPont DSC, without any permanent alterations so that it can

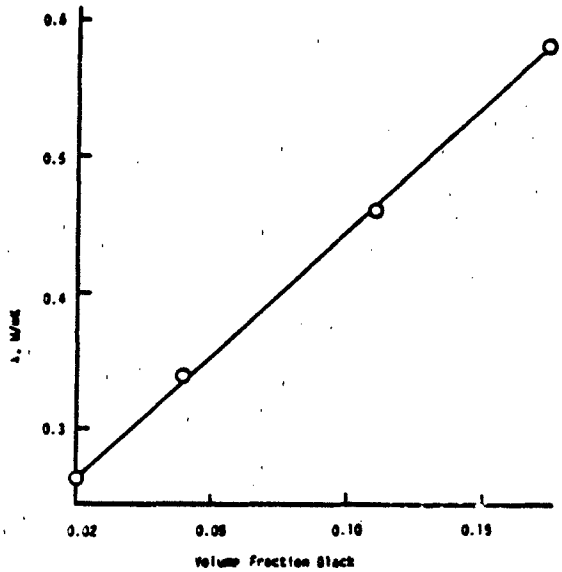


FIGURE 16. Effect of N-299 Black on Thermal Conductivity of a Bladder Compound (212).

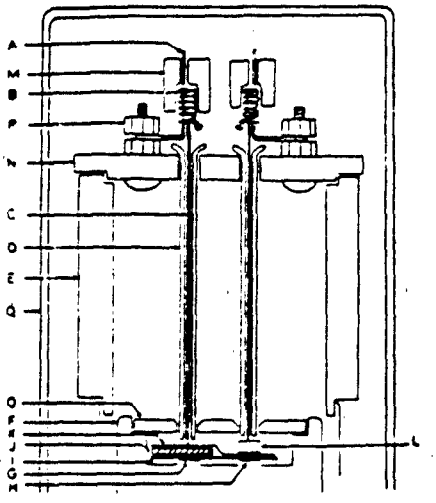
record resistivity as a function of temperature (120 to 500°C). The method was termed electrothermal analysis by Chiu. The modified DSC cell and the schematic are illustrated in Figure 17. Sircar (214, 215) used this method to determine the relationship of resistivity, with temperature of carbon black filled polymers. Figure 18 shows the resistivity vs. concentration of N-472 carbon black in EVA. The equipment was also used for quick scanning of different polymers and compounds for their usefulness as PTC (positive temperature coefficient of resistance) materials (215).

Prospect of Thermal Analysis in Elastomer Systems

There has been an extraordinary increase in the applications of the two main thermal analysis techniques (DTA or DSC and TG) in the physics and chemistry of elastomers in the last ten years. This is due to several circumstances. The most important being the availability of commercial instruments.

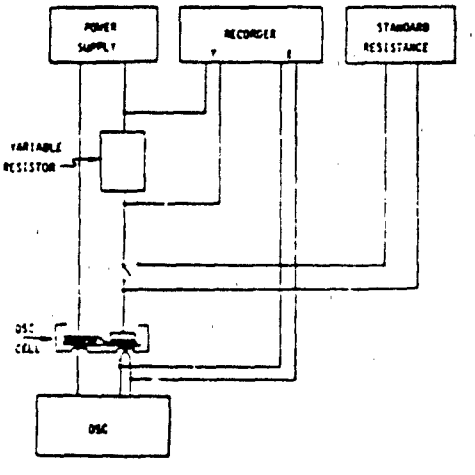
The design of sensitive and precise automatic equipment eliminated the disadvantages of polymers as objects for thermal analysis (low thermal conductivity, low phase transition heats, thermal gradient in measuring cells). Thermal analysis apparatus suitable for polymer research are offered at present by several tens of producers, and these apparatus have become

A



Cell for ETA measurement. (A) Copper conductor, (B) spring, (C) Pt electrode, (D) glass capillary, (E) extension tube, (F) DSC cell, (G) ref. platform, (H) sample platform, (I) glass slide, (J) asbestos pad, (K) Pt foil, (L) sample, (M) lead weight, (N) clear plexiglass cover, (O) aluminium cover, (P) terminal connection, (Q) glass bell.

B



Schematic for ETA measurements.

FIGURE 17. Electro Thermal Analysis: A - Cell for ETA Measurement (a) Copper Conductor; (b) Spring; (c) Pt Electrode; (d) Glass Capillary; (e) Extension Tube; (f) DSC Cell; (g) Reference Platform; (h) Sample Platform; (i) Glass Slide; (j) Asbestos Pad; (k) Pt. Foil; (l) Sample; (m) Lead Weight; (n) Clear Plexiglass Cover; (o) Aluminum Cover; (p) Terminal Connection; (q) Glass Bell (214); B - Schematic for ETA Measurements (214).

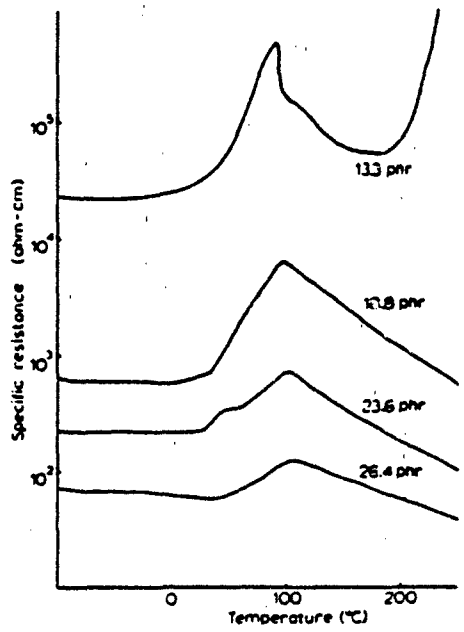


FIGURE 18. Electrothermal Analysis of Carbon Loaded EVA (215).

virtually standard equipment in laboratories studying the properties of elastomers from different aspects.

Thermal analysis is getting into all phases of the industrial laboratory work--research, quality control, process control, technical service. Most of these applications remain a trade secret and are not reported. Maurer (13,14) cites a few examples of the application of thermal analysis in quality, process, and product control in elastomer industries. Many others are available in the instrument manufacturers' literature.

DSC has virtually replaced the classical melting point apparatus for the determination of melting of polymers. Already there are a lot of uses for this very simple determination. An example is the polyethylene bag being dumped in the Banbury batch along with the contents (e.g., carbon black). The melting point of this bag, which can be determined by DSC in 15 minutes, is critical for its proper dispersion at the processing temperature.

A processing problem such as micro-incrustations in a customer's polymer film was traced by DSC to be due to undispersed initiator, which would severely reduce the area of the melting endotherm. These uses of the thermal analysis in quality, process and product control are being spurred by the availability of quality control related cheaper equipment. Brazier (15) thinks that increased acceptance of these methods will depend in part on the development of more rugged equipment which is better suited to the factory environment. In addition, he believes that more general acceptance of these methods will require in some cases an incubation period during which the industry becomes familiar with the techniques and then slowly displace some of the traditional methods of analysis.

From time to time new applications appear--for instance, estimatin of the molecular weight of polytetrafluoro ethylene by DSC (216) on the basis of the relationship between molecular weight and heat of crystallization. Another instance is the recent use of DTA to study the intermolecular bonding and morphology of the thermo-plastic polyurethane. The study gives information as to the optimum injection molding temperature--which gives best tensile, hysteresis, and fatigue properties (217). Certainly we can expect such new applications as well as a further quantitative extension of the main fields of application of DSC in the study of phase transitions, and of TG in the evaluation of the thermal stabilities and degradation of polymers. Novel ideas of hazard evaluation have found their way in completely new equipment as the "Accelerating Rate Calorimeter" (218). More demand is also expected for TMA for the various uses mentined. In the author's opinion, TMA is under utilized at present and its potential is only beginning to be realized.

As regards the possibilities of the particular TA techniques, the most promising appear to be the quantitative DTA or the DSC technique. Classical DTA has now been almost completely replaced by DSC and there does not seem to be any future for the former except for very high temperature (over 650°C), where design capability of some models limit the high temperature capability for DSC. DSC is fast becoming an important tool for the investigation of a wide range of properties, phenomenon, and processes in polymers. There are fields in which it has not fulfilled its expectations. One is the measurement of heat capacities of elastomers, although such measurements in other polymers have been reviewed (219). DSC can be routinely used for this purpose instead of adiabetic calorimeters. This would enable the rapid accumulation of the great mass of data necessary for the interpretation of the relation between the structure and heat capacity of polymers.

The survey of the literature by Gomory (220) does not confirm this expectation. Another would be the application of degradation kinetics (DSC, TG) in the prediction of service life. Although non-isothermal kinetics have, in general, attained great success, this has not trickled into the product applications.

The different new methods of analyses of elastomers have not yet found their way into specifications. This will come with the familiarity of the methods. The author used the different identification procedures mentioned earlier as a routine process for the identification of elastomers and blends in rubber products. Qualitative determination of the unknown recipe by combined DSC (for identification) and TG-DTG (for identification and quantitative evaluation) is believed to be getting popular. It is only a matter of time until these get into specifications.

Another particular advantage of the DSC technique is the comparative ease with which it can be adapted to measure other responses. One is the measurement of thermal conductivity. In view of the energy shortage and more awareness of heat conservation, there will be a great demand for heat conductivity data. The relative values of thermal conductivity can be very rapidly obtained by a simple modification of DSC (211). This, along with the heat capacity data so easily obtained from DSC, will allow the calculation of thermal diffusivity which is of importance in industrial processes such as vulcanization.

Another modification of DSC which measures electrical conductivity (213) has successfully been used by the author to determine thermal stability of elastomers (214) and to study positive temperature coefficient of resistance of carbon black loaded EVA (215). Such uses are expected to fluorish.

High pressure DSC is also commercially available but has not gained popularity except for special applications.

The coupled simultaneous techniques, i.e., combination of TA with some other method of structure analysis (mass spectrometry, gas chromatography, infrared) have great potential but probably suffer from the non-availability of commercially coupled instruments.

Recently, microprocessors have greatly improved the sensitivity and resolution of commercial instruments. Computerized data recording and storing capability have also been features of the new instruments. These developments will greatly expand the horizon of application of thermal analysis in the elastomer system for years to come.

ACKNOWLEDGEMENT

The author wishes to thank University of Dayton Research Institute for permission to publish this review. The contribution of his colleague at J. M. Huber Corporation, D. Sweigart, and J. L. Wells for experimental help to many of the author's thermoanalytical investigations over the last decade is gratefully acknowledged. The author sincerely appreciates the encouragement from his colleagues, R. P. Charvoff, J. A. Harvey, and I. O. Salyer during preparation of this paper. Sincere thanks and appreciation are also due to Julie Cochran and Margaret Bertke who typed this manuscript and to Judith N. Hecht for the literature search.

GLOSSARY OF ABBREVIATIONS

Abbreviation	Description of Chemical Name
BR	Poly(butadiene) rubber
SBR	Styrene - butadiene rubber
NR	Natural rubber
IR	Poly(isoprene) rubber
I-IR	Isobutene-isoprene or butyl rubber
EPM	Ethylene-propylene rubber (saturated)
EPDM	Ethylene-propylene-diene rubber
CR	Poly (chloroprene) rubber
NBR	Nitrile-butadiene rubber
CIIR	Chlorobutyl rubber
BIIR	Bromobutyl rubber
PMMA	Poly(methylmethacrylate)
PE	Polyethylene
PP	Polypropylene
CSM	Chloro-sulfonated polyethylene (Hypalon)
ABS	Acrylonitrile-butadiene-styrene polymer
EVA	Ethylene-vinyl acetate co-polymer
PVC	Poly(vinyl chloride)
ACM	Poly(acrylates)
FKM	Fluoroelastomers
CO	Epichlorohydrin Polymer
ECO	Epichlorohydrin-ethylene oxide copolymer

GLOSSARY OF ABBREVIATIONS (cont'd)

Abbreviation	Description of Chemical Name
DTA	Differential Thermal Analysis
DSC	Differential Scanning Calorimetry
DDSC	Derivative DSC
TMA	Thermomechanical Analysis
DTMA	Derivative TMA
TG	Thermogravimetry
DTG	Derivative Thermogravimetry
GC	Gas Chromatography

REFERENCES

1. Chem. Eng. News, (1969): 46.
2. Lab. Guide, Anal. Chem., (1972): 44,NO10
3. Teelsel, D. A. and Levi, D. W., Plastec Note, 1 (1963), 10 (1966), 20, (1969).
4. Wendlendt, W. W., Ed., Thermochim Acta, (Elsevier, Amsterdam), (1st issue 1970), published quarterly.
5. Buzagh, E. and Simon, J., Eds., J. Thermal Anal., Heyden & Sons, London (1st issue 1972), published bimonthly.
6. Redfern, J. P., Ed., Thermal Anal. Abstrs., McMillan, London, 1965, (1st issue 1972), published bimonthly.
7. Calorimetry, Thermometry, and Thermal Analysis (Japan), Soc. Calorimetry and Thermal Anal., Tokyo (1st issue 1974), published quarterly.
8. Sircar, A. K. (1980): "Rubber-80" International Conf., Dec. 28-30, 1980, Kharagpur, India.
9. Sircar, A. K. (1981): 120th Meeting of the Rubber Div., American Chemical Soc., Oct. 13-16, 1981, Cleveland, OH.
10. Sircar, A. K. (1982), J. Sci. & Indstr. Res. (India), 41: 536.
11. Maurer, J. J. (1969), Rubber Chem. Technol., 42: 110.
12. Brazier, D. W. (1980), Rubber chem. Technol., 53: 437-511.
13. Maurer, J. J. (1981): In Thermal Characterization of Polymeric Materials, Edited by E. A. Turi, pp. 571-708, Academic Press, New York.
14. Maurer, J. J., and Brazier, D. W. (1983), Kautsch. Gummi. Kunstst., 36:37.
15. Brazier, D. W. (1979): Natl. Bureau of Standards Special Publication #580, Proc. Workshop on State of the Art of Thermal Analysis, Gaithesburg, MD, May 21-22, 1979.
16. Wendlandt, S. S. (1974): Thermal Methods of Analysis, John Wiley & Sons, Inc., New York, NY.
17. Slade, P. E. Jr., and Jenkins, L. T. (1970): Thermal Characterization Techniques, Vol. 2, Mercel Decker. Inc., New York, NY.
18. Porter, R. S. and Johnson, J. G. (1968): Analytical Calorimetry, Vol. 1, Plenum Press, New York, NY.
19. Maurer, J. J. (1978): In: Thermal Methods in Polymer Analysis, Edited by S. W. Shalaby, Franklin Institute Press, PA.
20. Mackenzie, R. C. (1972): Differential Thermal Analysis, Vol. 2, Applications, Academic Press, London.
21. Pope, M. I. and Judd, M. D. (1977): A Guide to Technique and its Applicatons, Heyden & Sons, Ltd., London.
22. Chiu, J. (1974): Polymer Characterization by Thermal Methods of Analysis, Mercel Dekker, Inc., New York, NY

23. Blazek, A. (1974): Thermal Analysis, Van Nostrand, Reinhold Co., Ltd., London.
24. Mackenzie, R. C., Ed. (1970): Differential Thermal Analysis, Vol. I, Fundamental Aspects, Academic Press, London.
25. Schewenker, R. F. and Garn, P.D., Eds., (1969): Thermal Analysis, Vol I & II, Academic Press, New York, NY.
26. Keattch, C. J. and Dollimore, D., Eds., (1975): An Introduction to Thermogravimetry, Heyden & Sons, Ltd., London.
27. Brazier, D. W. (1980): In: Application of TG in the Study and Analysis of Elastomers and Elastomer Compounds, Edited by J. P. Redfern (in press).
28. Norem, S. D., O'Neill, M. J., and Gray, A. P. (1969): In: Proc. 3rd Toronto Symposium on Thermal Anal., p. 221.
29. Norem, S. D., O'Neill, M. J., and Gray, A. P. (1970): Thermochim Acta 1:29.
30. Garn, P. D., Menis, O., and Weldemann, H. G. (1981): J. Therm. Anal., 20:185.
31. McGhie, A. R., Chiu, J., Fair, P. G., and Blaine, R. L. (1983): Thermochim Acta, 67: 241.
32. Blaine, R. L. and Fair, P. G. (1983): Thermochim Acta, 67:233.
33. Gray, A. P. (1969): Perkin-Elmer Instr. News, 20: N01,10.
34. Instruction Manual, DuPont 941TMA, 900M11.
35. Brazier, D. W. and Nickel, G. H. (1978): Thermochim Acta, 26: 339; 1979: Rubber Chem. Technol., 52: 735.
36. Miller G. W. and Fitzsimmons, R. V. (1972): Thermochim Acta 4:425.
37. Byrne, L. F. and Hourston, D. F. (1979): J. Appl. Polym. Sci., 23: 1607.
38. Miller, G. W. and Sanders, J. H. (1969): J. Appl. Polym. Sci., 13: 1277.
39. Burfield, D. R. and Lim, K. L. (1983): Macromolecules, 16: 1170.
40. Miller, G. W. (1971): J. Appl. Polym. Sci., 15: 2335.
41. Strella, J. (1963): J. Appl. Polym. Sci., 7: 569.
42. Lambert, A. (1969): Polymer, 10: 319.
43. Strella, S. and Erhardt, P. F. (1969): J. Appl. Polym. Sci., 13: 1373.
44. Wunderlich, B., Boduly, D. M., and Kaplan, M. H. (1964): J. Appl. Polym. Sci., 35:1.
45. Maurer, J. J. (1970): In: Analytical Calorimetry, Vol. II, Edited by R. S. Porter & J. F. Johnson, Plenum Press. New York, NY, pp. 61.
46. Burfield, D. R. (1983): Polymer Communications, 24: 178.
47. Wood, L. A. (1958): J. Polym. Sci., 38: 319.
48. Maurer, J. J. (1965): Rubber chem. Technol. 39: 979.

49. Jorgensen, A. H., Chandler, L. A., and Collins, E. A. (1973): Rubber Chem. Technol. 46:1087.
50. Tokita, N. and Scott, R. (1969): Rubber Chem. Technol., 42: 944.
51. Ikeda, R. M., Wallsch, M. L., and Angelo, R. J. (1969): In: Block Polymers, Edited by S. L. Agarwal, Pergamon Press, New York, NY.
52. Gardiner, J. B. (1970): Rubber Chem. Technol., 43: 370.
53. Sircar, A. K. and Lamond, T. G. (1975): Rubber Chem. Technol., 48: 301.
54. Marsh, P. A., Voet, A., Price, L. D., and Mullens, J. J. (1967): Rubber Chem. Technol., 40: 344.
55. Landi, V. R. (1972): Rubber Chem. Technol., 45:222.
56. Sircar, A. K. and Lamond, T. G. (1975): Rubber chem. Technol., 48:653.
57. Callan, J. E., Hess, W. M., and Scott, C. E. (1971): Rubber Chem. Technol., 44:814.
58. Ceccorulli, G., Pizzoli, M., Scandola, M., and Pezzin, G. (1983): Polym. Communications, 24:107.
59. Gelling, I. R. and Smith, J. F. (1979): International Rubber Conf., Venice, Oct. 1979, pp. 140.
60. Davies, C. K. L., Wolfe, S. V., Gelling, I. R., and Thomas, A. G. (1983): Polymer, 24:107.
61. Burfield, D. R., Law, K. S., and Lim K. L. (in press): J. Appl. Polym. Sci.
62. Burfield, D. R., Lim, K. L., Law, K. S., and Ng, S. (1984): Polymer, 25:995.
63. Baker, C. S. L., Gelling, I. R., and Newell R. (1985): Rubber Chem. Technol., 58:67.
64. Ke, B. (1960): J. Polym. Sci., 42:15 (1962): J. Polym. Sci., 61:47.
65. Barrall, E. M., II, Porter, R. S., and Johnson, J. F. (1966): Rubber Chem. Technol., 39:1513.
66. Picón, P. R., Valles, E. M., and Capiati, N. J. (1984): Polymer Communications, 25:37.
67. Ke, B. (1966): In: Encyclopedia of Polymer Science and Technology, Vol. 5, Edited by H. F. Mark and N. G. Gaylords, John Wiley & Sons, Inc., New York, NY, p. 41.
68. Verstrate, G. and Wilchinsky, G. W. (1971): J. Polym. Sci., 9A-2:127.
69. Chakraborty, K. K. (1974): Rubber India, 26(2):14; 26(3):14.
70. Sircar, A. K. and Lamond, T. G. (1973): Rubber Chem. Technol., 46:178.
71. Morris, M. C. (1971): Rubber Chem. Technol., 40:341.
72. Marsh, P. A., Voet, A., and Price, L. D. (1968): Rubber Chem. Technol., 41:344.
73. Lee, B. and Singleton, C. (1979): J. Appl. Polym. Sci., 24:2169.

74. Ghijsels, A. and Mieras, H. J. M. A. (1972): J. Inst. Rubber Indst., 6:259.
75. Ghijsels, A. (1977): Rubber Chem. Technol., 50:278.
76. Brazier, D.W. and Nickel, G. H. (1975): Rubber Chem. Technol., 48:26.
77. Ranganathan, B.N. (1984): SAMPE, 15(2):1.
78. Bhaumik, M. L., Banerjee, D., and Sircar, A. K. (1962): J. Appl. Polym. Sci., 6:674.
79. Bhaumik, M. L., Banerjee, D., and Sircar, A.K. (1965): J. Appl. Polym. Sci., 9:1367.
80. Bhaumik, M. L., Banerjee, D., and Sircar, A.K. (1965): J. Appl. Polym. Sci., 9:1731.
81. Bhaumik, M. L., Banerjee, D., and Sircar, A. K. (1965): J. Appl. Polym. Sci., 9:2286.
82. Bhaumik, M. L., Banerjee, D., and Sircar, A. K. (1962): Proc. Fourth Rubber Technol. Conf., London.
83. Brazier, D. W. (1977): Thermochim Acta, 18:147.
84. Brazier, D. W., Nickel, G. H., and Szentgyorgy, Z. (1980): Rubber Chem. Technol., 53:160.
85. Chunhua, X., and Yizhen, L. (1984): Hecheng Xiangjiao Gongye, 7(2):134.
86. Wald, S.A. and Winding, C. C. (1971): Polym. Eng. Sci., 11:57,64,70.
87. Brazier, D.W. and Schwartz, N.V. (1980): Thermochim. Acta, 39:7.
88. Gusev, Y. K., Moiseev, D. I., Sigov, O. V., and Romanova, A. B. (1981): Kauch. Rezina, 11:19.
89. Markov, V. V., Privalikhina, N. P., and Zanemonets, N. A. (1973): J. Polym. Sci., 42:633.
90. Mihaila, D., Baeiu, D. and Suciv, P. (1970): Ind. Usoara, 17:624.
91. Mityushina, I. (1982): Vyssh. Uchebn. Zaved., Khim. Khim. Technol, 25(4):512.
92. Coran, A. Y. (1978): In: Science and Technology of Rubber, Edited by F. R. Birich, Academic Press, New York, NY, Ch. 7 and references therein.
93. Zanemonets, N. A., Igarova, S. A., Agayants, I. M., and Nekrasova, E. I. (1972): Sov. Rubber Technol., 3:20.
94. Crane, L. W., Dynes, P. J., and Kaelbe, D. H. (1973): J. Polym. Sci. Polym. Lett., 11:533.
95. Swarin, S. J. and Wims, A. M. (1974): Rubber Chem. Technol., 47:1193.
96. ASTM D-1160, Annual Book of ASTM Standards, Pt. 18, American Society for Testing and Materials, Philadelphia, PA, 19103, p. 231 (1973).
97. Wong, C. P. (1984): Polymers in Electronics Conf., American Chem. Soc.
98. Nosnikov, A.F. and Poznyakova, T. V. (1983): Vopr. Khim. Khim., 71:78.
99. Kleps, T. and Jaroszynska, D. (1983): Polimery, 28(9):328.

100. Sobczynski, T. and Kwaitkowski (1983): Zes. Z. Nauk-Acad. Ekon Poznaniu Ser. 1, 109:29.
101. Jaroszynska, D., Kleps, T., and Tutak, G. (1980): J. Thermal Anal. 19:69.
102. Sharma, K. K. and Varma, I. K. (1980): J. Appl. Polym. Sci., 25:1087.
103. Smith, D. A. (1966): Rubber Chem. Technol., 37:937.
104. Sircar, A.K. and Lamond, T. G. (1972): Rubber Chem. Technol., 45:329.
105. Strauss, S. and Wall, L. W. (1961): J. Res. Natl. Bur. Stand., A65:221.
106. Sircar, A. K. and Lamond, T. G. (1975): Rubber Chem. Technol., 48:640.
107. Maurer, J. J. (1970): Status of Thermal Analysis, Proc. Symp., NBS Special Publication #338, Gaithesburg.
108. Maurer, J. J. (1970): Rubber Age, 102:47.
109. Sircar, A. K. (1977): Rubber Chem. Technol., 50:71.
110. Brazier, D. W. and Nickel, G. H. (1975): Rubber Chem. Technol., 48:661.
111. Gelling, I. R., Loadman, M. J., and Sidek, B. J. (1979): J. Appl. Polym. Sci., 17:1383.
112. Sircar, A. K. and Lamond, T. G. (1978): Thermochim. Acta, 27:367.
113. Brazier, D. W. and Schwartz, N. V. (1978): Rubber Chem. Technol., 51:1060.
114. Dawson, B. and Sewel, P. R. (1975): J. Rubber Ind., 9:100.
115. Goh, S. H. (1980): Thermochim. Acta, 39:353.
116. Ponca-Velez, M. A. and Campos-Lopez, E. (1978): J. Appl. Polym. Sci., 22, 2485.
117. Instruction Manual, DuPont 951, Thermogravimetric Analyzer, PN 9510621.
118. Golub, M. A. and Garguilo, R. J. (1972): J. Polym. Sci., Polym. lett. 10:41.
119. Golub, M. A. and Sung, M. (1972): J. Polym. Sci., Polym. Lett. 12:89.
120. Sircar, A. K. and Voet, A. (1970): Rubber Chem. Technol., 43, 1327.
121. Sircar, A. K. and Lamond, T. G. (1973): J. Appl. Polym. Sci., 17(8):2569.
122. Brazier, D. W. and Schwartz, N. V. (1978): J. Appl. Polym. Sci., 22:113.
123. Zheyan, Z. and Guilin, Z. (1982): Zhongguo Kexueyuah Changchun Ying Yong Huaxue Yanjiuso Jekan, 19:121.
124. Sircar, A. K. and Lamond, T. G. (1978): Rubber Chem. Technol., 51:647.
125. Sircar, A. K. and Lamond, T. G. (1973): Thermochim. Acta, 7:283.

126. Sircar, A. K. and Lamond, T. G. (1975): Rubber Chem. Technol., 48:631.
127. Lazovenko, A.N., Ignatov, V.A., Ukolova, N.N., and Mityushina, V.I., (1982): IZV. Vyssh, Uchebon, Zaved., Khim. Khim. Technol. 25(4):512.
128. Maurer, J. J. (1974): J. Macromol. Sci. Chem., A8:73.
129. Budai, A. and Somlo,T. (1982): Muanyag Gumi, 19(10):293.
130. Wyden, H. (1982): Kunstst. Plast., 29(5):13-14,16.
131. Maurer, J. . (1968): Proc. Second International conf. Thermal Ana ., Worcestershire, ME.
132. Harris, J. (1977): Synthesis, 8:20.
133. Sickfield, J., Neubert, D., and Gross, D. (1983): Kautsch Gummi Kunstst., 36(9):760.
134. Schwartz, N. V. (1984): Gummi Fasern Kunstst., 37(6):274.
135. Schwartz, N.V. and Brazier, D. W. (1978): Thermochim. Acta, 26:349.
136. Pautrat, R. and Metrivier, B. (1976): 49:1060.
137. Chiu, J. (1966): J. Appl. Polym. Sci., Appl. Polym. Symp., 2:25.
138. Goh, S.H. (1980): Thermochim. Acta, 41:261.
139. May, W. R., Bsharah, L., and Merifield, D. B. (1968): Ind. Eng. Chem., Prod. Res. Develop., 7:57.
140. May, W. R. and Bsharah, L. (1969): Ind. Eng. Chem., Prod. Res. Develop., 8:185.
141. May, W. R. and Bsharah, L. (1970): Ind. Eng. Chem., Prod. Res. Develop., 9:73.
142. Smith, R. C., and Stephens, H. L. (1975): J. Elast. Plast., 7:156.
143. Gonzalez, V. (1980): Rubber Chem. Technol., 54:134.
144. Goh, S. H. (1977): J. Elast. Plast., 9:186.
145. Goh, S. H. and Pang, K. W. (1978): Thermochim. Acta, 25:109.
146. Miller, G. W. (1969): J. Appl. Polym. Sci., Appl. Polym. Symp., 10:35.
147. Marshall, D. L., George, E. J., and Turnispeed, J. M. (1973): Polym. Eng. Sci., 13(6):415.
148. Gomôry, I., Cech, K. (1971): J. thermal Anal., 3:51.
149. Horvath, J. W., Purdon, J. R., Meyer, G. E., and Naples, F. J. (1974): J. Appl. Polym. Sci., Appl. Polym. Symp., 25:187.
150. Kotoyori, T. (1972): Thermochim. Acta, 5:51.
151. Lye, P. H. and Toh, H. K. (1984): J. Appl. Polym. Sci., 29:2627.
152. Kissinger, H. E. (1956): J. Res. Natl. Bur. Stand., 57:217.
153. Doyle, C. D. (1961): J. Appl. Polym. Sci., 5(15):285.
154. Doyle, C. D. (1962): J. Appl. Polym. Sci., 6(24):639.
155. Ozawa, T. (1965): Bull. Chem. Soc. Jpn., 38:1881.

156. Ozawa, T. (1970): J. Thermal Anal., 2:301.
157. Grachok, M. A., Karaban, A. A., and Shramenok, V. D. (1981): Izv. Vyssh. Uchebn. Zaved., Khim. Khim. Technol., 24(11):1422.
158. Goh, S. H. (1984): Thermochim. Acta, 77:75.
159. Goh, S. H. and Lim, Y. B. (1979): Thermochim. Acta, 32:81 159(a) Goh, S.H. (1984): Thermochim Acta, 77:275.
160. Goh, S. H. (1984). Thermochim. Acta, 75:323.
161. Goh, S. H. (1984): Thermochim. Acta, 80:75.
162. Goh, S. H. (1984): Polym. Degrdn. Stability, 8:123.
163. Treherne, B. L. (1982): Elastomerics, pp. 25.
164. Maurer, J. J. (1973): Polymer Preprints, Am. Chem. Soc., Div. Polym. Chem., 14:518.
165. Spacsec, K., Somolo, A., and Soos, I. (1977): J. Thermal Anal., 11:211.
166. Jaroszynsak, D., Kleps, T., and Tutak, D. (1977): Int. J. Polym. Sci. Technol., 4:T20.
167. Charsley, E. L. and Dunn, J. G. (1981): Plast. Rubber Process. Appl., 16:3; (1982): Rubber Chem. Technol., 55:382.
168. Jaroszynska, D. and Kleps, T. (1977): Polimery, 22(18):292.
169. Toshinori, Y. (1984): Toyoda Gosei Giho, 26(2):57.
170. Toshinori, Y., and Hidenori, M. (1983): Toyoda Gosei Giho, 25(2):49.
171. Barral, E. M., II, Guide to Modern Methods of Instrumental Analysis, Edited by T. H. Gouw, Willey-Interscience, New York, NY.
172. Ozowa, T. (1976): J. Thermal Anal., 9:369.
173. Ozawa, T. (1975): J. Thermal anal., 7:601.
174. Freeman, E. S. and Carroll, B. (1958): J. Phys. Chem., 62:394.
175. Flynn, J. H. and Wall, L. A. (1966): J. Res. Natl. Bur. Stds., 70A:487.
176. Reich, L. and Levi, D. W. (1966): Encyclopedia of Polym. Sci. and Technol., Vol. 14, Edited by H. F. Mark and N. G. Gaylords, Interscience Publishers, New York, NY.
177. Garn, P. D. (1965): Thermoanalytical Methods of Investigation, Adacemic Press, Inc., New York, NY.
178. Rogers, R. N. and Smith, L. C. (1970): Thermochim. Acta, 1:1.
179. Michelson, R. W. and Einhorn, I. N. (1970): Thermochim. Acta, 1:147.
180. Anderson, D. A. and Freeman, E. S. (1961): J. Polym. Sci., 54:253.
181. Reich, L. (1966): J. Appl. Polym. Sci., 10:813.
182. Reich, L. (1966): Polym. Lett., 4:423.
183. Borchardt, H. J. and Daniels, H. (1957): J. Am. Chem. Soc., 79:41.

184. Gander, G. and Bloom, C. (1949): Z. Anarg. Chem., 258:249.
185. Ozawa, T. (in press): J. Thermal Anal.
186. Hampson, F. W. and Manley, T. R. (1977): Conf. on "How Long do Polymers Last in Service", Feb. 22, London.
187. Schneider, A. A. (1980): Polymer Bull., 2:551.
188. Toop, D. A. (1971): ERA Symp., London.
189. Howard, J. B., Bell Lab, Murray Hill, NJ.
190. Brown, G. P., Hill, S. A., and Murphy, C. B. (1961): J. Polym. Sci., 55:419.
191. Prime, R. B. (1978): Thermochim. Acta, 26:165.
192. Barrall, E. M., III, Flandera, M. A., and Logan, J. A. (1973): Thermochim. Acata, 5:415.
193. Barrall, E. M., III, James, P. A., Dawson, B., and Logan, J. A. (1974): J. Macromol. Sci., A8:135.
194. Gent, A. N. (1958): Trans. Inst. Rubber Ind., 34:46.
195. Ellerstein, S. M. (1977): Anal. Cal., 4:203.
196. Funkin, E.F. (1972): Wear, 19:277.
197. Hwo, C. H. and Johnson, J. F. (1974): J. Appl. Polym. Sci., 18:1433.
198. Fogiel, A.W., Frensdorff, H. K., and Maclachlan, J. D. (1976): Rubber Chem. Technol., 49:34.
199. Beatty, J. R. (1978): Rubber Chem. Technol., 51:1044.
200. Yanai, H.S., Freund, W. J., and Carter, O. L. (1972): Thermochim. Acata, 4:199.
201. Teitelbaum, B. Y. and Gubanov, E. F. (1964): Rubber Chem. Technol., 37:99.
202. Mark, H. F., Gaylord, N. G., and Bikales, N. M., Eds. (1970): Encyclopedia of Polymer Science and Technology, Interscience, New York, NY, Vol. 13, pp. 764.
203. Gehman, S. D. (1967): Rubber Chem. Technol., 40:36.
204. Hands, D. (1977): Rubber Chem. Technol., 50:480.
205. Hands, D. and Horsefall, F. (1977): Rubber Chem. Technol., 50:253.
206. Frensdorff, H. K. (1974): Rubber Chem. Technol., 47:849.
207. ASTM C-177,76; ASTM C-518, American Society for Testing and Materials, Philadelphia, 1965.
208. Brennan, W. P., Miller, B., and Whitewell, J. C. (1968): J. Appl. Polym. Sci., 12:1800.
209. Fujino, T., Kurosawa, T., Miyata, Y., and Naito, K. (1971): J. Phys. E., 4(1):51.
210. Larsen, F. N. and Long, C. L. (1975): 26th Pittsburgh Conf. on Anal. Chem., Appl. Spectr., Cleveland, OH, March 3.
211. Chiu, J. and Fair, P. J. (1979): Thermochim. Acta, 34:267.
212. Sircar, A. K. and Wells, J. L. (1981): Rubber Chem. Technol., 55:191.

213. Chiu, J. (1965): J. Polym. Sci., 8:27.
214. Sircar, A. K., Lamond, T.G., and Wells, J. L. (1980): Thermochim. Acta, 37:315.
215. Sircar, A. K. and Wells, J. L. (1981): Polym. Eng. Sci., 21:809.
216. Loft, B.C. (1975): J. Polym. Sci., Polym. Symp., 49:127.
217. Lawandy, S. N. and Hepburn, C. (1980): Elastomerics:45.
218. Townsend, D. I. (1979): North Amer. Thermal Anal. Conf., Chicago.
219. Richardson, J. J. (1978): In: Developments in Polymer Characterization - 1, edited by J.V. Hawkins, Applied Science Publishers, London.
220. Gomory, I. (1977): J. Thermal Anal., 11:10.
221. Prime, R. B. (1985): Polymer Prepints, 26:15.

THE CHROMATOGRAPHIC ANALYSIS OF ELASTOMERS

D. McINTYRE
Institute of Polymer Science, University of Akron, Akron, Ohio 44325

The most frequently used analytical method of analyzing molecular weights of elastomers is GPC. The analysis of natural rubber and other high molecular weight polymers will be discussed. Applications of these measurements to the thermal degradation of rubber have been made. Also, results from a new method of membrane viscometry are to be presented in terms of its possible use in evaluating other parameters such as microgel.

POLY(FLUOROALKOXYPHOSPHAZENE) ELASTOMERS -- PERFORMANCE PROFILE*

JEFFREY T. BOOKS
Ethyl Corporation, Baton Rouge, Louisiana 70898

INTRODUCTION

Fluoroalkoxy substituted phosphonitrilic polymers have been known for fifteen years[1] but have seen limited use due to cost and supply limitations. As the elastomer is now commercial, it seems appropriate to review the characteristics of these materials.

CHEMISTRY

Phosphazene elastomers are synthesized in two steps. First, a linear chloropolymer $(-PCl_2=N-)_x$ is prepared, normally from the cyclic trimer (Figure 1).

Secondly, the chlorine atoms are replaced with organic substituents. Note this process allows independent control of molecular weight, substituents, and substituent ratio. A wide variety of substituents has been examined, including alcohols, amines, and phenols.[2,3] This paper will confine itself to the commercial phosphonitrilic fluoroelastomer (Figure 2), formerly trademarked PNF^R by the Firestone Tire and Rubber Company and which Ethyl Corporation will produce and sell as EYPEL™-F phosphonitrilic fluoroelastomer. Significant early research on the synthesis, characterization and properties of these materials was conducted by or under contract to The Army Materials and Mechanics Research Center.[4]

This elastomer is substituted with two fluoroalcohols, trifluoroethanol and $HOCH_2(CF_2CF_2)_{1,3}H$. Nominally 65 mole percent trifluoroethanol is used and a small amount of an unsaturation site is also incorporated. This yields a gum with 54 weight percent fluorine and 1.4 percent hydrogen. The backbone contains only phosphorus and nitrogen and is

*Based on a paper presented at the 127th Meeting of the ACS Rubber Division.

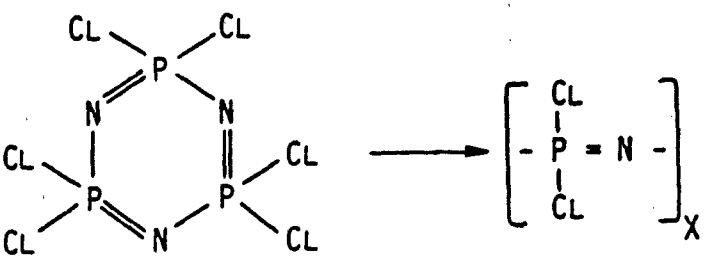
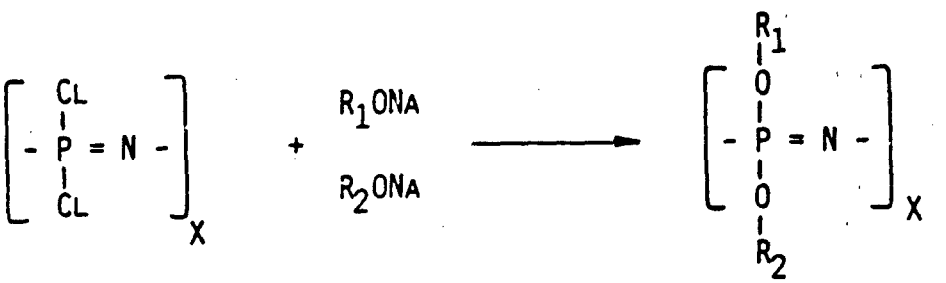


FIGURE 1. Synthesis of linear chloropolymer.



$R_1 = CF_3CH_2-$

$R_2 = H(CF_2CF_2)_{1-3}CH_2-$

FIGURE 2. Substitution of chloropolymer to form FZ elastomer.

insensitive to oxidative attack from oxygen or ozone.

Carbon black filled, silica filled, and mixed filler compounds are available providing compounds with durometers from 40-85A. Curing is accomplished through conventional peroxides. The characteristics of these compound types will be exemplified in the following sections.

EXPERIMENTAL

Fluoroalkoxyphosphazene compounds were obtained from the Firestone Tire and Rubber Co. This elastomer is identified as FZ in ASTM nomenclature. The compounds used are identified as follows:

EYPEL-F	7506	(PNF 275-006)	FZ 1
EYPEL-F	7003	(PNF 270-003)	FZ 2
EYPEL-F	8009	(PNF 280-009)	FZ 3
EYPEL-F	8011	(PNF 280-011)	FZ 4

Tensile properties were obtained using cut rings following ASTM D412, Method B. Compression set values were obtained using Type 1 buttons following Method B of ASTM D395. Fluid compatibility characteristics were evaluated using ASTM D471.

Dynamic moduli were obtained using a Polymer Laboratories instrument. Samples were run either in tensile or shear mode and were run at 1 HZ and a scanning rate of 5°C/minute.

Tests for sour crude oil resistance followed a variation of the National Association of Corrosion Engineers (NACE) Draft T-1G-17. The simulated crude oil (a hexane, octane, decane, toluene mixture) occupied 60% of the pressure vessel volume. Water occupied 5% of the vessel volume. Cut ring samples were suspended in the hydrocarbon phase. A mixture of 5% CO_2, 20% H_2S, and 75% CH_4 was added to the vessel at a pressure sufficient to achieve 6.2-6.9 MPa (900-1000 psi) at 100°C. The test was terminated after 168 hours exposure and samples were tested within two hours of removal from the pressure vessel.

INITIAL PROPERTIES

Properties obtained with several classes of FZ compounds are tabulated in Table 1. Compounds FZ 2 and 3 are silica filled materials. Compound FZ 4 is carbon reinforced, while FZ 1 contains both silica and carbon. In general, they have high initial moduli. Carbon filled compounds have somewhat higher tensile moduli and strength than those containing silica. The low compression set

TABLE 1

NOMINAL PHYSICAL PROPERTIES OF FOUR FZ COMPOUNDS

	FZ 1	FZ 2	FZ 3	FZ 4
50% Tensile Modulus, MPa (psi)	3.5 (510)	2.7 (400)	3.9 (570)	5.0 (730)
100% Tensile Modulus, MPa (psi)	8.6 (1240)	6.6 (979)	8.2 (1200)	
Tensile Strength, MPa (psi)	9.5 (1370)	8.9 (1300)	8.7 (1270)	12.3 (1780)
ELONGATION, %	110	135	100	110
DUROMETER, Shore A	74	68	80	75
Compression Set, % (70 hr. 149°C)	23	27	28	25

values are an indication of their suitability at moderately high use temperatures.

USE TEMPERATURE RANGE

The useful temperature range of FZ elastomers spans a broad range of applications. The glass transition temperature of the polymer is -64°C by DSC. Brittle Point and Clash Berg T10,000 values of FZ compounds are usually in the vicinity of -55° to -50°C. Thus unplasticized compounds can perform at the temperature extremes seen in Arctic service and in high altitude aircraft use.

Plots of tensile dynamic storage modulus and loss modulus are given for two compounds in Figures 3 and 4. It can be seen that the modulus and loss modulus are essentially invariant from ambient to 200°C at the test frequency. Thus the modulus and vibration dampening behavior remain nearly constant over this temperature range at low deformations and deformation rates.

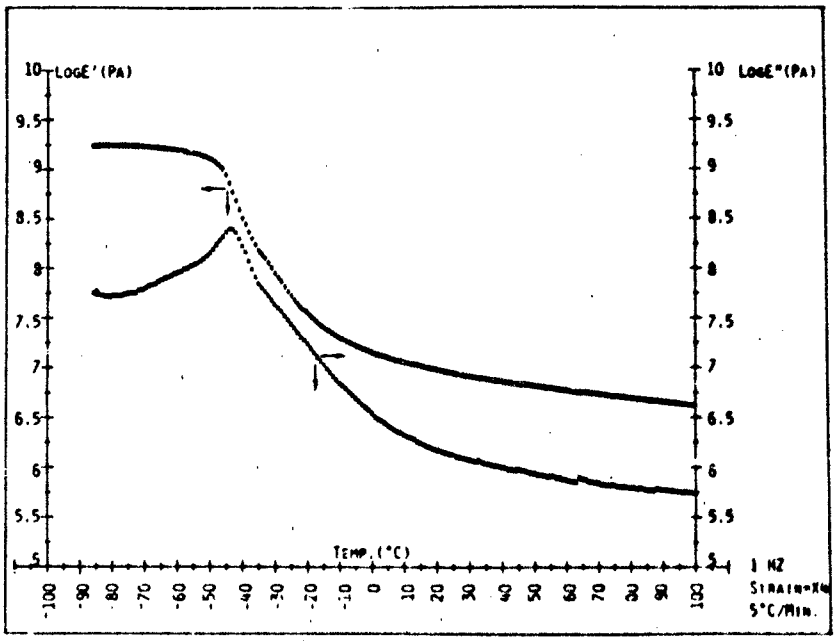


FIGURE 3. FZ 1 moduli/temperature plot.

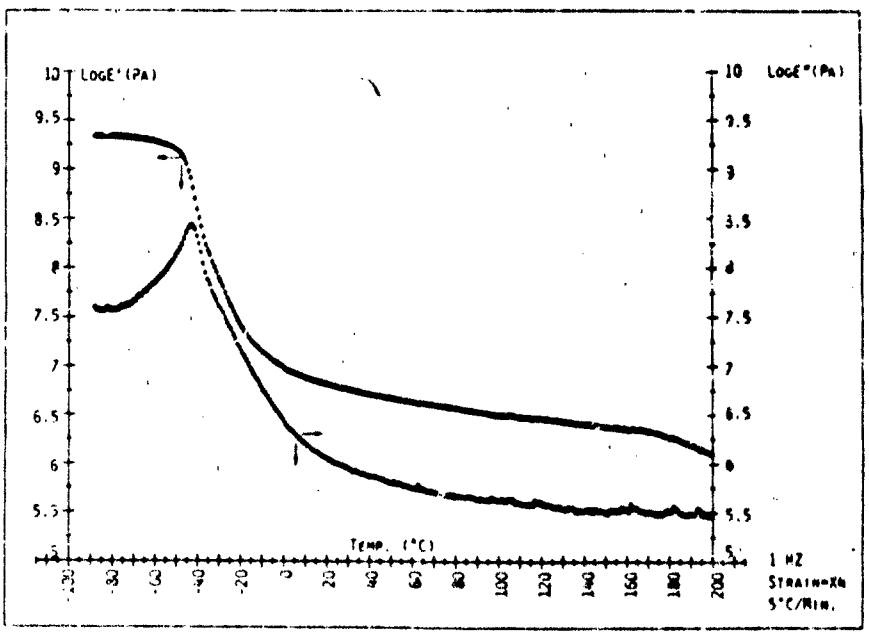


FIGURE 4. FZ 2 moduli/temperature plot.

The variation of ultimate properties with temperatures to 175°C is given in Figure 5 for two compounds. The ultimate properties vary more strongly with temperature than the dynamic moduli but less strongly than many elastomers with higher Tg values. The good high temperature strength retention aids demolding at cure temperature as well as providing toughness in high temperature use.

Retention of tensile properties at elevated temperature has been studied with FZ 2, a silica filled compound. The tensile strength decay approximately follows first order kinetics (Figures 6 and 7). FZ 2 is seen to retain over 50% of its tensile strength for 1000 hours at 175°C. An Arrhenius plot (Figure 7) provides half life data in the range of 150° to 200°C.

FLUID COMPATIBILITY

FZ elastomers are, not surprisingly, little affected by hydrocarbon fuels or hydraulic fluids. Polar organics

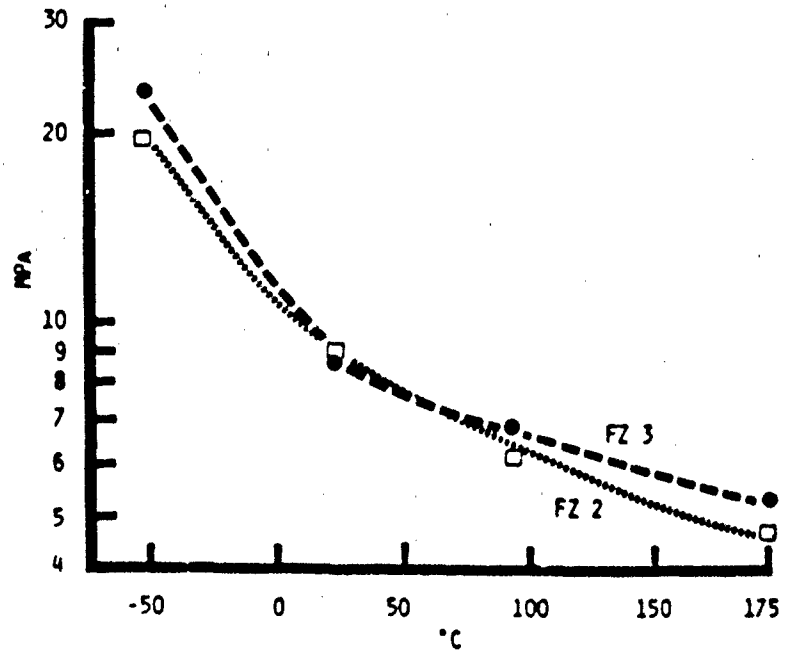


FIGURE 5. Temperature dependence of tensile strength for FZ 2 and FZ 3.

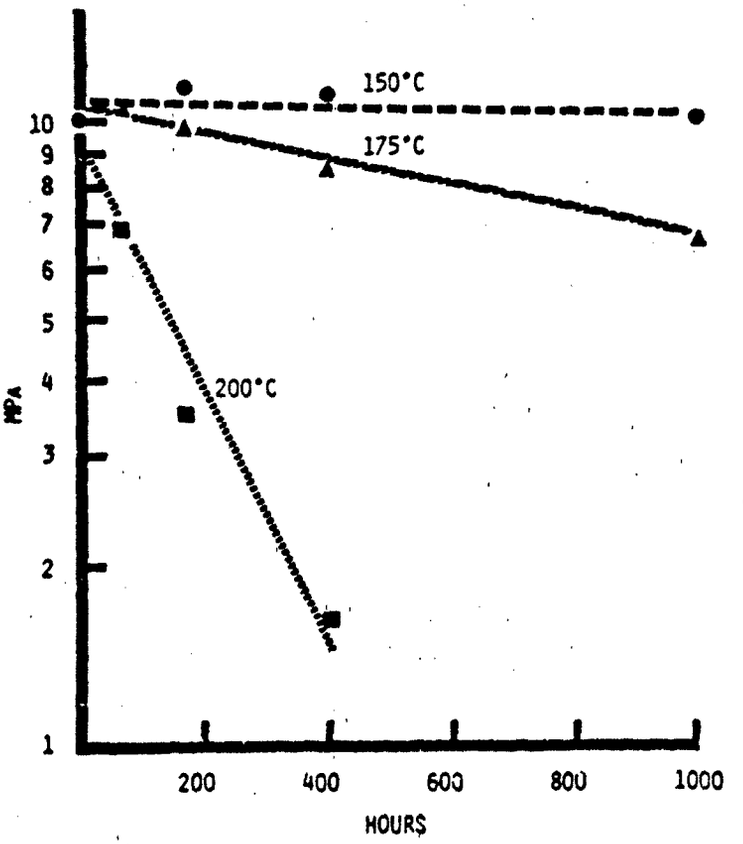


FIGURE 6. Tensile strength retention after aging at elevated temperatures.

swell these materials significantly more. Methanol, lower ketones, and dimethyl formamice are solvents for FZ, and thus swell the vulcanizate dramatically. FZ shares these solubility characteristics with other fluoroelastomers but is uniquely unaffected by aromatic solvents (Table 2).

One service environment getting much attention lately is oilfield wellhead service. Crude oil and gas exploration and production are occurring in ever more extreme conditions. Oils containing H_2S, CO_2, H_2O, and especially those containing amines to counteract the corrosive effects of this acid service, provide a severe challenge to any elastomer. FZ 4 provides property retention in a sour crude environment, as evidenced by results

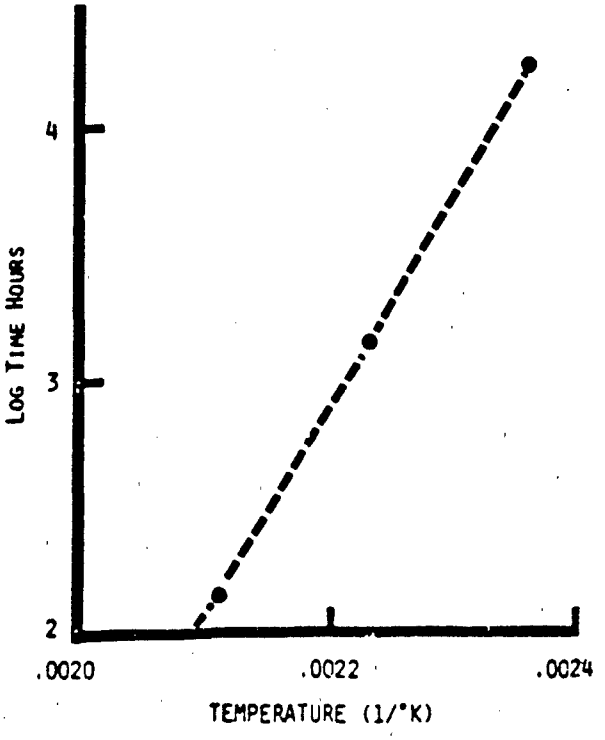


FIGURE 7. Time for 50% retention of tensile strength.

TABLE 2

VOLUME SWELL OF FZ 2 In SEVERAL FLUIDS AFTER ONE WEEK AT 23°C

ASTM Fuel C (50% Toluene/50% Trimethyl pentane)	12%
ASTM #3 Oil	0%
Ethyl Acetate	167%
Methylene Chloride	18%
Toluene	13%

obtained in a modified NACE procedure (Table 3). In addition, this resistance is coupled with the low temperature flexibility necessary in Arctic applications.

TABLE 3

RETENTION OF TENSILE PROPERTIES IN A SIMULATED SOUR CRUDE ENVIRONMENT

Test Temperature	100°C
50% Modulus, MPa	5.0
% Retained	89
Tensile Strength, MPa	12.3
% Retained	68
Elongation, %	110
% Retained	92
Durometer Shore A	75

APPLICATIONS

FZ elastomers have been used where their combination of use temperature range, fluid resistance, fatigue resistance, tear strength, abrasion resistance are critical. These include hydraulic seals in fighter aircraft where nitrile seals have failed due to embrittlement at high temperature. Vibration mounts for instruments on jet engines take advantage of the temperature and fuel resistance as well as the vibration dampening characteristics of FZ.

The hydrocarbon resistance, fatigue resistance, and low temperature flexibility of FZ compounds have proven useful in surge suppressors in liquefied natural gas pipeline service.

Fatigue resistance of a FZ compound is the principal attribute necessary in an air filter seal on the turbine engine for the M-1 battle tank. Seals of other rubbers had failed, leading to catastrophic engine failures.

Future applications will continue to benefit from FZ's combination of use temperature range, nonpolar and aromatic fluids resistance, fatigue life, and vibration dampening characteristics.

ACKNOWLEDGEMENT

I would like to thank the Ethyl Corporation for permission to publish this paper. A multitude of colleagues have contributed to various aspects of research on this material. Of these I would especially like to thank P. Robertson, G. S. Lum, and J. S. Arroyave for compound preparation and testing, and M. E. Kucsma (Ethyl Commercial Development) and D. F. Lohr (Firestone Tire & Rubber Co.) for many useful discussions.

REFERENCES

1. S. H. Rose (to Horizon Research, U. S. 3,315,688 (June 2, 1970).
2. H. R. Allcock, "Phosphorus Nitrogen Compounds", Academic Press, New York, 1972.
3. H. R. Allcock, Angew. Chem. Int. Ed. Eng. 16, 147 (1977).
4. R. E. Singler, N. S. Schneider and G. L. Hagnauer, Polymer Eng. and Sci. 15, 321 (1975).

A RATIONAL APPROACH TO ELASTOMER COMPOUND DEVELOPMENT

GEORGE C. DERRINGER
Battelle Columbus Division, 505 King Avenue, Columbus, Ohio 43201

INTRODUCTION

In developing a "clean sheet" elastomer formulation the compounder is faced with numerous choices. In a typical example there may be four candidate polymer types, ten candidate filler systems, and five types of plasticizer. The total number of combinations of just these three ingredients is 200 and variable levels have not yet been considered. If only three levels of each candidate material are evaluated the number of possible formulations is 5400. When the remaining ingredient types and levels are added to this the complexity of the problem becomes truly immense. Given such complexity it is hard to fault the compounder for using the "Edisonian" approaches to formulation development most commonly used today.

Edisonian approaches, however, are typically costly and are therefore often impractical in today's environment of limited research and development funding. Statistical approaches to formulation design have been shown to be efficient and cost-effective in comparison to "Edisonian" one-variable-at-a-time (OVAT) approaches (1, 2, 3). In a large program such as a "clean sheet" elastomer development program, however, a judicious mix of the appropriate types of statistical experimental designs along with appropriate statistical analyses is mandatory. How to achieve such a mix is the subject of this paper.

OBSTACLES TO BE OVERCOME

A methodology for development of a "clean sheet" elastomer formulation must address obstacles which in the form of three questions are:

1) How can two or more elastomer compounds be compared across several properties of interest?

2) How can different elastomers be compared given the broad spectrums of properties obtainable with various ingredient types and levels?

3) Once elastomer and ingredient types are chosen, how can the formulation be optimized to get all of the properties of interest into their required windows?

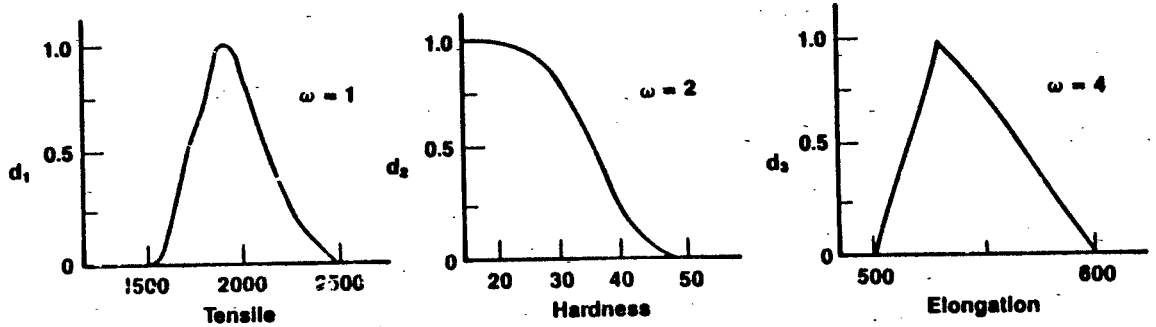
COMPARING COMPOUNDS ACROSS SEVERAL PROPERTIES

Suppose we have several unrelated elastomer formulations along with the properties of interest. The first thing that must be done is to translate property levels to a 0 to 1.0 desirability scale which represents how any property level translates into actual utility in the intended application. On the desirability scale 0 corresponds to a property level which would make the product useless. A desirability of 1.0 represents a property level which cannot be improved upon, again for the intended application. Intermediate desirability levels correspond to intermediate utility.

A desirability function can be defined as a table, graph, equation, or any set of rules which transforms a property level to a 0 to 1.0 desirability scale. Figure 1 illustrates the concept. The three graphs (Figure 1a) translate tensile strength, hardness, and elongation at break to corresponding desirability values. For example, for a tensile value of 2000 psi we would simply read the corresponding desirability value off the y-axis as shown. The D value is approximately 0.75. The table under the graphs (Figure 1b) presents tensile, hardness, and elongation data for four candidate formulations. Beside each property level is the corresponding desirability value taken from the graphs. For example, Formulation 1 exhibits desirabilities of 0.6, 0.07, and 0.67 for tensile, hardness, and elongation, respectively.

To get a single measure of performance the individual desirabilities are combined into a composite desirability D using the geometric mean of the individual desirabilities as shown in the equation for the unweighted case. In most instances, however, different elastomer properties are not of equal importance. Therefore, weights are assigned to each property and are shown beside each graph. Elongation was judged four times more important than tensile, and hardness twice as important. The weights are represented by exponents in the weighted desirability function shown at the bottom of Figure 1. The last two columns of the table show both weighted and unweighted desirabilities. For the unweighted case Formulation 1 with D = 0.304 is the best formulation. For the weighted case, however, Formulation 3 is the best with a D value of 0.384. As can be seen, once the weights and desirability functions are available, it is easy to translate each formulation to a single number representing utility.

Where, however, do the desirability functions and weights come from? In most cases they represent individual or group judgments. Often, of course, a specification must be met in



a. Graphs of Desirability Values for Tensile, Hardness, and Elongation

Candidate Formulation	Tensile	d_1	Hardness	d_2	Elongation	d_3	Composite Desirability	
							Unweighted	Weighted
1	1750	0.60	45	0.07	550	0.67	0.304	0.345
2	2000	0.75	30	0.75	500	0	0	0
3	1600	0.25	45	0.07	525	1.00	0.260	0.384
4	1600	0.25	45	0.07	585	0.20	0.152	0.153

b. Tensile, Hardness, and Elongation Data for Four Candidate Formulations

$$D = (d_1\, d_2\, d_3)^{1/3} \text{ (Unweighted)}$$

$$D = (d_1^1\, d_2^2\, d_3^1)^{1/7} \text{ (Weighted)}$$

FIGURE 1. Desirability optimization example for discrete formulation case.

which case upper and/or lower limits will be dictated. The shape of the desirability function, however, is still a matter of judgment. Similarly, the property weights are judgments, in the best case, from a consensus of individuals most closely associated with the technology. It is recommended that a lot of thought be given to the weights and desirability function shapes because if these judgments are not the best available, the methodology will not produce the best compound.

COMPARING ELASTOMER TYPES

Suppose that several elastomer types are judged to have the potential of meeting a specific application. What is the most efficient way of selecting the best candidate given the wide range of properties attainable within each material? This is difficult and there are many approaches. The approach recommended involves statistical screening designs. Screening designs are patterms of experiments which permit variable effects to be elucidated in a small number of experiments (i.e., formulations). A simple example is presented in Figure 2. Here three formulation variables are studied in only four formulations. The three formulation variables are (1) filler level, (2) cure system level, and (3) oil level. Each cell represents a single formulation. For example, the upper left cell corresponds to low filler level, low oil level, and low cure system level. In screening designs such as this, one generally sets each variable at the extremes of its practical range. In that way the full potential effect of each variable is elucidated.

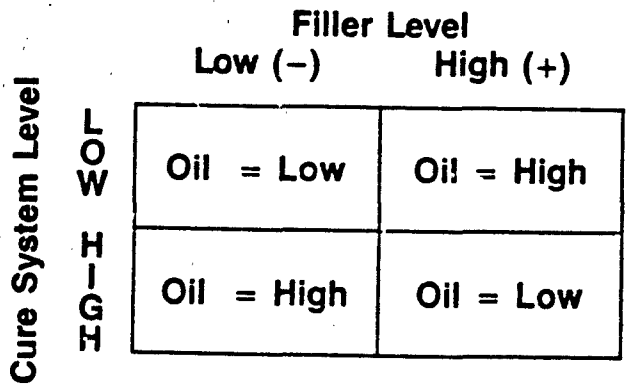


FIGURE 2. Four-run, three-variable screening design.

Screening designs of various sizes can be found in the literature (1, 2, 3). The size of the design will be dictated by the number of ingredients to be evaluated. This too is a matter of judgment and of course also will depend upon available assets. An eight-run design capable of evaluating up to seven ingredients is shown in Figure 3. The columns A, B, C, D, E, F, and G represent the seven variables and the rows of the matrix represent formulations to be mixed. The plus and minus signs represent the two levels of each ingredient to be evaluated. It should be noted that instead of levels, types of ingredient may be used. For example, two types of cure system, two types of filler, etc., may be used for any of the column assignments. Furthermore, it is not necessary in such a screening design to use all of the columns; in fact, there are advantages to leaving some of them unassigned.

In practice this part of the methodology involves the following steps:

1) Selecting ingredients to be studied for each elastomer system of interest

2) Selecting a suitable screening design

3) Selecting the levels (quantitative or qualitative) for each variable (i.e., ingredient or group of ingredients) for each elastomer type

4) Mixing and testing the indicated formulations

5) Calculating desirabilities for each formulation

6) Selecting the most promising elastomer type

Formulations	Variables						
	A	B	C	D	E	F	G
1	−	−	−	+	+	+	−
2	+	−	−	−	−	+	+
3	−	+	−	−	+	−	+
4	+	+	−	+	−	−	−
5	−	−	+	+	−	−	+
6	+	−	+	−	+	−	−
7	−	+	+	−	−	+	−
8	+	+	+	+	+	+	+

FIGURE 3. Seven-variable, eight-formulation screening design.

Example

Suppose that elastomer types I, II, III, and IV are candidates and that for each system the three ingredients judged to be most important are evaluated as described above in a three-variable, four-run experiment. The results might appear as in Table 1. The three variables are A, B, and C, and the two "levels" of each are denoted as A1, A2; B1, B2; and C1, C2. The identity of variables A, B, and C, will not necessarily be the same for all four elastomers and in fact usually will not be. The last four columns then each represent the four calculated composite desirabilities from each of the four screening designs. In a way we can think of these desirabilities as representing the potential capability for each elastomer type with respect to the target application.

TABLE 1

SCREENING RESULTS FOR THREE-VARIABLE, FOUR-RUN EXPERIMENT

Formulation	Variables			Composite D's Elastomers			
	A	B	C	I	II	III	IV
1	A1	B1	C2	0.0	0.5	0.8	0.4
2	A2	B1	C1	0.0	0.4	0.6	0.5
3	A1	B2	C1	0.1	0.0	0.1	0.5
4	A2	B2	C2	0.0	0.0	0.2	0.3

This becomes progressively a more accurate assessment as the size of the screening designs is increased. In this example Elastomer I can safely be eliminated as a serious candidate since the largest D value was 0.1 and three of the four values were zero. Elastomer III resulted in the highest single desirability, but Elastomer IV resulted in the highest minimum desirability so depending on the strategy believed to be most appropriate either III or IV could be selected for optimization.

FINE TUNING SELECTED INGREDIENT LEVELS

Once elastomer and ingredient types are chosen, we should have zeroed in on one or two promising elastomer types for fine tuning. The steps in the fine tuning process are as follows:

1) Select ingredients to be fine tuned

2) Select ranges for each of these ingredients

3) Select an appropriate (response surface) experimental design

4) Run the formulations dictated by the design

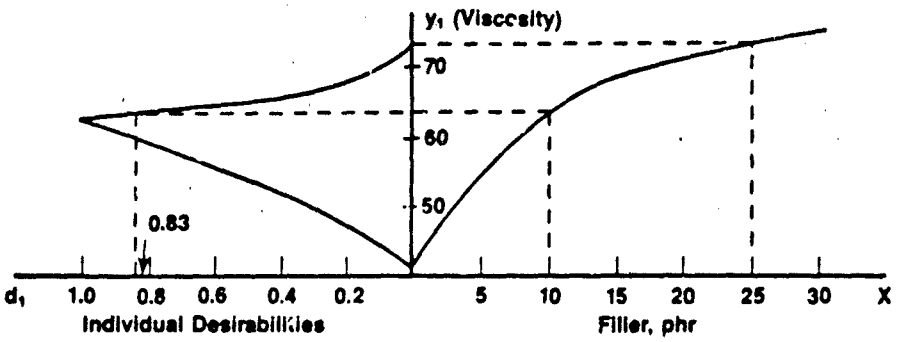
5) Fit prediction equations to the resulting data using multiple linear regression analysis

6) Transform each property desirability curve to a mathematical equation

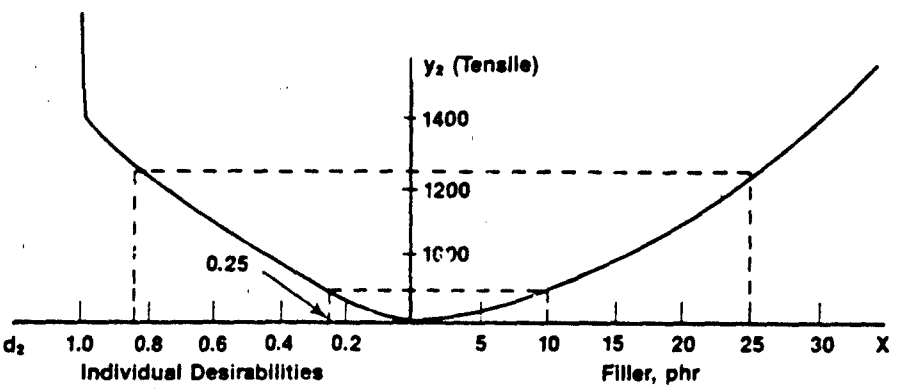
7) Use a computer maximization algorithm to maximize the composite desirability function over the independent (ingredient) variables.

Example

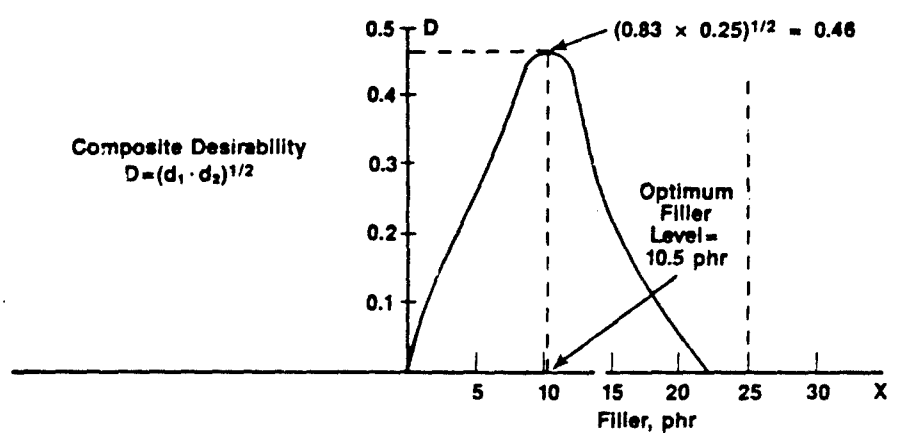
A simplistic example of these steps is illustrated in Figure 4. Suppose we have evaluated four or five filler levels in order to arrive at mathematical relationships relating viscosity and tensile strength to filler level. These relationships are shown as smooth curves in Figure 4a and 4b. Now, for each property axis the curve relating property to desirability is drawn. In this case the property axis becomes the abscissa for the desirability. We can now calculate tensile and viscosity desirabilities given only a specified filler level. For example, for 10 phr filler we can predict viscosity and tensile by drawing vertical lines until they intersect the property curve. We get approximately 63 and 800, respectively. Now from these points on the property curves we draw horizontal lines until they intersect the desirability curves. For viscosity we get a value of 0.83, and for tensile a value of about 0.25. The composite, unweighted desirability can then be calculated by taking the geometric mean of the two individual desirabilities. This value turns out to be 0.46.



a. Viscosity and its Desirability as a Function of Filler Level



b. Tensile and its Desirability as a Function of Filler Level



c. Composite Desirability as a Function of Filler Level

FIGURE 4. Viscosity, tensile, and desirabilities as a function of filler level.

This operation can be repeated for any filler level within the range of validity of the property versus filler curves (equations). The results for a series of such evaluations can be represented as a single curve showing composite desirability as a function of filler level (Figure 4c). This curve exhibits a maximum D at a filler level of approximately 10.5 phr. Therefore, 10.5 phr represents the best filler level given the individual desirability relationships.

In general such fine tuning is carried out over two or more ingredient variables and over 5 to 15 property variables including in most cases, cost. It is for this reason that the entire procedure must be translated into mathematical terms. The mathematical steps involved are as follows:

$$1)\ Y_k = B_o + \sum_{i=1}^{p} B_i X_i + \sum_{j=1}^{p} \sum_{i=1}^{p} X_i X_j$$

$$2)\ d_k = f_k\left(Y_k\right)$$

$$3)\ D = \left[d_1^{\omega_1} \cdot d_2^{\omega_2} \cdot d_3^{\omega_3} \cdots d_q^{\omega_q}\right]^{(1/\Sigma\omega_k)}$$

In Equation 1 each property variable is represented as a polynomial function, normally of second order, of the independent (i.e., ingredient) variables denoted as subscripted X's. In Equation 1, Y_k is the property variable, the B's are fitted regression coefficients and the X_i's are ingredient variables. The relationships are obtained by fitting the property, ingredient variable data obtained according to a response surface experimental design using multiple linear regression analysis.

In Equation 2 the relationships between desirability and each property are expressed mathematically. The procedures for doing this are discussed by Derringer (8) and Derringer and Suich (7).

In Equation 3 the individual desirabilities d_i are combined by way of a weighted geometric mean into a composite desirability D as discussed in an earlier section. In this

case it will be noted that since D is a mathematical function of the individual d_i's, the d_i's are mathematical functions of the Y_i's and the Y_i's are mathematical functions of the X_i's, it follows that D is ultimately a mathematical function of the individual X's. Therefore, D can be maximized over the X variables to arrive at the "optimal" formulation. A plot of such a D function is shown in Figure 5. Here the top of the hill represents the combination of HMM and RF resins which result in the best combination of three properties optimized in the example. This figure is a three dimensional version of the one shown in Reference 8.

CONCLUSIONS

The problem of building an elastomer formulation from scratch is complex and can easily entail thousands of choices by the elastomer technologist. In common practice, practical formulations usually evolve by a hit-or-miss strategy. This is a workable approach but the result is usually far from optimum. The approach outlined in this paper, although it too has deficiencies, is more systematic and gives the better formulations the best chance to emerge.

REFERENCES

1. Hunter, W. C. and Hoff, M. E. (1967): Industrial and Engineering Chemistry, 59, 43.
2. Derringer, G. C. (1980): Kautschuk und Gummi-Kunststoffe, 33, Jahrgang Nr. 8, 619.
3. Derringer, G. C. (July 1983): Elastomerics, 26.
4. McLean, R. A. and Anderson, V. L. (1984): Applied Factorial and Fractional Factorial Screening Designs. Marcel Dekker Inc., New York.
5. Box, G.E.P., Hunter, W. G., and Hunter, J. S. (1978): Statistics for Experimenters. John Wiley and Sons.
6. Diamond, W. G. (1981): Practical Experiment Designs for Engineers and Scientists. Lifetime Learning Publications, Belmont, California.
7. Derringer, G. C. and Suich, R. (1980). Journal of Quality Technology, 12 (4).
8. Derringer, G. C. (May 1983): Kautschuk und Gummi-Kunststoffe, 36. Jahrgang, Heft, Seiten 349-352.

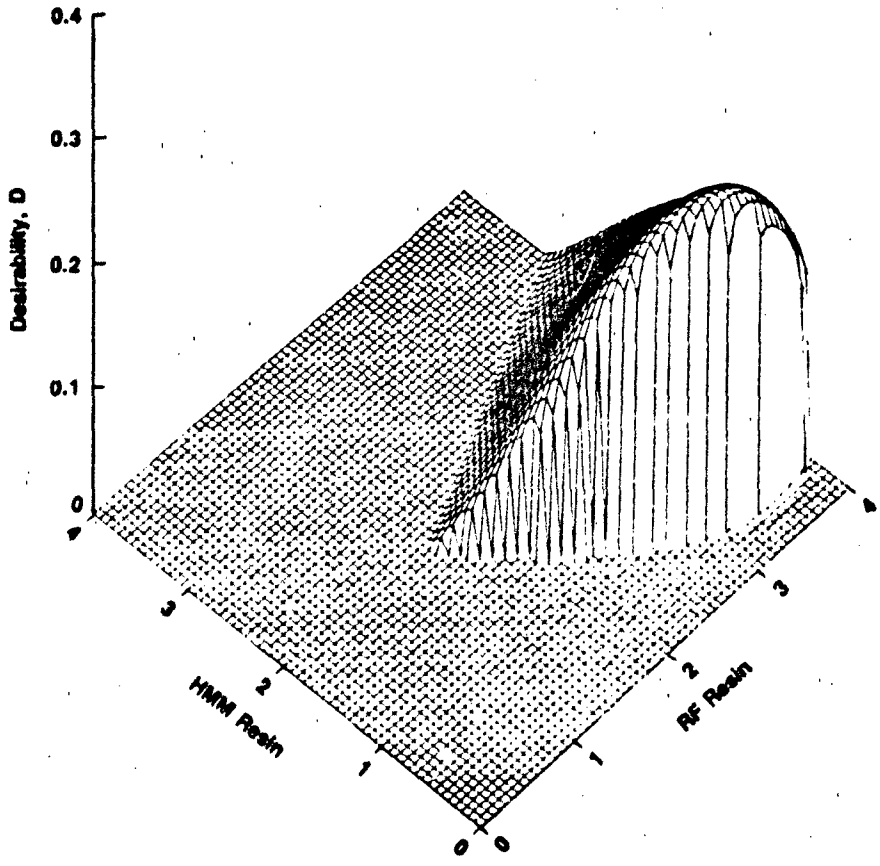


FIGURE 5. Three-dimensional plot of desirability surface.

BIMODAL NETWORKS AND NETWORKS REINFORCED BY THE *IN SITU* PRECIPITATION OF SILICA

JAMES E. MARK
Department of Chemistry and the Polymer Research Center, The University of Cincinnati, Cincinnati, Ohio 45221

ABSTRACT*

The goal of primary interest in these investigations was the development of novel methods for preparing elastomeric networks having unusually good ultimate properties. The first technique employed involves endlinking mixtures of very short and relatively long functionally-terminated chains to give bimodal networks. Such (unfilled) elastomers show very large increases in reduced stress or modulus at high elongations because of the very limited extensibility of the short chains present in the networks. The second technique employs the *in situ* precipitation of reinforcing silica either after, during, or before network formation. The reaction involves hydrolysis of tetraethylorthosilicate (TEOS), using a variety of catalysts and precipitation conditions, and the effectiveness of the technique is gauged by stress-strain measurements carried out to yield values of the maximum extensibility, ultimate strength, and energy of rupture of the filled networks. Information on the filler particles thus introduced is obtained from density determinations, light scattering measurements, and electron microscopy.

INTRODUCTION

Preparing an elastomer by endlinking polymer chains permits control of the network structure (1,2), in particular the network chain length distribution. One important result of this new synthetic versatility is the ability to form bimodal networks which consist of mixtures of very short and relatively long chains (3-10). Such bimodal elastomers have been prepared from poly(dimethylsiloxane) (PDMS) $[-Si(CH_3)_2O-]$ and found to have unusually good ultimate properties, even in the unfilled state, as is documented in the present review. A variety of experimental studies show that this improvement in properties is primarily due to the very limited extensibility of the short chains present in the networks (5). This limited extensibility and its effects on elastomeric properties are being investigated using a non-Gaussian theory of rubber-like elasticity based on network distribution functions generated from Monte Carlo simulations utilizing rotational isomeric state information on the chains of interest (11-13).

---

* Reprinted from British Polymer Journal, Vol. 17, 144, 1985.

Silica may be prepared by the hydrolysis

$$Si(OC_2H_5)_4 + 2H_2O \rightarrow SiO_2 + 4C_2H_5OH$$

of tetraethylorthosilicate (TEOS), in the presence of any of a variety of catalysts. There are three techniques by which silica thus precipitated can be used to reinforce an elastomeric material. First, an already-cured network, for example prepared from PDMS, may be swollen in TEOS and the TEOS hydrolyzed in situ (14-18). Alternatively, hydroxyl-terminated PDMS may be mixed with TEOS, which then serves simultaneously to tetrafunctionally endlink the PDMS into a network structure and to act as a source of SiO_2 upon hydrolysis (19-21). Finally, TEOS mixed with vinyl-terminated PDMS can be hydrolyzed to give a SiO_2-filled polymer capable of subsequent endlinking by means of a multifunctional silane (22). Some mechanical properties of typical PDMS elastomers reinforced in these ways are described, as are results on the average size, size distribution, and extent of agglomeration of the filler particles (15).

BIMODAL NETWORKS

Typical Experimental Results

In elongation measurements, the elastomeric quantity of primary interest is the reduced stress or modulus (3,23)

$$[f^*] \equiv f^* /(\alpha-\alpha^{-2}) \qquad (1)$$

where $f^* \equiv f/A^*$ is the nominal stress, f the equilibrium elastic force, A^* the undeformed cross-sectional area of the sample, and $\alpha=L/L_i$ the relative length or elongation. It is generally plotted as a function of reciprocal elongation as suggested by the semi-empirical equation of Mooney and Rivlin (24,25)

$$[f^*] = 2C_1 + 2C_2\alpha^{-1} \qquad (2)$$

where $2C_1$ and $2C_2$ are constants independent of elongation.

Some typical isotherms obtained for bimodal PDMS networks are shown in Figure 1 (7). Of particular interest here are the

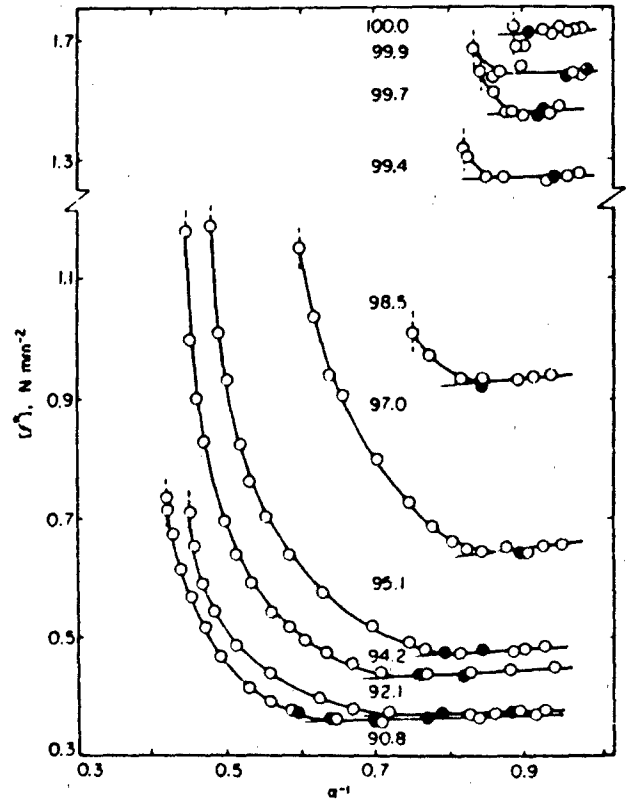


Fig. 1 Stress–strain isotherms (25°C) in the Mooney–Rivlin representation for (unfilled) PDMS bimodal networks in which the short chains have a number-average molecular weight of 660 g mol $^{-1}$, and the long chains 21.3×10^{3} g mol $^{-1}$.[7] Each curve is labelled with the mol % of short chains present in the network. The open circles locate the results obtained using a series of increasing values of the elongation α, and filled circles the results obtained out of sequence to test for reversibility. The short extensions of the linear portions of the isotherms help locate the values of α at which the upturn in $[f^*]$ first becomes discernible. The linear portions of the isotherms were located by least-squares analysis. (Reprinted from ref. 6 by courtesy of John Wiley & Sons, Inc.)

large, reversible increases in modulus observed at high elongations.

Origin of Improvement in Properties

The observed increases in modulus represent an important improvement in the ultimate strength of an elastomer, and their origin is therefore of considerable interest. A variety of

experimental studies (4,5,9,10) are relevant in this regard. The effect of temperature on the stress-strain isotherms is of particular importance with regard to the possibility of strain-induced crystallization in the network. Temperatures were found to have little effect on the elongation at which the upturn in [f*] becomes discernible, the elongation at rupture, and the magnitude of the increase in [f*] (5). These results thus indicate that the anomalous behaviour is not due to strain-induced crystallisation.

Also relevant here are force-temperature ("thermoelastic") results (5) obtained at elongations sufficiently large to give large increases in [f*] in the stress-strain isotherm. Such curves show no deviations from linearity which could be attributed to strain-induced crystallisation, or to other intermolecular orderings of the network chains.

The most striking evidence involves the effect of swelling on the isotherms. Results on unfilled PDMS networks as is illustrated in Figures 2 and 3 (9), show that swelling does not diminish the upturns in modulus and, in fact, frequently enhances them.

Similar results are obtained for filled PDMS networks, as is shown by the results presented in Figure 4 (10).

All of the above experimental results indicate that the increases in [f*] are due to an intramolecular effect, specifically to the limited extensibility of the very short network chains (3,11-13,26).

Theoretical Interpretation

Since the above results demonstrate that the upturns in modulus are due to limited chain extensibility, it becomes important to interpret them in terms of a non-Gaussian theory of rubber-like elasticity. A recent novel approach (11-13) to this problem utilises the wealth of information which rotational isomeric state theory (27) provides on the spatial configurations of chain molecules. Specifically, Monte Carlo calculations based on the rotational isomeric state approximation are used to simulate spatial configurations, and thus distribution functions for the end-to-end separation of the chains (28). These distribution functions are used in place of the Gaussian function in the standard three-chain network model (24) in the affine limit to give a molecular theory of rubber-like elasticity which is very useful for the interpretation of elastomeric properties at high elongations.

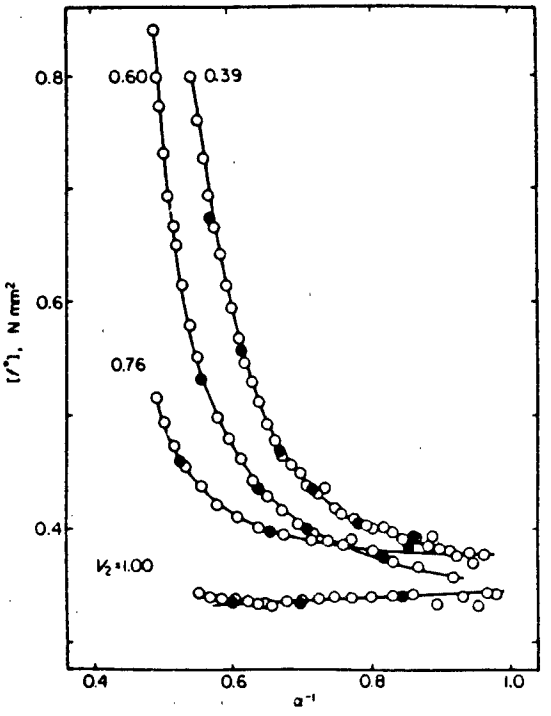


Fig. 2 The effect of swelling on isotherms (25°C) for unswollen and swollen (unfilled) PDMS bimodal networks (220, 18.5×10^3 g mol^{-1}) containing 85 mol % of the short chains.* Each curve is labelled with the volume fraction v_2 of polymer present in the network; the diluent was a linear DMS oligomer having 8–11 repeat units. (Reprinted from ref. 9 by courtesy of the American Chemical Society.)

NETWORKS REINFORCED BY IN SITU PRECIPITATION OF SILICA

After Crosslinking

Figures 5 and 6 show typical elongation isotherms obtained for PDMS networks reinforced by swelling with TEOS, which was subsequently hydrolyzed in situ to give silica filler particles (17). Increase in reaction time is seen to increase the amount of filler precipitated, as evidenced by increases in moduli, in upturns in moduli, and in toughness.

During Crosslinking

It would of course be advantageous if the in situ precipitation could be carried out simultaneously with the curing reaction. Filled PDMS networks have in fact been prepared in this way, using hydroxyl-terminated chains and sufficient TEOS

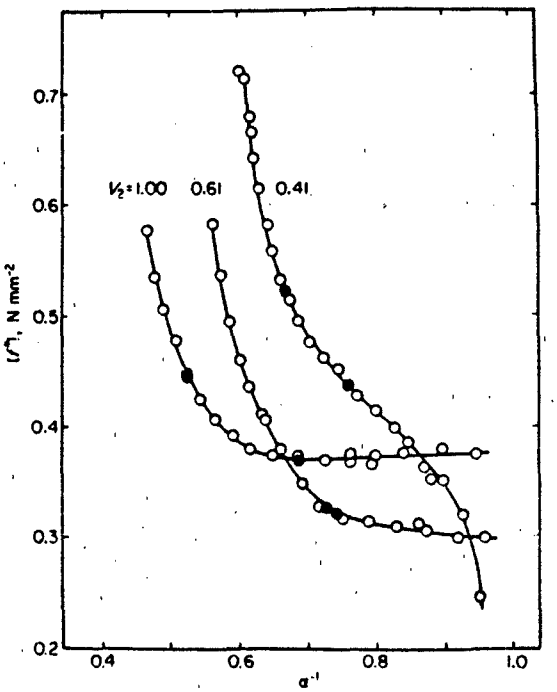


Fig. 3 The effect of swelling on isotherms for (unfilled) PDMS bimodal networks containing 90 mol % of the short chains;[9] see legend to Fig. 2. (Reprinted from ref. 9 by courtesy of the American Chemical Society.)

for both the endlinking process and the hydrolysis reaction to form the filler. Isotherms obtained for some of these networks are shown in Figure 7 (20). Again, very good reinforcement is seen to occur.

In the experiments cited (20), the ratio r of TEOS ethoxy groups to PDMS hydroxyl end groups, a measure of the excess TEOS available for hydrolysis, ranged from 1.0 to 150. The effect of this variable on the weight percent filler precipitated is shown in Figure 8 (20). Estimates obtained from the densities of polymer, silica, and filled network are seen to be smaller than those obtained directly from the increase in weight of the network. This indicates that either the filler particles have not been completely converted to silica or the particles contain a significant number of voids (29). In any case, the increase in r increases the amount of filler introduced and, as shown in Figure 9 (20), increases elastomer toughness (as measured by the energy E_r, required for rupture).

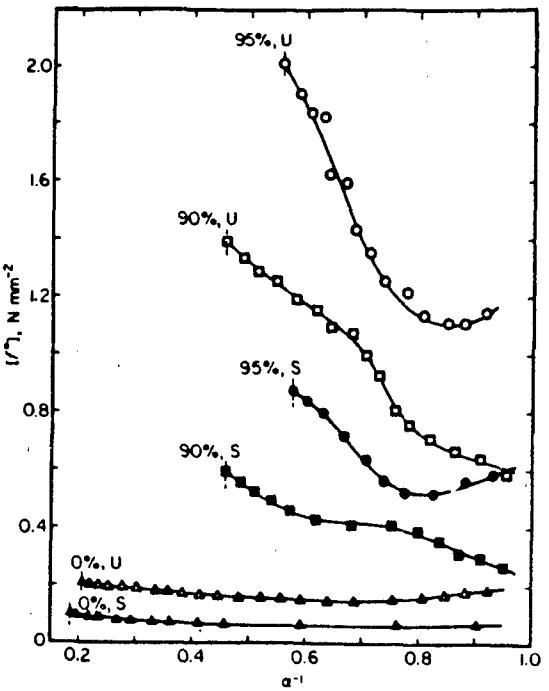


Fig. 4 The effect of swelling on isotherms for fume silica-filled bimodal networks of PDMS (860, 21.3×10^3 g mol^{-1}) in the unswollen (U) state and swollen (S) with *n*-hexadecane to $v_2=0.3$.[9] The numbers specify the mol % of short chains present in the network. Fume(d) silica refers to a commercial grade precipitated from the vapour phase. (Reprinted from ref. 10 by courtesy of John Wiley & Sons, Inc.)

Before Crosslinking

In the above 'in situ' techniques, removal of the by-product C_2H_5OH and unreacted TEOS causes a significant decrease in volume, which could be disadvantageous in some applications. For this reason a technique was developed for the precipitation of the silica into samples of PDMS to give stable polymer-filler suspensions which remained capable of being endlinked, subsequently, with no substantial changes in volume.

In brief, TEOS was added to vinyl-terminated PDMS and then hydrolysed to give polymer-filler suspensions which showed no signs of particle agglomeration or settling. After drying, the viscous liquids could be endlinked with a multifunctional silane to give filled elastomers with very good mechanical properties.

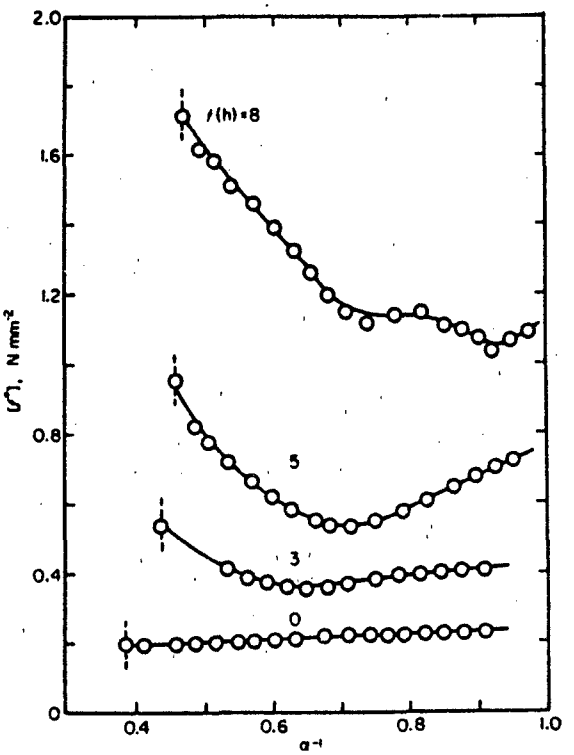


Fig. 5 Isotherms for a (unimodal unswollen) PDMS elastomer (8.0×10^3 g mol^{-1}) which was silica-reinforced by hydrolysis of tetraethylorthosilicate (TEOS) present as diluent in the network.[17] The reaction was carried out at 53% relative humidity, and each curve is labelled with the reaction time. (Reprinted from ref. 17 by courtesy of Dr. Dietrich Steinkopff Verlag.)

Characterisation of Filler Particles

Transmission electron microscopy (15) and light scattering measurements (30) are being used to study the filler particles. As illustration, an electron micrograph for a PDMS elastomer in which TEOS had been hydrolysed is shown in Figure 10 (15). The existence of filler particles in the network, originally hypothesised on the basis of mechanical properties (14), is clearly confirmed. The particles have average diameters of approximately 250 Å, which is in the range of particle sizes of fillers typically introduced into polymers in the usual blending techniques. The distribution of sizes is relatively narrow, with most values of the diameter falling in the range 200-300 Å (15).

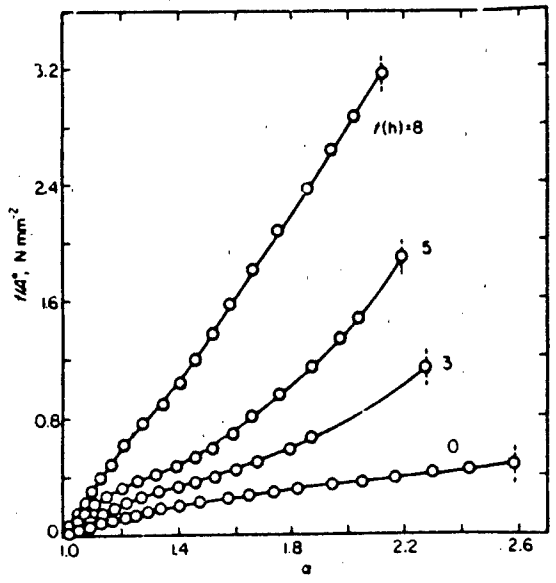


Fig. 6 The nominal stress shown as a function of elongation for the same networks characterised in Fig. 5.[17] In this representation, the area under each curve represents the energy E_r required for network rupture. (Reprinted from ref. 17 by courtesy of Dr. Dietrich Steinkopff Verlag.)

Most strikingly, there is virtually none of the aggregation of particles essentially invariably present in the usual types of filled elastomers. Therefore, these materials should be extremely useful in characterising the effects of aggregation, and could be of considerable practical importance as well (15).

ACKNOWLEDGEMENTS

It is a pleasure to acknowledge the financial support provided by the National Science Foundation through Grant DMR 79-18903-03 (Polymers Program, Division of Materials Research) and by the Air Force of Scientific Research through Grant AFOSR 83-0027 (Chemical Structures Program, Division of Chemical Sciences).

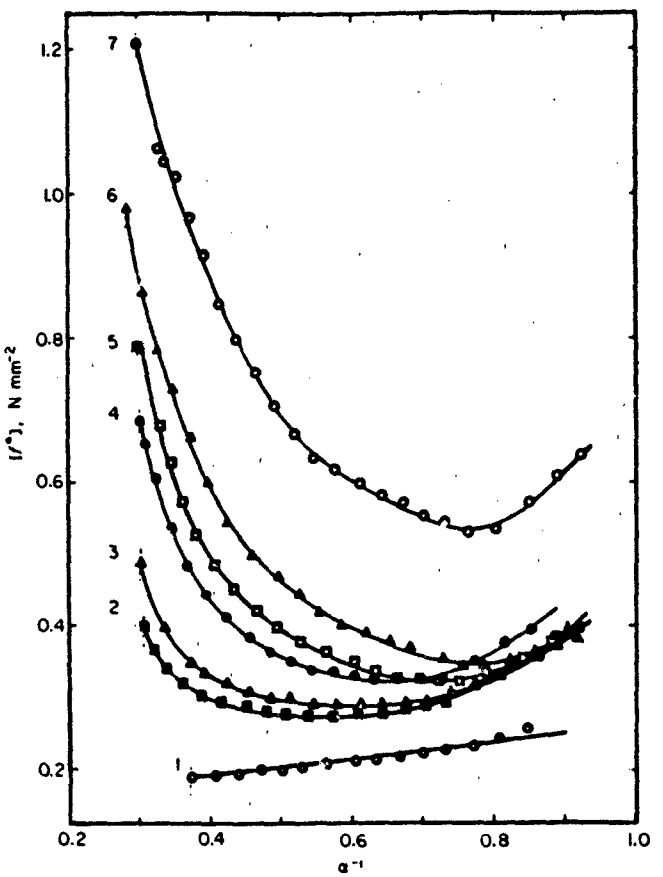


Fig. 7 Isotherms for PDMS networks prepared using TEOS to simultaneously endlink hydroxyl-terminated chains (21.3×10^3 g mol^{-1}) and to provide filler upon its hydrolysis.[20] For samples 1–7, the filler thus incorporated amounted to 0.0, 2.28, 4.56, 6.75, 8.83, 10.8 and 14.6 wt %, respectively. Additional information on these samples is given in Figs 8 and 9. (Reprinted from ref. 20 by courtesy of the American Chemical Society.)

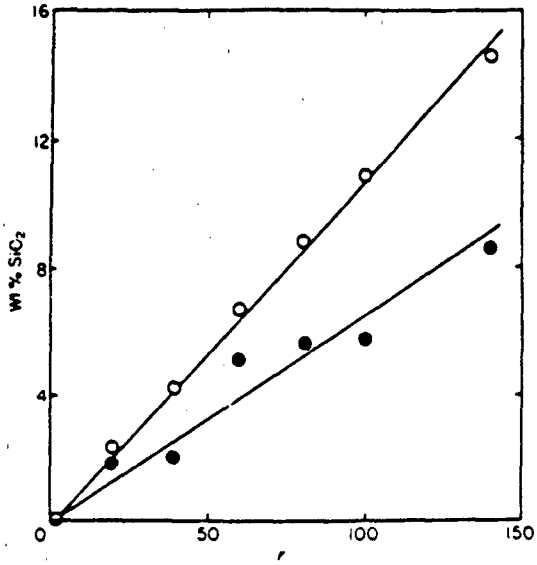


Fig. 8 The wt % filler precipitated within the PDMS networks shown as a function of the feed ratio $r=[OC_2H_5]/[OH]$, where the $-OC_2H_5$ groups are on the TEOS and the $-OH$ groups are on the ends of the polymer.[20] The open circles show the results obtained from the change in weight of the polymer and the filled circles from the density of the filled network. See legend to Fig. 7. (Reprinted from ref. 20 by courtesy of the American Chemical Society.)

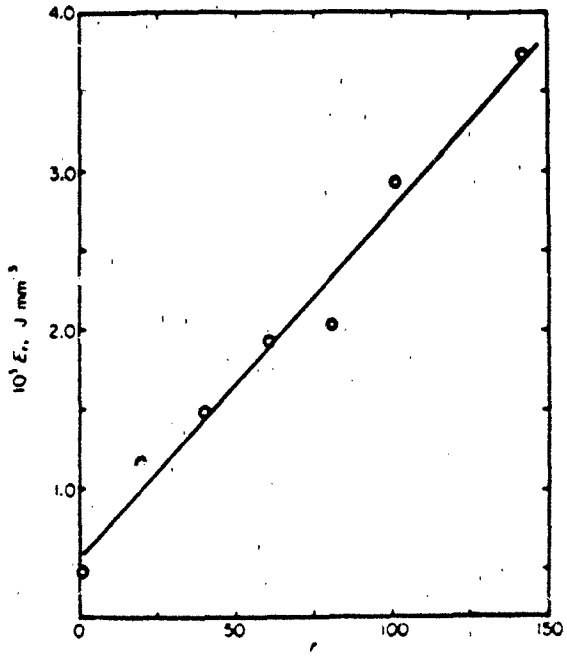


Fig. 9 The effect of the feed ratio on the energy required for network rupture.[20] See legend to Fig. 7 (Reprinted from ref. 20 by courtesy of the American Chemical Society.)



Fig. 10 Transmission electron micrograph at a magnification of 118800× for an *in situ* filled PDMS network containing 34.4 wt % filler. The length of the bar corresponds to 1000 Å. (Reprinted from ref. 22 by courtesy of John Wiley & Sons, Inc.)

1. Mark, J. E. (1979): Makromol Chemie, Suppl. 2, 87.
2. Mark, J. E. (1981): Rubber Chem. Technol., 54, 809.
3. Mark, J. E. (1982): Adv. Polym. Sci., 44, 1.
4. Mark, J. E. (1982): Elastomers and Rubber Elasticity, Edited by J. E. Mark and J. Lal, Washington: American Chemical Society.
5. Zhang, Z.-M. and Mark, J. E. (1982): J. Polym. Sci., Polym. Phys. Ed., 20, 473.
6. Mark, J. E. and Tang, M.-Y. (1984): J. Polym. Sci., Polym. Phys. Ed., 22, 1849.
7. Tang, M.-Y. and Mark, J. E. (1984): Macromolecules, 17, 2616.
8. Tang, M.-Y., Garrido, L., and Mark, J. E. (1984): Polymer, 25, 347.
9. Mark, J. E. (1984): Macromolecules, 17, 2924.
10. Jiang, C.-Y., Mark, J. E., and Stebleton, L., (1984): J. Appl. Polym. Sci., 29, 4411.
11. Mark, J. E. and Curro, J. G. (1983): J. Chem. Phys., 79, 5705.
12. Curro, J. G. and Mark, J. E. (1984): J. Chem. Phys., 80, 4521.
13. Mark, J. E. and Curro, J. G. (1984): J. Chem. Phys., 80, 5262.

14. Mark, J. E. and Pan, S.-J. (1982): Makromol. Chemie, Rapid Comm., 3, 681.
15. Ning, Y.-P., Tang, M.-Y., Jiang, C.-Y., Mark, J. E., and Roth, W. C. (1984): J. Appl. Polym. Sci., 29, 3209.
16. Jiang, C.-Y. and Mark, J. E. (1984): Makromol. Chemie, 185, 2609.
17. Jiang, C.-Y. and Mark, J. E. (1984): Coll. Polym. Sci., 262, 758.
18. Ning, Y.-P. and Mark, J. E. (1985): Polym. Eng. Sci., 25, 824.
19. Tang, M.-Y. and Mark, J. E. (1985): Polym. Eng. Sci., 25, 29.
20. Mark, J. E., Jiang, C.-Y. and Tang, M.-Y. (1984): Macromolecules, 17, 2613.
21. Tang, M.-Y., Letton, A. and Mark, J. E. (1984): Coll. Polym. Sci., 262, 990.
22. Ning, Y.-P. and Mark, J. E. (1985): J. Appl. Polym. Sci., 30, 3519.
23. Mark, J. E. and Flory, P. J. (1966): J. Appl. Phys., 37, 4635.
24. Treloar, L.R.G. (1975): The Physics of Rubber Elasticity, Oxford: Clarendon Press.
25. Mark, J. E. (1975): Rubber Chem.Technol., 48, 495.
26. Mark, J. E. (1985): Polym. J., 17, 265.
27. Flory, P. J. (1969): Statistical Mechanics of Chain Molecules, New York: Interscience.
28. Conrad, J. C. and Flory, P. J. (1976): Macromolecules, 9, 41.
29. Rigbi, Z., private communication.
30. Schaefer, D. W., Ning, Y.-P., and Mark, J. E., unpublished results.

INTERFACIAL ADHESION IN POLYMER BLENDS

A J TINKER
Malaysian Rubber Producers' Research Association
Tun Abdul Razak Laboratory
Brickendonbury
Hertford SG13 8NL
England

INTRODUCTION

Blending two or more polymers to give a material with a combination of the desirable properties of the constituent polymers is a well-established practice. Unfortunately, the outcome often falls short of the expectation for a number of reasons. One common reason is a lack of interfacial adhesion between the components of the blend due to a large difference between the solubility parameters of the polymers. This paper considers one possible means of improving interfacial adhesion in a blend - the formation of copolymeric species of the constituent polymers during blending. The blend considered is polypropylene blended with natural rubber (cis-1,4-polyisoprene) to improve the impact strength of the polypropylene.

The factors which govern the impact properties of blends of a thermoplastic with a rubber are well-known, namely phase morphology, composition, interfacial adhesion, and degree of crosslinking of the rubber phase (1). All four factors have been studied for blends of polypropylene with NR. The first two will not be considered here, except to the extent necessary to present the topics of primary interest. Even when these two parameters were optimised, the low temperature impact strength of blends of polypropylene and natural rubber did not meet expectations. Scanning electron micrographs of fracture surfaces of the blends suggested that rubber particles were debonding from the polypropylene matrix, that is there was evidence of a insufficient interfacial adhesion between the components of the blend.

The improvement of the impact properties of a polypropylene/natural rubber blend by the addition of low levels of m-phenylenebismaleimide was described briefly recently (2). The rationale behind the use of this additive was that it may be viewed as a multifunctional radical acceptor capable of reacting with the polymer radicals formed by chain scission during blending in an internal mixer. m-Phenylenebismaleimide is well-known as a co-agent in the peroxide vulcanization of

rubbers and has also been quoted in patents as as improving sag resistance of polypropylene by linking radicals formed by chain scission during mixing, when used at higher level than considered here, and as improving the adhesion of polypropylene to fillers by combining with radicals and interacting with the fillers (3,4). It was proposed that the m-phenylenebismaleimide added during blending was reacting with the natural rubber and polypropylene radicals to give copolymeric species. It is well-established that the presence of block or graft copolymers composed of the components of a blend greatly improve interfacial adhesion in the blend (1). However, it was recognised that m-phenylenebismaleimide is capable of introducing a low degree of crosslinking in the natural rubber phase of the blend. It is reported that low degrees of crosslinking of the rubber phase of a rubber-modified thermoplastic increases impact strength (1,5), although high degrees of crosslinking are deleterious in this respect. It was considered that the m-phenylenebismaleimide may act both by improving interfacial adhesion between the disperse NR phase and the polypropylene matrix and by introducing a low degree of crosslinking into the NR phase.

The contributions of these two mechanisms to the increase in impact strength of these blends are resolved here, and it will be shown that both are important. The potential for applying the technique of improving interfacial adhesion used here to other blend systems is also considered briefly.

One outcome of the earlier study of the effect of composition on the impact properties of blends of polypropylene with natural rubber is the observation that, in a comparison at a given blend stiffness, blends based on copolymer grades of polypropylene have higher impact strength than blends based on homopolymer grades of polypropylene. For this reason much of the current work has been performed on blends of copolymer grade polypropylene, although the findings have also been shown to apply equally to blends based on homopolymer grade polypropylene. Furthermore, it has been found that the incorporation of a small amount of high density polyethylene (HDPE) benefits the impact properties of the blends. Ternary blends of polypropylene, natural rubber, and HDPE have therefore also been considered here.

MATERIAL AND METHODS

A viscosity-stabilized grade of NR with a Mooney viscosity (ML1+4,100°C) of 60, SMR CV, was used.

The copolymer grade of polypropylene, Propathene GWM 101 (ICI Ltd), has a flexural modulus of 1350 MPa and a melt flow index (MFI) of 4g/10min. A homopolymer grade of polyprcpylene, Propathene GWM 22 (ICI Ltd), with a melt flow index of 4 was also used. When reference is made to polypropylene below and the grade is not specified, the polypropylene under consideration is GWM 101.

The HDPE used in ternary blends was a homopolymer grade (Rigidex 006-60, BP Chemicals) with a melt flow index of 0.7.

m-Phenylenebismaleimide (HVA-2, du Pont), sulphur, tetramethylthiuram disulphide, zinc stearate, phenolformaldehyde resin (SP1045, Schenectady-Midland Ltd), stannous chloride dihydrate, and the antioxidants (Permanax WSO, Vulnax International Ltd, and Irganox PS800, Ciba-Geigy Industrial Chemicals) were used as supplied.

The blends were prepared in a BR Banbury internal mixer on a 1 kg scale. The Banbury was heated with 0.28 MPa steam and mixing was for 5 min at 116 rpm. All times were taken from the initial seating of the ram. Antioxidants (0.2 pphp Permanax WSO and 0.2 pphp Irganox PS800) were added either with the polymers or after 4.5 min, when additives were used. Melting of the polypropylene is accompanied by an increase in the power drawn by the mixer. Power consumption then falls as the temperature of the melt increases and the viscosity falls. The addition of additives was made at or shortly after this peak in power consumption, to make best use of the high shear at the lower melt temperature but to avoid premature reaction with the rubber by those additives capable of causing crosslinking. The temperature of the blends at dump was in the range 180-186°C.

Melt flow indices were determined under condition P of ASTM D 1238 (190°C/5 kg). Die swell was determined for the cold extrudate by measuring the cross-sectional area of three pieces of extrudate and comparing the mean with the diameter of the die.

Izod impact strength was determined on injection-moulded, BS-notched specimens (notch radius 1 mm) at temperatures between -50 and 0°C.

Fractured Izod test pieces were coated with Au-Pd and examined by scanning electron microscopy (SEM) using an Hitachi S-500 microscope.

RESULTS

In order to resolve the effects of crosslinking of the NR phase and the proposed increase in interfacial adhesion on the properties of the blend, blends were prepared with the addition of low levels of other compounds which can be considered as multifunctional radical acceptors but which do not crosslink NR under the conditions of use. Sulphur, tetramethylthiuram disulphide (TMTD), and phenolformaldehyde resin, when added individually, satisfy these criteria. The addition of a low level of any one of these materials to a blend during mixing increases the viscosity of the blend, as indicated by the reduction in MFI, although the effect is not so great as observed previously for HVA-2 (Tables 1 and 2). Die swell during the MFI test is increased by the addition of these materials.

TABLE 1

FLOW PROPERTIES OF 15:85 BLENDS OF NR AND POLYPROPYLENE GWM101

Material	Additive	Amount (pphp)	MFI[a] (g/10min)	Die swell (%)
Blend	None	-	11	51
Blend	HVA-2	0.5	2.1	-
Blend	Sulphur	0.5	4.6	77
Blend	TMTD	0.7	3.6	59
Blend	TMTD/ZnSt[b]	0.7/3.0	3.2	22
PP[c]	None	-	11	52
PP[c]	Sulphur	0.5	11.6	56
PP[c]	SP1045	1.0	11.3	59
PP[c]	None	-	9.0	-
PP[c]	TMTD	0.7	8.1	-

a At 190°C under 5 kg load.
b Zinc stearate
c Masticated in the internal mixer under the conditions used in the preparation of the blends.

As demonstrated previously for HVA-2 (2), the addition of these materials during the mastication of polypropylene under the conditions used in the preparation of the blends does not

reduce the MFI of the masticated polypropylene (Table 1). Die swell during the MFI test is also not much affected.

TABLE 2

FLOW PROPERTIES OF 15:75:10 BLENDS OF NR, POLYPROPYLENE GWM 101 AND HDPE

Additive	Amount (pphp)	MFI[a] (g/10min)	Die swell (%)
None		8.5	62
SP1045[b]	1.0	2.5	116
SP1045/$SnCl_2$	1.0/0.3	3.2	13
TMTD/ZnSt[c]	0.3/1.5	2.6	49
TMTD/ZnSt	0.7/3.0	2.0	22
TMTD/ZnSt	1.0/4.5	2.8	19

a At 190°C under 5 kg load.
b Phenolformaldehyde resin
c Zinc stearate

Thus, the increase in viscosity of the blend due to the addition of these materials cannot be attributed to either crosslinking of the natural rubber or to a change in the flow properties of the polypropylene matrix. Some other mechanism, such as the formation of a copolymeric species, must be invoked. It is known that the formation of graft copolymers causes an increase in the viscosity of a blend (6,7). The increase in die swell caused by the addition of these materials to the blend may be explained by greater deformation of the disperse phase at the entry to the die, which would be consistent with greater interfacial adhesion.

The effects of sulphur or TMTD on the notched Izod impact properties of the blend are similar, but much less marked than that of HVA-2. Izod impact strength is increased, but the effect is only pronounced at the lowest temperatures (Figure 1). The large increase in impact strength above ca -30°C caused by the addition of HVA-2 is lacking.

When zinc oxide and stearic acid or zinc stearate are present in the blend and TMTD is added, crosslinking of the natural rubber phase will occur during blending. The MFI of

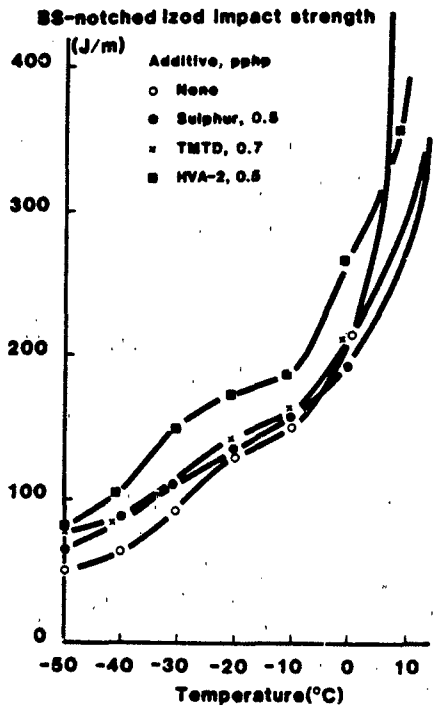


FIGURE 1. Impact strength of 15:85 NR:PP blend - effect of additives.

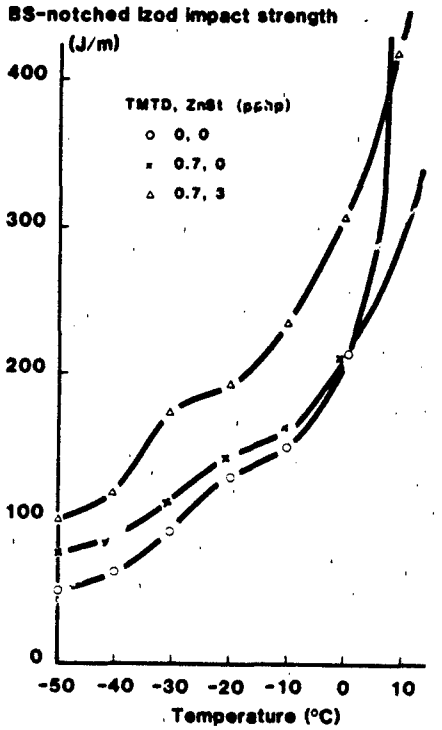


FIGURE 2. Impact strength of 15:85 NR:PP blend - effect of crosslinking the NR phase.

such a blend is closely similar to that of a comparable blend prepared with TMTD alone, but the die swell is much reduced (Table 1). Stannous chloride dihydrate catalyses the crosslinking of NR by phenolformaldehyde resin. When phenolformaldehyde resin was added to a blend containing stannous chloride dihydrate to give a combination which had been shown to crosslink NR under the prevailing conditions, the resulting blend also had a similar MFI and much lower die swell than those of the blend prepared without the stannous chloride (Table 2). It is known that the presence of a crosslinked, and hence less deformable, phase gives a reduction in die swell.

The impact properties of a blend are markedly improved by the introduction of crosslinking in the NR phase. This is illustrated in Figure 2, which allows a comparison of notched Izod impact strength as a function of temperature for blends prepared in the presence of TMTD alone and in the presence of both TMTD and zinc stearate. The increase in impact strength

due to crosslinking of the NR phase is most marked at temperatures above ca -30°C, but it is substantial over the entire range considered. A similar effect is apparent for blends containing phenolformaldehyde resin with and without stannous chloride. Thus the beneficial effect of a low degree of crosslinking of the rubber phase on the impact properties of a rubber-toughened thermoplastic reported for other systems (1,5) is confirmed here for polypropylene modified with NR.

It must be emphasized that the degree of crosslinking considered here is very low, and would not qualify as such in the conventional rubber technology sense. Some qualitative impression of the effect of the degree of crosslinking of the NR may be gained by varying the amount of crosslinking agent added to the blend. The MFI of blends containing 0.3 - 1 pphp TMTD are similar but the die swell decreases progressively, though the difference in die swell between the blends containing 0.7 and 1 pphp TMTD is only slight (Table 2). The attainment of a limiting MFI at a very low level of additive has been observed for other additives, for instance HVA-2 as noted above. There is also a tendency to approach a limiting die swell, as suggested by the values for the blends containing different levels of TMTD, but this happens at a higher level of additive.

The effect of the different levels of crosslinking agent on the notched Izod impact properties of the blend is illustrated in Figure 3, which indicates that there is an optimum degree of crosslinking of the NR in respect of impact properties. For the crosslinking system considered here, this corresponds to ca 0.7 pphp TMTD, although the precise amount may depend on the blending conditions used due to changes in the efficiency of crosslinking. The problems in estimating the degree of crosslinking of the disperse NR phase in such a blend, even relative to another blend, are formidable and this task has not yet been undertaken. The observation of an optimum degree of crosslinking at a low level is in accord with the behaviour of polystyrene toughened with poly(butadiene-co-styrene) rubber (5).

The effect of additives such as HVA-2 on the impact properties of NR/polypropylene blends are not peculiar to blends based on copolymer grades of polypropylene. The addition of HVA-2 during the preparation of blends of homopolymer grade polypropylene with NR gives similar increases in Izod impact strength (Figure 4).

The ultimate properties of a blend in which interfacial adhesion is lacking are improved when interfacial adhesion is increased by, for instance, including a suitable block or graft

copolymer in the blend (7). The tensile strength of a blend of polypropylene with 15% natural rubber is increased by the addition of a low level of TMTD alone (Table 3). Yield stress is also increased. The introduction of crosslinking into the natural rubber phase, by including zinc stearate in the blend, does not give any further significant change in tensile strength or yield stress. Blends prepared with the addition of HVA-2 also show increased tensile strength and yield stress (2).

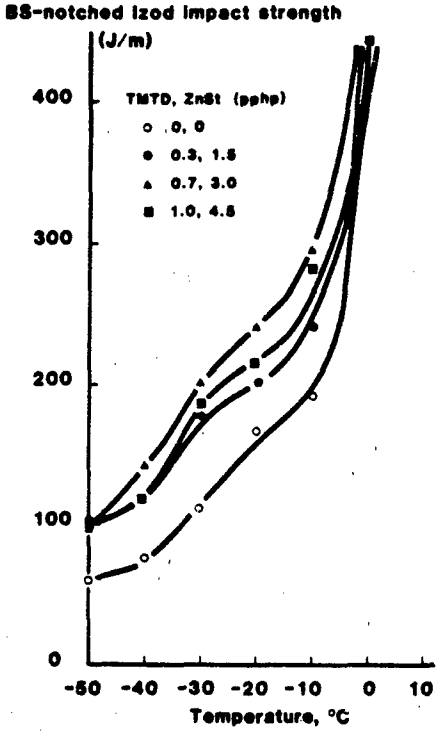


FIGURE 3. Impact strength of 15:75:10 NR:PP:HDPE blend - effect of crosslinker level.

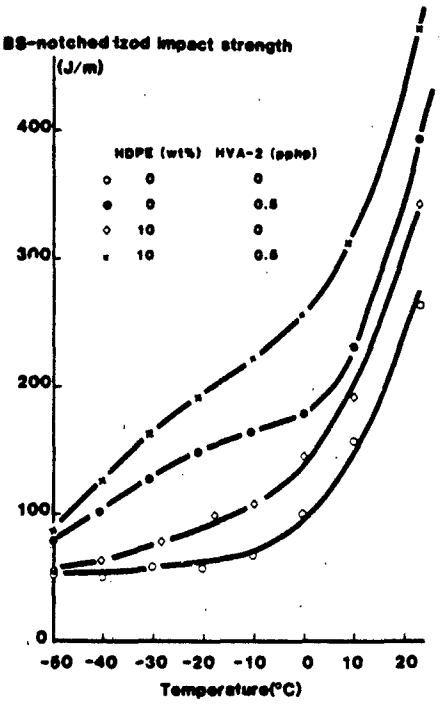


FIGURE 4. Impact strength of homoPP blends containing 15% NR - effect of HVA-2.

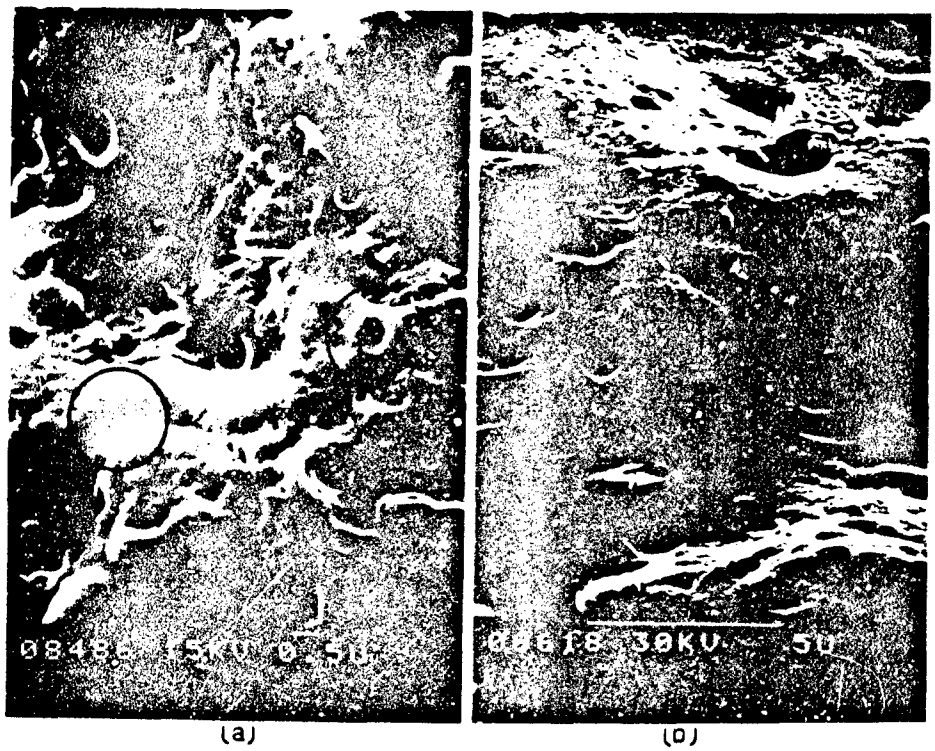
More direct evidence of changes in interfacial adhesion may be obtained by microscopy. A scanning electron micrograph of a cryogenic fracture surface of a blend containing 15% natural rubber reveals a number of features which may be ascribed to debonding of rubber particles (Figure 5a). In addition, there are a few smooth features which appear to be level with the

TABLE 3

EFFECT OF ADDITIVES ON THE PROPERTIES OF 15:85 NR:PP BLEND

Additive	Amount (pphp)	Yield stress (MPa)	Tensile strength (MPa)
None	-	18.5	27.2
TMTD	0.7	19.9	30.9
TMTD/ZnSt[a]	0.7/3.0	20.3	30.4
HVA-2	0.5	20.3	30.8

a Zinc stearate



(a) (b)

FIGURE 5. SEM micrographs of fracture surfaces of 15:85 NR:PP blends containing no additive (a) or 0.5 pphp HVA-2 (b). Some features representing debonded NR particles are circled, some smooth, level features are arrowed.

otherwise rough matrix. This roughness is probably a reflection of the nodular texture of the polypropylene matrix. The smooth features are on the scale of the rubber particles and may represent particles through which the fracture has passed. Micrographs of similar fracture surfaces of blends prepared in the presence of HVA-2 or TMTD with zinc oxide and stearic acid show few, if any, features which may be readily ascribed to the fracture following a weak interface between the matrix and rubber particles (Figures 5b and 6a). However, there are many features, on the scale of the rubber particles, which are smooth and essentially level with the rough surface of the matrix. Furthermore, the particles are generally somewhat irregular in shape, as the rubber particles are known to be in these blends because of the effect of crosslinking during mixing. These features may by identified as rubber particles and suggest that

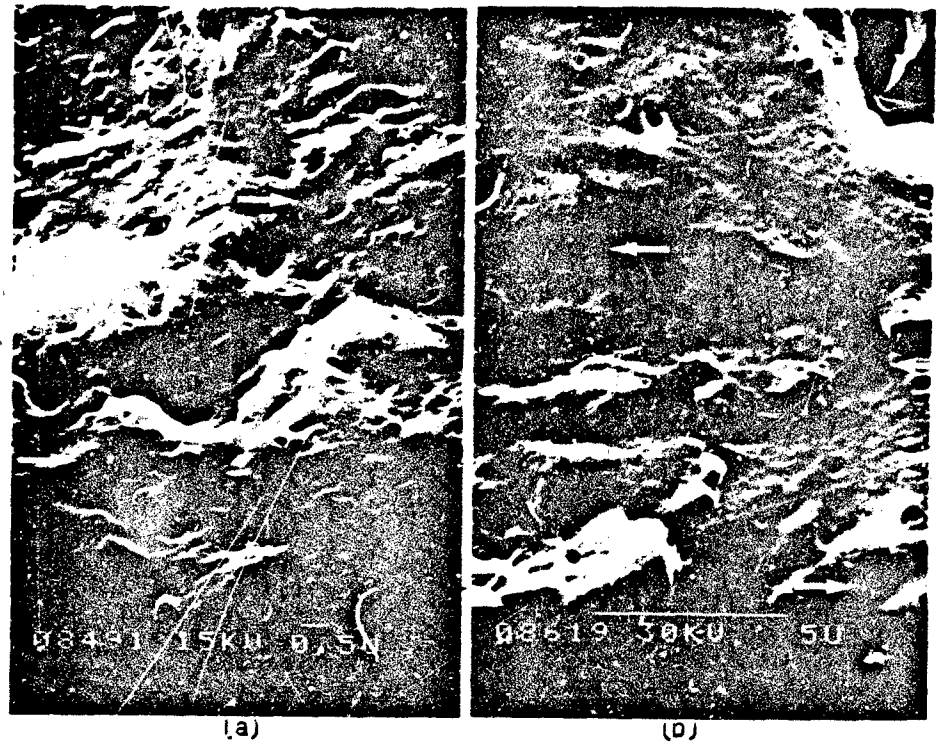


FIGURE 6. SEM micrographs of fracture surfaces of 15:85 NR:PP blends containing 0.7 pphp TMTD with ZnO/stearic acid (a) or alone (b). Some smooth, level features are arrowed.

the fracture has passed through the rubber phase rather than around a weak interface with the matrix. The micrograph of a blend prepared in the presence of TMTD alone shows similar smooth features, though regular in shape because the rubber phase was not crosslinked under these conditions (Figure 6b).

DISCUSSION

The results demonstrate that the substantial increase in the Izod impact strength of a polypropylene/NR blend given by additives such as HVA-2, which are capable of lightly crosslinking the NR phase under the conditions used in the preparation of a blend, is largely associated with the introduction of the low degree of crosslinking into the NR phase. The observation of a smaller increase in Izod impact strength by additives which do not crosslink the NR phase during blending suggests that there is also a contribution from another source, and the evidence of flow properties, ultimate properties, and SEM study of fracture surfaces suggests that this is increased interfacial adhesion.

The effect of these two factors on the impact properties of the blends is interpretable in terms of the known fracture mechanism of polypropylene. At the low temperatures and high rates of deformation experienced in the Izod test, plastic deformation of polypropylene is by crazing (8). When interfacial adhesion is poor, the rubber particles caught in a craze may debond from the matrix generating a void within the craze, which can grow into a crack and precipitate failure. Increasing the interfacial adhesion allows the particle to withstand a greater stress before debonding. However, the rubber particles will have limited cohesive strength, and cohesive failure of a particle being deformed in a craze will also generate a void. Crosslinking the rubber phase will increase cohesive strength and allow the rubber particle to undergo greater deformation before cohesive failure. As the degree of crosslinking increases, the modulus of the rubber particle increases and hence the stress across the interface increases for a given extent of deformation of the rubber particle. Failure may then again occur by debonding of the rubber particle as the adhesive strength of the interface is exceeded. The two factors may therefore been seen as complimentary in their effect on the impact properties of the blend.

It is proposed that the improvement in interfacial adhesion arises through reaction of the polymer radicals generated by

chain scission during blending with the additives to give block/graft copolymers. This means of improving interfacial adhesion is open to other blends of polymers which undergo chain scission under the conditions of blending. However, it may be anticipated that there will be some limit to the difference in solubility parameters between the components beyond which the technique will not be applicable, due to i sufficient opportunity for reaction of the dissimilar radicals with the additive.

The application of the technique to rubber-rubber blends which have processing difficulties and limited durability due poor interfacial adhesion is currently under investigation. The formation of cooolymers in these blends should improve their processing characteristics by increasing interfacial adhesion. Durability should also be improved as covulcanization is increased through both the direct participation of the copolymer in the two rubber networks and an increase in the thickness of the mixed interphase, caused by the presence of the copolymer, in which covulcanization can occur. In the latter context, it has been demonstated that, for blends in which covulcanization occurs readily such as NR with SBR, the act of covulcanization increases the thickness of the mixed interfacial region (9). This has been ascribed to the formation of copolymers as a part of the process of covulcanization.

ACKNOWLEDGEMENTS

This work forms part of a project for which funds have been provided to the United Nations Industrial Development Organization as a special purpose contribution by the Federal Republic of Germany. Thanks are due to these parties and to the board of the MRPRA for permission to publish.

REFERENCES

1. Bucknall, C. B. (1977): Toughened Plastics. Applied Science, London, p. 209

2. Tinker, A. J. (1984): Polypropylene/natural rubber blends having high impact strength at low temperatures, Polym Commun, 25:325-326

3. JP 58,132,037

4. EP 73,485

5. Morton, M., Cizmecioglu, M., and Lhila, R. (1984): Model studies of rubber additives in high-impact plastics. In: Advances in Chemistry Series Volume 206: Polymer blends and composites in multiphase systems. American Chemical Society, Washington DC.

6. Campbell, D. S., Mente, P. G., and Tinker, A. J. (1981): Polystyrene graft copolymers of natural rubber, Kaut Gummi Kunst, 34:636-640

7. Ide, F., and Hasegawa, A. (1974): Studies on polymer blend of nylon 6 and polypropylene or nylon 6 and polystyrene using the reaction of polymer, J Appl Polym Sci, 18: 963-974

8. Jang, B. Z., Uhlmann D. R., and Vander Sande J. B. (1984): Ductile-brittle transition in polymers, J Appl Polym Sci, 29:3409-3420

9. Braun, H-G., and Rehage, G. (1985): Compatability and molecular structure of rubbers, Angew Makromol Chem, 131:107-115

FAILURE PROCESSES IN ELASTOMERS

A. N. GENT
Institute of Polymer Science, The University of Akron,
Akron, Ohio 44325

SUMMARY

Studies of several failure processes in model elastomers are described. In unfilled elastomers a splitting of the tear front is ascribed to the presence of inherent stress-raisers about 100 μm apart. When tensile stresses are applied to an elastomer containing a single spherical inclusion the elastomer either pulls away at a critical stress or a void forms within the elastomer itself near the surface of the inclusion. If two inclusions are close together, a void forms midway betweem them and grows catastrophically. Profuse voiding is observed in carbon-black-filled rubber, each void being initiated by a particle about 0.5 μm in diameter. The implications of these observations for the reinforcement of elastomers is discussed.

INTRODUCTION

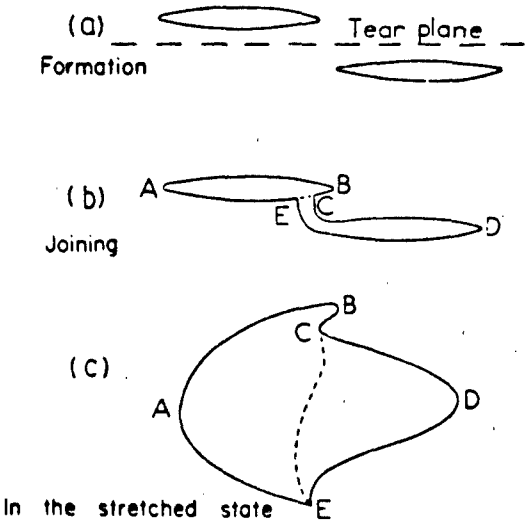
Much can be learnt about mechanisms of failure by direct observation. The results of two recent studies are summarized here. They deal with the way in which a tear propagates in elastomers, by a series of secondary tears developed at the tear front (1), and with the failure processes that occur near or at the surface of a rigid spherical inclusion (2).

TEAR PROPAGATION IN UNFILLED ELASTOMERS

Uniform advance of a smooth tear along a broad front is intrinsically unlikely. Instead, small secondary cracks develop at the tear tip, at points where the local stress is unusually high. If the material is highly-stretched at the tear tip, these secondary cracks are not co-linear, in general, but are separated somewhat in the vertical (strain) direction, Figure 1. Then, as they grow in size, they eventually link up by the deviation of one or both of them, as shown schematically in Figure 1b, under the influence of the complex stress field set up where they come into proximity.

This hypothesis accounts successfully for the formation of steps of the characteristic shape observed on fracture surfaces, shown schematically at point E in Figure 1b, and also for the appearance of webs in the stretched state, as sketched in Figure 1c.

Fig. 1. Formation of steps at the crack front by the joining of secondary cracks



It is noteworthy that the average distance between steps in a fully-developed tear surface, in the range 10-100 μm, is similar in magnitude to the inferred size of natural flaws or defects in elastomers, from which tensile or mechanical fatigue failures originate (3). If stress-concentrating features are commonly present in elastomers at a general spacing of 10-100 μm, then cracks or defects of this size would also be expected.

TEAR OF CARBON-BLACK-FILLED ELASTOMERS

Elastomers are commonly reinforced by the incorporation of large amounts of finely-divided particulate fillers, notably carbon black. The mechanism of reinforcement is still obscure, however. A photograph of the tear tip in a carbon-black-filled polybutadiene vulcanizate is shown in Figure 2. Many carbon black aggregates, about ½ μm in diameter, are visible at the tear tip and in the torn surfaces.

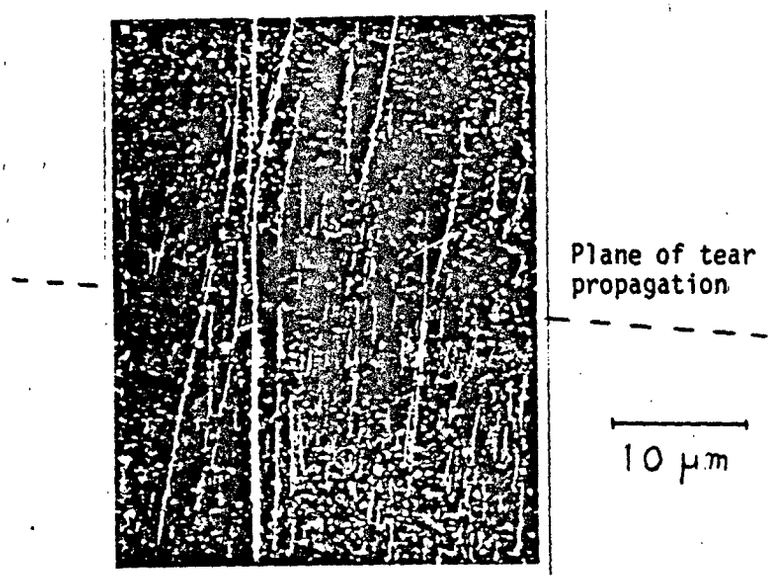


Fig. 2. Tear tip of carbon-black-filled polybutadiene vulcanizate C.

The tear tip is seen to be split by numerous vertical tears. Careful inspection shows that each tear is associated with a carbon black particle. Thus, each particle appears to have acted as a local stress-raiser and provided a potential nucleus for a secondary crack. The reinforcing action of carbon black thus appears to consist, paradoxically, of inducing many small tears to form in the highly-strained material at the tear tip, and in this way to blunt the effective tip diameter.

The particle size is extremely important for this reinforcement mechanism to operate. If the particles are much smaller than 1 μm, say, then detachment or tearing in their vicinity becomes improbable because the stresses required become extremely large (see below). On the other hand, when the particles are much larger than about 1 μm, then they do not confer significant advantages because unfilled elastomers appear to have inherent stress-raising defects at spacings of 10-100 μm, as discussed earlier.

FAILURE PROCESSES IN ELASTOMERS AT OR NEAR A RIGID SPHERICAL INCLUSION

An experimental study has also been carried out of two distinct failure phenomena, cavitation and debonding, in an

elastomer containing a rigid spherical inclusion. Several elastomers were employed, containing glass beads of various diameters with well-bonded beads ranging from 60 to 5000 μm, and with chemically different surfaces. The critical stress for cavitation was found to depend upon both Young's modulus, E, of the elastomer and the diameter of the bead. By extrapolation, it was found that the stress for cavitation near an infinitely-large bead is given by 5E/12, as predicted by theory (4). In contrast, the critical stress for debonding from less-well-bonded beads was found to decrease somewhat with increasing Young's modulus of the elastomer. This is attributed to a concomitant decrease in the strength of adhesion between the elastomer and the bead surface, due to rheological effects.

The stresses for both cavitation and for debonding were found to vary approximately with the negative half-power of the bead diameter. This suggests that a similar Griffith mechanism governs both failure processes when the bead size is small.

A study of cavitation and debonding in the presence of two glass beads was also carried out. As predicted from theoretical considerations, both stresses were found to decrease as the distance between the two beads was decreased, irrespective of the diameter of the bead and Young's modulus of the elastomer. At higher strains, however, a second cavitation process was found to take place at a point midway between the beads, Figure 3. Catastrophic tensile fracture of the specimen resulted from unrestrained lateral growth of this second cavity.

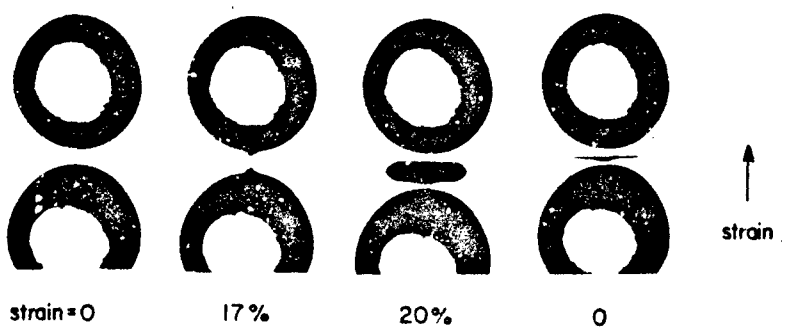


Fig. 3. Progress of cavitation in a silicone elastomer, E = 2.2 MPa, containing two glass beads of 1.25 mm diameter bonded to the elastomer. Direction of applied tension: vertical.

ACKNOWLEDGEMENTS

This work was initiated under a research grant from the Engineering Division of the National Science Foundation (NSF-ENG-16982) and completed under a research grant from the Office of Naval Research (ONR-N00014-76-C-0408). Additional support by Cabot Corporation and Lord Corporation is also gratefully acknowledged.

REFERENCES

1. A. N. Gent and C.T.R. Pulford, J. Mat.Sci. 19, 3612-3619 (1984).
2. A. N. Gent and B. Park, J. Mat. Sci. 19, 1947-1956 (1984).
3. A. N. Gent, P.B. Lindley and A.G. Thomas, J. Appl. Polymer Sci. 8, 455-466 (1964).
4. A. N. Gent and P.B. Lindley, Proc. Roy. Soc. (London), A249, 195-205 (1958).

APPLICATIONS OF THE J-INTEGRAL TO FRACTURE OF NON-ELASTIC RUBBER

J.A. DONOVAN, D.J. LEE, AND R.F. LEE
Department of Mechanical Engneering, University of Massachusetts, Amherst, MA 01003.

INTRODUCTION

It is difficult to determine valid fracture characterizing parameters for non-linear, non-elastic materials like carbon black filled, natural rubber. The classic tearing energy approach developed by Rivlin and Thomas (1) must be modified for the energy dissipated by hysteresis (2). The J-integral approach introduced by Rice (3) and initially applied by Begley and Landes (4) to metals and by William (5) to polymers has been shown to yield valid parameters that characterize crack initiation in these non-elastic materials. Oh (6) showed in rubber that the J integral gave the same results as the tearing energy method at deformations less than required to initiate crack growth. The objective of the current study was to develope test procedures based on the J integral concept, and determine the critical J for initiation of crack growth, and evaluate the critical parameters as material properties.

Carbon black filled, natural rubber was chosen because it is a highly dissipative material and a severe test of the validity of the J integral concept. The J integral was evaluated by 1) multiple specimen tests of Mode I (tension) and mixed mode (tension plus shear) and 2) single specimen tests of the effect of carbon black on crack initiation. The results show that the J integral provides a basis for valid and relatively simple evaluation of fracture resistance in highly dissipative elastomers.

J-INTEGRAL CONCEPT

The J-integral on any path Γ surrounding the crack tip is defined as

$$J = \int_{\Gamma} \left(W dy - T \frac{\partial u}{\partial x} \, ds\right) \qquad (1)$$

where W is the strain energy density, T is the traction vector, $\frac{\partial u}{\partial x}$ is the displacement gradient, and s is the arc length (3). It can be represented equally well by

$$J = -\frac{1}{B}\frac{\partial U}{\partial a} \qquad (2)$$

i.e., the negative change in potential energy U per unit thickness B for an incremental change in crack length a. That is, J is proportional to the area between the load-displacement curves of specimens with cracks of length a and a + da, respectively (Fig. 1). For conditions that satisfy linear elastic fracture mechanics $J = (1 - \nu^2) K^2/E = G$, where K is the stress intensity, E is the modulus, ν is Poisson's ratio and G is the strain energy release rate. The J-integral may be interpreted in two ways: (a) the intensity of the elastic-plastic deformation and stress field in the crack tip region or (b) the change in energy of the cracked body due to a small extension of the crack.

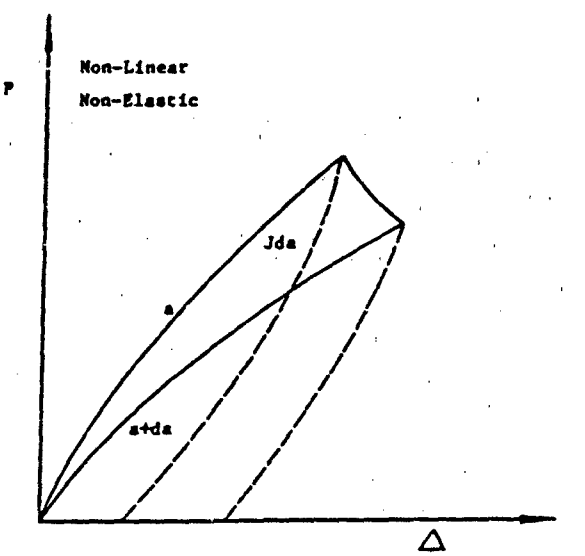


FIGURE 1. Load-displacement curves for specimens with cracks of size a and a+da. The dashed lines represent the un-loading curves.

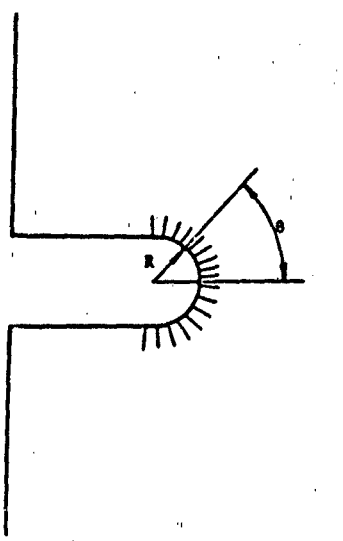


FIGURE 2. The geometry of a blunt notch with fiducial lines for local measurement of extension.

Begley and Landes (4) proposed that the value of J at crack initiation J_c be a fracture criterion and showed it to be a material property for specimens that exhibit large amounts of plasticity before fracture. Hence, J_c can be used to characterize fracture in ductile materials and is known as the ductile fracture toughness, analogous to G_c in linear elastic fracture mechanics. However, since sustained crack growth in ductile materials requires additional energy. the J-integral value for initiation is conservative.

Schapery (7) theoretically justified the use of the J-integral as a failure criterion in non-homogenous, viscoelastic media.

The line integral definition provides an analytical method for evaluating the J-integral and has been shown by Oh (6) to represent the state of stress and strain in elastomers. Rice (8) also showed that if the intergration path was taken along a blunt notch, rather than for a sharp crack,

$$J = \int W \, dy \qquad (3)$$

and provided another method, particularly interesting for the study of elastomers. In fact Thomas (9) arrived at the equivalent expression of tearing energy

$$T = R \int W \, d \sin\theta \qquad (4)$$

where R is the notch tip radius, W the local strain energy density and θ the angle from the center line of the notch, Figure 2, about 30 years ago.

EXPERIMENTAL PROCEDURE

A natural rubber recipe, compounded by B.F. Goodrich, with carbon black contents of 0, 10, 25 or 40 pph was used for all tests. The multiple specimen results for Mode I and mixed mode loading were done only with 40 pph carbon black, while the results based on the crack tip region were obtained with all four carbon black compositions.

Single edge notched specimens with sharp or blunt notches of different lengths, widths and pre-crack lengths were tested at 21°C and a displacement rate of 1 cm/min. The sharp cracks were made by cutting the rubber with a razor blade; the crack angle (β) varied between 0 and 65° (Fig. 3a). The blunt notches were made by drilling a hole with a sharp hollow circular cutter lubricated with water. Blunt notches with radii 1, 2 and 3 mm were made, then the sides of the notches were cut away with a sharp razor blade (Figure 3b).

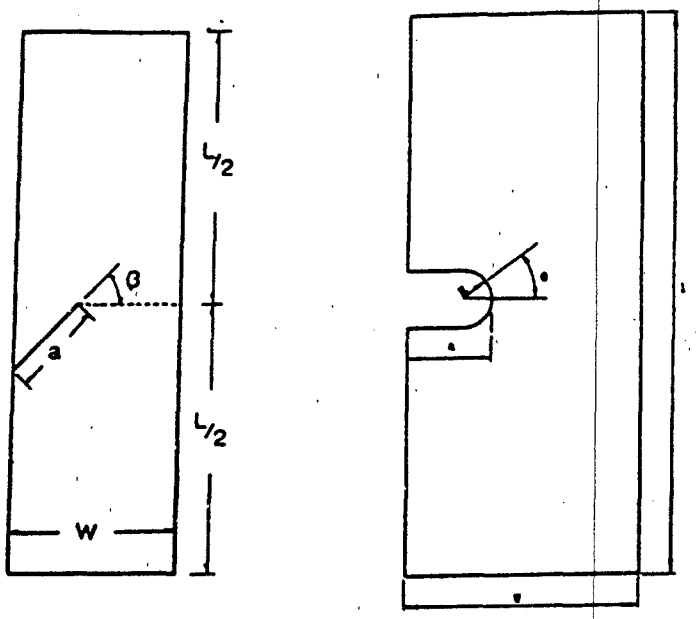


FIGURE 3. The specimen dimensions for a) pre-cracked and b) pre-notched specimen.

The region around the notch tip was coated with white powder so that a series of fine radial lines could be made in the notch tip region. The spacing between the lines was measured with the aid of a 10 x filar eyepiece. Based on these measurements the extension ratio as a function of position was determined and was the basis for calculating the critical J integral at initiation.

The above procedure is not applicable for sharp cracks, therefore J_δ, suggested by results for a Dugdale Zone (8), was defined as

$$J_\delta = \int \sigma d\delta \qquad (5)$$

where σ is the net section stress and δ the crack tip diameter. J_δ was determined and compared to J_θ.

Crack initiation was identified by coating the crack surface with the white powder, as loading increased the region in the crack tip developed a new surface delineated by the white powder was taken as crack initiation in the multiple specimen tests. Crack initiation as defined differenly for the single specimen tests as the first visible sign of peeling. Therefore, the results are consistently higher for the single specimen tests compared to the multiple specimen tests. Additional work is being done to refine identification of the initiation event.

Conventional tensile tests (smooth specimens) to determine stress-extension ratio curves and the stored energy as a function of extension ratio were also measured at 21°C and a displacement rate of 1 cm/min.

RESULTS

Mode I

Initial loading of the pre-cracked specimens (β=0) blunted the razor cut until a crack initiated. Since initiation was relatively easy to observe, the load and extension at initiation were easily determined. Almost immediately after the crack initiated renewed blunting of the crack occurred a the load increased. The initiation event was not apparent on the load-extension curve. Blunting, with little slow stable crack growth, continued with extension until unstable crack growth fractured the specimen.

The area under the load extension curve is the energy stored in the specimen. In the pre-cracked or pre-notched specimens the force-displacement field is non-uniform, therefore the energy density is non-uniform and greatest in the vicinity of the crack tip. The total energy, the area under the load-extension Δ curve, is shown in Figure 4 a a function of pre-crack length for various values of extension. The slope of these curves ($\frac{\partial U}{\partial a}$) gives J and it is shown in Figure 5 as a function of extension. $J(\lambda)$ and extension ratio at initiation are sufficient to determine J at initiation.

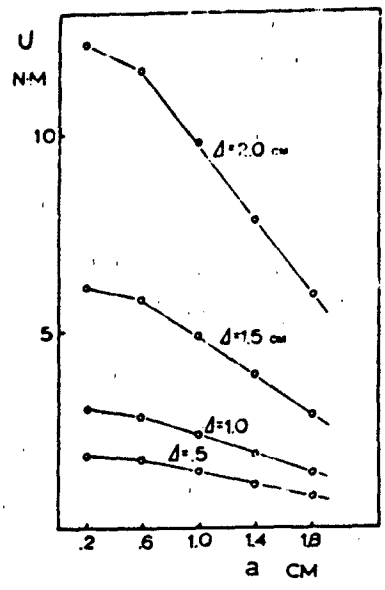


FIGURE 4. Stored energy as a function of pre-crack size at different extensions.

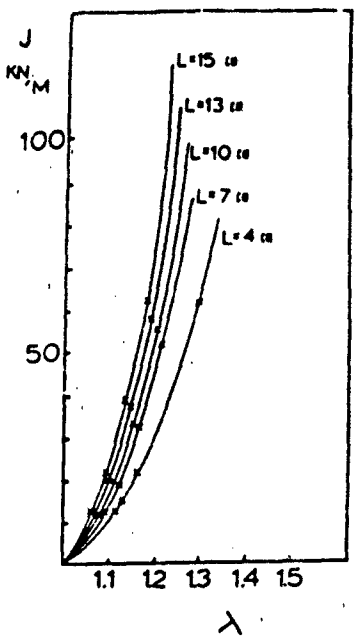


FIGURE 5. The J-integral as a function of extension ratio; the "X" marks the initiation for a specific pre-crack size.

The critical values of J at initiation were determined from Figure 5 for values of the extension at initiation and are shown in Figure 6 as a function of specimen length and pre-crack size. The critical J value is a function of the pre-crack size, but independent of specimen length. However, Figure 7 shows that the critical extension at initiation is a linear function of specimen length and the curves extrapolate to a common intercept, similar to results found by Agarwal et al (10) for composites. These data, therefore, allow the energy release rate to be partitioned between the crack tip region and away from the crack tip.

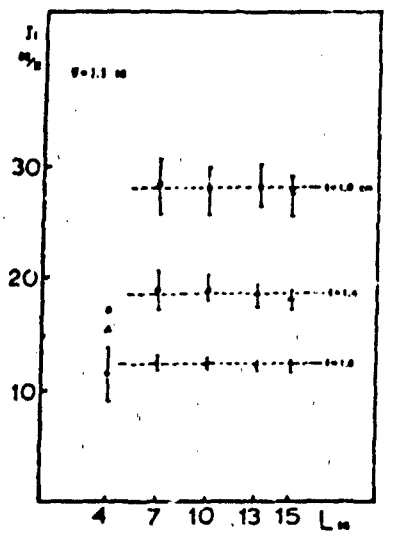


FIGURE 6. Critical J-integral as a function of specimen length and pre-crack size.

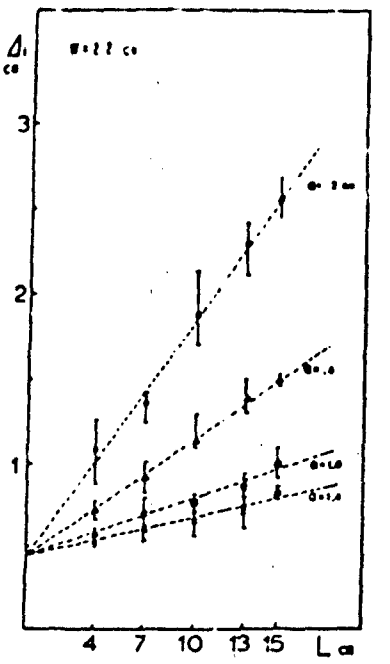


FIGURE 7. Critical extension as a function of specimen length and pre-crack size.

The J value obtained at the critical extension in the hypothetical zero length specimen Δ_o represents the critical energy release rate in the crack tip region to initiate a crack, which is independent of specimen length and crack size. This value was obtained by converting the extension for the hypothetical zero length specimen to the extension ratio for the actual length of the tested specimen $\lambda_o = (\Delta_o + \ell_o)/\ell_o$. With this λ_o the J value representing the critical strain energy release rate in the crack tip region was found from Figure 5 to be 10.8 kN/m for all specimen lengths tested.

The total energy stored in the pre-cracked specimens at initiation as a function of specimen length is shown in Figure 8. These data for a specific pre-crack size can be extrapolated as straight lines to zero specimen length and this energy also can be interpreted as the energy required in the crack tip region to initiate the crack.

Since J is defined as $-\frac{1}{B}\left(\frac{\partial U}{\partial a}\right)$ then the slope of U for $\ell = 0$ as a function of pre-crack length would be equivalent to the critical J value for the crack tip region to initiate the crack. These data are shown in Figure 9 and the slope of the line is 12 kN/m virtually the same as obtained from the critical extension at $\ell = 0$, and Figure 5.

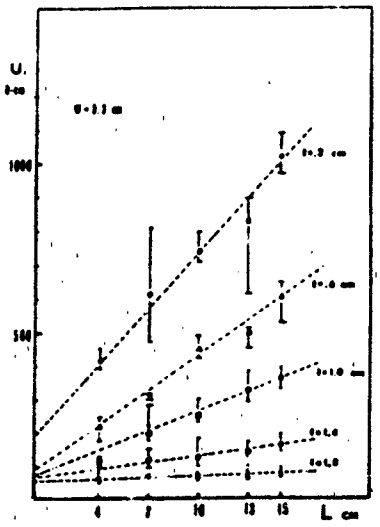


FIGURE 8. Stored energy at initiation as a function of specimen length and pre-crack size.

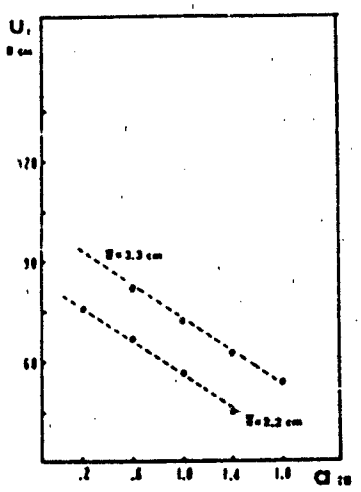


FIGURE 9. Total stored energy at initiation in a "zero" length specimen.

Mixed Mode

The results of the multiple specimen tests to determine the critical conditions for mixed mode loading conditions were analyzed in the same way as the results for Mode I studies. Attempts to measure the critical conditions for pure Mode II were unsuccessful because the specimen buckled due to the loading conditions. The results for the critical J value in the crack tip region as a function of β are shown in Figure 10.

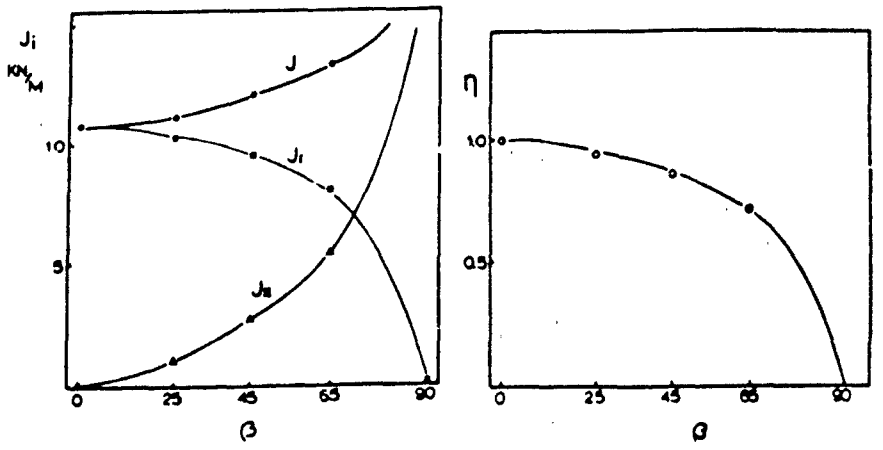


FIGURE 10. Critical J-integral for initiation as a function of crack angle. And, the contribution of J_I and J_{II}.

FIGURE 11. The ratio of crack opening displacement in mixed mode to pure Mode I at the critical extension for a "zero" length specimen.

Mode II loading does not cause any crack tip opening, therefore as a means for partitioning the contribution of Mode II to the fracture process the crack opening displacement δ was measured at the critical extension ratio for the zero length specimen as a function of β. The ratio η of crack opening displacement δ for any value of β to $\delta(\beta=0)$ is shown in Figure 11. Based on this experimental result and since it is known that J_I is proportional to δ (3) then

$$J_I = \eta J_{Ic}$$

Ishikawa et al (11) analytically proved that

$$J_{I,II} = J_I + J_{II}$$

then it follows that

$$J_{I,IIc} = \eta J_{Ic} + (\gamma) J_{IIc}$$

where γ is an unspecified proportionality factor. $J_{I,IIc}$ as a function of η is shown in Figure 12 and a linear extrapolation of the data gives the critical J_{II} as 19 kN/m and $\gamma = (1 - \eta)$.

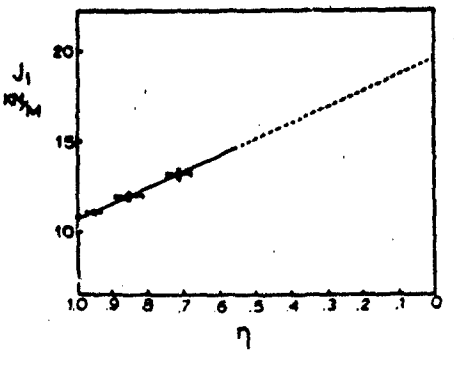


FIGURE 12. Critical mixed mode for J-integral as a function of crack opening displacement ratio.

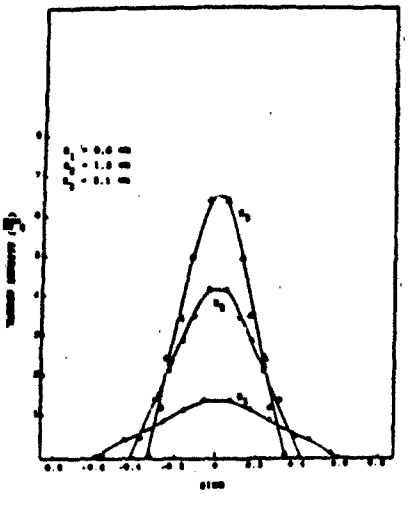


FIGURE 13. Energy density a a function of sinθ for a specimen with an initial radius of 2mm.

Crack Opening

The extension ratio as a function of position along the notch tip for different notch radii were measured, converted to energy density obtained from tensile tests, and are shown in Figure 12 as a function of sin θ for different imposed notch radii. These data were obtained in specimens of different length ℓ, width w, pre-notch radius R_p and pre-crack length a. The data were independent of these variables, except for R_p, within experimental error. The J-integral was then determined according to Equation 4 by intergrating the area under the W-sin θ curve and is shown in Figure 13 as a function of the notch tip radius and shows that it is independent w, ℓ, and a. The J value required for initiation of crack growth from a blunted pre-crack can be obtained by this procedure if the notch radius at initiation is known. Similar data were obtained as a function pre-notch tip radius, specimen geometry and carbon black content.

This procedure is tedious and cannot be applied to sharp cracks. Therefore, the net section stress was measured as a function of crack tip radius and found to be independent of ℓ, w and a (Figure 14). These data were used in Equation 5 to calculate J_δ and are shown in Figure 15. The J_θ was found to be equal to 2.04 times J_δ with a standard deviation of 0.14 for 35 different combinations of ℓ, w, a and carbon black content.

The critical value of J_θ and J_δ were determined by following the above procedures and noting the critical radius at crack initiation; Figure 16 shows J_δ as a function of the pre-notch radius and carbon black content. J_δ is a linear relation of pre-notch radius, including the data obtained for a sharp pre-crack, and also carbon black content increases the critical energy release rate necessary for crack initiation.

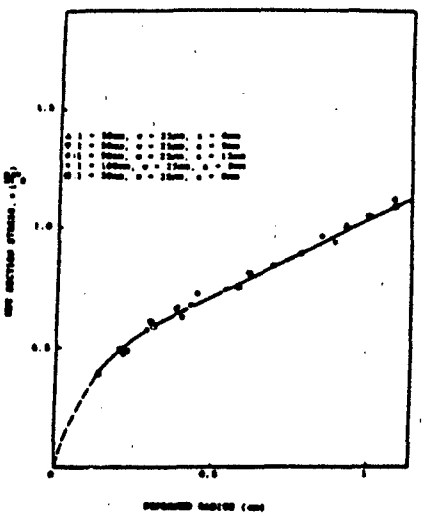


FIGURE 14. Net section stress as a function of crack tip radius in different geometry pre-cracked specimen.

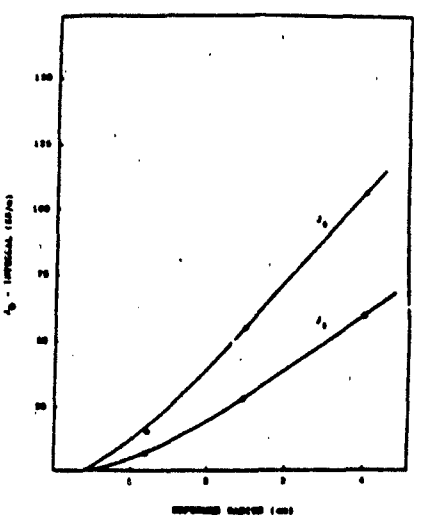


FIGURE 15. J_θ and J_δ as a function of notch radii.

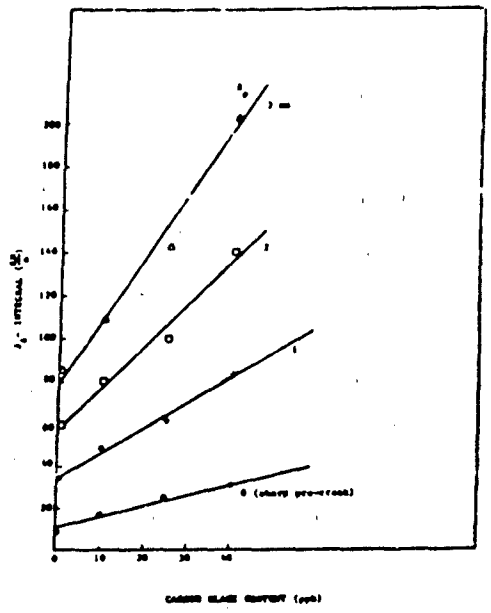


FIGURE 16. J_c at crack initiation as a function of carbon black content for specimen with different pre-notch radii.

DISCUSSION

It has been demonstrated that the J integral describes the critical conditions for crack initiation in carbon black filled, natural rubber, a non-linear, non-elastic material. However, the critical values determined by the multiple specimen method decrease with increasing pre-crack size. But, analysis of the critical extension as a function of crack size and specimen length shows that a unique value of the extension, independent of the crack size and specimen length is obtained for the hypothetical zero length specimen. Calculating the critical J with this value of extension gives a geometry independent material property that is a valid measure of the resistance of the rubber to crack initiation. This critical J is the critical strain energy release rate in the crack tip region for crack initiation. The J value determined by the usual multiple specimen procedure represents the total J required and is not independent of crack size.

The J integral approach also allows the determination of the critical conditions for crack initiation under mixed mode loading conditions. Mixed mode loading may be important for some practical situations. such as wear. By measuring the critical J value as a function of β it was possible to estimate the critical J value for pure Mode II loading as about 18 KN/m. The basis for this prediction involves two assumptions: 1) that the crack opening in mixed mode loading is due to the Mode I contribution alone and 2) that the relationship of $J_{I\ II,c}$ to η is linear over the entire range of η. The first assumption seems realistic, but the second is less certain. However, actual measurements of J_{IIc} don't appear to be possible because of buckling of the specimen, therefore this extrapolated value is believed to be the best approximation available.

The experimental procedures used to determine the critical J values by the multiple specimen procedure are involved and time consuming. However, by considering the net section stress and deflection in the crack tip region it is possible to determine the critical strain energy release rate in the crack tip region from a single specimen test. That is the material property that is a measure of the resistance of the material to crack initiation. It was shown that

$$J_\delta = \int_{\delta_0}^{\delta_1} \sigma \, d\delta$$

equals one half the true J_{IC} value that follows from measurements of the local strain energy density and crack tip diameter as suggested by Thomas (9) and Rice (8). This therefore makes it possible to measure the material property in a highly dissipative material simply by measuring the load and crack tip diameter.

Based on this simple single specimen procedure it was easy to show the linear dependence of the fracture properties on carbon black content. Therefore, this procedure provides an interesting and simple way to study the effect of carbon black on fracture properties.

CONCLUSIONS

It was shown that the critical J integral for crack initiation in carbon black filled, natural rubber is a valid material property (independent of specimen geometry) that describes the materials resistance to crack initiation. Either multiple or single specimen procedures could be used to study the effect of other variables, such as carbon black content, on fracture properties.

ACKNOWLEDGEMENTS

The financial support of the US Army Research Office-Durham and the Transportation System Center, US Department of Transportation of this work is gratefully acknowledged. One of us, R.F. Lee, also appreciates the award of a Cabot Foundation Fellowhip. We would like to thank the B.F. Goodrich Co. for supplying the material.

REFERENCES

1. R.S. Rivlin and A.G. Thomas, "Rupture of Rubber, I. Characteristic Energy for Tearing", J. of Polymer Science, 10, (1953) 291.
2. A. Ahagon, A.N. Gent, H.J. Kim and N. Kumagai, "Fracture Energy of Elastomers in Mode I and Mode III," Rubber Chem. Tech. 48 , (1975) 896,
3. J.R. Rice, "Mathematical Analysis in the Mechanics of Fracture," in Fracture - An Advanced Treatise, 2, Academic Press NY (1968) 191.
4. J.A. Begley and J.D. Landes, "The J-integral as a Fracture Criterion," in Fracture Toughness ASTM STP 514, Phil. (1972) 1.
5. J.M. Hodgkison and J.G. William, "J and G analysis of the Tearing of a Highly Ductile Polymer," J. Mat. Sci. 16 (1981) 50.
6. H.L. Oh, "A Simple Method for Measuring Tearing Energy of Nicked Rubber Strips," Mech. of Crack Growth, ASTM STP 590 (1976) 104.

7. R.A. Schapery, "On the Analysis of Crack Initiatin and Growth in Non-Homogenous Viscoelastic Media," Fracture Mechanics, Am. Math. Soc., SIAM-AMS Proceedings, 12 (1978) 137.
8. J.R. Rice, "A Path Independent Integral and the Approximate Analysis of Strain Concentration by Notches and Cracks," J of Appl. Mech. 35 (1968) 379.
9. A.G. Thomas, "Rupture of Rubber. II. The Srain Concentration at An Incision," J. of Polymer Science," 18 (1955) 177.
10. B.D. Agarwal, B.S. Patro, and P. Kumar, "J Integral as Fracture Criterion for Short Fiber Composites: An Experimental Approach, Eng. Frac. Mech, 19, (1984) 675.
11. H. Ishikawa, H. Kitegawa, and H. Okamura, "J Integral of a Mixed Mode Crack and its Application," ICM 3, 3, Cambridge, England, August (1979).

PROSPECTS FOR THE APPLICATION OF NONLINEAR FRACTURE MECHANICS TO ELASTOMERS

C.F. SHIH, R.D. JAMES, M. ORTIZ, S. SURESH, J. DUFFY
Division of Er jineering, Brown University, Providence, Rhode Island 02912

Recent developments in the theoretical foundations of the phencmenological theory of nonlinear fracture mechanics are reviewed. Small and finite deformation asymptotic fields for nonlinear elastic and elastic-plastic solids together with the full-field numerical results will be discussed. We examine the relevance of these crack-tip fields (and their characterizing parameters) for correlating crack initiation and growth in elastomers.

EFFECT OF CARBON BLACK ON DYNAMIC MECHANICAL PROPERTIES OF RUBBER*

A. I. MEDALIA
Consultant, 30 Dorr Road, Newton, Massachusetts 02158

Carbon black, which is the preeminent reinforcing filler for rubber, has a profound effect on the dynamic properties of rubber; i.e., the behavior under repeated strain cycling. The nature, loading, and dispersion of the carbon black are all important in these respects. Other compositional factors include the use of different elastomers and blends, cross-link density, oil extension, and plasticizers. Important dynamic mechanical properties are elastic modulus and loss parameters, including hysteresis and heat buildup.

The effects of carbon black on the dynamic properties of rubber are of great importance in many practical applications, such as compound design for automobile passenger tires, off-the-road tires, and tank track pads.

* Based on author's paper in (1978) Rubber Chemistry and Technology, Vol. 51, p.437.

COMPRESSIVE FATIGUE OF ELASTOMERS

D. DWIGHT[1], N. LAWRENCE[1]*, L.C. LOPEZ[1], JACOB PATT[2]
(1) Department of Materials Engineering, Virginia Polytechnic Institute and State University, Blacksburg, Virginia 24060;
(2) Track and Suspension Group, U.S. Army Tank Automotive Command, Warren, Michigan 48090

Our initial studies of field failures on track pads lead to a basic research program: compressive fatigue of elastomers is carried out in a Goodrich Flexometer simulating 20 and 40 mph with and without stress raisers and with various degrees of static and dynamic strain. Specimens were prepared with controlled variations in blending conditions, cure cycles, and rubber compounding ingredients (e.g. SBR, NR and triblends, 7% to 60% carbon black, Kevlar filled, curing systems).

Analyses of the mechanothermal hysteresis behavior will be reported, together with diagnoses of fatigue micromechanisms via swelling, ESCA, and SEM.

This study was sponsored by the U.S. Army Tank Automotive Command.

*Present address: FMC Corporation, San Jose, California.

THE INFLUENCE OF CAVITATION IN THE MECHANICAL BEHAVIOR OF FILLED POLYMERS AND HEAT BUILD UP IN NONHYSTERETIC ELASTOMERS

R. J. FARRIS, R. FALABELLA
Polymer Science and Engineering Department, University of Massachusetts, Amherst, MA 01003

INTRODUCTION

The mechanical behavior of phase separated polymer blends and composites is complicated by many factors of which the formation of crazes and vacuoles appears to be the dominant factor governing the stress-strain response (1-10). Crazes and vacuoles are the result of strong local variations in stress and strain at the microstructural level. When the material is subjected to high loads, vacuoles or crazes form in the high stress regions of the microstructure and upon doing so greatly relieve the local multiaxial state of stress. In systems where these crazes cannot readily propagate, crazing will occur throughout the microstructure. Generally speaking the onset of microstructural crazing causes a volume dilatation, a loss in modulus reinforcement, and an irreversible degradation of the microstructure due to mechanical loads (1,2,6,7).

It has been generally concluded that the mechanisms of craze formation and growth are the mechanisms which distinguish the energy absorption capabilities of phase separated polymeric systems. Since most very high impact polymers are of the crazing variety, there must be some truth to these arguments. It is important to note however that over a decade ago the same reasoning was being put forth with regard to the mechanical behavior of very highly filled elastomers. It was erroneously concluded that because of the large amounts of near rigid particulate filler that these systems contained, vacuole formation and growth was to be expected and was in fact the mechanism that permitted these systems to exhibit high elongations. Years later, when experiments were conducted under high superimposed pressure (1,2), it was found that pressure greatly suppressed vacuole formation and growth and generally resulted in a marked improvement in all mechanical properties, especially the stress and energy absorption characteristics. Interestingly, in the range of strain before vacuole formation, pressure had no influence on the mechanical properties.

The main purpose of this paper is to demonstrate the striking similarity between the behavior of particulate filled polymers and phase separated polymers. The changes in mechanical properties of these materials with deformation is almost

totally dependent upon the vacuole formation process and the factors controlling this process are not that well understood. The interesting conclusion one can draw from the experiences of researchers who work with highly filled polymers is that if craze formation could be suppressed, then the mechanical properties of high impact polymers could be improved. This observation is contrary to the thoughts of many in the polymer community who believe that craze formation and growth is one of the main mechanisms leading to very high impact characteristics.

Another interesting observation is that many thermoplastics plastics that have been tested in a uniaxial tension mode in our laboratories exhibit negative volume changes in the strain region before yield. Others before have observed the same or equally confusing results and many researchers dismiss such observations as experimental errors. It is demonstrated that such observations can be real and are possible within the framework of linear elastic theory.

EXPERIMENTAL

All of the data discussed in this paper was obtained using a gas dilatometer (9) in conjunction with a standard tensile tester. These dilatometers yield simultaneous and continuous measurements of stress, strain and volume dilatation over a wide range of test conditions including strain rate, temperature and superimposed hydrostatic pressure. Stress and strain are measured in the usual manner within the dilatometer which is equipped with internal force transducers. Volume dilatation is assessed by measuring the change in pressure of the gas surrounding the uniaxial test specimen as it is deformed in a constant volume chamber. The instrument is quite accurate and only responds to changes in sample volume. Under normal operating conditions the instrument can detect changes in volume of ±.02 percent and greater accuracy can be achieved if measures are taken to control temperature and minimize the free air volume within the test cavity.

Filled Elastomers

The stress-strain-dilatational response of filled polymers is very sensitive to material factors such as particle size, filler concentration, coupling agents to enhance adhesion and

matrix modulus and strength (6). It is also sensitive to test conditions such as strain rate, temperature, and stress field. Generally speaking any modifications to the material that will reduce vacuole dilatation, such as reducing the particle size, greatly improves the properties of these materials (6). Figure 1 illustrates the behavior of three highly filled elastomers. From this data it is clear that yielding or stress softening is a direct result of volume dilatation caused by the formation and growth of vacuoles. The effect of superimposed pressure on the stress-strain volume dilatation properties are shown in Figure 2 and 3 for another highly filled rubber based solid propellant for two different strain rates. These data clearly demonstrate that reduction in vacuole formation and growth via high pressure greatly improves their mechanical properties, especially strength and strain energy to rupture. With these low modulus composites, high pressure acts like a super bonding agent and does not allow for much vacuole formation.

Vacuole dilatation information itself is not simply interpreted. The data instead are best understood through models of microstructural failure (1). Assuming a single size of spherical filler particles encompassed by elliptically shaped voids that form arbitrarily in strain, and once formed grow at a constant rate with further deformation, then one can readily separate vacuole growth from vacuole formation. Models such as the one described above have been substantiated by microscopic studies. The solution of such models (1) indicates that the first derivative of vacuole dilatation with respect to

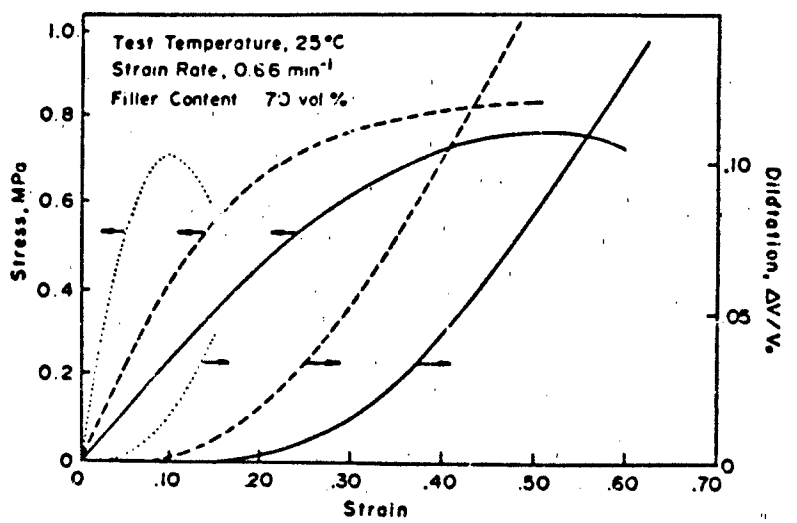


FIGURE 1. Stress-strain dilatational behavior of three highly filled elastomers.

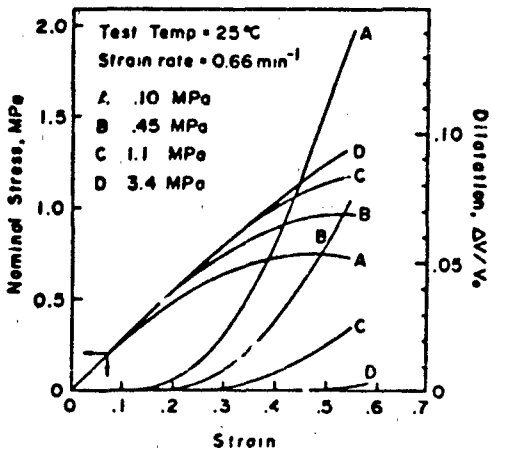


FIGURE 2. Stress-strain dilatational behavior of a 63.5 vol % filled elastomer at a series of hydrostatic pressures.

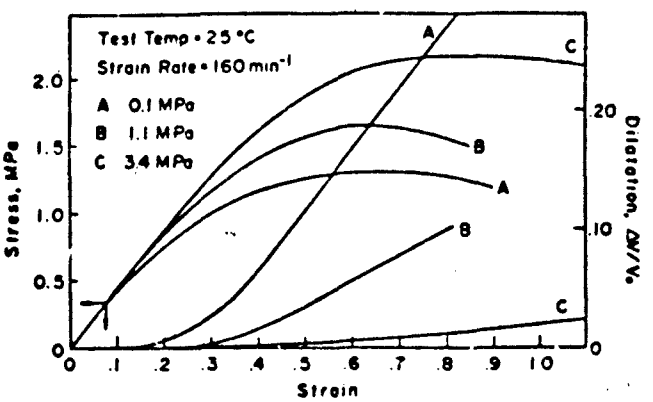


FIGURE 3. Stress-strain dilatational behavior of a 63.5 vol % filled elastomer at a series of hydrostatic pressures at a high strain rate.

strain, ε, is directly proportional to the cumulative number of vacuoles per unit volume, n, that exist at any strain. The second derivative is then directly proportional to the instantaneous frequency distribution of vacuole formation. These two results can be expressed mathematically as

$$n = c\,\frac{d(\Delta V/Vo)}{d\varepsilon} \qquad (1)$$

$$\frac{dn}{d\varepsilon} = c\,\frac{d^2(\Delta V/Vo)}{d\varepsilon^2} \qquad (2)$$

Figure 4 illustrates the typical volume dilatation-strain behavior along with the first and second derivatives. Clearly these measures are realistic in that the derivatives do take on the character of cumulative and instantaneous frequency distributions. Similar models can be constructed to relate the loss in stiffness to the number of vacuoles that have formed resulting in very simple but accurate stress-strain relations (1).

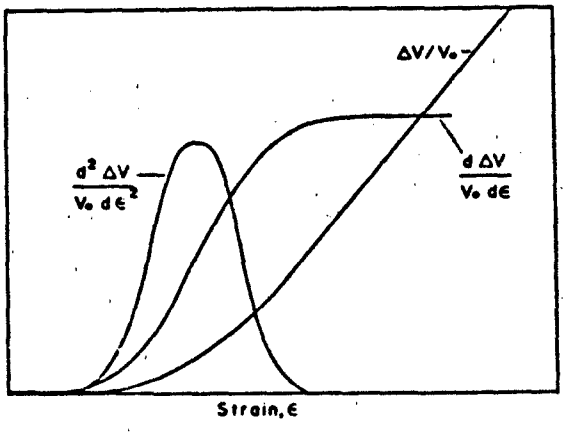


FIGURE 4. Schematic of the dilatation-strain relationship and its first and second derivatives.

Phase Separated and Filled Thermoplastics

Data similar to that obtained on highly filled elastomers was recently taken on a variety of thermoplastics. These data are illustrated in Figure 5 for a particulate filled polyethylene with and without a bonding agent. Figure 6 and 7 illustrate similar data for an ABS polymer with and without chopped glass fiber reinforcement. Additional data on nylon and polypropylene, Figures 8 and 9, has been obtained and

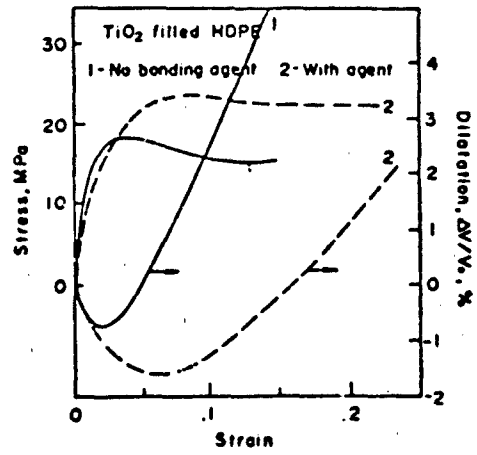


FIGURE 5. Stress-strain dilatational behavior of a filled high-density polyethylene with and without a coupling agent.

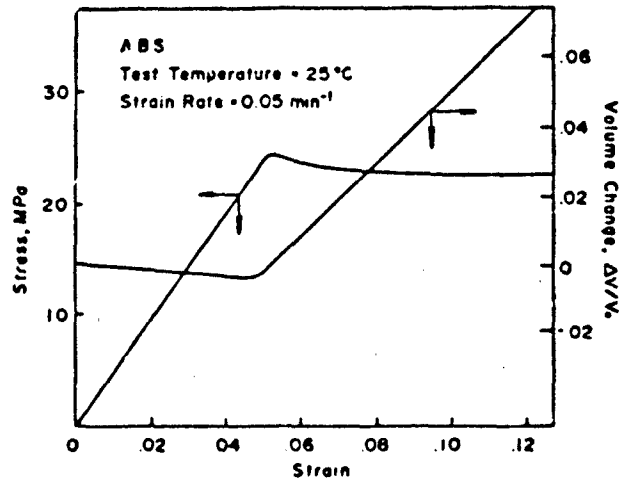


FIGURE 6. Stress-strain dilatational behavior of ABS.

several other polymeric systems also show similar results in that yielding is caused by cavitation of the microstructure. These data were all obtained using injection molded samples provided by the polymer manufacturer. In every situation using these samples negative volume changes have been observed prior to yielding followed by a sudden increase in volume rate at yield. The instrument was checked several times and it

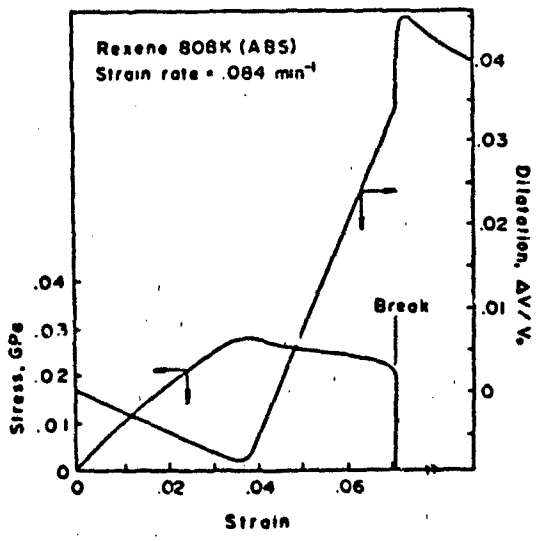


FIGURE 7. Stress-strain dilatational behavior of filled ABS.

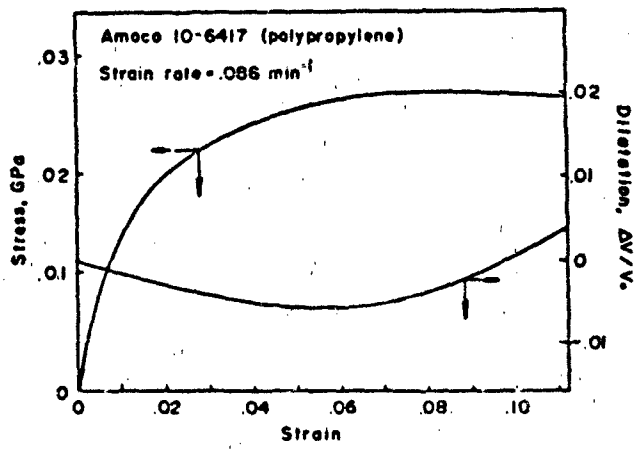


FIGURE 8. Stress-strain dilatational behavior of nylon.

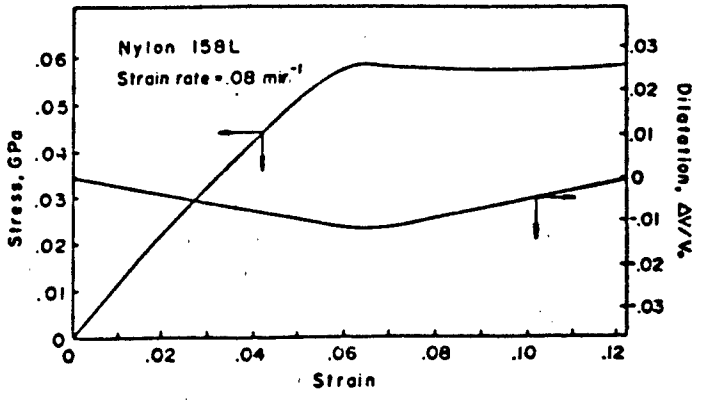


FIGURE 9. Stress-strain dilatational behavior of polypropylene.

demonstrated no sensitivity to load or stroke. After determining that these negative volume changes were real it was thought that the effect could be induced by the method of gripping the samples. However, considerable variations in gripping methods showed no significant change in the observations. Consequently, the effect is considered real and a logical explanation must exist. The only possible explanation considered that is consistent with all of our observations is that of anisotropic behavior. The reason most people dismiss such observations to "poor experimental technique" is that they restrict their thinking to isotropic linear elasticity wherein such observations are impossible and a contradiction to theory. With that interpretation these data would yield a value for Poisson's ratio greater than 0.5, which is of course impossible for an isotropic linear solid. The restrictions on Poisson's ratio in elasticity theory come about by imposing a positive definite strain energy requirement, that is if the body is in a deformed state it must possess a finite positive strain energy density. For a linear elastic isotropic solid the constitutive equation can always be expressed as

$$\begin{bmatrix} \varepsilon_1 \\ \varepsilon_2 \\ \varepsilon_3 \end{bmatrix} = \frac{1}{E} \begin{bmatrix} 1 & -\upsilon & -\upsilon \\ -\upsilon & 1 & -\upsilon \\ -\upsilon & -\upsilon & 1 \end{bmatrix} \begin{bmatrix} \sigma_1 \\ \sigma_2 \\ \sigma_3 \end{bmatrix} \qquad (3)$$

where ε_i = principal strains
σ_i = principal stresses
E = Young's modulus
υ = Poisson's ratio

For the energy to be positive definite the compliance matrix must satisfy certain conditions which can be summarized as follows

(a)every diagonal element must be greater than zero

(b)the determinant of each submatrix remaining when the row and columns containing a diagonal element are deleted must be positive

(c)the determinant of the compliance matrix must be positive.

For an isotropic linear elastic solid the first condition is automatically satisfied since each diagonal element is unity. The second condition results in three identical equations

$$1 - \upsilon^2 > 0 \quad \text{or} \quad -1 < \upsilon < 1 \tag{4}$$

The final condition yields a stronger constraint

$$1 - 3\upsilon^2 - 2\upsilon^3 > 0 \quad \text{or} \quad -1 < \upsilon < 1/2 \tag{5}$$

In a uniaxial tensile test the volume dilatation simply becomes

$$\Delta V/Vo = \frac{\sigma}{E}(1 - 2\upsilon), \tag{6}$$

which demands that the stress and dilatation have the same sign if υ is to be no larger than 0.5.

Using identical methods one can write the stress-strain equation for an orthotropic linear elastic solid in terms of the principal values of stress and strain as

$$\begin{bmatrix} \varepsilon_1 \\ \varepsilon_2 \\ \varepsilon_2 \end{bmatrix} = \begin{bmatrix} C_{11} & C_{12} & C_{13} \\ C_{12} & C_{22} & C_{23} \\ C_{13} & C_{23} & C_{33} \end{bmatrix} \begin{bmatrix} \sigma_1 \\ \sigma_2 \\ \sigma_3 \end{bmatrix} \tag{7}$$

where the compliance matrix must be symmetric if the state of strain energy is to be unique and only a function of the final state of stress and strain.

In order to have a positive definite strain energy density the conditions cited above demand that

$$\begin{aligned}
&\text{(a) } C_{11},\ C_{22},\ C_{33} > 0 \\
&\text{(b) } C_{11}C_{22} - C_{12}^2 > 0 \\
&\text{(c) } C_{11}C_{33} - C_{13}^2 > 0 \\
&\text{(d) } C_{22}C_{33} - C_{23}^2 > 0 \\
&\text{(e) } C_{11}C_{22}C_{33} + 2C_{12}C_{23}C_{13} - C_{22}C_{13}^2 - C_{33}C_{12}^2 - \\
&\qquad C_{11}C_{23}^2 > 0
\end{aligned} \tag{8}$$

The volume change in a uniaxial tensile test for the orthotropic case simply becomes

$$\frac{\Delta V}{V_o} = (C_{11} + C_{12} + C_{13})\sigma \tag{9}$$

In order to have negative volume changes in a tensile test one must require that

$$C_{11} + C_{12} + C_{13} < 0 \text{ if } \frac{\Delta V}{V_o} < 0 \text{ when } n > o \tag{10}$$

Therefore equation 8 must be satisfied to yield a valid constitutive equation from an energy perspective and equation 10 must be satisfied to yield the experimental observations. It can be shown that the conditions of equations 8 and 10 can be met, however the proof is a tedious algebraic problem. An indirect proof by example is just as valid since if these conditions are met there are no other restrictions that can be

imposed from a thermodynamic point of view. Consider the compliance matrix

$$C_{ij} = \begin{pmatrix} 1 & -.7 & -.7 \\ -.7 & 3 & -.2 \\ -.7 & -.2 & 3 \end{pmatrix} \qquad (11)$$

This matrix clearly satisfies all our conditions yet yields a value of Poisson's ratio of 0.7 and strong negative volume changes in a tensile test. Consequently small amounts of anisotropy can result in negative dilatation. It is believed that the anisotropy is caused by the orientation of the melt and subsequent rapid cooling in these injection molded samples, which are known to contain orientation and residual stress effects.

With the exception of the negative volume changes prior to cavitation the behavior illustrated in Figures 5 through 9 for thermoplastics are remarkably similar to that observed in filled elastomers where vacuole dilatation is known to lower the properties of the composite material. These data indicate that if vacuole dilatation could be minimized, the strain energy characteristics to rupture could be increased resulting in an improvement of impact properties. What factors control the vacuole process in incompatible polymer blends or semicrystalline polymers is not known; however, the effect should be strongly dependent upon the sizes and concentrations of each phase and the coupling between phases in a manner similar to that observed with filled elastomers. It would appear that systematic dilatational studies on these systems could shed considerable light on the mechanisms leading to high impact performance.

Energy Dissipation in Polymeric Materials

The measurement of stress and strain provides valuable information about the deformation processes in polymers; however, this conjugate variable pair is but one of several thermodynamic variables of fundamental interest. A corresponding measurement of the heat of deformation as well as the work enable one to calculate internal energy changes for

deformation using the first law of thermodynamics. It seems likely that internal energy changes during deformation would be extremely sensitive to both morphological and molecular changes.

One of the first people to recognize the importance of deformation calorimetry was F.H. Muller who, with A. Engelter, introduced a new method of measuring heat flow during solid deformation (12). This deformation calorimeter consisted of a constant volume sealed sample chamber and sensor which compared pressure in this chamber to the pressure in a reference chamber. The pressure change due to heat flow during deformation was compensated by an electrical heat generated in the reference chamber. Similar instruments were constructed by Morbitzer, et al.(13) and Foster and Benner (14). An alternate type of deformation calorimeter is based on the Tian-Calvet principle. This instrument operates by measuring temperature differences between the calorimeter inner and outer walls and relating these temperature differences to heat fluxes. The total heat may be calculated from heat fluxes. Instruments of this type have been constructed by Godovskii (15), Andrianova (16) and Hohne and Killian (17). A novel deformation calorimeter was developed in this laboratory to measure the thermodynamic quantities for the deformation of various polyurethane elastomers. The motivation for the thermodynamic measurements on polyurethanes was the use of these substances as the working material in a rubber heat engine. These detailed studies were done by Lyon (18-21).

When materials are deformed, the work required to deform the material goes into changing the material's kinetic energy, heat and changes in internal energy. In most materials, that portion of the work that does not go into kinetic energy eventually appears as heat and no internal energy change is observed. This observation is especially true in materials capable of large amounts of energy disipation such as liquids and the plastic deformation of metals. Similar observations hold for ideal rubbers and viscoelastic phenomena. There is essentially no limit to the amount of energy these materials can dissipate, provided the heat is transferred to the surroundings to eliminate the possibility of thermal degradation. There is also no real limit to the strain capabilities of soft metals which can be drawn almost endlessly. So-called polymeric thermoplastics are really not "plastic" in the sense that metals are plastic in that, in metals, a real "flow" is achieved and all the dissipation is released as heat. Polymeric thermoplastics, unlike fluids, metals undergoing plastic deformation and viscoelastic materials do not readily convert work into heat. One observes that, with both semi-crystalline and amorphous thermoplastics, 30 to 50% of the work

of deformation does not get released as heat and consequently must change the material's internal energy. These changes in internal energy at constant temperature really reflect changes in the make-up of the material. Factors that can change the internal energy are changes in crystallinity or crystal type, primary or secondary bond rupture, and latent free energy. Unlike energy disssipated as heat, there would appear to be limits to the amount one can change the internal energy.

With thermoplastic elastomers the problem is more complex. The hard segments that phase separate and form either crystalline or glassy physical crosslinks are really thermoplastics and can be plastically deformed and can yield large changes in internal energy. This problem of flow of the hard segments is pronounced at high stress levels and elevated temperatures. Hence, if normal dissipation leads to heat build-up, hard segment flow and internal energy changes are likely. If thermoplastic elastomers are to behave like crosslinked elastomers over a broad range of conditions, especially those involving energy dissipation, it is important that they behave similarly to crosslinked elastomers, namely, no large changes in internal energy. By contrasting the thermodynamics of deformation of these thermoplastic elastomers with crosslinked elastomers as a function of stress level, strain and temperature, one can better assess just how these materials dissipate energy and how the chemical structure influences such behavior.

The first law of thermodynamics when written in differential form applies only to smooth or continuous stresses and deformations. Shocks are not included in this type of derivation. There are special types of dissipation that are available in shock or wave motion and can occur in purely elastic materials such as gases or elastomers. For example, in the free expansion of an ideal gas, no work is done and no heat is transferred. Consequently, if one repeatedly compresses a gas adiabatically and expands it freely, the temperature will rise without limit. One puts in work during the compression raising the internal energy, and the internal energy remains unchanged during the free expansion. Hence, the internal energy is raised with each cycle. For such mechanisms to be of importance, the material must be capable of storing large amounts of mechanical energy. Gases and elastomers are about the only two classes of materials in this category and are capable of storing hundreds of times more energy than other materials. Any mechanisms leading to shocks or free contractions in a material can lead to heating that cannot be explained by normal viscoelastic arguments. Such mechanisms are possible in belts and tires and possibly tank pads. Analyses of this type of problem should be pursued and related to the performance of elastomeric treads.

REFERENCES

1. R.J. Farris, Trans. Soc. Rheol. 12, 308 (1968).
2. R.J. Farris, Trans. Soc. Rheol. 12, 315 (1968).
3. T.L. Smith, Trans. Soc. Rheol. 3, 113 (1959).
4. F.R. Schwarzl, "On the Mechanical Properties of Unfilled and Filled Elastomers", MECH. AND CHEMISTRY OF SOLID PROPELLANTS, Proc. 4th. Symp. Naval Structural Mechanics, Pergamon Press, New York, 1965.
5. A.E. Oberth and R.S. Bruenner, Trans. Soc. Rheol. 9, 165 (1964).
6. A.E. Oberth, Rubber Chem. Technol. 40, 1337 (1967).
7. R.J. Farris, "The Stress-Strain Behavior of Mechanically Degradable Polymers," in POLYMER NETWORKS: STRUCTURAL AND MECHANICAL PROPERTIES,ed. A.J. Chompff and S. Newman, pp. 341-394, Plenum, New York, 1971.
8. W.M. Hess and F.P. Ford, Rubber Chem. Technol. 36, 1220 (1963).
9. R.J. Farris, J. Appl. Polym. Sci. 8, 25 (1964).
10. H.F. Schnippel, Ind. Eng. Chem. 12, 33 (1920).
11. L.C. Cessna, Polym. Eng. Sci. 14, 697 (1974).
12. F.H. Muller and A. Engelter, Rheol. Acta, 1, 39 (1985).
13. L. Morbitzer, G. Mentze and R. Bonart, Moll. Z.Z. Polym., 216/217, 137 (1967).
14. M.O. Foster and R.E. Benner, Proc. Fourth Int. Cong. Rheol., Part 2, 121 (1965).
15. Yu K. Godovskii, G.L. Slonimskii and V.F. Alekseyev, Polymer Science U.S.S.R., 11(5), 1345 (1969).
16. G.P. Zndrionova, B.A. Arutyunov, Yu V. Popov., J. Polym. Sci., Polym. Phys. Ed., 16, 1139 (1978).
17. G.W.H Hohne, H.G. Killian and P. Trogele, Thermal Analysis, Vol. II, 955, B. Miller, ed., John Wiley and sons, New York (1982).
18. R.E. Lyon, D.X. Wang, R.J. Farris and W.J. MacKnight, J. Appl. Polym. Sci. and Eng., 29, 2859 (1984).
19. R.E. Lyon and R.J. FArris, Polym. Sci. and Eng., 24, 908 (1984).
20. R.E. Lyon, "Thermodynamics of Deformation," Ph.D. Dissertation, University of Massachusetts, Amherst, MA (1985).
21. R.E. Lyon, R.J. Farris and W.J. MacKnight, J. Polym. Sci., Polym. Lett. Ed., 21, 323 (1983).

ACKNOWLEDGEMENTS

The authors wish to express their appreciation to the Materials Research Laboratory of the University of Massachusetts, Amherst, MA 01003.

COMPUTER MODELING OF TANK TRACK ELASTOMERS

D. R. LESUER, A. GOLDBERG
Lawrence Livermore National Laboratory
Livermore, CA 94550

J. PATT
U. S. Army Tank Automotive Command
Warren, MI 48090

ABSTRACT

Computer models of the T142, T156 and the British Chieftain tank tracks have been studied as part of a program to examine the tank-track-pad failure problem. The modeling is based on the finite element method with two different models being used to evaluate the thermal and mechanical response of the tracks. Modeling has enabled us to evaluate the influence of track design, elastomer formulation and operating scenario on the response of the track. The results of these analyses have been evaluated with experimental tests that quantify the extent of damage development development in elastomers and thus indicate the likelihood of pad failure due to "cutting and chunking." The primary characteristics influencing the temperatures achieved in the track are the heat-generation rate and the track geometry. The heat-generation rate is related to the viscoelastic material properties of the elastomer, track design and loading/operating scenario. For all designs and materials studied stresses produced during contact with a flat roadway surface were not considered large enough to damage the pad. Operating scenarios were studied in which the track pad contacts rigid bars representing idealized obstacles in cross country terrain. A highly localized obstacle showed the possibility for subsurface mechanical damage to the track pad due to obstacle contact. Contact with a flat rigid bar produced higher tensile stresses that were near the damage thresholds for this material and thus capable of producing cutting and chunking failures.

INTRODUCTION

Computer modeling of tank tracks can provide significant insight into the field response of track. Lawrence Livermore National Laboratory (LLNL) has been involved in a study of the tank track-pad-failure problem for the U. S. Army Tank-Automotive Command. The problem is one of limited service life and high replacement costs associated with the premature failure of the pads. A portion of this study has involved developing finite element models. Two different models were studied. One is a mechanical model in which the solid

mechanics response of the track in typical operating scenarios can be evaluated. From the results of this analysis, we typically examine the stresses and the irreversible mechanical work done in various rubber portions of the track. The second is a thermal model in which the temperatures developed during vehicle operation are determined.

Both models were generated and analyzed using finite element codes developed at LLNL. Our purpose here was to apply these codes to the track-pad-failure problem. The primary codes used in this study were NIKE2D and TACO2D. NIKE2D is a two-dimensional finite deformation code[1] that solved the mechanics problem represented by the mechanical model. TACO2D is a two-dimensional finite element heat transfer code[2] used in the thermal modeling.

The NIKE2D code has a number of features that make it particularly suitable to the study of track problems. One of these features is the slideline capability that permits accurate modeling of material contact problems. Such a capability is highly desirable in track problems in that the weight of the tank is transferred to the track by means of a rolling roadwheel; and, modeling the interaction between a track pad and the terrain is of critical importance. Another feature is that the code is non-linear and is capable of solving finite strain problems associated with the deformation of the rubber portions of the track.

The computer models of track can be used to study the influence of design and material changes on the track-pad-failure problem. It also can be used to evaluate the influence of track operating parameters (such as operating scenario and vehicle weight) on the problem. The methodology that was used is shown schematically in Figure 1. The track design, material properties, and characteristics of the operating scenario are represented in the models and are inputted into the codes. The results of the finite element analyses are examined primarily for the stresses, temperatures, and irreversible mechanical work done. The irreversible mechanical work can be used to calculate the heat-generation rate for rubber elements in the track. The heat-generation rate, in turn, is one of the input quantities for the thermal code.

Tank track pads are known to fail by a number of different mechanisms. In one of the most common, known as cutting and chunking, the initiation and propagation of cuts causes small pieces of rubber to be torn from the track pad. The failure evaluations discussed in this report address this failure mode. The temperatures and stresses predicted by the models together with these failure evaluations can be used to determine the likelihood of pad failure.

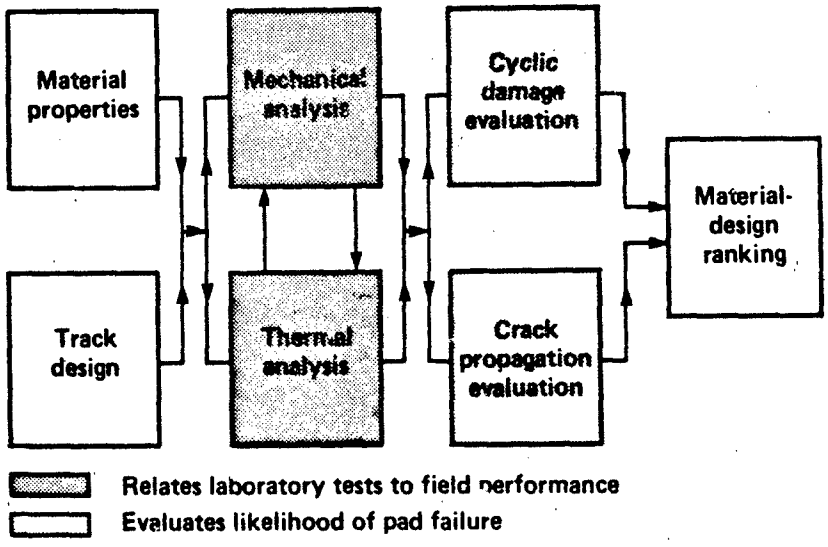


FIGURE 1. Methodology used to study the track pad failure problem.

MECHANICAL MODEL

Both thermal and mechanical models for all track designs studied were based on a cross section of track. The shoe and relevant sections of the T142 track are shown in Figure 2. The mesh, boundary conditions and slidelines used in this problem are shown in Figure 3. Notice that the roadwheel and the road surface are incorporated into the model. A frictionless slideline was used between the roadwheel and roadwheel path. This permitted the rolling of the roadwheel to be simulated by frictionless sliding. The weight of the tank is applied to the track through this roadwheel which then rolls across the track section. The roadwheel traverses the track section three times so as to achieve a steady-state hysteresis loop representative of multiple roadwheel passes. The tension placed on the modeled section of track by neighboring sections was also represented as shown in Figure 3. A slideline was placed between the bottom of the pad and a rigid flat surface to realistically represent contact with a roadway.

The stress-strain behavior of the elastomer was represented by the linear viscoelastic material model contained in NIKE2D. In this material model the shear behavior is considered to be viscoelastic and is derived from a three element standard linear solid. The bulk behavior is considered to be elastic. The suitability of this material model has been evaluated for the large strain problems encountered in this study[3]. The model does have limitations. However it can provide a reasonable engineering representation of the stress-strain behavior for reinforced rubber subject to large deformation in a primarily

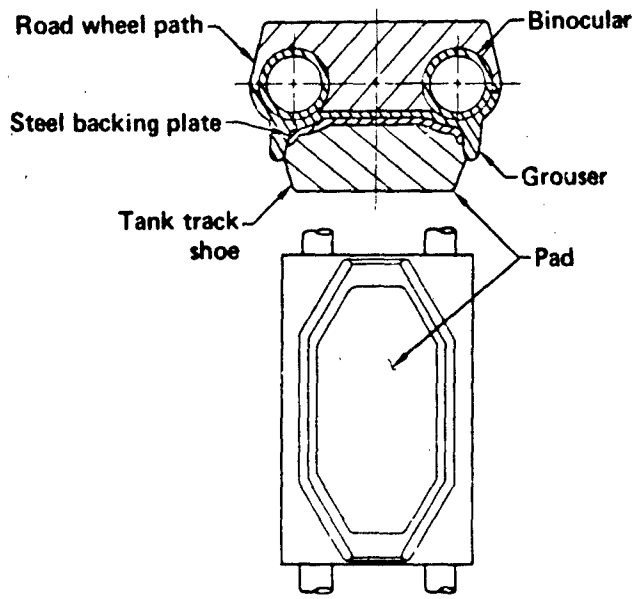


FIGURE 2. Shoe and relevant sections of the T142 track. Thermal and mechanical models were based on a cross section of track.

compressive strain field provided the material parameters are evaluated at the strain range and loading frequency of interest. Material parameters were evaluated from rubber cylinders that were loaded in compression in a cyclic manner in a servo-hydraulic test system. Three different elastomer formulations were tested and evaluated in the modeling work reported in this paper. Two of the elastomers were obtained from commercial track pads -- a T142 track pad and a softer formulation from a T156 track pad. We also evaluated the response from a very stiff elastomer containing 35 weight percent (62.9 phr) carbon black. The formulation for this material has been given previously[4]. Linear elastic behavior was assumed for all metal components of the track.

THERMAL MODEL

In the thermal model, heat transfer was considered to occur in the track section under study (as shown in Figure 2). Because of the high length to width ratio of the track pad and the poor thermal diffusivity of rubber, heat losses at the end of the pad have relatively little influence on temperatures in interior sections. Thus, for interior sections, heat flow occurs only in the plane section under study. We

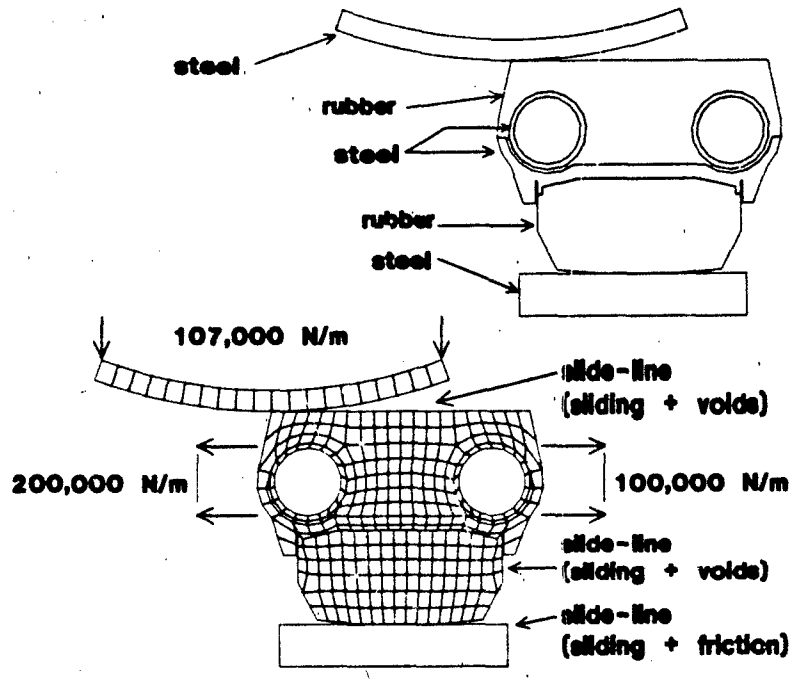


FIGURE 3. Mesh, boundary conditions and slidelines used in the mechanical model of the T142 track.

have found that boundary conditions can be represented well by convective heat transfer at all external surfaces of the track. The convective film coefficient was obtained from surface temperature-time measurements made in the field on a moving M60 tank[5].

Thermal properties (density, heat capacity, thermal conductivity) were determined from experimental tests. The heat-generation rate also needs to be used in the thermal model. It was obtained for each element from the mechanical work done as determined from the mechanical model. The most suitable approach for studying this problem would use coupled thermal and mechanical codes in which an update on material properties for both codes (in this case primarily the viscoelastic properties and the heat-generation rate) is done as the problem is run. However, coupled codes did not exist at the time; thus, we took advantage of two physical characteristics of this problem in obtaining a solution. The first is that the temperature in a cyclically loaded track pad rises very slowly (requiring more than 1.5 hours to

reach steady state); thus, the temperature of the rubber experiences virtually no change during the loading and unloading process. The second characteristic is that the viscoelastic material constants decrease with increasing temperature and change very little above 100° C. Thus, we assumed that when all rubber elements of the track are above 100° C there is no change in mechanical response and, therefore, no change in heat-generation rate. Therefore, we evaluated the mechanical model (and the heat-generation rates for each element) at ambient temperature and 100° C. The heat-generation rate for each element is assumed to vary in a linear fashion with temperature between these two temperatures. It is assumed to be constant above 100° C. Analysis for temperature build-up in the thermal model was done for a speed of 20 mph. Additional details can be found in reference 6.

OPERATING SCENARIO STUDIES

We evaluated the response of the T142 track pad upon contact with a flat rigid surface (roadway) and two different rigid localized obstacles. Results for the flat surface scenario are shown in Figure 4 for two different temperatures of operation, 25° C and 100° C. Material constants were obtained from the rubber in a T142 track pad. In both cases all elements were given properties determined at the particular temperature. The 100° C study represents the correct mechanical response if all elements are at 100° C or above, since, as noted before, the viscoelastic mechanical properties of the material studied show little change above 100° C.

Results of the mechanical model are presented primarily in terms of maximum principal stress; and either damage development or failure is examined assuming a maximum principal stress criterion. Contour plots in Figure 4 show that the maximum principal stresses are not strongly influenced by temperature. The Mohr's circle in Figure 4 shows the state of stress at point x for the 25° C case. Stresses are small with no tensile stresses being present. Thus, as observed in field-tested T142 track pads, cutting and chunking failures are not expected during vehicle operation on a paved surface.

One of the more important quantities that can be calculated in the analysis of any track model is the work done. This quantity represents the strain energy stored in the rubber which can be used to calculate the heat-generation rates for individual rubber elements. Contour plots of the work done at two different locations of the roadwheel are shown in Figure 5. The value of these plots is that they show where the maximum energy is stored. They also provide an indication of how the heat generation rate varies throughout the pad. Actual contour plots of heat generation rate are not available. The heat-generation rate is a maximum within the track pad underneath the binocular tube.

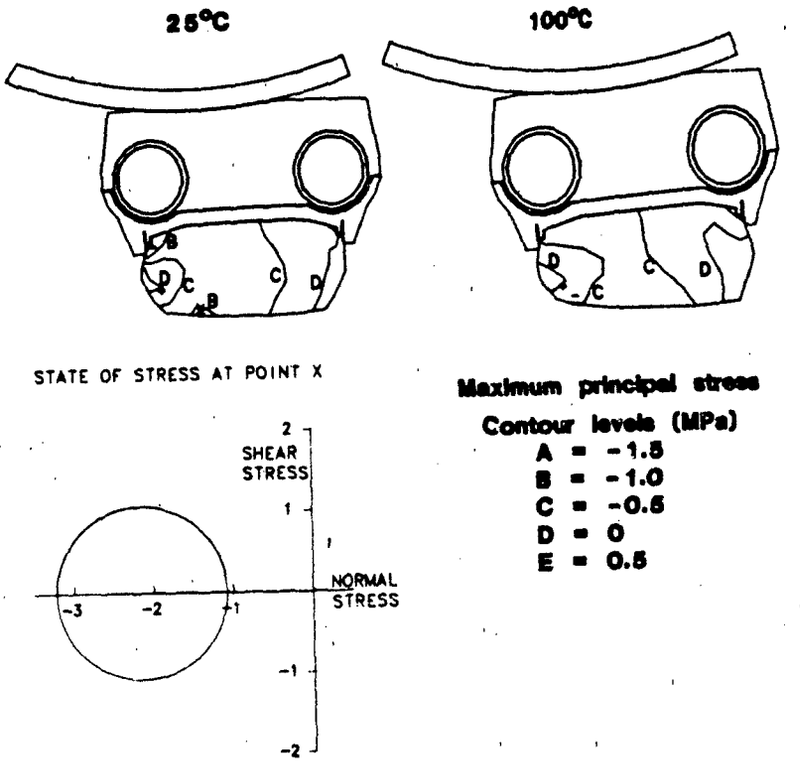
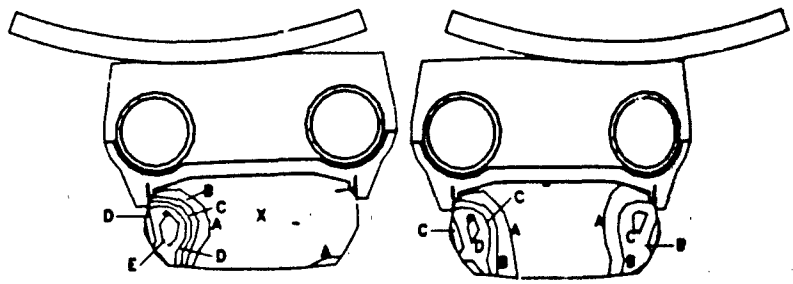


FIGURE 4. Contours of maximum principal stress for the T142 track during contact with a flat roadway surface. Results are given for two different operating temperatures, 25° C and 100° C. The Mohr's circle shows the state of stress at point "x".



Contour levels ($Nm/m^3 \times 10^6$)

A = .04
B = .08
C = .12
D = .16
E = .20

FIGURE 5. Contour plots of work done for the T142 track at two different locations of the roadwheel.

Temperature contours developed in the T142 track after 1.7 hours of continuous operation on a paved roadway are shown in Figure 7. The interior regions of the pad achieved temperatures that were over 50° C hotter than those at the surface. The maximum temperature was 152° C whereas surface temperatures were about 100° C. In our first studies of the thermal model[5], heat generation rates were obtained from field data. Surface and internal pad temperatures were measured on a T142 track operated at constant velocity on a paved course. Results are shown in Figure 8. Thermal model calculations predicted a temperature-time response that was within 6° C of the temperature-time response measured in the field.

Obstacle scenarios studied contact between the T142 track pad and two different rigid bars that represent idealized obstacles which might be encountered in cross country terrain. Both studies were done in plane strain assuming the weight of the vehicle was uniformly distributed among the 24 roadwheels. Figure 9 shows the results for a bar providing highly localized contact with the track pad. Examination of contours for maximum principal stress shows that tensile stresses are produced in this operating scenario and that the largest stresses are produced in the interior of the track pad. Figure 9 also shows the state of stress in the region where the tensile stress is largest. A comparison with the state of stress produced during contact with a rigid roadway surface shows that for this obstacle-contact scenario the shear stress and maximum principal stress are significantly larger than those for

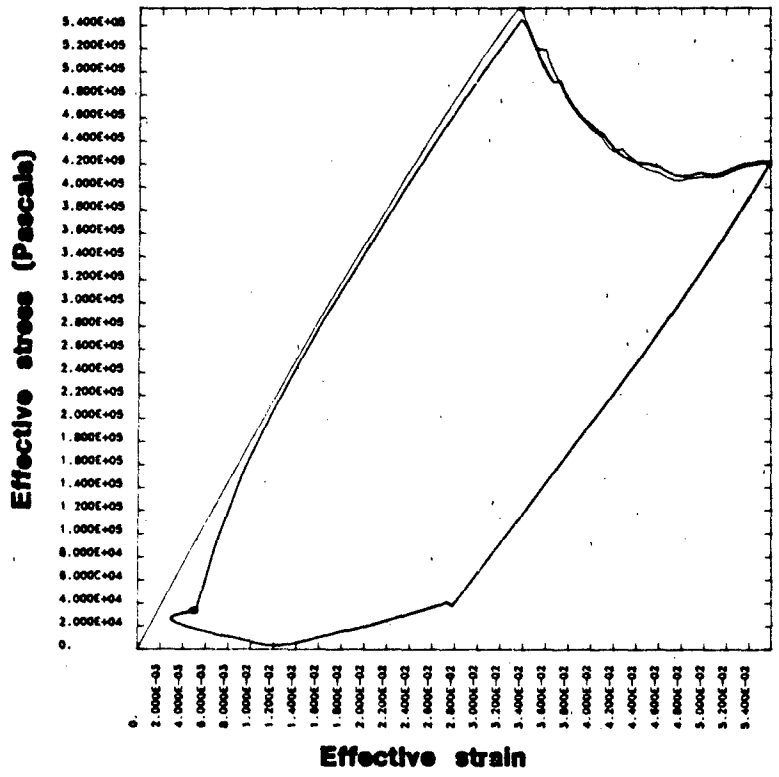


FIGURE 6. Effective stress versus effective strain curve for an element at point "x" shown in Figure 5. The strain energy density dissipated as heat is equal to the area within the loops.

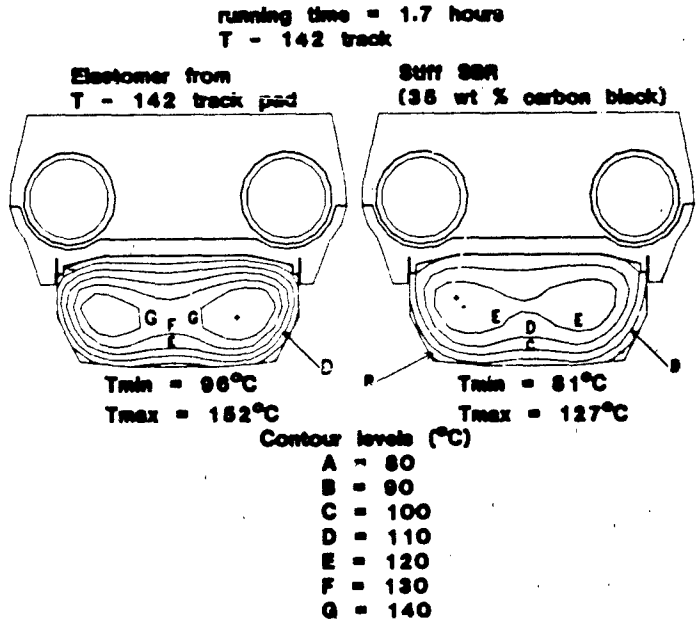


FIGURE 7. Contour plots of temperature for the T142 track after 1.7 hours of continuous operation on a paved course. Results are given for two different elastomers.

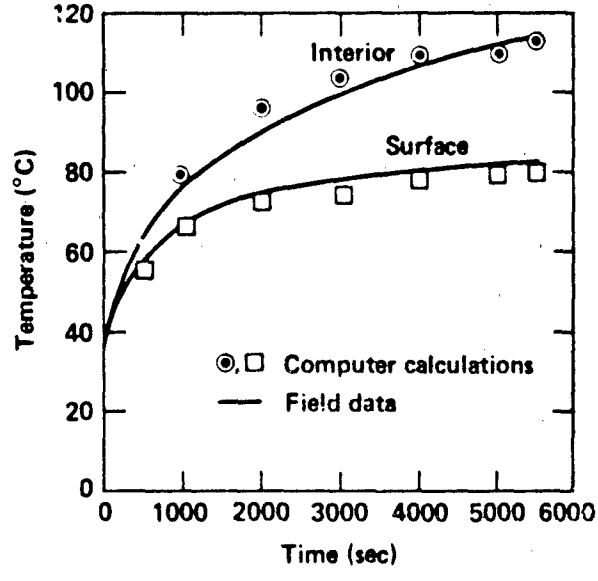


FIGURE 8. Temperature-time response for surface and internal locations of the T142 track. Solid curve is derived from field data; individual points are derived from the thermal model.

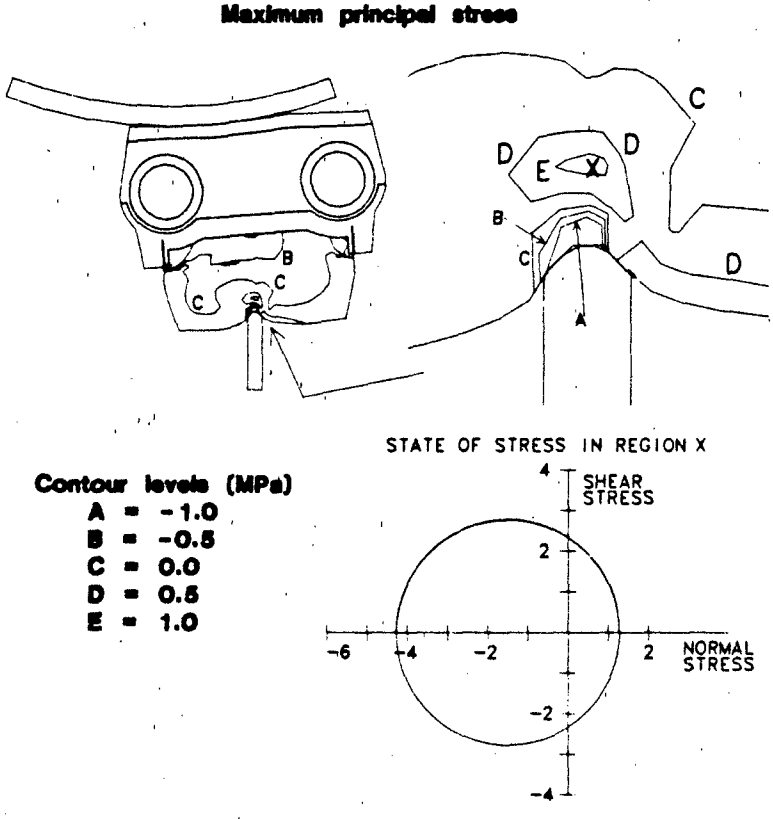


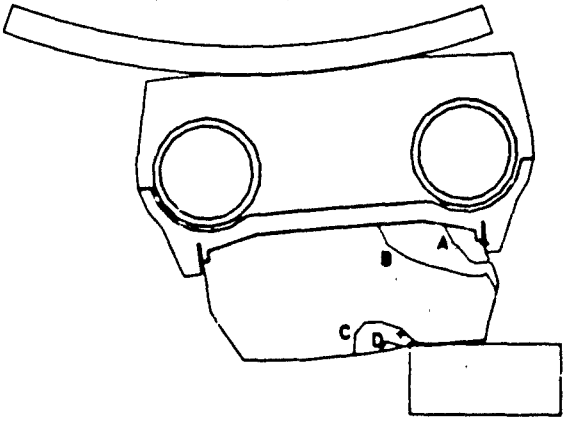
FIGURE 9. Contours of maximum principal stress for the T142 track contacting a rigid bar. State of stress at point "x" is indicated by the Mohr's circle.

road contact. As we will see in the final section of this paper the tensile stresses do not exceed identifiable damage thresholds. However the results do show the possibility for subsurface mechanical damage to the track pad during contact with highly localized rigid obstacles.

We also analyzed the problem of the T142 track contacting a bar of rectangular cross section. Results are shown in Figure 10. Tensile stresses are produced in this operating scenario. However they are larger than in the previous example (Figure 9) with the largest stresses being produced near the surface of the pad. These tensile stresses also increase somewhat as the roadwheel runs across the track which is consistent with field observations. As we will see in a later section these stresses are near the damage thresholds for this material and thus are capable of producing cutting and chunking failures.

TRACK DESIGN STUDIES

Three widely different track designs that are currently being used on heavy tanks were studied using the computer modeling methodology. In addition to the T142 track discussed above we studied



Maximum principal stress

Contour levels (MPa)
A = -1
B = 0
C = 1
D = 2

FIGURE 10. Contours of maximum principal stress for the T142 track contacting a rigid bar of rectangular cross section.

the track used on the British Chieftain tank and the T156 track which is currently used on the U.S. Army M1 tank. Analyses of these design changes and the material changes (described in the next section) were made for the track striking a flat, rigid roadway surface. In Figure 11 we compare the contours of maximum principal stress for the three track designs. For both the British Chieftain and the T156 track material constants used in the analyses were derived from rubber samples obtained from a T156 track shoe. Stress distribution and contour levels are very similar in all three designs and we would expect little chunking or damage to be produced in the track pad. The big and significant difference between the different designs is in the heat-generation rate. The heat-generation rates were highest in the T156 track and lowest in the British Chieftain.

The heat-generation rates had a strong effect on the temperatures developed in the track. Contour plots showing temperatures developed in the T156 and British Chieftain tracks after 1.7 hours are given in Figures 12 and 13, respectively. Results for all three designs are summarized in Table 1. We also examined the ability of two track designs to dissipate heat. This was done by evaluating the thermal models for the T156 and British Chieftain with the same heat generation rate for all elements. As expected, maximum temperatures

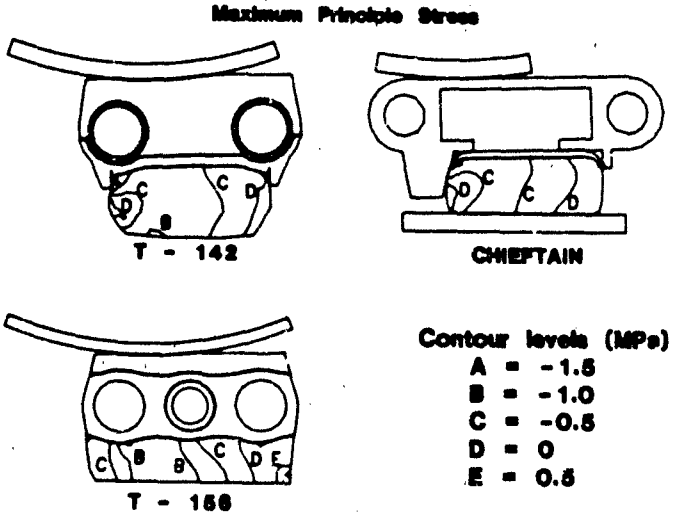


FIGURE 11. Contours of maximum principal stress for the three track designs studied.

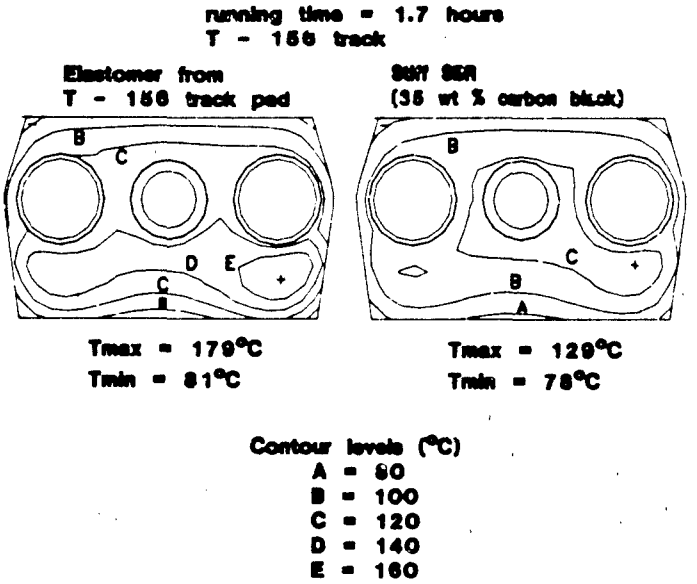


FIGURE 12. Contour plots of temperature for the T156 track after 1.7 hours of continuous operation on a paved course. Results are given for two different elastomers.

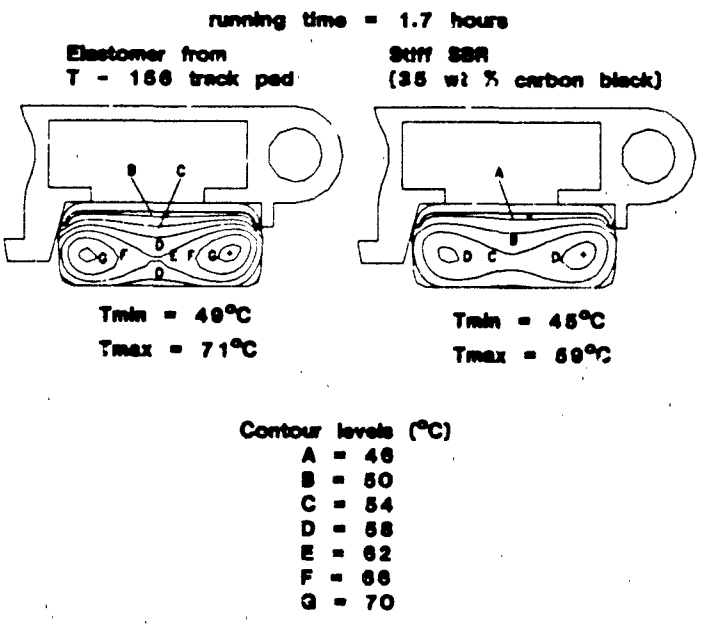


FIGURE 13. Contour plots of temperature for the British Chieftain track after 1.7 hours of continuous operation on a paved course. Results are given for two different elastomers.

in the T156 track were higher (by approximately 30° C) than those in the British Chieftain track. This is due to the thicker rubber sections in the T156 track which causes a longer thermal path.

TABLE I

MAXIMUM AND MINIMUM TEMPERATURES PRODUCED IN TRACK WITH DIFFERENT ELASTOMERS

ELASTOMER	TRACK T156 Max. Temp	T156 Min. Temp	T142 Max. Temp	T142 Min. Temp	British Chieftain Max. Temp	British Chieftain Min. Temp
Laboratory Formulation Containing 35 Weight Percent Carbon Black	129*	78	127	81	59	45
Elastomer From T142 Track Pad	--	--	152	96	--	--
Elastomer From T156 Track Shoe	179	81	--	--	71	49

*All temperatures in ° C.

MATERIAL STUDIES

As mentioned previously, three elastomers with widely different stiffnesses that were suitable for track use have been evaluated. Rubber obtained from a T156 track shoe was the softest elastomer studied; whereas, the laboratory formulation rubber containing 35 weight percent carbon black had the highest stiffness. Rubber obtained from a T142 track pad had a stiffness between the two formulations described above.

Contour levels for the maximum principal stresses were very similar for all materials studied. There was some difference in the minimum principal stresses and strains produced for the materials studied. However, these differences were judged not to be significant. The large and important difference between the elastomer formulations studied for a given track design was the heat generation rate. The influence of this on track rubber temperatures are evident from the contour plots shown in Figures 7, 12 and 13. Results are summarized in Table I.

Sensitivity studies were done on the influence of density, heat capacity, and thermal conductivity on the temperatures developed in the T156 track. The range in properties studied represents the maximum variation that has been measured in field-tested track pads. These property variations produced internal pad temperatures that differed by, at most, 18° C. This temperature change is small compared with temperature changes obtained with differences in design or viscoelastic material constants.

Thus the primary characteristics influencing the temperatures achieved in the track are the heat-generation rate and the track geometry. The heat-generation rate is related to the viscoelastic material properties of the elastomer, track design, and loading/operating scenario.

FAILURE EVALUATION

Quantitative evaluations of failure in tank track pads is a very complex problem. A portion of this complexity is the many possible failure mechanisms that are exhibited. In this portion of the study we consider only the so-called cutting and chunking failures which are associated with the accumulation of damage and loss of rubber pieces due to fatigue. We have quantitatively evaluated the extent of damage development due to fatigue. For this study we view damage as an irreversible degradation in mechanical properties and a precursor to failure.

Experimentally, these evaluations had a two-step procedure. The first step was to fatigue the material by cyclically loading a sample in an MTS servo-hydraulic test machine between zero and some predetermined tensile load at 1 Hertz for 100 cycles. The stress produced by this predetermined load will be referred to as the cycling stress. Testing was done at temperature on flat, dog-bone shaped samples that were obtained from T142 track pads. The second step in this procedure was to pull the sample to failure. This was done immediately after cyclic loading. The ultimate tensile strength measured in this test will be referred to as the residual strength, and can be used as a measure of the damage developed in the material due to cyclic loading.

Results are shown in Figure 14 for material obtained from two track-pad manufacturers. For both materials and temperatures shown in Figure 14 severe degradation takes place above a critical or threshold stress of about 2 MPa. Clearly for a given material any experimentally derived threshold stress is a function of a number of variables including temperature, environment, and number of fatigue cycles used. Our purpose here is to gain some quantitative understanding of the degradation behavior of typical tank-tread elastomers when subject to a limited number of high stress cycles.

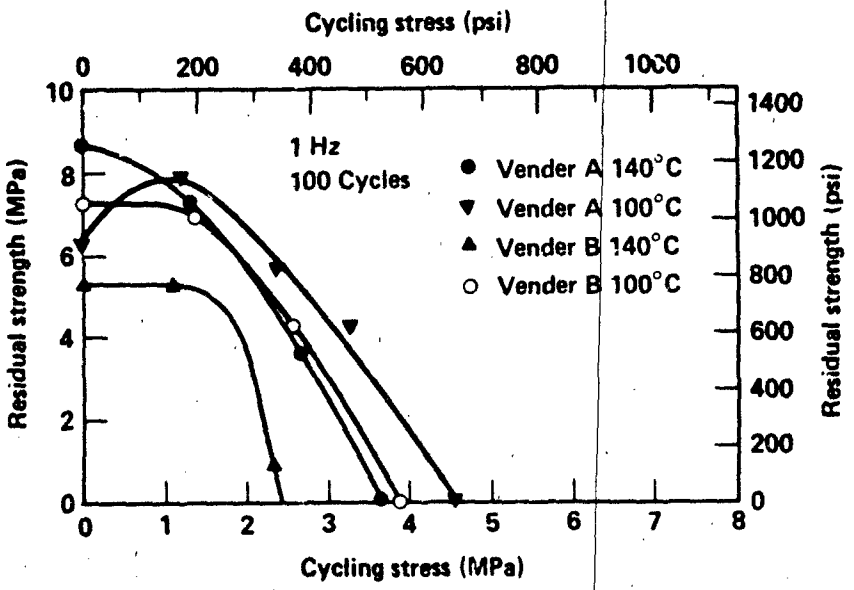


FIGURE 14. Residual stress versus cycling stress at 100° C and 140° C for rubber taken from commercial track pads.

Additional studies of damage development in elastomers have been presented elsewhere[7]. It is important to note that the threshold stress obtained from Figure 14 is comparable to the stress obtained in the obstacle contact scenario shown in Figure 10. Thus one would expect such obstacle contact to be a source of cutting and chunking. As observed in field tests significant track pad damage can take place with a limited number of stress applications in such operating scenarios at temperatures greater than 100° C.

ACKNOWLEDGMENTS

Work performed under the auspices of the U.S. Department of Energy by the Lawrence Livermore National Laboratory under Contract W-7405-Eng-48, with financial support by the U.S. Army Tank-Automotive Command. Contributions to the computer modeling were made by Mike Gerhard, Rick Wood, Ray Cornell and Diane Chambers. The damage development experiments were performed by Dave Hiromoto.

REFERENCES

1. J. O. Hallquist, NIKE2D - A Vectorized, Implicit, Finite Deformation, Finite Element Code for Analyzing the Static and Dynamic Response of 2-D Solids, Lawrence Livermore National Laboratory, Report UCID 19677 (1983).
2. P. J. Burns, TACO2D - A Finite Element Heat Transfer Code, Lawrence Livermore National Laboratory, Report UCID 17980, Rev. 2 (1982).
3. D. R. Lesuer, R. H. Cornell and S. D. Santor, "Cyclic Stress-Strain Behavior of Rubber", Proceedings of the 1982 Joint Conference on Experimental Mechanics Society for Experimental Stress Analysis, 779 (1982).
4. A. Goldberg, D. R. Lesuer, J. C. Stone, and J. Patt, "Tearing, Cut Growth and Fracture of Styrene-Butadrene Rubber and Natural Rubber Containing Various Amounts of Carbon Black", Lawrence Livermore National Laboratory, Report UCID 20287 (1984).
5. D. R. Lesuer, M. Zaslowsky, S. V. Kulkarni, R. H. Cornell, and M. D. Hoffman, "Investigation into the Failure of Tank Track Pads", Lawrence Livermore National Laboratory, Report UCID 19035 (1980).
6. D. Lesuer, M. Gernard, R. Wood, and D. Chambers, "Computer Modeling of the T156 and British Chieftain Tank Tracks", Lawrence Livermore National Laboratory, Report UCID 20668 (1986).
7. Donald Lesuer, Alfred Goldberg, David Hiromoto and Jacob Patt, "Damage Development During Fatigue of Carbon-Black Loaded SBR", Precedings of the 1985 SEM Spring Conference on Experimental Mechanics, 702 (1985).

MECHANISMS OF ELASTOMER DEGRADATION & WEAR

DAVID W. DWIGHT[1], H. R. NICK LAWRENCE[2], JACOB PATT [3]
(1) Professor, Materiels Science and Engineering, Virginia Tech, Blacksburg, VA 24060; (2) Deputy Program Manager, Combat Vehicles, FMC Ordnance Division, San Jose, CA 95108; (3) Mechanical Engineer, Track and Suspension Subfunction of the Systems Development Lab, TACOM, Warren, MI 48397-5000.

INTRODUCTION

Military tracked vehicles such as tanks, armored personnel carriers, self-propelled artillery and certain recovery vehicles utilize rubber pads for the purpose of damping vibration, reducing noise and preventing unnecessary damage to the built-up surfaces such as concrete, asphalt and macadam over which these vehicles must often travel. The majority of the track pads currently in use are the T142 model, used on the M48 and M60 series tanks, and the T130 model pads, used on the M113 series armored personnel carriers. As the M1 tank begins to see more field use, its T156 model pad will become a logistically more important commodity.

Similar materials are used in the manufacture of the T130, T142 and T156 model pads. The polymeric material currently used is a styrene-butadiene copolymer vulcanized into an elastromeric morphology using sulfur as a crosslinking agent and zinc-oxide as an accelerator. Additionally, reinforcing fillers (carbon black), processing aids, antidegradants and other diluents are added to form the final vulcanizate. The molded styrene-butadiene rubber (SBR) product is then bonded to a steel backing plate. This assembly is then bolted to the track and supports the weight of the vehicle.

The scope of work described herein was designed to study the wear mechanisms evident in military track pads. The authors believe that significant insight into pad wear and failure processes were developed by this investigation.

METHODS

Electron Spectroscopy for Chemical Analysis (ESCA)

One of the most ideally suited techniques to investigate the chemical nature of surfaces is Electron Spectroscopy for Chemical Analysis (ESCA). The instrument employed is composed of five basic components: (1) source, (2) sample compartment, (3) electron energy analyzer, (4) detector, and (5) read-out system. The source produces an x-ray beam which is directed into the sample compartment where it impinges upon the material

to be studied, causing the ejection of electrons. The electron energy analyzer sorts the resulting electrons according to their kinetic energies (KE) and focuses them on a detector at the output. The detector produces an electrical signal proportional to the intensity of the emitted photoelectrons from the specimen and the readout system translates it into graphic form. From the kinetic energy (KE) and the energy in the x-ray beam (hv), the binding energy (BE) of an electron can be calculated by the relationship BE (eV) = hv - KE(eV). The binding energy (BE) is characteristic of the element from which the electron is ejected. The quantity of electrons detected for each different KE value provide stoichiometric ratios of the detectable elements making up the analyzed specimen.

$$\text{Relative \% present} = \frac{\dfrac{(A_n)\ (AF_n)}{(PCS_n)\ (MFP_n)}}{\sum_{n=Cls}^{Cls} \dfrac{(A_n)\ (AF_n)}{(PCS_n)\ (MFP_n)}}$$

Where,
A = Spectrum peak area of component, n.
AF = Instrument attenuation factor for component, n.
PCS = Photoelectron cross-sectional area of component, n.
MFP = Mean free path of component, n.
And,
for oxygen (1s), (PCS) x (MFP) = 396.7 relative units.
for carbon (1s), (PCS) x (MFP) = 173.6 relative units.

Scanning Electron Microscope (SEM) and Energy Dispersive Analysis Using X-Rays (EDAX)

For the scope of this study, the SEM was used along with attachments to take fractographs (photographs of fractured surfaces) and to do an energy dispersive analysis using x-rays (EDAX). Electrons from a filament are accelerated by a voltage and directed down the center of the SEM electron column consisting of two or three magnetic lenses. These lenses cause a fine electron beam to be focused onto the specimen surface. Scanning coils placed before the final lense control the motion of the electron beam. The same circuit which controls the scanning coils also controls the coils in a cathode ray tube (CRT). As a result, the motion of the electron beam incident on the specimen surface causes various phenomena, of which the

emission of secondary electrons is the most commonly used. The emitted electrons strike a detector and the resulting current is amplified and used to modulate the brightness of the CRT. Consequently, an image of the surface is progressively built up on the CRT screen. Because of the preciseness of the SEM, the image produced is of dramatic three-dimensional quality and is known as a photomicrograph. Since the SEM has no imaging lenses, any signal that arises from the action of the incident electron beam upon the specimen (reflected electrons, transmitted electrons, emitted light, x-rays, etc.) can be used to form an image on the CRT screen.

In a different type of mode, the x-rays emitted from the sample are used to provide information about the nature and amount of elements present in the material. This type of analysis can be used on the surface or in the bulk of the material, depending on the energy of the incident electron beam and differs from ESCA insofar as the former provides a point chemical analysis. This method is known as energy dispersive analysis using x-rays (EDAX). In EDAX, the energy of an emitted x-ray photon is converted into an electric pulse which is proportional to the energy of the x-ray. This pulse is amplified, converted to a voltage pulse, and fed into a multi-channel analyzer. The analyzer sorts out the pulses according to their energy and stores them in the memory of the correct channel. The resulting spectrum can be displayed on a CRT, plotted on a chart, or printed out numerically. From this, the elements present can be determined since the individual energies of the x-rays emitted are characteristic of the different elements.

Swelling

A swelling experiment is designed to determine the relative amount of corsslinks between different samples on a comparative basis. This can be done since the percent weight gain is inversely proportional to the amount of crosslinks in the material.

The procedure for carrying out this swelling experiment is given as follows: Specimen weighing approximately 0.2g each are cut from the samples to be tested and are placed in a toppered flask containing enough swelling solvent, such as toluene, to cover the specimen. Periodically, the specimen are removed and rapidly weighed. (The work should be carried out rapidly to avoid loss of solvent by deswelling and evaporation, causing the sample weight to drift downward.) This should be repeated until the samples reach their equilibrium degree of swelling (2-3 days). When equilibrium is reached, the final

constant weight can be used to determine the percent weight gain from the following equations:

$$\% \text{ weight gain} = \frac{Ws - Wd}{Wd} \times 100$$

$$\text{relative crosslink density} = (\% \text{ weight gain})^{-1}$$

Where,

Wd = dry weight of SBR specimen (after deswelling)
Ws = swollen weight of SBR specimen and Toluene

TEST MATERIALS

The materials studied were actual T142 track pads sent to Virginia Tech's Materials Engineering Department by the United States Army's Tank-Automotive Command (TACOM.) These pads comprised a sample population of test batches initially sent to Yuma Proving Grounds (an Army test center) by each of four major rubber companies. While at the Yuma Proving Grounds, each pad sample was installed on an M60 tank track and subjected to only one of the four following service conditions:

1. 500 miles on paved surface
2. 1500 miles on paved surface
3. 250 miles of cross-country service
4. 1000 miles on gravel surface

New (pre-service) pads from each manufacturer were also provided so as to establish a baseline for analysis. Photographs of new pads and typical wear mechanisms of each of the three service conditions are shown in Figure 1.

Once the pads were received, catalogued and tagged with an identification code, specimen preparation began. Two sample populations were cut using a single-edged razor blade. Samples were taken from both the surface and the interior (bulk) regions of every pad. Each specimen measured approximately one centimeter in diameter by one millimeter in depth. Specimen weight averaged 0.2 grams. The first-sample population was used for SEM study only. The second sample population was first swollen (to determine relative crosslink density) and then analyzed by the electron spectrometer (to determine the relative oxygen to carbon ratio).

Although exact reproducibility in the experimental results was not expected, sample population size was large

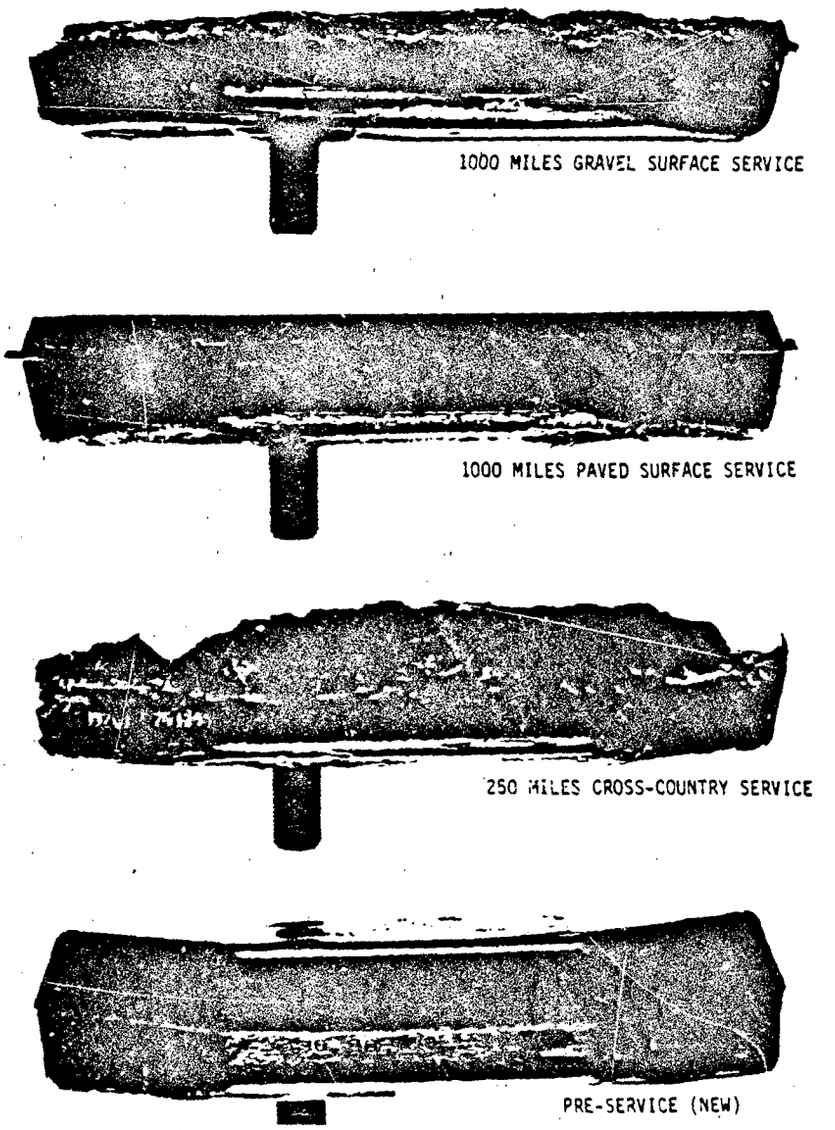


FIGURE 1. Comparative topography.

enough so as to ensure the identification of normative material characteristics.

RESULTS

Electron Spectroscopy for Chemical Analysis (ESCA)

In order to develop a relative stoichiometric understanding of what are the critical moities within the pad matrix, oxygen and carbon, a study of the oxygen ESCA peak intensity was ratioed against the carbon peak intensity. Table 1 provides the results of this ratio analysis.

TABLE 1

OXYGEN-TO-CARBON RATIOS VERSUS SERVICE LIFE OF SBR MATERIAL
OF SBR MATERIAL

	New	250 mile c-country	500 mile paved	1000 mile gravel	1500 mile paved
SURFACE	11%	21%	42%	46%	50%
BULK	6%	9%	17%	17%	18%

In general, ESCA analysis shows that the pad surface (that region within 10 nm of the pad surface) contains more oxygen than a bulk cross section. Clearly, this is due to the unavoidability of surface reaction with oxygen, having been exposed to air over a long period of time. Secondly, the amount of oxidation at the pad surface increases significantly with service mileage. In the bulk regions, less oxidation was observed; although the pads with gravel and paved-service histories did experience oxidative rate increases.

Scanning Electron Microscope (SEM) and Energy Dispersive Analysis Using X-Rays (EDAX)

The SEM is used to characterize and compare the general morphologies and topographies of track pad materials that have undergone specific service histories. Comparisons are made of both surface and bulk regions.

Surface Region. - The surface region is defined as that portion of the pad matrix that, when undergoing field use, experiences intimate ground contact. Figure 2 is an SEM magnification series of a rubber specimen cut from the surface of a pre-service (new) T142 track pad. The topography is relatively smooth although at higher magnifications natural flaws and small fracture lines are clearly evident. The existence of these flaws and naturally occurring fractures are not unexpected in new polymeric materials. Figure 3 shows the surface study of a T142 pad with 500 miles of paved-surface service history. At the lowest magnification, the surface topography is not unlike a pre-service pad, exhibiting relatively smooth contours. However, at higher magnifications, definite degradation is observed. Friction and subsequent abrasion experienced during service, has developed a topography characterized by craters approximately 50 nm in diameter. Inside these craters, granulated particles on the order of 1-10 nm are seen. After 1500 miles of paved-surface service (Figure 4), the craters are still observable but are smaller and more numerous. Granulation is still evident; however, the individual grains have increased in size when compared to pads with less paved-surface mileage.

Figure 5 characterizes the surface of a T142 pad with 250 miles of cross-country service. Note the extreme surface roughness even at low magnifications. Matrix granulation is again evident. Fracture wear is observed by the numerous, large and continuous stress lines that criss-cross the surface topography.

Figure 6 shows the photomicrographic study of a specimen taken from a pad with 1000 miles of gravel-surface service history. Granulation and cratering have taken place within the rubber matrix. Stress fracture lines are also readily observed; however, they are not as numerous as are the stress lines observed in the cross-country pads.

Bulk Region. - The bulk region is defined as that portion of the track pad that, when undergoing field use, does not experience intimate contact with either the ground or the atmosphere. Figure 7 shows that the cutting action of the

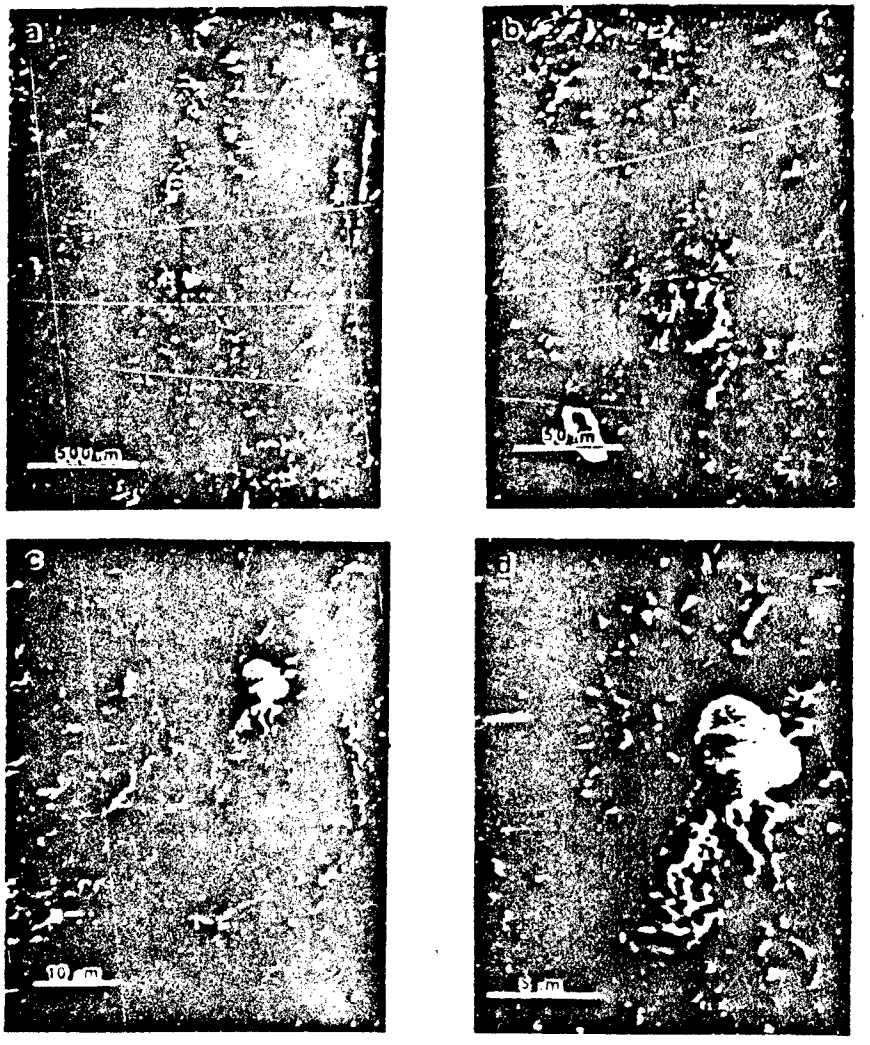


FIGURE 2. SEM photomicrograph pre-service pad surface

razor blade, used to remove the specimen from a new pad's bulk, caused few striations upon the material. At higher magnifications, the presence of rubber fibrils are observed. At high magnification (Figure 8), a particle (position 1) is shown to be slightly displaced out of the matrix. Using EDAX, this material flaw is identified as having a high zinc content; whereas, the surrounding matrix (position 2) has very little zinc. The presence of a zinc agglomeration is not unexpected

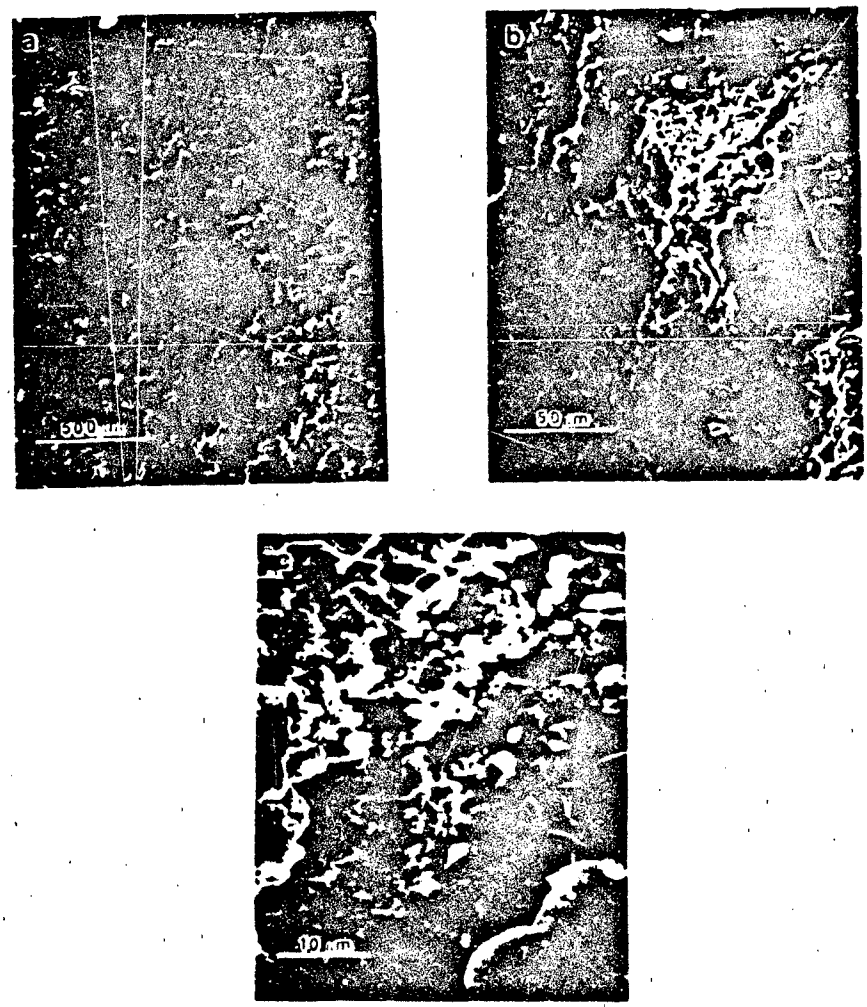


FIGURE 3. SEM photomicrograph, pad surface after 500 miles of paved surface service.

since zinc-oxide is used as an accelerating agent for crosslinking in the SBR recipe.

Figure 9 shows the topographical detail within the bulk of a T142 pad having 500 miles of paved-surface service history. Low magnification shows a topography characterized by many thin striations caused by the slicing of the razor through the matrix. These striations are more pronounced than those

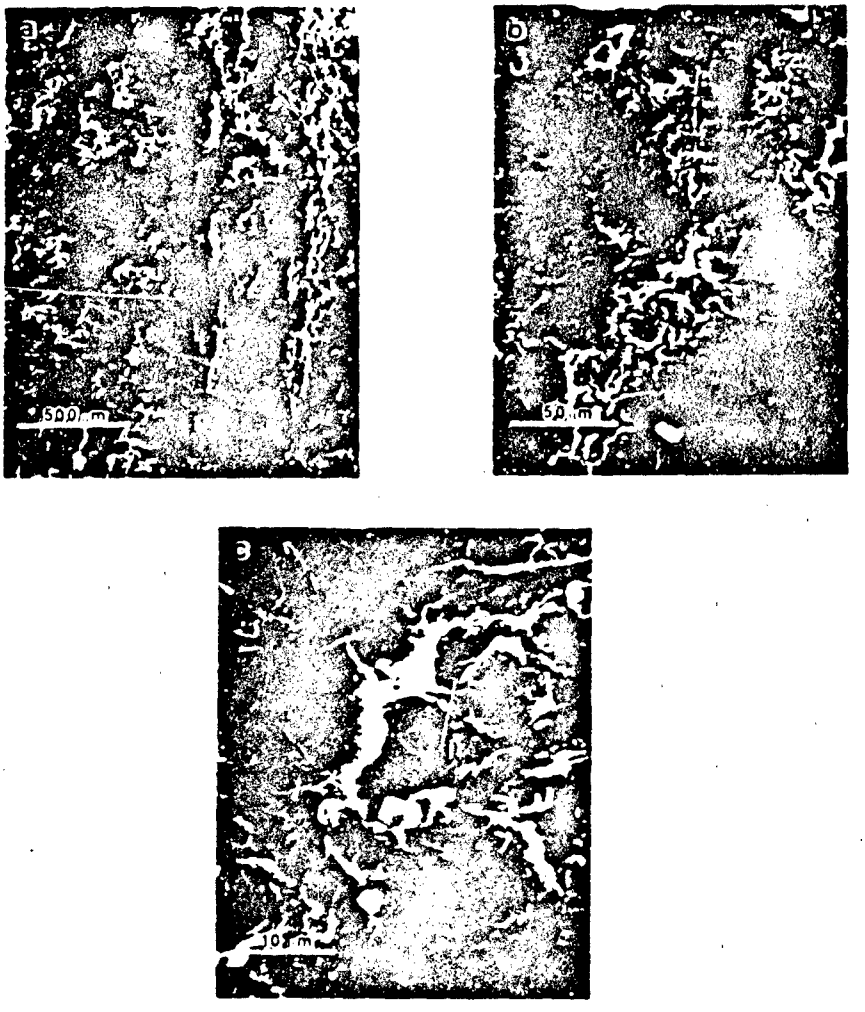


FIGURE 4. SEM photomicrograph, pad surface after 1500 miles of paved service.

observed in the pre-service pad (Figure 7). A second striking feature present in the 500 mile paved pad's bulk morphology is the system of cracks running throughout the material. Generally, these cracks appear to travel parallel to the razor-caused striations. However, this parallelism is often disrupted by material inhomogeneities. These inhomogeneities, as analyzed by the EDAX attachment to the SEM, are pieces of rock and gravel that would appear to have been worked into the

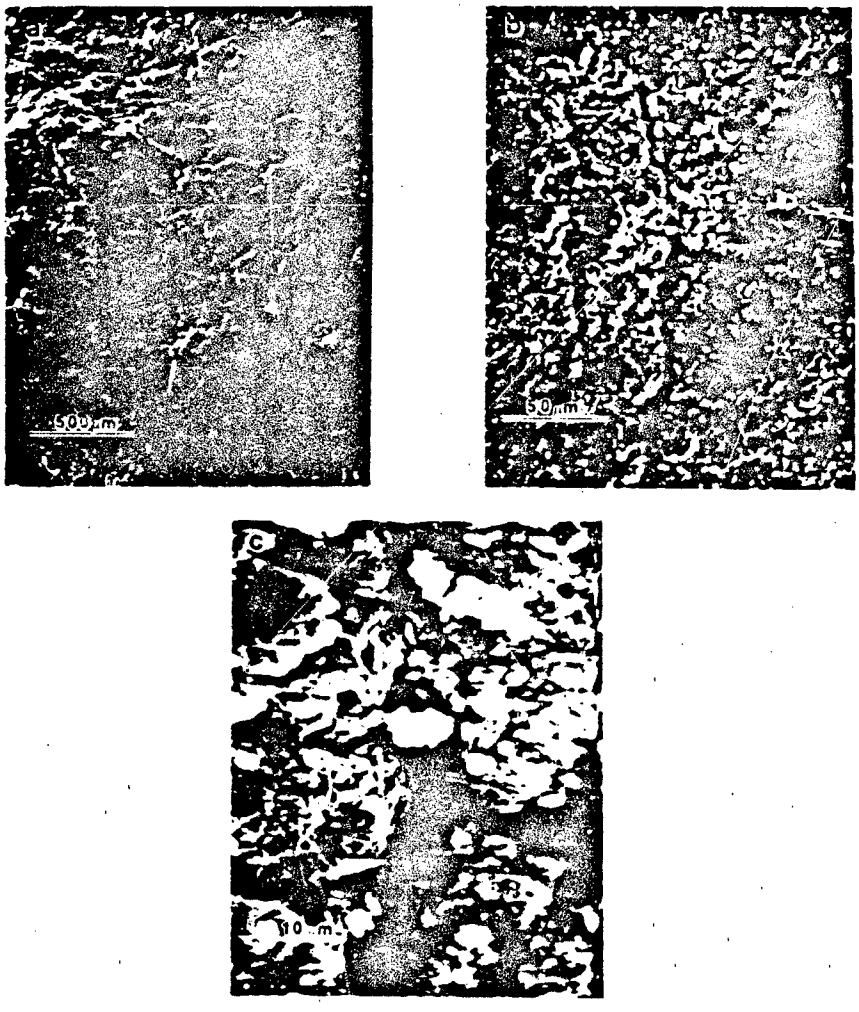


FIGURE 5. SEM photomicrograph, pad surface after 250 miles of cross-country service.

bulk of the matrix as the pad undergoes field use. Figure 10 is the bulk study of a T142 pad that has undergone 1500 miles of paved-surface service. The two most notable features are the lack of razor-caused striations and the many fibrillar features throughout the series of photomicrographs.

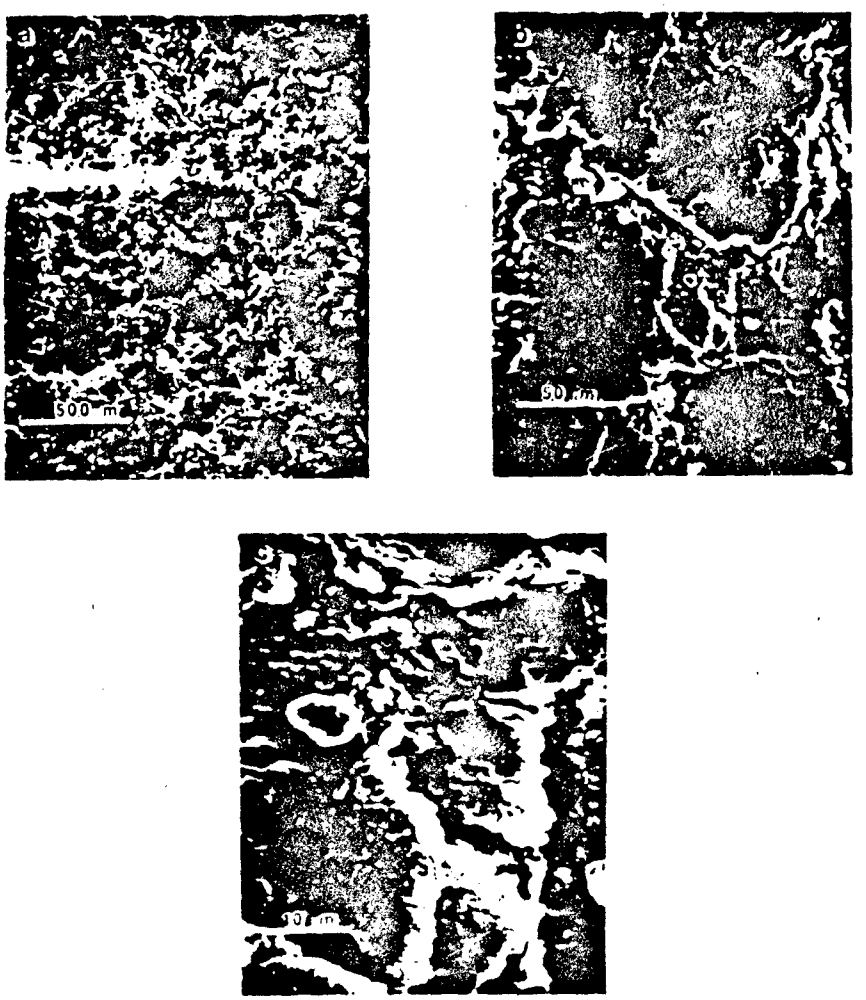


FIGURE 6. SEM photomicrograph, pad surface after 1000 miles of gravel service.

Low magnification of a bulk region within a cross-country pad (Figure 11) shows the most pronounced and numerous striation content of any of the pads with differing service histories. At higher magnifications, fibrils are noticeably absent. Stress induced cracks are evident and numerous throughout the matrix.

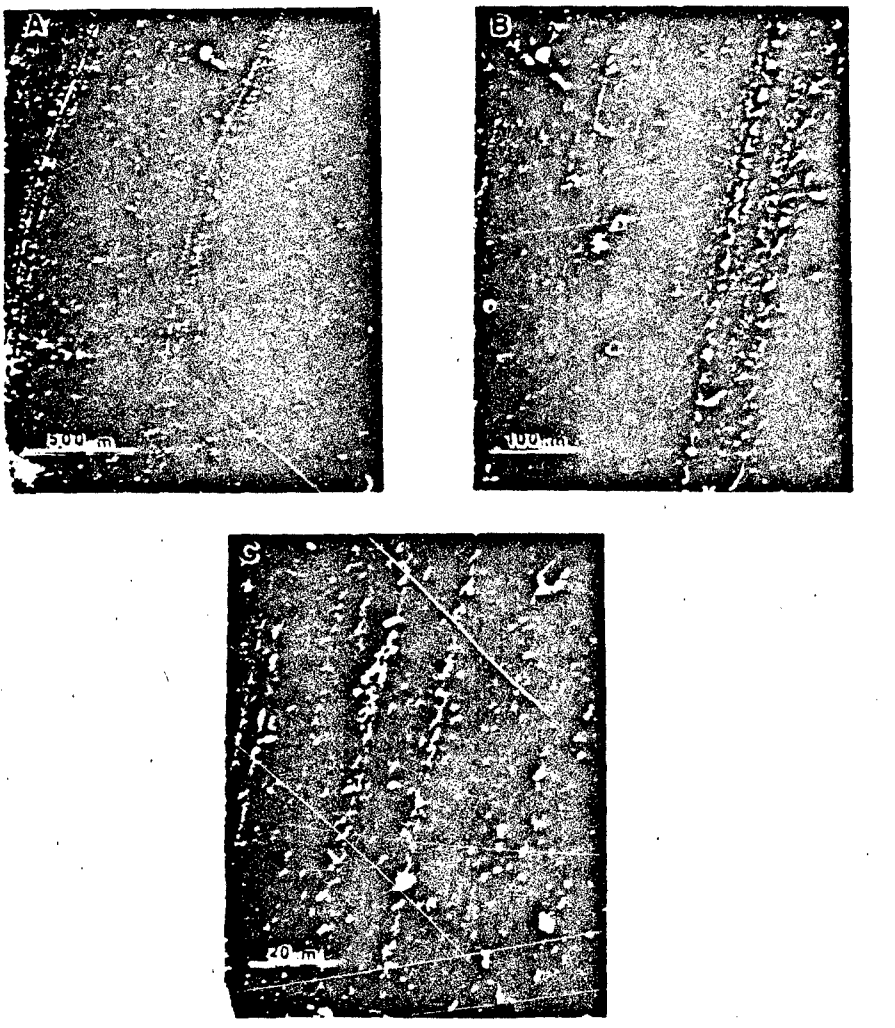


FIGURE 7. SEM photomicrograph, bulk region of pre-service pad.

Swelling

Relative crosslink densities calculated from the swelling data is given at Table 2. Several characteristics are shown by the tabulated data. First, cross-country and gravel service histories cause increases in the relative crosslink densities for both surface and bulk pad regions. The most significant

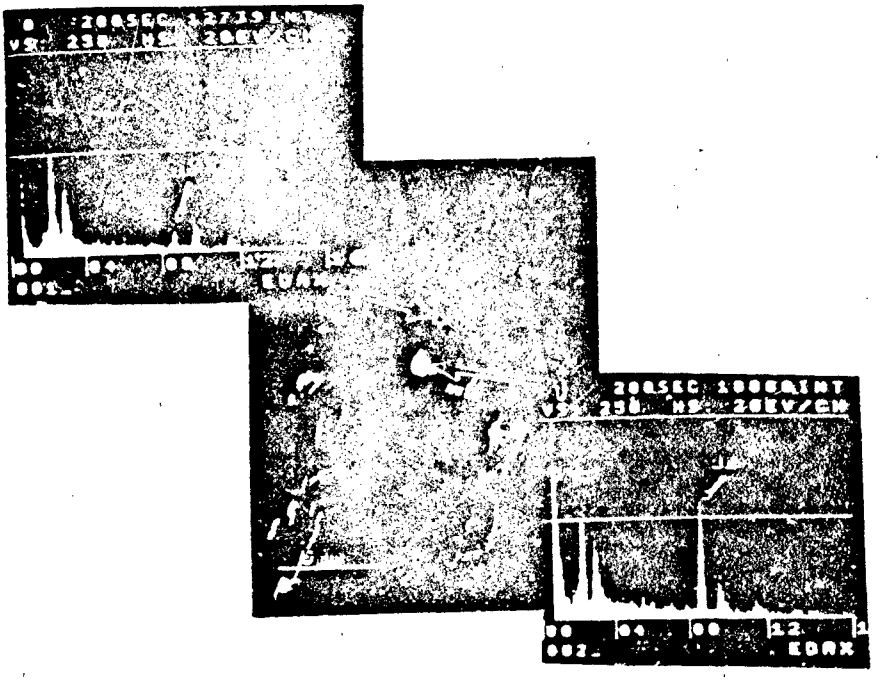


FIGURE 8. SEM/EDAX photomicrograph analysis showing material inhomogeneity within pad.

increases for both bulk and surface regions are measured in the cross-country pad. A general material morphological relationship is developed: the pad material experiences an increase in crosslink density with service life. Paved service initially follows this relationship. However, after prolonged paved surface service, there is a decrease in the relative crosslink density measurement. At 1500 miles of paved service, both surface and bulk regions show such a decrease.

The final characterizations derived from the tabulated data at Table 2 is that service effects on the relative crosslink density measurements are generally more pronounced in the bulk than at the surface. Thus, the most significant change in crosslink density occurs in the bulk of the cross-country pad.

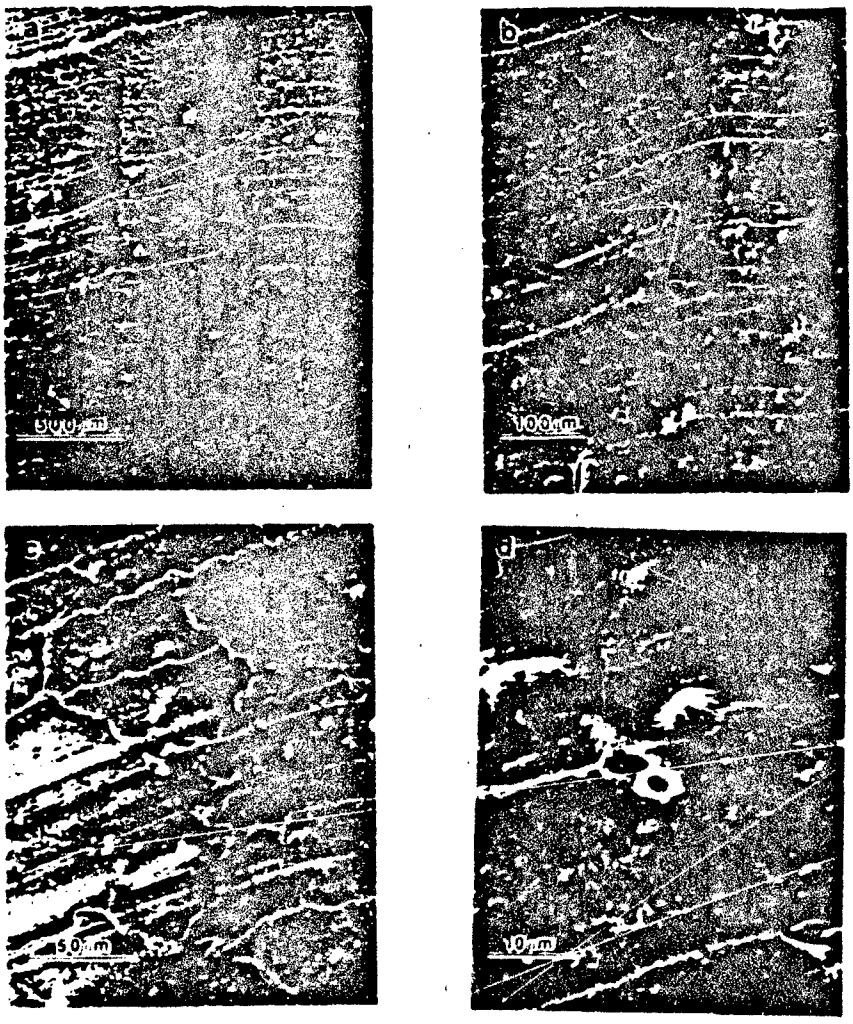


FIGURE 9. SEM photomicrograph, bulk region of a pad with 500 miles paved surface service.

DISCUSSION

Cross-Country Service

Clearly, Figure 1 indicates that cross-country service presents the most severe wear environment for military tracked-vehicle pads. Cross-country service is typified by the

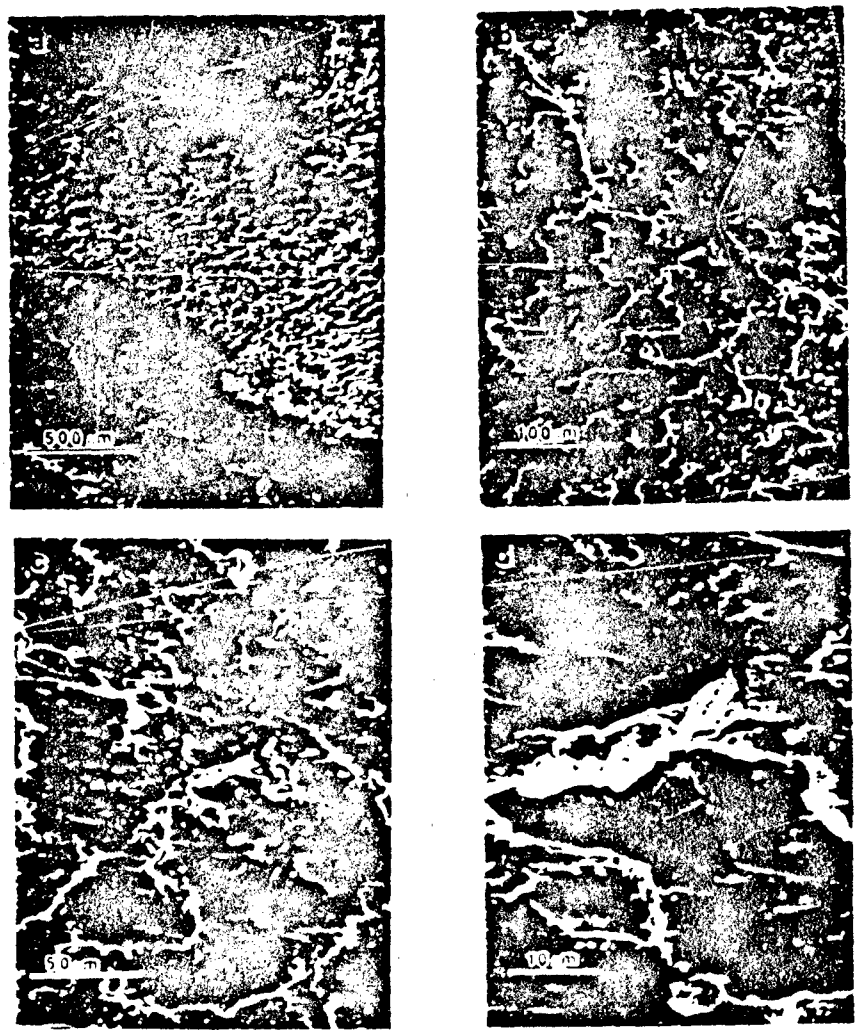


FIGURE 10. SEM photomicrograph, bulk region of a pad with 1500 miles of paved-surface service.

tracked vehicle traveling over terrain that is soft and compressive but has many large and rigid stress risers (large rocks, etc.) strewn over its surface. Vehicular velocity is usually slow and of relatively short duration. Since the substrate is generally compressive, little thermal build-up is experienced by the pad. The pad wear incurred during cross-country service is characterized by large-scale

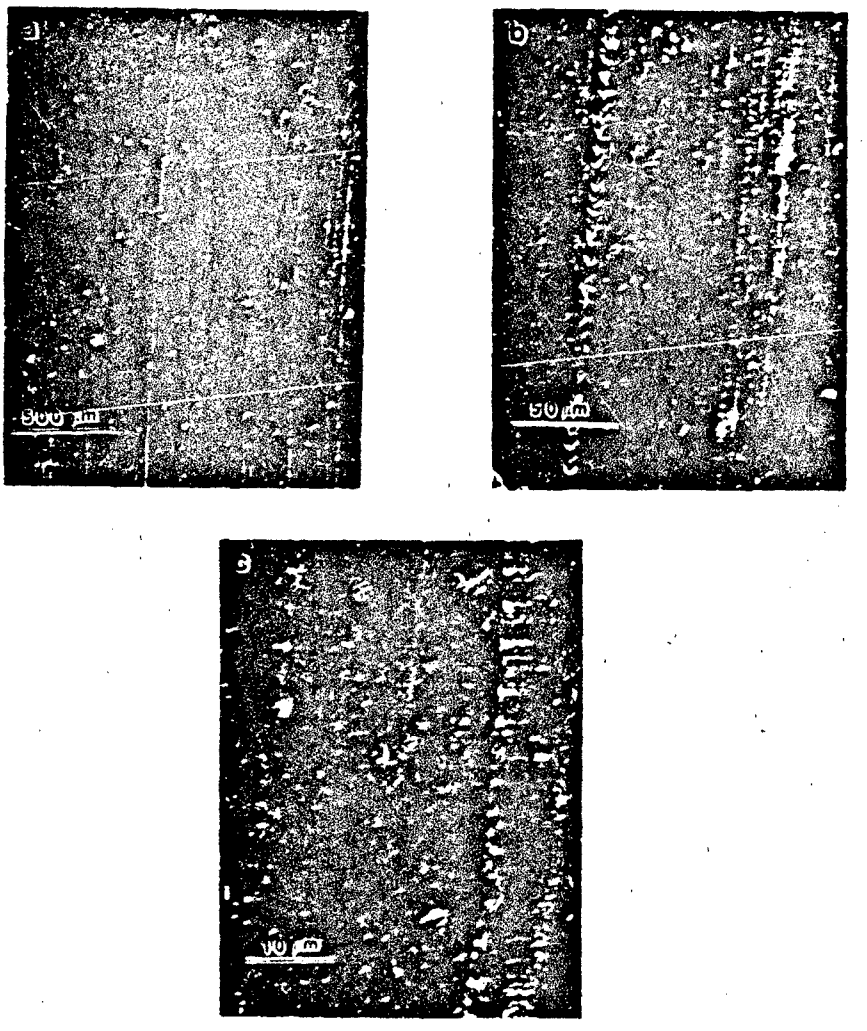


FIGURE 11. SEM photomicrograph, bulk region of a pad with 250 miles cross-country service.

fracture. Figure 1 shows that catastrophic fracture forms large cuts and chips on the pad surface. The equilibrium swelling data collected on pads with cross-country service history, shows a significantly large increase in the relative crosslink density. This increase is evident in both surface and bulk regions although the latter is more pronounced. Indeed, the SEM photomicrographs taken of a pad with

TABLE 2

RELATIVE CROSSLINK DENSITY VERSUS SERVICE LIFE OF TRACK PAD MATERIAL (SBR)

	New	1500 mile paved	500 mile paved	1000 mile gravel	250 mile c-country
SURFACE	0.50	0.44	0.51	0.56	0.57
BULK	0.49	0.47	0.57	0.58	0.60

cross-country service, reveal large fracture lines at the surface (Figure 5) and both fracture lines and large, well-defined striations in the bulk (Figure 11). In both of these SEM magnification series, fibrils are completely absent. The combination of the presence of large fracture lines, well-defined striations and the lack of fibrillar structures in the pad material (as shown by SEM), as well as an increase in the relative crosslink density (per swelling data), define an embrittled elastomeric matrix. Embrittlement is one of two primary phenomena that will occur with the application of a stress riser to the pad's elastomeric material. The second phenomenon is immediate macroscopic-level degradation where chunks of rubber are torn from the pad. This will occur only if the applied stress generates enough tear energy or is concentrated within the material so as to rupture an entire plane of network chains that connect two surface areas. Sharp terrain stress risers or material inhomogeneities (Figure 8) will cause these stress concentrations to occur. Immediate degradation is not as common as network embrittlement. The majority of applied stresses will have enough energy to tear only a portion of a molecular chain plane. When only a segment of a plane is fractured, the material retains its geometric integrity. Since these partially fractured planes contain ruptured molecular chains by homolytic chain scission, many free radicals are produced. These free-radicals, at the end of the ruptured chains, attack susceptible material within the pad's matrix. Such susceptible material can be radical scavangers, such as oxygen, or any unsaturated bond that exists within the network structure. Except for the surface regions, quantities of oxygen will not be present in the matrix to

convert these free-radicals. Substantial oxygen diffusion through an elastomeric matrix has been shown to proceed only at high temperatures. Since little thermal build-up is experienced during cross-country service very little oxidation of the matrix is expected. This is supported by ESCA data (Table 1). The free radicals generated during cross-country service will usually form bonds with other chains. These new intermolecular bonds will cause the material's crosslink density to increase and the pad to become embrittled. Matrix embrittlement lowers the amount of tear energy necessary to cause planar rupture. Therefore, as a track pad undergoes cross-country service, it becomes embrittled and will require progressively smaller applied stresses to precipitate rapid and catastrophic material failure.

Paved-Surface Service

Paved-surface service is typified by the tracked vehicles traveling over smooth terrain that is hard and incompressible. Stress risers are seldom present, and are usually very small (small pebbles, etc.). Vehicular velocity is usually quite high and of relatively long duration. Because of the high rate of vehicular speed and the long duration of travel on an incompressive substrate, high thermal build-up is experienced by the pad.

Two important conclusions are made from the study of the photographs in Figure 1. The first conclusion is that paved service is not as damaging to the T142 track pad as either the cross-country or the gravel service conditions. Secondly, the wear mechanisms involved during paved-surface service are very different from the cross-country wear mechanisms previously described. The photograph of a T142 pad with a paved-surface service history shows a relatively smooth surface topography that is characteristic of abrasive wear. The SEM surface studies of the same specimen (Figures 3 & 4) reveal a surface topography characterized by the development and wearing away of smooth granule particulate.

In the absence of significant terrain stress-risers, another mechanism must cause the molecular chain rupture so essential for material degradation and wear. This mechanism is provided by the high temperatures generated in the material during paved service. These high temperatures generate enough thermal energy within the matrix to disrupt certain intramolecular bonds. Bonds that are in a natural state of stress are particularly susceptible to thermal rupturing.

High temperatures not only precipitate bond rupture but also increase the ability of oxygen to diffuse throughout the elastomeric material. Indeed, specimen cut from pads with paved-service histories exhibit a significant increase in oxidative content as shown by ESCA (Table 1). Oxygen, acting as a radical scavenger, may "cap" the macro-radicals before they are able to link with other matrix chains. As a result, network morphology becomes more linear. The equilibrium swelling data collected from pads with extended paved service histories, shows such a decrease in the relative crosslink density (Table 2). This decrease is equally pronounced in both surface and bulk regions. SEM photomicrographs provide additional evidence of increased material elasticity as characterized by the many fibrils present in the pads shown in Figures 3 and 4. Paved service wear is less severe than cross-country service because the major wear mechanism abrasion, is generally confined to surface regions. Chain rupture by thermal build-up occurs at random locations throughout the matrix. Hence, the planar fracturing necessary for chunking and chipping to take place seldom occurs. However, the presence of large natural flaws (Figure 2) or gross inhomogeneities (Figure 8) within the material may serve as an internal mechanism for stress concentration and precipate future failure under paved conditions.

Gravel Service

Gravel service is typified by the tracked vehicle travelling over rough terrain that is hard and incompressible. The terrain is covered with small stress-risers (small rocks). Vehicular velocity is usually quite high and of relatively long duration.

The data collected in this study indicate that pads with gravel service show wear mechanisms common to both cross-country and paved service conditions. Photographs of pads with gravel service histories reveal a topography that exhibits both material fracture and surface abrasion. ESCA data shows distinct oxidation of the matrix indicating thermal build-up during service. The equilibrium swelling experiment reveals evidence of material embrittlement. It is noted that the level of pad oxidation during gravel service approaches the levels achieved during paved service. However, material embrittlement is not as severe in the gravel case when compared to pads with cross-country service histories. Thermal build-up and the accompanying oxidation of the pad material tends to lessen the degree of matrix embrittlement resulting from stress induced chain fracture.

SUMMARY

Cross-country service

- Cross-country is the most severe operational environment for vehicle track pads.
- Degradation is characterized by homolytic chain scission, rapid matrix embrittlement, and the subsequent chipping and chunking of large pieces of pad material.
- The wear mechanism is primarily mechano-chemical in nature.

Paved service

- Paved-surface service induces thermal build-up, random chain rupture, oxidation of the pad matrix, and subsequent material softening.
- Degradation is characterized by surface abrasive wear.
- The wear mechanism is primarily thermo-oxidative in nature.

Gravel service

- Gravel-surface service exhibits mechanisms of wear common to both paved and cross-country service conditions.
- Oxidation of the matrix decreases the degree of embrittlement experienced in the pad during field service.

Material Characterization

- The SBR matrix exhibits natural flaws. These natural flaws may precipitate fatigue failure under all service conditions.
- The SBR matrix exhibits material inhomogeneity within the bulk. These flaws will concentrate applied stresses and may lead to internally nucleated crack growth.

THERMOMECHANICAL DEGRADATION OF ELASTOMERS

J.L. MEAD[1], S. SINGH[1], D.K. ROYLANCE*[1], J. PATT[2]
(1)Department of Materials Science and Engineering, Massachusetts Institute of Technology, Cambridge, MA 02139; (2)U.S. Army Tank-Automotive Command Warren, MI 48090.

INTRODUCTION

Military tracked vehicles, such as tanks and personnel carriers, use rubber pads on their tracks to reduce road damage, damp vibrations, and reduce noise. With the high loads and speeds encountered by modern tracked vehicles, the rubber pads often fail in an undesirably short time. This study was undertaken to investigate the types of damage which occur under repeated cyclic loadings similar to those found in normal service. Under these conditions substantial heat build-up occurs, leading to permanent thermomechanical degradation. This research has been directed at determining what failure mechanisms occur under cyclic compression loading, and the fatigue effects on physical properties.

MATERIALS AND METHODS

The material chosen for this study was a commercial polyether polyurethaneurea system, prepared from a toluene diisocyanate (TDI) prepolymer and a diamine curative, trimethylene glycol-di-p-amino benzoate. The stoichiometry (curative/polymer weight ratio) used was 85%. This material has shown good wear resistance in rough-terrain track testing, and is a possible replacement for more traditional rubber compounds. Further, the urethane is not so highly compounded as the traditional elastomers, and this simplifies many of the analytical techniques needed for its analysis.

A servohydraulic Instron model 1331 was used for fatigue loading. Compression-compression fatigue data were obtained at a frequency of 6.5 Hz

and a 0.1 ratio of minimum to maximum stress. The specimens were tested between two parallel flat plates, with a sinusoidally varying load. The testing was done in load control mode on the Instron, because it was felt this would more accurately simulate tank track pad conditions. The temperature of the blocks was monitored by a thermocouple which had been inserted in a hole drilled to the center of the block. The final temperatures and stresses are shown in Table 1 for the polyurethane system. Blocks numbered 1-3 and 10 were obtained commercially, and blocks numbered 4-9 were prepared by us. The maximum temperature measured is shown next to the cycle count at which the maximum temperature was measured. Often the final test temperature could not be measured because of thermocouple failure. All blocks were 2.5" x 2.5" x 2.5" with the exception of blocks number 2 and 3, which were 3" high.

TABLE 1

Fatigue Test Data

Specimen	Max Load(lb)	Max Temp(C)	Failure Cycles
1	variable	177	failure
2	6,000	170–8,240	failure–9,270
3	6,000	140–7,416	stopped–7,416
4	8,000	?	failure–3,714
5	6,000	156–3,710	failure–5,355
6	5,000	170–8,285	failure–8,367
7	5,000	155–7,975	stopped–8,000
8	6,000	173–2,725	stopped–4,284
9	6,000	120–2,110	stopped–3,214
10	4,500	91–54,000	stopped–2,182,610

A typical temperature versus number of cycles plot is shown in Figure 1 for blocks number 5, 8, and 9. The testing we have done is not fatigue testing in the usual sense due to the small number of blocks examined. The extensive analysis required for each block, in order to determine the failure

mechanism, limited the total number of blocks that could be tested.

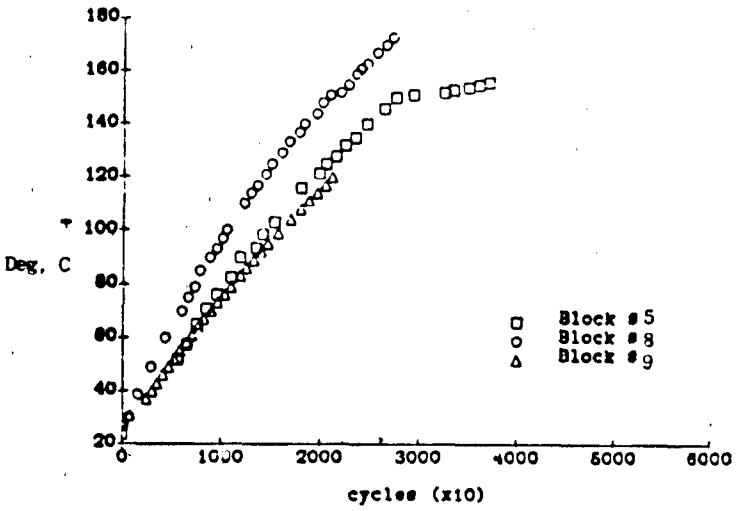


FIGURE 1. Center Thermocouple Temperature (6,000 lbs maximum load).

RESULTS

Differential Scanning Calorimetry

Since polyurethane block copolymers are generally two-phase systems, the degree of phase mixing will affect the transition temperatures of both hard and soft segments. Mixing of hard and soft segments has been used to explain the increase in soft segment T_g with increasing hard segment content (1). Differential scanning calorimetry (DSC) can be used to study the transition temperatures of unfatigued and fatigued specimens.

DSC analysis was run on a Perkin-Elmer DSC IV with a heating rate of 10°C/min. There appear to be two high temperature transitions in unfatigued material, one occurring at around 180°C, and the

other at around 205°C. When specimens are taken to failure there is only one transition, which is at nearly the same temperature as the higher temperature transition for the unfatigued material. This is shown in Figure 2.

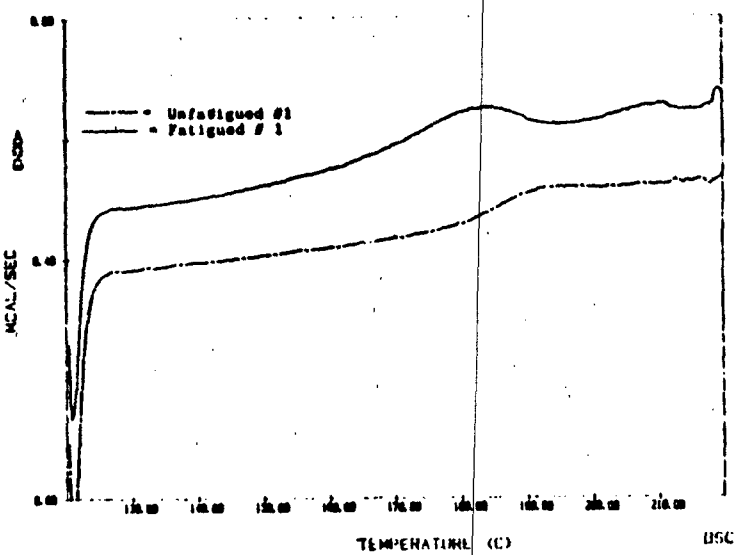


FIGURE 2. Hard Segment Transition Temperatures for Unfatigued and Fatigued Material (Specimen #1).

The data for all the fatigue tests is shown below in Table 2. By comparison of values shown for specimen #9, it is evident that no changes occur in transition temperatures with blocks fatigued to this level.

TABLE 2

DSC Analysis

Specimen #	Transition Temp.(C)	
1 unfatigued	176	204
1 fatigued	187	
2 fatigued	213	
3 fatigued	178	204
4 unfatigued	178	204
4 fatigued		202
5 unfatigued	179	
5 fatigued		207
6 unfatigued	179	205
6 fatigued		213
7 unfatigued	180	206
7 fatigued	182	213
8 unfatigued	179	208
8 fatigued		192
9 unfatigued	178	209
9 fatigued	178	209

The changes in transition temperature appear to be due only to thermal annealing because heating a sample in the DSC also moves the lower temperature transition upward. High temperatures may produce some kind of annealing effects which could increase the amount of phase separation or improve the ordering of the hard segment. Both these phenomena would increase the hard segment T_g. Since no improved order after annealing was reported in similar systems (2), increased phase separation may be the most a viable explanation, but if this were the case we would expect the T_g of the soft segment to also show changes, which it does not.

Cain (3) studied a polyurethane system very similar to ours, prepared from PTMEG, TDI, and MOCA, and found the presence of two high temperature transitions. Annealing either moved the lower transition upwards or caused it to disappear. Cain, with the aid of IR measurements at high temperatures, was able to correlate the transitions

to hydrogen bonding in the urethane carbonyls (lower temperatures) and urea carbonyls (higher temperatures). It is quite reasonable that our system shows similar behavior. Although we cannot be exactly sure what changes occur to the hard segment structure after annealing, we can conclude that the changes seen in the DSC scans after fatigue are merely the result of thermal treatment at the high temperatures observed during testing.

Swelling Studies

One method of measuring the mechanochemical degradation is to measure the changes in crosslink density (ν_e/V). The crosslink density can be measured by the application of the Flory-Rehner equation to solvent swollen samples (4).

$$\frac{\nu_e}{V} = -\frac{1}{V_s} \times \frac{\ln (1-v_r) + v_r + \chi v_r^2}{v_r^{1/3} - 2v_r/f}$$

ν_e/V is the crosslinking density (mole/cm^3), V_s is the molar volume of the solvent, χ is the polymer solvent interaction parameter, v_r is the volume fraction of rubber in the swollen sample, and f is the functionality of the crosslink. v_r can be calculated by the weight of the specimen while swollen and after removal of the solvent, if the density of the polymer and solvent are known.

For the polyurethaneurea under investigation the swelling solvent chosen was dimethylformamide (DMF). It is believed that this solvent may break up the hard segment hydrogen bonding to allow measurement of the primary crosslink density.

For swelling measurements specimens weighing approximately 0.4 grams were placed in 80 ml of DMF and allowed to swell for 25 hours at 25°C. The specimens were removed and weighed in sealed jars. The deswollen weight was obtained by drying the specimens in a 60°C vacuum oven overnight.

To obtain absolute values from swelling measurements, the value of χ must be known. To find a value for χ one can determine the crosslink density by measuring the elastic modulus of swollen specimens (no hard segment stiffening) using the following equation (5).

$$\nu_e/V = F\ v_r^{1/3} / \{ART(\alpha - \alpha^{-2})\}$$

where ν_e/V is the moles of effective network chains per unit volume of polymer, F is the force to obtain an extension α, v_r is the volume fraction of elastomer in the swollen specimen, A is the unswollen cross-sectional area, R is the gas constant, and T is the temperature. This value of the crosslink density can then be used in the Flory-Rehner equation to calculate χ.

By inserting the crosslink density obtained from stress-strain measurements on swollen samples into the Flory-Rehner equation a value for χ of 0.468 was obtained. The crosslink densities calculated by the Flory-Rehner equation with χ = 0.468 are shown in Table 3. The values reported are the average of at least two runs.

Significant changes after fatigue can be seen only in specimen #1. Specimens 6 unfatigued and 8 fatigued showed large percentages of soluble material, but this may be nothing more than variability from sample to sample, perhaps due to slight variations in the cure temperature. For the most part no significant changes can be seen in the swelling behavior of any of the other blocks after fatigue. Specimen 5 does show an increase in crosslink density after fatigue. Unfatigued specimens were taken from the outer surface of the blocks before testing, and perhaps the outer surface was improperly cured in the case of specimen 5. The values for the fatigued material represent average values for the specimens, since the test specimen was exposed to a variation in temperature, with the middle portions experiencing higher temperatures than the outer portions. For the most part there is no significant breakdown in the crosslink density,

TABLE 3

CROSS-LINK DENSITY FROM SWELLING

Specimen	% Soluble	v_r	ν_e/V (moles/cm^3)
1 unfatigued	2.3	.183	1.00×10^{-4}
1 fatigued	36.6	.046	3.95×10^{-6}
2 fatigued	2.6	.253	2.47×10^{-4}
3 fatigued	3.7	.207	1.38×10^{-4}
4 unfatigued	2.8	.247	2.27×10^{-4}
4 fatigued	1.5	.293	3.73×10^{-4}
5 unfatigued	6.9	.122	3.89×10^{-5}
5 fatigued	2.1	.240	2.10×10^{-4}
6 unfatigued	11.6	.210	1.52×10^{-4}
6 fatigued	1.5	.275	3.11×10^{-4}
7 unfatigued	4.5	.173	9.10×10^{-5}
7 fatigued	2.6	.257	2.54×10^{-4}
8 unfatigued	2.6	.244	2.21×10^{-4}
8 fatigued	16.2	.292	3.73×10^{-4}
9 unfatigued	3.4	.198	1.39×10^{-4}
9 fatigued	2.0	.250	2.40×10^{-4}
10 unfatigued	3.5	.220	1.64×10^{-4}
10 fatigued	3.2	.234	1.98×10^{-4}

even though the blocks taken to failure cracked during testing. The results for block #10 show that fatigue at low loads for long periods of time does not explain the increased swelling found for block #1. It may be that this block was different from the others, perhaps the starting materials had been degraded in some way, or the processing conditions were different.

From the swelling experiments it can be concluded that no significant permanent chain scission is required for failure of polyurethane elastomers under compression loading. If chain scission did occur, the bonds must have reformed before the samples were analyzed, and this seems unlikely.

Dynamic Mechanical Analysis

Above T_g amorphous polymers exhibit a slight plateau in the temperature dependence of the modulus due to chain entanglements. With crosslinking this plateau region is extended. In phase separated systems, such as polyurethanes, the hard segments tend to reinforce the structure, producing an extended plateau region, until the hard segment T_g is reached (6).

The elastic modulus in the plateau region can be used to determine the crosslink density through the theories of rubber elasticity. The stress-strain relation can be expressed as: (7)

$$f = E/3(\alpha - \alpha^{-2})$$

where f is the force per unit unstrained cross-sectional area, E is the Young's modulus, and α is the elongation. Assuming Poisson's ratio is 0.5, then (7)

$$E = 3G = 3RT(\nu_e/V)$$

We can relate the elastic modulus E' to the crosslink density by the use of this equation. All the values for crosslink density calculated by this method are higher than by swelling analysis. This is not unexpected since the modulus measurements include the reinforcing effect of the hard segment domains. The modulus of the specimens goes down with temperature indicating that ideal rubber elasticty is not attained (8), possibly due to internal energy contributions. However, these data may still give an approximate estimate of the degradation occurring.

From Figure 3 it can be seen that fatigued specimens showed a significant decrease in the elastic modulus values (E'), even though swelling measurements showed little change. Fatigued specimens from blocks not taken to failure showed

less modulus reduction, which would be expected if fatigue causes a progressive modulus reduction.

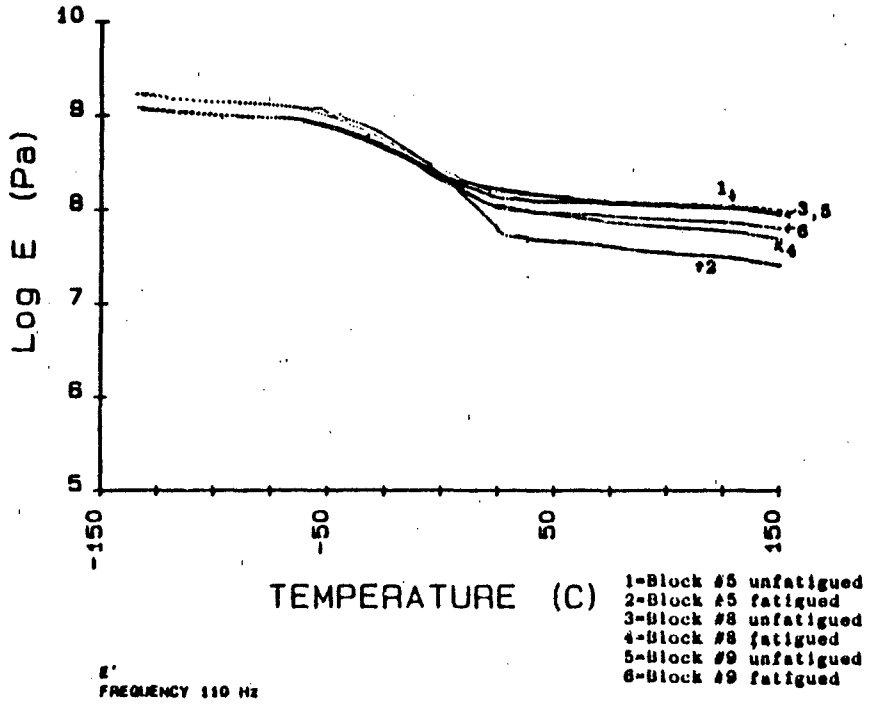


FIGURE 3. Comparison of Elastic Modulus (E') (6,000 lbs maximum load).

A calculation of the percent reduction in elastic modulus after fatigue was done for specimens number 5-10 and is shown in Table 4. This should allow us to compare the differences in loadings and number of cycles for each block.

The modulus clearly decreases after fatigue, indicating some type of permanent change. Thermal annealing tests showed no permanent change in the elastic modulus, indicating that high temperatures alone do not produce these changes.

TABLE 4

PERCENTAGE DECREASE IN RUBBERY MODULUS

Specimen	T=50°C	T=75°C	T=100°C
Block #4	52%	40%	43%
Block #5	67%	68%	70%
Block #6	42%	49%	51%
Block #7	15%	18%	20%
Block #8	37%	39%	41%
Block #9	24%	26%	28%
Block #10	–	12%	10%

A probable explanation for this modulus reduction is the "Mullins Effect", which was originally found in filler-loaded rubbers, but has since been found in polyurethane elastomers (9). Trick (9) found a reduction in modulus with repeated extension; almost all of the reduction occurred in the first cycle. The stress-softening phenomenon is believed to be caused by the disruption of the glassy domains under repeated stretching (10).

Kaneko et al. (11) studied the cut growth fatigue of polyurethanes prepared from PTMEG, TDI, MOCA, and hexamethylene diisocyanate (HMDI). After constant load fatigue they measured the changes in elastic modulus with the Rheovibron. For all fatigued samples a decrease in the elastic modulus was encountered, but the authors did not investigate if the amount of change was dependent on the number of fatigue cycles. Kaneko et al. suggested that the differences they noted after fatigue could be due to orientation under stress.

Either orientation or disruption of the hard domains is a possible explanation for the changes seen in compression fatigue tests. The changes seen in the modulus are clearly not caused by high temperatures alone, but require the application of

stress. The continuous increase in temperature leads to softening of the material, thus increased deformation. This increased deformation amplitude will lead to continued softening (10). Because of the heat build-up stress softening continues to occur throughout the test, rather than mainly in the first cycle. Thus, we can expect the material properties of polyurethanes to continuously change as fatigue degradation occurs. As evidenced by the results from block 10, when cycled at low load levels with little heat build-up, the modulus values show only a slight reduction.

Mechanical Failure Analysis

To understand the failure mechanism under compression loading, we need to be aware of the mechanical stresses that the compressed block experiences. For blocks that are bonded to end plates, the force applied can be viewed as being composed of two portions: one part is responsible for the surface displacement and a second shear displacement is added to restore points on the rubber surface to their original positions on the compression surface (12). For a linearly elastic, incompressible, and isotropic material this stress state produces a hydrostatic pressure component within the block. This hydrostatic pressure has a maximum at the center and a parabolic decrease towards the outside. As the height of the block increases the maximum internal pressure decreases (13). When the thickness of the block increases the effect of the constrained surfaces (shear forces) will contribute less to the stress distribution in the block (13).

Reed and Thorpe (14) determined the shear stresses in a compressed block by finite element analysis. The shear stresses were found concentrated in the top outside corners and negligible at the center. Therefore, although there may well be some small amount of shear stresses at the center of the block, their contribution to the failure mechanism is likely to be small.

For a compressed sample with frictionless surfaces, Treloar (15) states the equilibrium strain

in a compressed block is the same as the equilibrium strain for a specimen biaxially strained perpendicular to the loading direction. For Treloar's case no bulging effects occur as in our test.

Under fatigue all blocks taken to failure exhibit cracks formed at the center of the specimen. These cracks run perpendicular to the loading direction. Figure 4 shows the internal cracks, generated during fatigue testing, on a cut section of one of our specimens. Figure 5 shows the internal cracks for a clear polyurethane of a different composition than our specimens.

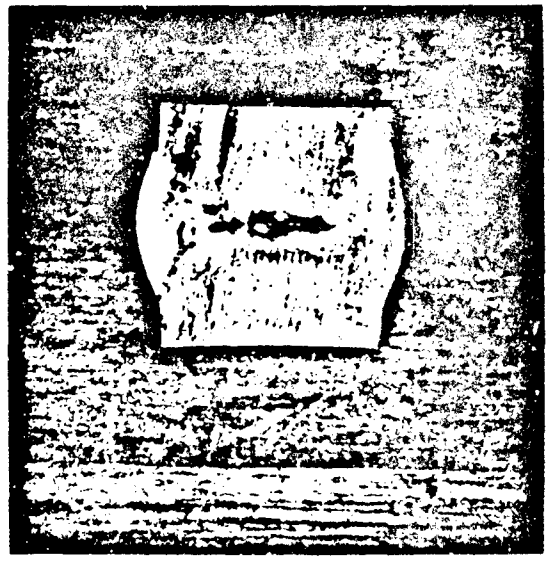


FIGURE 4. Specimen Cut Open To Reveal Internal Center Cracks After Failure.

Buckley (16) ran compression tests on cylindrical specimens of styrene-butadiene rubber in a Goodrich Flexometer. He found a similar type of

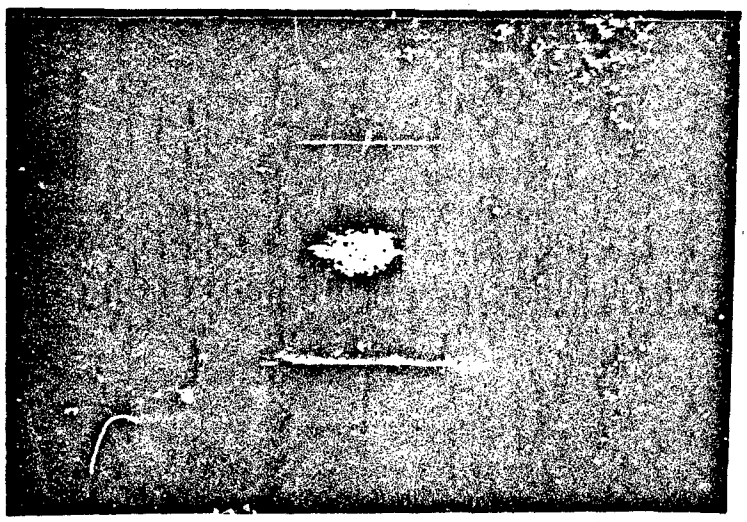


FIGURE 5. Uncut Specimen Showing Internal Cracks.

failure, with internal and/or external cracks running perpendicular to the loading direction. Although Buckley felt the stress state in his test would be much more complex than Treloar described for uniaxial compression, Buckley suggested the observed failures could be due to biaxial extension. The strains in the center of the specimen would be similar to a flat sample extended in two directions. The model which Buckley used to describe his failures is shown, with changes to represent a square cross-sectional surface as in our specimens, in Figure 6.

In this model the compressed specimen exhibits bulging. A slice taken from the center of the specimen, perpendicular to the loading direction, shows extensions similar tc those of a biaxially

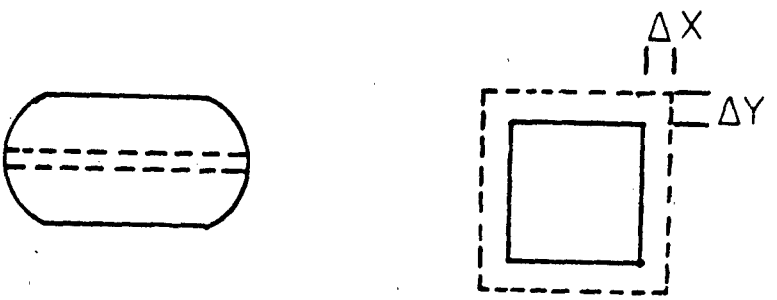


FIGURE 6. Biaxial Extension Model of a Compressed Block.

stretched sample. These extensions are believed to cause biaxial tensile failure of the specimen (16).

Recently, Stevenson (17) studied the formation of cracks in bonded rubber blocks. He found cracks to initiate at the bonded surfaces under tensile stress concentrations. In contrast to Buckley's results, he found no evidence for much heat build-up or internal cracking.

The results of our testing correlate well with the experiments of Buckley. It may be that heat build-up changes the characteristics of the failure so that only internal cracking initiates the failure, with external cracking appearing only at the very end of the test. Under compression cycling heat build-up occurs; the hottest portion of the specimen being the center of the block. The center portion of the block is subjected to extensional strain, and as the temperature at the center of the block approaches the hard segment transition temperature, the material properties at the center of the specimen will degrade. This weakening of the center portion of the specimen, in conjunction with

the extensional strain, causes failure at the center of the specimen.

CONCLUSIONS

Under three different loading conditions it was possible to fail specimens through cracks generated at the center of the test specimen. DSC analysis showed an increased hard segment transition temperature, caused by thermal annealing at the high temperatures of the fatigue test. Swelling analysis indicated that no significant breakdown in crosslink density is required for failure of specimens in compression loading.

All samples had a decreased elastic modulus (E') after fatigue; the percentage decrease grows with increasing number of fatigue cycles. The internal temperature also increases with the number of cycles, and the continuous increase in temperature leads to softening of the material and increased deformation. Stress-softening continues with increased amplitude of deformation, so the modulus decreases throughout the duration of the test. The modulus reduction is not caused by mechanical stress or thermal annealing alone, but requires the interaction of both.

The blocks fail under heat build-up with the generation of cracks at the center of the test specimen. Under compression cycling heat build-up occurs; the hottest portion of the specimen being the center of the block. The center portion of the block is subjected to extensional strain, and as the temperature at the center of the block approaches the hard segment transition temperature, the modulus of the material will decrease rapidly. This leads to higher and higher extensions, and finally, rupture of the specimen. This weakening of the center portion of the specimen, in conjunction with the extensional strain, causes failure at the center of the specimen, rather than surface failure initiation. There is scant experimental evidence for chain scission; however, it is possible that the urethane and urea bonds could dissociate at high

temperatures and subsequently reform as the material is cooled.

From this work it seems that the hard segment transition temperature determines the fatigue life of a compressed polyurethane block. For long part lifetimes the polyurethane must possess a very high temperature hard segment transition, or the heat build-up characteristics of the material must be such that the service temperature of the part is well below the hard segment transition.

ACKNOWLEDGEMENTS

The authors gratefully acknowledge the support of the U.S. Army Tank-Automotive Command for this work. We also wish to thank Mr. Preston Kemp and Ms. Linda VanDuyne, undergraduate assistants, and Dr. Kenneth Scott and Mr. Cal Harmon of Goodyear for providing technical assistance. Finally, we were most fortunate to have the technical assistance of the Army Materials and Mechanics Research Center in performing several of the analyses discussed here.

REFERENCES

1. C.S.P. Sung and N.S. Schneider, Macromolecules, Vol. 8, pp.68-77 (1975).
2. N.S. Schneider, C.S.P. Sung, R.W. Matton, and J.L. Illinger, Macromolecules, Vol. 8, pp. 62-67 (1975).
3. E.T. Bishop and S. Davison, Journal of Polymer Science - Part C, Vol. 26, pp. 59-79 (1969).
4. A. R. Cain, W. R. Conard, S. E. Schonfeld, and B. H. Werner, Polymer Preprints, Vol. 17, pp. 580-584 (1976).
5. E.F. Cluff and E.K. Gladding, Journal of Applied Polymer Science, Vol. 3, pp. 290-295 (1960).
6. S.L. Cooper and A.V. Tobolsky, Textile Research Journal, Vol. 36, pp. 800-803 (1966).
7. G. Allen, P.L. Edgerton, and D.J. Walsh, Polymer, Vol. 17, pp. 65-71 (1976).
8. T.L. Smith and A.B. Magnusson, Journal of Polymer Science, Vol. 42, pp. 391-416 (1960).

9. G. S. Trick, Journal of Applied Polymer Science, Vol. 3, p. 252 (1960).
10. S. L. Cooper, D. S. Huh, and W. J. Morris, Industrial Engineering and Chemistry - Product Research and Development, Vol. 7, pp. 248-251 (1968).
11. Y. Kaneko, Y. Watabe, T. Okamoto, Y. Iseda, and T. Matsunaga, Journal of Applied Polymer Science, Vol. 25, pp. 2467-2478 (1980).
12. Gent, A. N. and Meinecke, E. A., Polymer Engineeering and Science, Vol. 10, pp. 48-53 (1970).
13. Holownia, B. P., Journal of Strain Analysis, Vol. 7, pp. 236-242 (1972).
14. Reed, A. J. and Thorpe, J., in Elastomers: Criteria For Engineering Design, by C. Hepburn and R. J. W. Reynolds, Applied Science Publishers, Ltd., London, Chapter 11 (1979).
15. Treloar, L. R. G., The Physics of Rubber Elasticity, Clarendon Press, Oxford (1975).
16. Buckley, D. J., Paper presented at Rubber Division, A.C.S., May, 1974.
17. Stevenson, A., International Journal of Fracture, Vol. 23, pp. 47-59 (1983).

NATURAL RUBBER FROM GUAYULE

RICHARD WHEATON
Director, Critical Agricultural Materials Office, U.S. Department of Agriculture, Washington, D.C. 20250

A national concern over the availability of nonfuel minerals and materials considered essential or critical to the Nation's industrial base during either peacetime, demand surges, or emergency mobilization has been a longtime issue.

It has become a national policy to reduce America's materials vulnerability through dependency on foreign supplies for strategic and essential industrial materials. To implement this national policy, it has become a national goal to conduct research and development programs to provide for: the Nation's security, the Nation's economy, and adequate supplies of essential materials.

Natural rubber is an essential material for which the Nation is totally dependent on foreign sources. Domestic production would provide an alternative to this dependency and economic benefit to industry and the population in general.

The Critical Agricultural Materials Act of 1984 places responsibility with the U.S. Department of Agriculture to research and develop a domestic source of natural rubber from a native arid land plant called guayule. Current research on rubber processing is indicating that guayule can be economically competitive with imported hevea rubber. Byproduct yields, through technological advances, are being enhanced and provide new incentives for the research and development of a domestic natural rubber industry.

This economic competitiveness will make it possible to domestically produce needed quantities of natural rubber to meet any potential shortfall or disruption from foreign supplies. Domestic production would primarily address these issues should it become necessary to provide a larger share of the Nation's needs. A domestic source of natural rubber provides protection through a degree of self-sufficiency for one of the Nation's essential materials.

MICROSCOPIC CHARACTERIZATION OF CARBON BLACK DISPERSION IN RUBBER

ABRAM O. KING
Materials Characterization Division, U.S. Army Materials and Mechanics Research Center, Watertown, Massachusetts 02172

Carbon black dispersion is one of the key factors influencing tensile strength, abrasion, tear resistance, and other important properties of rubber.

The mixing process regulates the particle size, distribution, and degree of uniformity of aggregate/carbon dispersion within the final bulk rubber vulcanizate.

The work presented here is an optical microscopy study of a few commercial rubber samples selected for their potential use as track pad materials. These rubbers were produced by different vendors, each using a standardized formulation supplied by the U.S. Army Materials and Mechanics Research Center and showing variations in particle/aggregate size and dispersion.

THERMAL AND DYNAMIC MECHANICAL PROPERTIES OF ELASTOMERS

JOEY L. MEAD, ELIAS R. PATTIE
Composites Development Division, U. S. Army Materials and Mechanics Research Center, Watertown, Massachusetts 02172

ABSTRACT

Heat build-up measurements were taken on a variety of elastomer formulations under compression-compression fatigue in order to correlate material properties with tank track performance. Computer calculations of the effect of test piece geometry on heat build-up were made. Tan delta measurements were taken in the low strain regions with a Rheovibron, and hysteresis values were calculated using the values of tan delta obtained. These hysteresis values could not be correlated to the hysteresis values as obtained under compression test conditions. This indicates the need for dynamic mechanical tests under high strains, which will be addressed in future work.

I. Introduction

A. Heat build-up in tank pads can lead to failure

B. Material property tests should be used to predict performance

II. Experimental

A. Fatigue testing

1. Compression-compression fatigue
2. Stress ratio 0.1, 20 Hz, maximum load 4,500 lbs
3. Test specimens 2.5" x 2.5" x 0.63
4. Monitor internal temperature

B. Dynamic Mechanical Properties

1. Low strains--Rheovibron
2. Compare tan delta values

C. Hysteresis

1. Calculate hysteresis from tan delta and compare with actual hysteresis from test

a. Calculated hysteresis =

$$\frac{(\sigma_1 2 - \sigma_2 2)\pi \tan \delta}{E}$$

b. Compression modulus from fatigue test and tan δ from Rheovibron

TABLE 1

HYSTERESIS VALUES

Sample	Temp (C)	Hysteresis Calc. (lb-in)	Hysteresis Actual lb-in
TR-129	106	59	41
TR-130	91	97	52
TR-86	53	92	44
TR-92	141	96	44
TR-128	84	121	46
TR-127	48	79	40

TABLE 2

EFFECT OF VOLUME ON TEMPERATURE RISE

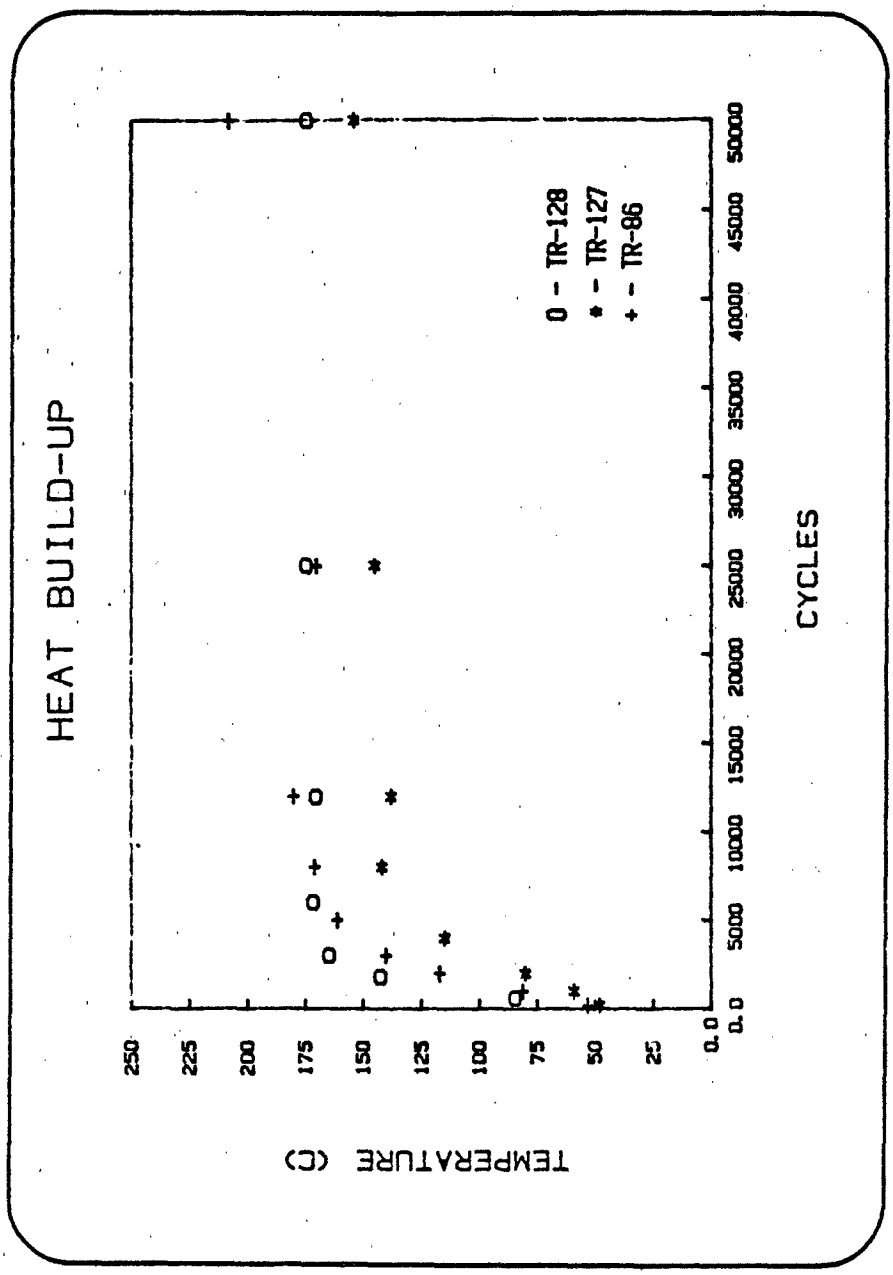
Width (cm)	Height (cm)	Temperature Rise (C)
6.35	1.52	18
12.70	3.04	72
19.05	4.56	162
25.40	6.08	283

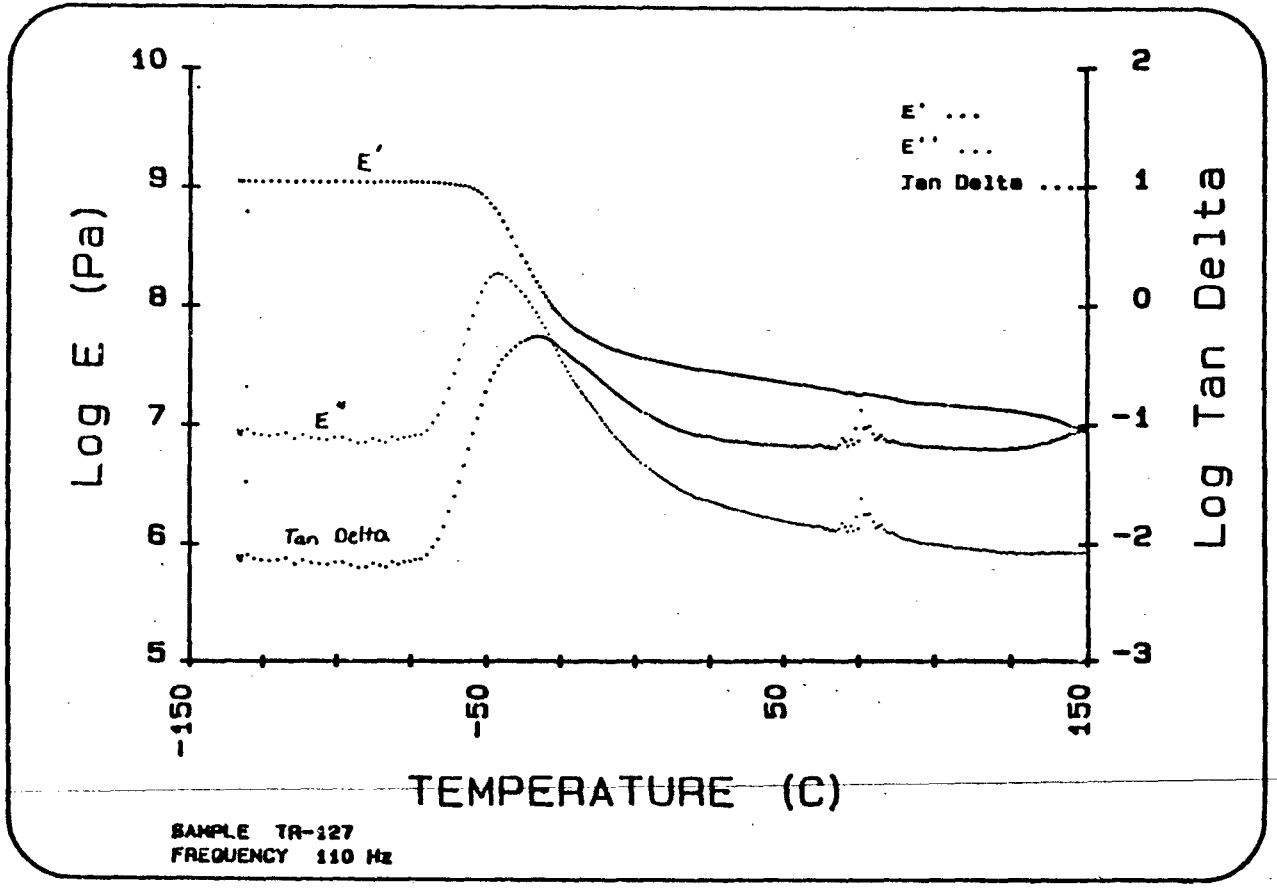
Shape Factor 1.04

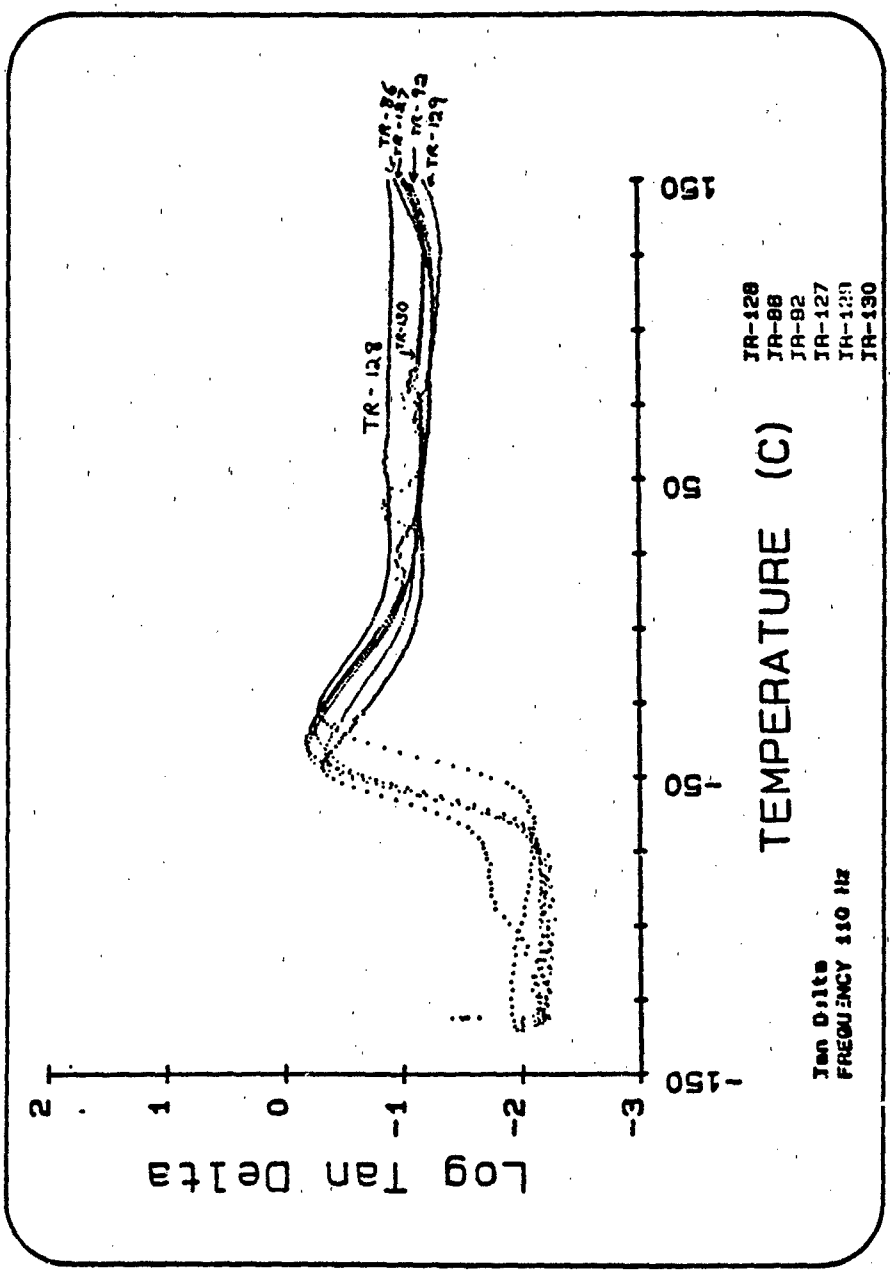
III. Conclusions

A. Calculated hysteresis values cannot be correlated with actual test hysteresis values

B. Dynamic mechanical tests under high strains will be required


HEAT BUILD-UP
TEMPERATURE (C)
CYCLES
O - TR-128
* - TR-127
+ - TR-86
250
225
200
175
150
125
100
75
50
25
0.0
5000
10000
15000
20000
25000
30000
35000
40000
45000
50000


10
9
8
7
6
5
Log E (Pa)
2
1
0
-1
-2
-3
Log Tan Delta
E' ...
E'' ...
Tan Delta ....
E'
E''
Tan Delta
-150
-50
50
150
TEMPERATURE (C)
SAMPLE TR-127
FREQUENCY 110 Hz


Log Tan Delta
2
1
0
-1
-2
-3
-150
-50
50
150
TEMPERATURE (C)
TR-128
TR-88
TR-92
TR-127
TR-129
TR-130
Jan Data
FREQUENCY 110 Hz

HEAT BUILD-UP CALCULATION

In order to obtain a rough estimate of the heat build-up in the blocks, a sample calculation was run for a urethane system. The equilibrium temperature rise above ambient (ΔT) can be calculated from (1)

$$\Delta T = RQ/60KA$$

where A is the surface area, Q is the heat input in cal/min, R is the distance from the center to the surface, and K is the coefficient of thermal conductivity in cal-cm/s-cm^2 - °C. Q can be calculated from the following equation

$$Q = 0.143\ E_H$$

where E_H is the heat energy input in N-cm/s. We can determine E_H for a given cyclic loading by (1)

$$E_H = (\sigma_1^2 - \sigma_2^2) w\ f_d/E_C$$

where σ_1 and σ_2 are the maximum and minimum stresses, w is the test frequency, f_d is the damping factor, and E_C is the compression modulus.

E_C is a function of the shape factor (S) of the test piece, where S is defined as the ratio of the loaded area to the force free area. The compression modulus can be calculated by (2)

$$E_C = E_O\ (1+2kS^2)$$

where E_O is the Young's modulus of the material, S is the shape factor, and k is a numerical factor.

From Rheovibron data a value for E_O was determined to be 1.89×10^9 dynes/cm^2. The values for E_O will vary with the temperature and the amount of deformation, but for a first approximation E_O was assumed independent of these variables. The value of k was assumed to be 0.5, K was taken to be 0.002, and f_d was assumed to be 0.15. For a fatigue test with

4,500 lbs maximum load, 450 lbs minimum load, and a frequency of 6.5 Hz, the equilibrium temperature rise was calculated for varying values of S. The test specimen was assumed to have a length and width of 2.5 inches, and the height of the specimen was varied to obtain changes in S. A second calculation was done, but with the shape factor constant and the volume of the block increasing. The cyclic stress was maintained the same for all sizes of the block.

REFERENCES

1. Sprey, R. (February 24, 1983): Avoiding Destructive Hysteresis in Elastomers. Machine Design.
2. Lindley, P. B. Engineering Design With Natural Rubber. NR Technical Bulletin. The Malaysian Rubber Producer's Research Association, Hertford, England.

SCANNING AUGER IMAGES OF ADDITIVE DISPERSION IN RUBBER

SIN-SHONG LIN
U. S. Army Materials and Mechanics Research Center, Watertown, Massachusetts 02172

ABSTRACT

Auger electron spectroscopic technique for examining additive dispersions of commercial rubber has been developed. This technique not only reveals inhomogeneous elemental distributions of rubber in micro-domains, but also can be used to deduce the probable chemical compositions of the heterogeneous sites. The particle sizes as well as aggregations of additives are determined within the electron beam width of the analytical instrument. Thus elemental distributions, additive dispersions, and chemical compositions of intimate mixtures can be studied by direct Auger imaging.

The preparation of the specimen is crucial for the success of the present technique. Frozen rubber is first sectioned into 10 to 20 um thick slices and then the slices are either mounted on an adhesive copper tape or back-coated with a noble metal. The sectioned surfaces are analyzed by scanning Auger microscopic imaging for elemental distributions, and by Auger spot spectra for chemical compositions. The spectra are used to calculate atomic concentrations from known elemental sensitivity factors. Examples obtained from commercial rubber will be illustrated and essential factors affecting the analysis will be discussed.

INTRODUCTION

The recent development of analytical instrumentation has accelerated advancements of scientific frontier in discovery and understanding of new phenomena. Application of Auger electron spectroscopy (1-3) (AES) in scientific fields has expanded from the initial stage of laboratory curiosity (4) to every corner of material sciences (5, 6). This technique has features uncommon to other electron beam methods. One of the notable characteristics of this technique is its ability to study the chemical environment of surface elements in the most efficient and effective way. The instrument has a high sensitivity for the light elements commonly observed in organic materials. This contrasts with X-ray fluorescence analysis where the fluorescence yield is very small for these elements.

The degree of additive dispersions in rubber is one of the important factors that influence physical properties of vulcanized rubber (7). The significance of carbon black dispersion on mechanical properties of rubber has been discussed in the literature (8, 9). However the dispersion of other additives, such as sulfur and sulfur containing molecules, zinc oxide, and organic acids, is not well understood. It is generally believed that these additives are chemically well dispersed into the interiors of the rubber matrix, and due to their small quantities, the properties of the rubber are less affected by the extent of their dispersions.

The information obtainable from the AES study of the dispersion of the additives excluding carbon black includes: (1) the dimensions and the distributions of additives or additive agglomerates, (2) the chemical natures of these particles and agglomerates, and (3) the chemical differences of the surface irregularities. In this paper, the technique for studying additive dispersions is described. The Auger images of commercial rubber are illustrated and the dominant factors influencing the analysis are discussed.

EXPERIMENT ANALYSIS

Sample Preparation

Preparation of specimen for AES analysis is crucial for success of the present technique. The rubber to be examined is first sectioned into a suitable thickness, followed by proper mounting on a specimen holder before it is placed into the analytical chamber of the Auger instrument.

Sectioning of Rubber. The procedure for sectioning vulcanized rubber has been well documented in ASTM tests (10, 11), so it will not be repeated here. The main features of the present preparation are not quite as strict as those described in the ASTM methods. The rubber is first frozen below the glass transition temperature so that a smooth cutting can take place. The easiest way to do this is to pick up a chunk of rubber from liquid nitrogen and mount it on the microtome instrument for immediate slicing until the rubber is defrosted. Usually, the cutting period can be extended by spraying with Freon coolant. The surface contamination of the coolant was found to be negligible after vacuum outgassing. The best thickness of slices is approximately 10 to 20 um, since for thinner slices the surface is easily destroyed by the analytical electron beam, while for thicker slices no Auger signal can be obtained due to poor electrical conductance.

Therefore, an appropriate thickness is determined by the conductance as well as by the electron beam density of the analytical instrument.

Mounting of Slices. For Auger electron spectroscopic analyses, a good signal is obtained only when the surface to be examined is conductive and is firmly grounded. For this reason, the surface should have a good electric connection to a supporting fixture. This is accomplished by either conducting adhesives or by evaporation coating of Pd/Au onto the backside of the sliced surface. By a trial and error method, it is found that intimate adhesion of the surface can be made by a conductive copper tape commercially available. Care should be exercised not to expose excessive adhesive on the front surface. It should be stressed that intimate adhesion between rubber and copper has been made by repeatedly pressing the rubber surface against the underlying copper tape. The use of tweezers and forceps is highly recommended to avoid surface contamination. In the case of the conductive coating, Pd/Au alloy commonly used in the SEM specimen preparation (12) is employed. The metal coating on the surface is about 1 um thick. Due to the elastic nature of rubber, frequent bending of the back surface during handling may displace the evaporated layer. Consequently it might produce a small electrically isolated domain. After careful mounting, the specimen is ready to clip onto the carousel of the analytical instrument.

Instrument and Procedures

The instrument used in the present investigation is PHI model 548 ESCA/Auger manufactured by Physical Electronics Ind., with a scanning Auger microscopic (SAM) attachment. The instrument is depicted in Figure 1 and the Auger transition is briefly illustrated in Figure 2. For the present analysis, the electron energy is fixed at 5 kV and 1 uA. with modulation frequencies of 6 eV for SAM and 3 eV for stationary Auger spot analysis. Under this setting, the electron beam width is about 4 um. The setting is chosen because of convenience as well as minimal distortion of Auger images with a maximum area of analysis. The SAM images are recorded by using the magnitudes of the negative peak heights at a speed of 2.5 minutes/frame. The identification of an element is established from the energies of emitted Auger electrons. From the magnitudes of Auger peak heights recorded on the spectra, the chemical composition can be estimated (13).

Heating Effect. The primary electron beam has a tendency to heat the surface, resulting in evaporation, charring, and

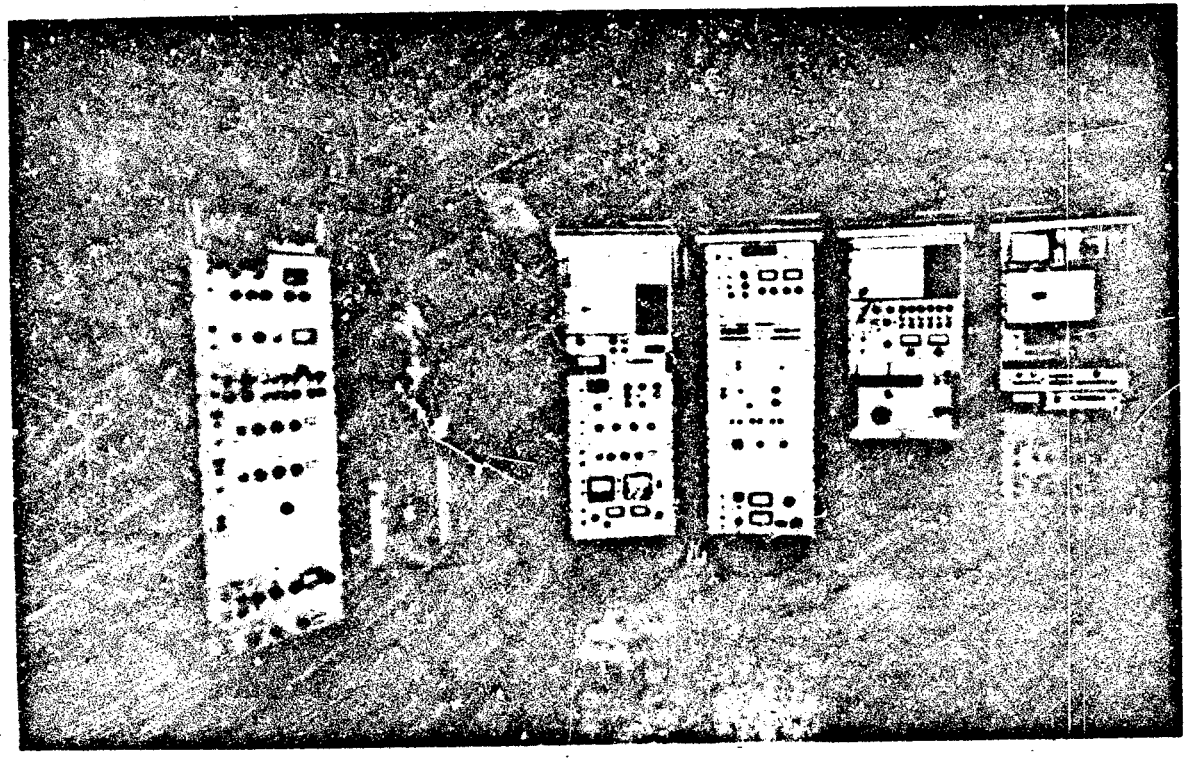


FIGURE 1. The surface analytical instrument, PHI Model 458 manufactured by Physical Electronics Ind., Perkin Elmers Corp. From left (1) Scanning Auger microscope and TV monitor, (2) Vacuum chamber including two ion guns, two electron energy analyzers, specimen stage, X-ray generator, quadrupole mass spectrometer, etc. (3) Auger spectrometer control, (4) Auger control and data processing, (5) Depth profiling and X-ray power source, and (6) Secondary ion mass spectrometer panel.

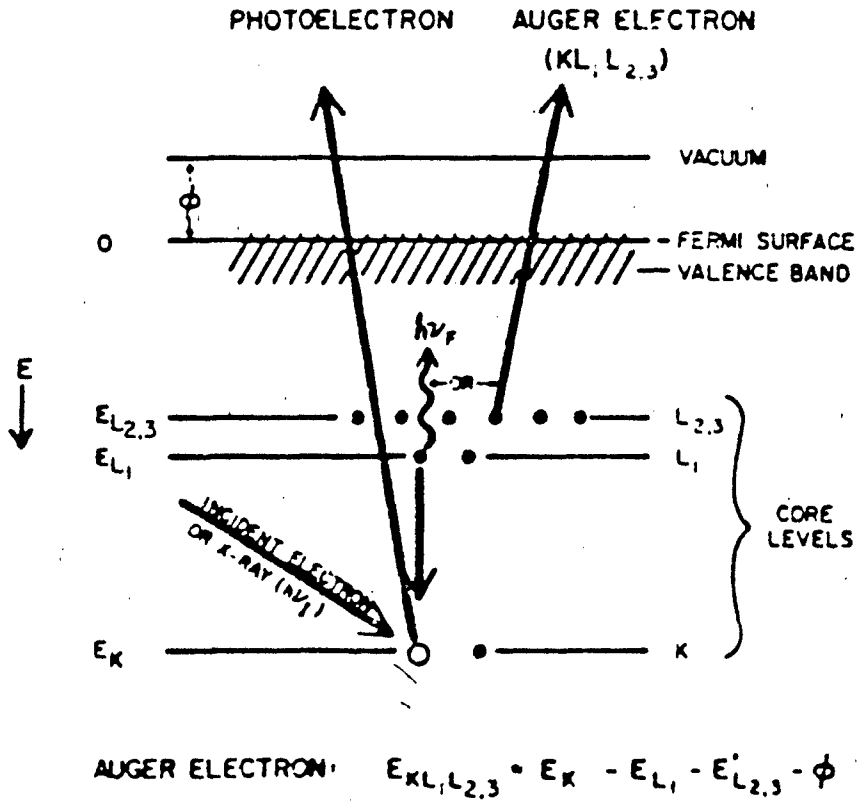


FIGURE 2. Illustration of Auger electron transition. There are three steps: (1) creation of vacancy in the inner atomic orbital (K shell) by an electron beam of X-ray radiation. (2) the electron transition from the upper level (L_1 shell) to the vacant orbital (K shell), and simultaneously, (3) the emission of Auger electron from the adjacent atomic orbital ($L_{2,3}$ shell).

destruction of the analyzed area. Heating by primary electron beam causes serious problems in the analysis. The heat induced by the electron beam not only introduces physical damage to the surface, such as cracking and shrinking, but it also creates unwanted chemical transformation on the surface. Thus, the image obtained at the end of the scanning will be distorted; and in the extreme case, the surface is entirely different from that at the beginning.

Charging Effect. The effect of sample charging (14) due to electrically isolated domains should be avoided as much as possible during the preparation. The effect can be reduced by lowering the primary analytical electron energy, tilting the sample surface, and using a neutralization gun. The floating potential surface yields drastic changes in SAM images and AES spectra. The interpretation of the image and the spectrum becomes difficult and erroneous. In an extreme case of the charge effect, the AES spectrum consisted of several large off-scale signals occurring at low electron energy. In a lesser extent of the charge effect, the Auger peak positions are shifted toward higher electron energy. Since the magnitude of the energy shift is not predictable, the Auger peak positions in the spectra become meaningless. The SAM images under a mild charging condition show extreme bright spots indicating excessive accumulations of electrically charged islands.

Chemical Contrast

The versatility of the Auger electron spectrosopy is due in great measure to its detection of a rich variety of chemical elements present on the top surface. Therefore, the chemical treatment can be employed to produce high contrast in SAM images revealing differences in chemical binding states of the heterogeneous surface in addition to particle inclusions and agglomerations. By a suitable choice of chemical reactants, it is possible to reveal heterogeneities in the binding states of elastomer surfaces. Chemical oxidizing reagents such as $KMnO_4$, OsO_4, Br_2, and HBr can be used to monitor heterogeneous micro-domains in rubber structures by varying degrees of reaction. The results obtained from the $KMnO_4$ and OsO_4 solutions will be illustrated here.

RESULTS AND DISCUSSIONS

The example of poor dispersion with many heterogeneous sites taken from commercial tread ruober is shown in Figure 3. The terrain with many particle inclusions is shown (Figure 3a and 3b). The SAM image of carbon (Figure 3c) and those (Figures 3d to 3f) of oxygen, sulfur, and zinc are complimentary. The site at the center of the frame (Figure 3b) shown on the AES spectrum (Figure 4a) reveals a rather high concentration of oxygen. The presence of oxygen without accompanying cation indicates that oxygen is probably present as organic acids, carbonyl, or highly oxidized polymers. Two bright spots are observed in the sulfur image (Figure 3e), but one of them has no corresponding spot in the oxygen and zinc images (Figure 3d and 3f). The stationary AES analyses (Figure 4c) of the latter

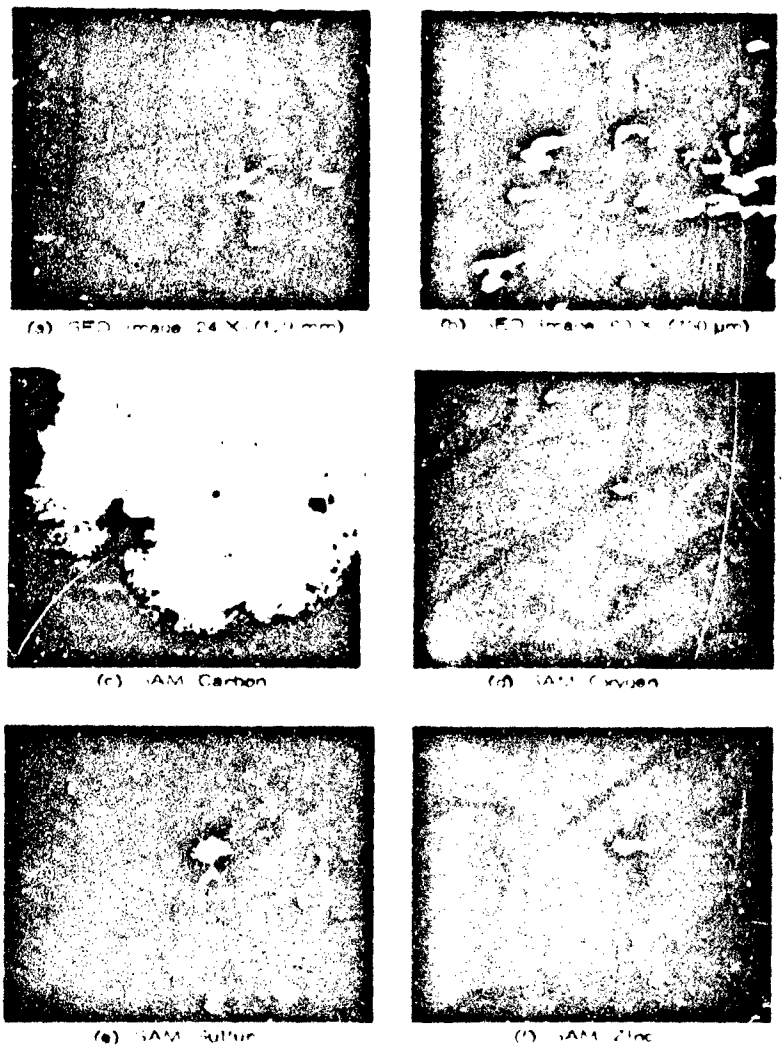


FIGURE 3. Scanning Auger microscopic images of rubber surface (TP#48). Two bright spots, A and B, in the S image are observed, but only "B" has corresponding spots in the Zn and O images.

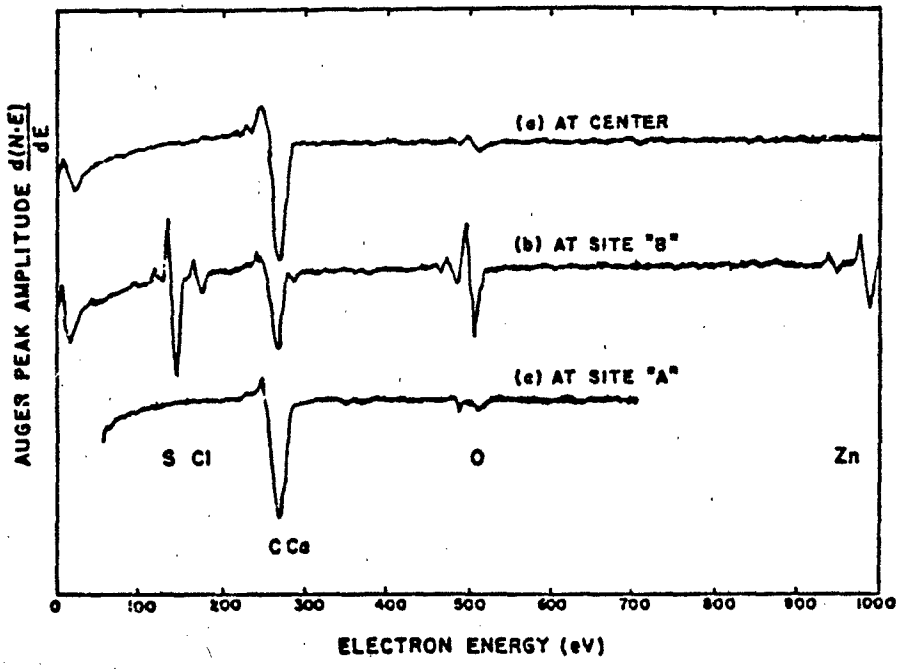


FIGURE 4. Auger electron spectra of rubber surface (TB#4B). Refer to Figure 3b: (a) at the center, (b) at site "B", (c) at site "A".

spot (designated as "A" in Figure 3e) reveals no sulfur signal. This might be due to the evaporation of free sulfur by excessive heat produced by the electron beam during the spot analysis. The sulfur image taken after the spot analysis and the prolonged exposure to the electron beam, shows the absence of this bright spot. The stationary analysis (Figure 4b) of the site (designated as "B") in (Figure 3c) indicates the presence of Zn, S, O, Ca, and Cl in addition to C. The atomic concentrations of the first three elements are roughly in a proportion of 21:15:17. Thus the site probably contains ZnO, ZnS, and CaO in addition to Zn/Ca chlorides. After the magnification of 500X (frame width 150 um) as shown in Figure 5a, the site is found to consist of at least two, possibly three, large aggregates under the present limited resolution. From the SAM images shown (Figure 5b to 5d), it can be speculated that the site is an agglomeration consisting of several particles containing ZnO and ZnS in a matrix of elastomer and carbon black. The present observation suggests that ZnO has reacted with S to form ZnS. During the fabrication of vulcanized rubber, the

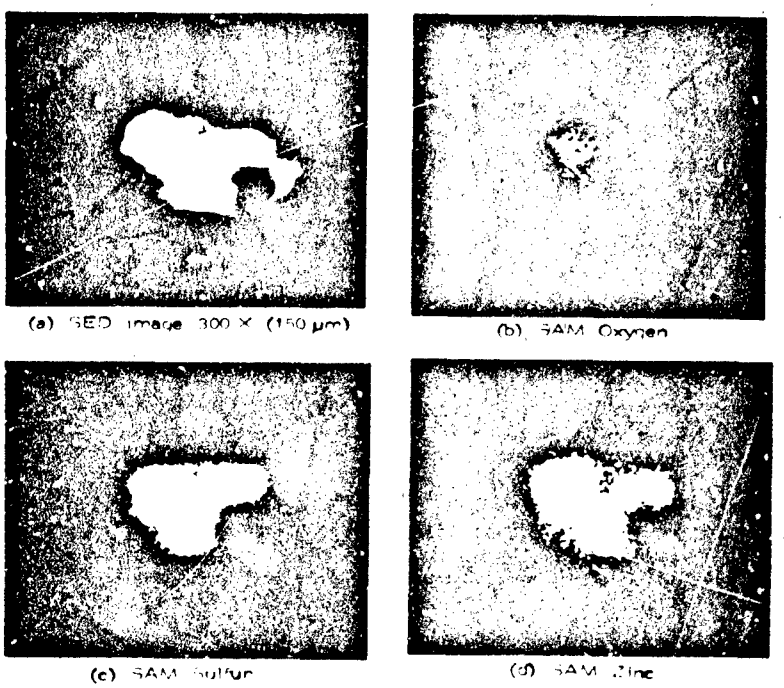


FIGURE 5. Scanning Auger microscopic images of rubber surface (TP#4B1). The enlargement of the site "B" in Figure 3. The site is an agglomeration of many ZnO and ZnS small particles.

sequence of the blending process might adversely lead to the formation of ZnS instead of S cross-linkage.

One set of the interesting SAM images containing many exotic particle inclusions is shown in Figure 6. Several bumps and nodules are clearly shown on SED photograph (Figure 6a). Two spots partially immersed in rubber matrix are found to have high oxygen concentrations (Figure 6c). The stationary analyses (Figure 7) of these sites indicate that the "A" location has chemical constituents of Al, Si, Ti and O, while the "B" location has a negligible amount of oxygen only. In the latter case, the particle might have been removed by the electron beam. In the S image (Figure 6d), two high concentrations of sulfur are observed, but no sulfur is detected in the AES spectra (Figure 7c and 7d). The "C" location is found to have a large amount of CaO while the "D" site shows only carbon. The absence of sulfur is probably due to evaporation by the electron beam heating. In other instances, foreign particles of Fe, Cr, and Ni oxides are found (not shown) to embed into the rubber matrix. These are contaminations probably introduced during fabrication.

In Figure 8, the surface treated with $KMnO_4$ with the reference image (Figure 8a) followed by the SAM images of C, O, and Mn (Figures 8b to 8d, respectively) is shown. The topography of the surface (Figure 8a) after the treatment is fairly smooth with fewer numbers of bumps and nodules scattered on the surface. The SAM C image (Figure 8b) reveals that except for a few sites, carbon C is distributed evenly. The SAM images (Figures 8c and 8d) of O and Mn are very similar except for relative contrast. The distribution of these two elements are not homogeneous due to the varying degrees of chemical reactions which occurred between the permanganate solution and the rubber surface. The reaction (15) is thought to remove noncrystalline material preferentially in polyethylene. The high concentrations of Mn and O are observed in the upper left corner of the both frames (Figures 8c and 8d). The high density of Mn shown on the image is probably derived from a high reactivity of the surface and a formation of stable Mn compounds. The chemical contrast has been also produced by the treatment of the rubber surface with a 1 percent OsO_4 solution. This oxidative treatment affects only residual olefine double bonds (16) in rubber. The SAM Os image (not shown) shows no enrichment of Os indicating that no appreciable amount of olefin double bonds remains in the rubber matrix.

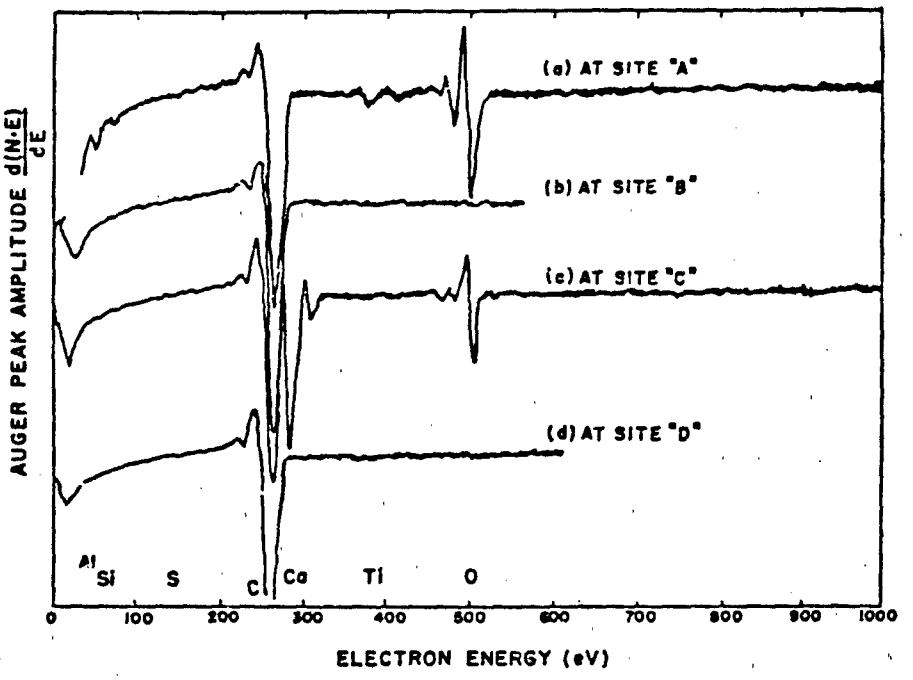
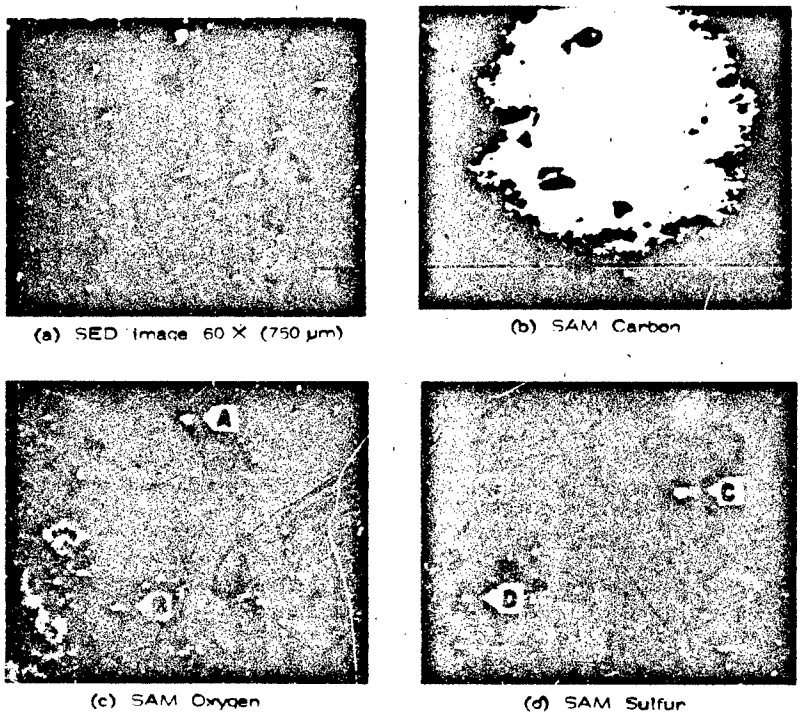


FIGURE 6. Scanning Auger microscopic images of rubber surface (TP#10B). Four heterogeneous sites are observed in the S and O images designated as A, B, C, and D. The compositional analyses of these sites show exotic chemical constituents.

CONCLUSIONS

Auger electron spectroscopy is a versatile tool in studying the chemical constituents of dispersions in rubber. This technique combined with the SAM analyses produces two dimensional images which are useful in the elucidation of aggregations and dispersion states of the rubber additives. Especially particle inclusions and agglomerations can be studied together with the topographic features of the complimentary SED image. Additional information concerning the binding states of elastomers and additives, aggregations of excessive cross-linkages, unsaturated double bonds, and large hard segments of polymers can be imaged with the aid of chemical reactants.

The success of the present AES technique depends on the proper preparation of sample surfaces. A conductive surface is an essential factor in the analyses of additive dispersions.



(a) SED Image 60 X (750 μm)

(b) SAM Carbon

(c) SAM Oxygen

(d) SAM Sulfur

FIGURE 7. Auger electron spectra of rubber surface (TP#10B). Refer to Figure 6a: (a) at "A", (b) at "B", (c) at "C" and (d) at "D". Many particle inclusions are observed.

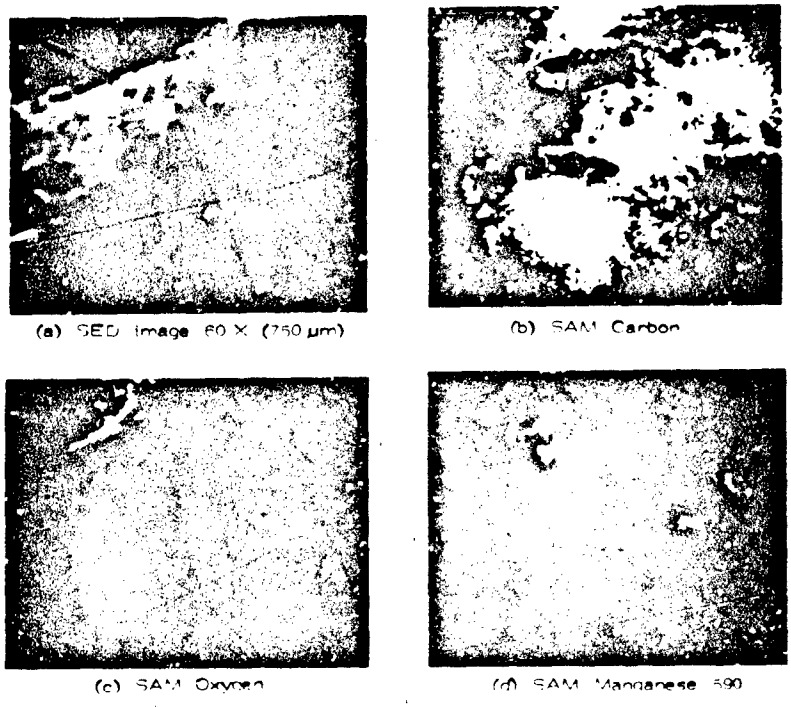


FIGURE 8. Scanning Auger microscopic images of rubber surface after chemical treatment with $KMnO_4$. The sectioned rubber is treated with a saturated $KMnO_4$ solution to reveal the heterogeneous chemical nature of the surface. The Mn and O images are similar due to the chemical reaction.

The heating of the surface by the electron beam as well as the alternation of the surface topology by electron specimen interactions should also be considered in the correct interpretation of the observed images. Artifacts associated with the analysis should be carefully examined so that they might reveal information about tne composition and heterogeneity.

ACKNOWLEDGMENT

The author wishes to express many thanks to Dr. R. E. Singler, of AMMRC, for his assistance and discussion during the preparation of the manuscript, and especially for his enthusiastic support of the research program.

REFERENCES

1. Chang, C. C. (1976): Characterization of Solid Surface, edited by P. E. Kane and G. B. Larrabee, Plenum Press, New York, Chapter 20, 509 pp.
2. Grant, J. T. (1977): Characterization of Metal and Polymer Surface, edited by L. H. Lee, Academic Press, Inc., New York, 133 pp.
3. Joshi, A., Davis, L. E., and Palmberg, P. W. (1975): Methods of Surface Analysis, edited by A. W. Czanderna, Elsevier Scientific Pub. Co., New York, Chapter 20, 159 pp.
4. Auger, P. (1926): Ann. Phys., Paris, 6, 183.
5. Turner, N. H., Dunlap, B. I., and Colton, R. J. (1984): J. Anal. Chem. 56, 373r.
6. Grant, J. T. (1982): Surf. Sci. 13, 35.
7. Gent, A. N. (1978): Strength of Elastomer. In: Science and Technology of Rubber, edited by F. R. Eirich, Academic Press, New York.
8. Boonstra, B. B. and Medalia, A. E. (1963): Rubber Age, 92, 892.
9. Boonstra, B. B. and Medalia, A. E. (1963): Rubber Age, 93, 82.
10. ASTM 09.01, D3849-80 (1983): Primary aggregate dimensions from Electron Microscopic Image Analysis.
11. ASTM 09.01, D2663-83 (1983): Dispersion of Carbon Black.
12. Newbury, D. E. and Yakowitz, H. (1977): Practical Scanning Electron Microscopy, edited by J. I. Goldstein and H. Yakowitz, Plenum Press, New York, 211 pp.
13. Davis, L. D., et al. (1976): Handbook of Auger Electron Spectroscopy, Physical Electronics Industries, Inc.

14. Oatley, C. W. (1972): The Scanning Electron Microscope, The University Press, Cambridge.
15. Barnes, S. R. (1980): Polymer, 21, 723.
16. Hobbs, S. Y. and Watkins, V. H. (1982): J. Polym. Sci., 20, 651.

ASPECTS OF THE SYNTHESIS OF POLY(DICHLOROPHOSPHAZENE)

MICHAEL S. SENNETT
U. S. Army Materials and Mechanics Research Center, Watertown, Massachusetts 02172

INTRODUCTION

The thermal polymerization of $(NPCl_2)_3$, I, is the principal synthetic route to poly(dichlorophosphazene) $(NPCl_2)_n$, II. The uncatalyzed polymerization is difficult to control, particularly its tendency to produce insoluble, crosslinked polymer at high conversions (1). Understanding and treating this problem is made more difficult by the lack of reproducibility observed from batch to batch of I. The polymerization of I has been studied extensively and is reviewed in recent literature (2). It is generally agreed that it is a cationic chain-growth polymerization, initiated either by ring opening of I or by chloride dissociation from I (3-5).

Catalysis has been considered as a possible solution to the problems encountered in the polymerization of I and a great many materials have been tested for catalytic activity (6,7). Although many materials are capable of accelerating the reaction or lowering the temperature required to induce polymerization, most also tend to promote crosslink formation. Boron trichloride (BCl_3), is catalytically active and promotes polymerization at temperatures as low as 150°C although gel formation is still encountered under some conditions. Performing the polymerization with dilute solutions of I has been shown to help control crosslinking (8), and BCl_3 catalyzed solution polymerizations of I in 1,2,4-trichlorobenzene (TCB) produce high yields (> 80 percent) of soluble, high molecular weight II.

This paper presents the results of an investigation of the BCl_3 catalyzed solution polymerization of I. The use of laser Raman spectroscopy to monitor the concentration of $(NPCl_2)_3$ throughout the course of the reaction represents a great improvement over gravimetric methods previously employed to determine polymerization rates. Characterization of the polymeric products of the reaction by size exclusion chromatography (SEC), light scattering, membrane osmometry, and dilute solution viscosity (DSV) techniques provided information important to understanding the reaction mechanism.

EXPERIMENTAL SECTION

Toluene and heptane were distilled from CaH_2 under N_2 and stored under N_2. HPLC grade TCB (Fisher) was saturated with N_2 upon opening and stored under N_2. HPLC grade THF was used as received from Burdick and Jackson Labs and stored under helium. $(NPCl_2)_3$ (Phosnic 390, Inabata Co., Japan) was purified by repeated recrystallization from heptane and sublimation. BCl_3 (99.95 percent) was used as received from Matheson Gas Products. Polymerizations monitored by Raman spectroscopy were carried out in heavy walled pyrex tubes (5 mm o.d. x 200 mm long, approx. vol. 2 mL). Larger ampoules (approx. vol. 30 mL) were used to prepare polymers for characterization studies.

In a typical experiment, a flame dried polymerization tube was filled in the drybox with a TCB solution of I. The filled tube was then degassed outside the drybox using a vacuum line and ultrasonic agitation. A measured quantity of BCl_3 was then condensed at 77 K into the tube which was then sealed with a flame. Polymerization was carried out in a thermostatted aluminum block heater controlled to within 1°C of the desired temperature. Laser Raman spectroscopy was performed using a Spex Industries model 1401 spectrometer coupled to a Spex Datamate system and a Spectra-Physics 2 watt argon-ion laser. The initial Raman spectrum of the polymerization solution was recorded at room temperature from 280 to 420 cm^{-1}. The sample was then heated to polymerization temperature. The reaction was halted at intervals by cooling to room temperature and the Raman spectrum recorded again. The areas of the peaks at 327 cm^{-1}, 361 cm^{-1}, and 390 cm^{-1} (TCB, I, TCB) were calculated and the ratios of the peak areas (361/327, 361/390) were used to determine the concentration of I.

After polymerization, II was characterized by SEC and DSV then reacted with THF solutions of $NaOCH_2CF_3$ in the drybox at room temperature to produce the stable polymer $(NP(OCH_2CF_3)_2)$, III, for further characterization by light scattering and membrane osmometry (9). SEC was carried out on a Waters 244 ALC/GPC instrument with 6000A solvent delivery system, U6K injector and a R400 refractive index (RI) detector coupled to a Spectra-Physics SP4000 data system. Additional chromatography was performed on a Waters 150 ALC/GPC instrument coupled to a Waters Data Module (9). Light scattering was performed on a FICA model 50 instrument. Membrane osmometry measurements were made on a Hewlett Packard Mechrolab model 501 high speed membrane osmometer equipped with an Arro Laboratories Type 600 cellulose acetate membrane. DSV measurements were made using Cannon Ubbelohde type viscometers immersed in a 40 L water bath controlled to within 0.1°C of the desired temperature.

RESULTS AND DISCUSSION

Polymerizations were carried out using 0.54 molal (m) solutions of I in TCB and BCl_3 concentrations ranging from 0 to 5.4 m. The reaction temperature was varied between 170 and 230°C.

Molecular Weight Determinations

Monitoring the molecular weight of the product polymer as a function of extent of reaction showed that $\bar{M}_w$ increased throughout the course of the reaction, suggesting the absence of a termination step. A typical molecular weight distribution (determined by SEC) was essentially uni-modal and broad, with dispersity ($\bar{M}_w/\bar{M}_n$) values ranging from 2 to 7. This contrasts the typically complex molecular weight distributions of polymers produced in uncatalyzed polymerizations (10). As the BCl_3 concentration was increased from 0 to 1.08 m at 190°C and constant I, the polymer molecular weight increased reaching a maximum at 0.16 m BCl_3 then decreased (Figure 1). This effect can be attributed to the variation of the relative rates of propagation and initiation. As the temperature was increased from 170 to 230°C at constant concentration of reactants (0.54 m BCl_3, I) the polymer molecular weight increased as shown in Figure 2. This suggests that the activation energy for propagation is greater than that for initiation. At very high [BCl_3] (> 5.0 m), high polymer did not form.

Rate Determination

Plots of log [$(NPCl_2)_3$] vs. time were linear through at least one-half life at constant temperature and [BCl_3] indicating first order behavior of the reaction under these conditions. Varying the BCl_3 concentration caused the observed rate constant k_{obs} to vary as shown in Figure 3. The rate of polymerization decreased dramatically when BCl_3 was removed from the system in mid-reaction. These observations suggest a complex rate constant incorporating a pre-equilibrium step. The effect of temperature on the observed rate constant is illustrated in Figure 4. From these data it was possible to determine the rate constants for propagation and the values of the pre-equilibrium constant for propagation at temperatures from 170 to 230°C (Table 1).

The thermodynamic parameters for the propagation reaction and for the formation of the catalytically active species were determined by analyzing the temperature dependence of k_3 and K_2, respectively. The activation energy for propagation determined in this manner is 36 kcal/mole and the heat of

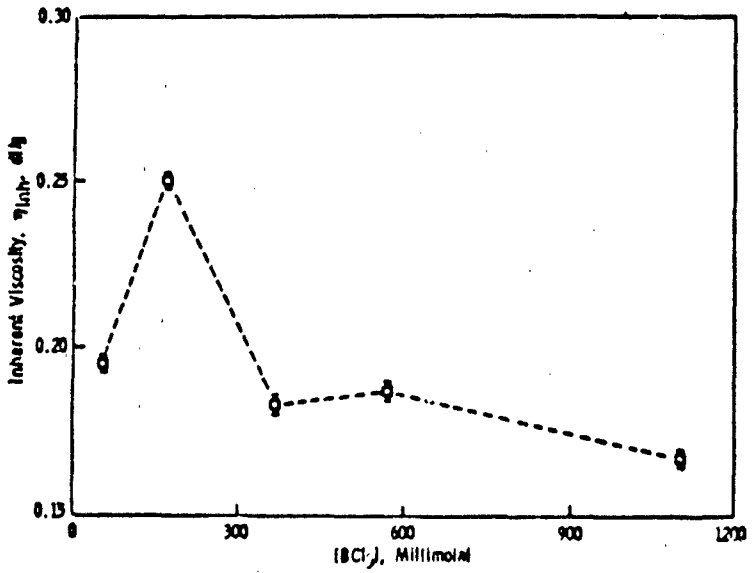


FIGURE 1. Dependence of the inherent viscosity of III on $[BCl_3]$. Polymerization at 190°C and $[I]_o$ = 0.54 m, carried to 60 percent conversion.

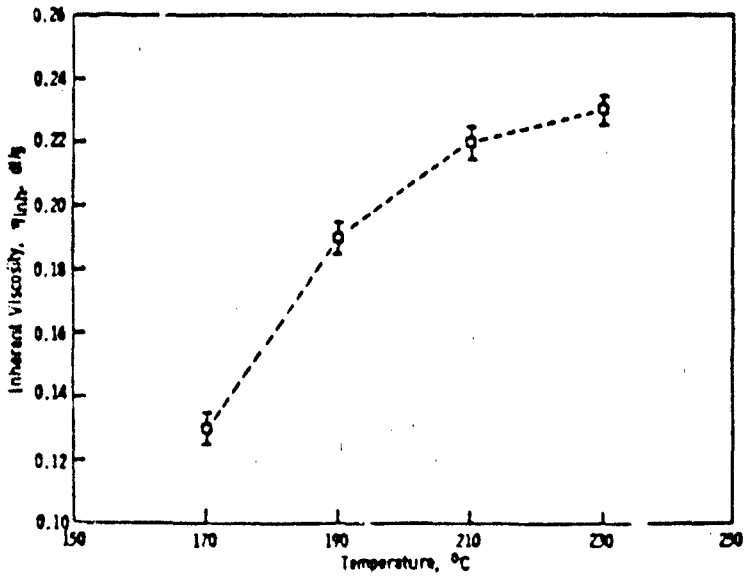


FIGURE 2. Dependence of the inherent viscosity of III on polymerization temperature at $[BCl_3] = [I]_o = 0.54$ m. Polymerizations carried to 60 percent conversion.

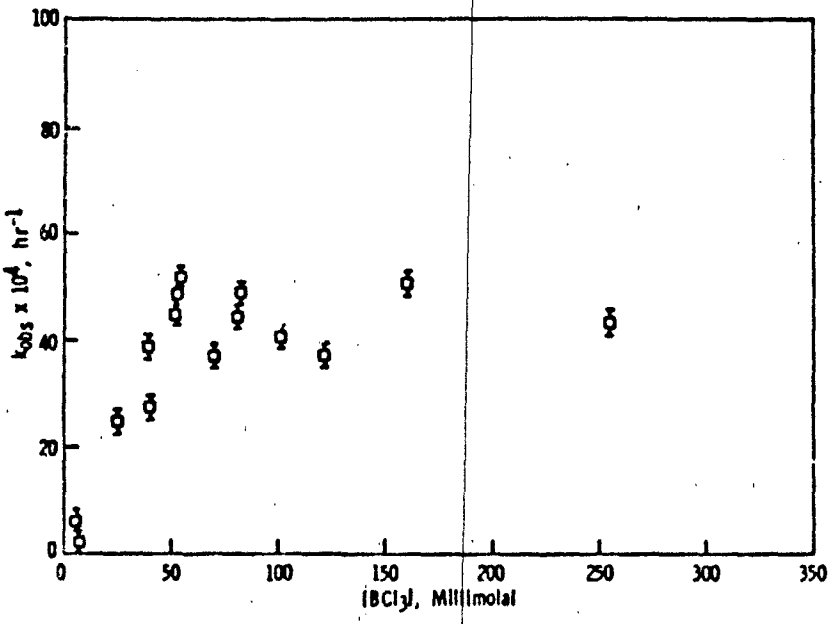


FIGURE 3. Dependence of the observed rate constant on [BCl_3] at 170°C and $[I]_0$ = 0.54 m

formation of the catalytically active species is -28 kcal/mole. As the BCl_3 concentration was increased above 0.50 m at 170°C, the overall reaction rate decreased sharply to a minimum at about 0.60 m, then slowly increased. This behavior coincided with a decrease in the production of high polymer, indicating inhibition of propagation by concentrations of BCl_3 consistent with the findings of Horn et al. (11). This inhibition is attributed to the formation of an acid-based adduct between BCl_3 and I which is deactivated to propagation.

Catalysis Mechanism

The proposed reaction mechanism is illustrated in Figure 5. Evidence for the equilibrium K_2 includes the dependence of the reaction rate on the BCl_3 concentration and the reversibility of the reaction when BCl_3 is removed from the system. This behavior was consistent over the entire temperature range studied. The nature of the interaction between BCl_3 and the growing chain end is speculative. The proposal is based on the known chemistry of BCl_3 and I, in particular the compounds prepared by Moran (11): $(Cl(Cl_2PN)_3PCl_3^+)^3PCl_6^-$ and $Cl(Cl_2PN)_3PCl_3^+BCl_4^-$. The proposed formation of the BCl_3:I

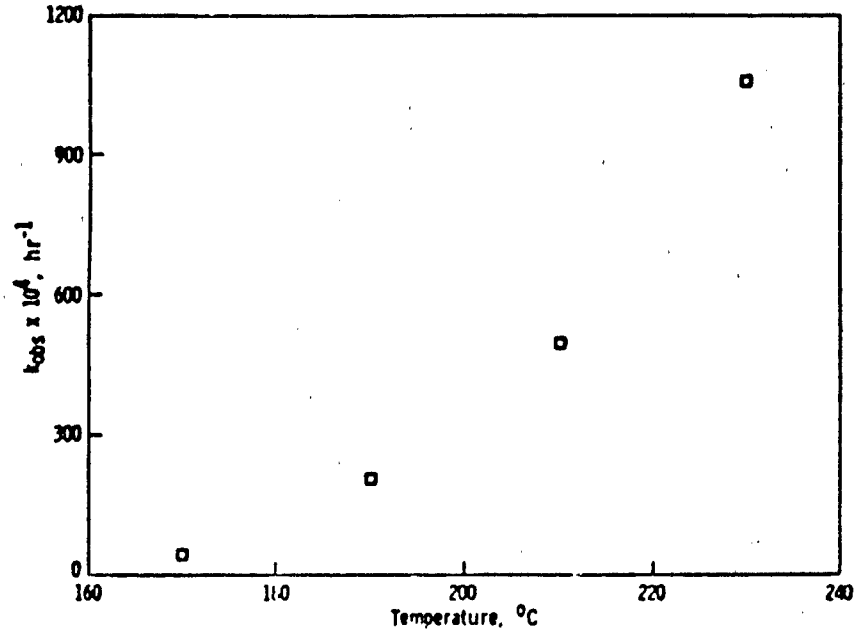


FIGURE 4. The effect of temperature on observed rate constant.

TABLE 1

TEMPERATURE DEPENDENCE OF THE RATE CONSTANT k_3 AND THE EQUILIBRIUM CONSTANT K_2 FOR PROPAGATION

Temperature, °C	k_3, hr^{-1}	K_2, kg sol'n/mol
170	6.56×10^{-3}	33.0
190	3.69×10^{-2}	5.3
210	1.61×10^{-1}	2.2
230	8.12×10^{-1}	0.68

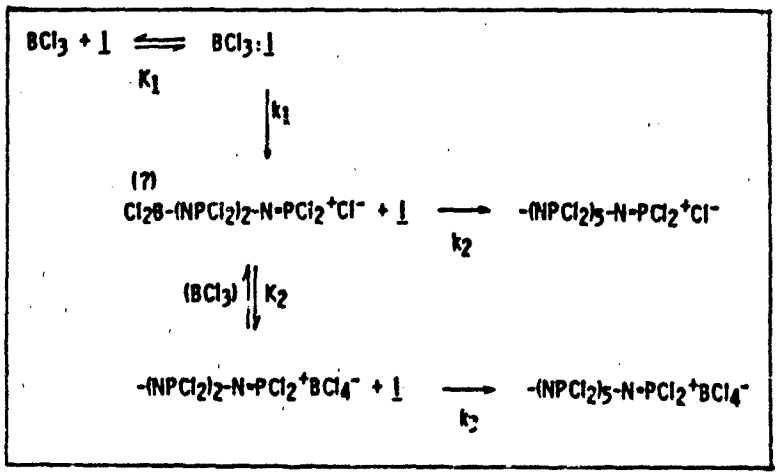


FIGURE 5. Proposed reaction mechanism for the BCl_3 catalyzed polymerization of I.

adduct in the initiation step is necessary to explain the inhibition of propagation by high concentrations of BCl_3. The formation of such an adduct is supported both by precedent (the well known BX_3-amine adducts) and by Horn's ^{31}p NMR observations of derivatives of I in the presence of BCl_3 (13). Given the high electron affinity of BCl_3 and the fact that I is the strongest base in the system, the association seems inevitable. The absence of a termination step is indicated by the polymer molecular weight dependence on conversion.

Ongoing research is directed at positive identification of the polymer end groups and further enhancement of the reactivity of the growing chain end.

REFERENCES

1. Allcock, H. R. (1972): Phosphorus Nitrogen Compounds. Chapter 15, Academic Press, New York.
2. Hagnauer, G. L. (1981): J. Macromol. Sci-Chem., A16(1), 385.
3. Konecny, J. O. and Douglas, C. M. (1959): J. Polym. Sci., 36, 195.
4. Knoessel, R., Parrod, J., and Benoit, H. (1960): C.R. Acad. Sci., 25, 2944.
5. Allcock, H. R. and Best, R. J. (1964): Can J. Chem., 42, 447.

6. Snyder, D. L., Stayer, M. L., and Kang, J. W. (1978): U. S. Patent #4, 123,503.
7. Devadoss, E. and Nair, C.P.R. (1984): Ind. Eng. Chem. Prod. Res. Dev., 23, 272.
8. Retuert, J., Ponce, S., and Quijada, J. P. (1979): Polym. Bull., 1, 653.
9. Sennett, M. S. (1985): Ph.D. Thesis. Northeastern University.
10. Hagnauer, G. L. and Koulouris, T. N. (1981): Liquid Chromatography of Polymers and Related Materials III, edited by Jack Cazes, Marcel Dekker Inc., New York.
11. Horn, H.-G. and Kolkmann, F. (1982): Makromol. Chem., 183, 1833.
12. Moran, E. F. (1968): J. Inorg. Nucl. Chem., 30, 1405.
13. Horn, H.-G. and Kolkmann, F. (1982): Makromol. Chem., 183, 1843.

APPLICATIONS OF HIGH PERFORMANCE LIQUID CHROMATOGRAPHY FOR RUBBER ANALYSIS

DAVID A. DUNN
Polymer Research Division, U.S. Army Materials and Mechanics Research Center, Watertown, Massachusetts 02172

High performance liquid chromatography (HPLC) methods have been developed for the solution characterization of elastomers. The relative molecular weight (MW) and molecular weight distribution (MWD) of uncured natural and synthetic elastomers have been determined using size exclusion chromatography (SEC). Application of this method for a series of synthetic elastomers showed differences in the respective MW values. Two samples of the same material, obtained on different dates, showed significant differences. Natural rubber (guayule) samples were also analyzed by SEC. These samples were obtained over a 4-month period and the MW values determined show the difference between the samples. SEC is a valuable technique for determining the relative MW values of elastomers. Methods are being developed for the analysis of additives in extracts of uncured and cured compounded rubber samples. UV and fluorescence detectors are being used in this work.

ANALYSIS OF CARBON BLACK FILLED ELASTOMERS BY FT-IR

JAMES M. SLOAN, HARRY HART, AND MICHAEL J. MAGLIOCHETTI
Polymer Research Division, U. S. Army Materials Technology Center, Watertown, Massachusetts 02172-0001

INTRODUCTION

The rubber industry is a major user of infrared spectroscopy (1, 2). Many problems associated with rubber samples can be solved by using this technique. The most frequently used analyses required are the identification of the base elastomers, identification of inorganic fillers, and the quantitation of individual elastomers in elastomer blend compounds.

Interactable materials, such as cured rubber compounds filled with carbon black present a difficult problem for infrared spectroscopists. The carbon black acts as light sinks toward the IR radiation with little or no radiation reaching the detector. Many sampling methods have been devised to overcome this difficulty, such as microtomed thin slices (3, 4), attenuated total reflectance employing Ge as the reflectance crystal, grinding (5), and pyrolysis (6).

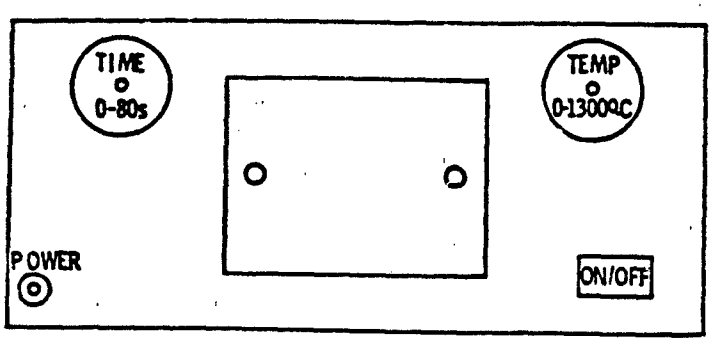
In this work, the methods of analysis of elastomeric materials used in the track pad materials are presented. This work has been limited to natural, butadiene, and styrene-butadiene elastomers, and their respective di and triblends. These blends are the primary rubber compounds used in track pads to date. We have used pyrolysis as the sampling technique and used a curvefit software routine (7, 8) to yield a best fit between the known individual IR spectra to that of the unknown blend spectra. In addition, data derived from ATR and grinding into a KBr matrix are presented.

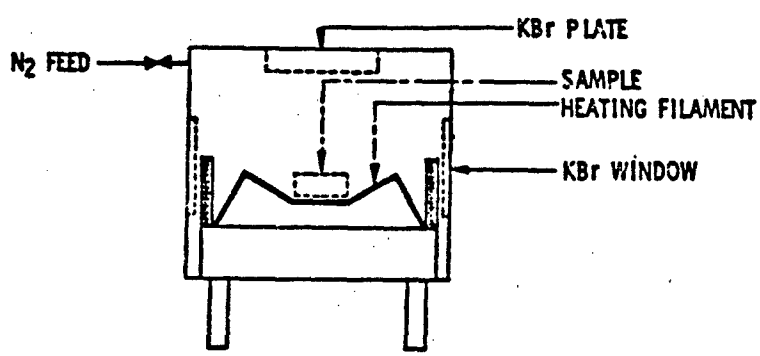
EXPERIMENTAL

The materials used in this study were either laboratory compounds provided by FT Belvoir R&D Center or Red River Army Depot (RRAD), known samples from commercial sources, or production samples provided by the Tank Automotive Command (TACOM or RRAD). Production smaples were purchased by the Army under contract to private industry.

Pyrolysis of rubber compounds were carried out in a Wilks Model 40 Pyro-Chem pyrolysis accessory. Rubber samples were extracted in acetone before introduction into the accessory.

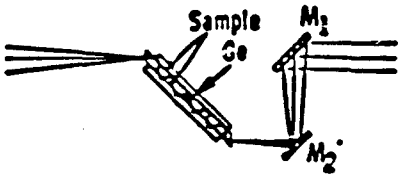
The accessory was then purged with dry nitrogen gas prior to pyrolysis, to inhibit oxidation of the resulting pyrolyzate. The pyrolysis temperature was set at 450°C for 45 seconds. The pyrolyzate was deposited on a KBr salt plate which replaced the normally used Krs-5 internal reflectances crystal in the accessory. This was done to obtain direct transmission measurements, which allow more accurate quantitative IR spectra to be obtained. Figure 1 shows a schematic drawing of this accessory, a Harrick Model 4X-TBC-VA ATR accessory. The internal reflectance element (IRE) was a rhomohedral-shaped germanium crystal with dimensions of 50 mm x 3 mm x 2 mm. Figure 2 shows the schematic drawing of this accessory.





FOXBORO ANALYTICAL PYRO-CHEM PYROLYSIS UNIT

FIGURE 1. Schematic diagram of the pyrolysis chamber used.



$$d_p = \frac{\lambda / n_{Ge}}{2\pi \left[\sin^2\theta - (n_{SAM}/n_{Ge})^2\right]^{1/2}}$$

d_p = depth of penetration into sample ($n_{Ge} > n_{SAM}$)

λ = wavelength of radiation in μm

n_{Ge} = refractive index of germanium

n_{SAM} = refractive index of sample

θ = angle of incidence of radiation

INTERNAL REFLECTANCE SPECTROSCOPY

FIGURE 2. Schematic diagram of the internal reflectance accessory.

RESULTS AND DISCUSSION

Figure 3 shows the spectra of the three most commonly used elastomers for track pad applications. Using these spectra as references, the type of base elastomer can be determined.

Figure 4 demonstrates the use of a curvefit software routine to allow qualitative analysis of blends to be obtained. Each of the three IR pyrolyzates are known di or triblends. The printout from this curvefit analysis is shown next to their respective IR spectra. Table 1 gives a comparison between known blend compounds and the curvefit values obtained.

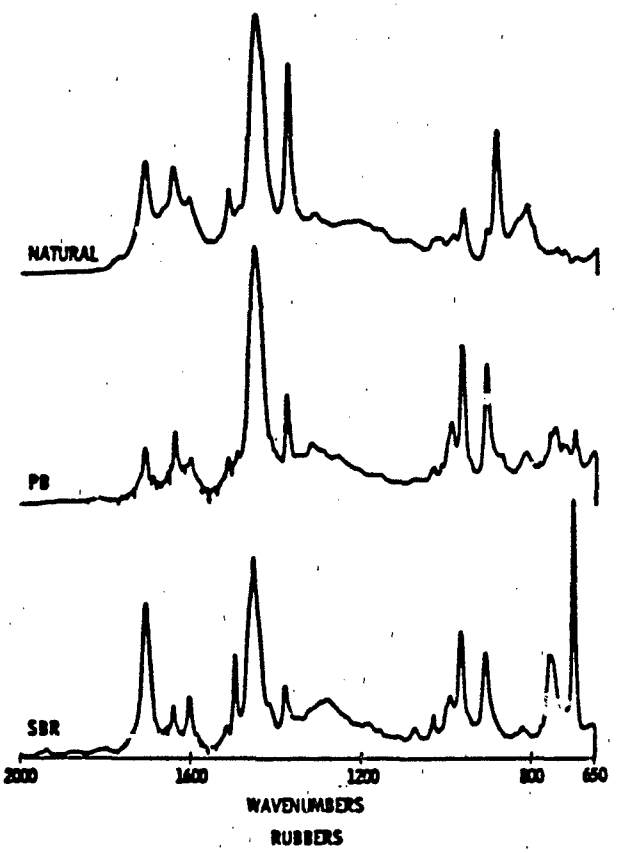


FIGURE 3. Pyrolysis spectra of three standard elastomers: natural rubber, butadiene rubber, and stryrene-butadiene rubber.

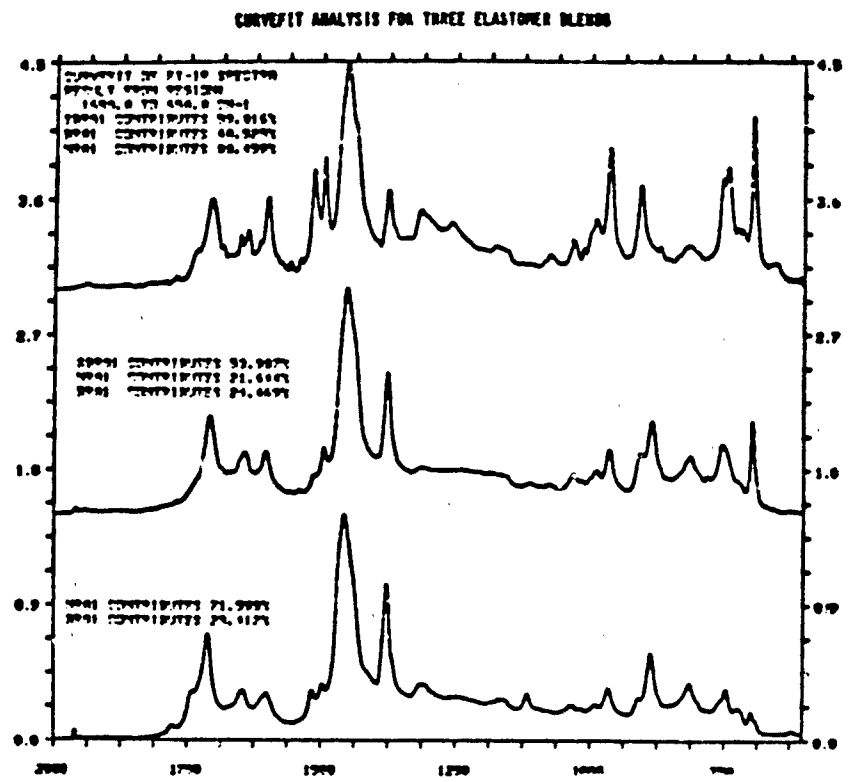


FIGURE 4. Typical curvefit analysis for three elastomer blends compounds. Each compound spectrum has the corresponding curvefit printout next to it with the relative percentages of individual elastomer.

TABLE 1

COMPARISON OF UNKNOWN AND KNOWN BLEND COMPOSITIONS USING CURVE-FIT ANALYSIS OF PYROLYSIS SPECTRA

SAMPLE ID	CURVEFIT VALUES	KNOWN VALUES
TR 96	SBR 59 BR 41	SBR 60 BR 40
TR 21	SBR 71.5 BR 28.5	SBR 70 BR 30
TR 40	SBR 98.6 BR 1.4	SBR 100
TR 76	SBR 78.6 BR 21.4	SBR 80 BR 20
TR 127	SBR 60 NR 40	SBR 60 NR 40
TR 44	SBR 2.1 NR 98	SBR 0 NR 100
TR 113	SBR 42 BR 27 NR 31	SBR 35 BR 30 NR 35

The results in Table 1 suggest that the accuracy for di-blend compounds in between ±3 percent. While the accuracy for triblend compounds is much worse, somewhere around ±10 percent.

ATR

Figure 5 shows the IR-ATR spectra of the three most commonly used elastomers for track pad applications. These are used as reference spectra for identification of base elastomers. This sampling technique, samples the only surface of the elastomer (between 0.25 mm - 2.5 mm) depending on the wavelength of the IR beam.

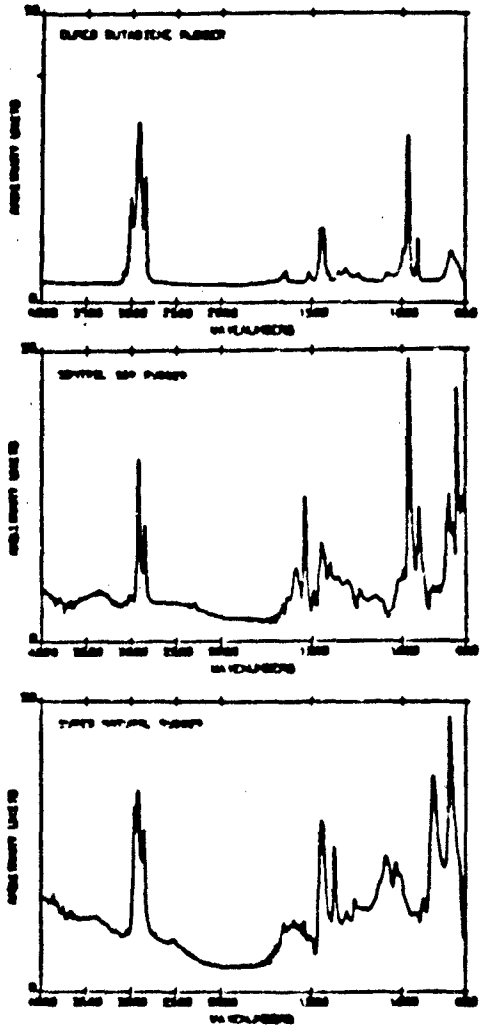


FIGURE 5. Attenuated total reflectance spectra of three commonly used elastomers for track pad applications.

Figure 6 shows how this sampling technique might be used to analyze track pad materials. This figure shows the surface of the used track pad (top spectrum) compared to the interior portion of the same track pad (middle spectrum). The bottom spectrum is a sample test sheet of the same compound shown for comparison. The surface of the rubber show all the same IR bands except that several new bands can be seen between

1000 cm^{-1} - 1200 cm^{-1}. The bands are not due to the deterioration but are in fact due to the presence of silica, which probably has been imbedded into the track pad from field use.

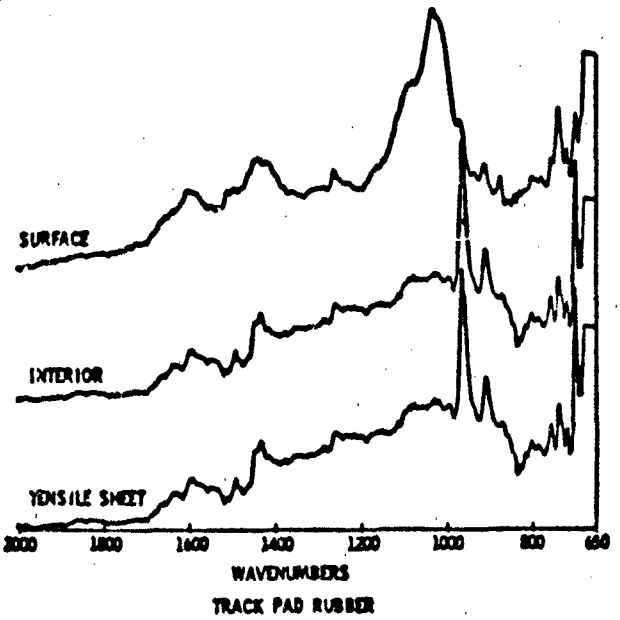
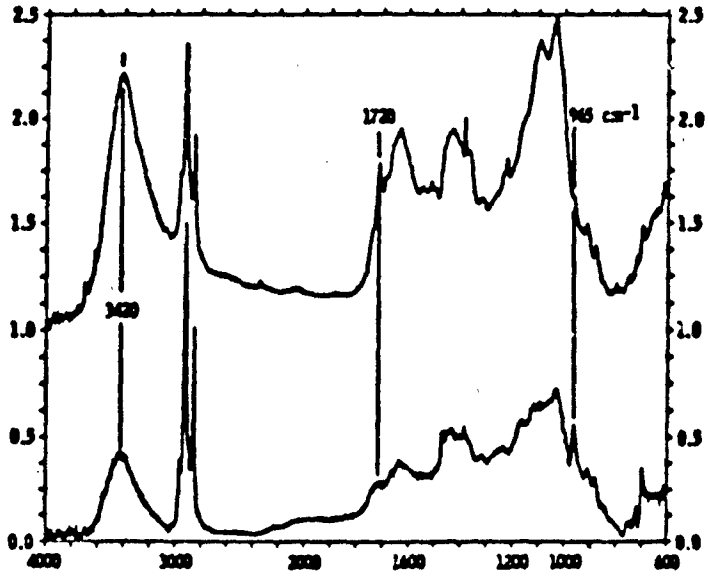


FIGURE 6. ATR spectra of deteriorated M-1 track pad.

Grinding in KBr Matrix

Figure 7 shows the determination of the same M-1 tank track pad as in the previous figure. The top spectrum shows the surface of the same track pad. The degraded surface shows some IR bands attributed to oxidative degradation. The 1720 cm^{-1} band, indicative of carbonyl formation, and the 3420 cm^{-1} indicative of hydroxyl groups are examples of this.



TOP: SURFACE OF USED TRACK PAD
BOTTOM: INTERIOR PART OF SAME TRACK PAD

FIGURE 7. KBr pellet IR spectra of degraded M-1 tank track pad.

CONCLUSION

Various sampling techniques have been employed to study M-1 tank track pad materials. Each technique yields different information about the individual track pad compound. Pyrolysis yields information on the identification of the base elastomer as well as quantitation on the respective amounts of individual elastomers in blend compounds. ATR-Ge reveals information on the structure of the elastomer at the surface of the rubber compound. Effects such as degradation and imbedded particles from service can be detected by this method. Finally, grinding the sample into a KBr matrix reveals information on the structure of the polymer without destroying the polymer backbone as with the pyrolysis technique.

REFERENCES

1. Method for Identification of Rubbers. (1967): British Standard 4181.
2. Jasper, B. T. (1970): The Identification and Determination of Selected Polymers with a Unicam SP200 Infrared Spectrophotometer. Spectrovision, 23, 4-7 pp.
3. Corish, P. J. (1960): J. Appl. Polymer Sci., 4, 86.
4. Corish, P. J. (1961): J. Appl. Polymer Sci., 5, 53.
5. Hart, W. W., Painter, P. C., Koenig, J. L., and Coleman, M. M. (1977): Appl. Spec., 31, 220.
6. Pattacini, S. C. The Identification of Cured Rubber Compounds Using Infrared Spectroscopy. Perkin-Elmer Infrared Bulletin, 52.
7. Fortran Application Programs. (1960): Bio-Rad, Digilab Division, Users Manual M091-0121C.
8. Antoon, M. K., Koenig, J. H., and Koenig, J. L. (1977): Appl. Spect., 31, 518.

CHARACTERIZATION OF ELASTOMERS FOR ARMY APPLICATIONS BY THERMAL ANALYSIS

DOMENIC P. MACAIONE, ROBERT E. SACHER, ROBERT E. SINGLER, AND WALTER X. ZUKAS
U. S. Army Materials and Mechanics Research Center, Watertown, Massachusetts 02172-0001

ABSTRACT

Thermal methods of analysis measure the change in some physical or chemical property as a function of temperature. Modern thermal analysis techniques have proven extremely useful in the compositional analysis of the complex mixtures we refer to as rubbers.

Thermal analysis, in its various forms, has provided valuable insight into the analysis of rubber materials. Of the several thermal analysis techniques available this presentation is concerned with the following:

- Thermogravimetric Analysis--TGA. Measures mass loss of sample as a function of temperature.
- Differential Thermogravimetry--DTG. Measures rate of sample mass loss.
- Differential Scanning Calorimetry--DSC. Measures energy or thermal difference.
- Thermomechanical Analysis--TMA. Measures dimensional changes.
- Dynamic Mechanical Analysis--DMA. Measures modulus or loss tangent.

THERMOGRAVIMETRIC ANALYSIS AND DIFFERENTIAL THERMOGRAVIMETRY

Figure 1 shows the classical thermogravimetric analysis/differential thermogravimetry curve obtained upon analysis of an elastomer in nitrogen atmosphere from ambient temperature to 600°C followed by a change to air atmosphere from 600 to 950°C. The corresponding DTG curve indicates the temperature at which maximum weight loss occurs and the DTG maximum for the elastomer component has been found to be characteristic of the elastomer. Figure 2 shows similar curves for mono, di, and triblend elastomer compositions. One misconception, as shown in the figure, is the inability of the DTG data to distinguish

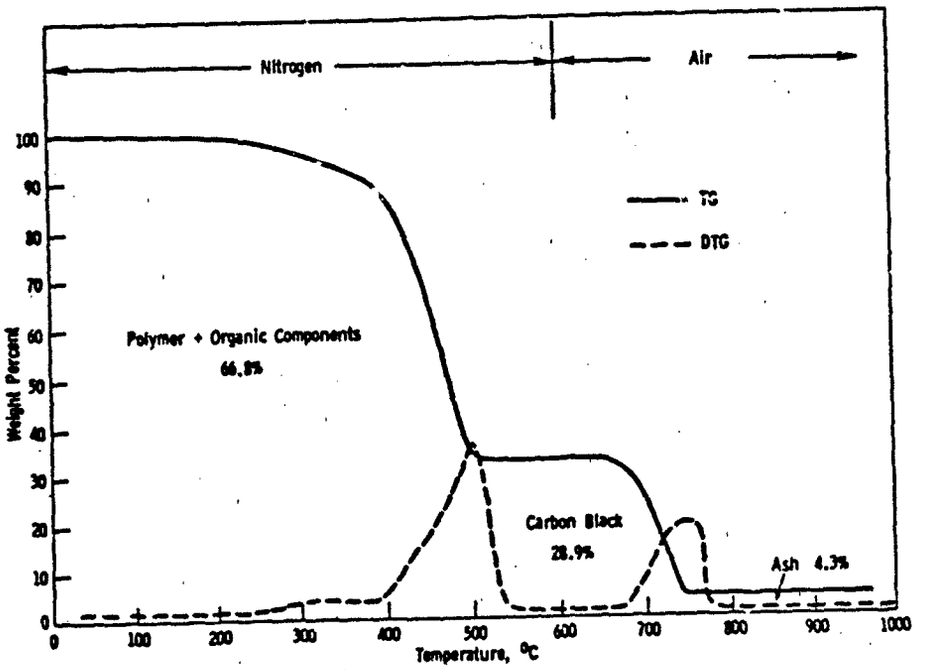


FIGURE 1. Thermogravimetric analysis of a styrene-butadiene (SBR) rubber vulcanizate showing weight losses for organic, carbon black, and inorganic components.

between SBR and BR when both elastomers are present in a formulation.

Tables 1 and 2 show the formulations for a natural rubber and a synthetic rubber composition followed by the results of thermal analysis for the three main portions of the composition. These data indicate that a reasonably accurate thermogravimetric analysis of elastomer compositions is possible.

DIFFERENTIAL SCANNING CALORIMETRY

Figure 3 shows a wide spectrum DSC curve over the temperature range--100°C to greater than 600°C (D. W. Brazier, NBS Publication #580, pg. 72, 1979), indicating the typical transitions observable by DSC. Unlike TGA, the DSC mode can distinguish cured and uncured elastomer compositions. Accelerated sulfur cures exhibit a broad exotherm in the 150 to 220°C region. Figures 4 and 5 show the DSC results for uncured and

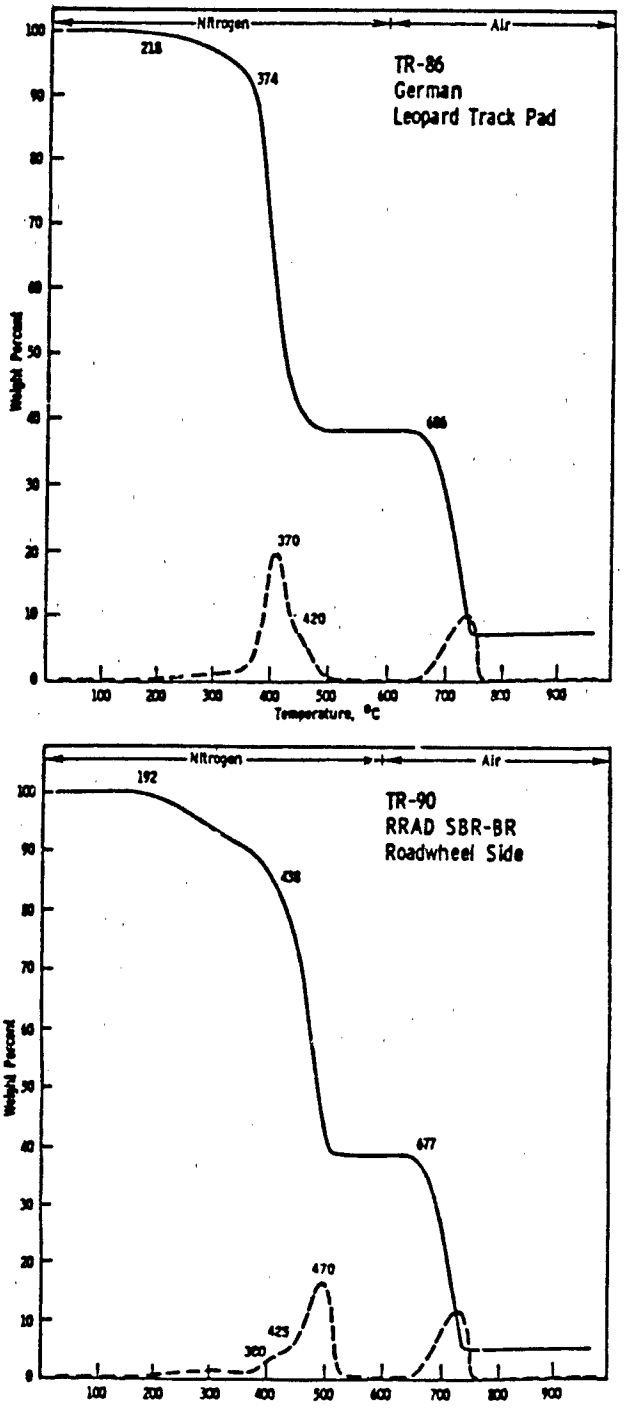


FIGURE 2. Thermogravimetric analysis (TGA-DTG) curves for three elastomer compositions.

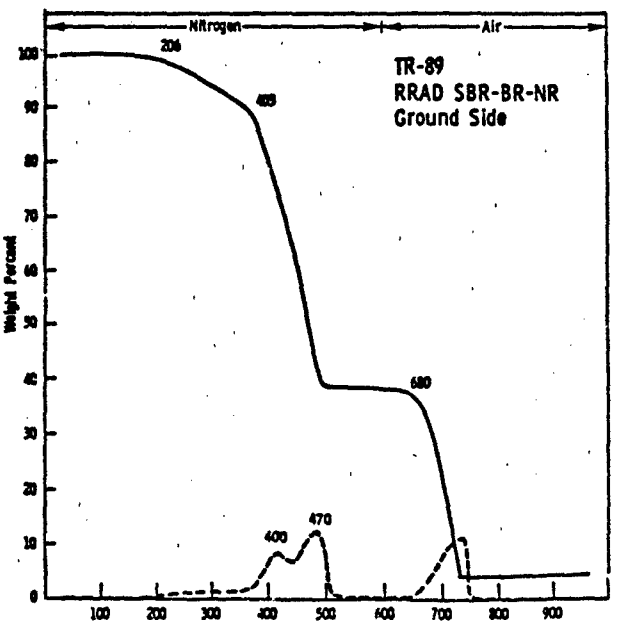


FIGURE 2. Thermogravimetric analysis (TGA-DTG) curves for three elastomer compositions (continued).

cured TR-40, respectively, an accelerated sulfur cure SBR elastomer composition.

THERMOMECHANICAL AND DYNAMIC MECHANICAL ANALYSIS

Thermomechanical and dynamic mechanical analysis techniques are useful for identifying elastomers by glass transition temperature (Tg).

TABLE 1

NATURAL RUBBER COMPOSITION AND THERMAL ANALYSIS

15NAT2B	TR-41 (UNCURED)	
	PARTS	%
NATURAL RUBBER	100.0•	63.37
ZINC OXIDE	4.0†	2.53
STEARIC ACID	2.0•	1.27
CARBON BLACK	45.0†	28.52
ANTIOXIDANT	0.5•	0.32
ANTIOZONANT	3.0•	1.90
SULFUR	2.5•	1.58
ACCELERATOR	0.8•	0.51
	157.8	100.00

COMPONENT	CALCULATED	FOUND
•POLYMER, ORGANICS, VOLATILES	68.95	68.00
†ASH	2.53	3.17
†CARBON BLACK	28.52	27.93

The following tabulation lists the Tg values for the three elastomers found in formulations of interest to this presentation, both in the uncured and cured states.

Rubber	Glass Transition Temperature (Tg)°C Uncured	Cured
Natural (NR)	-60	-56
cis-Polybutadiene (BR)	-105	-95
Styrene-Butadiene (SBR)	-49	-47

Uncured diblends and triblends exhibit more than one transition by DMA and a single transition by TMA. In diblends of SBR and BR, the Tg of the blend lies somewhere between the

TABLE 2

SYNTHETIC RUBBER COMPOSITION AND THERMAL ANALYSIS

15SBR25	TR-40 (UNCURED)	
	PARTS	%
SBR	100.0*	62.35
ZINC OXIDE	4.0†	2.49
STEARIC ACID	2.0*	1.24
CARBON BLACK	45.0‡	28.05
ANTIOXIDANT	0.5*	0.31
ANTIOZONANT	3.0*	1.87
SULFUR	0.75*	0.46
ACCELERATOR	4.625*	2.88
WHITING	0.5†	0.31
	160.38	99.96

COMPONENT	CALCULATED	FOUND
*POLYMER, ORGANICS, VOLATILES	69.24	69.28
†ASH	2.80	2.20
‡CARBON BLACK	28.05	28.55

Tg values of the individual elastomers and will shift with changes in composition. Cured samples exhibit one transition by either TMA or DMA. Typical data to illustrate the response of uncured and cured compositions to TMA and DMA experiments is given next.

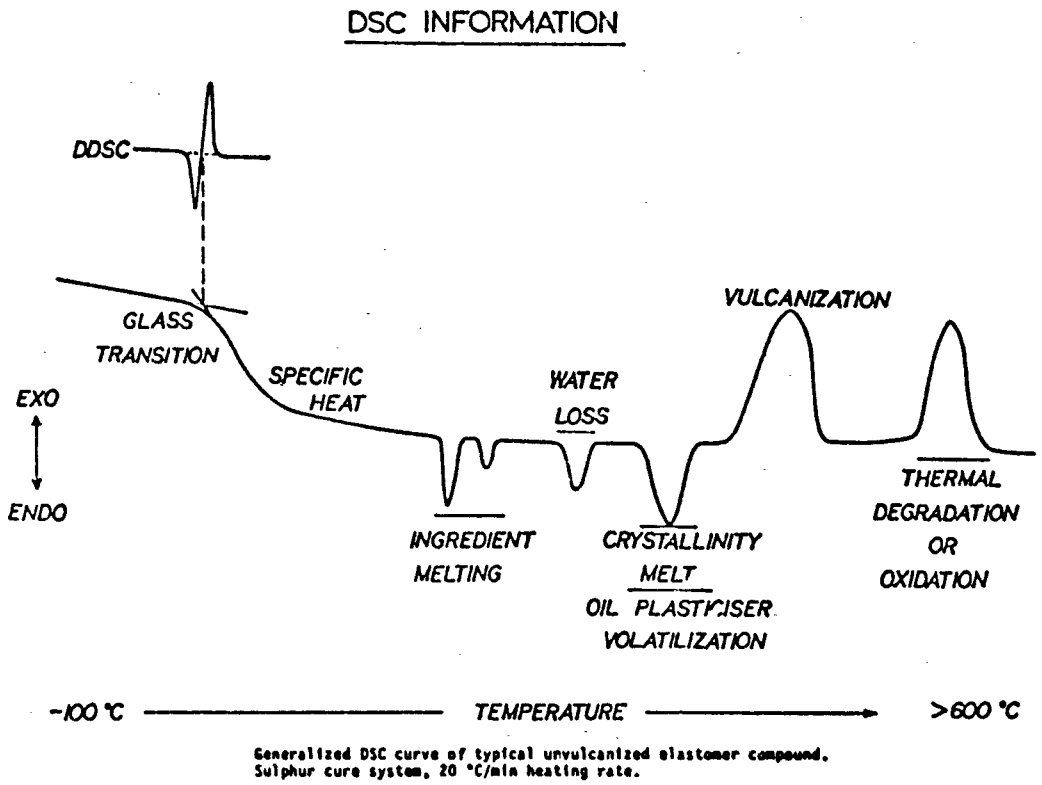


FIGURE 3. DSC curve over a temperature range.

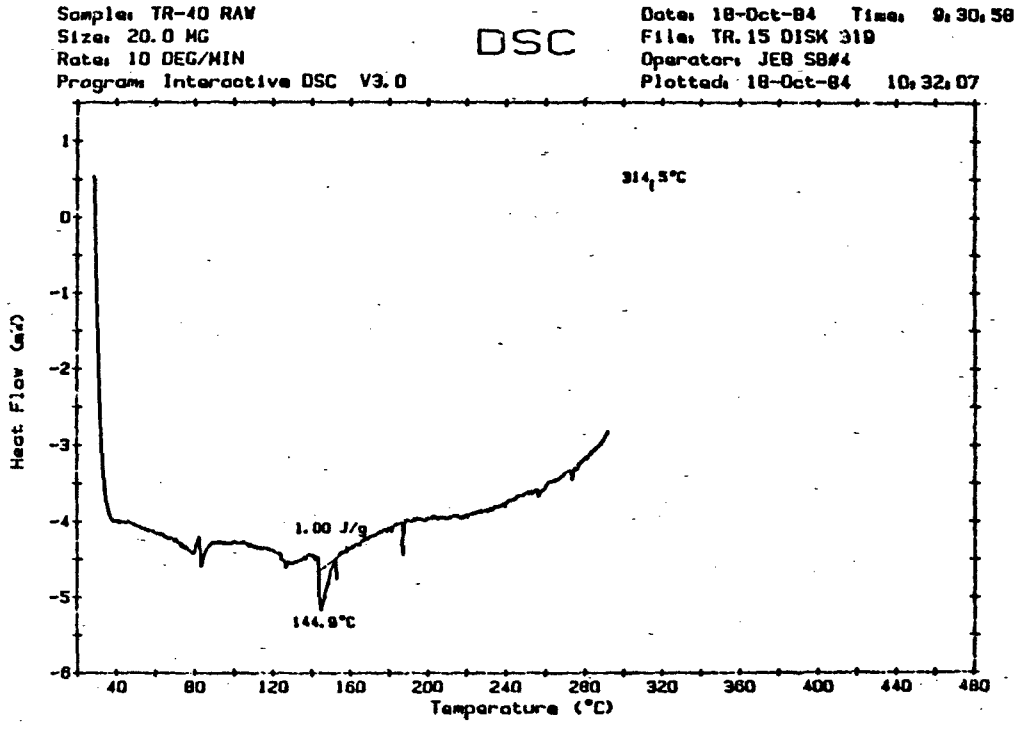


FIGURE 4. DSC results for uncured TR-40.

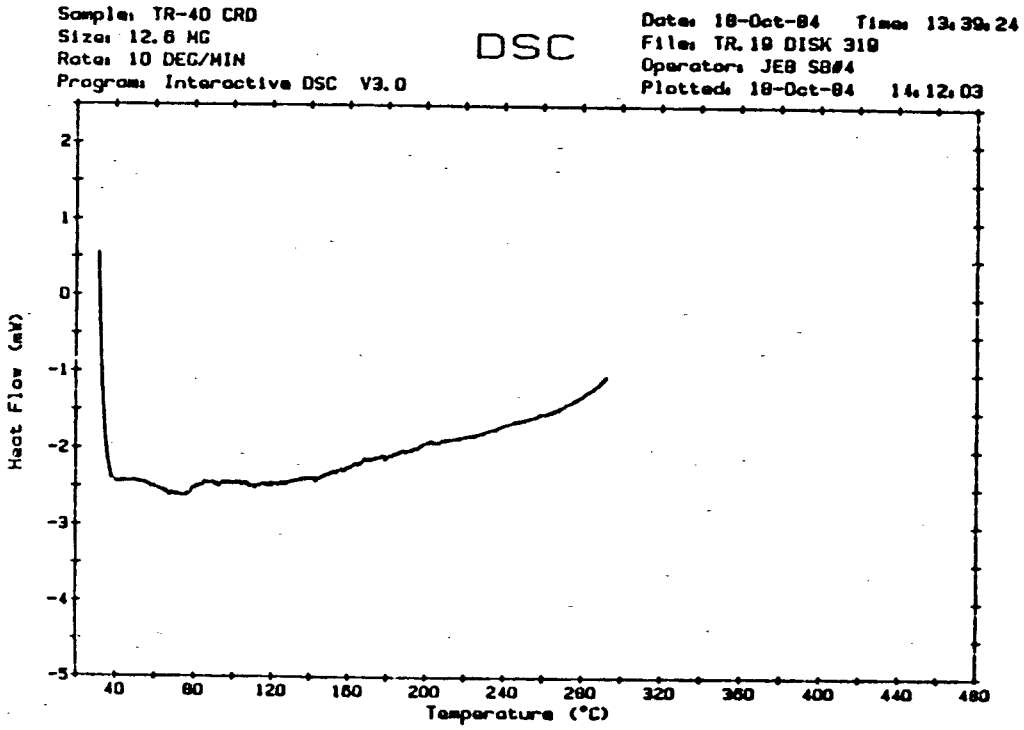


FIGURE 5. DSC results for cured TR-40.

TR#	Composition	Glass Transition Temperature (Tg)°C TMA	DMA*
111	SBR-BR, uncured	-57	-48,-98
112	SBR-BR, cured	-59	-59
113	SBR-BR-NR, uncured	-64	-49,-98
114	SBR-BR-NR, cured	-59	-59

* Constant Oscillation Amplitude Procedure.

Oscillating Disk Rheometry (ODR) is another dynamic mechanical method applied to elastomers. It monitors that portion of the DSC curve under "Vulcanization" (in Figure 3) and yields data on minimum torque, scorch time, cure time, and maximum torque. As part of one segment of the elastomer program, ODR and DSC were applied to two MIL-T-11891 rubber compounds. Figure 6 shows a standard ODR reference curve, Table 3 is the actual formulation of the rubber compounds used in the experiment, in accord with the specification, and Figure 7 shows the actual ODR curve obtained in the laboratory.

Figure 8 shows the results of isothermal curing of the rubber at the indicated temperatures. The vulcanization reaction i observed as an exothermic reaction or downward fluctuation in the DSC trace. To improve the accuracy of the heat evolution vs. time trace, a second dynamic DSC method was employed. A sample of uncured elastomer was rapidly heated at an isothermal cure temperature for a predetermined time, corresponding to a point on the ODR curve, and then quenched. The sample was then put through the dynamic DSC program to determine the degree of cure. Figure 9 shows the results of this investigation, and indicates that at T max either the material is not fully cured or that some reversion has occurred. Table 4 presents the corresponding inverse peak minima and thermal values. This aspect of the investigation is in the initial stages of organization and will be expanded in the future.

CONCLUSIONS

- Classical thermal analysis techniques give rapid results.
- Each technique contributes to the overall information available from each sample.

- Accuracy and precision are sufficient to justify routine use of the technique.
- Thermal analysis data will facilitate analyses by other analytical methods.

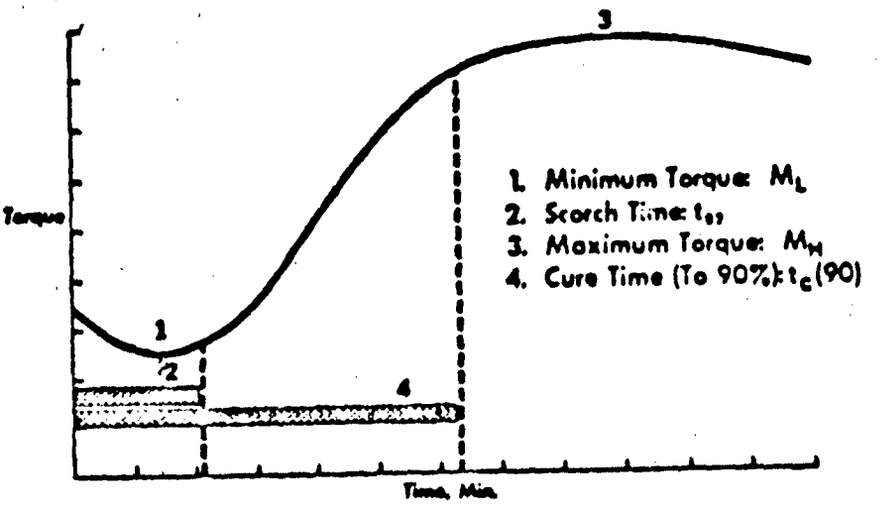


FIGURE 6. Rheometer reference curve.

TABLE 3

FORMULATION OF RUBBER COMPOUNDS

MIL-T-11891
TRACK BLOCKS AND PADS
RUBBER COMPOUNDS

MATERIALS	PARTS PER HUNDRED RUBBER-PHR	
	GROUND SIDE	WHEEL SIDE
STYRENE-BUTADIENE SBR-1500	35	60
POLYBUTADIENE TAKTENE-220	30	40
NATURAL RUBBER SMR-20	35	0
N220 CARBON BLACK	65	65
ZINC OXIDE	3	3
STEARIC ACID	1.50	1.50
SUNOLITE 100 - HYDROCARBON WAX	1.50	1.50
SANTOFLEX 13 - ANTIDEGRADANT	3	3
FLECTOL FLAKES - ANTIDEGRADANT	2	2
SUNDEX 790 - HIGH AROMATIC OIL	4	4
SULFUR	1.3	1.3
DIBS SULFENAMIDE ACCELERATOR	3.2	3.2
SANTOGARD PVI	0.2	0.2
	184.70	184.70

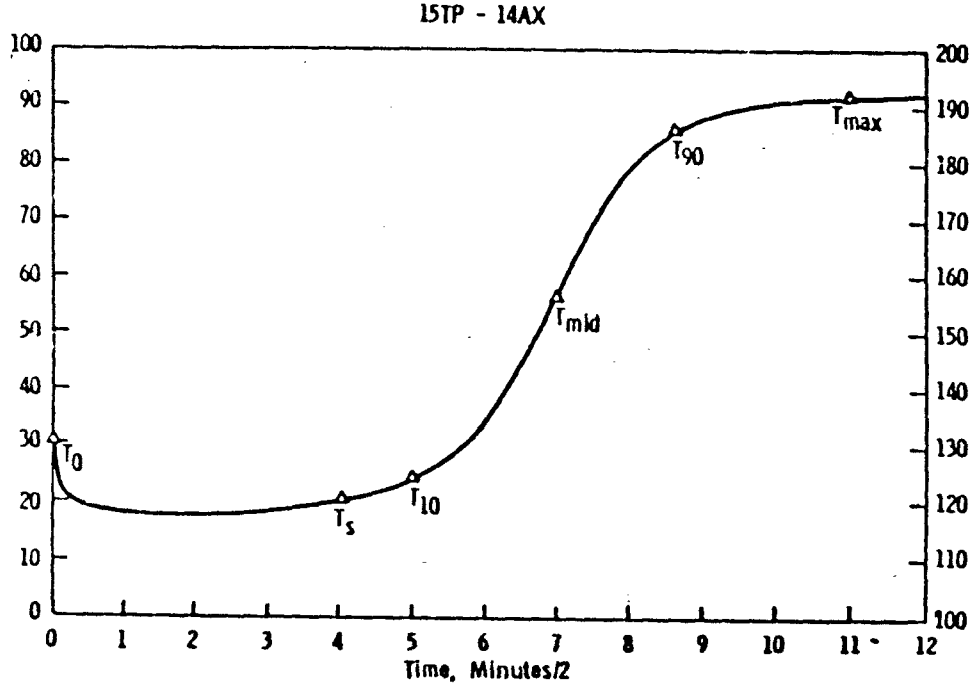


FIGURE 7. Actual ODR curve.

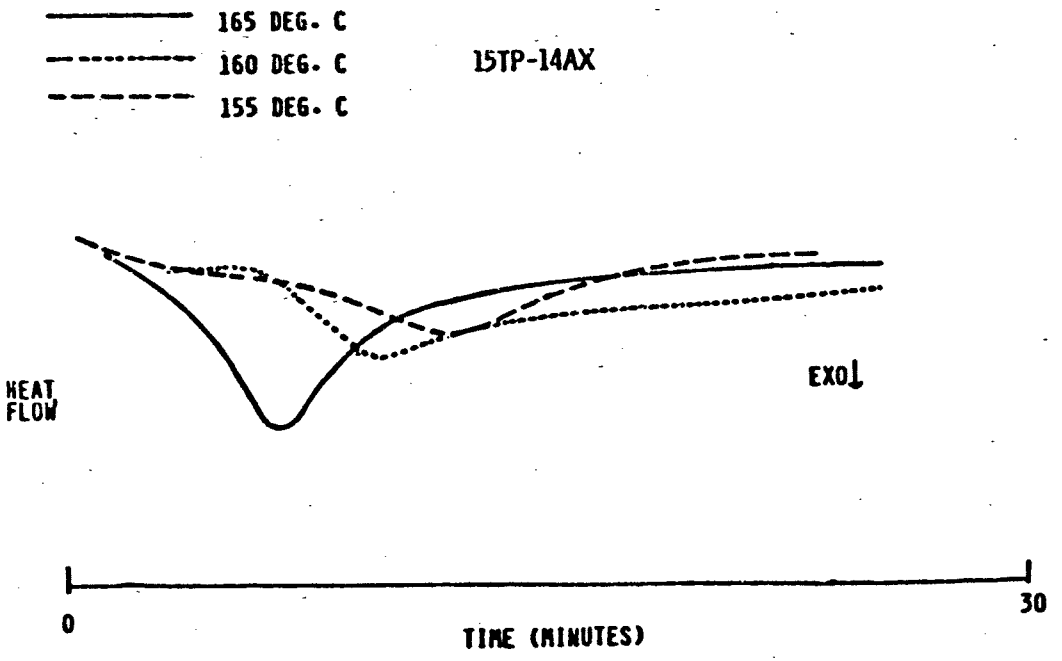


FIGURE 8. Results of isothermal curing of rubber at specific temperatures.

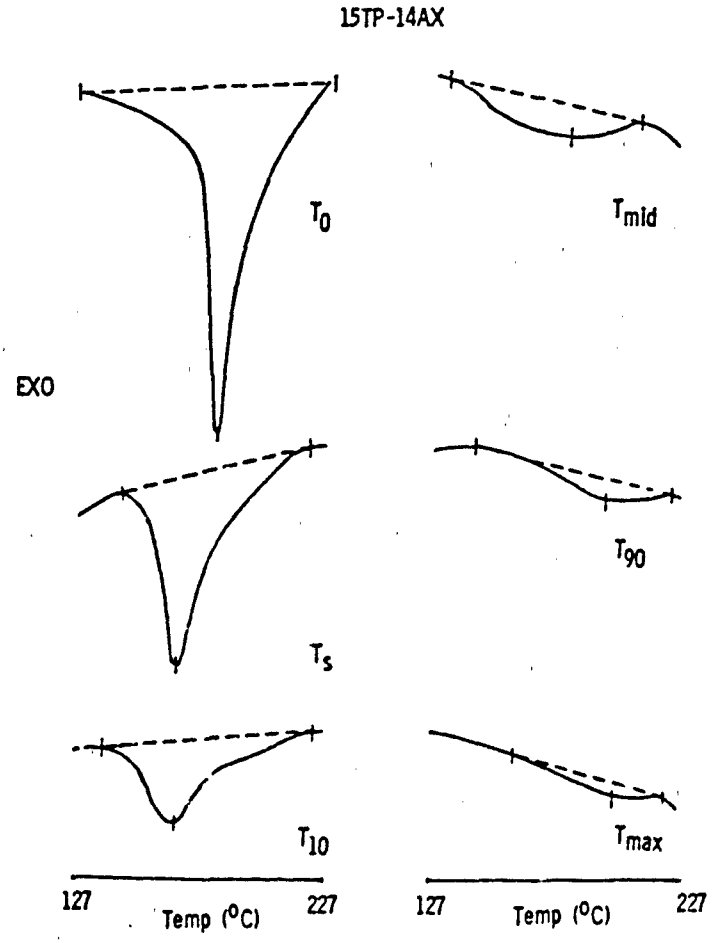


FIGURE 9. Results after a second dynamic DSC method was employed.

TABLE 4

UNCURED ELASTOMER INVERSE PEAK MINIMA AND THERMAL VALUES

15TP-14AX

	min. peak, °C	ΔH, J/gm (# of samples)
T_0	184.5	17.4 ± 5.9(7)
T_s	168.4	8.0 ± 1.4(4)
T_{10}	167.7	5.5 ± 0.2(2)
T_{mid}	184.8	3.5 ± 0.5(4)
T_{90}	191.4	1.4(1)
T_{max}	196.9	0.7(1)

FAST ATOM BOMBARDMENT--MASS SPECTROMETRY OF ELASTOMER ADDITIVES

ALFRED J. DEOME, PETER J. KANE
U.S. Army Materials and Mechanics Research Center, Watertown, Massachusetts 02172

ABSTRACT

Fast Atom Bombardment (FAB) is a specialized mass spectrometry ionization technique particularly well suited for organic molecules which do not yield sufficiently stable mass spectra under electron ionization conditions. While this technique has been used with increasing success in biochemical and pharmaceutical applications, its adaptability and application in the characterization of conventional vulcanized elastomer systems has just begun. The efforts presented in this research address the development of new FAB matrices which permit the direct analysis of mixtures of elastomer additives without chromatographic separation. Primary emphasis in this work is directed toward characterization of the new M-1 Abrams T-156 elastomer triblend systems using fast atom bombardment ionization techniques with both low and high resolution mass spectrometry.

INTRODUCTION

The complex nature of vulcanized elastomers presents a significant challenge for any singular analytical technique. While pyrolysis-gas chromatography-mass spectrometry has been shown to be a viable approach to selectively separating and identifying the individual components of an elastomer system, it involves a chromatographic separation of a pyrolyzate (1). This separation cannot only be time consuming, but thermally labile materials may not survive introduction to the mass spectrometer via pyrolysis, thereby invalidating a portion of the characterization process.

Recent developments in ionization techniques, such as FAB, have shown promise as a means of elucidating structural information by producing both positive and negative molecular ionic species of intractable polar materials (2,3). FAB is generally accepted as a "soft ionization" process, facilitating adduct formation of protons, metal cations, or matrix ions to the molecule of interest (4). The resulting adduct ion most commonly formed is a positively charged protonated molecular ion (M+1).

The resulting molecular ion information attained by FAB ionization may not be possible under normal electron ionization conditions for two reasons. First, the heat involved in EI can pose a problem for thermally labile samples. Heat is evolved from the solid probe for sample vaporization, the gas chromatograph for vaporization and separation of components, and the heated ion source itself. This may act to decompose the sample, thus, no molecular ion information is obtained. Secondly, the energy imparted on the sample by the electron beam may act to decompose the sample during ionization. The resulting spectra may be predominantly low mass ions with no characteristic molecular information.

FAB ionization is unique in that it produces a long lasting mass spectrum, in the order of minutes. Conventional solid probe techniques rely on the volitility of the sample at a given temperature. As the probe tip is heated, the sample is vaporized into the ion source. The time frame of vaporization and ionization can be short, in the order of seconds, making various high resolution or metastable experiments for structural elucidation of molecules difficult (5). Gas chromatography-mass spectrometry has the same basic flaw of short durations of compounds eluting from the column.

The long duration of FAB experiments is attributable to three basic factors. First, the sample is dissolved in a high viscosity low vapor pressure liquid matrix that can withstand the high vacuum of the mass spectrometer ion source. The liquid acts to replenish sample to the area of ionization by the beam of atoms. In this way the sample is not depleted as in some other ionization techniques. Secondly, the mass spectrometer source and inlet system are maintained at ambient temperature to decrease sample/matrix vaporization rate. Additionally, the potential of producing intact molecular ions of thermally labile samples is enhanced. Thirdly, the neutral beam of xenon atoms, produced by the FAB gun, impacts on the sample/matrix target and displaces a relatively small portion of the sample (1,2). These factors allow for the production of a continuous mass spectrum of sample and matrix.

FAB has been used to some extent to evaluate additives in vulcanized and unvulcanized elastomers systems (6). The focus of efforts presented here is a preliminary evaluation of FAB ionization mass spectrometry as a viable approach to direct mixture analysis of the T-156 triblend vulcanized elastomer system. The novel approach to this type of study involves the selection, evaluation, and optimization of a number of matrix components both singularly and in combination (7,8). The final

result is a composite mass spectrum qualitatively characteristics of the additives in the elastomers under investigation at this research center.

EXPERIMENTAL

All FAB spectra were obtained using a Finnigan/MAT model 8230 mass spectrometer system equipped with an Ion Tech Ltd. model FAB11NF gun. Mass spectral acquisition and subsequent analysis was performed on a PDP 11/34 computer operating under RSX-11M and SSX-300 software. Fast atom bombardment was accomplished using xenon atoms accelerated by an 8 KV potential in the FAB gun. A mass range of 60 to 1,000 AMU was scanned at 5 seconds/decade.

A series of elastomer additives which represent the known formulation of the T-156 triblend reference system (MIL-T-11891C) was selected for initial evaluation of the matrix selection. Samples of the respective additives were weighed and dissolved in spectroquality grade methylene chloride (DCM) to which an equal volume of experimental matrix was added. The DCM was evaporated using a stream of nitrogen, resulting in a sample-matrix solution. Approximately one microliter of the sample-matrix combination was applied to the FAB target probe tip. Subsequently, the target was placed in the ion source and the sample was ionized via the atom beam and mass analyzed.

RESULTS AND DISCUSSION

The additives evaluated and the results obtained from the matrix evaluation appear in Table 1. Nitrophenyl-octyl ether (NPOE) appears to be the most suitable of the matrices evaluated. Although glycerol and oleic acid show good results in most instances, NPOE exhibits a greater versatility for a broad range of additives which have dissimilar structures.

The FAB ionization procedure is relatively simple to perform. However, parameter optimization and data interpretation of the resulting FAB spectra can be complex. Matrix selection for additive analysis is crucial. Solubility of the additives in the matrix is essential for production of viable spectra.

The least successful experiments were encountered with the thiuram class of accelerators. Tetramethylthiuram disulfide demonstrated marginal solubility in all matrices resulting in low intensity molecular ion species.

TABLE 1

MATRIX EVALUATION

EVALUATED ADDITIVE	MATRIX SOLUTION GLYCEROL	OLEIC ACID	2-NITROPHENYL-OCTYLETHER
POLYMERIZED 2,2,4-TRIMETHYL-1,2-DIHYDROQUINOLINE (ANTIOXIDANT)	+	+	+
N-(CYCLOHEXYLTHIO)PHTHALIMIDE (RETARDER)	o	+	+
N-(1,3-DIMETHYLBUTYL)N-PHENYL-P-PHENYLENE DIAMINE (ANTIOZONANT)	+	+	+
TETRAMETHYLTHIURAM DISULFIDE (THIURAM ULTRA ACCELERATOR)	-	-	o
N-OXYDIETHYLENE BENZOTHIAZOLE-2-SULFENAMIDE (ACCELERATOR)	+	+	+
2-MERCAPTO BENZOTHIAZOLE (ACCELERATOR)	+	+	+
N,N-DIISOPROPYL-2-BENZOTHIAZYL-SULFENAMIDE (ACCELERATOR)	-	+	+

+=INTENSE MOLECULAR ION

o=WEAK MOLECULAR ION

--=NO SPECTRUM OBTAINABLE

The ability to identify individual components from a mixture using FAB ionization was experimentally evaluated by preparing a mixture of polymerized 2,2,4-trimethyl-1,2-dihydro-quinoline (antioxidant), N-(cyclohexylthio) phthalimde (retarder), and N-oxydiethylene-benzothiazole-2-sulfenamide

(accelerator) in NPOE matrix. Figure 1 shows the FAB fragmentation of the NPOE matrix. The molecular ion of 252 m/z represents the protonated species of the actual molecular ion 251 m/z. Significant fragmentation clusters are found at m/z 235, 140, 123, and 111. While they are characteristic of the matrix spectrum, they can in fact interfere in identifying the presence of important additive sample ions. This is clearly evident in the additive mixture and NPOE FAB analysis shown in Figure 2 where the matrix ions dominate. By subtracting a standard intensity reference spectrum of the NPOE matrix, however, the diagnostic ions indicative of the additives become apparent as shown in Figure 3. The diagnostic ions for each of the additives in Figure 3 are shown in Table 2.

The differentiation of matrix ions from sample ions can be enhanced further through the use of high resolution (greater than 2,500 resolution) (9). Figure 4 represents a low resolution (1,000 resolution) acquisition of 250-255 amu range of N-oxydiethylene benzothiazole-2-sulfenamide (MW = 252) in NPOE (MW = 251). The unresolved mass ions at m/e 251, 252, and 253 can be separated using a high resolution acquisition as shown in Figure 5.

The additional separation of ions afforded by higher resolution in conjunction with matrix ions for reference masses makes accurate mass mapping possible. The data system can be used to reduce the information to provide potential elemental composition of additive ions. This affords more conclusive identification of additives.

CONCLUSION

The results derived from the Fast Atom Bombardment experiments presented here demonstrate the preliminary application of analysis of additive mixtures without chromatographic separation. While a considerable amount of experimentation remains to be done in matrix-additive evaluation, the technique shows significant promise in enhancing the characterization techniques for complex rubber vulcanizates.

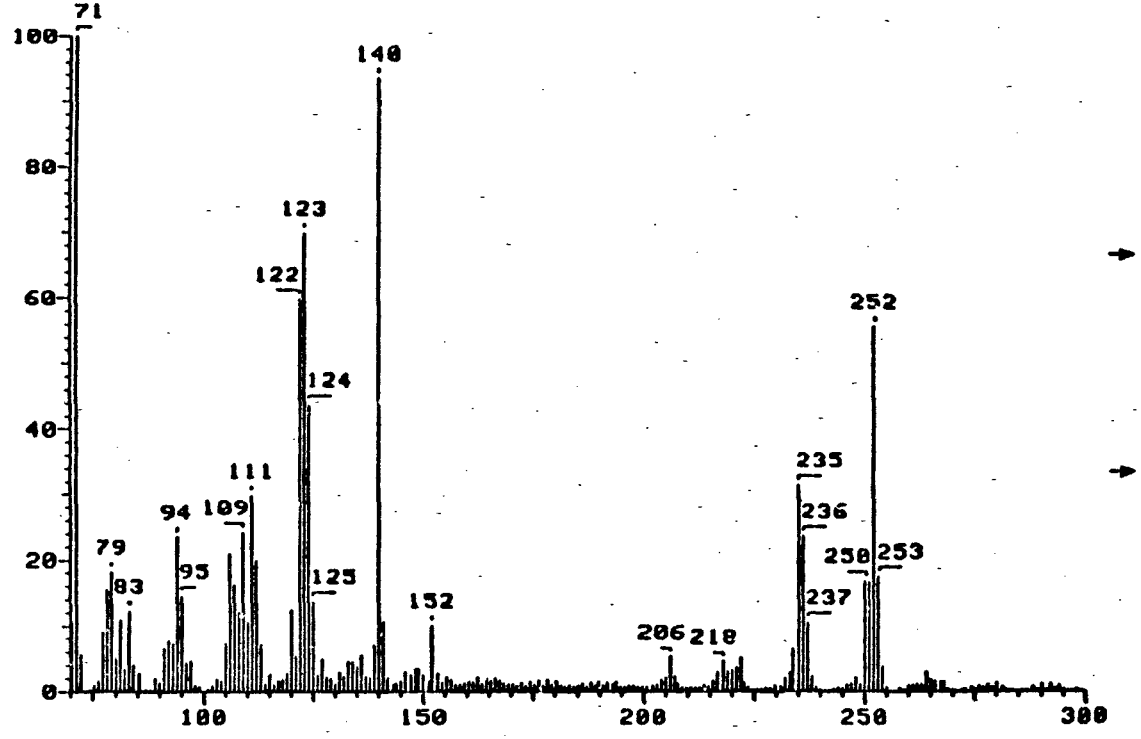


FIGURE 1. Fast atom bombardment mass spectrum of nitrophenyloctyl ether matrix (8KV).

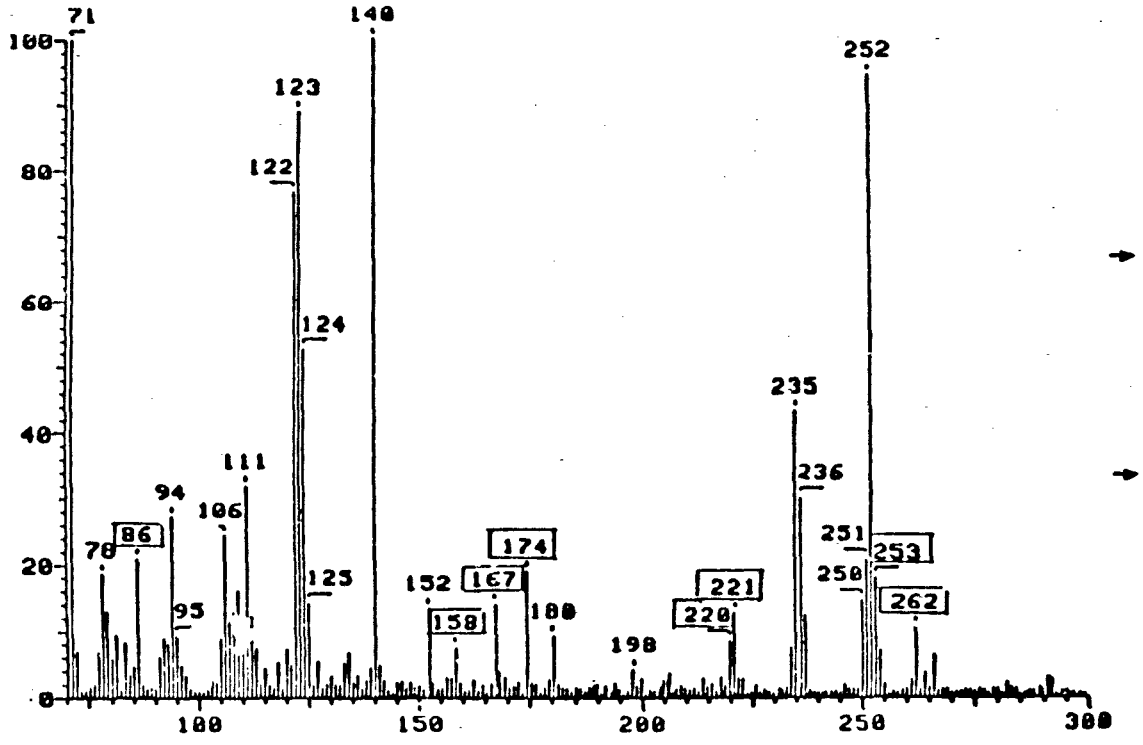


FIGURE 2. Fast atom bombardment mass spectrum of polymerized 2,2,4-trimethyl-1,2-dihydroquinoline, N-(cyclohexylthio) phthalimide, and N-oxydiethylene benzothiazole-2-sulfenamide in a nitrophenyloctyl ether matrix.

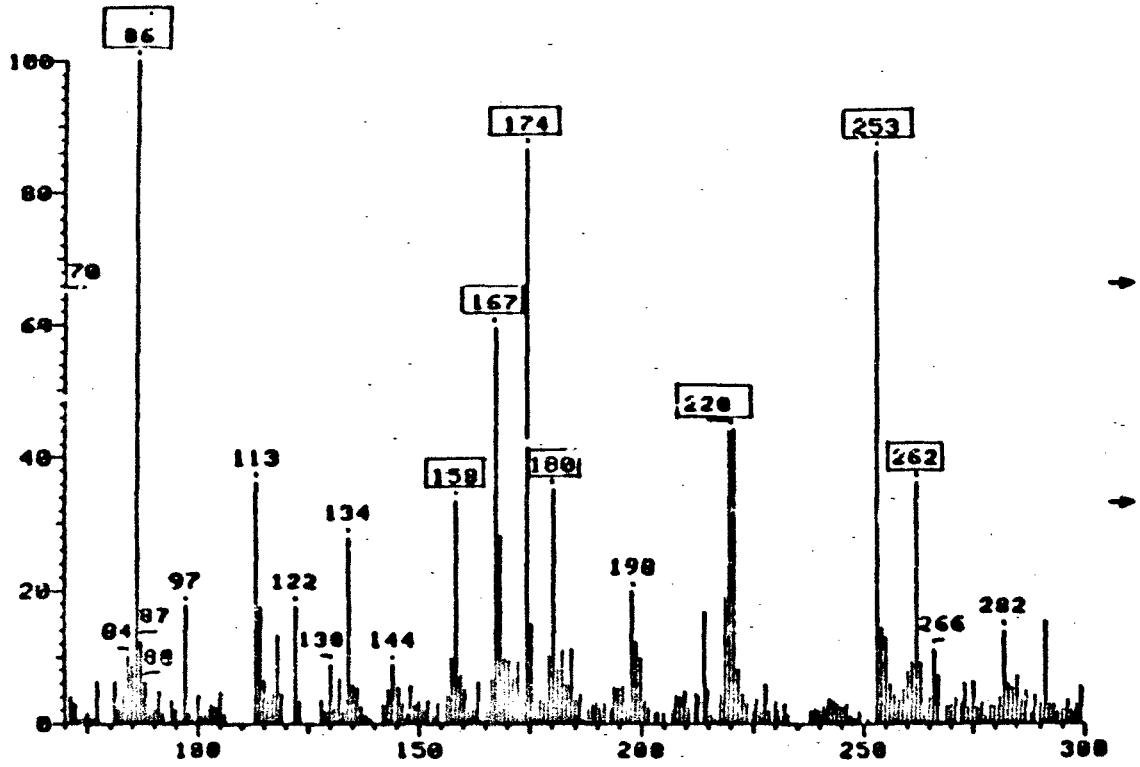


FIGURE 3. Composite fast atom bombardment mass spectrum of the three additives in Figure 2, with the reference spectrum of nitrophenyloctyl ether removed by spectrum subtraction.

TABLE 2

CHARACTERISTIC ADDITIVE IONS OF FIGURE 3

ADDITIVES	DIAGNOSTIC IDENTIFICATION IONS
1. POLYMERIZED-2,2,4-TRIMETHYL-1,2-DIHYDROQUINOLINE	m/z 174, 158
2. N-(CYCLOHEXYLTHIO)PHTHALIMIDE	m/z 262, 180
3. N-OXYDIETHYLENE BENZOTHIAZOLE-2-SULFENAMIDE	m/z 253, 221, 220, 167, 86

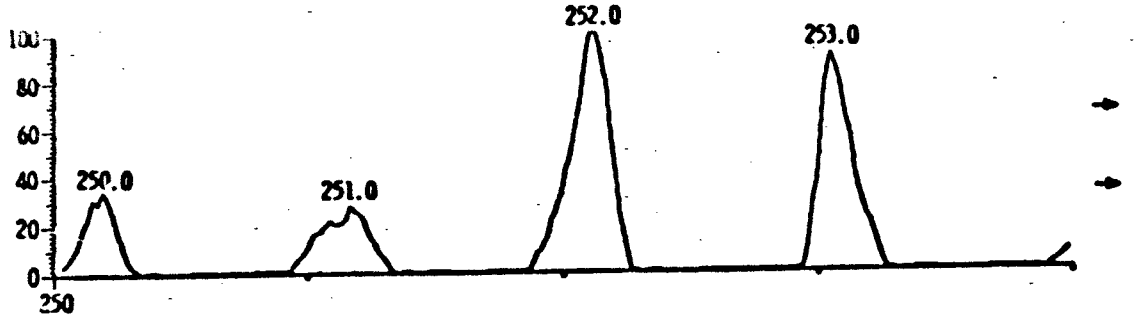


FIGURE 4. The low resolution FAB spectrum of N-oxydiethylene benzothiazole-2-sulfenamide (accelerator) in nitrophenyloctyl ether matrix (8KV).

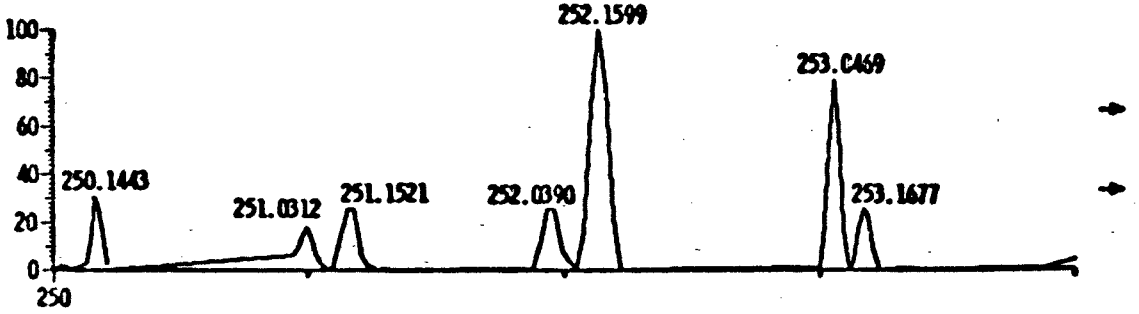


FIGURE 5. The high resolution FAB spectrum separating isobaric masses:
--N-oxydiethylene benzothiazole-2-sulfenamide, mass 251.0312, 252.0390, 253.0469
--Nitrophenyloctyl ether, masses 250.1443, 251.1521, 252.1599, 253.1677.

REFERENCES

1. Deome, A. J., Kane, P. J., and Patt, J. The Determination of Temperature Dependent Degradation Mechanism in Track Pad Elastomers by PY-GC-MS. AMMRC Technical Report, 82-53 pp.
2. Barber, M., Bordeli, R. S., Sedgwick, R. D., and Tyler, A. N. (1981): J. Chem. Soc. Chem. Commun., 7: 325-327.
3. Barber, M., Bordeli, R. S., Elliot, R., Sedgwick, D., and Tyler A. N. (April 1982): Anal. Chem., Vol. 54, No. 4, 645A-657A pp.
4. Lehmann, W. D., Kessler, M., and Konig, W. A. (1984): Biomedical Mass Spectrometry, Vol. II, No. 5.
5. Taylor, L., Hazelby, D., and Wakefield, C. J. (1983): Inter. J. of Mass. Spec. and Ion Phy., 46, 407-410 pp.
6. Lattimer, R. P., Harris, R. E., Ross, D. B., and Diem, H. E. (1985): Rubber Chem. and Tech., Vol. 57, 1013-1022 pp.
7. Martin, S. A., Costello, C. E., and Biemann, K. (1982): Anal. Chem., 54, 2362-2368 pp.
8. Meili, J. and Seibl, J. (1983): Inter. J. of Mass. Spec. and Ion Phy., 45, 367-370 pp.
9. Clay, K. L. and Murphy, R. C. (1983): Inter. J. of Mass. Spec. and Ion Phy., 53, 327-330 pp.

RUBBER DISPERSION USING DARK FIELD MICROSCOPY

GUMERSINDO RODRIGUEZ
Materials, Fuels and Lubricants Laboratory, U.S. Army Belvoir Research, Development, and Engineering Center, Fort Belvoir, Virginia 22060-5606

The importance of carbon black dispersion to the end use performance and economical aspects of rubber compounding has been well documented. Large inhomogeneities in the rubber matrix resulting from grossly incomplete dispersion generally affect failure properties, such as tensile strength, tear strength, fatigue, and abrasion resistance. The ease of attaining good dispersion depends upon the behavior of the elastomer, that of the carbon black and other additives, the mixing equipment configuration, and the mixing operating conditions. To understand how dispersion affects physical properties requires consideration of all these aspects.

Because of this extreme dependence of final product properties on the state of filler dispersion, several methods for estimating this parameter have evolved over the years. Studies on the dispersion process have been primarily involved in two areas. One is the direct examination of the state of dispersion, which is done effectively with microscopes. The other is the indirect characterization of the progress of dispersion by measuring a processing or vulcanizate property of the stock. The response of the compound to these tests relates to the state of the disperse phase within the polymer. Commonly used tests are viscosity, tensile strength, and elongation at break, among many others.

The system described here makes use of a dark-field microscope, high resolution TV camera with monitor and a waveform analyzer. The surface of the rubber is displayed on the TV monitor and its video signal is analyzed with a Data 6000 waveform analyzer. From the waveform analyzer we can obtain the mean peak height measurement and the estimate of standard deviation for a given surface and trace. The mean peak height produces a quantity associated with the average level of the rubber surface while the standard deviation is a function of the variability of that surface. Figure 1 shows a sketch for dark field microscopy.

A number of rubber formulations have been evaluated using the described technique. Table 1 summarizes the data obtained on some rubber compounds. Low mean peak height and standard deviation, conforms with good dispersion, the values for the glass surface serve as baseline. There is a marked difference

in values between SBR-1 and SBR-2, which are identical compounds except that SBR-2 was mixed in an overloaded mixer condition; the same holds for the natural rubber compounds. The results of NAT-38 shows the effect of using a larger particle size carbon black in the same polymer matrix.

Figure 2 correlates certain physical properties with the waveform analysis results. The correlation is evident, generally for lower tensile strength, tear strength, and resistance to crack. The results of the waveform analysis, (peak height, standard deviation) are higher for any given polymer.

The technique gives results which are sufficiently discriminating to allow correlation of filler dispersion with some physical properties. An additional advantage of the method is that the results of the analysis can be treated statistically to develop a rating method .

DARK FIELD MICROSCOPY

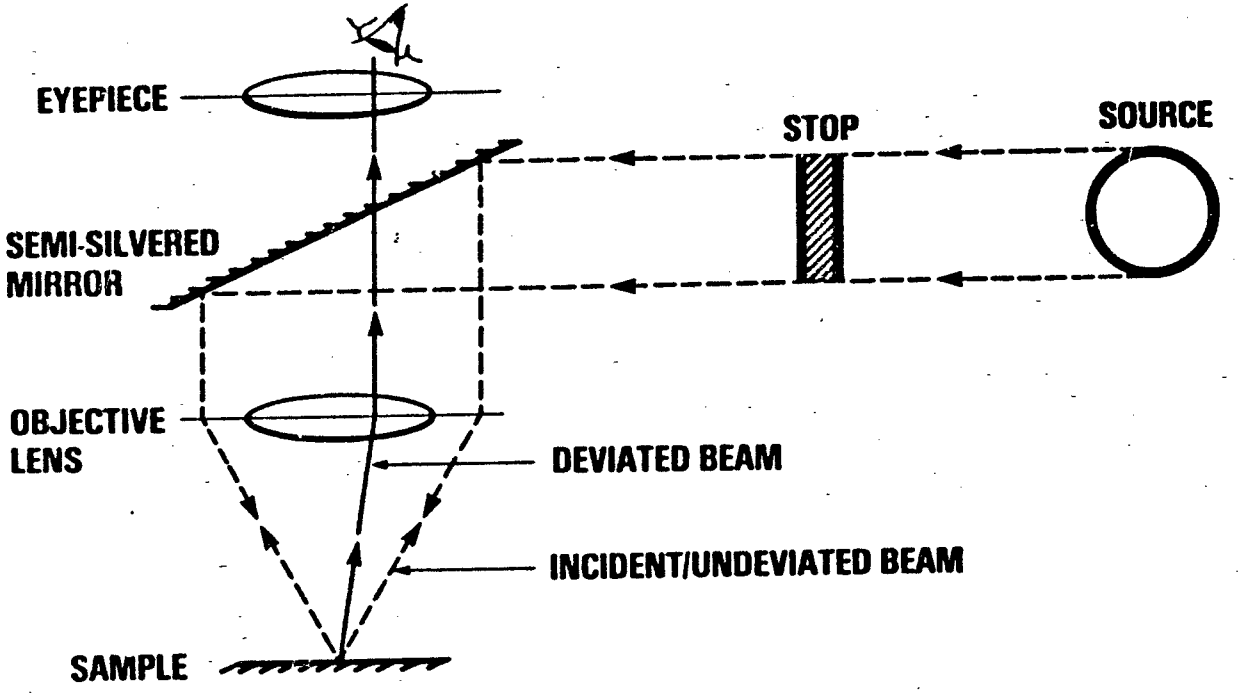


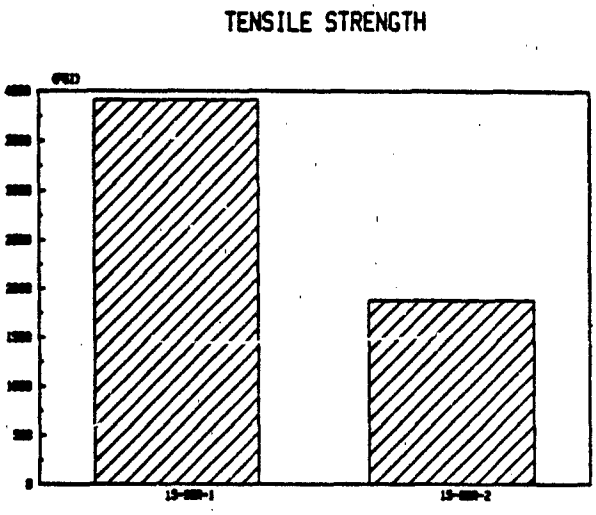
FIGURE 1. Dark field microscopy.

TABLE 1

WAVEFORM ANALYSIS

WAVEFORM ANALYSIS

COMPOUNDS	MEAN (MV)	S DEV (MV)	ENERGY $(v)^2$-S	AREA (MV-S)	MAX (MV)
SBR-1	217.960	66.4022	308.382	1.2944	277.483
SBR-2	200.764	93.7442	510.904	1.6366	416.85
CR-1	254.05	71.7143	408.55	1.48880	344.35
TP-D	267.020	70.4644	448.224	1.56900	356.853
NAT-1	218.424	57.0280	293.730	1.25891	266.860
NAT-2	249.52	60.934	387.400	1.4654	299.981
NAT-38	259.671	68.9020	420.060	1.5136	320.610
GLASS	163.120	42.4974	169.530	0.9734	200.612



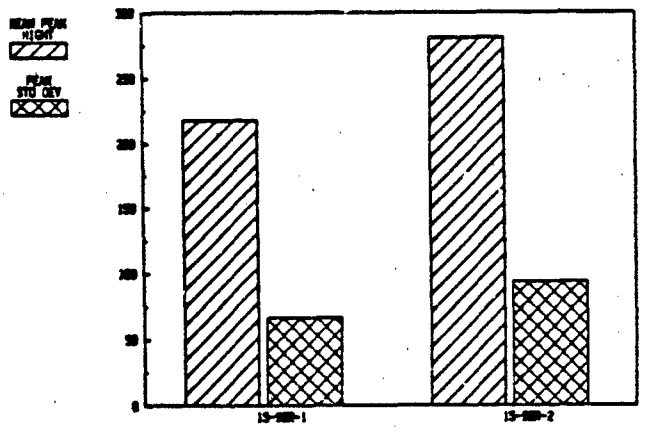


FIGURE 2. Correlation of physical properties with the waveform analysis results.

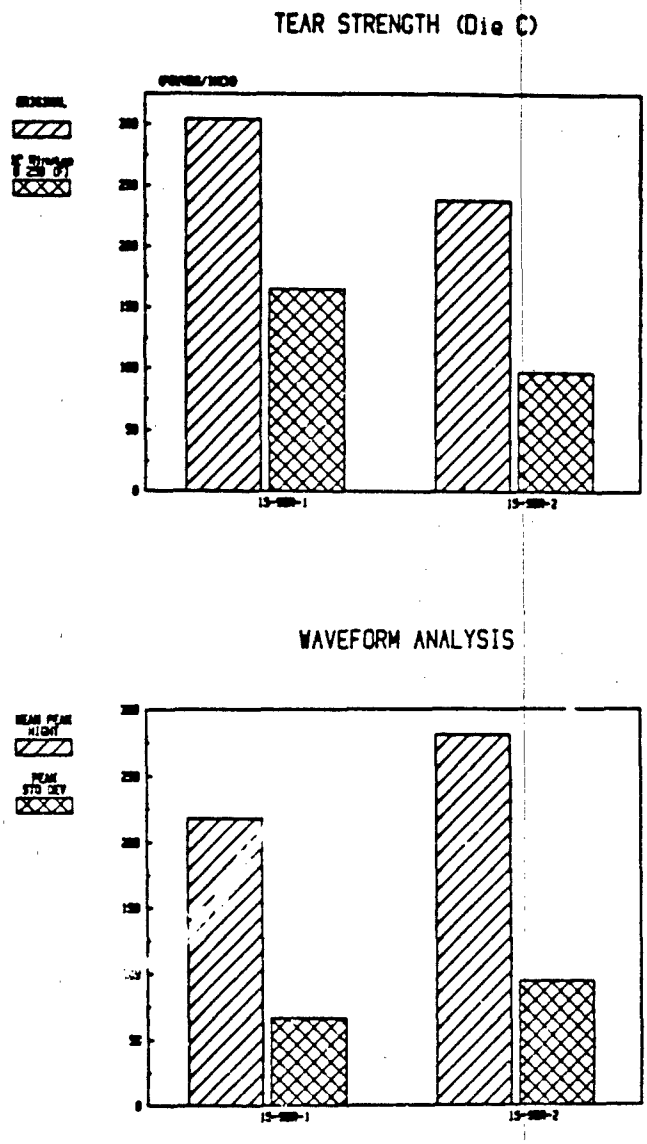
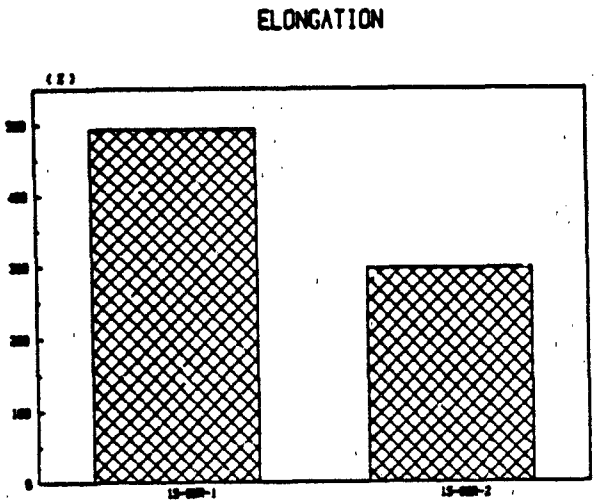


FIGURE 2. Correlation of physical properties with the waveform analysis results.(Continued)



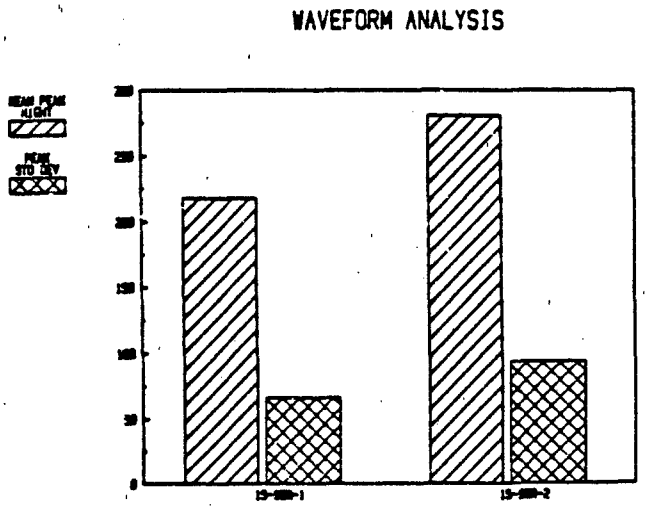


FIGURE 2. Correlation of physical properties with the waveform analysis results. (Continued)

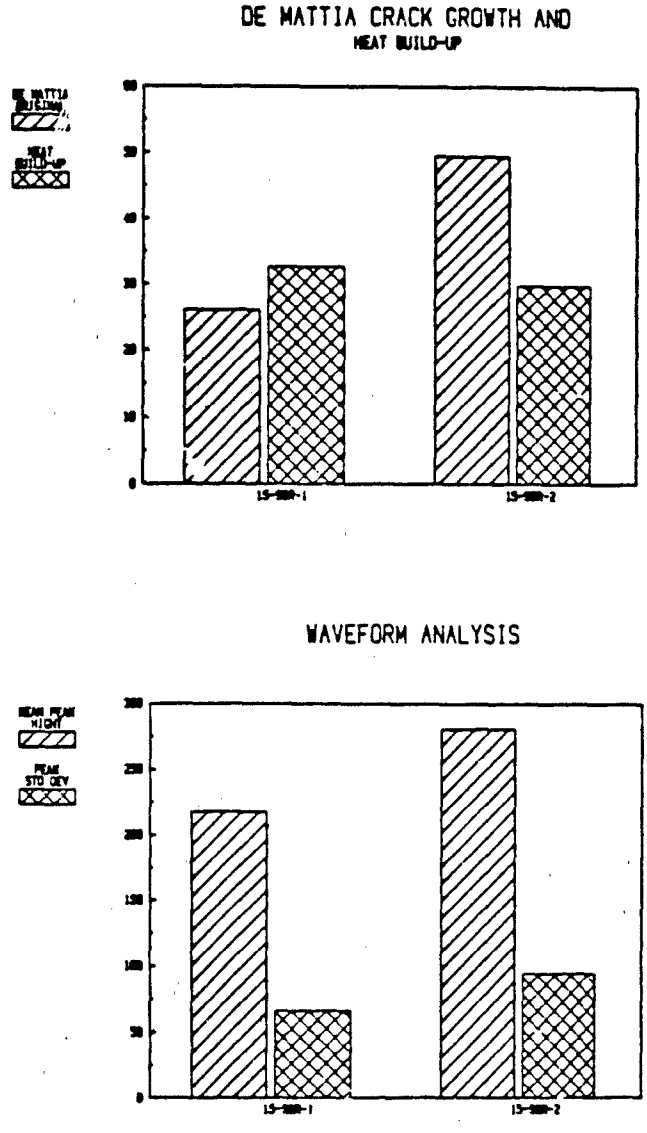


FIGURE 2. Correlation of physical properties with the waveform analysis results. (Continued)

MASS SPECTROMETRY OF ELASTOMER SYSTEMS

ALFRED J. DEOME, DAVID A. BULPETT, AND CHRISTOPHER J. KULIG
U. S. Army Materials and Mechanics Research Center, Watertown, Massachusetts 02172

ABSTRACT

Serial chromatopyrography-mass spectrometry is presented as a novel, rapid, and accurate analytical technique for deformulation of complex vulcanized elastomer systems. The technique has been developed at the U.S. Army Materials and Mechanics Research Center to monitor discreet alterations in formulations, to evaluate thermal degradation mechansisms within the polymer matrix, and to evaluate the technology of manufacturer supplied elastomer end-items. This technique has been in development for approximately 3 years with primary emphasis directed toward improvement of the M-1 Abrams Tank T-156 track pad elastomer system. Results are presented in this paper for several different vulcanizates to demonstrate the versatility of the methodology and the compatibility of the technique with different polymer formulations.

INTRODUCTION

Previous work in the area of pyrolysis-gas chromatography-mass spectrometry (1-5) has shown that this technique is a powerful analytical tool well suited for studying the complex composition of intractable materials such as vulcanized elastomers. An interesting and particularly valuable application of the many pyrolysis techniques available is Serial Chromatopyrography-Mass Spectrometry (Ser-Py-GC-MS). This technique appears to be very applicable to separating residual vulcanizate formulation components from polymer composition without the need for complicated sample manipulation procedures. Instrumental techniques employing a combination of serial pyrolysis techniques, high resolution capillary gas chromatography, and mass spectrometry have been developed at the U.S. Army Materials and Machanics Research Center in collaboration with the U.S. Tank Automotive Command (TACOM) in Warren, Michigan 48090, during the past several years. The technique is used as a means of accurately accessing and reconstructing formulations of vulcanized elastomers where few, if any, straightforward analytical procedures are available for this type of work.

The complex nature of industrial elastomer systems provides a significant analytical challenge. Compound analysis is predicated on the availability of numerous instrumental techniques and a complement of procedures to analyze polymers, additives, and fillers in a single elastomer system. Because compounding produces the optimum physical characteristics in an elastomer system, it is possible to create a tremendous number of diverse elastomers by varying the polymer ratios, additive and filler types, or by varying the mixing and processing techniques. The statistical combinations are virtually endless, each variation resulting in a specific system with new and different physical and compositional characteristics.

The use of Ser-Py-GC-MS has successfully been developed at this research center to avoid manipulative ASTM procedures, reduce analysis time, increase accuracy, and generally provide more specific information about elastomer systems that could previously be obtained by combinations of wet chemistry analysis, extractions, and instrumental identifications.

Three proprietary elastomer systems are presented in this paper to demonstrate the application of the technique as well as to illustrate the format and nature of results. The elastomers presented in this paper include 1) a T-156 track pad elastomer system; 2) an experimental proprietary natural rubber; and 3) an Advanced Attack Helicopter (AAH) self-sealing fuel hose.

EXPERIMENTAL

All samples were pyrolyzed using a Chemical Data Systems (CDS, Oxford, PA) Model 122 Pyrolysis unit interfaced to a Hewlett-Packard Model 5996 gas chromatograph-mass spectrometer system controlled by a Hewlett-Packard Model 1000-E series computer operating under RTE-6/VM Rev. C software. A sample, weighing approximately 5 mg., of each elastomer system is placed in a quartz pyrolysis tube and inserted into a CDS interface maintained at 250°C. The initial pyrolysis temperature of 300°C is used to thermally desorb the organic fraction of the formulation additives without disintegration of the intact polymer matrix. Without removing the sample from the interface, the sample is pyrolyzed at 600°C. This serial pyrolysis temperature serves to fragment the polymer matrix, already free of additive and formulation components, into its monomeric species and associated pyrolysis rearrangement species which are used for further identification of the whole system.

The pyrolyzate resulting from each pyrolysis experiment was chromatographed on a 12 meter capillary column of cross-linked methyl silicone (SE-30). The gas chromatograph was programmed from 50°C to 260°C at 8°C/min and the final temperature was maintained for 10 minutes. A mass range of 33 to 300 amu was scanned repeatedly at approximately 1.4 second intervals and the electron ionization mass spectra (70 eV) of the pyrolyzate components were collected by the computer acquisition software. Data reduction of the mass pyrograms was accomplished using on-line software programs designed to display individual mass spectra and to compare the spectrum of interest to standard reference spectra contained in the 46,000 NBS (National Bureau of Standards) Mass Spectral Reference Library.

RESULTS AND DISCUSSION

The respective sets of serial pyrolysis experiments for each sample are provided. One of the important aspects of using mass spectrometry as a specific detector for this type of work is that it provides conclusive evidence of the organic structure of the chromatographed pyrolyzate. The ambiguity of pyrolysis-gas chromatography, conventionally used to produce a "fingerprint" of vulcanizate composition, is virtually eliminated; the components can be evaluated for molecular ion information as well as for structure. In many respects this technique is definitive for composition.

The T-156 analysis shown in Figures 1 and 2 provides a set of data which elucidates a formulation of accelerator, antioxidants, and extenders or processing aids (Py at 300°C). The mass pyrogram derived from the second step of the experiment (Py at 600°C) clearly shows the monomeric species of 1,3-butadiene (m/z 54) and styrene (m/z 104). Other aromatic decomposition products derived from the polymer matrix also produce ions indicative of the styrene-butadiene (SBR) polymer.

The proprietary natural rubber formulation shown in Figures 3 and 4 displays pyrolytic products with gas chromatographic retention times similar to those in the styrene-butadiene formulation in Figure 1. Mass spectrometric identification of the chromatographic effluent, however, shows not only the essential organic formulation and polymer, but also essential oils and fatty acids which serve to further classify the polymer as being derived from SMR (Standard Malaysian Rubber) rather than from synthetic cis-1,4-polyisoprene. The conventional use of Py-GC pattern recognition techniques between Figure 1 and Figure 3 would

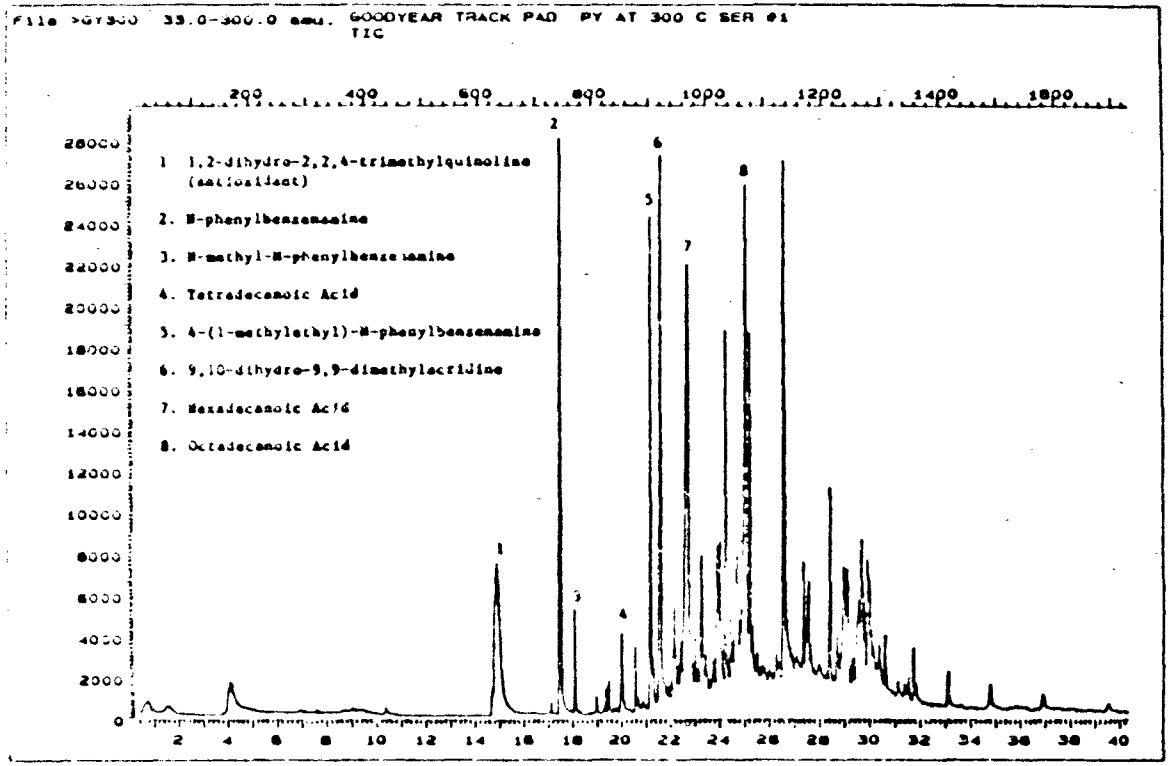


FIGURE 1. Serial mass chromatopyrogram #1 of T-156 track rubber pyrolyzed at 300°C.

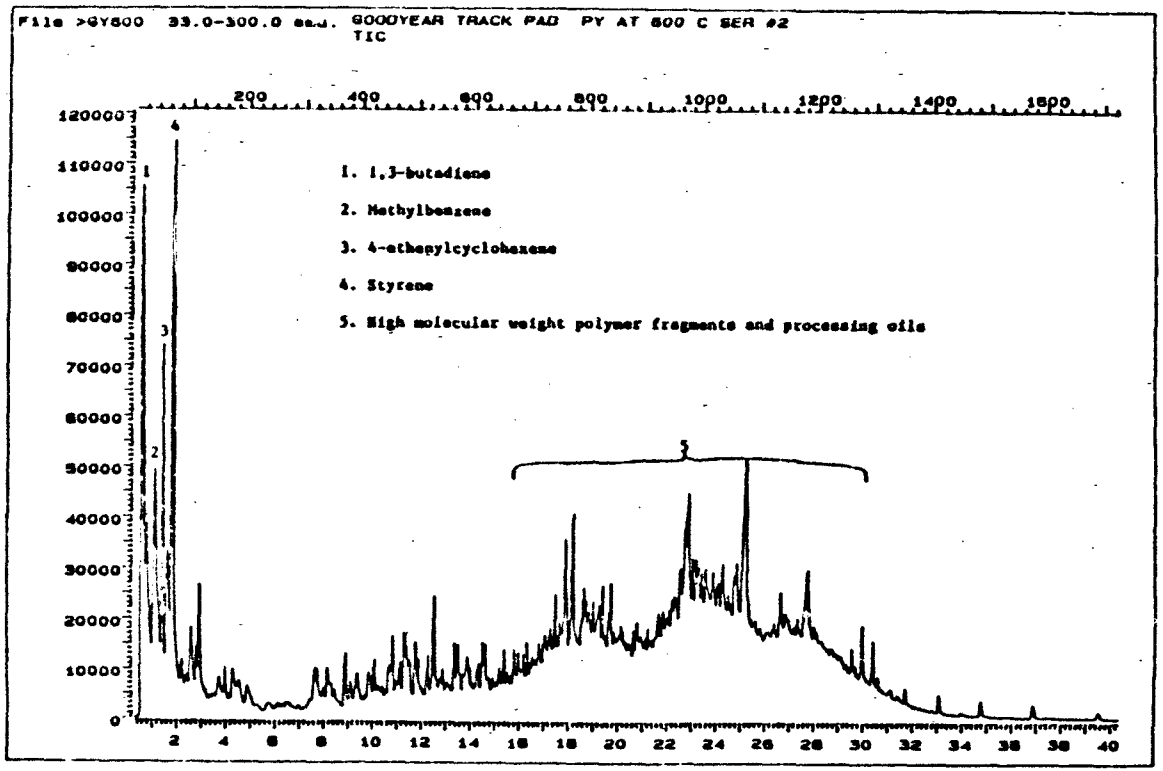


FIGURE 2. Serial mass chromatopyrogram #2 of T-156 track rubber pyrolyzed at 600°C.

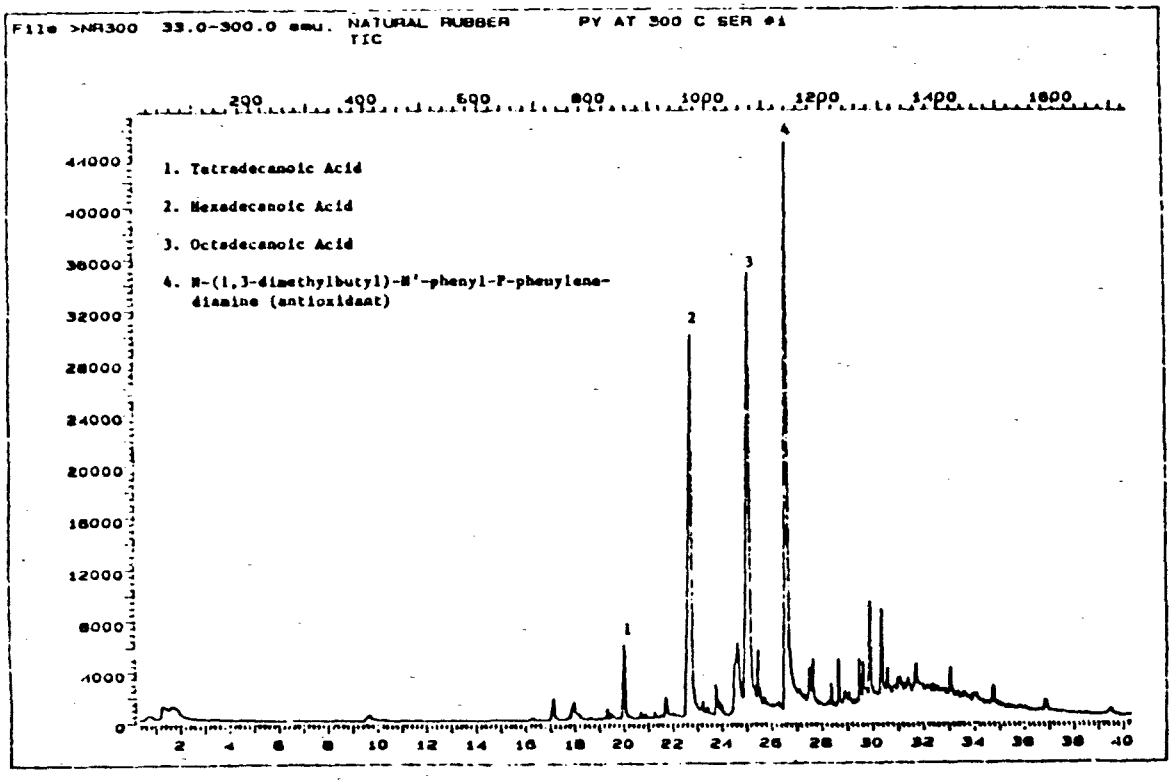


FIGURE 3. Serial mass chromatopyrogram #1 of a natural rubber vulcanizate pyrolyzed at 300°C.

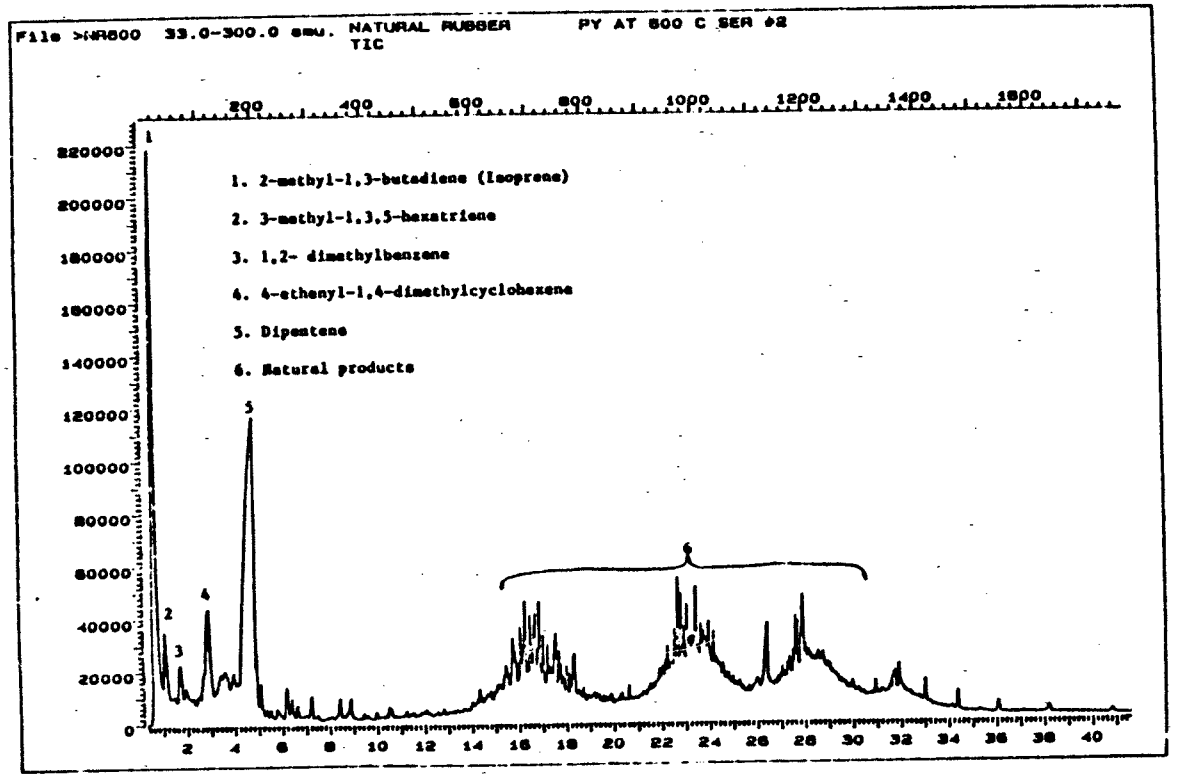


FIGURE 4. Serial mass chromatopyrogram #2 of a natural rubber vulcanizate pyrolyzed at 600°C.

produce vague and questionable identifications; mass spectrometry clearly differentiates the two dissimilar systems without relying on gas chromatographic retention time comparisons.

The 300°C mass chromatopyrogram of the fuel hose in Figure 5 reveals a highly specialized formulation which is quite different from the previous two examples. This material is formulated with 2,5-dimethyl-2,5-(t-butylperoxy)-hexane as a cross-linking agent as well as 4-morpholinyl-2-benzothiazole disulfide as an accelerator for the sulfur curing system. The two mechanisms of cross-linking are required to effect vulcanization of the polymer system derived in the 600°C pyrolysis. Figure 6 shows that the polymer is in actuality a combination of nitrile rubber with styrene-butadiene rubber. The peroxide cross-linking agent is recommended for the NBR fraction while the sulfenamide accelerator provides maximum strength and wear qualities for the SRF fraction. The dibutyl phthalate provides a softening characteristic for the SBR rubber. Octyldiphenylamine is the primary antioxidant for the entire system. Dibetanaphthyl-p-phenylenediamine is also used as an antioxidant as well as a copper inhibitor, most likely serving as a protective mechanism for the copper braid grounding wound around the entire hose under the protective covering. The construction of the hose is such that NBR, on the interior of the hose, provides a fuel resistant layer while the exterior of the hose is a softened SBR rubber. If the hose is penetrated, fuel will swell the softened SBR which may seal the puncture. Again, this example illustrtes the versatility of this technique, providing significant analytical capability to discern formulations designed for complex elastomer systems having specialized applications.

CONCLUSIONS

Serial pyrolysis-gas chromatography-mass spectrometry is a highly specialized analytical technique which reduces complex, vulcanized elastomer systems to selective, thermally degraded states. The data derived from this type of analysis provide essential information about the elastomer formulation and polymer while reducing sample manipulations to an absolute minimum. In many cases, extractions and multiple analytical steps advocated in conventional ASTM procedures are eliminated. Ser-Py-GC-MS, as a method, represents a powerful means of elastomer characterization providing rapid, reproducible, and accurate data which transcend conventional pyrolysis applications. Particularly in the case of vulcanized elastomers, the pyrolysis data may be extrapolated into performance behavior,

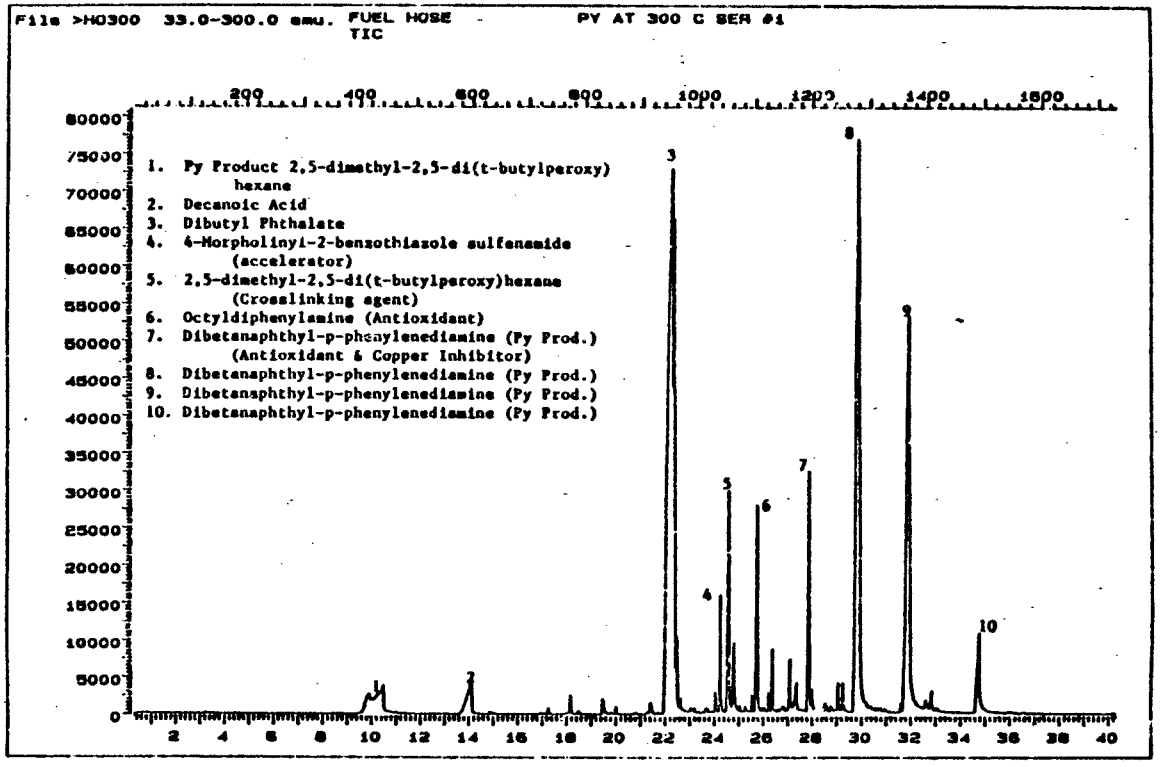


FIGURE 5. Serial mass chromatopyrogram #1 of AE-502 fuel hose pyrolyzed at 300°C.

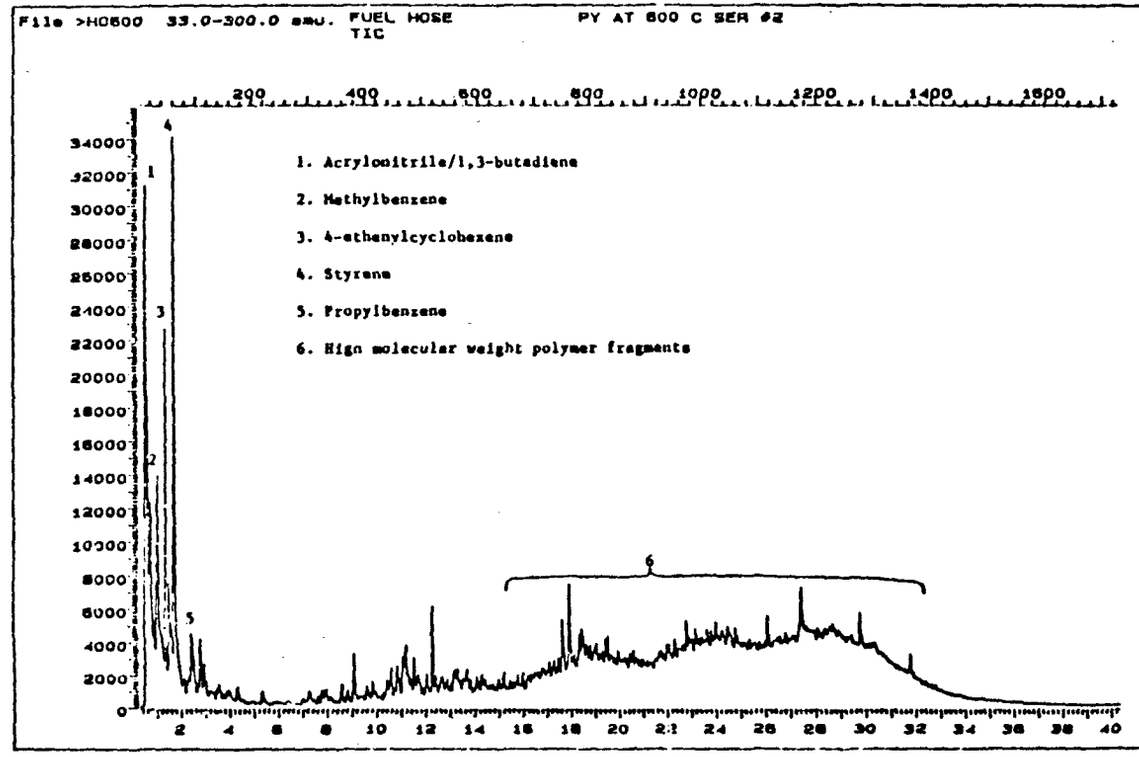


FIGURE 6. Serial mass chromatopyrogram #2 of AE-502 fuel hose pyrolyzed at 600°C.

correlated to quality assurance, and serve as a materials profile to predict the overall integrity of the elastomer.

REFERENCES

1. Deome, A. J., Kane, P. J., and Patt, J. (October 1982): The Determination of Temperature-Dependent Degradation Mechanisms in Trade Pad Elastomers by Pyrolysis-Gas Chromatography-Mass Spectrometry. AMMRC TR 82-53.
2. Deome, A. J. and Hagnauer, G. L. (1981): Pyrolysis-Gas Chromatography-Mass Spectrometry of AE502 Fuel Hoses. AMMRC TR 81-12.
3. Wuepper, J. L. (1979): Pyrolysis Gas Chromatography-Mass Spectrometric Identification of Intractable Materials. Anal, Chem., 51:997.
4. Iglauer, N. and Benley, F. F. (1974): Pyrolysis GLC for the Rapid Identification of Organic Polymers. J. Chromatog. Sci., 12:23.
5. Chih-An Hu, J. (1977): Pyrolysis Gas Chromatography Analysis of Rubbers and Other High Polymers. Anal. Chem., 49:537.

CHARACTERIZATION OF ELASTOMERS USING NEUTRON ACTIVATION AND HIGH RESOLUTION GAMMA RAY SPECTROSCOPY

FORREST C. BURNS
Materials Characterization Division, U.S. Army Materials and Mechanics Research Center, Watertown, Massachusetts 02172

Elastomer samples are difficult to analyze using conventional analytical techniques because they are composed of many different materials and are therefore hard to get into solution. It is not necessary to process the elastomers in any way to be able to use thermal or fast neutron activation analysis. The sample is simply irradiated with a standard containing the elements of interest and each is then counted using a gamma ray spectrometer. Since very small samples (less than 10 milligrams) can be irradiated and analyzed the homogeniety of an elastomer can be determined.

In addition to quantitative results being possible for many elements; a gamma ray "fingerprint" is also obtained. This is unique for each batch of material. Even if the elements are the same the ratios of the concentrations depicted by the peak heights of the energy peaks in the gamma ray spectra are different. Therefore, if it were ever necessary to trace the origin of a sample it would be possible.

Fast neutron activation is the only nondestructive method for obtaining quantitative elemental bulk oxygen analyses of elastomers. Using this technique it is possible to determine the amount of oxidation that has taken place at the surface of a tank pad as opposed to the unexposed surface.

In this presentation examples of gamma ray "fingerprints" will be shown. Also a table of oxygen analyses of tank pads from different manufacturers will be presented.

DEFORMATION OF MICROPHASE STRUCTURES IN POLYURETHANES

C.R. DESPER[1], N.S. SCHNEIDER[1], J.P. JASINSKI[1]*, J.S. LIN[2]
(1) Organic Materials Laboratory, U.S. Army Materials and Mechanics Research Center, Watertown, Massachusetts 02172;
(2) National Center for Small Angle Scattering Research, Oak Ridge National Laboratory, Oak Ridge, Tennessee 37830

Microstructure deformation in three selected polyurethanes has been studied quantitatively by SAXS during macroscopic tensile strain. The results demonstrate three possible modes of response at the level of the microphase structure: a shear mode, a tensile mode, and rotation or translation of independent particles. In the shear mode, as seen in an amine-cured polyurethane, the hard segment lamellae tilt away from the stretch direction, while the soft segment microphase deforms in shear. In the tensile mode, exemplified by a diol-cured polyurethane, the lamellae orient normal to the stretch direction, while the soft segment microphase deforms in tension. For a triol-cured polyurethane, the local deformation mode is ambiguous. Results are interpreted in terms of either rotation or translation of microparticles.

*Intergovernmental Personnel Act (IPA) fellowship: on leave from the Chemistry Department, Keene State College, Keene, New Hampshire 03431.

RELATIONSHIP BETWEEEN CHEMICAL COMPOSITION AND HYSTERESIS IN POLYURETHANE ELASTOMERS

CATHERINE A. BYRNE
U.S. Army Materials and Mechanics Research Center, Polymer Division, Watertown, Massachusetts 02172-0001

INTRODUCTION

Polyurethane elastomers are promising materials for solid tires and track pads for tanks. There is little systematic study reported of the relationship between the specific chemical compositions of a series of chemically similar polyurethanes and their hysteresis and other properties thought to influence elastomer performance on heavy vehicles[1]. In this work, the characteristics of a group of promising polyurethanes are being studied, including the thermal properties, mechanical properties at elevated temperatures, hardness, tear strength and compressive fatigue behavior. Abrasion resistance is also an important property, but the correlation between laboratory tests and road tests is frequently poor. Abrasion resistance will not be discussed here.

The polyurethanes chosen for the study are based on 1,4-diisocyanatocyclohexane (CHDI, 99% trans isomer, Akzo Chemie America) poly(tetramethylene oxide) soft segment of different molecular weights (PTMO), chain extender 1,4-butanediol (BD) and crosslinker trimethylol propane (TMP). Polyurethanes from CHDI have been compared to those from several other diisocyanates in a study by Wong and Frisch[2]. In general, the stress properties of the CHDI samples were poorer at room temperature but better retention of strength occurred at higher temperatures, in the range examined, up to 150°C. A linear CHDI sample with Shore A hardness 97 showed a stress of approximately 15 MPa at 300 percent elongation and 25°C and 8 MPa at 150°C. An MDI sample of similar hardness, but higher hard segment content, showed 17 MPa at 25°C and about 4 MPa at 150°C.

Polyurethanes from CHDI also exhibit better retention of tear resistance at elevated temperatures.[3] A comparison was made of polyurethanes prepared from PTMO 1000 and MDI having 33.9 weight percent hard segment and a similar CHDI polymer having 27.2 weight percent hard segment. Split tear resistance (ASTM D1938) values of 44.0 kN/m (252 pli) at 25°C and 2.8 kN/m (16 pli) at 150°C were observed for the MDI polyurethane and 37.5 kN/m (214 pli) and 25.2 kN/m (144 pli) at the respective temperatures for the polymer prepared from CHDI. While the tear resistance of the latter materials is lower at

room temperature it retains 67 percent of that value at 150°C. The polymer prepared from MDI retains only 6 percent of its tear resistance at 150°C.

EXPERIMENTAL

The synthesis involved formation of a prepolymer, followed by chain extension. Samples were prepared as 50 mil (1.3 mm) sheets using 0.0009 weight percent T-12 catalyst or as 2-1/2 x 2-1/2 x 5/8 inch (63.5 x 63.5 x 15.9 mm) blocks using no catalyst. The preparation of 100g batches of polyurethane and casting as blocks was not possible when a catalyst was used, because the larger samples set up too quickly. The CHDI is intermediate in reactivity between MDI and hydrogenated MDI (H_{12}MDI) and so good elastomers could be made without a catalyst. The infrared spectra of thin films of the samples prepared with a catalyst showed a trace of free isocyanate at 2255 cm^{-1}. When the attenuated total reflectance method was used, the polyurethane surfaces showed no free isocyanate.

Thermomechanical analysis was performed using Perkin-Elmer TMS-1 with a Perkin-Elmer Model UU-1 temperature program controller. Samples were heated in a helium atmosphere from

Table 1

THERMOMECHANICAL ANALYSIS RESULTS

moles/1 mole/moles/mole CHDI/ PTMO/ BD / TMP	Transitions (°C)	
1.9 - 2000 - 0.8 - 0.13	-72	217°
2.0 - 2000 - 0.8 - 0.13	-71	225°
2.1 - 2000 - 0.8 - 0.13	-71	244°
2.1 - 2000 - 0.9 - 0.066	-72	256°
2.1 - 2000 - 0.6 - 0.266	-74	241°
2.5 - 2000 - 1.2 - 0.2	-70	251°
2.6 - 2000 - 1.2 - 0.2	-74	253°
2.4 - 2000 - 1.2 - 0.2	-74	241°
2.6 - 2000 - 1.35 - 0.1	-69	258°
2.6 - 2000 - 0.9 - 0.4	-74	251°
2.6 - 1000 - 1.2 - 0.2 PTMO 1000	-68	265°
2.6 - 2000 - 1.2 - 0.2 Postcure 125°	-74	247°
2.6 - 2000 - 1.2 - 0.2 Postcure 150°	-74	236°

-100°C to the softening point of the sample at 20°C/minute. The weight used in the TMA was 40 grams in most cases, 20 grams for one or two samples.

A Perkin-Elmer DSC-2 cooled with liquid nitrogen and purged with helium was used for DSC. Sample size was 10 - 15 mg. The heating rate was 20° per minute. A Perkin-Elmer Thermal Analysis Data Station was used to determine the temperatures of the transitions.

A Rheometrics Dynamic Spectrometer, RDS-7700, was used for dynamic mechanical analysis. The samples were cut to 13 by 64 mm and were 1.3 to 1.6 mm thick. A liquid nitrogen controller was used to achieve the desired temperature. Measurements were taken at 10° temperature increments, with an equilibration time of two minutes at each temperature. The range studied was from -100 to 160°C, with a strain setting of one percent and a rate of 6.28 radians per second.

During Rheometrics analysis, a torsional motion is imposed on the sample and the torque and normal forces resulting from the motion are measured by a transducer. From these values can be calculated the storage modulus, G', the loss modulus, G" and the ratio of the latter to the former, the loss tangent ($\tan\delta$).

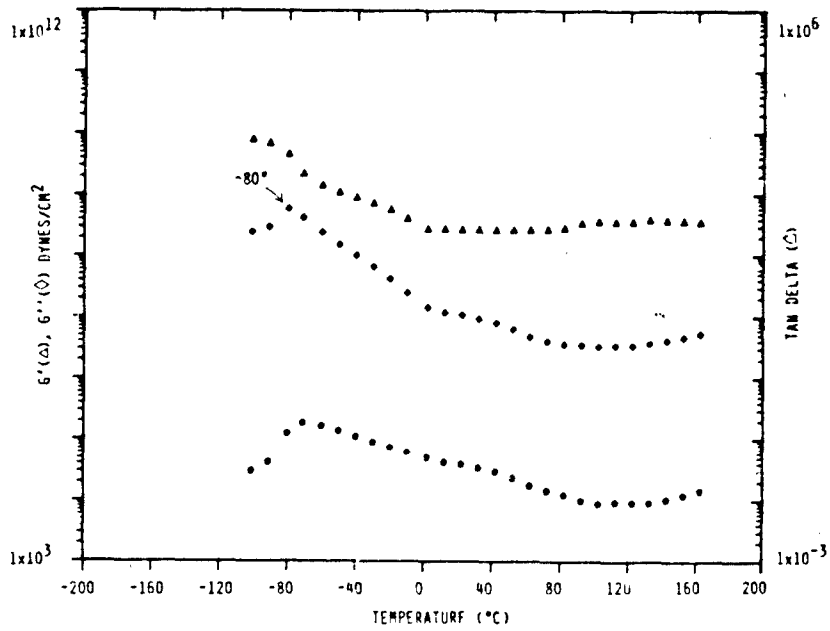


FIGURE 1. The Dynamic Mechanical Spectrum for sample 2.5-2000-1.2-0.2. Modulus values can be converted to Pascals by reducing the ordinate values by an order of magnitude.

Tear resistance was measured using a trouser tear specimen described in ASTM D470-82. The crosshead speed was 500 mm/min. The data reported is the average of results for six specimens. A hand-held Shore durometer, hardness type "A-2" was used to determine the haruness of the samples, accordingly to ASTM D2240-75. Specimens were rectangular, 25 mm in length by 13 mm wide. Four plies of sample were used to achieve a thickness of 6.4 mm. Three readings were taken, 6 mm apart on the surface of the four plies. Hardness values measured on the blocks tended to be up to 5 units lower.

Internal heat generation was measured during fatigue loading of a series of the polyurethane elastomers described above. Compression-compression fatigue testing was performed on sample blocks at 18.5 Hertz with a maximum load of 4500 pounds (20,000 N) and a ratio of minimum to maximum load of 0.1. The testing continued for 200,000 cycles and a time of 180 minutes.

An Instron model 1322 servohydraulic test machine was used for all fatigue tests. Throughout the test, load and stroke data were acquired using a Nicolet digital oscilloscope. These data were stored on floppy disks for post-test reduction. The internal temperature of each block was measured using a J type thermocouple inserted through a drilled hole into the center of the block. Temperature was recorded by an Electronic Controls Design Datalogger Model DL 2020 at time intervals which varied depending on the rate of temperature rise.

The Nicolet oscilloscope is microprocessor based and data reduction can be performed internally. The data were reduced by displaying and plotting load versus stroke at various times during each fatigue test. Hysteresis was calculated from the area between the loading and unloading curves using a program supplied by Nicolet. Each value represents an average of five to six successive cycles of loading.

RESULTS AND DISCUSSION

Initially, the TMA curves for a number of samples were examined. It is important that the samples have final softening temperatures well above the temperature experienced by the samples in compressive cycling. All the samples tested exhibit two transitions shown in Table 1, one due to the T_g of the PTMO soft segment and the other to the final softening, considerably above the temperatures occurring during compressive cycling and also higher than final softening values for many polyurethanes. An increase in NCO/OH leads to a higher

Table 2

SHORE A HARDNESS AND TEAR STRENGTHS OF POLYURETHANES

moles/1 mole/moles/moles CHDI/ PTMO/ BD / TMP	Hardness	NCO/OH	Tear Strength (pli)	(kN/m)
2.0 - 2000 - 0.8 - 0.13	-	1.0	15.61	2.73
2.1 - 2000 - 0.8 - 0.13	84	1.05	62.13	10.87
1.9 - 2000 - 0.8 - 0.13	87	0.95	131.86	23.08
2.1 - 2000 - 0.9 - 0.066	85	1.05	-	-
2.1 - 2000 - 0.6 - 0.266	87	1.05	23.03	4.03
2.1 - 1000 - 0.8 - 0.13	97	1.05	79.71	13.95
2.6 - 1000 - 1.2 - 0.2	95	1.05	77.29	13.53
2.0 - 2695 - 0.8 - 0.13	81	1.0	-	-
2.5 - 2000 - 1.2 - 0.2	86	1.0	131.61	23.03
2.4 - 2000 - 1.2 - 0.2	88	0.95	146.11	25.57
2.6 - 2000 - 1.35 - 0.1	95	1.05	-	-
2.6 - 2000 - 0.9 - 0.4	90	1.05	21.84	3.82
2.6 - 2000 - 1.2 - 0.2	91	1.05	50.72	8.88

final softening, presumably due to allophanate crosslinking. An assumption was made at the outset, that the best hysteresis properties would be observed for crosslinked samples. All the samples discussed in this work are crosslinked by TMP. It was assumed that crosslinking would reduce the compressibility of the samples and the heat generated would be lower. The assumption has not been tested, and may be incorrect for samples prepared with such a compact diisocyanate.

An increase in the amount of crosslinking by TMP leads to a decrease in the final softening temperature. This is attributable to poorer order in the hard segment regions due to the crosslinking. An increase in weight percent hard segment, effected either by increasing the amount of CHDI or by using PTMO 1000, both cause an increase in final softening. Post cures of six hours at 125 and 150°C cause a lowering of the final softening temperatures, to the extent of 5 to 20°C. A post cure had been suggested as a method of improving the mechanical properties of these polymers. Since the reduced final softening temperatures indicate some degradation, the temperatures which were chosen are possibly too high.

DSC experiments were run on two crosslinked samples, 2.1-2000-0.9-0.067 and 2.6-2000-1.35-0.1. Both samples have soft segment T_g's of -82°C, indication of a very high degree

Table 3

THE RESULTS OF COMPRESSION TESTING

moles/1 mole/moles/moles CHDI/ PTMO / BD / TMP	Hysteresis (in-lb)	(N-m)	Maximum Temp (°C)	Time to Maximum
2.0 - 2000 - 0.8 - 0.13	9.9	1.1	57*	85 min
2.1 - 2000 - 0.8 - 0.13	14.2	1.6	86	177 min
2.0 - 2000 - 0.9 - 0.066	14.0	1.6	87	180 min
2.1 - 2000 - 0.9 - 0.066	12.0	1.4	72**	137 min
2.0 - 2000 - 0.6 - 0.266	13.5	1.5	82**	103 min
2.5 - 2000 - 1.2 - 0.2	6.4	0.7	57	185 min
2.5 - 2000 - 0.9 - 0.4	13.2	1.5	88	182 min
2.0 - 2695 - 0.8 - 0.13	16.0	1.8	100	182 min
2.5 - 2695 - 1.2 - 0.2	23.8	2.7	100	176 min

* Thermocouple failed, temperature still rising
** Thermocouple failed, temperature leveling off

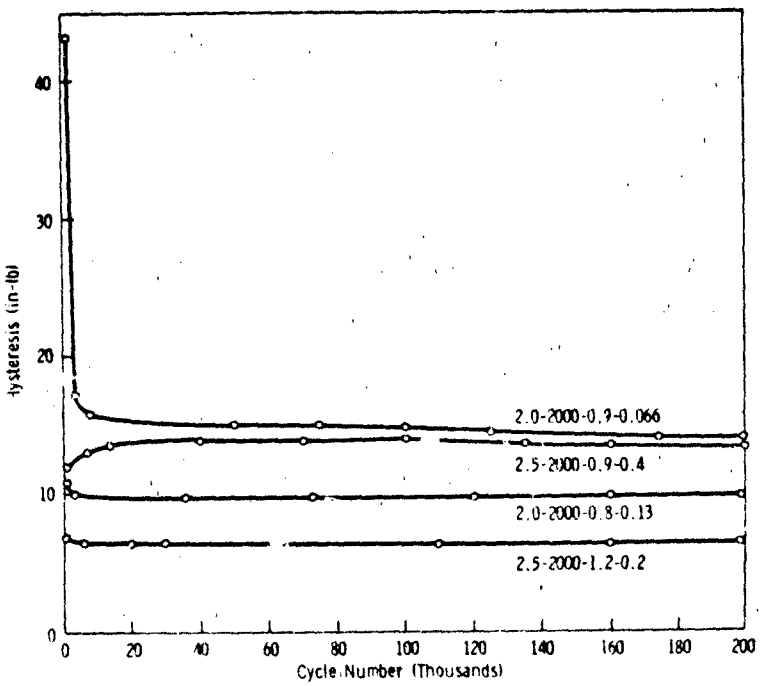


FIGURE 2. The hysteresis during compressive fatigue at 18.5 Hertz.

of purity in the soft segment phase. The pure PTMO has a T_g of -85°C. Each also exhibits an endotherm at -6 to -8°C, which is probably soft segment crystalline melting. In the sample with 2.6 moles CHDI, another transition is apparent at the highest temperature to which the experiment was run, 200°C. A sample without TMP crosslinking, 2.6-2000-1.5 exhibits a very small hard segment T_g with onset temperature 76°C. This is not observed in the crosslinked samples. The maximum temperature attained in compressive cycling in the best samples shown in Table 3 is lower than the hard segment T_g. This factor is important in keeping the hysteresis low. The dynamic mechanical spectrum for 2.5-2000-1.2-0.2 is shown in Figure 1. The curve for loss modulus (G") shows a transition due to the soft segment T_g at -80°C, a change in slope due to soft segment melting at about 0°C and possibly another transition occurring between 0° and 60-70°C. The last behavior is not explainable at present. The sample retains its strength until at least 160°C, which is above the temperatures attained in compressive cycling.

Thermal analysis combined with information about the hardness values for the samples, led to the choice of samples for initial compressive testing. Hardness values were considered important because many of the commercially important compounded elastomers have lower hardness values than these polyurethanes. Increasing the weight percent soft segment by using PTMO 2695 was one way to reduce the hardness. Reducing

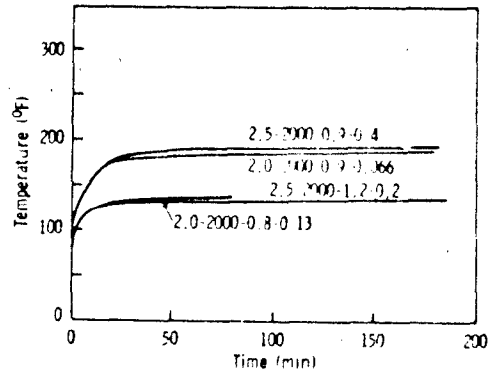


FIGURE 3. The temperature at the center of the sample blocks during compressive fatigue at 18.5 Hertz.

the weight percent hard segment by using 2 moles CHDI also produced softer samples. Another method which has not been tried would be to prepare the polyurethanes by a one step technique rather than by the prepolymer method. This would probably lead to softer samples with more poorly organized hard segment phases. Unfortunately, increasing the softness frequently also leads to an increase in hysteresis. It should be noted that polyurethanes prepared from CHDI exhibit unusually high Shore A hardness values at low weight percent hard segment, ranging from 17.3 to 22.8 weight percent for sample compositions shown in Table 2 prepared with PTMO 2000.

The results of compression testing of the sample blocks are shown in Table 3 and Figures 2 and 3. The hysteresis changes initially, but then levels off and the blocks generally attain a steady elevated temperature. The hysteresis values are very high initially for three of the samples, exemplified by 2.0-2000-0.9-0.066 in Figure 2. In the others the initial change is small. A more or less constant hysteresis value and temperature is attained in all cases except one before 3,000 cycles have been completed. The sample prepared with 2.5 CHDI and PTMO 2695 was the only sample tested which showed a continuing increase in hysteresis and temperature throughout the 180 minute experiment. Some type of change in polymer chain organization was undoubtedly continuing in that sample. The reasons why some samples show large hysteresis values initially and others do not is uncertain. Experiments could probably be designed to study this behavior using annealing with and without compressive stress.

The softest samples tested, prepared with PTMO 2695, exhibited the highest temperature during testing, approximately 100°C. This is a moderate temperature, the same as that used for curing the samples. In several cases noted in Table 3, thermocouple failure occurred. The hysteresis values in the table are all values found at the end of the tests, since the hysteresis could still be obtained after the internal temperature could no longer be measured.

The sample in the table with the smallest temperature rise after the completed experiment contains 2.5 moles CHDI. This indicates that increasing the CHDI content from 2 moles to 2.5 moles, which increases the weight percent hard segment and the hardness may not by itself effect the hysteresis. There is insufficient data to make conclusions about the effect of crosslinking, either by allophanate or by TMP, on the hysteresis. All of the samples exhibit small temperature rises, low hysteresis and in general, judging from their unchanged

appearances, withstand the test very well. Samples which nave not withstood the test well show evidence of internal melting and severe distortion of the block shape.

Another factor which would be important in resistance to wear on rough surfaces is tear resistance. Values for tear strength are shown in Table 2. A trouser tear test was used in a effort to reduce the tensile contribution to the result. Reduction of NCO/OH below 1.0 improves the tear strength. An increase in crosslinking by TMP reduces the tear strength. Use of PTMO 1000 improves the tear strength over samples with the same molar composition when PTMO 2000 is used. The tear resistance values at the elevated temperatures reached during compressive fatigue should also be measured.

All the results together indicate that the best sample examined so far is 2.5 - 2000 - 1.2 - 0.2 which exhibited the lowest hysteresis and also high tear strength. Results of the tear strength tests indicate that hysteresis testing of samples with isocyanate to hydroxy group ratio less than 1.0 should be done, since their tear strengths are the highest of any in the table.

ACKNOWLEDGMENTS

The author would like to thank Richard W. Matton for the synthesis, Elias R. Pattie for the Fatigue Testing and Anthony L. Alesi and William W. Houghton for helpful discussions. A special thanks is due to Walter X. Zukas for presenting the poster at the Elastomer Conference a week before Fritz was born.

REFERENCES

1. Anthony L. Alesi, William W. Houghton, Margaret E. Roylance and Robert W. Simoneau, Proc. 42nd SPE Annual Tech. Conf. 583 (1984).

2. S.-W. Wong and K. C. Frisch, Advances in Urethane Science and Technology 8, 75 (1981).

3. Unpublished results, Akzo Chemie America, Chicago, Illinois.

CHEMICAL SCREENING STUDIES OF RUBBERS

ANTHONY F. WILDE, GEORGE W. BATTLE, AND CARYN F. MEE
U. S. Army Materials and Mechanics Research Center, Watertown, Massachusetts 02172-0001

INTRODUCTION

The purpose of this presentation is to describe some of the recent efforts at AMMRC concerned with the screening of commercial and military rubbers against the effects of selected organic liquids.

The objectives of this program are outlined in Table 1. The Army is dependent upon many types of rubber materials. Successful choice and/or development of suitable rubbers will be facilitated by a materials interaction data base. The interactions of concern are listed in the table. Specialized liquids were selected to serve as simulants for chemical agents. The structures of the liquids are also given in the table, along with selected properties. The solubility parameter (δ) of a substance is a measure of the attractive energy between its component molecules and is used to correlate and predict solubilities and miscibilities of one material or substance with another.

The screening was accomplished by immersion testing of the rubbers in the respective liquids. The advantages of immersion testing are listed below and are derived largely from the simplicity and utility of the method.

- Simple experiment requires no complex instrumentation, equipment, or training.
- Treatment of raw data is simple and straightforward.
- Estimates of fundamental parameters of liquid/polymer interactions are provided.
- Specimens which are suitable for post-exposure mechanical testing can be used.
- Screening to begin assembly of a materials interaction data base is relatively rapid.

The AMMRC immersion test procedure is outlined in Table 2. The specimens are small disks cut from sheet stock, usually of thickness ranging from 0.040 to 0.100 inch. The test is continued until the occurrence of one of the events listed in the

TABLE 1

OBJECTIVES OF THE CHEMICAL SCREENING STUDIES OF RUBBERS

PURPOSE

- •INVESTIGATE INTERACTIONS OF RUBBER MATERIALS WITH SELECTED ORGANIC LIQUIDS
- •RESULTS OF THESE SCREENING TESTS WILL PROVIDE A MATERIALS INTERACTION DATA BASE
- •INTERACTIONS OF INTEREST
  - •SORPTION
  - •DIFFUSION
  - •PERMEATION
- •SPECIALIZED LIQUIDS OF INTEREST TO THE ARMY

NAME	1,5-DICHLOROPENTANE	DIISOPROPYL METHYL PHOSPHONATE
ABREV	DCP	DIMP
STRUCTURE	$Cl\text{-}CH_2\text{-}CH_2\text{-}CH_2\text{-}CH_2\text{-}CH_2\text{-}Cl$	$(CH_3)_2CH\text{-}O\text{-}P(=O)(CH_3)\text{-}O\text{-}CH(CH_3)_2$
MOL. WT.	141	180
MOLAR VOL., $cm^3/MOLE$	128	184
EST. δ, $[J/cm^3]^{1/2}$	19.3	16.2

table. Test data are taken at decreasing frequencies, as indicated, until termination of the test.

EXAMPLES OF WEIGHT CHANGE BEHAVIOR DUE TO IMMERSION

Various types of immersion test response of rubbers are illustrated in the following figures.

Figure 1 (Silicone in DIMP) shows a very rapid weight gain process, essentially complete in about 6 hours, indicating a large diffusion coefficient of the liquid in the rubber.

Figure 2 (Viton in DIMP) illustrates a very large weight gain, more than 240 weight percent. This process is complete in about 40 hours. Figure 3 (Fluorosilicone in DIMP) shows a

TABLE 2

AMMRC IMMERSION TEST PROCEDURE

- PREPARE SPECIMEN DISK (1 OR 1-1/2 INCH DIAMETER)
- WEIGH SPECIMEN TO 0.0001 gm
- IMMERSE SPECIMEN IN 50 ml LIQUID FOR SPECIFIED TIME
- REMOVE SPECIMEN AND BLOT THOROUGHLY ON FILTER PAPER
- WEIGH SPECIMEN IN TARED WEIGHING BOTTLE
- REIMMERSE IN LIQUID
- REPEAT AT APPROPRIATE TIME INTERVALS UNTIL OCCURRENCE OF
  - EQUILIBRIUM WEIGHT GAIN, OR
  - PEAK WEIGHT GAIN, OR
  - SIGNIFICANT WEIGHT LOSS, OR
  - SPECIMEN DISINTEGRATION
- TYPICAL IMMERSION TIMES

  FIRST DAY: 1,2,3,4,6 HOURS
  SECOND DAY: 24,30 HOURS
  THIRD DAY: 48,54 HOURS
  UP TO ONE WEEK: DAILY
  UNTIL TERMINATION: WEEKLY OR BIWEEKLY

very large weight gain followed by disintegration of the specimen after 2 days. Figure 4 (Butyl in DIMP) shows an extremely slow weight gain process still progressing after 2 months, indicating that the diffusion coefficient of DIMP in that rubber is very small.

Figure 5 (EPR in DIMP) illustrates an immediate and steady weight loss process still continuing after 8 days. Weight gain followed by weight loss is evident in Figure 6 (EPDM in DCP). This suggests that weight gain and weight loss are occurring simultaneously, with the former predominating at early stages, and the latter one at longer times. Weight loss is probably due to extraction or leaching of some of the compounding ingredients present in the cross-linked polymer network.

In Figure 7 (Butyl in DCP) we see what appears to be an ideal Fickian process, i.e., a perfectly linear weight gain as a function of the square root of time for more than one-half of the total weight gain process. Figure 8 (Urethane in DIMP) illustrates a two-stage weight gain process followed by disintegration of the specimen. Presumably the two-phase

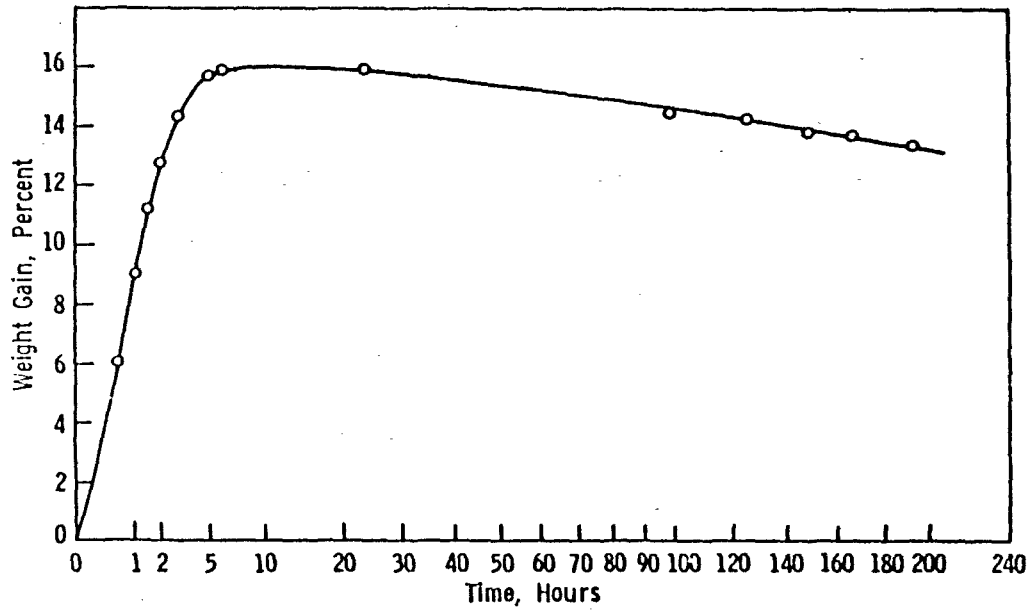


FIGURE 1. Silicone 600 in DIMP.

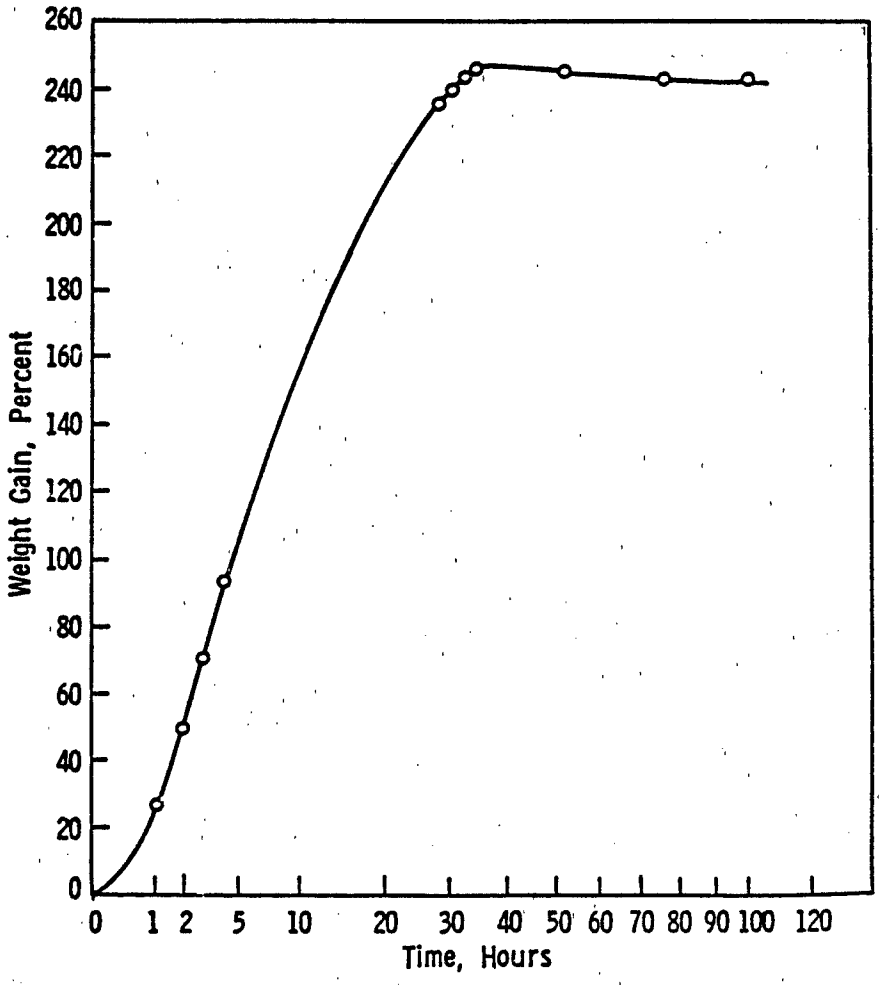


FIGURE 2. Viton 4900 in DIMP.

microdomain structure of the urethane elastomer is responsible for the individual weight gain steps evident in this test.

Some immersion tests have been conducted with rubber disk specimens, both uncoated and coated with a fluoroelastomer film. A comparison is shown in Figure 9 (Nitrile substrate in DCP). The uncoated specimen was highly susceptible to the liquid, gaining 100 weight percent in less than 1 day. The coated specimen underwent little weight gain, only a few

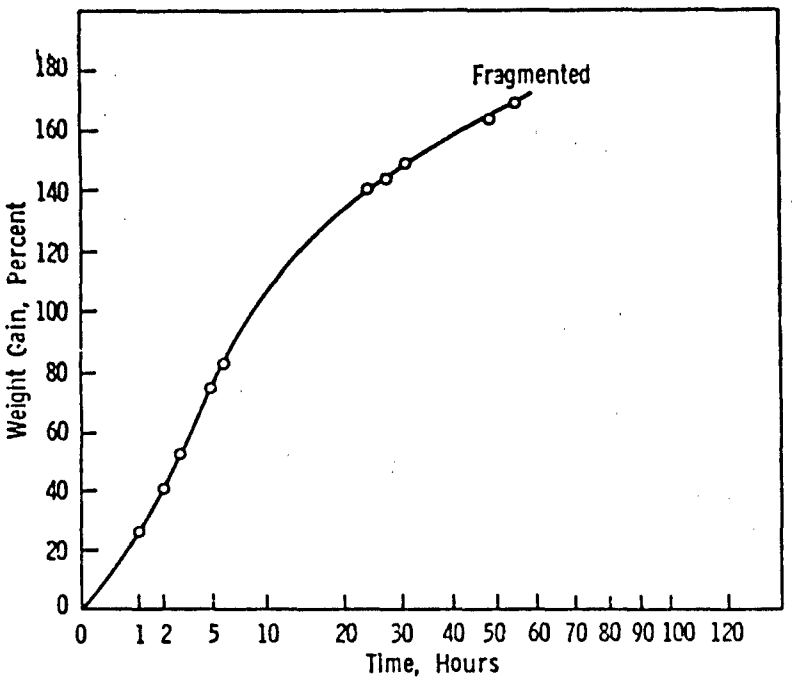


FIGURE 3. Fluorosilicone FS5C in DIMP.

percent after 2 months. This may suggest a practical approach toward protection of susceptible military items by a suitable coating material.

SOLUBILITY PARAMETER PLOTS

Attempts have been made to correlate the equilibrium weight gains of these rubbers with their solubility parameters (δ_2). The maximum weight gain is expected for those polymers whose δ_2 values are very close to the δ_1 value of the immersion liquid. Figure 10 is a plot of the rubbers which have reached an equilibrium weight gain in DCP (δ_1 value estimated as 19.3 $[J/cm^3]^{1/2}$). In general, the largest weight gains are for polymers of δ_2 value in this vicinity. Exceptions to this trend are the phosphazenes (PNF) and the silicones (SIL), possibly because both types do not have carbon-carbon backbone structures.

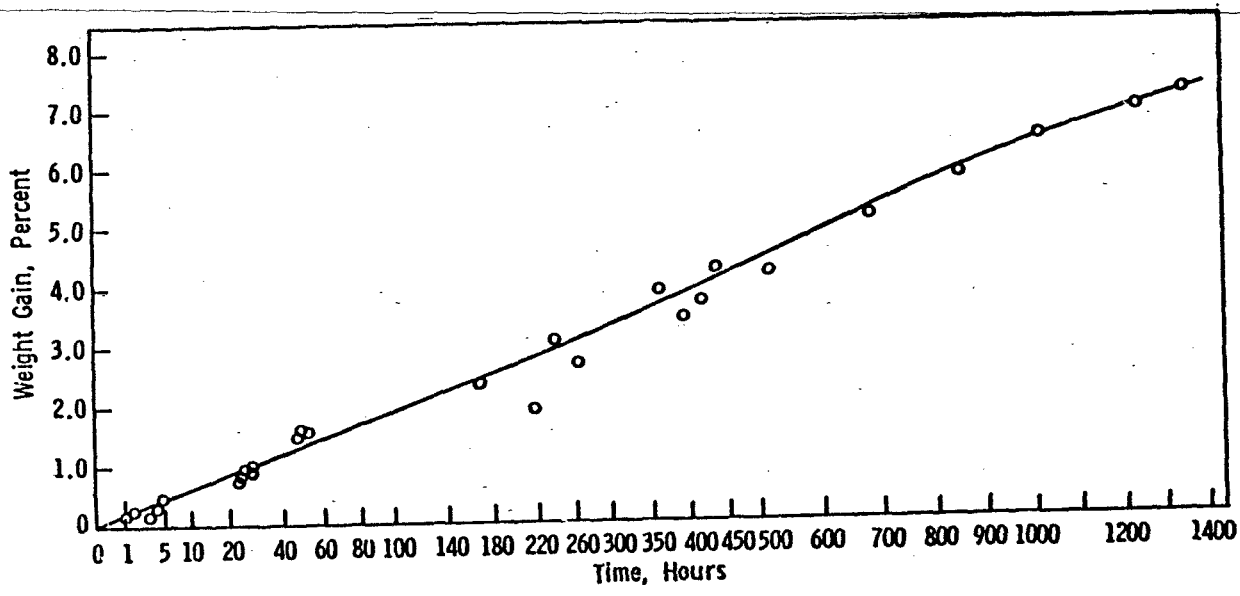


FIGURE 4. Butyl B7A in DIMP.

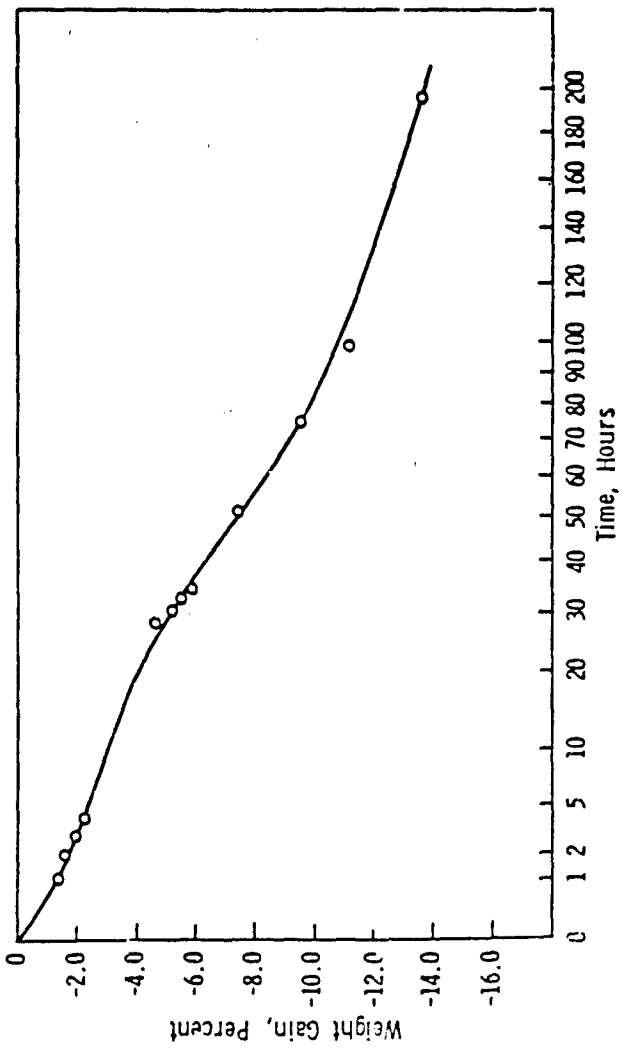


FIGURE 5. EPR 6260 in DIMP.

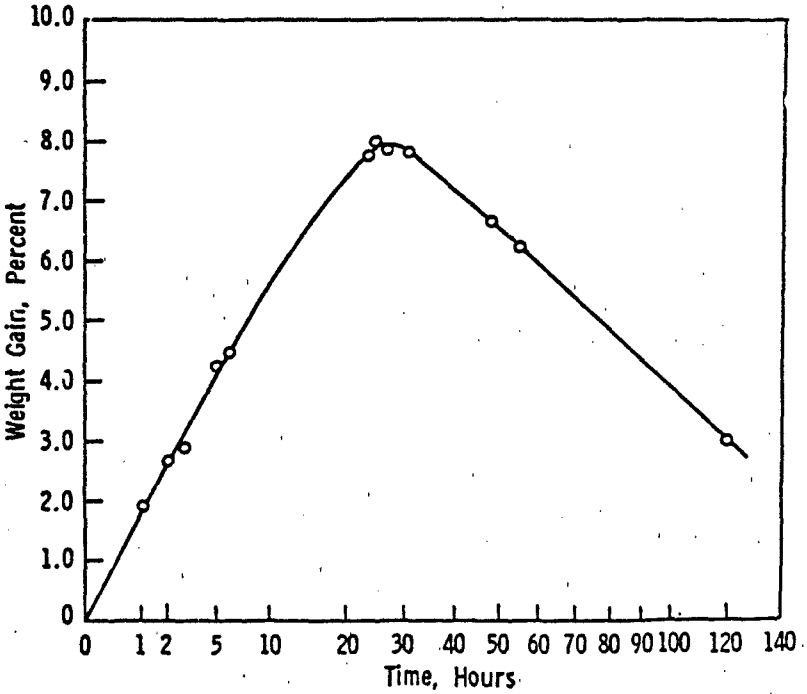


FIGURE 6. EPDM EP8A in DCP.

Figure 11 is a similar plot of those rubbers which have attained an equilibrium weight gain in DIMP (δ_1 value estimated as 16.2). Peak weight gains are near δ_2 values of 18, although the Hydrin (HYD) shows a peak at about 22. This suggests that the effective δ_1 value may be higher than 16.2. In addition, other rubbers with δ_2 between 18 and 20 exhibit relatively low values of weight gain, indicating further problems with this particular solubility parameter correlation.

The above plots do not express a quantitative estimate of the expected weight gain or sorption of liquid by the polymers; they simply indicate where on the solubility parameter scale the maximum should occur. Alternatively, it is possible to use the Flory-Rehner theory to estimate the magnitude of liquid sorbed by the polymer as a function of the value of ($\delta_1 - \delta_2$), designated as $\Delta\delta$ in the plot of Figure 12. Application of the theory also requires knowledge of the average molecular weight between cross-links (M_C) for the rubber. As an example, Figure 12 is a plot of the theoretical volume fraction ratio of

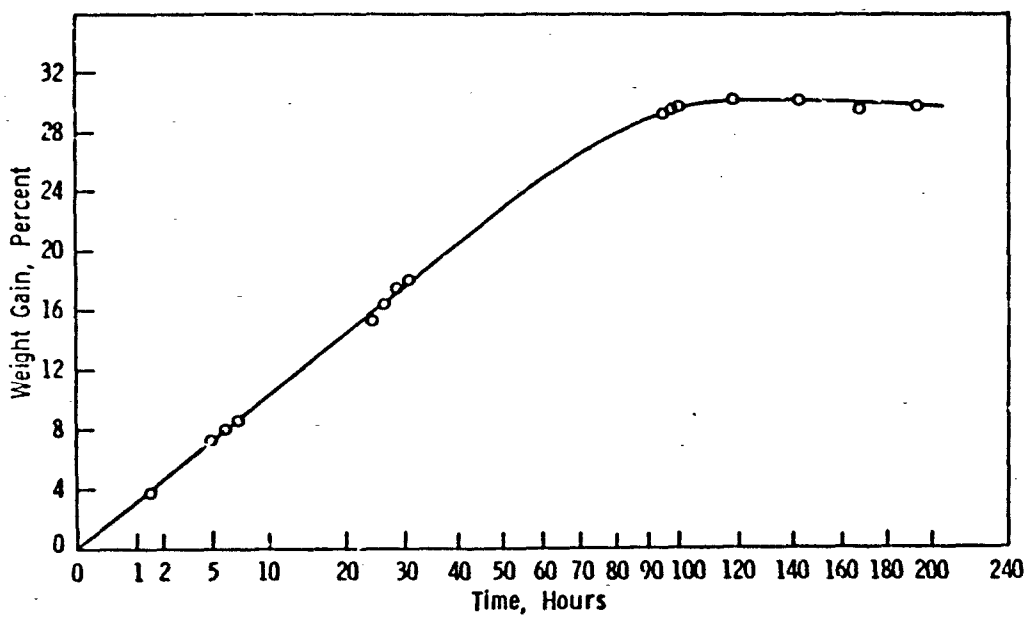


FIGURE 7. Butyl B7A in DCP.

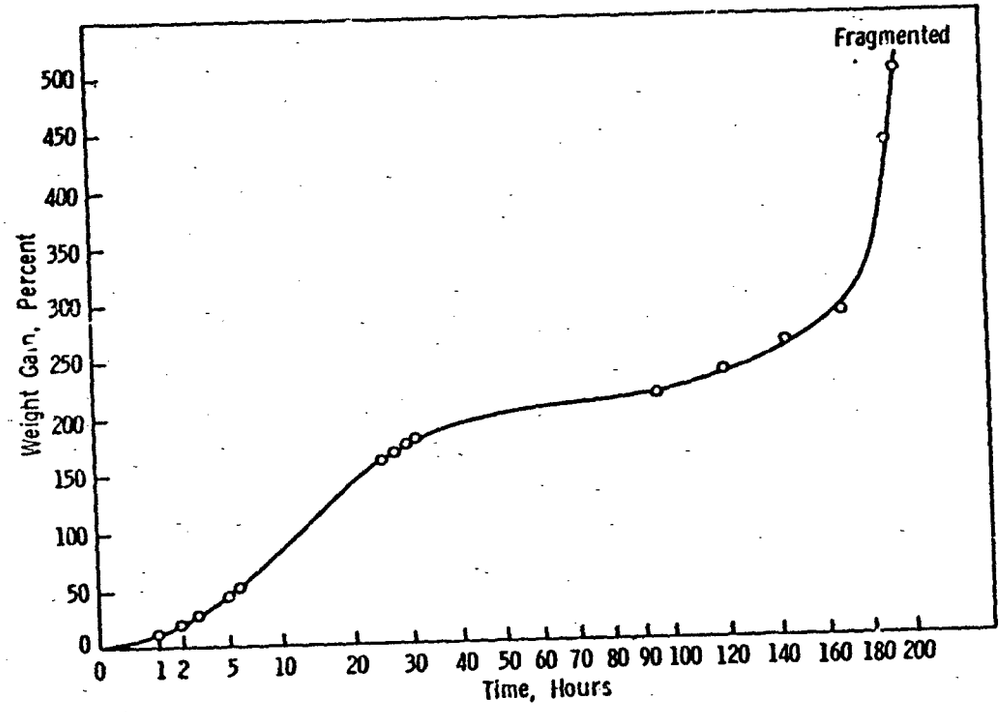


FIGURE 8. Urethane P6E in DIMP.

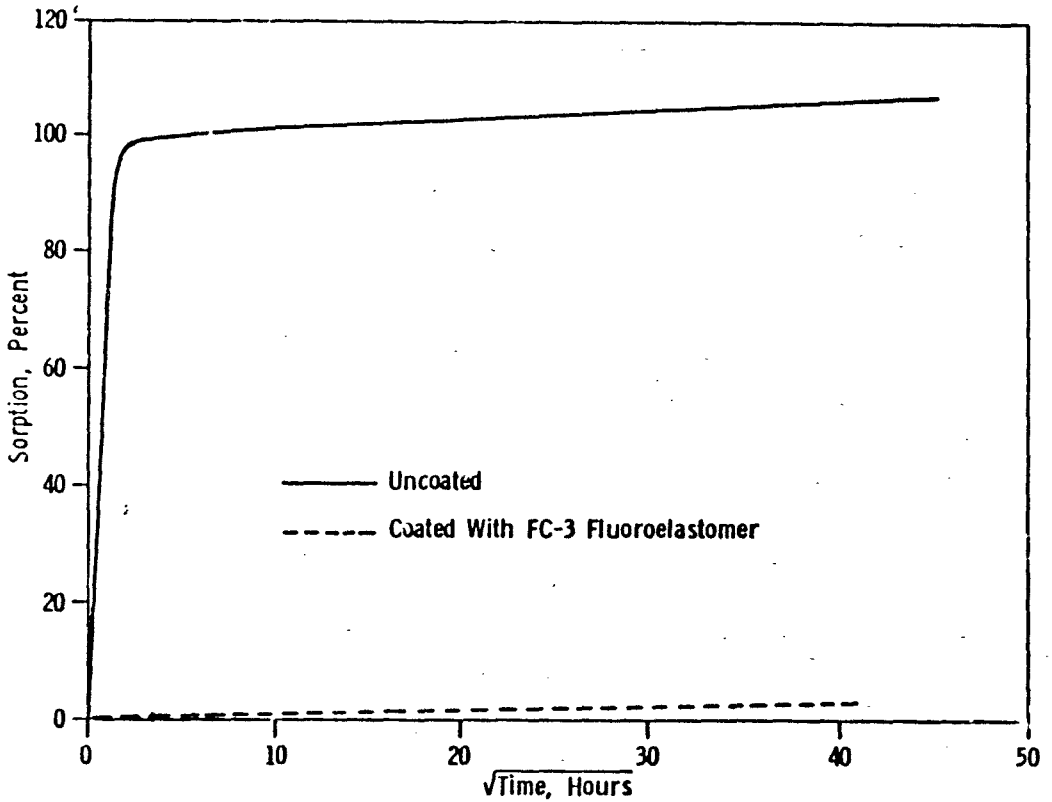


FIGURE 9. Immersion of Nitrile rubber in DCP (uncoated and fluoroelastomer coated).

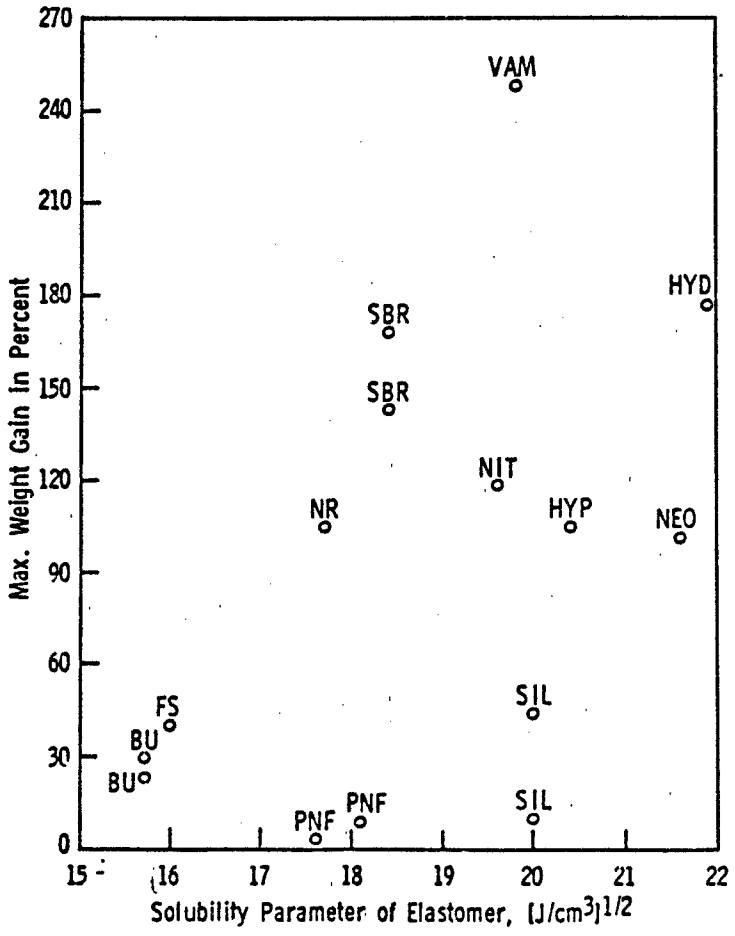


FIGURE 10. Immersion of rubbers in DCP.

DCP to polymer, $\emptyset_1/\emptyset_2$, as a function of $\Delta\delta$ for three different values of M_c. Superimposed upon these curves are the experimental data points of Figure 10, where $\Delta\delta = 0$ for the theory is aligned horizontally with $\delta_1 = 19.3$ for the DCP. The experimental weight gain data have been normalized to the organic contents of the rubbers, and then converted from weight fractions to volume fractions to be consistent with the $\emptyset_1/\emptyset_2$ values of the theory. It is evident that most of the rubbers fall near to M_c values ranging from 1000 to 5000, a reasonable result. Perhaps the phosphazenes and silicones, mentioned above, are more highly cross-linked (lower values of M_c), thus falling well below the curve for $M_c = 1000$.

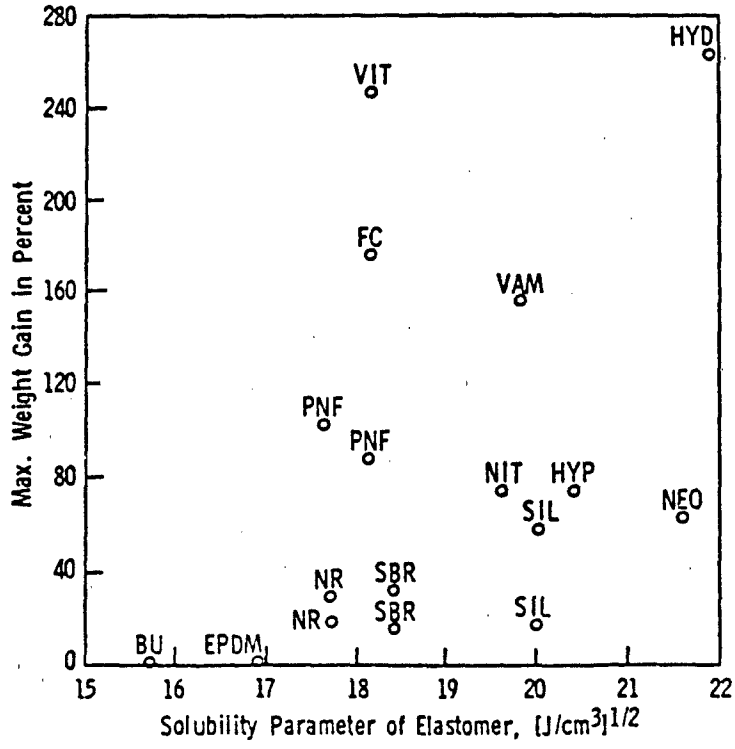


FIGURE 11. Immersion of rubbers in DIMP.

FURTHER CALCULATIONS

Immersion test data can be used for the estimation of the diffusion coefficient (D) of the immersion liquid in the polymer specimen. Figure 13 indicates the method. The $t_{1/2}$ is defined as the time required for one-half of the maximum weight gain. Similarly, the immersion test results can provide estimates of the liquid transmission rate or flux through a given thickness, l, of the polymer film. Table 3 shows the derivation for the steady-state permeation rate.

SUMMARY TABLES

A summary of experimental weight gain data, estimated values of diffusion coefficients, and permeability rates are tabulated in Tables 4 through 6 for a series of commercial rubbers immersed separately in three liquids. The third liquid, DS-2, is a decontaminant solution of complex composition.

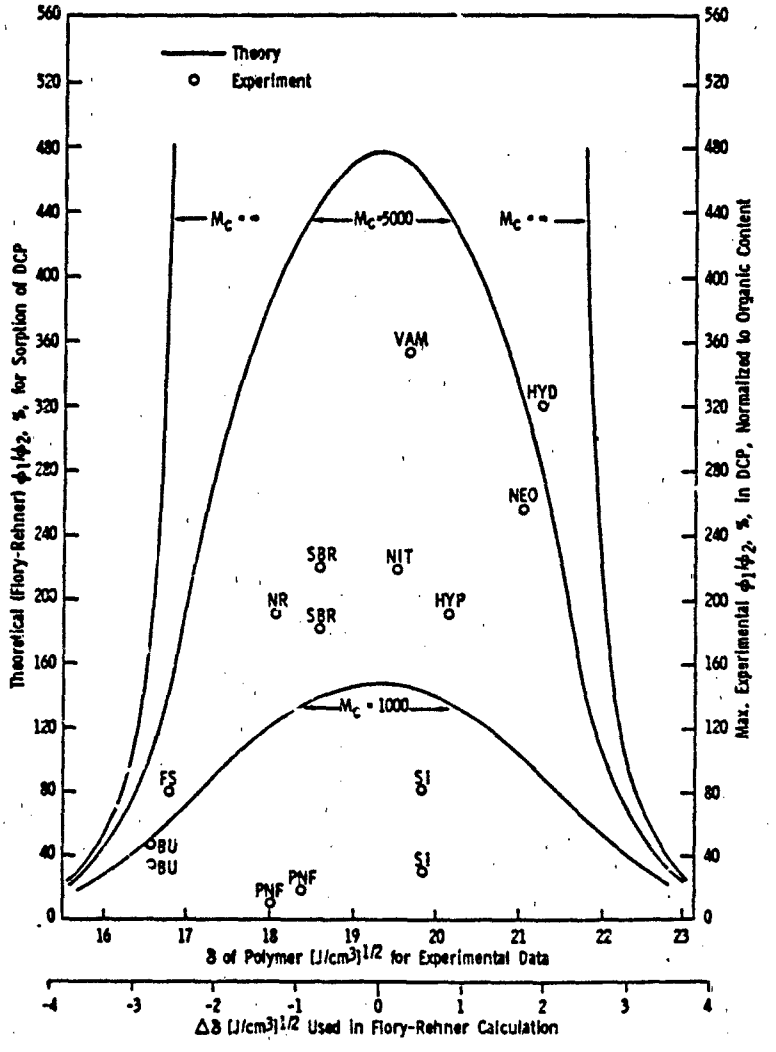
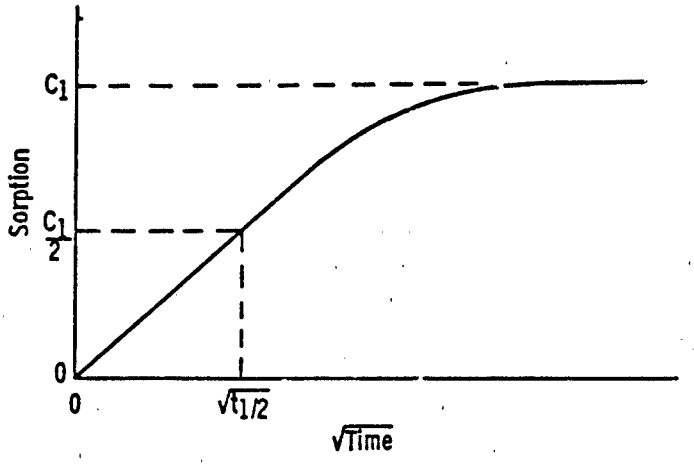


FIGURE 12. Solubility parameter plot of rubbers in DCP (theoretical and experimental).

This kind of tabular summary can serve as the nucleus of a materials interaction data base.



FOR ONE-DIMENSIONAL DIFFUSION

$$D = \frac{0.049\,\ell^2}{t_{1/2}}$$

WHERE D = DIFFUSION COEFFICIENT

ℓ = SPECIMEN THICKNESS

FIGURE 13. Diffusion coefficient in polymer film.

TRACK AND SUSPENSION RUBBERS

Similar immersion testing has been carried out with a series of track and suspension rubbers. Plots of weight gain behavior of selected specimens are illustrated in Figure 14 for immersion in DCP and, in Figure 15 for immersion in DIMP. The former shows a large and rapid liquid uptake, complete in about 1 day. The latter indicates a somewhat smaller and less rapid uptake completed within 2 days. Subsequent weight loss in DIMP suggests extraction of compounding ingredients from the rubbers.

Thermogravimetric analysis was used for the estimation of organic material content of these proprietary rubbers. Figure 16 is a plot of the maximum weight gain in DIMP as a function of the organic material content of the rubber. Although there is significant data scatter due to other unknown differences in compound formulation, the upward trend for the

TABLE 3

LIQUID TRANSMISSION RATE OR FLUX THRU POLYMER FILM

FICK'S FIRST LAW OF DIFFUSION

$$J = -D\frac{\delta C}{\delta x}$$

J = FLUX

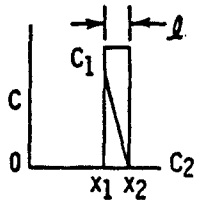
D = DIFFUSION COEFFICIENT

C = CONC. OF LIQUID IN FILM AT DISTANCE x

x = DISTANCE IN FILM FROM SURFACE

ASSUME UNIFORM CONCENTRATION GRADIENT

$$J = -D\frac{C_1-C_2}{x_1-x_2}$$



BUT $x_1 - x_2 = \ell$

ASSUME $C_2 = 0$

HENCE $J = -D\frac{C_1}{\ell}$

WHERE C_1 IS THE EQUILIBRIUM CONCENTRATION OF SORBED LIQUID

SBR compounds is clearly seen. This would be expected from a simple consideration of organic material and carbon black, regarding their relative susceptibilities to swelling by organic liquids.

To eliminate the relative effects of the fillers, the maximum weight gains of the rubbers were normalized to their organic material contents. Similarly, the initial modulus of the rubbers (approximated by the 100 percent modulus) was divided by the weight fraction of filler to provide a relative measure of the degree of cross-linking. A plot of one versus the other is shown in Figure 17. The expected inverse relationship is evident, in spite of the data scatter, thus

TABLE 4

WEIGHT GAIN DATA FOR ELASTOMERS IMMERSED IN VARIOUS LIQUIDS

ELASTOMER	MAXIMUM WEIGHT GAIN IN PERCENT DS-2	DCP	DIMP
HYDROCARBONS			
NAT RUBBER 470 (unfilled)	>11	212	32
EPR 6260	1.0	11▲	Lost >13%
BUTYL 6660	0.06	2%	0
BUTYL B7A	>4.2*	30	>7.2*
SBR 1500	5.6	14%	1%
EPDM EP8A	>2.7*	8.0▲	=0
NAT RUBBER R4A	9.0	>416	28
SBR G4A	2.5	169	33
FLUOROCARBONS			
VITON A900	0.85	>5.9*	245
FLUOROCARBON V7D	0.9	>11*	174
SILICONES			
SILICONE 600	Fragmented after 0%	10.7	15.9
FLUOROSILICONE FS5C	>7.7*	40	Frag. after 168%
SILICONE S5B	Lost >62%	44	56
PHOSPHAZENES			
PNF-LT	7.0	8.8	87
PNF-200	5.3	3.4	101
MISCELLANEOUS			
NITRILE N7A	9.7	119	73
NEOPRENE C6A	0.7▲	102	62
HYPALON H8E	Fragmented after ~25%	105	73
URETHANE P6E	Fragmented after ~20%	>164*	Frag after 498%
VAMAC M6E	48	248	155
HYDRIN Y6E	164	177	260

*Experiment Continuing
▲Then lost weight abruptly

indicating that the more highly cross-linked rubbers tended to pick up less of the DCP.

SUMMARY AND CONCLUSION

Immersion testing constitutes a useful method for screening of rubber materials to the effects of organic liquids. In addition to the simple quantity of weight gain, the experimental data can provide estimates of other fundamental parameters of interaction, such as diffusion coefficients and permeability rates. Some correlation of data has been achieved by use of solubility parameter concepts. Further analyses have been performed with the track rubber immersion results to provide some rough correlations with gross estimates of compound formulation and rubber morphology. The results

TABLE 5

DIFFUSION COEFFICIENT VALUES FOR ELASTOMERS IMMERSED IN VARIOUS LIQUIDS

ELASTOMER	DIFFUSION COEFF IN 10^{-6} cm^2/sec DS-2	DCP	DIMP
HYDROCARBONS			
NAT RUBBER 470 (unfilled)	+	9.5	5.9
EPR 6260	2.3	+	+
BUTYL 6660	+	4.6	+
BUTYL B7A	<0.21[a]	2.7	<0.17[a]
SBR 1500	0.84	11	0.36
EPDM EP8A	<0.80[a]	+	+
NAT RUBBER R4A	0.93	< 2.6	2.3
SBR 6A	1.3	21.0	4.7
FLUOROCARBONS			
VITON A900	1.9	<0.039[a]	5.6
FLUOROCARBON V7D	63	<0.19[a]	8.9
SILICONES			
SILICONE 600	+	100	53
FLUOROSILICONE F55C	<0.31[a]	130	+
SILICONE S5B	+	62	37
PHOSPHAZENES			
PNF-LT	6.2	11	17
PNF-200	15	2.3	16
MISCELLANEOUS			
NITRILE N7A	1.8	30	9.7
NEOPRENE C6A	+	18	7.4
HYPALON H8E	+	7.7	1.5
URETHANE P6E	+	6.4α	8.1α
		<0.10 β	<0.37 β
VAMAC M6E	0.17	20	6.3
HYDRIN Y6E	0.78	7.6	8.5

[a] Experiment Continuing
+ Insufficient Data
α First sorption process
β Second sorption process

described in this presentation can serve as the core of a materials interaction data base.

TABLE 6

PERMEABILITY RATES FOR ELASTOMERS IMMERSED IN VARIOUS LIQUIDS

ELASTOMER	CALCULATED FLUX THROUGH 0.010-INCH FILM IN 10^{-9} $\frac{gm}{cm^2 \cdot sec}$		
	DS-2	DCP	DIMP
HYDROCARBONS			
NAT RUBBER 470 (unfilled)	*	7136	670
EPR 6260	11	*	*
BUTYL 6660	*	519	*
BUTYL B7A	4.2β	383	5.7β
SBR 1500	22	7483	24
EPDM EP8A	5.2β	*	*
NAT RUBBER R4A	40	5110β	1100
SBR G6A	15	16,780	711
FLUOROCARBONS			
VITON 4900	12	1.7β	10,260
FLUOROCARBON V7D	426	16β	11,580
SILICONES			
SILICONE 600	*	5054	3982
FLUOROSILICONE FS5C	11β	24,560	*
SILICONE S5B	*	12,890	9788
PHOSPHAZENES			
PNF-LT	322	725	11,060
PNF-200	591	58	12,090
MISCELLANEOUS			
NITRILE N7A	80	16,860	3345
NEOPRENE C6A	*	8673	2168
HYPALON H8E	*	3817	520
URETHANE P6E	*	8384α 9.0β	38783 520β
VAMAC M5E	39	23,100	4620
HYDRIN Y6E	756	7950	13,060

*Insufficient Data
βCurrent Estimate
αFirst sorption process
βSecond sorption process

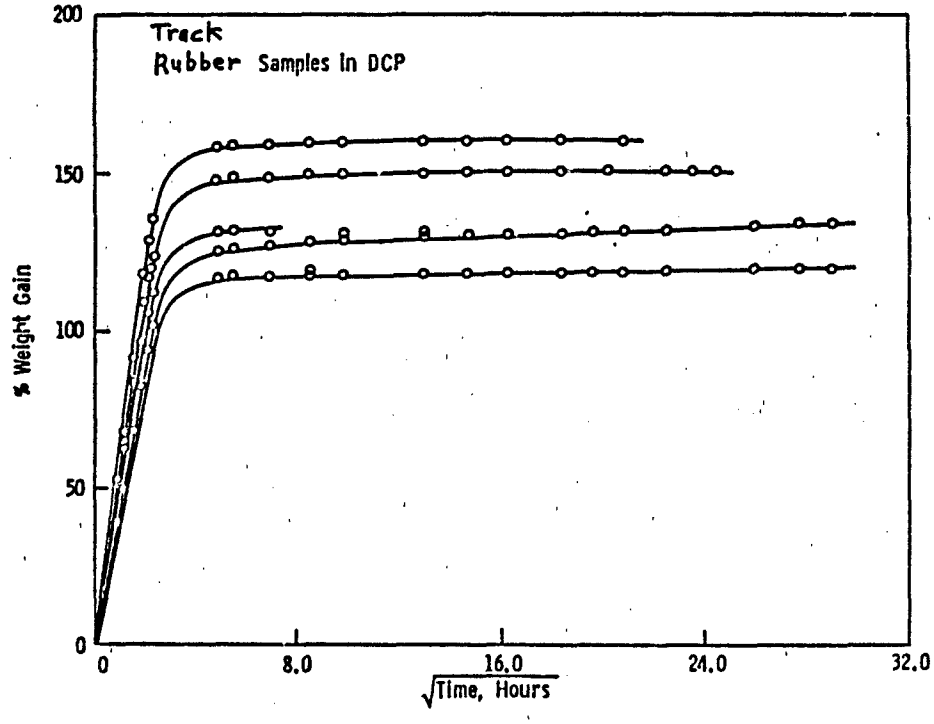


FIGURE 14. Plot of weight gain for specimen immersed in DCP.

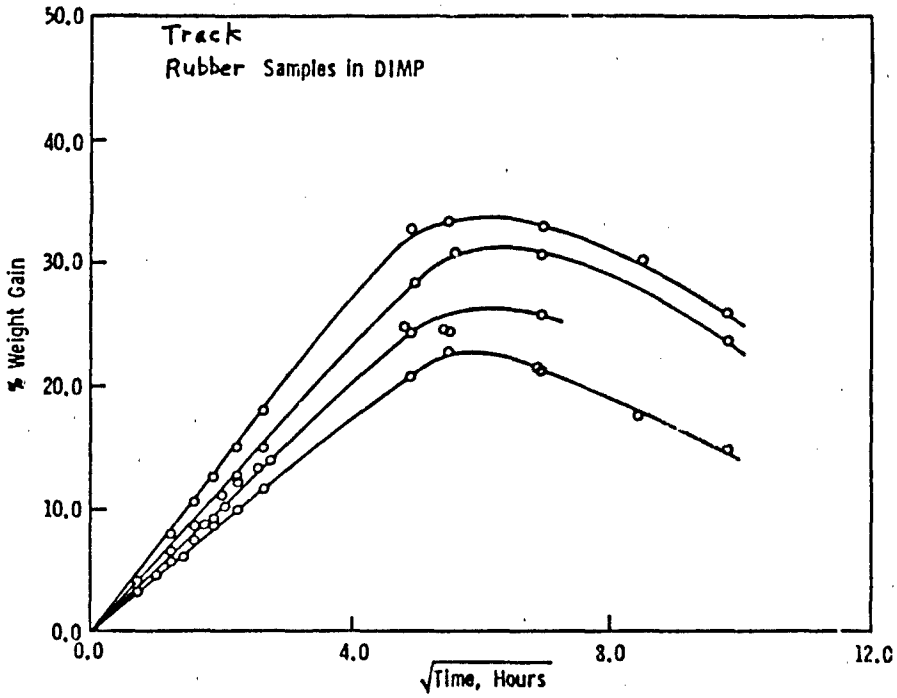


FIGURE 15. Plot of weight gain for specimen immersed in DIMP.

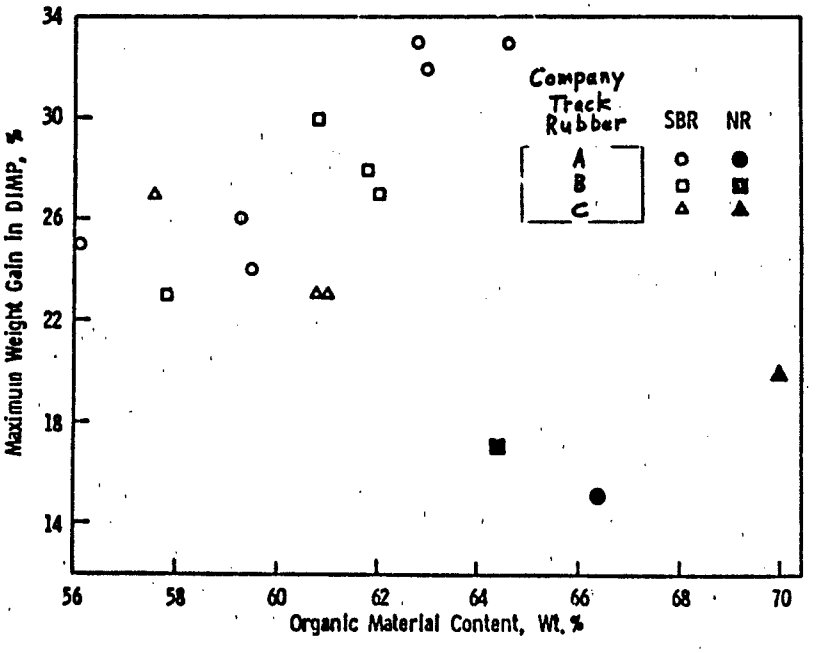


FIGURE 16. Effect of organic material content upon weight gain.

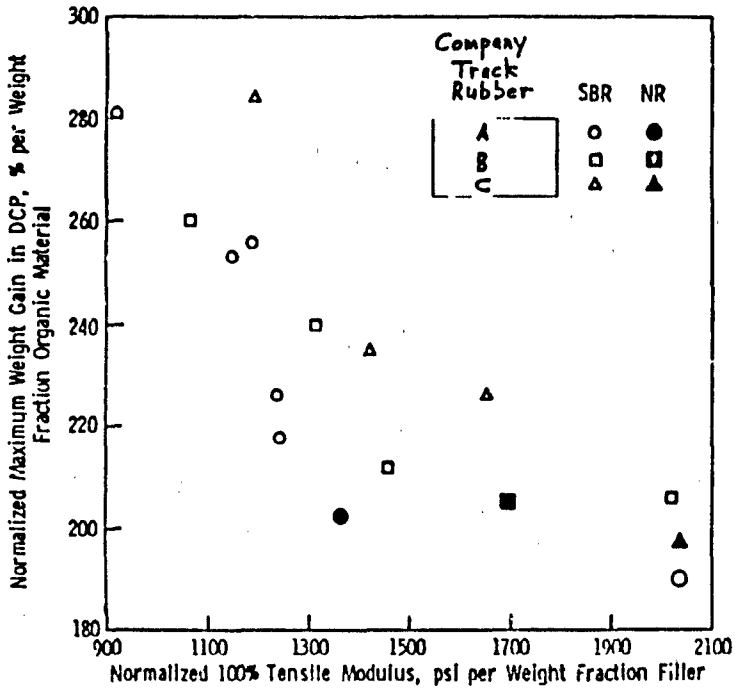


FIGURE 17. Effect of cross-linking upon weight gain.

PROPERTIES OF ELASTOMER BLENDS

EMILY A. McHUGH[1], EUGENE WILUSZ[2]
(1) Polymer Research Division, U.S. Army Materials and Mechanics Research Center, Watertown, Massachusetts 02172;
(2) U.S. Army Natick Research and Development Center, Natick, Massachusetts 01760

The objectives of this study are to prepare and characterize blends of two elastomers as a function of composition and compounding ingredients, and to determine the effects on mechanical properties and the interaction with chemical agent simulants. Samples of neoprene and hydrin rubbers and blends of varying composition, both with and without carbon black loading, were prepared at the U.S. Army Natick Research and Development Center. Three types of hydrin rubber were included: Hydrin 100, the epichlorohydrin homopolymer, Hydrin 200, a copolymer with ethylene oxide, and Hydrin 400, a terpolymer. Tg behavior for the Neoprene-Hydrin 100 system indicates that these two elastomers are incompatible, and suggests that this is also true for the Hydrin 200 and Hydrin 400 systems. Results illustrate the significance of blend composition and carbon black loading on the 100 percent modulus and swelling characteristics.

VAPOR INTERACTIONS WITH A PHASE SEGREGATED POLYURETHANE

CARYN F. MEE, ROSEMARY GOYDAN, NATHANIEL S. SCHNEIDER
U.S. Army Materials Technology Laboratory, Polymer Research Division, Watertown, Massachusetts 02172-0001

ABSTRACT

Heterophase polymers represent a class of increasingly important materials, exemplified by the several varieties of thermoplastic elastomers of which the segmented polyurethanes are the most important representative. The response of the polyurethane to solvent exposure will depend on whether swelling is limited to the soft segment phase or also affects the hard segment domains. Incremental sorption measurements with hexane vapor in an Estane polyurethane result in a low solubility and uncomplicated sorption and diffusion behavior. This suggests that swelling is limited to the elastomeric matrix. With orthodichlorobenzene, high sorption levels and two stage sorption behavior are observed. The two stage behavior is analyzed by a combined Fickian and relaxation model and suggests the occurrence of hard segment swelling.

INTRODUCTION

The current military applications for segmented polyurethanes are three fold as a flexible lens in the current Air Force version of the Army XM30 mask; as a moisture permeable, but waterproof, coating for clothing; and as a candidate for tank track pads. The military is investigating the effects of CW agents on these polymers to gain an understanding of the factors controlling the rate and extent of contamination by hazardous chemicals. The present work was carried out to determine how the two phase structure of a typical polyurethane elastomer effected the interaction with two different types of solvents.

The polyurethane used in this study is an Estane material produced by B. F. Goodrich. The soft segment is a 1000 molecular weight polytetramethlyeneoxide (PTMO). The urethane segment consists of diphenyl methyl diisocyanate (MDI) extended with butanediol (BD). The components exist in a molar ratio of 3:2:1 respectively, which corresponds to 52% by weight soft segment. The soft segment, which is flexible at room temperature, has a T_g of -80°C whereas the hard segment has a rather high T_g of 130°C. The hard segment undergoes phase segregation due to its incompatibility with the soft

segment matrix, thereby creating a morphology consisting of discrete glassy domains dispersed in a rubbery matrix.

EXPERIMENTAL

Incremental vapor sorption experiments were carried out using a vacuum system as diagrammed in figure 1. After evacuating the system, a sample of known dry weight was suspended from the quartz spring balance. The sample chamber was then closed off and the pressure in the ballast volume was set, using the vapor source, to obtain the desired vapor activity. The sample chamber was then opened to the vapor in the ballast volume at a time designated as t=0. The displacement of the quartz spring balance was recorded as a function of time until a stable weight was reached. The sample chamber was then closed off and the ballast volume was set to the next incremental pressure step. This procedure was repeated until a full range of vapor activities was traversed.

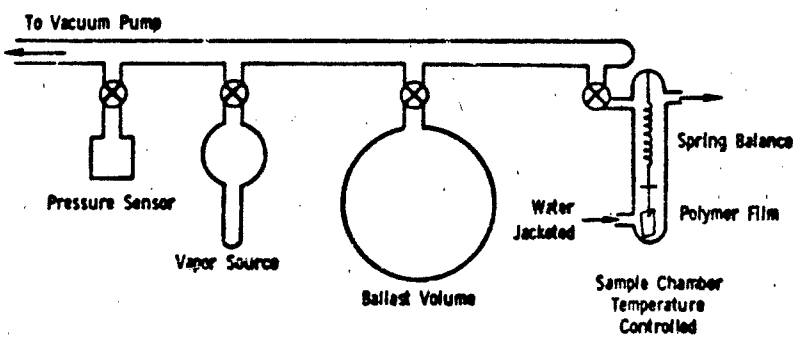


Figure 1. Vacuum Sorption Rig

RESULTS AND DISCUSSION

Experiments were performed with both n-heptane, a nonpolar solvent, and orthodichlorobenzene, ODCB, a polar aprotic solvent. The results from the liquid immersion studies show that the sample reached a maximum uptake of 6.5% when immersed in n-heptane and 230% when immersed in ODCB. This rather large weight gain is also characteristic of the high degree of swelling expected from CW agent HD.

The vapor sorption results from the heptane studies correspond to ideal Fickian diffusion. The weight uptake as a function of time can be calculated from Crank's solution of Fick's law for diffusion in a plane sheet (1). The sorption process is linear with the square root of time over the initial 70% of the weight uptake and then rapidly attains its equilibrium weight as seen in figure 2. The equilibrium values obtained from the plateau portion of the sorption curve can be described by Henry's Law, c=KP, (K=solubility coefficient) where the sorbed concentration, or percent sorption, is proportional to the vapor pressure (see the lower curve in figure 3). The diffusion coefficient increases linearly with concentration and shows good agreement for sorption and desorption runs (see figure 4).

With ODCB the sorption isotherm (upper curve in figure 3) shows pronounced upward curvature above an activity of 0.4. The sorption of ODCB results in various nonFickian anomalies. At low activities the sorption and desorption curves are Fickian in appearance (figure 5). However, the curve for desorption lies above that for sorption (figure 6). This is in conflict with Fick's law which requires that sorption be

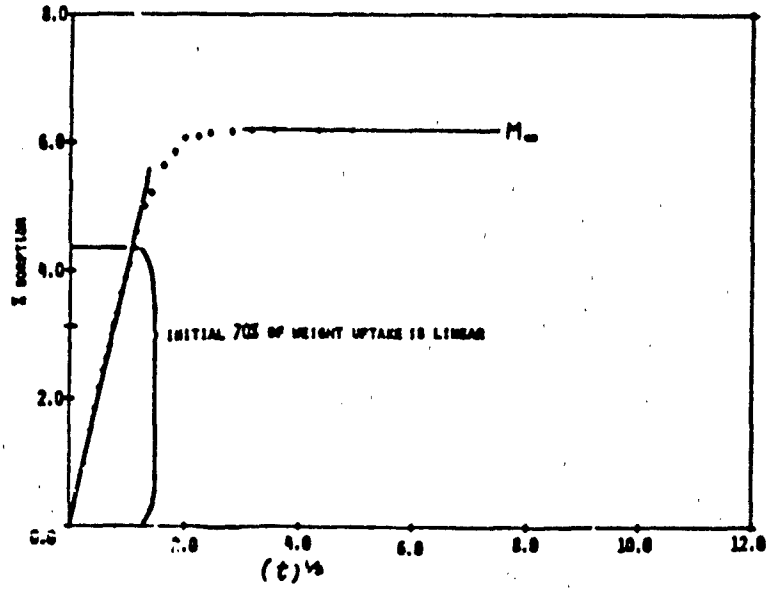


Figure 2. Sorption Time Behavior

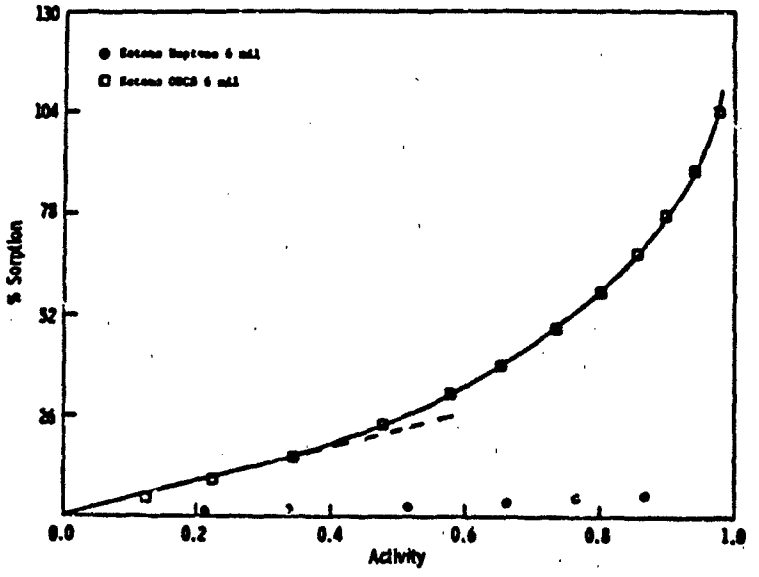


Figure 3. Sorption Isotherm

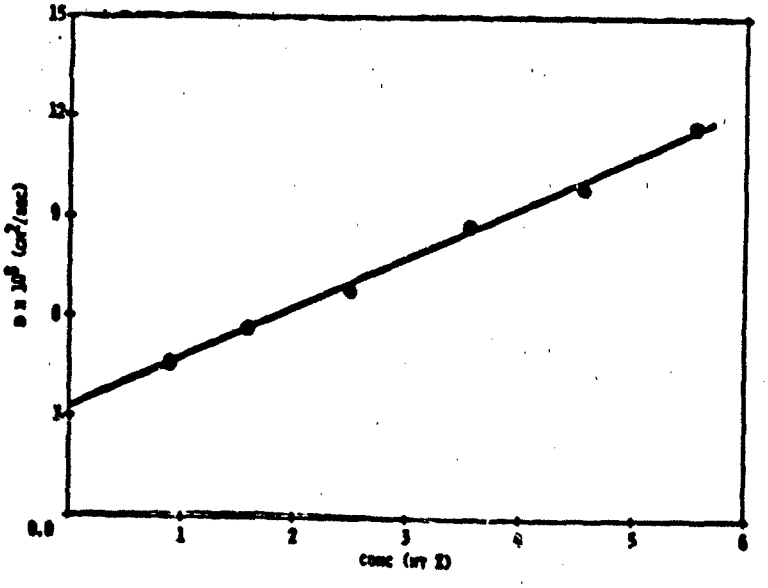


Figure 4. D vs. C Behavior - Concentration Dependence

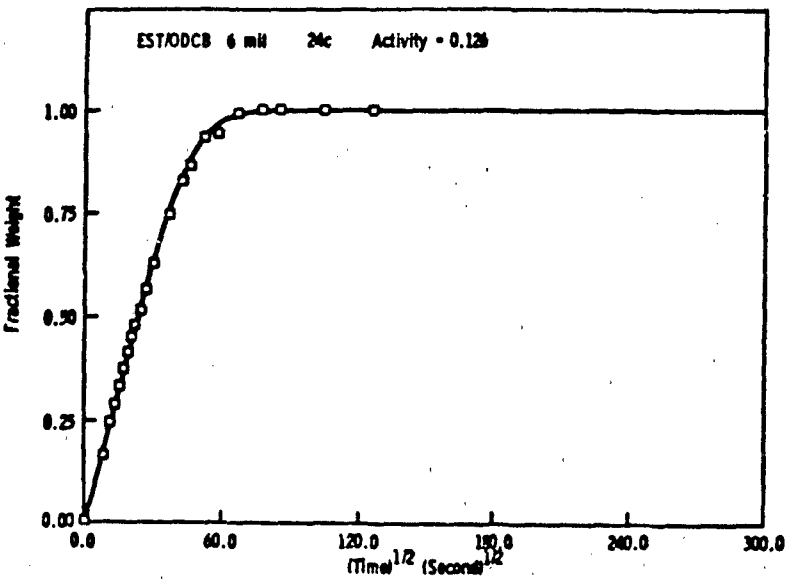


Figure 5. Sorption - Time Behavior Low Activity

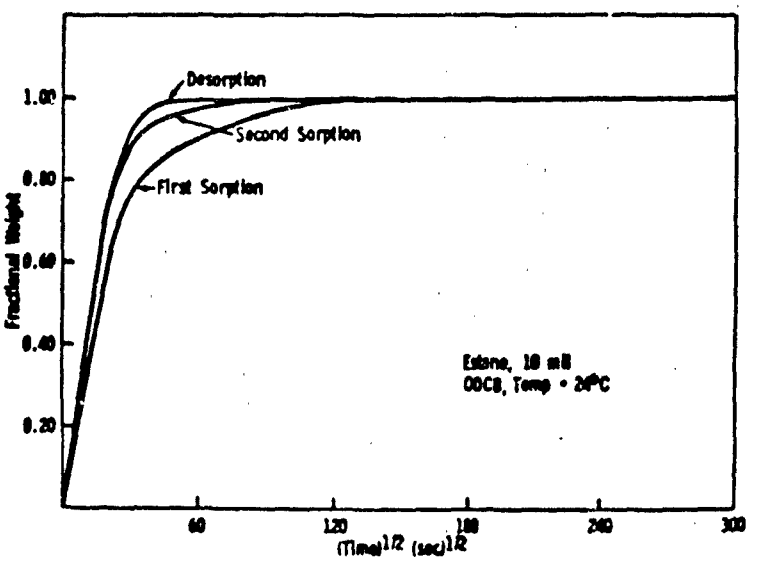


Figure 6. Sorption - Desorption Behavior

faster than desorption when the diffusion constant increases with concentration as expected here. At intermediate activities the sorption process shows a marked departure from Fickian appearance (figure 7) which becomes increasingly evident at still higher activities where two stage behavior is observed (figure 8). The desorption curves generally remain Fickian in appearance.

The two stage sorption curves have been analyzed by a model proposed by Berens and Hopfenberg (2). In this model the total amount of sorption is assumed to be the sum of independent contributions from two processes; that due to Fickian diffusion and to relaxation:

$$M_T = M_{T,F} + M_{T,R}$$

where:

M_T = total amount of sorption (gms) at time T.

$M_{T,F}$ = weight uptake due to Fickian diffusion (gms).

$M_{T,R}$ = weight uptake due to relaxation of polymer (gms).

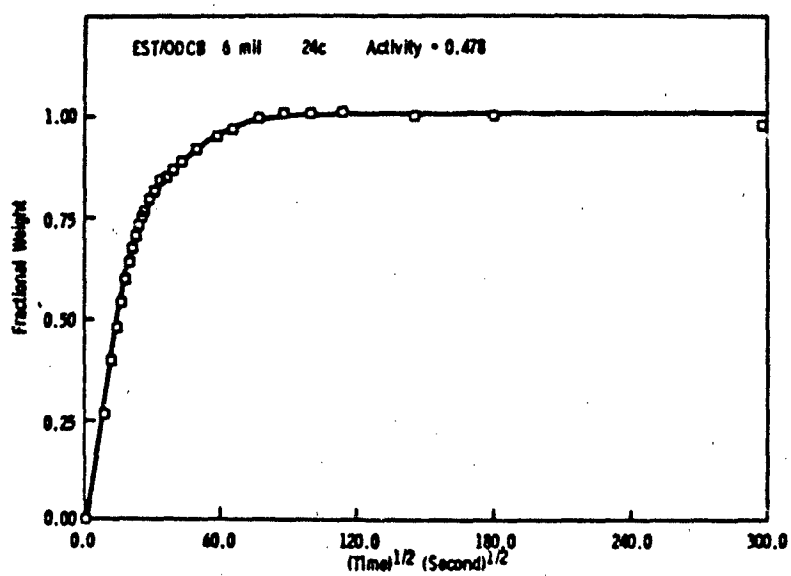


Figure 7. Sorption - Time Behavior Intermediate Activity

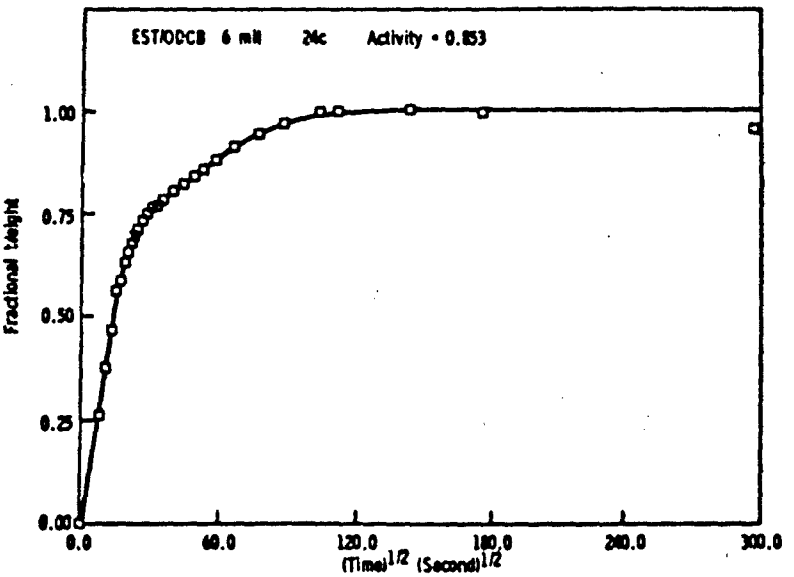


Figure 8. Sorption - Time Behavior High Activity

$M_{T,F}$ is the Fickian contribution as described by Fick's first law and involves the diffusion constant, D, and the equilibrium Fickian uptake $M_{\infty,F}$. $M_{T,R}$ is the relaxation contribution described by a first order rate equation which depends on the rate constant k_R and the total uptake due to relaxation $M_{\infty,R}$. The parameters were obtained by assuming that the long time second stage sorption was due solely to relaxation and by fitting the data to a first order rate equation in the linearized form obtained by plotting log (M_T - M_T) versus log (T). The earlier time data was then treated in a similar fashion to obtain the Fickian constants by subtracting the relaxation contribution based on the parameters which had been determined from the relaxation process.

The concentration dependence of D for the films of three different thicknesses as obtained from desorption runs is shown in figure 9. The sorption runs yield similar curves, using the values of D obtained from the Berens/Hopfenberg analysis of the two stage behavior which occurs at intermediate and high activities. The pronounced maximum in D versus concentration is unusual and is difficult to explain. The marked thickness dependence apparent in the figure is largely an artifact, due to the need to correct for pressure changes which occur during the run as a result of the low vapor pressure of the solvent and the high solubility of the solvent in the polymer. The necessary equations are presented

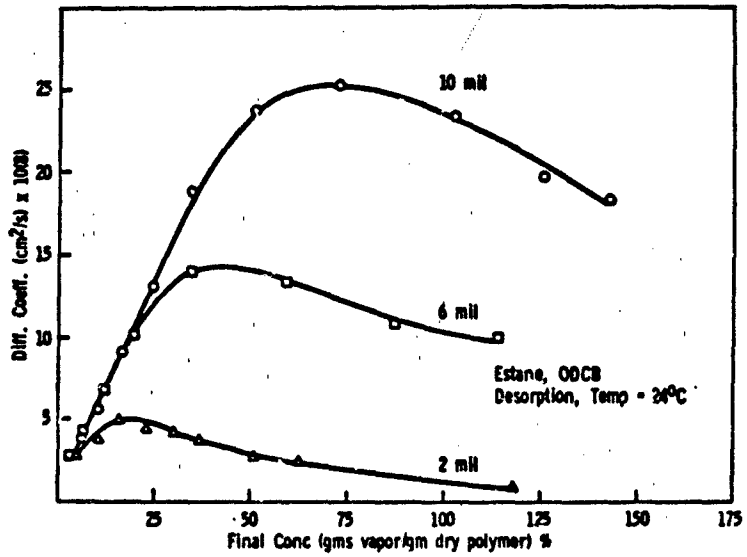


Figure 9. Thickness Dependent - D vs. C Behavior

in Crank, but could not be applied in the time available. The trend of the relaxation rate constants with concentration, in figure 10, is also unexpected. In a glassy polymer, k_R should increase with solvent concentration and with corresponding increases in free volume and segmental mobility. However, the data in figure 10 show a uniform decrease in k_R with increasing concentration for all thicknesses.

CONCLUSIONS

The results show that the sorption of heptane, a non polar solvent, follows classical Fickian behavior. This implies that the sorption is limited to the soft segment phase and does not perturb the hard segment structure. With orthodichlorobenzene, strong swelling occurs accompanied by two stage sorption behavior and various types of anomalies. The results strongly suggest that solvent interactions occur with the hard as well as the soft segment phases. However, the anomalies, such as the maximum in the D versus C curve, cannot be explained simply by the occurrance of sorption at different rates in the soft and hard segment phases (3). While it is difficult to offer a physical explanation of this behavior, it is not peculiar to the polyurethanes. An equally pronounced maximum in D versus C has been reported in SBS triblock co-

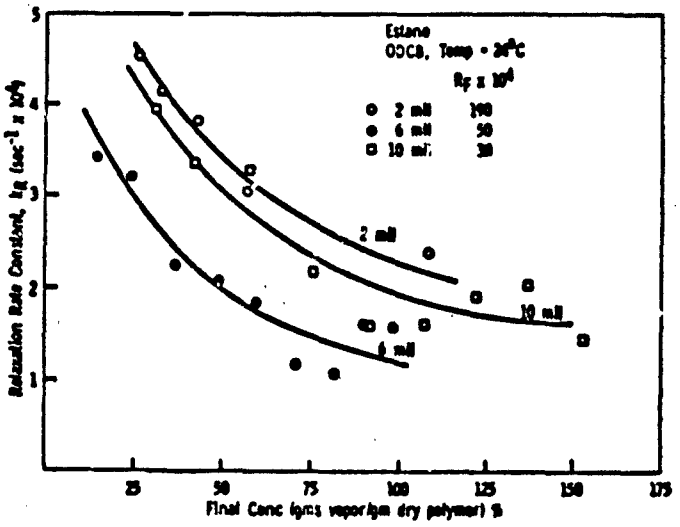


Figure 10. k_R vs. C Behavior

polymers and might prove to be characteristic, in some general way, of segmented and block copolymers with glass microdomains.

REFERENCES

1. Crank, J. Mathematics of Diffusion, 2nd Ed. Oxford University Press, London, 1975.

2. Berens, A. R. Hopfenberg, H. B. J. Polym. Sci., - Polym. Phy. Ed., 17, p. 1757, 1979.

3. Meldon, J. H., Kang, Y., Sung, N. "An Analysis of Transient Permeation and Sorption in Heterophase Media", paper presented at AICHE Conference in San Francisco, 1984.

REINFORCEMENT OF TRACK PAD ELASTOMERS FOR GREATER MILEAGE

ANTHONY L. ALESI[1], PAUL TOUCHET[2], JACOB PATT[3]
(1)U. S. Army Materials and Mechanics Research Center, Watertown, Massachusetts 02172-0001; (2)U. S. Army Belvoir R&D Center, Fort Belvior, Virginia; (3)U. S. Army Tank and Automotive Command, Warren, Michigan.

INTRODUCTION

The rubber pads with which tracked combat vehicles travel on roads and cross country are generally subjected to severe use. Service life measured in miles is low and replacement costs per mile are high. The M-1 Tank, the nation's newest, heaviest, and fastest, is the prime example.

It is possible to conclude from a long history of formulating track pad compounds that conventional rubbers cannot be significantly further improved in durability. Reinforcement of elastomers, conventional and otherwise, is now being considered and tested as a possible approach to greater mileage. This paper outlines how short fibers and continuous cords are being tried to improve the wear properties of conventional rubbers.

WORK IN PROGRESS

Proprietary tank pad elastomeric materials and off-the-road tire (OTR) compounds have been obtained from industry to develop a data base. As part of the overall support program, the physical and dynamic properties of these materials are being obtained for later use to determine whether field performance can be correlated with laboratory results. This is being done in such a way that all compounds are coded to retain vendor's privacy. To date, more than 17 OTR compounds from six suppliers and more than 20 tank pad compounds from eight suppliers have been evaluated. At least six OTR compounds are being considered for fabrication into experimental tank pads.

Materials containing short fibers have been mixed in house and also obtained from industry for laboratory evaluation. Although laboratory data do not indicate outstanding properties, OTR compounds containing fiber reinforcement have exhbited marked improvements in service life of tires used under severe conditions. Property data for OTR compounds, proprietary tank pad rubbers, and fiber reinforced rubbers are given in Tables 1, 2 and 3, respectively. Evaluation of additional compounds is continuing.

TABLE 1

PROPERTIES OF COMMERCIAL OFF-THE-ROAD TIRE COMPOUNDS

Properties	OTR 1	OTR 2A	OTR 5	OTR 7	OTR 10	OTR 12	OTR 14	14AX STD
Original Properties								
Tensile Strength, psi	3030	3143	3187	2557	3123	3267	3717	2853
200% modulus, psi	947	1060	660	663	610	617	710	1445
Elongation, %	467	463	547	570	563	560	557	340
Hardness, IRHD, pts.	67	74	67	70	64	58	63	73
Rebound, %	44	38	33	29	47	43	44	35
Taber Abrasion, Gr./1000 cys	.0629	.0914	GUMMY	.0128	.0208	.0331	.0233	.0338
Tear Strength, ASTM Die C								
Unaged, lb/in	310	596	675	336	323	557	511	243
At 250°F, lb/in	228	285	>254	188	214	304	258	156
Flex Fatigue Test								
Demattia, Crack Growth								
Unaged, mil/min	15.0	7.8	5.5	20.8	16.4	7.8	5.7	35.5
After 20 hrs at 250°F, mil/min	3000	21.1	152	716	976	24.2	51.7	333
Goodrich Flex								
Temperature Rise, °C	22.5	15.7	28.5	37.7	23.7	21.7	17.0	35.0
Blow Out Time, min	52.4	76.7	32.3	30.5	43.	21.0	<120	25.4
Heat Resistance (250 F)								
F/Fo = 70%, min	100	140	185	177	72	40	110	398

TABLE 2

PROPERTIES OF COMMERCIAL TANK TRACK PAD COMPOUNDS

Properties	TP-A	TP-B	TP-C	TP-E	TP-F	TP-K	TP-Q	TP-R
Original Properties								
Tensile Strength, psi	2817	2667	2883	3100	3250	4123	2727	2977
200% modulus, psi	575	802	1500	887	757	1063	680	1217
Elongation, %	513	500	350	507	503	500	443	407
Hardness, IRHD, pts.	69	80	75	76	69	66	70	80
Rebound, %	36	32	33	32	36	49	44	27
Taber Abrasion, Gr./1000 cys	.0364	.1415	.0415	.1816	.0175	.0338	.1001	.0210
Tear Strength, ASTM Die C								
Unaged, lb/in	310	326	335	299	270	554	209	264
At 250°F, lb/in	115	124	109	120	171	320	102	184
Flex Fatigue Test								
Dematti, Crack Growth								
Unaged, mil/min	24.2	32.8	37.2	38.8	23.2	12.2	20.8	28.7
After 20 hrs at 250°F, mil/min	>435	>435	3000	>435	139.0	27.1	39.2	246
Goodrich Flex								
Temperature Rise, °C	29.8	40.3	28.8	33.2	27.0	14.7	41.7	28.3
Blow Out Time, min	37.0	9.7	>120	33.0	61.5	>120	13.0	28.3
Heat Resistance (250 F)								
F/Fo = 70%, min	203	328	140	245	120	243	14000	740

TABLE 3

PROPERTIES OF RUBBER COMPOUNDS WITH FIBER REINFORCEMENT

Properties	150TR 15	150TR 16	150TR 17	15NSP 33	15NSP 34	14AX STD
Original Properties						
Tensile Strength, psi	3997	3297	3017	3063	3027	2853
200% modulus, psi	720	593	720	1980	1577	1445
Elongation, %	563	590	530	303	297	340
Hardness, IRHD, pts.	60	66	67	80	76	73
Rebound, %	44	36	35	35	36	35
Taber Abrasion, Gr./1000 cys	.3749	.353	.1814	.0185	.0098	.0338
Tear Strength, ASTM Die C						
Unaged, lb/in	553	526	290	297	263	243
At 250°F, lb/in	258	248	194	151	167	156
Flex Fatigue Test						
Demattia, Crack Growth						
Unaged, mil/min	8	9	11	55.2	32.3	35.5
After 20 hrs at 250°F, mil/min	629	246	251	1579	1338	333
Goodrich Flex						
Temperature Rise, °C	15.7	19.0	25.0	35.0	29.0	35.0
Blow Out Time, min	76.7	51.0	59.4			25.4
Heat Resistance (250 F)						
F/Fo = 70%, min	140	143	185	205	505	398
Fiber Content, PHR	1.50	2.24	2.50	4	0	0
	Treated Cellulose Fiber			Kevlar Pulp		

Short fiber reinforced rubber will be tested on a M-1 tank. Fiberglass (Owens Corning RICS) has been incorporated to the extent of 5 percent in the Red River Army Depot 14A tri-blend (Natural/SBR/Butadiene) and will be tested in the field this summer. Other fibers that will be tried include treated cellulose fiber (Monsanto Santoweb), nylon and aramid. Fiberglass tire cord has also be molded into track shoes for field testing this summer. These have been spaced in the horizontal, vertical, and 45 degree planes to determine the effect of cord orientation. Nylon and aramid cords will be tested later.

Elastomers other than conventional rubbers are also under evaluation. Thermosetting cast polyurethanes and thermoplastic co-polyester (Du Pont's Hytrel) will be in this summer's field test. The polyurethanes were selected on the basis of hysteresis characteristics and chemical composition. With the wide range of hysteresis values present, it may be possible to establish a limit below which catastrophic blowout of the track pad can be avoided. The different chemistries, listed below, may be identified with resistance to wear.

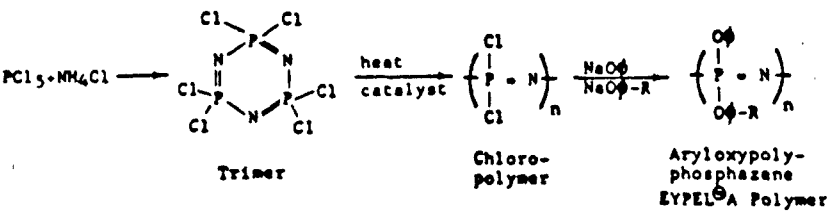
	Diisocyanate	Polyglycol	Curative
1.	TDI (Toluene diisocyanate)	Polyether	MOCA (methylene-bis o-chloroaneline)
2.	TDI	Polyester	MOCA
3.	MDI (methylene-bis-p-phenyliso-cyanate)	Polyether	Polyol
4.	MDI	Polyether	Amine
5.	TDI	Polyester	Amine
6.	NDI (napthalene diisocyanate)	Polyester	Glycol

All the polyurethane were in the Shore A hardness range of 74 to 89. The second formulation in the above tabulation was also cast into an aluminum sponge reinforcement that would stiffen the pad and dissipate the heat from hysteresis.

ARYLOXYPOLYPHOSPHAZENE APPLICATIONS: NON-HALOGENATED FIRE RETARDANT SPECIALTY POLYMERS

WARREN B. MUELLER
Ethyl Corporation,Ethyl Tower,451 Florida,Baton Rouge,La. 70801

Polyphosphazene polymers represent a class of semi-inorganic polymers possessing virtually unlimited synthetic versatility. The alternating nitrogen and phosphorus backbone with two labile chloride groups on the phosphorus atom provides the starting point for a variety of synthetic pathways leading to polymers which can be tailor made to fit a wide range of end use applications. The details of polyphosphazene synthesis have been published elsewhere[1] and can be succinctly summarized in the following manner:



Early investigators recognized that a nearly limitless variety of substituents could be attached to the inorganic backbone to modify polymer chemical and mechanical properties. Applications work originally funded by the Navy[2] and later carried on elsewhere, including the Ethyl Corporation, determined that true elastomers possessing inherent flame retardance with low smoke characteristics could be produced from polyphosphazene chloropolymer which had been substituted with phenoxy and substituted phenoxy groups. The importance of this observation has continued to grow in significance as fire safety research has indicated a need to achieve flame retardance in some product applications without the use of halogenated polymers or additives.

An application which has developed a tremendous amount of interest in fire resistant material is the shipboard insulation area, where a combination of factors such as ship layout, large crew population, and a requirement for the highest level of operational readiness has prompted the U.S. Navy to actively pursue materials which are flame retardant, low smoking, and produce combustion products with relatively low toxicity and corrosivity[3].

Ethyl Corporation has developed a low density foam insulation based on EYPEL-A Aryloxypolyphosphazene which meets the Navy's desired end-use properties. EYPEL-A Foam Insulation can be processed on conventional rubber compounding equipment followed by heat activation of a chemical blowing agent to give the desired closed-cell foam structure. Typical properties for 4.0 lb/ft^3 foam are given in Table 1, but these can be significantly varied by choosing different density targets.

TABLE 1

EYPEL-A INSULATION FOAM PROPERTY SPECIFICATIONS

Flammability	Test Methods, Units	Typical Value
Limiting Oxygen Index	ASTM D-2863	46
NBS Smoke Density	ASTM E-662 Non-Flaming	25
	Flaming	49
Surface Burning	ASTM E-84 Flame Spread	20
Characteristics*	@ ½" Smoke Developed	60
NBS Quarter Scale		No
Test	640 BTU/min heat input	Flashover
Mechanical		
Density	ASTM D-1622, lb/ft^3	4.0
Compressive Resistance	ASTM D-1056, psi	2.0
Tensile Strength	ASTM D-412, psi	17.0
Compression Set	ASTM D-1667, %	25.0
Noise Reduction		
Coefficient	ASTM C-423 at 1.0 inch	.3
Thermal Conductivity		
75°F mean	ASTM C-518	.28
140°F mean	BTU-in/hr. ft^2.°F	.31
Other		
Water Vapor	ASTM C-355 wet cup,	
Permeability	perm-in.	.19
Oil Resistance	MIL-15280H, 4.6.9	No Swell
Dimensional Change	MIL-15280H, 4.6.8, %	.8

* The flamespread rating determined by ASTM E-84 under controlled laboratory conditions is not intended to reflect the fire risk presented by this or any other material under actual fire conditions.

In numerous NBS Quarter Scale Flammability Test runs, Ethyl's EYPEL-A Foam Insulation has met the Navy's targeted requirement of no flash-over[4]. In addition, specially instrumented tests have shown that EYPEL-A Foam Insulation is not only fire retardant but also acts as a fire blocking material which provides fire protection to underlying substrates[5]. As a closed cell elastomeric foam, EYPEL-A Foam Insulation functions as a superb water vapor barrier and is easily fabricated and installed with readily available contact adhesives. While a judicious choice of compounding ingredients is necessary to achieve the high levels of flammability performance exhibited by EYPEL-A Foam Insulation, the inherent flammability is determined by the fire resistant nature of the polyphosphazene polymer.

Potential EYPEL-A Foam Insulation shipboard applications include submarine thermal/acoustical insulation, bulkhead thermal/acoustical insulation, elastomeric foam pipe insulation, and HVAC duct insulation. In addition to the high performance fire retardance properties offered by Ethyl's EYPEL-A Foam Insulation, it also has the potential for providing more efficient installation than some presently used materials.

Preliminary evaluations of EYPEL-A Foam Insulation in acoustic applications are underway to study the sound absorption and sound transmission loss characteristics of specially designed and constructed EYPEL-A Foam Insulation composite materials. Presently used materials in these applications are often difficult to fabricate, labor intensive to apply, and unpleasant to work with.

Wire and cable jacketing is another application generating a high level of interest in flame retardant, low smoke material with no halogen content. Plenum wire & cable is a particularly active area because of new demands being placed on the plenum areas of office buildings by the upcoming "computerized office".

More immediate concern for high performance wire & cable jacketing having high levels of flame retardance with low smoke generation, and low toxicity combustion products is clearly spelled out in Mil-C-24640, the Navy's new specification for lightweight shipboard cable. In a move away from PVC jacketed cables, Mil-C-24640 specifically limits halogen content to .2% by weight. EYPEL-A Wire & Cable Jacketing has passed all of the Mil-C-24640 specifications for which it has been tested, including the IEEE-383 vertical burn test. Typical properties for EYPEL-A Wire & Cable Jacketing are given in Table 2 and compared to Navy targets outlined in Mil-C-24640.

TABLE 2

EYPEL-A WIRE & CABLE JACKET COMPOUND

PROPERTIES

	Typical Value	Mil-C 24640 Spec. Minimum
Tensile Strength (psi)	1420	1300
Elongation (%)	360	160
Tear Strength (psi)	76	35
Halogen (% max)	.05	0.2
Water Absorption (mg/in^2, max)	7	(25 draft)
Heat Aging Dry & Oil		
Tensile % orig	100-112 @ 158°C Dry	60
Elongation % orig	45-65	60
Flame Propogation (IEEE 383)	Passed	Pass
Smoke Index (max)	17	25
Acid Gas, (% max)	0	2
LOI	44	--
Durometer Shore A	80	80

Cable production on commercial equipment has shown EYPEL-A Wire & Cable Jacketing compound to be easy to extrude and handle with the ability to effect final crosslinking using heat or radiation. In addition to its excellent flammability characteristics, EYPEL-A Wire & Cable Jacketing has exhibited excellent resistance to ASTM #1, #2, and #3 oils (low volume swell) and in initial laboratory testing has demonstrated the potential for receiving a UL 125°C temperature rating.

In conclusion, EYPEL-A Polyphosphazenes comprise a versatile family of polymers which can be designed to optimally serve many potential end uses. With general properties such as high performance flame retardance, low smoke development, low toxicity combustion products and non-halogenated composition, EYPEL-A Polyphosphazenes are particularly well suited to tackle today's end use applications where maximum fire safety is an important product performance requirement in addition to mechanical property characteristics.

References

1. Allcock, H.R. (1985): Inorganic Macromolecules, Chem. and Eng. News, March 18:22-36.
2. Gerber, A.H. and Peterson, T.C.: Poly(Aryloxyphosphazene) Foamed Thermal Insulation, N00173-77-C-0286, Horizons Re-

search Incorporated, Cleveland, Ohio, 1978, 8 pp.
5. Passive Fire Protection Symposium, October 16, 1984, Naval Research Laboratory and Naval Sea Systems Command.
6. Lee, B.T. and Breese, J.N.: Submarine Compartment Fire Study - Fire Performance Evaluation of Hull Insulation, NBSIR 78-1584, National Bureau of Standards, Washington, D.C., 1979, 42 pp.
7. Ethyl Corporation, internal results.

ENHANCEMENT OF RUBBER PROPERTIES VIA SHORT ARAMID FIBERS

ANDREW P. FOLDI
C & C Consultants
2833 W. Oakland Drive
Wilmington, DE 19808

INTRODUCTION

In the rubber industry, especially in the tire and mechanical goods sectors, carbon black has been used traditionally as a most effective reinforcing agent. However, the improvements in tensile properties -- obtained through higher and higher loadings of carbon black -- are offset both by increasing processing difficulties and by deterioration of other properties, especially heat buildup. With compounds of very low green (i.e., uncured) strength, adding more carbon black to improve cured tensile properties leads to unacceptably high levels of breakouts and/or bagginess on the rubber mill rolls. In addition, increased levels of carbon black cause drastic changes in curing behavior, usually making the compound too scorchy. Also, carbon blacks cannot be used for light colored compounds, for obvious reasons. By using the appropriate short fibers -- at relatively low loadings -- one can both avoid some of the above problems and also impart many desirable, up-to-now unobtainable properties to rubber articles.

The use of short fibers is not new, but only recently have short fiber forms been developed solely or mainly as an engineered reinforcement of rubber. With the development of these new reinforcing fibers came systematic studies on how these fibers influenced various basic properties of the fiber/rubber composite systems (References 1 to 5). This paper deals with the reinforcement of various rubber compounds by short aramid fibers, both staple and "pulp". It describes how these improvements are obtained, and points out the most common pitfalls.

EXPERIMENTAL

Specimens

The aramid pulp used in these investigations was a commercial product of the Du Pont Company known as "Dry Kevlar® Pulp, Merge 6F218" with a nominal average fiber length of 2 mm (for detailed description see Reference 5). This unique material consists of short, random-length fibers of varying cross-section

---

Kevlar® is a Registered Trademark of the Du Pont Company

with fibrils extending over the entire surface. The high length over diameter ratio of the fiber core, coupled with the high surface area provided by the fibrils, causes good mechanical locking to the rubber matrix, especially under tension. This pulp exhibits high tensile modulus and strength as well as the inherent thermal and chemical stability associated with all aramids.

The aramid staple was produced from 1.5 dpf (denier per filament), 12 μm diameter Kevlar® yarn by precision cutting to 1/16 inch (~1.6 mm) staple length which is comparable to the average pulp length. During the vigorous processing steps both the pulp and the staple retain their original lengths, unlike glass which breaks up severely. Unlike asbestos, these aramid fibers -- which had no adhesive treatment on the surface -- have shown no adverse physiological effects.

Sample preparation

All samples were prepared by adding the fibers onto a rubber mill during compounding of the rubber. Good mixing and dispersion could be achieved with the staple (up to 20 phr) by using the customary "cut and fold" and "cigaring" methods. Above this level of loading, clumping of the fiber is very likely to occur. These fiber clumps cannot be removed by further processing of the rubber, and become a site of weakness. With the pulp, this method of "sprinkling" the fibers onto the rolling bank of the mill was too time consuming and limited the scale of production and level of loading to a point as to be impractical. For this reason, a new, proprietary masterbatch -- developed by DuPont -- was used. This masterbatch, which consists of Kevlar® pulp, the elastomer, and a filler, not only facilitates the handling and dispersion of the pulp but also permits high levels (up to 70 %) of pulp in the masterbatch. The "MB" suffix was used to identify whenever this masterbatch technology was used during compounding.

Sample testing

When available, ASTM test methods were used:

Tensile properties (to break)	D412 (Die C)
Hardness	D2240
Winkleman tear	D624-54, Type B
Abrasion resistance (NBS)	D1630-61

Green tensile properties were measured on rectangular specimens at 500%/minute strain rate. Surface tack was eliminated by "surface precuring" at 121°C for two minutes.

Cyclic extension testing was performed on rectangular samples because this permitted better precision of testing than the standard dumbbell shape. The frequency of cycling was low: less than 10/minute.

Compression testing was carried out on cylindrical pellets (normally used for heat buildup measurement) with a height to diameter ratio of 2:1. When cycling, the frequency of cycling was less than 10/minute.

Bending stiffness was measured in a 3-point bending mode similar to ASTM D790-81, Figure 1a. The tangent modulus of elasticity in bending was calculated according to the cited ASTM method:

$$E_B = \frac{L^3 m}{4bd^3}$$

where: E_B = Modulus of Elasticity in Bending, MPa

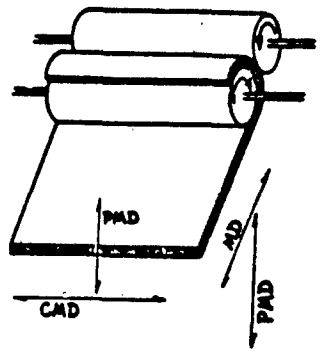
m = Slope of initial tangent of load/deflection curve, N/mm
L = Length of support span, mm
b = Width of "beam", mm
d = Thickness of "beam", m

Tongue tear (also known as "Trousers test or tear") was measured on rectangular samples prenotched (cut) to a depth of at least 25 mm prior to the pull. The test and its validity are described in detail in Wellington Sears Handbook of Industrial Textiles, 1963, page 489.

The **penetration resistance** test was developed by the author and is described in detail in the Appendix.

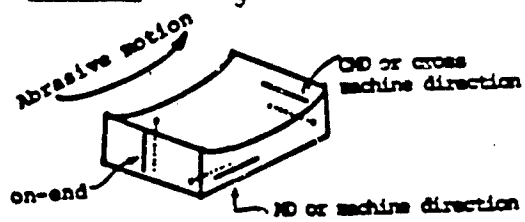
Fiber orientation

Depending on the fiber type and loading, and on the kind of rubber stock used, it is not difficult to orient the majority of the fibers **once good dispersion has been achieved**. The ease of fiber orientation (or reorientation, as it may be the case) depends on the magnitude of the shear in the last preparative step. A practical way of judging the degree of orientation is to compare properties obtained in the machine direction (MD) to the same properties obtained in the cross machine direction (CMD). We found low-elongation modulus (in rubber technology, modulus always means secant modulus) -- at 100% or, preferably, lower elongations -- to be a good indicator of orientation. The three major directions of testing, as well as of "orientation", are:



MD, machine direction (which is parallel to the direction most fibers are pointing); CMD, cross machine direction; PMD, perpendicular to both MD and CMD.

We found the need to describe a fourth testing direction, called "**on-end**", for the abrasion testing of fiber-loaded samples. The sketch explains the three possible directions of fiber orientation in abrasion testing:



RESULTS AND DISCUSSION

The success of short fiber reinforcement of rubber in general depends on a few key requirements. Of these, uniform dispersion is the most important since fiber clumps -- instead of reinforcing -- may act as actual failure sites. High surface area and mechanical/thermal integrity are requirements either for actual end use and/or during the manufacturing process. Aramid pulp and staple are eminently suitable to meet these requirements.

The obtainable improvements and side effects with **properly dispersed and oriented** aramid pulp are shown in Table 1. One must keep in mind that, because of the orientation effect, the "demonstrated levels" are always those in the direction of optimum orientation. Optimum orientation varies according to the property, and will be mentioned individually with each property discussed. The ablative behavior of aramid reinforced rubber is outside the scope of this paper, and is mentioned only for completeness.

TABLE 1

GENERAL EFFECT OF ARAMID PULP ON ELASTOMER PROPERTIES

BENEFITS	DEMONSTRATED LEVELS
• In the Green (uncured) State	
-- Increased Yield Strength	30X
-- Tougher, Much Harder to Cut	
-- Curing Requirements Unchanged	
• In the Cured State	
-- Greater **Hardness**	+10 Units
-- Much Higher Low-Elongation **Tensile** Modulus	5X
- Steeper Stress/Strain Curve	
- Increased Break Strength at Elevated Temperatures	2X
-- Tougher **Compressive** Behavior	4X
- Higher Heat Buildup at Constant Stroke but only Slightly Higher at Constant Load	
-- Higher Bending **Stiffness**	3-4X
-- Better **Penetration** Resistance	2X
-- **Tear** Properties (greatly affected by shape and direction)	2X
• Excellent Ablative Behavior	
• Non-Asbestos; Environmentally Safe	

The increase in **green** strength is the most pronounced with relatively weak rubber stocks. For instance, with a weak neoprene compound (Table 2), the 100% modulus improvement was 7.8X and the hardness increase was 10 Shore A units. These levels were only 1.8X and 4 units, respectively, with a compound of a strong Hypalon® synthetic rubber. In **cured** rubber compounds, the presence of fibers always manifests itself in higher hardness, steeper stress/strain (i.e., load/elongation) curve, and much higher initial and low-elongation moduli. While at room temperature this rapid shift in the stress/strain curve is accompanied by a reduction in break elongation **and** break strength, at elevated temperatures the presence of aramid fibers compensates for the inherent deterioration of the rubber matrix, thus resulting in higher break strength.

Upon compression, the fibers -- when oriented parallel to the compressive force -- contribute very little. However, if aligned in such a way that the filaments can go into tension, they

TABLE 2

COMPARISON OF GREEN STRENGTH IMPROVEMENT WITH WEAK AND STRONG RUBBER COMPOUNDS

Effect of Fiber Loading on Green Properties

Aramid pulp, phr:	0	2	5
	Neoprene Stock**		
100 % Modulus, KPa	393	1724	3068
200 % Modulus, KPa	434	1875	3220
300 % Modulus, KPa	552	2055	--
Green (Yield) Strength, KPa	1276	2510	3192
Green Elongation, %	840	576	261
"Orientation" ≈ Δ 100 % Modulus**	14	993	2296
Hardness, Shore A	36	42	46
	Hypalon* Stock***		
100 % Modulus, KPa	4500	5960	8050
200 % Modulus, KPa	5520	6330	7160
300 % Modulus, KPa	6390	6610	--
Green (Yield) Strength, KPa	7260	6600	6990
Green Elongation, %	547	423	222
"Orientation" ≈ Δ 100 % Modulus**	400	1300	2600
Hardness, Shore A	86	89	90

** Δ (MD-CMD), KPa

*** 100 phr Hypalon* 45

**** 70 phr Neoprene W, 30 phr Neoprene WHV

* DuPont registered trademark

All properties measured MD, except "Orientation" and Hardness (which was measured PMD)

contribute significantly to the inherent resistance to compression by the rubber matrix. Under such conditions, if one subjects a sample to, say, the standard BFGoodrich "Flexometer" heat buildup test, the compressive stroke with constant deflection causes significant heat generation. In reality, there are few applications where the deformation is caused by a fixed compressive strain but rather by a fixed compressive load. Under such circumstances, since the fiber reinforced article will deform much less, the fiber-caused heat generation will be less significant.

Due to the increased composite tensile modulus, fibers aligned parallel to the "beam" axis will cause higher bending stiffness, while penetration resistance will increase to a different degree depending on fiber orientation. While tear resistance always increases if the tear has to propagate across the fibers -- such as shown in Table 3.

TABLE 3

EFFECT OF ARAMID FIBERS ON TEAR RESISTANCE ACROSS THE FIBER

Fiber:	None	Aramid 5 phr Staple	Aramid 5 phr Pulp
Tongue Tear, N•mm^{-1}	20.1	42.0	32.4
Winkleman Tear, N•mm^{-1}	105	155	133

Commercial "Adiprene M467 Polyurethane Prepolymer
Chain extended with Butanediol

In some instances and depending on the test method(s) used, this resistance can be so great as to channel the tear's propagation in a direction 90 degrees to the original tear. When this happens, the fibers can actually facilitate the tear (although in the "wrong" direction). Proper recognition of this phenomenon and proper engineering of the rubber article can alleviate this problem.

The fact that aramid fibers do not have the safety problem associated with asbestos has already secured a considerable segment of the friction products (brake, clutch facings), as well as seal and gasket markets for aramids.

We conducted very extensive studies based on a 100% natural rubber composition. However, the trends -- discussed in detail below -- are applicable to other elastomers, too.

As far as **stress/strain** properties are concerned, short aramid fibers provide -- at ≥10 phr levels -- more than 3X enhancement in low-elongation modulus in the machine direction (Figure 1). Initially, both pulp and staple show very much the same reinforcing effects but as one exceeds the break elogation (~4%) of the fibers, a rheological separation has to take place, since the fibers are so strong that they would not break. The pulp with its highly branched surface maintains its rheological integrity longer than the staple does. However, when tested in the cross machine direction, there was no initial modulus enhancement.

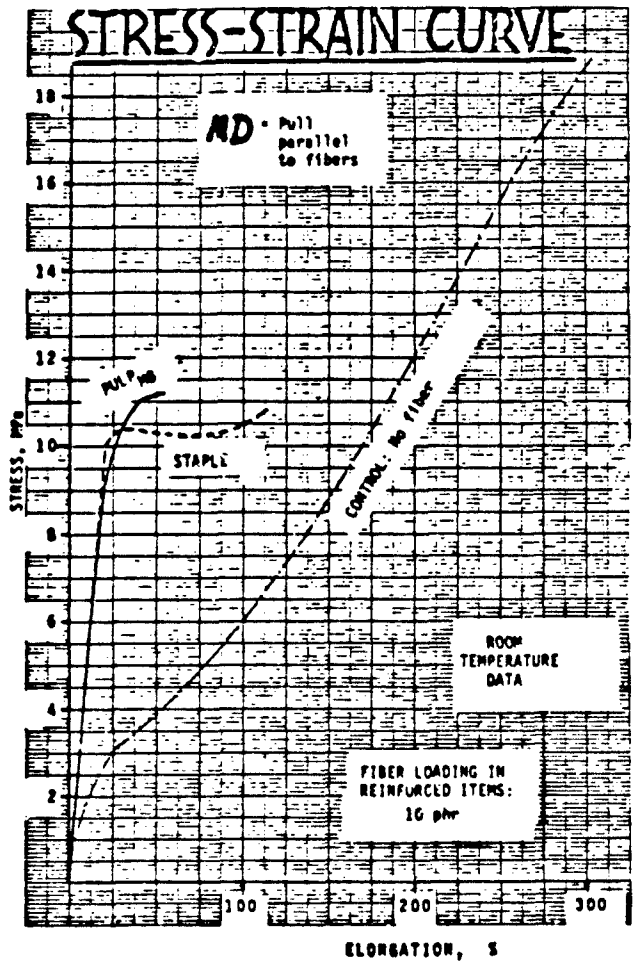


FIGURE 1. Typical stress-strain curve of aramid reinforced rubber, measured in the machine direction on 100 phr natural rubber stock, compared to the fiberless control.

The importance of orientation can be shown by comparing the 20% tensile moduli of compounds reinforced with both aramid pulp and staple (Figure 2) as a function of fiber loading. There is hardly any enhancement in the cross machine direction. This very limited enhancement in the cross machine direction is the result of the fibers originally oriented not exactly 90° to the direction of the pull: as the rubber is extended, these fibers -- out of geometric necessity -- get more and more aligned in the direction of pull.

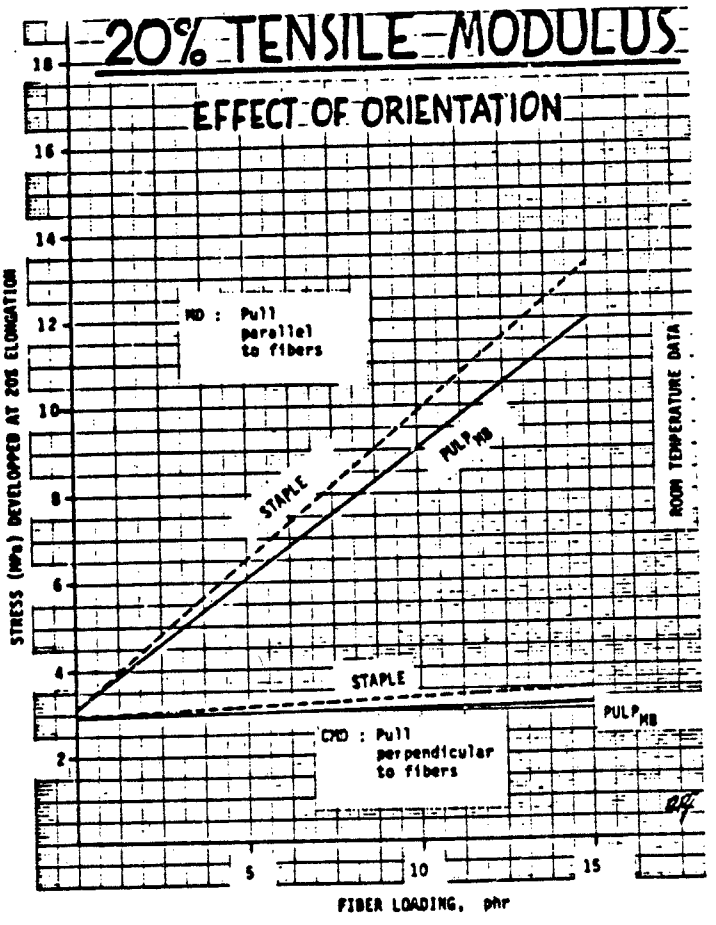


FIGURE 2. Effect of orientation on 20% modulus in 100 phr natural rubber compound as a function of fiber loading.

It was of some concern how the enhancement obtained with the fibers would be retained after **cyclic extension**. Test strips subjected to 2% cyclic extension indicated (Figure 3) that even after extensive (50) cycling, the fiber reinforcers still provide 2X to 3X enhancement, although the cycling did cause some loss -- even with the no-fiber control compound. The biggest loss was experienced during the first two extensions, the further losses gradually diminishing. Nearly steady state condition was reached by the 10th cycle. The cyclic extension experiment was repeated at 20% strain -- a strain way beyond the break elongation of the fibers --, yet the fibers continued to provide substantial

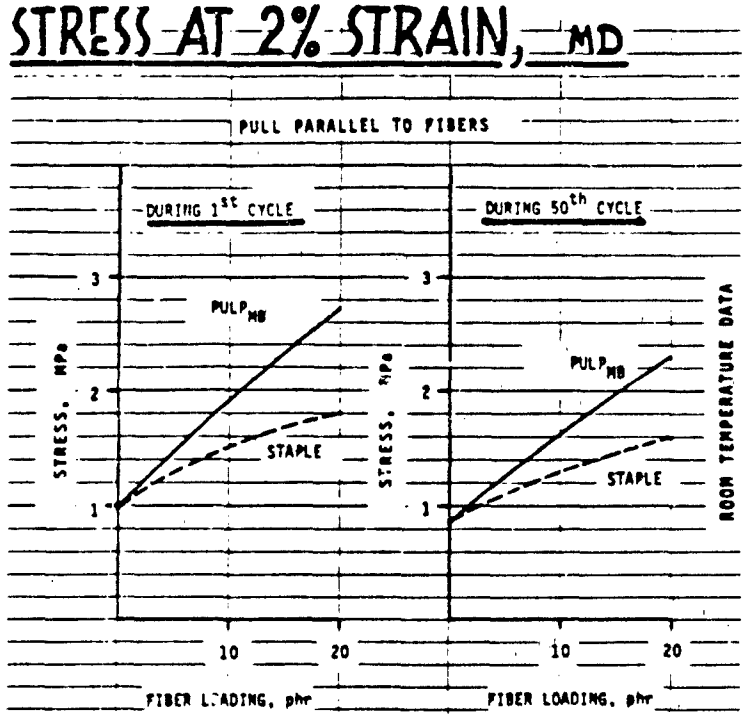


FIGURE 3 Effect of cyclic extension to 2% strain in the machine direction at various fiber loadings (100 phr natural rubber stock).

reinforcement (Figure 4). Even after cycling at elevated temperature (149°C), the fibers still provided 2X to 3X enhancement.

During **compression**, the fiber reinforced specimens responded in a unique manner. When the fibers were oriented parallel to the direction of compressive force, there was hardly any increase in the stresses generated. However, when the fibers were oriented perpendicular to the force of compression, a very substantial increase in the resistance to compression occurred. The reason for this is that when rubber is compressed, it wants to bulge out in the direction perpendicular to the compression, thus putting under tension the fibers oriented in that (perpendicular) direction. The stresses generated can be quite formidable as shown by the 40% compression data (Figure 5): at 20 phr loading, the stresses about tripled when the sample was compressed to 60% of its original height. Although cyclic compression causes some losses -- mainly during the first cycle --, the proportional reinforcement remains the same after cycling.

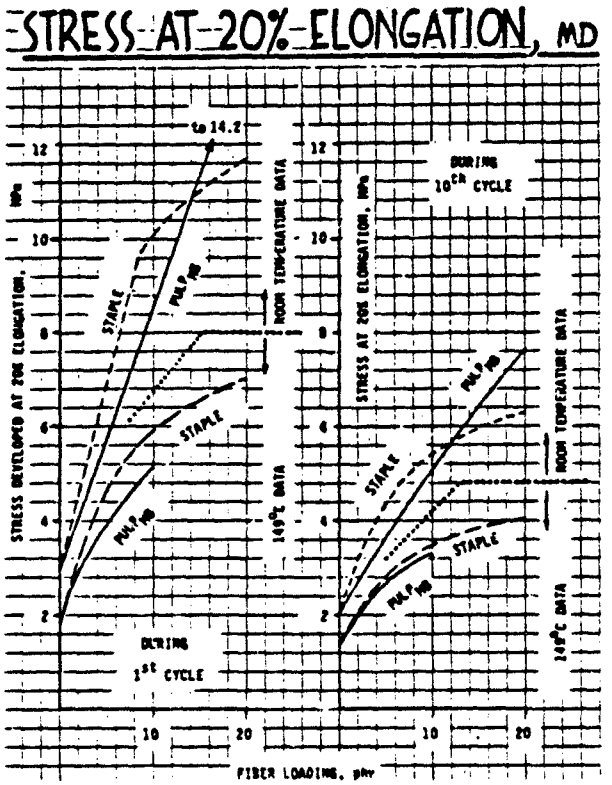


FIGURE 4. Effect of elevated temperature and cycling to 20% strain on stress as a function of fiber loading. Measured in the machine direction on 100 phr natural rubber compound.

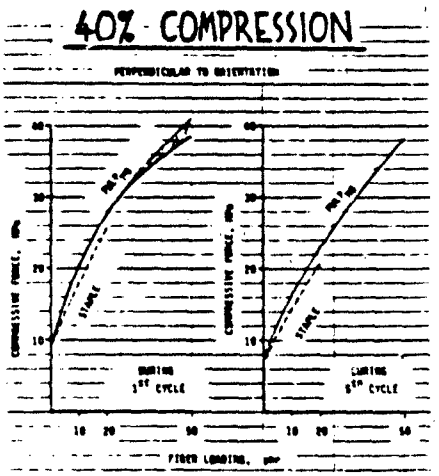


FIGURE 5. Effect of cycling at 40% compression as a function of fiber loading. Fibers perpendicular to the compressive force. 100 phr natural rubber compound.

In **bending**, the effect of orientation is even more dramatic (Figure 6). In a 3-point bending test, pulp and staple behaved very much the same: when the fibers were oriented in such a way that they were subjected to tension, the improvement in bending stiffness was substantial (3X at 20 phr). With the fibers oriented in such a way that they were subjected to neither extension nor compression, the presence of the fibers actually weakened the response.

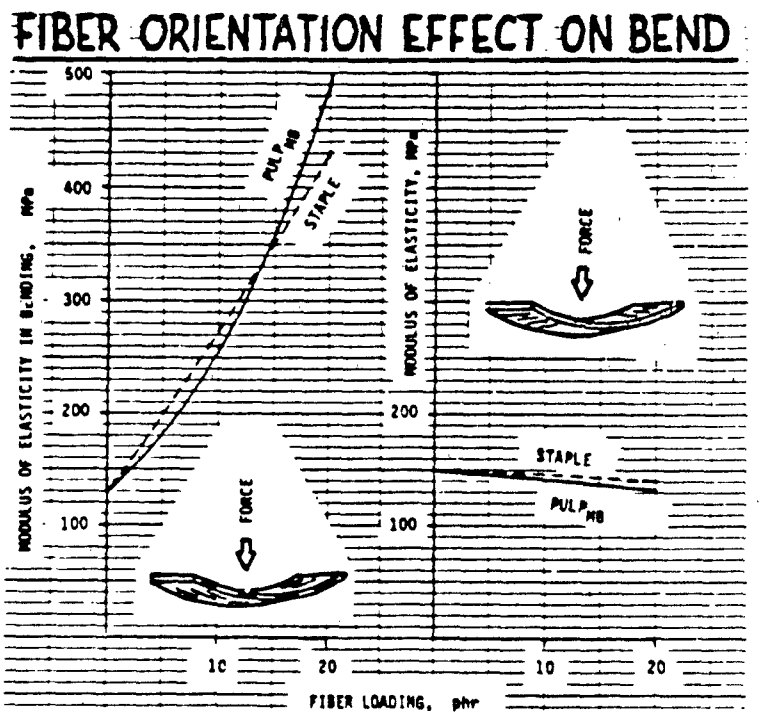


FIGURE 6. Effect of fiber orientation on bending stiffness as a function of fiber loading; 100 phr natural rubber compound.

When studying the effects of fiber orientation on **penetration resistance**, we found that both MD and CMD directions provided reinforcement, the reinforcement in CMD (i.e. when the fibers were perpendicular to the penetrating probe) being much greater (Figure 7). This can be easily explained by studying the components of penetration: the forces needed (a) to repeatedly initiate a wound (i.e. to propagate a wound front); (b) to spread apart the already developed wound; and (c) to overcome friction between the rubber and the penetrating object. We found

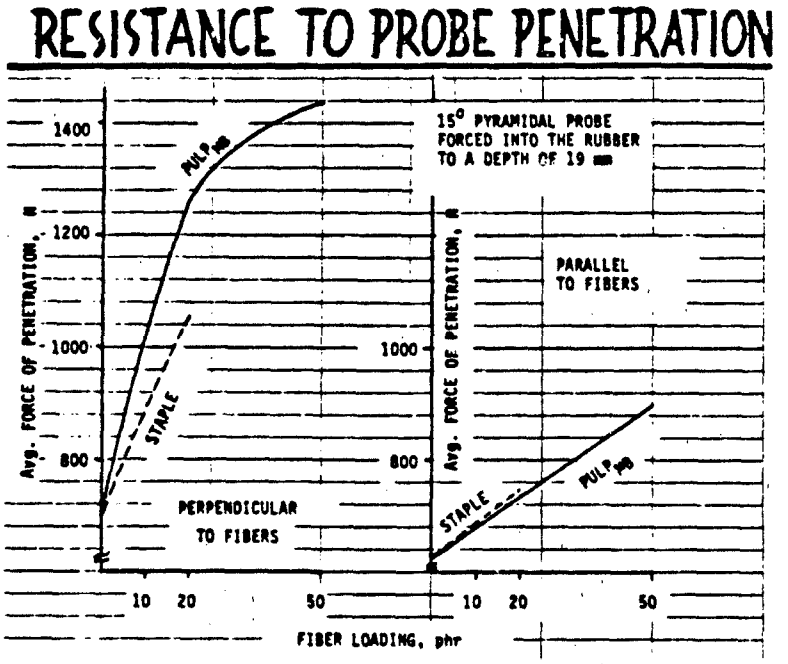


FIGURE 7. Effect of orientation on penetration as a function of fiber loading; 100 phr natural rubber compound.

that ~60% of the total force was used up for spreading of the wound (Figure 8), regardless of fiber orientation. The absolute force needed to overcome friction was independent of fiber orientation, and ~20% of the total force was used up for the wounding. We used the following experimental technique to separate the various components of penetration: First, we measured the force needed for the initial penetration; this gave us the combined effects of initiating the wound + spreading the wound + overcoming friction. Then we retracted the probe and carefully reentered the seemingly "healed" wound. In doing so, the force needed to penetrate was the sum of spreading the wound + overcoming friction. We again retracted the probe but before reentering the wound, we applied a lubricant (water is excellent in this case) onto and into the wound (capillary forces sucked the lubricant into the wound). Reentering with the probe, we then measured only the force needed for spreading the wound.

When the fibers are perpendicular to the penetrating probe, they reinforce because they are subjected to tension as the probe initiates and spreads the wound. The stresses so generated are similar to the ones seen upon compression. When the fibers are parallel to the penetration, the penetrating probe causes somewhat of a bending and the increase in the force needed to penetrate is caused by the increased composite bending stiffness.

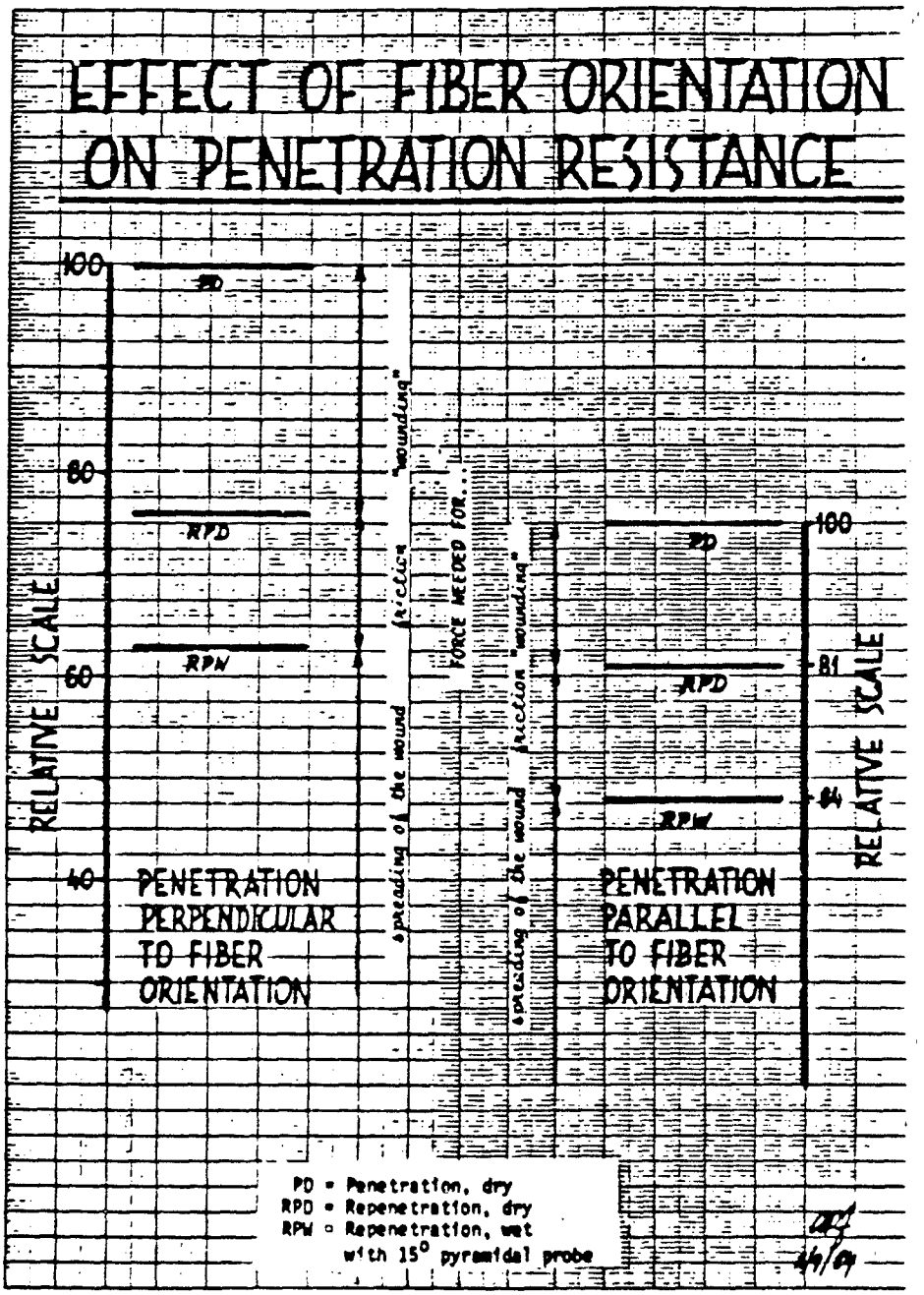


FIGURE 8. Effect of fiber orientation on the components of penetration resistance, 100 phr natural rubber compound.

For **abrasion resistance**, the only fiber orientation which offered improvement was the "on-end", that is when the fibers were perpendicular to the surface being abraded (Figure 9). Other orientation directions actually cause a greater abrasive loss. Close scrutiny of the literature (References 6 to 8) gave a reasonable explanation for these findings. According to Schallamach and Thomas, the abrasion of rubber occurs through a wavelike abrasion ridge-pattern propagation, due to crack growth propagation at the base of the ridges. Whenever the fibers are perpendicular to this crack (which they are only in the "on-end" configuration), crack propagation will be hindered and -- thus -- abrasive wear will be diminished. The other orientations actually promote crack propagation by acting as sites of inhomogeneity.

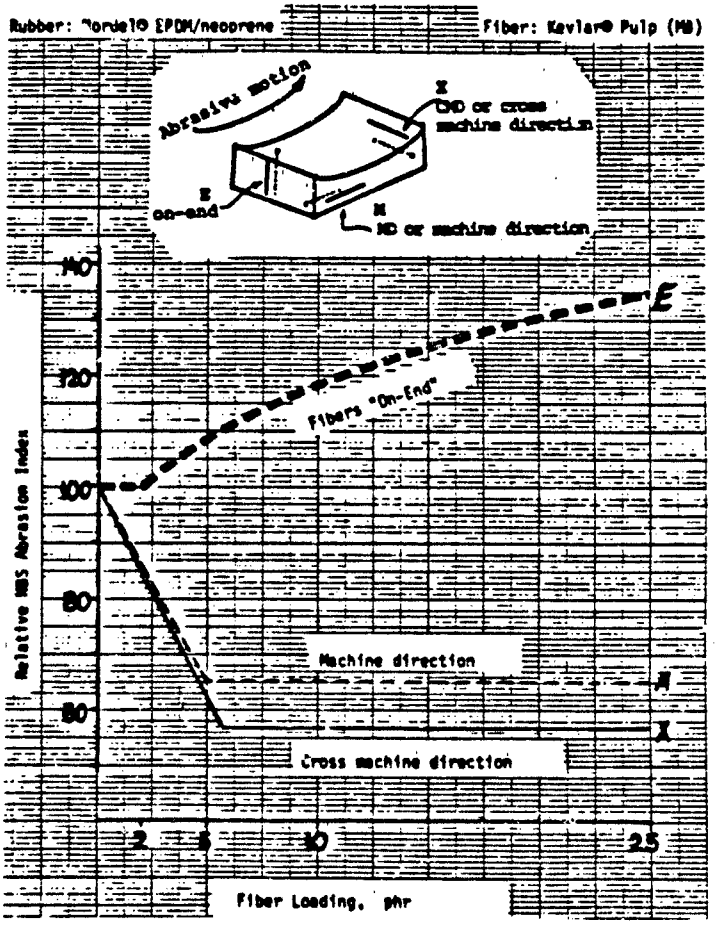


FIGURE 9. Effect of fiber loading and orientation on abrasive behavior, measured on 80/20 phr EPDM/neoprene compound.

SUMMARY AND CONCLUSIONS

Cured rubber compounds are deficient in low-elongation tensile properties, are too compliant under compression, hardly resist bending forces, and are easily cut, torn, and penetrated (especially when wet). The following technical **advantages** from aramid fiber reinforcement were demonstrated which may alleviate these deficiencies: much higher initial tensile modulus; better cut, tear, wear and penetration resistance; increased compressive response, greater bending stiffness; and higher steady-state, dynamic reinforcement-- provided that one uses the appropriate fiber orientation. The other benefits, good thermal stability and no need for adjustment of curing conditions, are not dependent on orientation. The technical **limitations** one may encounter are: lower break elongation (an unavoidable "by product" due to rheological changes); greater compression set (again, a manifestation of the restricted rheological behavior imparted by the fibers); greater hardness, when this may be objectionable; and high anisotropy. This latter may be bothersome if one needs isotropic composite behavior; complete isotropy can be achieved only by layering techniques. The technical **barriers** are: higher heat build-up at fixed displacement only (associated with any high-modulus, high-performance fiber); and uneven fiber dispersion (because this results in sites of weakness and early failure).

Aramid fiber reinforced rubbers are a new kind of engineering material with greatly enhanced properties over conventional rubber compounds. This enhancement is limited by one's ability to orient the fibers in the desired direction or to incorporate the needed amounts of fiber. The extent of reinforcement depends on the homogeneity of the product and on the concentration of the fiber(s). A clear understanding of the mechanism of reinforcement is **crucial** for success.

ACKNOWLEDGEMENTS

This paper is based on the research conducted by the author while working at Textile Research Laboratory, Chestnut Run, E. I. du Pont de Nemours & Co., Inc. Most of the findings were presented at the Scandinavian Rubber Conference (Reference 9) and at the 32nd Sagamore Conference (Reference 10). The help and cooperation of Polymer Products Department (formerly Elastomers Division) of the Du Pont Company at Chestnut Run, Wilmington, Delaware -- especially of W. Roman and T. E. Schroer -- is gratefully acknowledged. R. Strengari provided valuable help in the preparation of this paper.

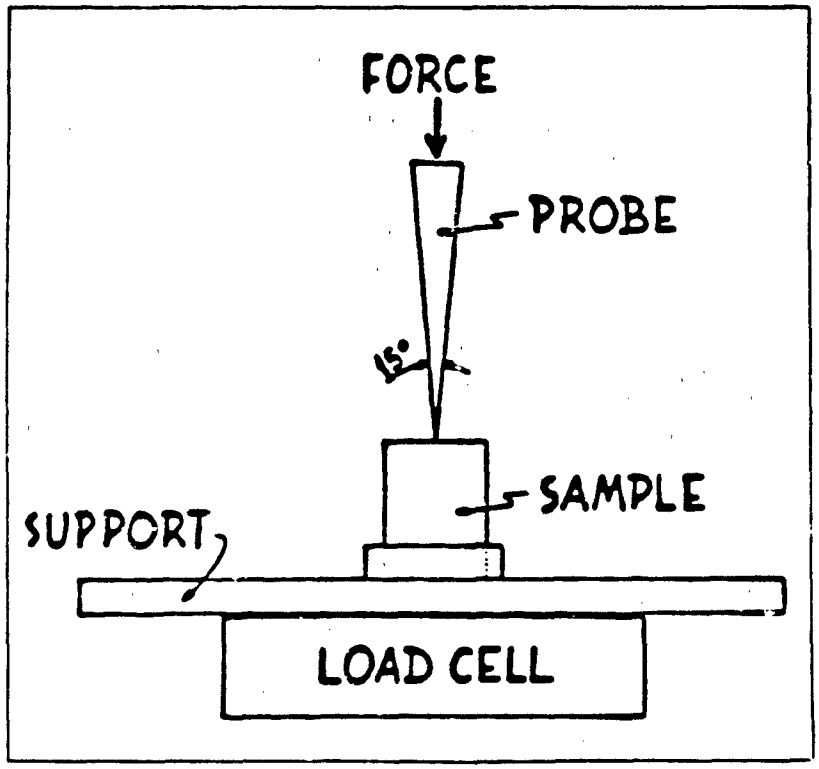
REFERENCES

1. G. C. Derringer, J. Elastoplast. **3**, 230 (1971)
2. L. F. Marker, **USP** 3 570 575 (March 16, 1971)
3. K. Boustany et al., **USP** 3 697 364 (October 19, 1972) and Rubber Chem. Technol. **47**, 396 (1974)
4. A. P. Foldi, Rubber Chem. Technol. **49**, 379 (1976)
5. A. P. Foldi et al., J. Industrial Fabrics, **1**, #2 (1982)
6. C. T. R. Pulford: " Failure of Rubber by Abrasion" (ACS Rubber Div. Mtg., Indianapolis, May 1984)
7. A. G. Thomas and E. Southern: " Plastics and Rubber : Materials and Application", November 1978, p. 133
8. A. Schallamach, Trans. Inst. Rubber Ind., **28**, 256 (1952)
9. A. P. Foldi and W. Nuesch, Paper presented at the Scandinavian Rubber Conference, Copenhagen, June 11, 1985
10. A. P. Foldi, Poster presentation at the Thirty-second Sagamore Army Materials Research Conference, Lake Lucerne, NY, July 25, 1985

APPENDIX

PENETRATION RESISTANCE TEST

A four-sided, polished steel pyramid with a 15° angle at the apex was forced into a 12.7 mm diameter, 25.4 mm high rubber cylinder in which the fibers were oriented either parallel to the axis or perpendicular to it. The force required to move the pyramid 19 mm into the cylinder, held in place by a narrow steel collar, was used to describe penetration resistance. The probe was honed to an extremely sharp (yet 15°) point. Wet testing was performed by first placing a drop of water on the cylinder's face through which the probe was then pushed.



Schematic of Penetration Resistance Test

OLIGOMERIC DIAMINOBENZOATES - A UNIQUE CLASS OF LONG-CHAIN REACTIVE AMINES

D. J. FINOCCHIO AND E. L. McINNIS *
Polaroid Corporation, Commercial Chemicals Department, 238 S. Main Street, Assonet, MA 02702

ABSTRACT

Oligomeric diaminobenzoates (ODAs) represent a unique class of reactive amines which have utility in the areas of cast urethane elastomers, coatings, and rubber-modified epoxies[1].

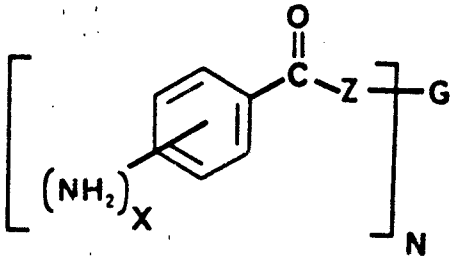


FIGURE 1. Oligomeric Diaminobenzoates; X = 1, 2, or 3, Z = O or NH, G = N valent radical, N = 2, 3, or 4

The reactivity of the aromatic amine is modified by the neighboring carboxylate group[2] so that controlled polymerizations with methylene diphenylisocyanate (MDI) can be effected, a capability not found with other reactive amines.

Although a number of different backbone materials have been examined (G = polycarbonate, polypropyleneoxide, and polyester), optimization and characterization efforts have centered on the di-p-aminobenzoate containing a polytetra-

methyleneoxide backbone (Figure 2)

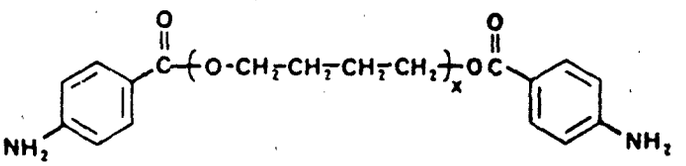


FIGURE 2. Polytetramethyleneglycol Oligomeric di-p-amino-benzoate (PTMEG-ODA) X = 13.6, ODA-1000, X = 27.5, ODA-2000.

The true benefits of ODA-MDI formulations derive from the fact that these systems are liquid-liquid and can be cured at room temperature. The tensile and hardness properties of an ODA 1000-modified MDI system cured at ambient temperature develop rapidly (Figure 3).

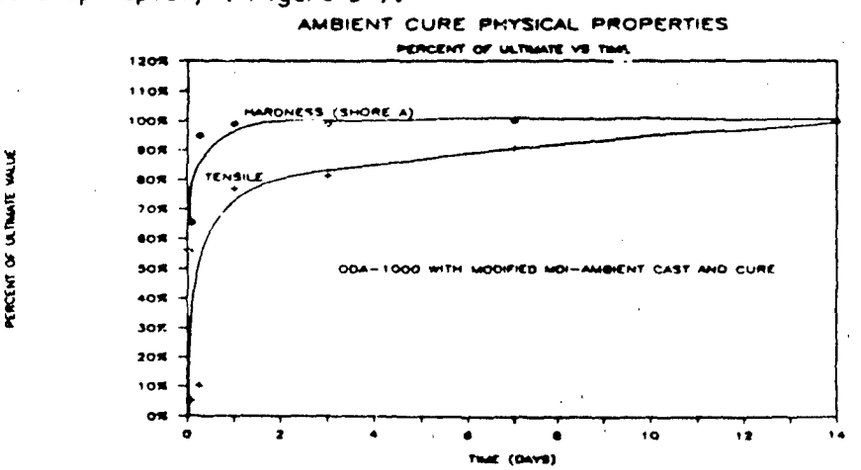


FIGURE 3. The development of hardness and tensile properties for an ambiently processed and cured ODA-1000

In many applications, the time to gelation (pot-life) and the exotherm associated with the curing reaction are important considerations. ODA-MDI systems can be catalyzed

with traditional acid or amine catalysts to obtain pot-lives as low as 1 minute without sacrificing physical properties (Figure 4).

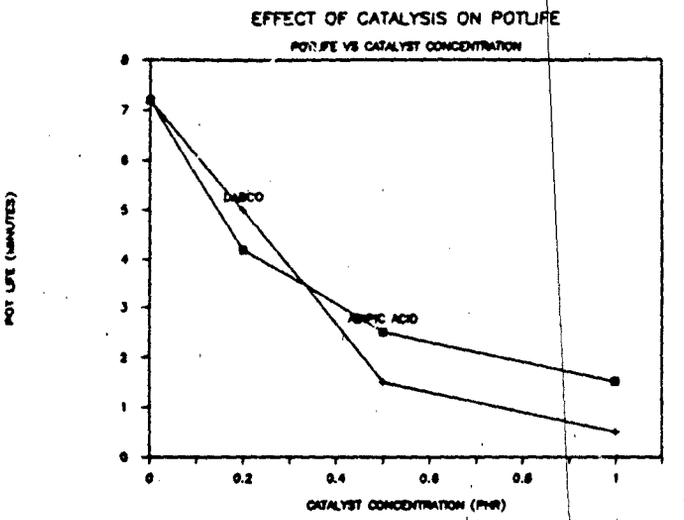


FIGURE 4. Effect of triethylenediamine or 1, 4-diaza [2.2.2] bicyclooctane (DABCO) and Adipic Acid on ODA-MDI Pot-Life.

Moderate exotherms are observed in both catalyzed and uncatalyzed systems cured at room temperature (Figure 5).

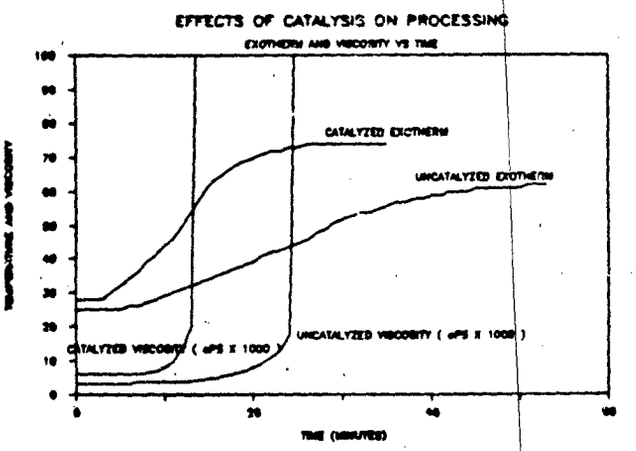


FIGURE 5. Effect of Catalysis on ODA-MDI Viscosity and Exotherm Profiles.

A high performance elastomer can be prepared under conditions in which elaborate processing and curing equipment is not available (Table 1).

TABLE 1

PHYSICAL PROPERTIES OF ODA-1000-MDI FORMULATIONS CURED AT ROOM TEMPERATURE

MDI	RUBINATE® XI-208	ISONATE® 143-L	ISONATE® 240 1	ISONATE® 181
% NCO	31	29	19	23
Cure Temp. (°C)	25	25	25	25
Cure Time (Days)	7	7	7	7
Tensile	10000	5800	7500	5200
Elongation	420	460	510	690
100 % Modulus	1230	1000	1000	970
300 % Modulus	2100	1400	1200	970
Tear Die-C	370	420	400	410
Tear D-470	110	150	120	120
Hardness	95A	95A	95A	95A
Rebound	53	49	56	55
Compression Set	64	49	64	75

Isonate® is the registered trademark of the Upjohn Company and Rubinate® is the registered trademark of Rubicon Chemicals Inc.

Deficiencies in the compression set of ODA-MDI can be remedied by increasing the extent of crosslinking present in the elastomer. This has been accomplished by incorporating a trifunctional polypropyleneoxide ODA (PPG-ODA) in the formulation. Compression set decreases linearly with increasing trifunctional ODA content (Figure 6).

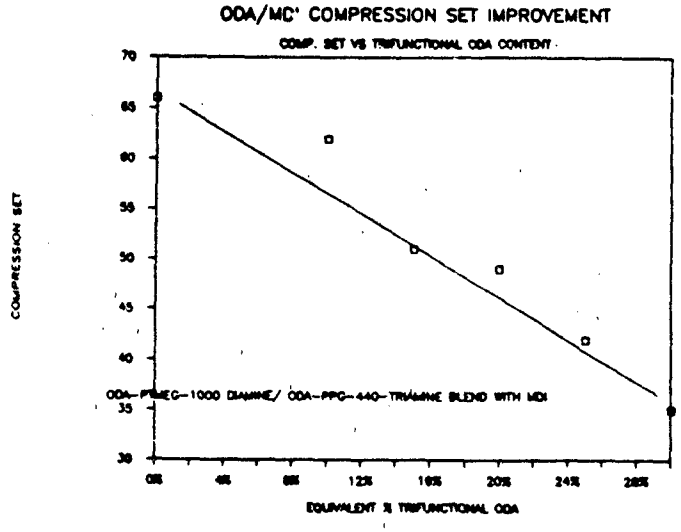


FIGURE 6. Effect of Increasing Trifunctional ODA Content on Elastomer Compression Set

REFERENCES

1. U. S. Patent 4,328,322
2. Baron, Cerankowski, Mattucci, and Taylor, J. Appl. Polym. Sci., 20(1):285-286.

STRETCHING IN AN ELASTOMER CYLINDER DURING AN AXIAL PROBE PENETRATION

A. R. JOHNSON [1], C. J. QUIGLEY [1], I. FRIED [2]
(1)Mechanics of Materials Branch, Mechanics and Structural Integrity Laboratory, U. S. Army Materials and Mechanics Research Center, Watertown, Massachusetts 02172-0001; (2)Department of Mathematics, Boston University, 111 Cummington Street, Boston, Massachusetts 02215.

ABSTRACT

A finite element algorithm is developed to analyze elastomer cylinders subjected to axisymmetric probe loading. A form of the Valanis - Landel energy density functional is used to model the material behavior of the elastomer. The nonlinear finite element equations are found by computing the gradient and tangent matrices of the total potential energy and are solved using the Newton - Raphson method. A penalty method, based on minimizing the distance between the probe surface and the contacting nodes in the finite element mesh of the elastomer, is used to model the probe loading. Stretch ratios in excess of 2.0 are computed for a 0.25 in. radius hemispherical ended probe penetrating 0.50 in. into a 1.0 in. radius cylinder 2.0 in long.

INTRODUCTION

The Army is evaluating new elastomer materials for use in tank track pads. The pads are repeatedly loaded to large strains when the tank travels on roads and to larger strains when the pad is penetrated by sharp objects or rocks off the road. In the process of evaluating the new materials, cylindrical samples are tested in the laboratory. This poster paper summarizes a finite element algorithm developed to analyze an elastomer cylinder axially loaded by a hemispherically ended probe penetrator.

LARGE AXISYMMETRIC DEFORMATIONS

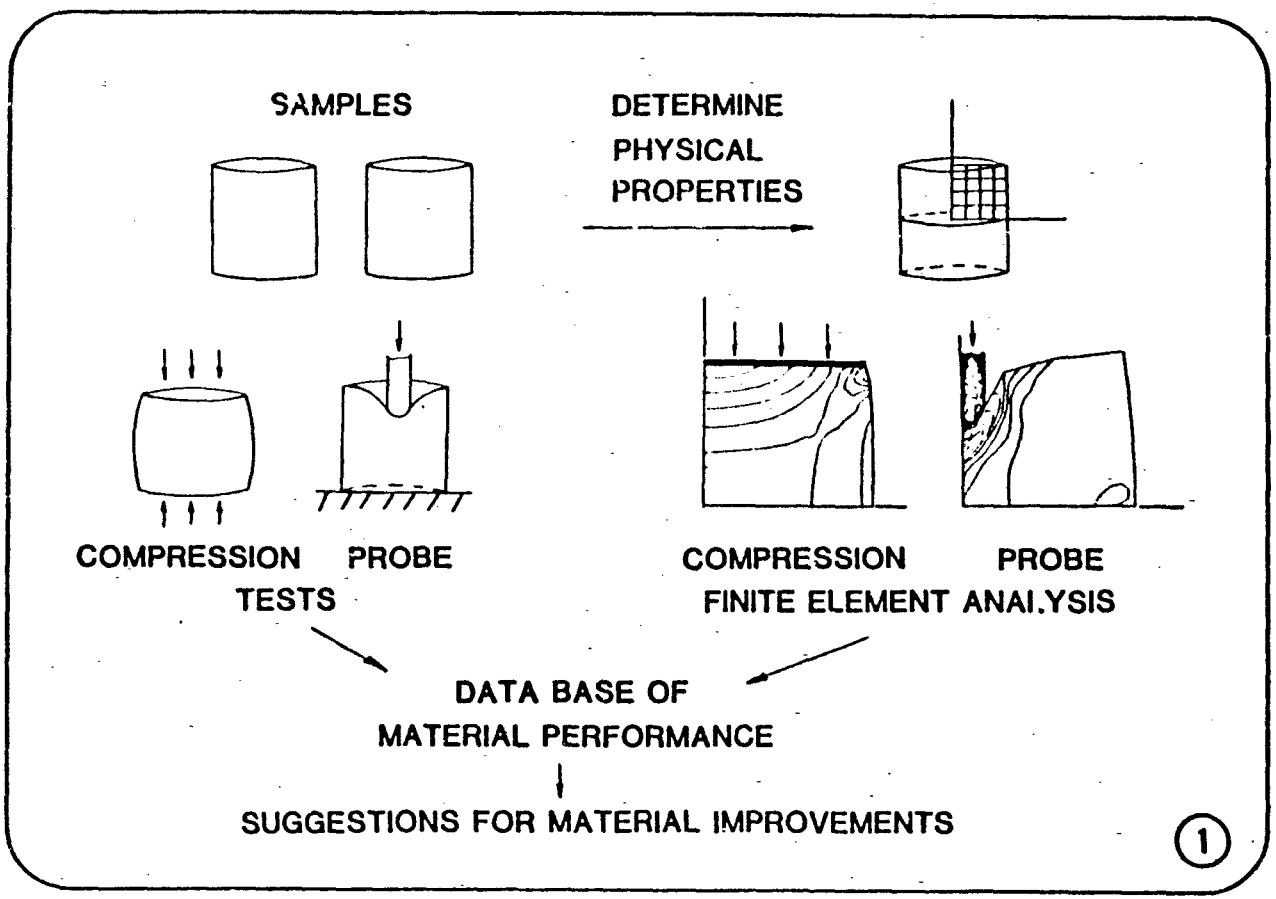
The relationship between the testing and analysis is shown in Illustration 1.* Materials are tested and data is collected at a limited number of points (heat buildup at center, strains on outside, etc.) The analysis effort allows for field representation of the strains, temperatures, etc. and assists the analyst in understanding the details of the response. The notation used to describe the axisymmetric deformations is shown in Illustration 2. The line segment $\bar{\delta}_1$ represents an infinitesimal material line at angle θ as shown in the undeformed cylinder. After deformation the line segment stretches and rotates to $\bar{\delta}_2$. The constitutive relations for elastomers require that the principal stretch ratios (maximum and minimum values of $|\bar{\delta}_1|/|\bar{\delta}_2|$) be determined. The calculation of these principal stretch ratios λ_1 and λ_2 are shown on Illustrations 2 and 3 using the (α,β) coordinates to describe the undeformed material and (r,z) coordinates for the deformed.

With the principal stretch ratios λ_1 and λ_2 determined we develop an axisymmetric triangular finite element. The element is shown in Illustration 4. The potential energy is interpolated using the elements and is expressed in terms of nodal variables. The gradient and tangent matrices of the energy are then found so that the Newton - Raphson method can be used to obtain the extreme values of the energy. Illustration 5 shows the bilinear interpolation used. Then, Illustrations 6 through 10 present some of the details of the computations of the gradient and tangent matrices.

A summary of the finite element algorithm developed here is shown in Illustration 11 followed by an example showing some details of how to use the Valanis - Landel form of the energy density in Illustration 12. Plots of the deformed mesh, profiles of radial and axial displacements, profiles of the principal stretch ratios λ_1, λ_2 and λ_3, and the profiles of $\sqrt{I_3}$ (representing the volume change) are given in Illustrations 13 through 19 for a 35% probe penetration as described in the abstract.

---

* Illustration numbers are given at the bottom right-hand corner of each illustration.


SAMPLES
DETERMINE
PHYSICAL
PROPERTIES
COMPRESSION
TESTS
PROBE
COMPRESSION
FINITE ELEMENT
PROBE
ANAI.YSIS
DATA BASE OF
MATERIAL PERFORMANCE
SUGGESTIONS FOR MATERIAL IMPROVEMENTS
1

LARGE AXISYMMETRIC DEFORMATIONS

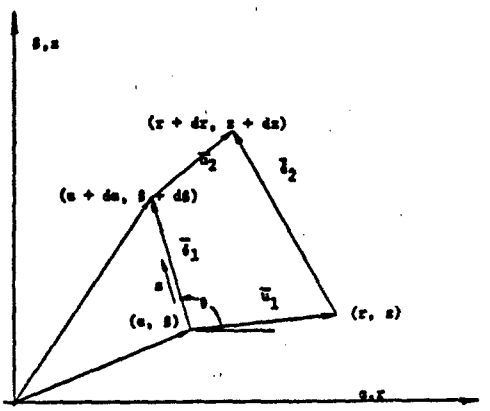


Figure 1. Notation for material line deformations.

Geometry

$$\bar{\delta}_1(\theta) = d\alpha\hat{\alpha} + d\beta\hat{\beta} = (\cos\theta\ \hat{\alpha} + \sin\theta\ \hat{\beta})ds$$

$$\bar{\delta}_2(\theta) = dr\hat{\alpha} + dz\hat{\beta} = (r_s\hat{\alpha} + z_s\hat{\beta})ds$$

Stretch Ratio

$$\lambda(\theta) = |\bar{\delta}_2| \ / \ |\bar{\delta}_1| = (\ r_s^{\,2} + z_s^{\,2})^{1/2}$$

Total Langrangian Assumption

$$r = r(\alpha(s),\beta(s))$$

$$z = z(\alpha(s),\beta(s))$$

(2)

PRINCIPAL STRETCH RATIOS

$$r_s = r_\alpha \cos(\theta) + r_\beta \sin(\theta)$$

$$z_s = z_\alpha \cos(\theta) + z_\beta \sin(\theta)$$

$$\lambda^2(\theta) = (r_\alpha^2 + z_\alpha^2)\cos^2(\theta) + 2(r_\alpha r_\beta + z_\alpha z_\beta)\cos(\theta)\sin(\theta) + (r_\beta^2 + z_\beta^2)\sin^2(\theta)$$

$$\lambda^2(\theta) = [\cos\theta \ \sin\theta] \begin{bmatrix} r_\alpha^2 + z_\alpha^2 & r_\alpha r_\beta + z_\alpha z_\beta \\ r_\alpha r_\beta + z_\alpha z_\beta & r_\beta^2 + z_\beta^2 \end{bmatrix} \begin{bmatrix} \cos\theta \\ \sin\theta \end{bmatrix}$$

Eigenvalue analysis yields

$$\lambda_1^2 = 1/2(A + B + ((A - B)^2 + 4C^2)^{1/2})$$

$$\lambda_2^2 = 1/2(A + B - ((A - B)^2 + 4C^2)^{1/2})$$

where

$$A = r_\alpha^2 + r_\beta^2$$

$$B = r_\beta^2 + z_\beta^2$$

and

$$C = r_\alpha r_\beta + z_\alpha z_\beta$$

Hoop Stress Ratio

$$\lambda_3^2 = r^2/a^2$$

(3)

FINITE ELEMENT FORMULATION

$$\Pi = \int_\tau U(\lambda_1,\lambda_2,\lambda_3)\, d\tau - W$$

$$\lambda_i = \lambda_i(r_1,z_1,r_2,z_2,r_3,z_3) = \lambda_i(u)$$

Gradient

$$g = \frac{\partial \Pi}{\partial u^T} = \pi r_c \Delta \frac{\partial U}{\partial u^T} - \frac{\partial W}{\partial u^T}$$

Tangent Matrix

$$k = \frac{\partial^2 \Pi}{\partial u \partial u^T} = \pi r_c \Delta \frac{\partial^2 U}{\partial u \partial u^T} - \frac{\partial^2 W}{\partial u \partial u^T}$$

Triangular 3 – Node Element

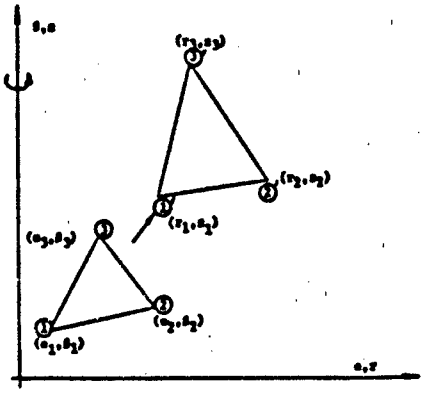


Figure 1. Node numbering and coordinates for element.

$$d\alpha_1 = \alpha_3 - \alpha_2 \qquad d\alpha_2 = \alpha_1 - \alpha_3 \qquad d\alpha_1 + d\alpha_2 + d\alpha_3 = 0$$

$$d\beta_1 = \beta_3 - \beta_2 \qquad d\beta_2 = \beta_1 - \beta_3 \qquad d\beta_1 + d\beta_2 + d\beta_3 = 0$$

(4)

Bilinear Interpolation

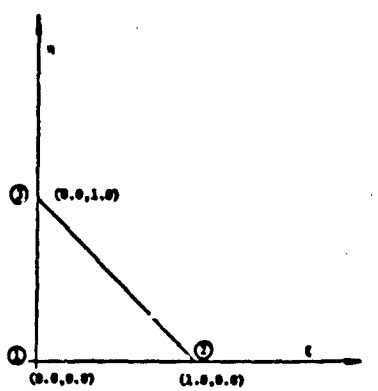


Figure 3. Unit triangle used for interpolation.

$$\alpha = \alpha_1(1 - \xi - \eta) + \alpha_2\xi + \alpha_3\eta$$

$$\beta = \beta_1(1 - \xi - \eta) + \beta_2\xi + \beta_3\eta$$

$$\begin{bmatrix} d\xi \\ d\eta \end{bmatrix} = \frac{1}{\Delta}\begin{bmatrix} -d\beta_2 & d\alpha_2 \\ -d\beta_3 & d\alpha_3 \end{bmatrix}\begin{bmatrix} d\alpha \\ d\beta \end{bmatrix} \quad \text{where}$$

$$\Delta = d\alpha_2\, d\beta_3 - d\alpha_3\, d\beta_2$$

Similarly

$$r = r_1(1 - \xi - \eta) + r_2\xi + r_3\eta$$

$$z = z_1(1 - \xi - \eta) + z_2\xi + z_3\eta$$

where

$$u^T = (r_1, z_1, r_2, z_2, r_3, z_3)$$

$$\begin{bmatrix} dr \\ dz \end{bmatrix} = \begin{bmatrix} dr_3 & -dr_2 \\ dz_3 & -dz_2 \end{bmatrix}\begin{bmatrix} d\xi \\ d\eta \end{bmatrix}$$

(5)

$$x_\alpha = -\frac{1}{A}\sum x_i\, d\beta_i \qquad x_\beta = -\frac{1}{A}\sum x_i\, d\beta_i \qquad i = 1,2,3$$

$$z_\alpha = -\frac{1}{A}\sum z_i\, d\beta_i \qquad z_\beta = -\frac{1}{A}\sum z_i\, d\alpha_i$$

STRAIN ENERGY FOR ELASTOMERS

$$U(\lambda_1,\lambda_2,\lambda_3) = \sum F(\lambda_i)$$

GRADIENT OF U (ELEMENT LEVEL)

$$u^T = (x_1, z_1, x_2, z_2, x_3, z_3)$$

$$\frac{\partial U}{\partial u^T} = \sum_{i=1}^{3} U_i\, \lambda_{i,u}$$

where

$$U_i = U_{,\lambda i}$$

$$\lambda_{i,u} = \begin{bmatrix} \lambda_{i,x1} \\ \lambda_{i,z1} \\ \cdot \\ \cdot \\ \cdot \\ \lambda_{i,z3} \end{bmatrix}$$

TANGENT MATRIX FOR U

$$\frac{\partial^2 U}{\partial u\, \partial u^T} = \sum_{i=1}^{3} \left[U_{ii}\lambda_{i,u}\lambda_{i,u}^T + U_i\lambda_{i,uu}\right] + \sum_{\substack{i=1 \\ j=2,3\ (j>i)}}^{3} U_{ij}\left[\lambda_{i,u}\lambda_{j,u}^T + \lambda_{j,u}\lambda_{i,u}^T\right]$$

(6)

where

$$\lambda_{i,uu} = \begin{bmatrix} \lambda_{i,r1r1} & \lambda_{i,r1z1} & \lambda_{i,r1r2} \cdots \\ & \lambda_{i,z1z1} & \lambda_{i,z1z2} \cdots \\ \text{(sym)} & & \lambda_{i,r2r2} \cdots \end{bmatrix}$$

and

$$\lambda_{i,u}\lambda_{j,u}^{T} = \begin{bmatrix} \lambda_{i,r1} \\ \lambda_{i,z1} \\ \\ \lambda_{i,z3} \end{bmatrix} \begin{bmatrix} \lambda_{j,r1} & \lambda_{j,z1} & \cdots & \lambda_{j,z3} \end{bmatrix}$$

Calculation of $\lambda_{i,u}$ and $\lambda_{i,uu}$

$\lambda_i = \lambda_i(A,B,C) \quad i = 1,2$

$\lambda_3 = u^T\phi / a$

$\lambda_{3,u} = \phi / a$

$A = r_\alpha^2 + r_\beta^2$

$B = r_\beta^2 + z_\beta^2$

and

$C = r_\alpha r_\beta + z_\alpha z_\beta$

$$\lambda_{i,u} = \lambda_{i,A}A_{,u} + \lambda_{i,B}B_{,u} + \lambda_{i,C}C_{,u} \qquad i = 1,2$$

and

$$\lambda_{3,u} = t/a$$

(7)

$$\lambda_{i,uu} = \lambda_{i,A}A_{,uu} + \lambda_{i,B}B_{,uu} + \lambda_{i,C}C_{,uu} + \lambda_{i,AA}A_{,u}A_{,u}^T + \lambda_{i,BB}B_{,u}B_{,u}^T + \lambda_{i,CC}C_{,u}C_{,u}^T + \lambda_{i,AB}(A_{,u}B_{,u}^T + B_{,u}A_{,u}^T) + \lambda_{i,AC}(A_{,u}C_{,u}^T + C_{,u}A_{,u}^T) + \lambda_{i,BC}(B_{,u}C_{,u}^T + C_{,u}B_{,u}^T)$$

$i = 1,2$

and

$$\lambda_{3,uu} = 0$$

Calculation of $A_u\ A_{uu}\ B_u\ B_{uu}\ C_u\ C_{uu}$

$$r_c = (r_1 + r_2 + r_3)/3 = u^T t$$

$$r_\alpha = u^T p \qquad z_\alpha = u^T q$$

$$r_\beta = u^T r \qquad z_\beta = u^T s$$

where

$$p^T = -1/\Delta\ [d\theta_1\ 0\ d\theta_2\ 0\ d\theta_3\ 0]$$

$$q^T = -1/\Delta\ [0\ d\theta_1\ 0\ d\theta_2\ 0\ d\theta_3]$$

$$r^T = 1/\Delta\ [d\alpha_1\ 0\ d\alpha_2\ 0\ d\alpha_3\ 0]$$

$$s^T = 1/\Delta\ [0\ d\alpha_1\ 0\ d\alpha_2\ 0\ d\alpha_3]$$

(8)

Then,

$$A = u^T[pp^T + qq^T]u$$
$$B = u^T[rr^T + ss^T]u$$
$$C = u^T[pr^T + rp^T]u$$

$$A_{,u} = 2[x_\alpha p + z_\alpha q] \qquad B_{,u} = 2[x_\beta r + z_\beta s]$$
$$A_{,uu} = 2[pp^T + qq^T] \qquad B_{,uu} = 2[rr^T + ss^T]$$

and

$$C_{,u} = x_\alpha r + x_\beta p + z_\alpha s + z_\beta q$$
$$C_{,uu} = pr^T + rp^T + qs^T + sq^T$$

$\lambda_{i,A} \quad \lambda_{i,B} \quad \lambda_{i,C} \quad \lambda_{i,AA} \quad \cdots$

$$\lambda_1^2 = 1/2(A + B + ((A - B)^2 + 4C^2)^{1/2})$$

$$\lambda_2^2 = 1/2(A + B - ((A - B)^2 + 4C^2)^{1/2})$$

$$\lambda_{1,A} = \frac{1}{4\lambda_1}\left[1 + \frac{A - B}{\lambda_1^2 - \lambda_2^2}\right]$$

$$\lambda_{1,B} = \frac{1}{\lambda_1}\left[\frac{1}{2} - \lambda_1\lambda_{1,A}\right]$$

(9)

$$\lambda_{1,C} = \frac{C}{\lambda_1[\lambda_1^2 - \lambda_2^2]}$$

$$\lambda_{2,A} = \frac{1}{\lambda_2}\left[\frac{1}{2} - \lambda_1\lambda_{1'A}\right]$$

$$\lambda_{2,B} = \frac{\lambda_1\lambda_{1,A}}{\lambda_2}$$

$$\lambda_{2,C} = \frac{-\lambda_1\lambda_{1,C}}{\lambda_2}$$

$$\lambda_{1,AA} = \frac{1}{\lambda_1}\left[\frac{1}{4}\frac{(\lambda_1^2 - \lambda_2^2) - 2(A - B)(\lambda_1\lambda_{1,A} - \lambda_2\lambda_{2,A})}{(\lambda_1^2 - \lambda_2^2)^2} - \lambda_{1,A}^2\right]$$

$$\lambda_{1,AB} = -\lambda_{1,AA} - \frac{\lambda_{1,A}}{2\lambda_1^2}$$

$$\lambda_{1,AC} = \frac{1}{\lambda_1}\left[\frac{2C(\lambda_2\lambda_{2,A} - \lambda_1\lambda_{1,A})}{(\lambda_1^2 - \lambda_1^2)^2} - \lambda_{1,A}\lambda_{1,C}\right]$$

$$\lambda_{2,AA} = -\frac{1}{\lambda_2}\left[\lambda_{1,A}^2 + \lambda_{2,A}^2 + \lambda_1\lambda_{1,AA}\right]$$

$$\lambda_{2,AB} = -\frac{1}{\lambda_2}\left[\lambda_{1,A}\lambda_{1,B} + \lambda_{2,A}\lambda_{2,B} + \lambda_1\lambda_{1,AB}\right]$$

$$\lambda_{2,AC} = -\frac{1}{\lambda_2}\left[\lambda_{1,A}\lambda_{1,C} + \lambda_{2,A}\lambda_{2,C} + \lambda_1\lambda_{1,AC}\right]$$

$$\lambda_{1,BB} = -\frac{1}{\lambda_1}\left[\lambda_{1,A}\lambda_{1,B} + \lambda_{1,B}^2 + \lambda_1\lambda_{1,AB}\right]$$

$$\lambda_{1,BC} = -\frac{1}{\lambda_1}\left[\lambda_{1,A}\lambda_{1,C} + \lambda_{1,B}\lambda_{1,C} + \lambda_1\lambda_{1,AC}\right]$$

$$\lambda_{2,BC} = -\frac{1}{\lambda_2}\left[\lambda_{1,B}\lambda_{1,C} + \lambda_{2,B}\lambda_{2,C} + \lambda_1\lambda_{1,BC}\right]$$

(10)

$$\lambda_{1,cc} = \frac{1}{\lambda_1}\left[\frac{(\lambda_1^2 - \lambda_2^2) - 2C(\lambda_1\lambda_{1,C} - \lambda_2\lambda_{2,C})}{(\lambda_1^2 - \lambda_2^2)^2} - \lambda_{1,C}^2\right]$$

and

$$\lambda_{2,cc} = -\frac{1}{\lambda_2}\left[\lambda_{1,C}^2 + \lambda_{2,C}^2 + \lambda_1\lambda_{1,cc}\right]$$

SUMMARY

$$\Pi = \nu r_c \Delta U - W$$

$$g = \frac{\partial \Pi}{\partial u^T} = \nu r_c A \frac{\partial U}{\partial u^T} - \frac{\partial W}{\partial u^T}$$

and

$$k = \frac{\partial^2 \Pi}{\partial u \partial u^T} = \nu r_c A \frac{\partial^2 U}{\partial u \partial u^T} - \frac{\partial^2 W}{\partial u \partial u^T}$$

Newton - Raphson

$$u_2 = u_1 - k_1^{-1} g_1$$

(11)

MATERIALS

Valanis – Landel

$$U = 1/2\ \hat{\lambda}\ [\ln(\lambda_1\lambda_2\lambda_3)]^2 + 2\mu \sum_{i=1}^{3} \lambda_i[\ln(\lambda_i) - 1]$$

where $\hat{\lambda}$, μ = the Lamé constants.

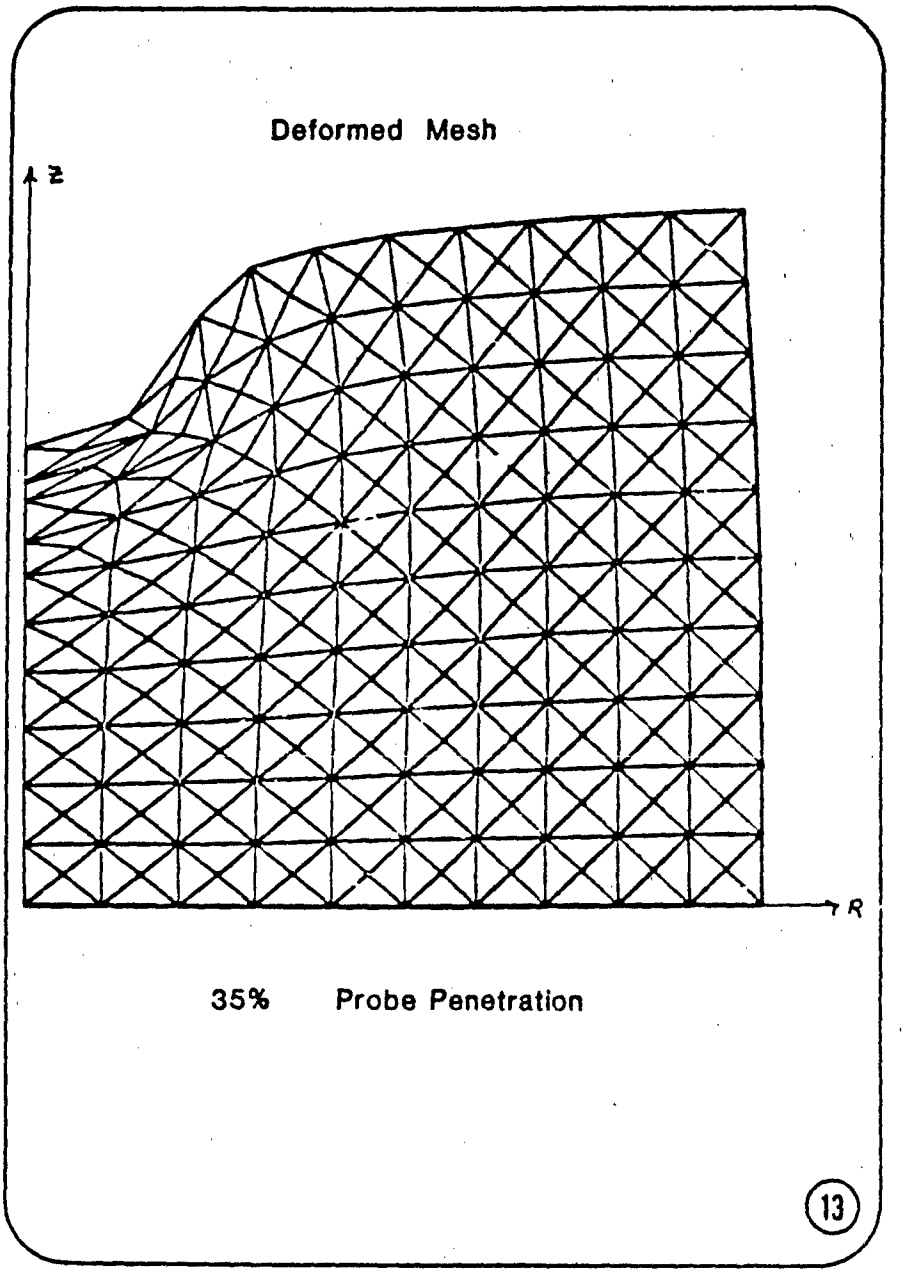
$$U_i = \frac{\hat{\lambda}}{\lambda_i} \ln(\lambda_1\lambda_2\lambda_3) + 2\mu \ln(\lambda_i) \qquad i=1,2,3$$

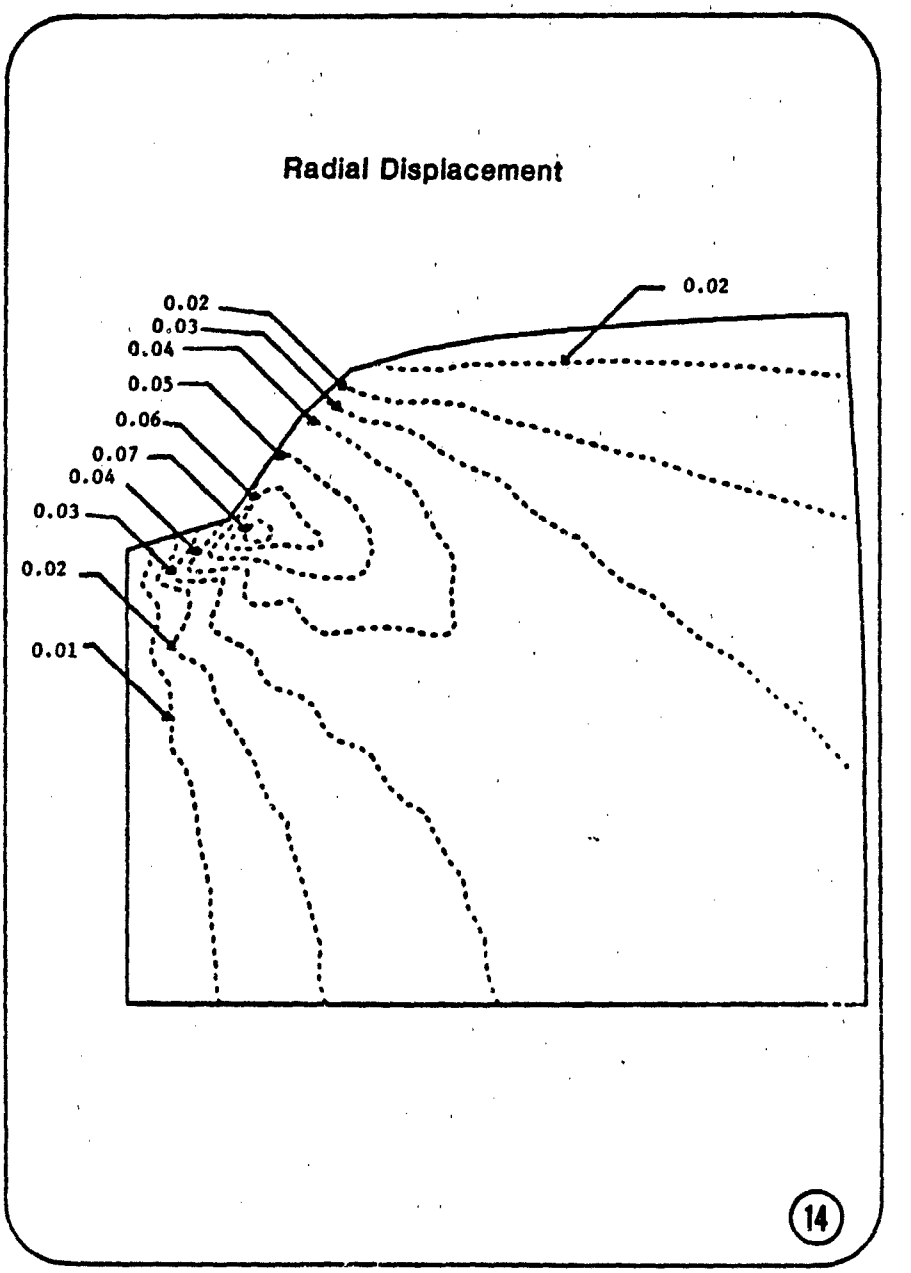
$$U_{ii} = \frac{1}{\lambda_i^2} [\ \hat{\lambda}[1 - \ln(\lambda_1\lambda_2\lambda_3)] + 2\mu\lambda_i] \qquad i=1,2,3$$

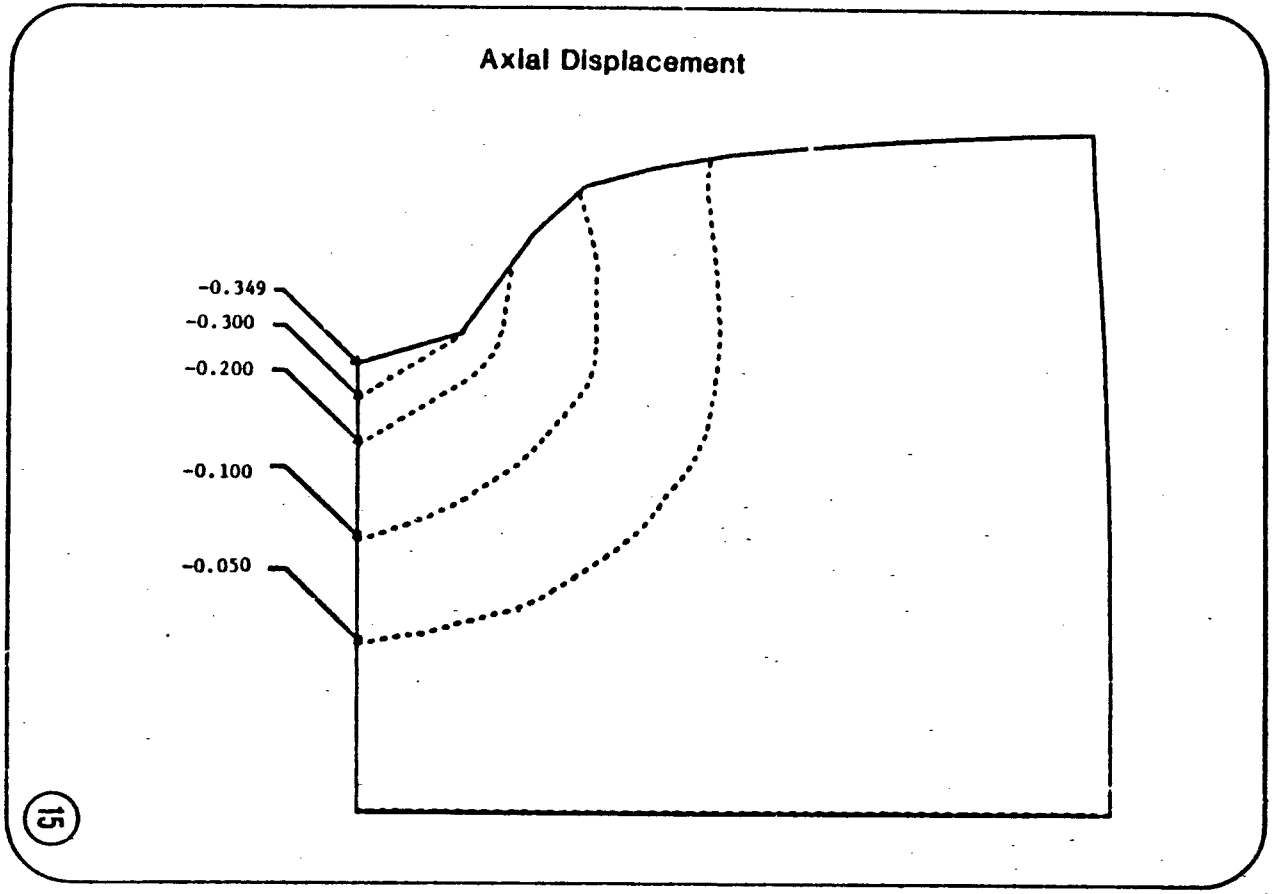
and

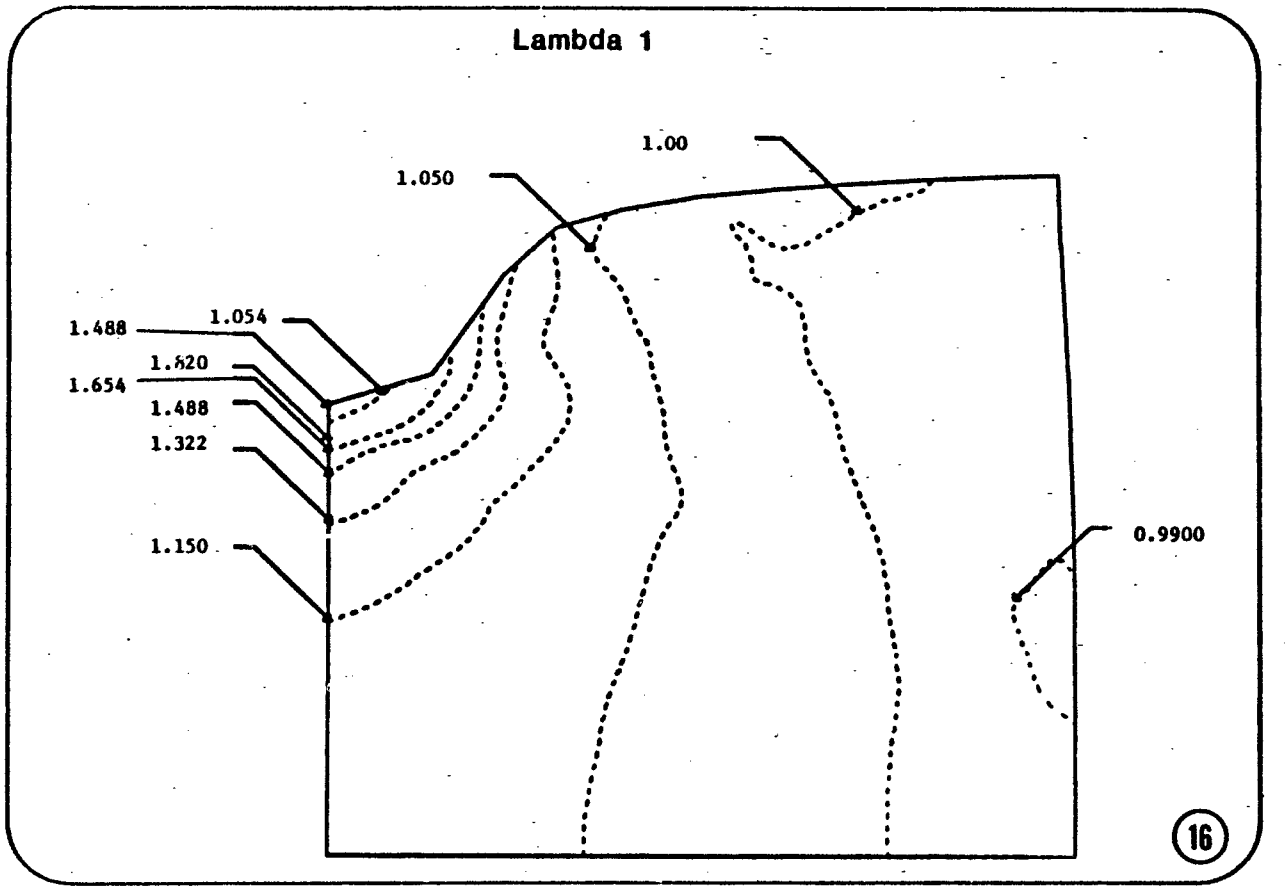
$$U_{ij} = \frac{\hat{\lambda}}{\lambda_i\lambda_j} \qquad i=1,2 \quad j=2,3 \quad j>i$$

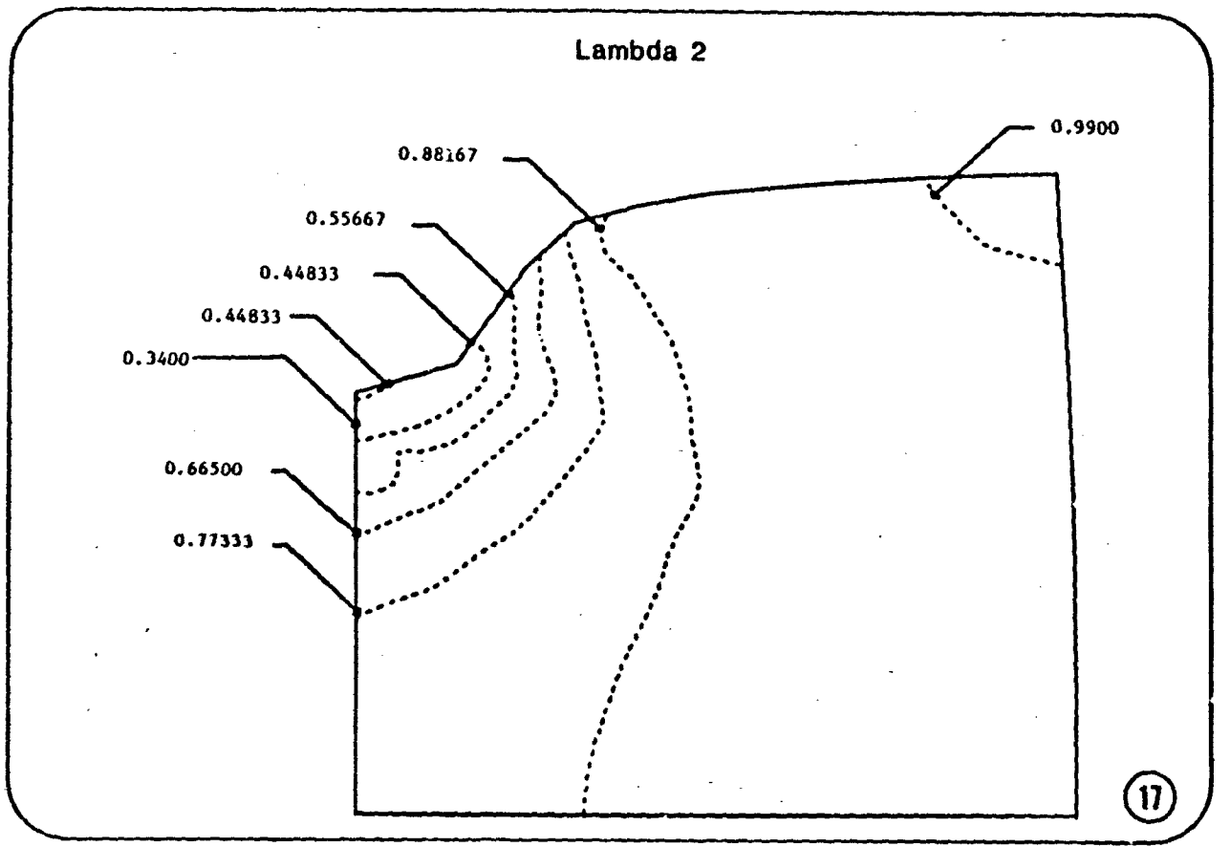
(12)

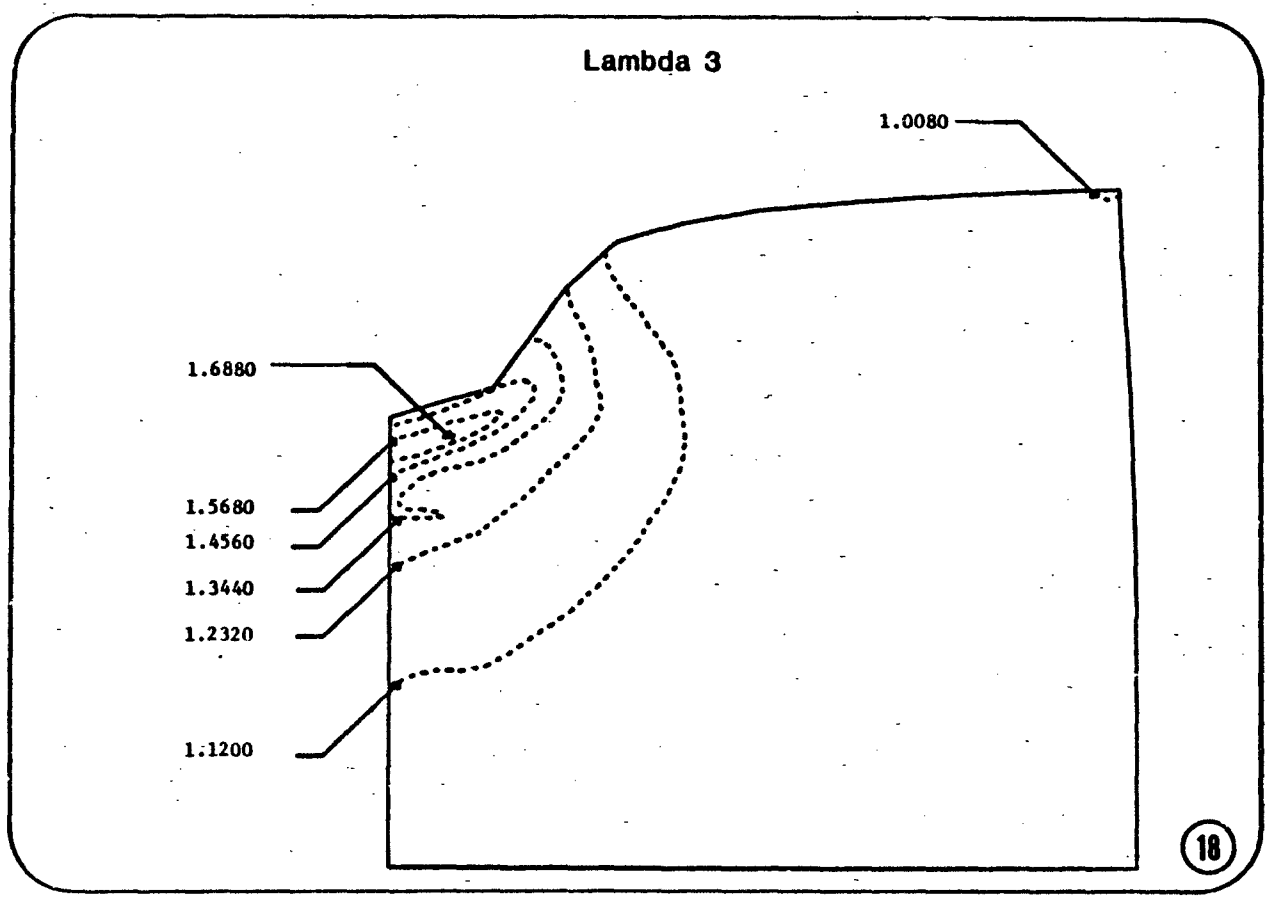

Deformed Mesh
Z
R
35% Probe Penetration
13

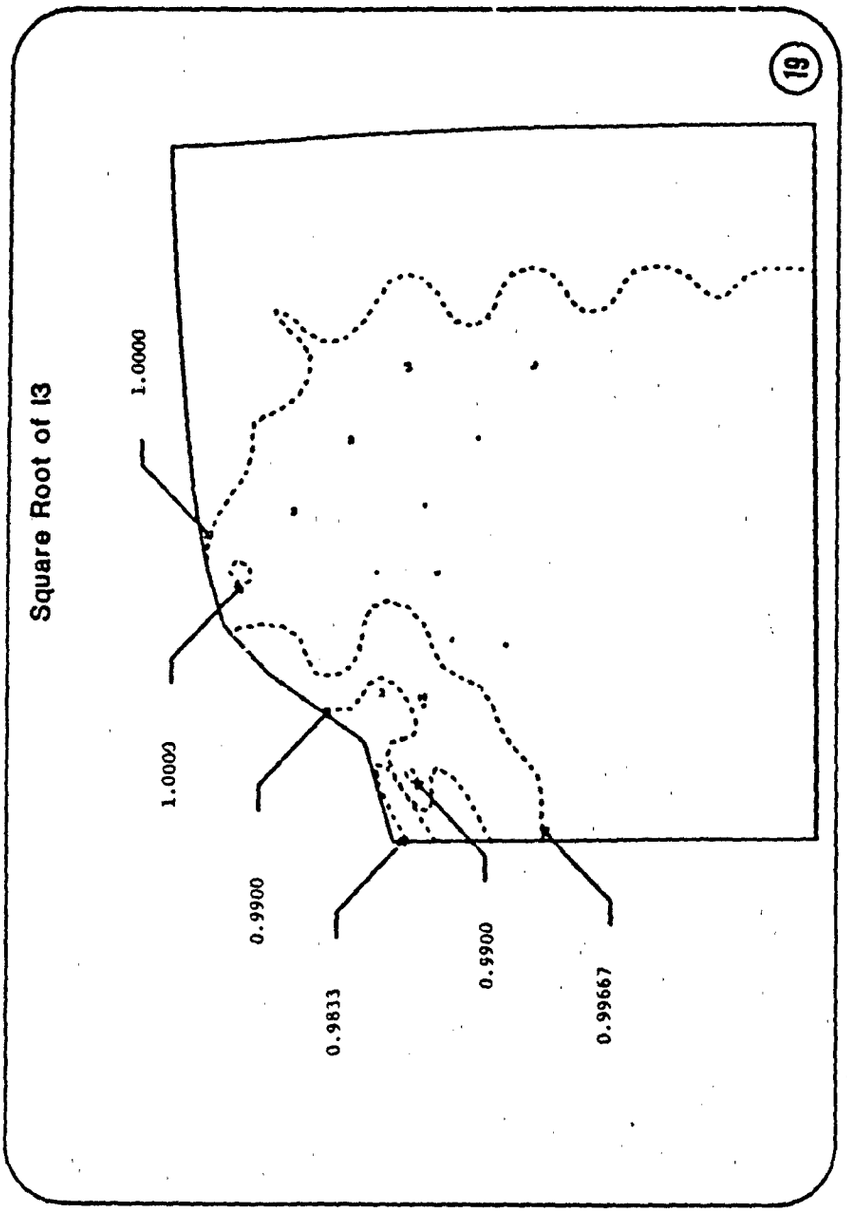

Radial Displacement
0.02
0.03
0.04
0.05
0.06
0.07
0.04
0.03
0.02
0.01
0.02
14


Axial Displacement
-0.349
-0.300
-0.200
-0.100
-0.050
15


Lambda 1
1.00
1.050
1.054
1.488
1.620
1.654
1.488
1.322
1.150
0.9900
16


Lambda 2
0.9900
0.88167
0.55667
0.44833
0.44833
0.3400
0.66500
0.77333
17


Lambda 3
1.0080
1.6880
1.5680
1.4560
1.3440
1.2320
1.1200
18


19
Square Root of I3
1.0000
1.0000
0.9900
0.9833
0.9900
0.99667

TRACK PAD MATERIALS STUDY

C. DEARDOFF
FMC Corporation, 1105 Coleman Avenue, Box 1201, San Jose, California 95108

ABSTRACT

Track pad performance and durability depend largely upon its elastomeric material of construction and environmental service terrain. With greater knowledge of elastomer chemistry, wear and failure mechanisms can be explained. Processing variations, including the use of different molding techniques, may also play a key role in overall component performance. FMC's goal is to improve component performance by increasing material wear resistance and improving current quality control methods. Efforts to data have focused on three areas of study:

- Investigation of current production T157 track pad materials service-tested separately under cross country and paved surface conditions. The goal of this ongoing effort is to perform a trend analysis of microscopic and macroscopic wear mechanisms using thermal, surface, and chemical characterization techniques.

- Trade off study of alternative elastomer materials to maximize abrasive wear resistance. Test plans are under way to evaluate 15 compounds under paved surface conditions, select the top performers, and evaluate pad durability under cross country service.

- Investigation of the current track elastomer specification (MIL-T-11891D) to suggest modifications addressing procurement problem areas and alternate quality control provisions.

FALURE MODE INVESTIGATION OF CURRENT TRACK PAD MATERIALS

This effort began in 1984 as an IR&D project "Failure Study of Elastomeric Material for Track".

Although elastomers are located in three track locations: roadwheels, bushings, and track pads, pads were focused upon due to the severe wear problems which had been reported and the available service testing capabilities.

The goal of this work is to increase elastomer durability and longevity by identifying the molecular and microscopic failure mechanisms in track pad materials. Defining failure modes may lead to suggestions for modifying rubber mixing and/or molding procedures.

TESTING AND RESULTS

Two complete sets of T157 (M2) track pads were procured from one vendor source. Certification verified that the pads, containing the base polymer styrene butadiene rubber (SBR), were molded from the same production run.

Preservice evaluation began with the removal of material samples from two different locations on selected pads. To determine if material variations exist due to production conditions, thermal, surface, and chemical characterization testing was performed using the following techniques:

TGA: Thermal Gravimetric Analysis
TMA: Thermal Mechanical Analysis
DSC: Differential Scanning Colorimetry
SEM/EDAX: Scanning Electron Microscopy/Energy Dispersive Analysis of X-rays
Auger Spectroscopy
Optical Microscopy
Solvent Swelling.

The important material test parameters under investigation include: elastomer cross-link density, butadiene rubber content, oxidative cross-linking tendency, and variations in the material microstructure.

The track pads were then subjected to the following field tests:

1) 3000 mile test at Camp Roberts, CA, on cross country terrain

2) 350 mile test at San Jose, CA, on a paved surface, 1 km, oval track.

Work pads were removed at nine intermediate mileage intervals from designated track locations. The removed pads were the same ones from which preservice samples were previously obtained. Weight measurements were subsequently taken. Figures 1 through 3 illustrate weight loss vs. mileage results for each service test and a comparison between the two. For

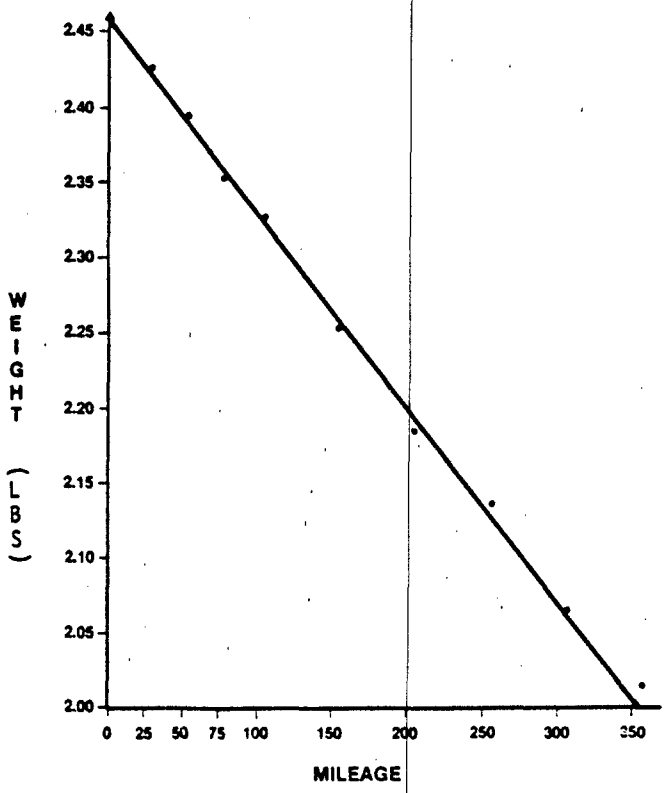


FIGURE 1. Paved wear: weight loss vs. mileage.

the first 300 miles of service, paved surface wear is 3.6 times that resulting from cross country wear.

Future plans include a trend analysis of the worn pads using the above described thermal, surface, and chemical characterization techniques and to compare these with the preservice baseline results.

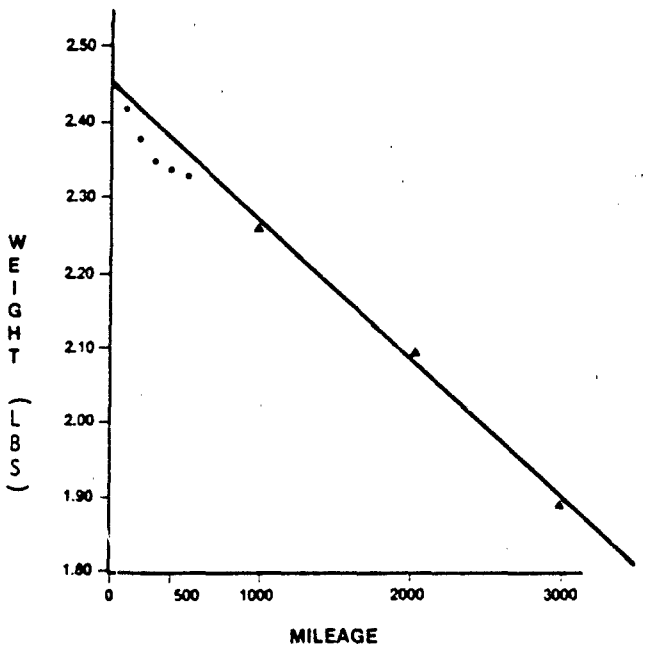


FIGURE 2. Cross country wear: weight loss vs. mileage.

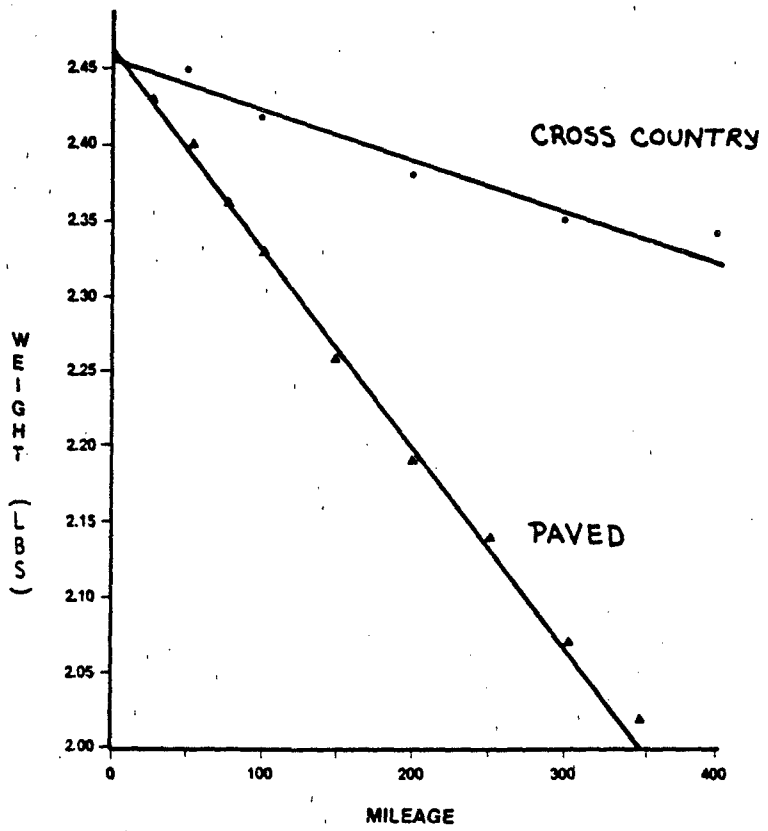


FIGURE 3. Comparison of paved and cross country wear weight loss vs. mileage.

TRADE OFF STUDY OF ALTERNATE ELASTOMER MATERIALS

This effort began in 1984 as part of an STS contract (#DAAE07-84-C-R006) titled "BFV Track Pad Life Improvement".

The goal of the project is to improve track pad abrasion resistance without significantly degrading the chunking and blowout resistance of current track pad materials. The scope of work is as follows:

1. Investigate natural rubber and other high potential candidate compounds for the T157 pad

2. Investigate increasing T157 pad thickness and/or surface area

3. Durability test the top performing material compounds determined from Task 1 with a new track design developed from Task 2 on cross country terrain

4. Investigate improving Q.C. techniques, and propose changes to MIL-T-11891D (AT) track pad procurement specification

5. Perform a trend analysis of paved worn pads (tested under the IR&D program) and compare with preservice baseline results.

To address Task 1, ten vendors were contacted and invited to participate. They were asked to submit compound information and prototype pad development requirements for materials they considered high potential for the track pad application. Although material property data were received for most of the candidate compounds, no suitable criteria exist to predict compound field performance from this information. Therefore, the field test program was developed to test a larger number of compounds than was originally anticipated.

Seven of the vendors and the two following government agencies involved in track pad elastomer R&D work:

- Ft. Belvoir Research and Development Center
  - contact: Paul Gatza

- Red River Army Depot
  - contact: George Kentros.

together, submitted a total of 15 material compounds for our evaluation.

A paved surface field evaluation has been completed. The test program involved five separate vehicle tests designed to evaluate three experimental compounds per test. The following lists important test parameters:

Course: FMC, San Jose, 1 km, paved oval track

Duration: 300 miles, (where track direction was changed every 12.5 miles)

Period of Performance: 7/85 to 10/85

Vehicle Weight: 50,000 $\pm$ 1000 lbs.

(ballisted)

Vehicle Speed: Constant lap speed, approximately 37 mph.

Consistency from test to test was of primary importance. Besides the above weight and speed parameters, vehicle stop times and the refueling schedule were held as consistent as possible. No pivot turns (which cause severe pad abrasion) were allowed at any time during testing. Pad height and weight measurement were made. Data analysis is scheduled for completion by end of 1985.

Figure 4 illustrates the track pad configuration used for field testing.

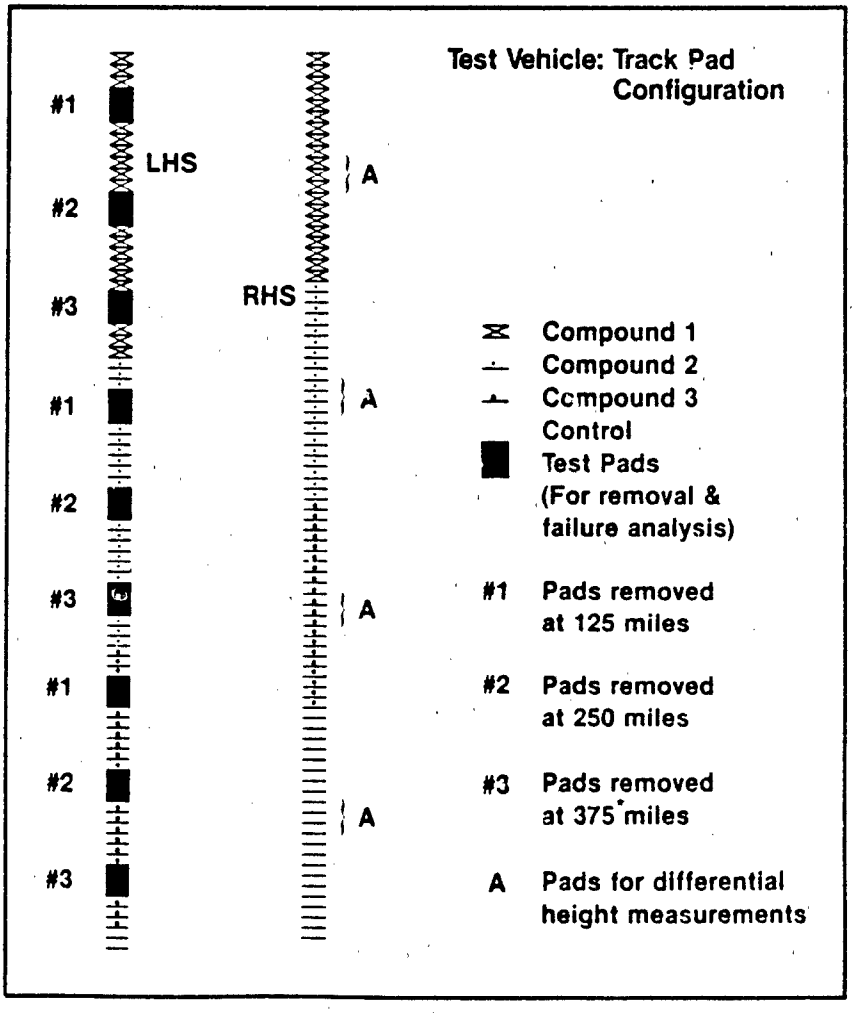


FIGURE 4. Test track configuration.

PROCUREMENT SPECIFICATION, PROBLEM AREAS, AND ALTERNATE QUALITY CONTROL PROVISIONS

Background

Changes to the long standing track procurement specification, MIL-T-11891B, were developed to keep pace with progressing rubber technology.

The new revisions were designed:

- To allow use of natural rubber in compound formulations
- To encourage continual improvement for elastomer formulations through cost incentive contracting
- To improve quality control by matching production material physical properties to those of qualified materials applying established tolerance constraints and infrared spectroscopy "finger printing".

Problem Areas

Although cost incentive contracting is an improvement, the necessary field testing is:

- Costly
- Time consuming
- Difficult to provide fairness to each participating vendor.

In addition, quality control which relies on end item defect detection, is outdated in view of statistical process control (SPC) techniques.

FMC's Commitment

FMC will investigate:

- The development of track pad material test methodology which can accelerate or otherwise improve the qualification process
- The application of SPC techniques to suggest modifications to the existing procurement

specification. SPC is working for the automotive industry, not only to improve product quality, but to lower production costs as well.

These investigations represent FMC's comprehensive commitment to solving track pad problems.

CONCLUSION

There does not appear to be any quick relief solutions to costly track pad wear problems. The ultimate solutions will evolve from the combined efforts of many; therefore, communication for information exchange is vital.

ACKNOWLEDGEMENTS

FMC Ordnance Engineering Staff:

W. Grusonik, manager, mechanical design: suspension group

H. R. Nick Lawrence, deputy program manager, combat vehicles

S. Ellery, technical leader, composite structure: component development

W. Bilkiewicz, senior staff engineer, mechanicl design: suspension group

D. Bird, manager: Purchasing Department

FMC Central Engineering Laboratory:

L. Peters, supervisor, non-metallics laboratory section

D. Beasley, D. Diaz, technicians.

HIGH PERFORMANCE POLYURETHANE ELASTOMERS

ANTHONY J. CASTRO[1], WALTER BRODOWSKI[2], EJAZ SYED[3]
(1)Akzo Chemie America, 2035 9th Avenue, San Francisco, California 94115; (2)Akzo Corporate Research, Obernburg, West Germany; (3)Akzo Chemie Deventer, The Netherlands.

Polyurethane elastomers, both thermoplastic and thermoset, have long been the material of choice when a particular application demanded exceptional resistance to abrasion, solvents, toughness and/or superior dynamic properties and the concomitant increase in these physical properties was sufficient to extend the lifetime of a part so as to compensate for any increase in raw material costs as compared to traditional elastomers. A more widespread use of polyurethane elastomers has been prevented by the rather low high-temperature softening point of conventional polyurethanes and the falloff of properties as the softening point is approached.

Since the high temperature properties of segmented elastomers are strongly dependent upon the nature and content of the "hard segment" portion of a polyurethane, our laboratories have attempted to develop high performance elastomer formulations based upon the use of two simple, rod-like molecules; 1,4-trans-cyclohexane diisocyanate (CHDI) and paraphenylene diisocyanate (PPDI) as the main hard segment portion.

Although diol cured thermoplastic formulations have been obtained with softening points too high to permit injection molding, use of mixed chain extenders to selectively disturb the crystallinity of the hard segments has led to a series of injection moldable thermoplastics with softening points in the range of 175°C-210°C (347°F-410°F).

Thermoset cast elastomers have been produced based upon diol chain extenders with properties comparable to MOCA cured systems while at least one CHDI/MOCA cured elastomer did not exhibit softening behavior until beyond 265°C (510°F).

Additionally, transparent, injection moldable, aliphatic polyurethanes have been produced with softening points in the range of 150°C-175°C (300°F-350°F).

Other physical properties, such as tensile strength, modulus, abrasion resistance, etc., of CHDI and PPDI derived polymers are not sacrificed in order to achieve better high temperature resistance.

As might be expected, highly ordered, phase separated polyurethanes exhibit enhanced resistance to hydrolysis as measured by change in tensile strength after immersion in 95°C water.

SANTOWEB® FIBER REINFORCEMENT OF RUBBER COMPOUNDS

LLOYD A. WALKER[1], WILLIAM W. PARIS[1], JOHN B. HARBER[2]
(1)Monsanto Polymer Products Company, Akron, Ohio; (2)Brad Ragan Rubber Company, Radford, Virginia

1. OFF-THE-ROAD (OTR) TIRE TREADS

INTRODUCTION

The large off-the-road (OTR) mining tires of today are frequently required to meet a variety of demands, depending on the application or use. In one case, the tires used on loader vehicles are commonly exposed to very rough, sharp surfaces with the result often being chipping/chunking of treads. Since most vehicles of this type operate at very low speeds, heat generation is sometimes a factor but not nearly to the extent it is in haulage equipment where large loads are carried at relatively high speeds. In many of these latter cases, the high heat build-up may be accompanied by some chipping/chunking, particularly if abrasive surfaces are present. To date, it has generally been observed that two or more distinct types of tread compounds are used to meet particular needs. The tread is referred to particularly because the tread provides most of the contact with damage-causing surfaces. Engineering and design are, of course, also critical in obtaining optimum durability but the work reported herein is directed to compounding only. The objective of this paper is to report advances in compounding leading to improved durability of both loader and hauler tires with the same compounds.

Initial efforts have been directed toward reducing heat build-up. Major improvements were realized in an all-natural rubber compound (no synthetic rubbers), by utilizing reduced reinforcing filler levels, accompanied by increased curative levels to maintain or improve other properties ([1]). Further improvements were observed through the use of reduced sulfur together with increased accelerator or sulfur donors. The primary variables and results of that work are summarized in Table 1. It will be observed that a combination of carbon black and bydrated silica is used for reinforcement, reflecting the industry thinking related to the beneficial effects of some silica on tear strength, which property, in turn, is thought to be related to chipping/chunking resistance. Thus, one sees in this initial effort our approaches to both reduced heat build-up and chipping/chunking resistance. An important note is to be made here: heat build-up/hysteresis properties can be measured in a number of ways in laboratory tests (and can usually be confirmed in tire tests), but chipping/chunking is another matter and it is very difficult to correlate lab tests with field service. With

TABLE 1*

EFFECTS OF REDUCED FILLER/INCREASED CURATIVES
TENSILE, TEAR, AND DYNAMIC PROPERTIES

	Control	Exp 1	Exp 2	Exp 3	Exp 4
N-231 Black	45	40	40	40	40
Silica	20	12	12	12	12
Oil	6	3	3	3	3
Sulfur	2.4	2.4	2.4	1.5	1.5
MBS	0.7	-	-	-	-
TBBS	-	1.2	0.7	1.5	0.7
DTDM	-	-	0.5	-	0.9
Optimum Cure @144°C					
Heat Build-up, °C	>60	15	16	-	-
Blow-Out Time, Mins.	2	21	18	-	-
Die C Tear, kN/m	60.4	112.7	132.1	-	-
6 Hours Cure @132°C					
Heat Build-up, °C	75	-	-	18	17
Die C Tear, kN/m	34.3	-	-	103.8	97.9
Tensile Strength, MPa	19.3	-	-	28.2	27.3

*Base Compound NR 100, Zinc Oxide 5.0, Stearic Acid 2.0, 6PPD, 2.(
TMQ 2.0.

the above as a base, the results of further compounding variations to yield further improvements in durability are described. These variables include a treated cellulosic fiber (TCF*), partial replacement of natural rubber with SBR, and combinations of these with semi-E.V. cures.

EXPERIMENTAL

Mixing: All masterbatches, less curatives, were prepared in a Laboratory "00" Banbury Mixer or in a Factory #11 Banbury Mixer (for tire tests) using conventional mixing techniques. Final addition of curatives was carried out by normal mill addition/mixing at 70°C or in a #9 Banbury Mixer with a maximum temperature of 94°C.

*Monsanto's Santoweb® DX.

Processing characteristics (Mooney Scorch) were measured on the Monsanto Mooney Viscometer (ASTM D-1646-81).

Curing characteristics were determined on the Monsanto Rheometer Model R-100 at desired curing temperatures (ASTM D-2084-81. Optimum cure was taken as time to 90% of the difference of maximum torque minus minimum torque. Preparation and curing of test samples followed ASTM D-3182-74. Retreaded OTR tires for these tests were produced by the Banlug† process in Brad Ragan Rubber Company shops.

Physical properties (stress-strain) were carried out as per ASTM D-412, using the Monsanto Tensometer 500. Hardness was measured as Shore "A".

Tear tests followed the Method in ASTM D-624 for the Die C Tear Strength as well as an internally developed Trouser Tear Test ([2]) and a test to measure tear of thick specimens (more practical). The latter test is described in Appendix A.

Tests for dynamic properties (heat build-up) were carried out as prescribed in ASTM D-623 for the Goodrich Flexometer. The Monsanto Fatigue-to-Failure Tester was used for fatigue testing. Rebound was measured with the Lupke Test. Abrasion resistance was measured as per ASTM D-2228 with the Pico Abrasion Tester.

Cut growth was measured with the DeMattia Flex Tester according to ASTM D-813 and with the BFG Ring Flex Tester (measure hours to growth of a cut - usually to 5X the original cut).

Tread performance was determined by visual inspections of tires on mining vehicles.

Chipping/chunking resistance was measured with an in-house built guillotine-type instrument ([3]), which records the number of blows to chunk-out or break. See Appendix B for details of the most recent procedure.

RESULTS

Treated Cellulose Short Fibers

The past decade has seen the development of a series of cellulose short fibers made dispersible in a number of elastomers through various treatments. The major uses of these fibers have been at relatively high levels (5-30 phr) to provide composites with high green strength, increased stiffness, reduced swell, and higher load bearing capacity among other improved properties. Such levels, however, were not compatible with tire tread processing. The properties obtained did provide a basis for speculation that

†Banlug is a registered trademark of Brad Ragan Co.

lower levels might provide some resistance to external forces in a mechanical manner.

Considerable laboratory ([4]) studies were made to define any possible indicators that tire performance might be improved. Unfortunately, nothing outstanding was observed to justify tire tests other than modest increases in tear strength; in fact, both abrasion resistance and heat build-up usually are slightly off with the TCF. However, the potential for improved chipping/chunking resistance was sufficient to initiate a joint test program between our companies to evaluate the effects of the fibers in retreaded OTR tires. As a result, one fiber grade designated as TCF, was chosen for its compatibility with conventional unsaturated elastomers. Tread compounds were factory mixed and tires ranging in size from 18.00 X 33 and 24.00 X 35 for haulers to 65.35 X 33 for loaders were retreaded. Tests were carried out in rock quarries and mines in many locations in the U.S.; e.g. Georgia, Florida, Pennsylvania, New York, and others where hundreds of tires were evaluated.

Initial tests included a combination of TCF and hydrated silica (7.0 phr) in comparison with a currently used and good performing all-natural rubber tread with all-black filler and both with conventional curing systems. Compared to the above referred to laboratory test results, the results in the field were outstanding to say the least. The following lists the advantages observed in this field test:

- Very smooth tread surfaces - very little, if any, chipping/chunking. See Figures 1 and 2.
- Large reductions in wear rate (50-100% increase in tread life).
- Periods of essentially no wear over many hours of service.

The basic variables and test results are seen in Table 2, where tear and chipping/chunking tests show only very modest indications of the resulting tire performance - of both loader and some hauler tires. It should be observed that cutting was not prevented, but growth of the cut was.

Since these initial trials contained two changes - both TCF and silica - and as usual with any new changes in the factory, a very slight increase in toughness seen at the mill was a mild source of complaint, a new test without silica was begun. These were again all-natural rubber treads with reduced black levels (lower viscosity and heat build-up) plus TCF but no silica. Hundreds of tires were also involved here. Table 3 shows the major variables and results in tests similar to those in the first trials. Here the durability is still significant, with negligible chipping/chunking, but slightly shorter tread life compared to the TCF/silica combination. In addition, the lab tests show significant reductions in heat build-up for the second compound



FIGURE 1. Control tread at 1100 hours service.



FIGURE 2. TCF/Silica tread at 2800 hours service.

TABLE 2

TCF/SILICA IN OTR TREAD COMPOUNDS (100 NR)

	Control	Experimental
Carbon Black	50.00	45.00
Silica	-	7.00
TCF	-	2.50
Sulfur	2.25	2.00
TBBS	0.60	1.00
Laboratory Tests		
Shore "A" Hardness	69	67
300% Modulus, MPa	12.14	7.81
Elongation, %	522	536
Die C Tear, Kn/m	65.6	81.9
Fatigue, KC to Fail (100% Extension)	29	54
DeMattia, KC to Break	250	100
Ring Flex, Hrs. to 5X	51	56
Chipping/Chunking Resistance Blows to Break	230	300
Tire Tests		
Hours to 50% Reduction in Tread Depth	1020	2180
Appearance of Tread	Rough/chunk-outs	Smooth
Predicted Life (Hours)	2000	4000+

(no silica, low black, TCF) and it may be more advantageous for haulers in hot weather areas. Chipping/chunking results were surprisingly low here as compared with previous results, but it may also point to the effect of silica on tear strength. A summary of the test results for both of the TCF-containing treads on tread wear is seen in Figure 3. It must be emphasized again at this point that the laboratory data still is not effective in predicting tire test results.

TABLE 3

TCF IN OTR TREAD COMPOUNDS (100 NR)

		Control	Experimental
Carbon Black		50.00	42.00
Process Oil/Pine Tar		10.00	4.00
TCF		-	2.50
Sulfur		2.25	2.25
TBBS		0.65	0.75
Laboratory Results			
Shore "A" Hardness		66	65
300% Modulus, MPa		13.19	11.05
Elongation,%		501	556
Trouser Tear F_1, N		14.23	20.46
Lupke Rebound, %	@24°C	63	71
	@70°C	72	78
Rate of Rebound Decay			
@24°C	(-)	0.159	0.120
@70°C	(-)	0.129	0.095
Fatigue, KC to Fail (100% Extension)		111	78
Goodrich Flexometer			
ΔT, °C		38	19
% Set		21.2	12.3
Pico Abrasion (R.I.)		156	133
BFG Ring Flex Hours to 5X		44	77
Chipping/Chunking Resistance Blows to Break		158	129
Tire Tests			
Hours to 50% Reduction in Tread Depth		1020	1900
Appearance of Tread		Rough/chunk-outs	Smooth
Predicted Life (Hours)		2000	3600

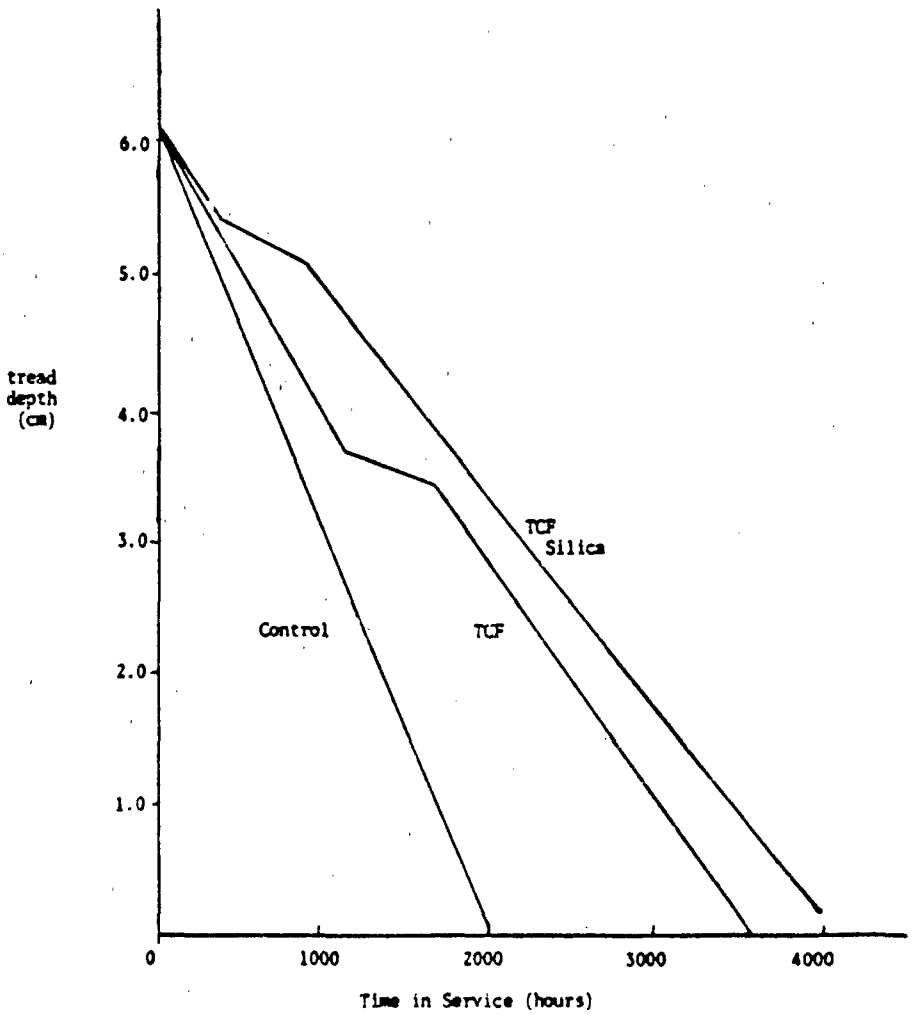


FIGURE 3. Effect of TCF on OTR tread wear.

These treads are still performing well but more is still to come, after the next phase of work on OTR tread durability.

Replacement of Natural Rubber With SBR

Initial work directed at replacing natural rubber with SBR was strictly cost related, based upon prevailing elastomer prices. The objective was to obtain hysteresis/heat build-up properties for 100% SBR which were equivalent to 100% natural rubber. This was accomplished by the use of lower carbon black levels (much

lower than usual for SBR but typical for NR) plus increased curatives - but with a large sacrifice in tear strength, which we have seen may be a key factor in service performance. With OTR tire performance in mind, it was then decided to investigate the partial replacement of NR with SBR to take advantage of properties of both elastomers. An extensive laboratory program was carried out with replacement of 20, 40, and 60% of the NR with SBR 1500. These variations were complemented with cure system modifications (semi-E.V.) and use of silica as a partial replacement of carbon black, along with other factors such as bonding agents (resorcinol and methylene donors). No attempt will be made to report the results of the whole program, but the critical results indicating possible improvements over past work are recorded as follows:

- A comparison of the various levels of SBR (Table 4) shows the best balance of properties for 60/40 NR/SBR ratio, especially related to tear and dynamic properties. This directs emphasis on tear to trouser tear, not Die C. Note slight adjustments in sulfur/accelerator ratios to accommodate the SBR.

- Partial replacement of carbon black with a hydrated silica provided definite improvements in chipping/chunking resistance and, as already observed, in tear strength.

Table 5 shows the significant results with both NR and NR/SBR (60/40) with the silica usage. Addition of bonding agents is somewhat questionable and requires additional curatives to maintain modulus (as does silica), but past work has shown some advantage in tear strength. Overall, however, the 60/40 NR/SBR with 40/10 carbon black/silica and a semi-E.V. cure system appears optimum.

- One would then conjecture that the compound mentioned above plus TCF would provide significantly improved field performance. The next phase of this work involved the application of much of the foregoing lab and field work results to further tire tests using retreads as before. The key changes made in this work were:

1. NR/SBR blends in place of all-NR.
2. Semi-E.V. cure system (1.5/1.5 accelerator/sulfur).
3. TCF - but no silica at this point.

Inspection of about 30 (out of 130) tires in underground mines were then made with the following observations:

- Operating conditions were very severe; in many cases, water and sharp objects combined. Considerable spinning in some areas.

- Previous tires have failed in 20 hours or less in a number of cases.

TABLE 4*

PARTIAL REPLACEMENT OF NR WITH SBR

	1	2	3	4
SMR-5CV	100.0	80.0	60.0	40.0
SBR 1500	-	20.0	40.0	60.0
Sulfur	2.2	2.0	2.0	2.0
MBS	0.8	1.0	1.1	1.2
Mooney Scorch @121°C				
Minutes to 5 Pt. Rise	42	55	62	67
Rheometer @150°C				
t_{90}, Minutes	15.2	19.8	23.7	27.8
300% Modulus, MPa	10.72	10.76	10.66	11.12
Die C Tear Strength, kN/m	112	123	45	40
Trouser Tear (All Knotty Tears)				
Max Tear, N	14.2	17.8	36.5	80.5
Frequency of Knots	18	13	8	4
Lupke Rebound				
% Rebound	69	66	65	65
Rate of Decay (-)	.144	.167	.166	.172
Goodrich Flexometer				
(.44 cm Stroke; 1.55 MPa Load; 100°C; 30')				
ΔT, °C	34	31	32	33
T Set	20.2	16.6	12.4	14.2

*Rubber 100, N-330 Black 50, Oil 5.0, Zinc Oxide 3.5, Stearic Acid 2.0, 6PPD 2.0, TMQ 1.0, Wax 1.5

• These tires have been in service up to one year now; thus, some new and others with several thousand hours.

• All appear the same - smooth surfaces with essentially no chipping/chunking. See Figures 4 through 6. Note also very little shoulder wear.

It is appropriate at this point to describe a new trouser-type tear test developed in the Brad Ragan laboratories. The major variation in this test from others in common use is the thickness

TABLE 5

EFFECTS OF SILICA AND BONDING AGENTS

	1	2	3	4	5
SMR-5CV	100.0	100.0	100.0	100.0	100.0
SBR 1500	-	-	-	40.0	40.0
N-330 Black	50.0	40.0	40.0	40.0	40.0
HiSil* 233	-	10.0	10.0	10.0	10.0
Sulfur	2.5	2.5	2.5	1.5	1.5
MBS	0.8	1.5	1.5	1.5	2.0
DTDM	-	-	1.0	0.6	1.0
Penacolite† B18S	-	-	3.5	-	3.5
HMMM	-	-	2.5	-	2.5
Mooney Scorch @121°C					
Minutes to 5 Pt. Rise	27.6	28.0	20.0	40.5	27.0
300% Modulus, MPa	13.62	12.96	12.18	12.41	11.33
2 Hrs. Cure @127°C					
Trouser Tear, N	8.9	6.2	13.3	34.7	19.6
Goodrich Flexometer					
(17.5% Deflection, 155 MPa Load, 100°C, 30')					
ΔT, °C	26	18.0	23.0	25.0	32.0
% Set	11.9	9.1	12.7	9.6	15.2
Chipping/Chunking Resist.					
Blows To Fail	328	402	371	493	386
Pico Abrasion					
Relative Index	171	187	149	185	122

*Registered trademark of Pittsburgh Plate Glass Co.
†Registered trademark of Koppers Co.

of the samples tested - which are more in line with large OTR treads than are thinner specimens normally used. This test has predicted, with considerable accuracy, the performance of OTR treads in the field, particularly tear and chipping/chunking resistance, and such was the case in the underground mine tires.



CTA Underground Mine-Retread (TCF) | Old Retread | New Tire (No TCF)

FIGURE 4. CTA tire with TCF vs. old retread and new tread.

The test apparatus consists of an air-operated cylinder with suitable controls and sample vise-clamps to pull the test sample apart. The force required to tear the specimen is measured on a spring scale connected to the opposite side of the specimen through a pulley linkage.

The sample is 0.635 cm thick, 18.42 X 18.42 cm sheet cured under appropriate conditions (usually 20' and 30' @148°C). Test specimens are cut running with the grain and across the grain as the stock comes from the laboratory mill. A slit of 1.27 cm is made at the center of one end to provide gripping for the clamps.

An example of the results of this test is seen in Table 6, where the new treads with TCF (CTA Premium) shows superb performance. Even the standard quality tread with TCF showed good chipping/chunking resistance. In fact, the treads with TCF did not tear to break due to limitations of the load (the general purpose did break). Since that time, a modified version using a tester with 500 lb./inch load capacity has been developed in the Monsanto laboratories (described in Appendix A). Table 7 illustrates even more the effect of the TCF using the modified test.

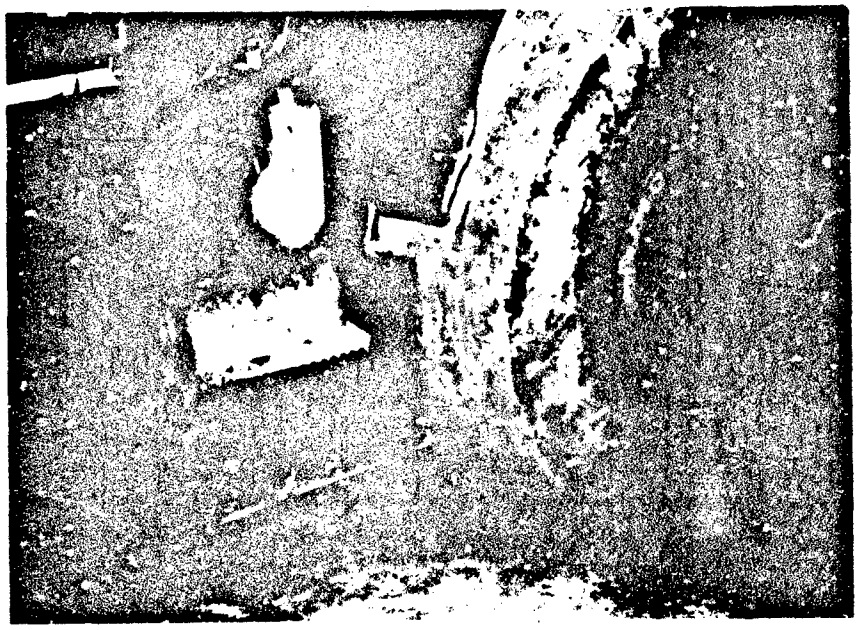


FIGURE 5. CTA tire in service.

CONCLUSIONS

Based upon these laboratory and tire tests, the following conclusions are drawn:

- There is little correlation of laboratory and field tire test data except for the "new" Trouser Tear Test, which does predict tire test results.

- The use of TCF does, without a doubt, improve resistance to chipping/chunking.

- Partial replacement of carbon black with hydrated silica does enhance performance in the lab and in the field.

- A combination of NR and SBR appears to be the overall best elastomer system when combined with semi-E.V. cures and the other variables already referred to (TCF, etc.).

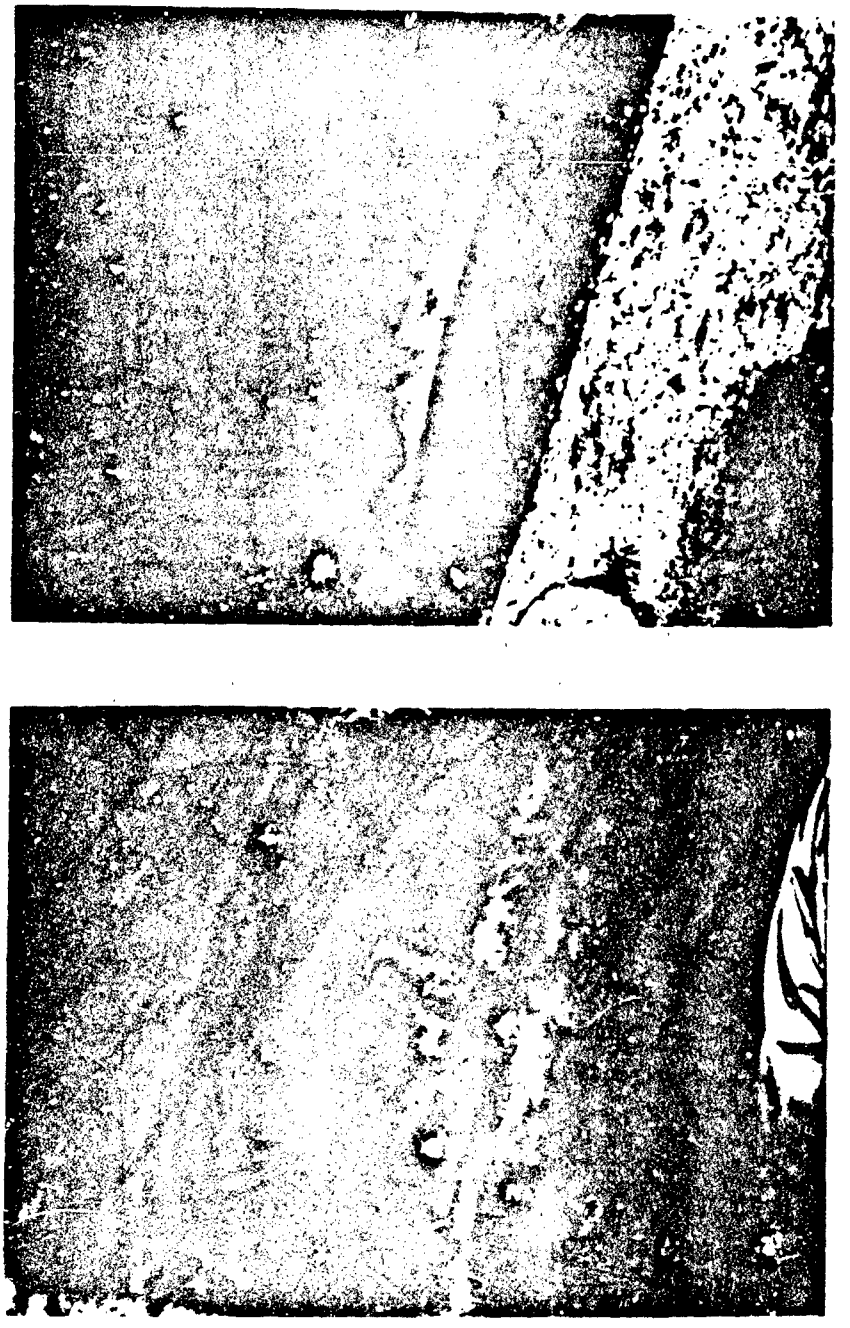


FIGURE 6. CTA tires - up to one year of service.

TABLE 6

NEW TROUSER TEAR TEST: CORRELATION WITH FIELD PERFORMANCE

	Laboratory		Field Performance
	Avg. Pull Kg	Std. Dev.	
Compound CTA (Underground Mine) Premium NR/SBR Semi-E.V. Cure/TCF	37.76	0.628	10 (No chipping/ chunking) Long wear
Q&H (Quarry and Haulage) Standard (with TCF)	37.2	2.2	9.0 (Very light chipping/chunking) Good wear
OEM (General Purpose) Tread (no TCF)	33.05	2.41	7.5 (chipping/chunking) Moderate wear

TABLE 7

MODIFIED TROUSER TEAR TEST (APPENDIX A)

Compound	Avg. Pull (Kg)	Std. Dev.
CTA (Underground Mine) Premium NR/SBR Semi-E.V. Cure/TCF	67.2	0.91
Q&H (Quarry & Hauler) Standard (with TCF)	59.9	2.1
OEM (General Purpose)	33.05	2.4

Thus, a typical compound to provide both hauler and loader treads of high performance is suggested as follows:

NR	60.0		TMQ	2.0		
SBR	40.0		6PPD	2.0		
N-231 Black	40.0		TCF	2.25		
Silica	10.0		Blended Wax	1.5		
Oil	3.0		Sulfur	1.5		1.5
Zinc Oxide	5.0	(MBS or TBBS)	Sulfenamide	1.5	or	0.7
Stearic Acid	2.0		DTDM	0.6		1.5

REFERENCES

1 L. A. Walker, Journal of Elastomers and Plastics, 10,327. (1978).

2 J. L. LeBlanc, "A Modified Trouser Specimen to Assess Tear Resistance of Rubber Compounds", Proceedings of the Fifth European Plastics and Rubber Conference, Paris, June 12-15 (1978), Vol. 2, pp. E.22.

3 J. R. Dunn, L. P. Gelinas, and R. C. Klingender, "Factors Influencing the Chipping Resistance of Polybutadiene Vulcanizates", Polymer Corporation Limited, Sarnia, Ontario, Canada. April 12, 1965.

4 Lloyd A. Walker and John B. Harber, "Improved Durability in OTR Mining Tires", Presented at the 126th American Chemical Society Rubber Division Meeting, Denver, Colorado, October 23-26, 1984.

APPENDIX A

BRAD RAGAN/MONSANTO TROUSER TEAR TEST

A. APPARATUS

1. DeMattia Flex mold - double specimen - See Figure 1.

2. Instron, T-10 or any suitable testing device with load cell 500 lb./in. load capacity.

3. 10" Hyde rubber knife.

B. MILLING AND CURING SAMPLE

Milling the compound:

1. Grain direction is very important regardless of the incorporation of Santoweb into the compound. Samples can be run with the grain and against the grain to determine optimum conditions. Sheet stock off mill at .255 - .260" and cut specimens to fit mold.

2. Curing: cure to optimum condition labeling sample clearly as to stock and grain direction.

C. SAMPLE PREPARATION

1. A DeMattia flex specimen approximately 2" X 6" is cut in two pieces at the curved indentation to obtain duplicate samples 2" X 3" in size. The DeMattia specimen is not necessarily required; any type roughly ¼" thick would be permissable. However, the DeMattia is recommended for ease of handling and efficiency/ reproducibility.

2. With a Hyde rubber knife or other suitable cutting tool, place a 1" cut in the center of each specimen cutting from the edge containing the indentation. (See Figure 2).

3. Label each sample.

D. PROCEDURE

1. Calibrate tensile tester for 500 lb./in. full scale, 5"/min C/H, 5"/min. recorder speed.

2. Appropriate clamping is important because of slippage and large amount of force needed to tear sample.

3. Clamp each end of the sample into the clamp, fasten securely. Note: prepared sample resembles a trouser tear configuration.

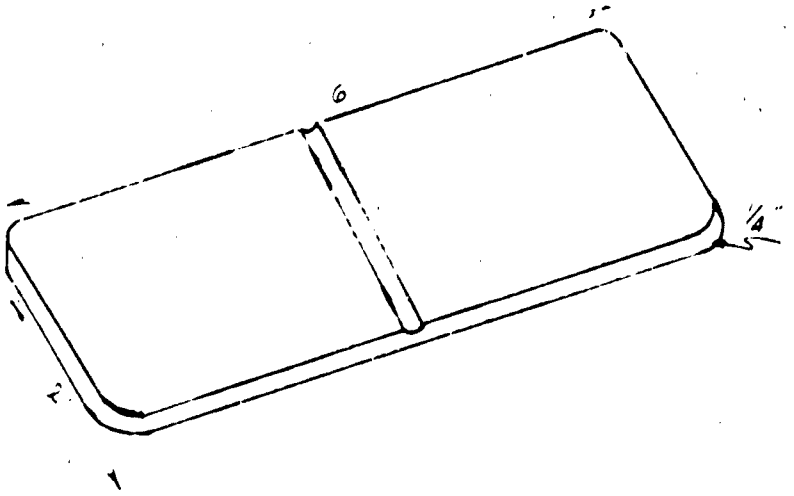


FIGURE 1. DeMattia flex specimen.



FIGURE 2. DeMattia flex specimen cut in center.

4. Start cross head and continue pull until sample separates (See attached chart).

5. Pull all samples in set using same procedure.

6. Save all samples for observation of tear characteristics.

APPENDIX B

MONSANTO CHIPPING AND CHUNKING TEST

SCOPE

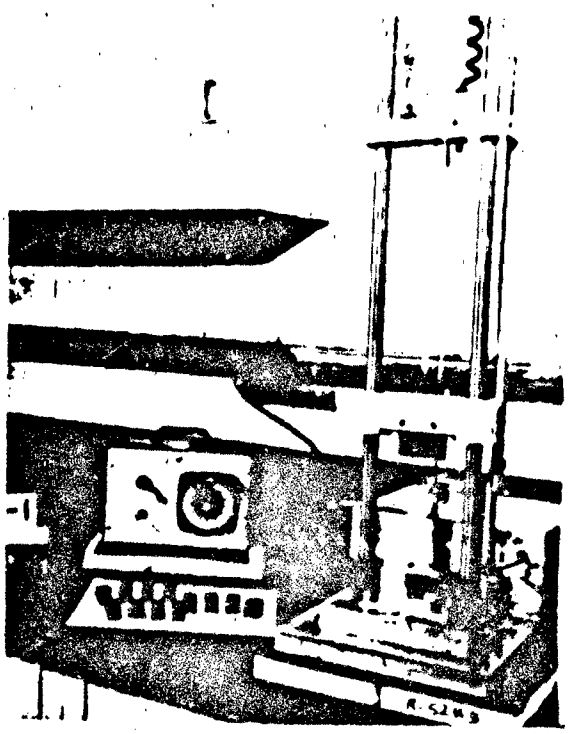
This method describes a laboratory test for the evaluation or the chipping and chunking resistance of rubber compounds.

APPARATUS

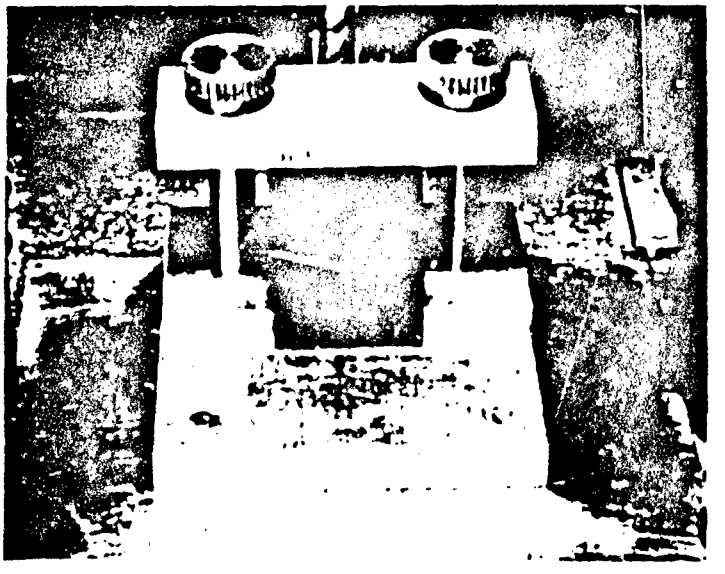
A. Press with a 680.4kg capacity and temperature control.

B. A three-piece, 6-cavity mold for curing 3.81cm long X 3.175cm wide X 1.27cm thick Chevron-shaped test specimen. The attached shows the individual test specimen and gives dimensions on molded samples.

C. A guillotine tester consisting of a blunt blade having a radiused edge 0.635cm thick inserted in a head of 2.27kg total weight. Any apparatus suitable for consistently dropping the blade from a height of 45.72cm may be used. An example is shown in the attached along with the dimensions of the blade and its position relative to the test specimen.



Guillotine tester.



Blunt blade and its postion to test specimen.

SAMPLE PREPARATION AND CURING PROCEDURE

A. Mill sheet of rubber to 0.635cm thickness. Ply pieces of stock together to form six specimens conforming to the general shape of mold (dimensions should be slightly greater than those of mold tc insure good fill but should not exceed measurements by more than 0.159cm).

B. Preheat press and mold at desired cure temperature.

C. As quickly as possible, remove mold from press, fill with pre-shaped specimens, close mold and replace in press.

D. "Bump" press (open and close) twice to remove air. Close press to 680.4kg and cure for desired length of time (due to thickness of sample, it suggested that five minutes be added to normal cure time to insure uniform vulcanization).

E. Remove specimen at end of cure time and cool in water.

TEST PROCEDURE

A. Each sample (a minimum of six samples per rubber stock is suggested) is preheated in an oven at 80°C for 20 minutes. After conditioning, it is placed in the sample holder which is maintained at 70°C. Each sample receives 50 blows (cycles) of the guillotine from a height of 45.72cm.

B. After the 50 cycles, the sample is inspected for the formation of cracks or chips.

C. If specimen is undamaged, it is aged for two days at 100°C and given a further 50 blows after conditioning as described in Step A.

D. The cycle of aging, conditioning, and testing is repeated until chipping or chunking has occurred on the test specimen.

REPORT

A. The average number of blows required to cause cracking or chipping on six specimens per rubber stock is reported.

2. THE MONSANTO COMPOSITE HOSE PROCESS

INTRODUCTION

Monsanto has developed a new process enabling low-to-medium pressure hose to be manufactured in one step, instead of the customary 3 steps; i.e. extrusion of innerliner, application of textile reinforcement by braiding or knitting, and extrusion of cover.

The advantages are that less equipment and manpower are required and cost reductions of up to 20% have been demonstrated.

It is based on the following concepts:

(A) The incorporation of Santoweb fiber into the matrix which reinforces the polymer. When bonded chemically to it, these short fibers replace the textile braiding or knitting.

(B) Extrusion of the short fiber/polymer composite through a specially designed die which preferentially orients the fibers in the circumferential direction. The anisotropy created gives the hose the necessary strength to resist cross sectional internal pressures but insures flexibility is maintained longitudinally. (For information on patents, see Appendix A).

After extrusion, a rubber hose can be vulcanized immediately without support and the fiber is sumultaneously crosslinked to the matrix. In the case of PVC, the bonding occurs by virtue of a patented bonding agent, and after cooling the hose requires no further treatment.

The basic process produces straight hose, but shaped hose can also be made either on mandrels or by direct extrusion shaping with a moving die.

If desired, a colored or protective cover can be co-extruded.

The principles of the process can also be applied to the reinforcement of the innerliner of high pressure hose. The presence of the fiber increases the strength and improves resistance to cord strike-through during both production and service.

This briefly describes the Monsanto process, highlighting its advantages and major technical features.

EXPERIMENTAL

Whenever a short fiber/polymer composite is made to flow in a given direction, the fibers become aligned parallel to the flow direction. Fiber orientation produces anisotropy which shows as differences in stress-strain properties when measured parallel (0°) and perpendicular (90°) to the fiber.

The simplest example of orientation produced by flow is in milling or calendering. Figures 1 and 2 illustrate the anisotropy in tensile modulus and elongation at break of typically milled composite sheets as it varies with fiber concentration.

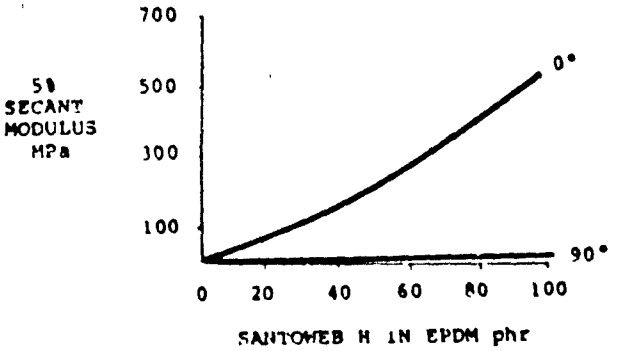


FIGURE 1. Variation of Modulus with Fiber Concentration.

In these milled sheets, physical properties are at a maximum when measured at an angle of 0° to the orientation and a minimum at 90° to it.

Similarly, if a composite is extruded through a conventional tube die, the flow will cause the fiber orientation to be in the length or axial direction. Such a tube/hose would be stiff and have no resistance to pressure because the maximum strength is perpendicular to the circumferential application of stresses.

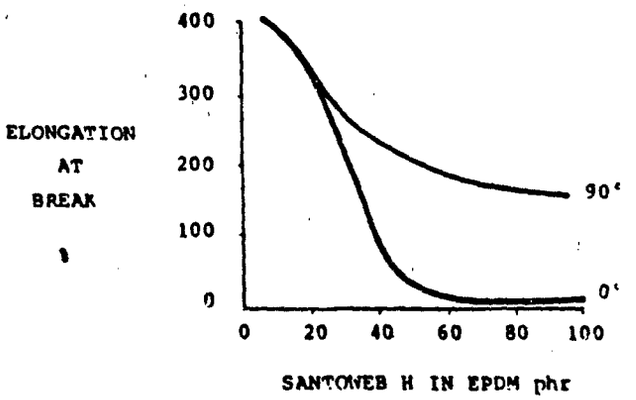


FIGURE 2. Variation of Elongation with Fiber Concentration.

This can be overcome if the fibers can be orientated in the circumferential direction during extrusion. Figures 3 and 4 illustrate the two contrasting orientation patterns.

The configuration in figure 4 can be achieved using the patented Monsanto conically expanding mandrel die.

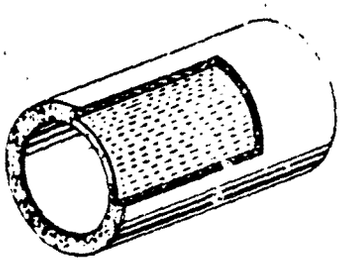


FIGURE 3. Short Fibers Orientated in Axial Direction.

The die functions on the principle that when a short fiber composite flows in an expanding channel, the matrix is stretched in a direction perpendicular to the forward flow, and this stretching effect turns the fibers progressively with respect to the forward motion - the angle of orientation of the fibers being related directly to the degree of expansion.

This effect is illustrated in Figure 5 which gives a diagrammatic impression of changes in fiber orientation.

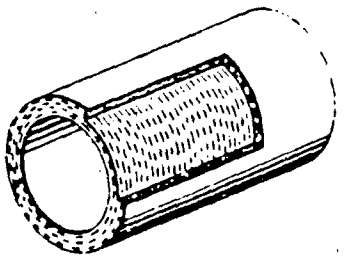


FIGURE 4. Short Fibers Orientated in Circumferential Direction.

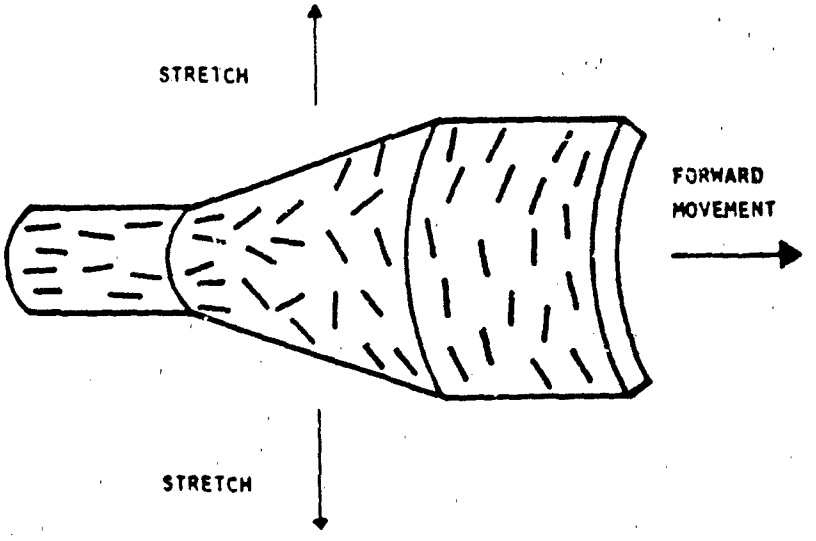


FIGURE 5. Diagramatic Illustration of Fiber Orientation on Passing Through a Conically Expanding Die.

A typical conically expanding mandrel die is shown in Figure 6.

FORMULATION OF THE COMPOSITE

The choice and concentration of ingredients used are critical in obtaining satisfactory performance.

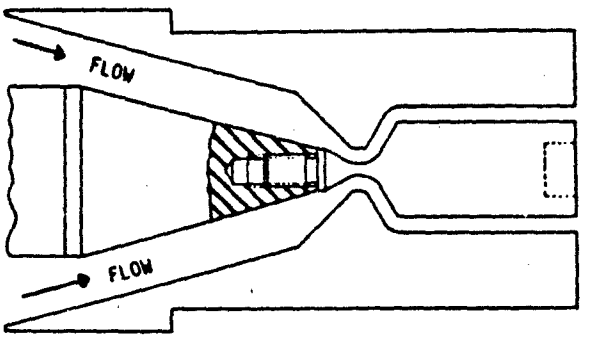


FIGURE 6. Monsanto Die.

Rubber Matrix

The choice of matrix is determined by the compatibility of the hose with the media that it will contact, both internally and externally. In general, EPDM or SBR/NR blends are used for hose which will transport water or aqueous fluids, and air: NBR or NBR/PVC blends are used for hose having contact with fuels. For long life, particularly under severe service conditions, silicone rubber is used.

Fiber loadings in the range 10-30% by weight are used for making fully reinforced hose: to increase the green strength of innerliners, loadings of 2-5% are suggested. Concentrations of other ingredients; e.g. black and oil, are chosen to give a compromise between ultimate physical properties, and good factory processability of the compound.

The ultimate strength of the hose depends on a balance of correct fiber loading, adequate fiber bonding, dispersion and orientation of the short fibers, and optimum vulcanization of the composite.

PVC Matrix

PVC compound formulations used for hose are much simpler than those used for rubber. Santoweb W is used in concentrations up to 10% by weight. A patented bonding agent is added to the compound to effect fiber bonding. Plasticizers and fillers are chosen to balance cost and hose flexibility requirements.

However, in contrast to the ease of incorporating Santoweb fiber into rubber, traditional powder mixing techniques for preparing PVC compounds need to be modified to provide adequate Santoweb fiber dispersion. The low shear in the high speed mixer is not sufficient by itself to separate fiber bundles, and a modified technique has been developed ([1]).

HOSE MANUFACTURE

The composite hose is made directly in a one-step process using the special die ([2]) fitted to a standard extruder. If required, a protective or decorative cover can be co-extruded using a crosshead extruder linked directly to the Monsanto die.

The major advantage of the short fiber system is the simplification of the manufacturing process. The hose is extruded directly and cured, compared to conventional hose production which requires tube extrusion, cord knitting or covering, cover extrusion, and curing. A comparison of these two hose processes is illustrated in Figure 7.

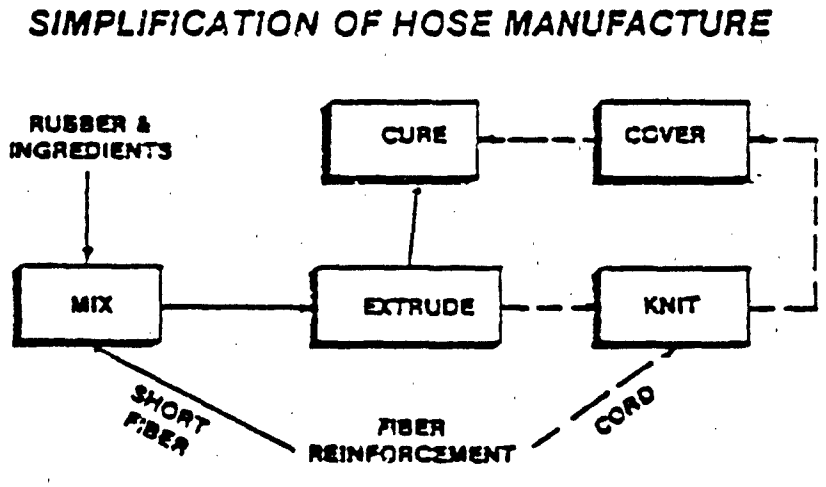


FIGURE 7. Simplification of Hose Manufacture.

Vulcanization and Shaping

Straight rubber hose can be vulcanized in steam autoclaves without support. Also, continuous vulcanization is possible because the green strength of the hose is high. PVC hose is cooled directly from the extruder and is ready for packing.

Shaped rubber hose; e.g. for automotive coolant systems, can be made by using internal mandrels or by an extrusion shaping technique ([3]). In this case the outer part of the extrusion die is moved in a plane perpendicular to the extrusion. When this is done in a controlled manner, it produces the desired shape. The shaped hose made in this way needs some external support during cure; e.g. a female mold. A two-dimensional die system is shown in Figures 8 and 9.

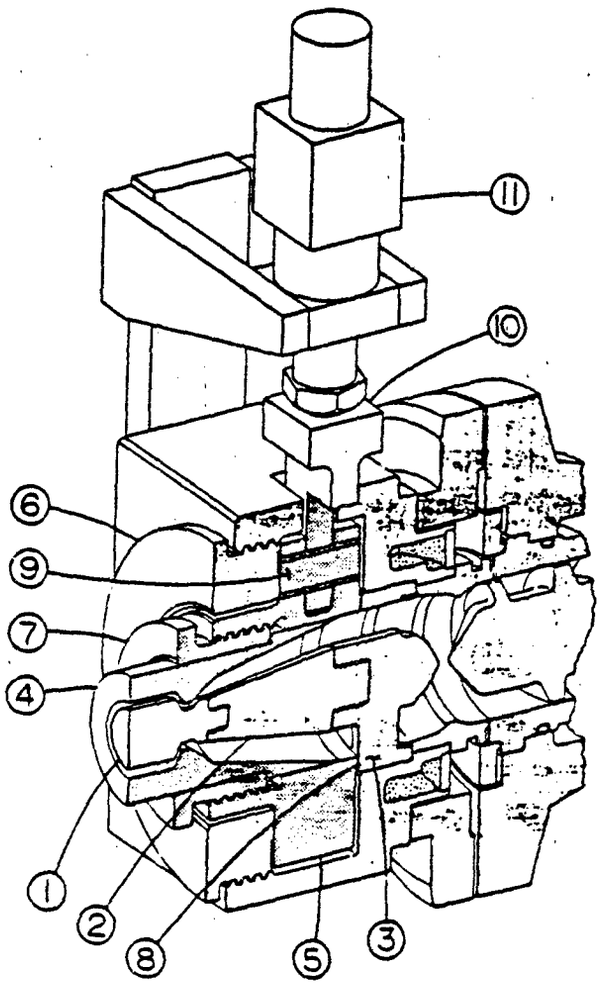


FIGURE 8. Assembly of Moving Parts in Die Head.

1--stationary die pin; 2--adapter; 3--spider; 4--moving outer die; 5--die holding ring, 6--die holding ring unit; 7--die holding unit; 8--sliding seals; 9--connecting pin; 10--ram; 11--drive cylinder.



FIGURE 9. Planar S-Bend Hose Shape. As it is Formed by Extrusion.

Hose Dimensions

Since the matrix of this hose is a homogeneous composite, the hose dimensions, and particularly the wall thickness, can be varied to change properties proportionally; e.g. burst strength. Burst strength is inversely proportional to hose diameter and is directly proportional to wall thickness.

Therefore, with a given compound, properties of a hose can be varied at will and can be predicted. Thus, if a given hose has an unnecessarily high burst pressure, the reduction in wall thickness needed to achieve the desired level can be calculated as well as the consequential cost saving.

Table 1 shows a comparison of 5/8" I.D. knitted vs. Santoweb fiber reinforced heater hose. Burst characteristics are very similar. The Santoweb reinforced hose had no failures in a 45,000 mile fleet test.

APPLICATIONS IN HIGH PRESSURE HOSE

Since the cord is under tension, applying steel cord reinforcement in hydraulic hose manufacture poses problems. The innerliner tube must resist penetration of the cord, and also longitudinal growth by a "squeezing out" effect. To solve these problems, the liner is usually frozen or made stiffer by adding fillers.

An alternative approach is to use Santoweb fiber in the innerliner. It may then be extruded using either a conventional die to give

TABLE 1

COMPARISON OF KNITTED VS. SANTOWEB® FIBER HOSE

	Commercial Knit Reinforced Heater Hose	Santoweb Fiber Reinforced Heater Hose*
Burst, psi @R.T.	285	235
Burst, psi @100°C	168	177
% Growth @75 psi, R.T.		
Hoop	8.2	4.0
Axial	-3.1	0.8
45,000 Mile Vehicle Test†	---	Passed

* 70 phr Santoweb® H (14 wt. %) in EPDM compound.

† Six vehicles used the Santoweb fiber reinforced hose under fleet test conditions No hose failed or resulted in leakage of coolant.

axial orientation or using a Monsanto die to give circumferential orientation, depending on the flexibility needed in the final hose.

The greatest resistance to cord strike through occurs when the cord is applied at right angles to the short fiber orientation; the effect of the cord is to extend the compound which increases the resistance to extrusion. The reverse is true when the cord is applied parallel to the short fibers; these effects are illustrated in Figures 10 and 11.

ADVANTAGES OF THE MONSANTO PROCESS OF HOSE MANUFACTURE

The key advantage in the Monsanto process is the lack of specialized equipment for applying continuous cord reinforcement; hence, the required capital investment is reduced. A comparison of the traditional and Monsanto methods is shown in Table 2.

Simplification of shaped hose production by extrusion shaping short fiber reinforced compounds with a Moving Die system is outlined in Table 3.

Examples

Examples of commercially produced hoses reinforced with Santoweb short fibers are shown in Figures 12 through 18.

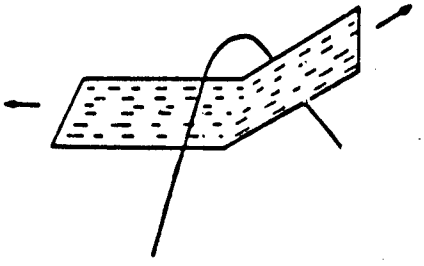


FIGURE 10. Cord Applied at Right Angles to Short Fibers-High Effective Green Strength.

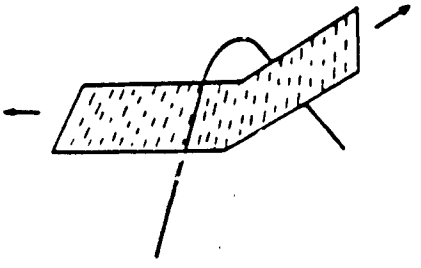


FIGURE 11. Cord Applied Parallel to Short Fibers-Low Effective Green Strength.

REFERENCES

(1) L. A. Goettler, Polymer Composites, October 1983, Vol. 4, No. 4.

(2) L. A. Goettler and A. J. Lambright, U.S. Patent #4,056,591 and 4,057,610 (1977).

(3) L. A. Goettler, A. J. Lambright, R. I. Leib, P. J. Dimauro, Rubber Chemistry and Technology, 54, 1981, pp 277-301.

TABLE 2

COMPARISON OF TRADITIONAL AND MONSANTO METHODS FOR MANUFACTURING LOW-TO-MEDIUM PRESSURE HOSE

FACTOR	TRADITIONAL	MONSANTO	ADVANTAGE OF MONSANTO PROCESS
Process	3-Step	Single-step	Reduced manpower. Reduced compound inventory. Reduced scrap.
Equipment	Straight head and crosshead extruders Braiding/knitting machines	Single extruder	Reduced capital; lower maintenance. Reduced manpower.
Materials	Separate liner and cover compounds essential	Only single composite necessary	Reduced compounding needs and inventory.
Reinforcement	Continuous cord applied at interface between liner and cover	Santoweb fiber incorporated into compound during mixing	Homogeneous reinforcement; no adhesion problems.
Cover	Essential integral part of hose: without it exposed cords easily damaged	Not essential: applied to give attractive finish or as protection.	Lower costs.
Cure (for rubber only)	Lead sheath plus internal support for autoclave cure	Free standing autoclave or CV cure line	Cheaper process. Reduced capital.
Recycle of compound	Not possible	Perfectly acceptable with PVC: to be used with discretion with rubber	Elimination of scrap and reduction in costs.
Dimensions	a) Thick wall b) Restriction on max. diameter related to size of knitting machines	a) Thin wall b) No restriction on diameter.	Lighter product. Good kink resistance. Good flexibility.

TABLE 3

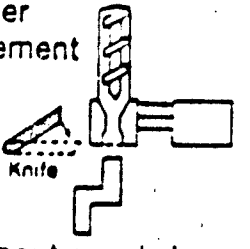
SHAPED AUTOMOTIVE HOSE

Conventional Process

1. Extrude tube
2. Apply cords
3. Extrude cover
4. Shape on mandrel
5. Cure on mandrel
6. Remove from mandrel
7. Trim

Short Fiber Process

1. Extrude shaped hose segments containing short fiber reinforcement



2. Cure without mandrel





FIGURE 12. Rubber Water, Compressed Air, and Fuel Hose.

COMMERCIAL EXAMPLES

General Purpose Hose

Domestic garden and professional irrigation hose are available in rubber or PVC: fuel hoses have been made in rubber, and either PVC or rubber can be used for compressed air.

Burst Pressures:
12.5mm ID garden hose in rubber or PVC, 1.8 MPa
7.5 mm ID fuel hose, 3.3 MPa
4.0 mm ID bicycle pump hose, 2.0 MPa



FIGURE 13. PVC Water and Compressed Air Hose.

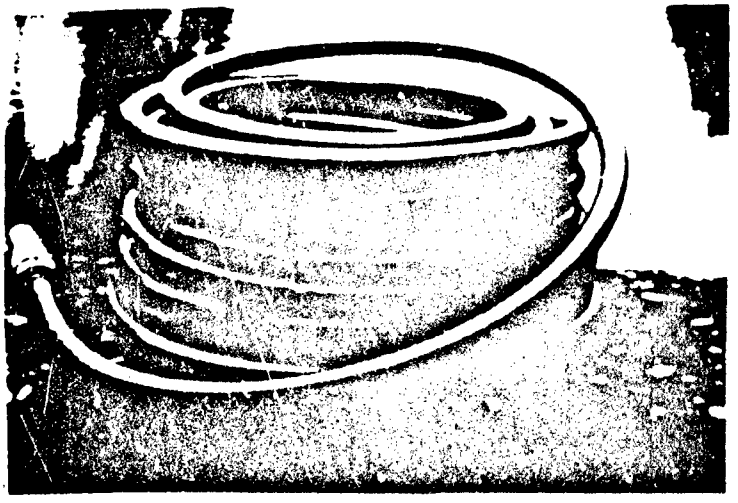


FIGURE 14. PVC Garden Hose.



FIGURE 15. Silicone Rubber Hose.

COMMERCIAL EXAMPLES - CONT'D.

Silicone Hose

Hose used in coolant systems for trucks and buses and other severe service conditions.

Burst pressure 32mm ID, 0.6 MPa.

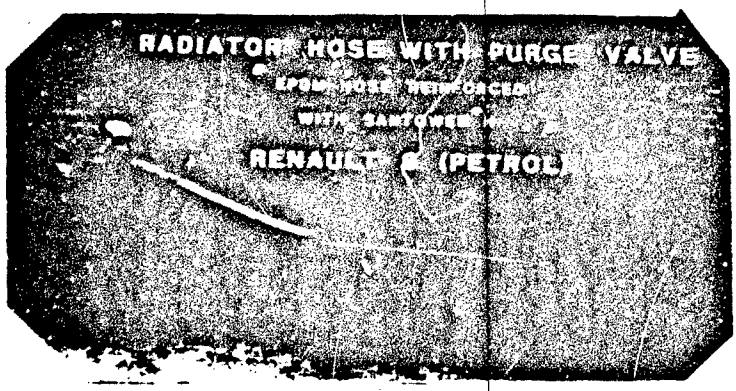


FIGURE 16. EPDM Radiator Hose for Petrol Engines, Original Equipment.

COMMERCIAL EXAMPLES - CONT'D.

Automotive Coolant Hose - EPDM

Hose is used for radiator and heater hose for both petrol and diesel engines as original equipment.

Burst pressures:

32mm ID radiator hose, 0.8 MPa
15mm ID heater hose, 1.6 MPa

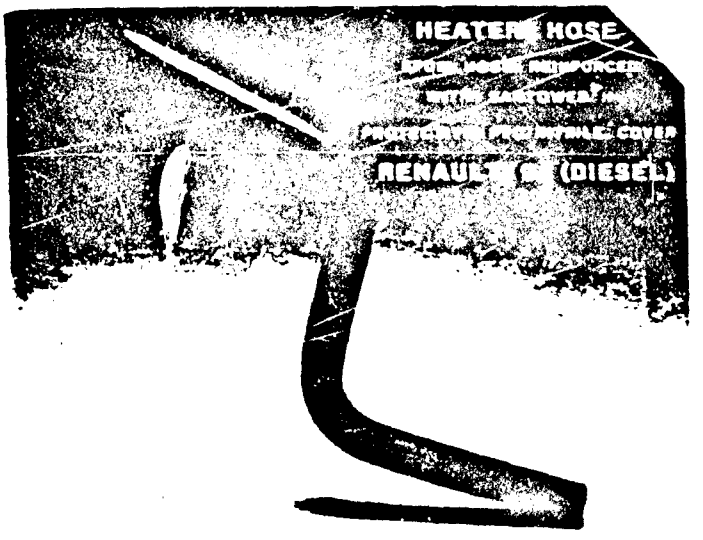


FIGURE 17. EPDM Heater Hose with NBR/PVC Cover for Diesel Engines, Original Equipment.

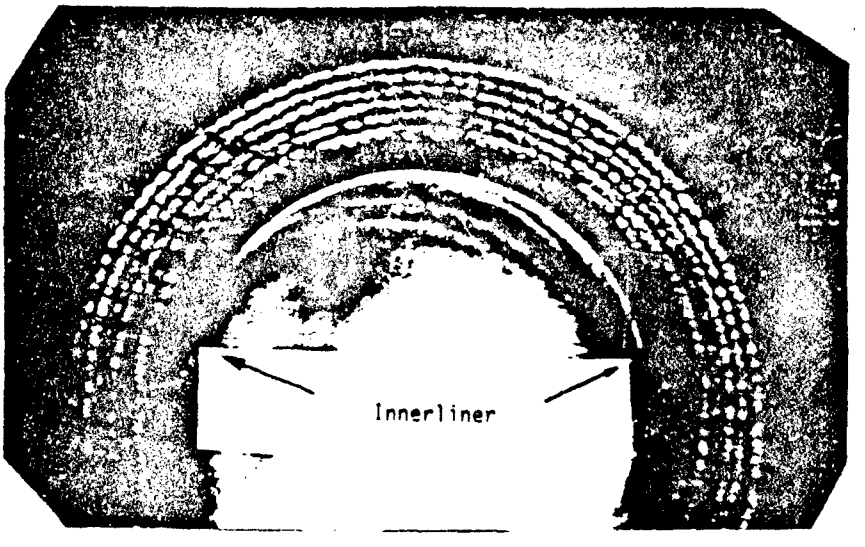


FIGURE 18. Hydraulic Hose with Santoweb Fiber Reinforced Inerliner.

COMMERCIAL EXAMPLES - CONT'D.

Hydraulic Hose Innerliner

Hoses tested with pulsation 0-400 ATU at 90°C for 400,000 cycles without failure.

APPENDIX

MONSANTO PATENTS AND LICENSING POLICY

The principle of control of short fiber orientation during extrusion, described in this bulletin is covered by a series of worldwide patents owned by Monsanto Company.

Monsanto Company is prepared to grant licenses under these patents for the commercial production of hose. Details of terms are available on request. The licenses cover the use of other fibers as well as Santoweb fiber; e.g. glass fiber in silicone hose for use at temperatures in excess of the decomposition temperature of cellulose.

In those countries where Monsanto Patents have not been filed, no license is required for the manufacture and sales within the country concerned. If, however, hose made in this way is exported to a country where patents exist, then a license is needed to sell in that country.

Monsanto also has patents covering the use of recommended bonding agents in the production of Santoweb fiber/PVC composites. Information on licenses under these patents will be supplied upon request.

DEVELOPMENT OF A 3500-POUND PIPE HANGER MOUNT FOR SHIPBOARD APPLICATION

MARSHALL L. SHERMAN
Ship Materials Engineering Department, David Taylor Naval Ship R&D Center, Annapolis, Maryland

A 3500-pound mount was developed as the last in a series of shear-type mounts to isolate vibration between piping systems and the hull of ships. This mount, designated 5M3500, has a natural rubber resilient element and a load rating of 2000 to 3500 pounds (908 to 1589 kilograms). It has a nearly constant dynamic spring rate over its load range and is unbiased when loaded in the vertical direction. The mount has a resonance frequency of 5 hertz when supporting its maximum rated load which meets the low frequency requirement for this application, and it is recommended for use of ships as a standard Navy mount.

FATIGUE OF A RUBBER TANK TRACK COMPOUND UNDER TENSILE LOADING

G. B. MCKENNA[1], G. W. BULLMAN[1], K. M. FLYNN[1], J. PATT[2]
(1)Polymers Division, National Bureau of Standards, Gaithersburg, Maryland 20899; (2)DRSTA-RCKT, U. S. Army Tank Automotive Command, Warren, Michigan 48090

INTRODUCTION

The mechanical durability of a rubber compound is an important property in its suitability for tank track applications. The evaluation of this property is a difficult and time consuming task. In this paper we present a methodology for evaluating the durability of carbon black filled rubber. This methodology is based upon the concept of a cycle shifted failure envelope which we have found previously (1) to be useful in describing the frequency and waveform dependence of the fatigue lifetimes of a carbon black filled butyl rubber.

In what follows we present the background which led to our development of a failure model and outline the failure model. We will subsequently present creep and fatigue data for a tank track rubber compound (15TP-14AX, MIL-T-11891) and show how the model applies to them. The results will be compared with those obtained previously for a filled rubber compound evaluated in this laboratory (1,2).

BACKGROUND

The phenomenon of stress softening is known to occur in both filled and some unfilled elastomers (3-9). Of particular interest is the work of Derham and Thomas (9) in which they reported on the creep behavior of a carbon black reinforced natural rubber subjected to load-unload cycling. They found that the creep rate was greater under cyclic loading than under static loading and that the rate of cyclic creep followed a logarithmic law (with cycle number) and did not tend towards a constant value. Figure 1 depicts their findings showing the "accelerated" creep due to cyclic loading.

In studying the failure behavior of filled rubber, McKenna and Penn (2) found that lifetime under load-unload cycling depends upon both frequency and waveform and that the dependence could not be described by either a time dependent cumulative damage approach (for which lifetime would be independent of test frequency) or a cycle dependent cumulative damage approach (for which the total number of cycles to failure would be constant independent of test frequency and waveform). As shown in Figure 2, lifetime for a carbon black filled polyolefin rubber was found to be much shorter than either the creep failure time or that expected from a cumulative damage prediction - thus, failure was "accelerated" due to the cyclic loading.

The failure model was developed in order to establish a link between the observed "accelerated" creep and the "accelerated" failure behaviors of carbon black filled rubber. The link was made through a failure envelope similar to that originally proposed by T. L. Smith (10-13). Details are presented in the next section.

The Failure Model

Some years ago, Smith (10-13) proposed the concept of a failure envelope for which the locus of stress-at-break (σ_b) vs strain-at-break

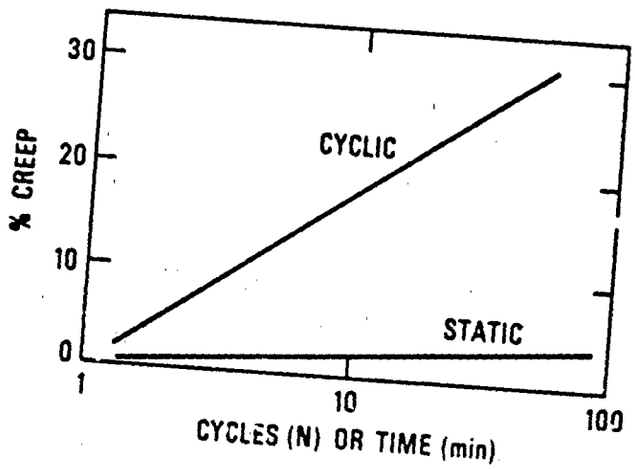


Figure 1. Schematic of the difference in creep behavior of a filled natural rubber in creep and static loading. [After Derham and Thomas (9)]

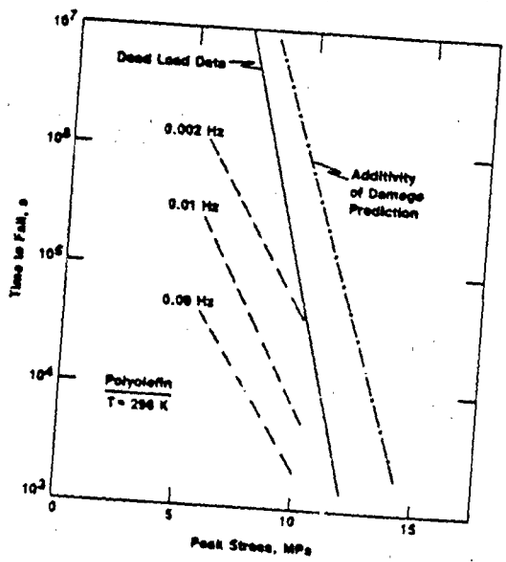


Figure 2. Lifetime vs (peak) stress for a filled polyolefin rubber comparing fatigue behavior with static behavior and prediction of fatigue lifetime from a cumulative damage law. [After McKenna and Penn (2)].

(ε_b) for a rubber can be represented as a unique curve independent of deformation or stress history. Figure 3 shows a typical failure envelope. (Note that the failure stress is reduced by the temperature to account for the modulus variation with temperature.) This is a reasonable approximation for simple deformation histories such as constant rate of deformation, stress relaxation or creep. However, in the presence of a stress softening effect, Smith found that the failure envelope could shift to larger strains (13,14).

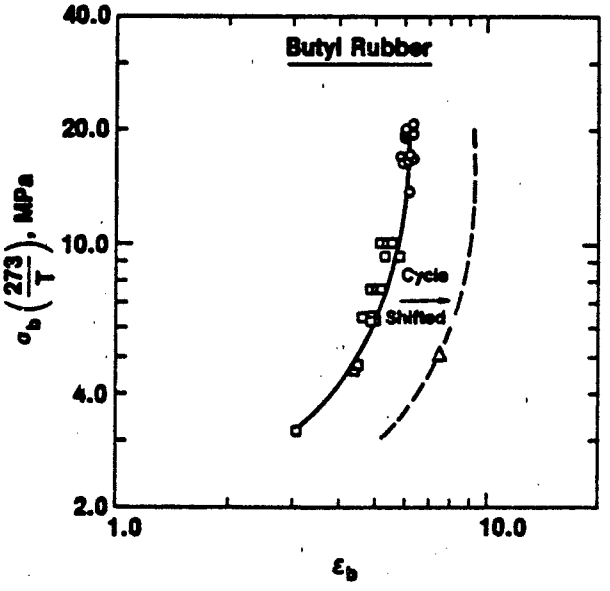


Figure 3. Failure envelope for a filled butyl rubber. (O) From constant rate of deformation experiments. (□) From creep to failure measurements. (Δ) Shifted envelope from cyclic loading. [After McKenna and Zapas (1)].

In our previous work (1), we were able to use creep data taken under cyclic loading conditions combined with the notion of a shifted failure envelope to account for the frequency and waveform dependence of the fatigue lifetime of a carbon-black filled butyl rubber. The shifted failure envelope is represented by a simple equation which relates the failure envelope in simple deformation histories to that in cyclic histories. For the strain-at-break we found (1):

$$\varepsilon_{bc} = a_0 \varepsilon_{bo} \qquad (1)$$

where ε_{bc} is the strain-at-break under cyclic load, a_0 is a shift factor (which may depend on the stress level, frequency, etc.) and ε_{bo} is the failure strain (at the same stress) in a simple deformation history. Then, if it is assumed that a_0 is a constant independent of stress, frequency, etc., then fatigue lifetime can be predicted simply by extrapolation of the cyclic creep curve to the ε_{bc} determined by equation (1) and a single set of failure data. For the filled butyl

rubber $\alpha_0 = 1.67$ was determined from failure data obtained at 0.09 Hz. Figure 4 shows a comparison of the lifetime predicted from the model and the lifetimes obtained experimentally. As can be seen the agreement is reasonable. We note that the extrapolations were made from short time creep data obtained for $.1\ N_f \leq N \leq .33\ N_f$ depending upon the test frequency and waveform.

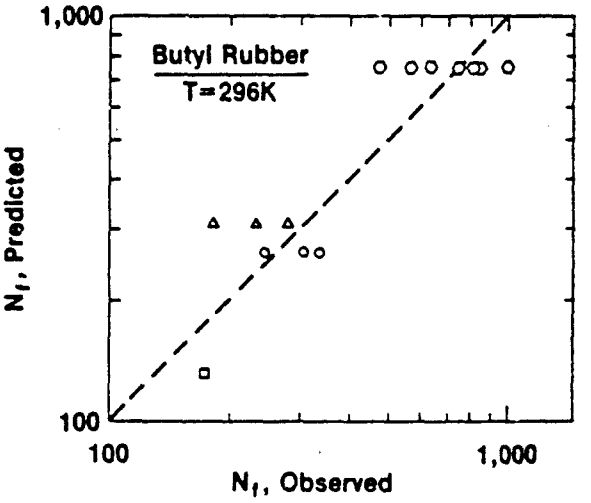


Figure 4. Comparison of number of cycles to failure predicted from cycle shifted failure envelope model with observed number of cycles to failure for a filled butyl rubber at a peak stress of 5.5 MPa (800psi). Zero-tension loading. Sinusoidal: (□) 0.0002 Hz; (0) 0.01 Hz; (○) 0.09Hz; (Δ) Squarewave with 52.4 s cycle [After McKenna and Zapas (1)].

MATERIALS AND METHODS

The rubber compound used in this study was a carbon black filled blend of SBR, Natural Rubber and Polybutadiene designated as 15TP-14AX, MIL-T-11891D. The material was provided to us in the form of cured sheets (6" x 6" x .08") (152mm x 152mm x 2mm) by P. Touchet of the U. S. Army Belvoir Research and Development Center. The Butyl rubber compound described in the prior study was made at NBS in the form of 6" x 6" x 0.04" (152mm x 152mm x 1mm) sheets. The rubber formulations are given in Table 1.

Creep data were obtained at room temperature (23°±1°C) by hanging weights from the samples and measuring the separation of two gage marks using a cathetometer. Time to rupture was recorded for each sample.

Table 1

COMPOUNDING FORMULATIONS FOR FILLED RUBBERS

Ingredients	Quantity, parts by mass
	Butyl Rubber*
NBS 388j, butyl rubber	100
NBS 370e, zinc oxide	3.00
NBS 371g, sulfur	1.75
NBS 372h, stearic acid	1.00
NBS 378b, HAF black	50.00
NBS 374c, tetramethylthiuram disulfide	1.00
	15TP-14AX**
SBR 1500	35.00
Polybutadiene (98% Cis)	30.00
Natural Rubber (SMR20)	35.00
N220 Carbon Black	65.00
Zinc Oxide	3.00
Stearic Acid	1.50
Waxy hydrocarbon blend (MP=65-70°C, SpGr=0.9-0.93)	1.50
3-Dimethylbutyl-N'-phenyl-p-phenylene-diamine	3.00
Polymerized 2,2,4-trimethyl-1, 2-dihydroquinoline	2.00
High Aromatic Oil, ASTM D2226, type 102	4.00
N-diisopropyl-2-benzothiazyl-sulfenamide	3.20
Sulfur	1.30
N-(cyclohexylthio)phthalimide	0.20

*Prepared according to ASTM D-3188-73, Formula 1A.
**Prepared per ASTM D3182.

Mechanical properties testing was performed on nonstandard size dumbbell samples in order that fatigue testing results could be compared with the results from creep and constant rate of deformation experiments. The nonstandard dumbbell specimens had a width in the gage section of 0.25 inch (6.4 mm) a gage length of 1.0 inch (25 mm), a maximum width in the grips of 0.5 in (13 mm) and an overall length of 3.0 in (75 mm).

Constant rate of deformation tests were performed using a screw driven machine. Crosshead displacement rates were varied from 0.04 in/min (1 mm/min) to 20 in/min (500 mm/min). Elongation was measured using a rule accurate to 0.1 in (2.5 mm) to measure the distance between gage marks on the samples originally separated by 0.5 in (12.7 mm). Data were obtained at temperatures of -40°, 0°, 23°, 50°, 75°, 100°, 125°, 150° and 175°C.

Fatigue data were obtained at room temperature (23°±1°C) using a servohydraulic testing machine with a total stroke capacity of 6 in.

(152 mm). The strain measurements under cyclic loading were obtained using the same procedure as above. Results are reported at the maximum load in the cycle. Tests were carried out in zero-tension sinusoidal loading at frequencies from 2×10^{-4} to 5×10^{-2} Hz. This range of testing frequency was chosen to assure that the tests were isothermal and that hysteretic heating did not occur. The number of cycles to failure was obtained for each sample.

RESULTS

In Figure 5 are depicted the Failure Envelopes for the 15TP-14AX rubber obtained from static testing, i.e., constant rate of deformation and creep experiments. There are two things to note from this figure. First, there is a considerable amount of dispersion in the results. This is possibly due to an inherent variability in the material response due to the fact that it is a highly filled, highly crosslinked material. Second, the creep data do not fall upon the same curve as the rest of the data. This may be due to the presence of strain crystallization which results in a nonunique failure envelope (see ref. 12) or due to the fact that the rubber in the longer time tests (lower σ_b) showed extensive surface damage typical of ozone cracking in the rubber.

Figure 6 depicts typical creep behavior of the 15TP-14AX rubber under both constant and cyclic loading conditions. As can be seen, the material creeps more rapidly under the cyclic loading. However, the "acceleration" of the creep rate under cyclic loading is not as great as we had observed previously for the butyl rubber (1) nor does it

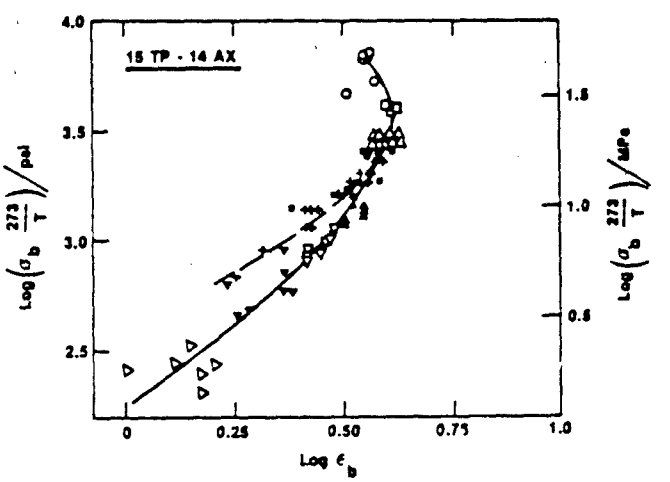


Figure 5. Failure envelope for 15TP-14AX rubber obtained from constant rate of deformation and creep experiments. Solid line is for constant rate: (○) -40°C; (□) 0°C; (△) 23°C; (●) 50°C; (■) 75°C, (▲) 100°C; (▽) 125°C; (▼) 150°C; (▷) 175°C. Dashed line is for creep: (+) 23°C.

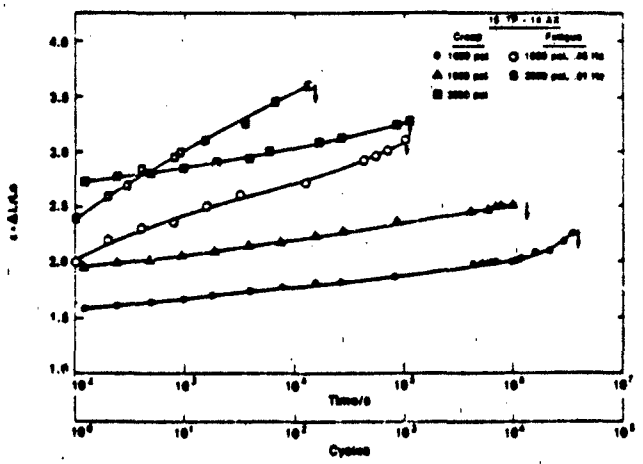


Figure 6. Typical creep behavior of 15TP-14AX rubber under cyclic (fatigue) loading and constant (creep) loading conditions at 23°C at (peak) loads and frequencies, as indicated.

appear to depend significantly upon peak stress level or test frequency, unlike what we observed previously with the filled butyl rubber.

In Figure 7 are shown the time to failure vs (peak) stress in creep and zero-tension sinusoidal loading. Interestingly, in creep loading there is a change in slope at σ=1750 psi which does not occur under cyclic loading at any frequency. The reasons for this are unclear, but may be related to a change in the mode of failure related to the onset of ozone attack of the rubber in the creep experiments in which the samples were subjected to the (peak) load for longer times than in the cyclic experiments. Of considerable interest, also, is that, concurrent with the previously mentioned fact that the creep rate under cyclic loading is not "accelerated" as much for this rubber as it was for the butyl rubber (1), the lifetime of the samples under cyclic loading is of the same order of magnitude as under static loading. This compares with the decrease of 2-4 orders of magnitude found for the filled butyl rubber (1) or a filled polyolefin rubber (2) (see Figure 2) under similar experimental conditions.

A point of importance needs to be made here about the common practice of using "high" frequency testing to "accelerate" failure. In Figure 8 are shown the lifetimes of the 15TP-14AX rubber vs test frequency at different stress levels. As can be seen the total lifetime decreases with testing frequency - the reason that high frequency testing is used. However, the slope of the lines of lifetime vs frequency is different from that which would be obtained were the number of cycles to failure, N_f, constant (cycle dependent fatigue). In fact, the difference is such that the number of cycles to failure decreases with decreasing test frequency and extrapolation of "high" frequency results to lower frequencies (assuming constant N_f) overestimates the durability of the rubber.

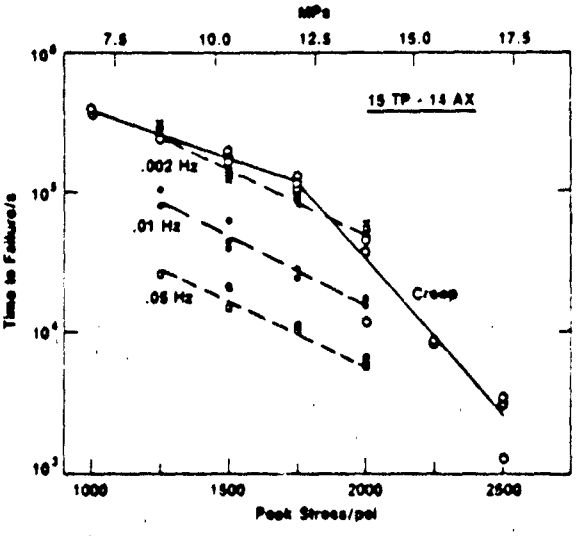


Figure 7. Time-to-failure vs (peak) load for 15TP-14AX rubber under static loading and zero-tension sinusoidal loading at different frequencies, as indicated.

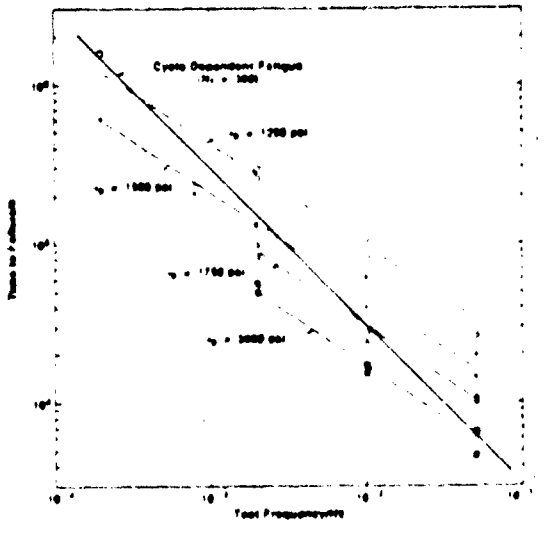


Figure 8. Lifetime vs test frequency for 15TP-14AX rubber subjected to zero-tension sinusoidal loading.

Figure 9 depicts the failure envelope for the 15TP-14AX rubber under constant rate of deformation tests, under creep loading and under cyclic loading. Unlike what has been observed previously (1) the failure envelope obtained under cyclic testing is significantly different from that obtained in the constant rate testing. Given the limited experimental data, the cyclic envelope appears to parallel the creep branch of the failure envelope but shifted by a factor $\alpha_\sigma = 1.08$. To our knowledge such behavior has not been observed previously. Thus, it appears that for the 15TP-14AX rubber the proposed failure model describes failure when the cyclic failure envelope is shifted relative to the creep failure envelope. The reasons that the creep and constant rate failure envelopes differ are uncertain at this time.

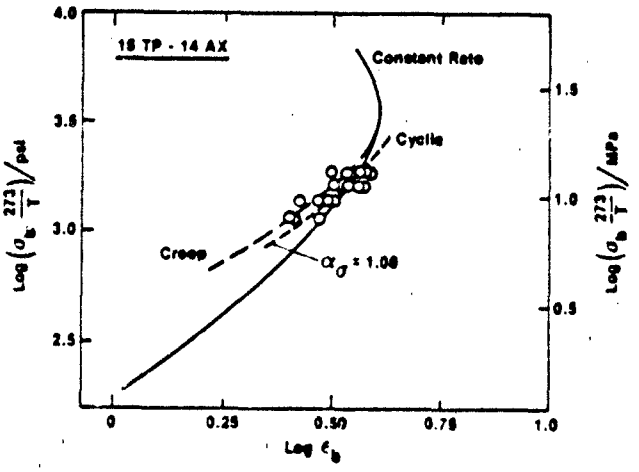


Figure 9. Failure envelopes for 15TP-14AX rubber under different loading conditions, as indicated. Points are data for cyclic loading.

ACKNOWLEDGMENTS

This work is being supported by the U. S. Army Tank Automotive Command under MIPR Number W56HZW-85-EKE-02. Thanks to P. Touchet for providing us with the rubber samples used in this study.

REFERENCES

1. G. B. McKenna and L. J. Zapas, Rubber Chem. Technol. 54, 718 (1981).
2. G. B. McKenna and R. W. Penn, J. Biomed. Matls. Res., 14, 689 (1980).
3. L. Mullins, Rubber Chem. Technol., 42, 339 (1969).
4. J. B. Donnet and A. Voet, Carbon Black: Physics, Chemistry, and Elastomer Reinforcement, Marcel Dekker, Inc., New York (1976).

5. E. M. Dannenberg and J. J. Brennan, Rubber Chem. Technol., 39, 597 (1966).
6. E. M. Dannenberg, Rubber Chem. Technol., 48, 410 (1975).
7. J. A. C. Harwood, A. R. Payne and J. F. Smith, Rubber Chem. Technol., 43, 687 (1970) also Kautsch. Gummi. Kunst. 22, 548 (1969).
8. A. I. Medalia, Rubber Chem. Technol., 45, 1171 (1972).
9. C. J. Derham and A. G. Thomas, Rubber Chem. Technol., 50, 397 (1977).
10. T. L. Smith, J. Polym. Sci., A, 1, 3597 (1963).
11. T. L. Smith and R. A. Dickie, Rubber Chem. Technol., 43, 714 (1970) also J. Polym. Sci., A-2, 7, 635 (1969).
12. T. L. Smith, J. Polym. Sci., 32, 99 (1958).
13. T. L. Smith, as cited by R. F. Fedors in "Uniaxial Rupture of Elastomers" in The Stereo Rubbers, ed. by W. M. Saltman, John Wiley and Sons, New York (1977).
14. T. L. Smith, "Strength and Extensibility of Elastomers," in Rheology, Vol. 5, ed. by F. R. Eirich, Academic Press, New York (1969).

PAUL TOUCHET
U.S. Army Belvoir Research, Development, and Engineering Center, Fort Belvoir, Virginia 22060-5606

Performance in the field of the elastomeric components of track assemblies of vehicles such as the M-60, M1, and Bradley tanks has been poor, with the service life expectancy limited to as low as 400 miles in off-the-road service. Consequently, the assistance of the Rubber and Coated Fabrics Group from the Belvoir R&D Center was requested to conduct processing and compounding studies to improve the service life of the elastomeric tank pads.

Processing studies were conducted on Stryrene-Butadiene and Natural Rubber compounds, typical of those used in fabricating tank track pads. The effects of purposely implemented alterations in formulating, mixing, and molding of the compounds were ascertained through visual examination of ingredient dispersion and physical/mechanical testing of vulcanized samples obtained for each variation. Results are analyzed in terms of the ultimate positive or negative impact upon quality and expected performance of the end item.

Compounding studies are being conducted to determine the effects of carbon blacks, various curing systems, types of polyisoprene polymers and other polymer types of properties being used to evaluate the potential of materials for tank pad applications.

A processing study to determine the effect of compounding variations on the physical properties of SBR and natural rubber compounds was conducted. A standard mixing procedure and compound formulation was selected to introduce the variations. These variations ranged from increasing and decreasing mixing times, temperature, and molding pressure to variations in the level of curing ingredients, fillers, and the use of predispersed ingredients. Table 1 shows a summary of the mixing procedures and findings of this processing study.

To determine the effect of changing the grade of natural rubber in an otherwise similar formulation, a study was conducted with eight grades of natural rubber and one compound using Guayule.

From Table 2 the tensile strength did not vary much among the 10 compounds, however, the difference is more obvious for the 200 percent modulus where the synthetic natural rubber had the lowest modulus and SMR-L the highest one. Another

TABLE 1

PROPERTIES STUDIED

TEST	TEST METHOD
• MOONEY VISCOSITY AND CURVE	ASTM D1646
• RHEOMETER DATA AND CURVE	ASTM D2084
• PROPERTIES OF CURED RUBBER RUN AT ROOM TEMPERATURE:	
• SPECIFIC GRAVITY	ASTM D297, PARA 15
• TENSILE STRENGTH	ASTM D412
• ELONGATION	ASTM D412
• 100 AND 200% MODULUS	ASTM D412
• HARDNESS, IRHD	ASTM D1415
• RESILIENCE, BASHORE REBOUND	ASTM D2632
• TEAR STRENGTH, DIE C AND DIE B	ASTM D624
• TROUSER TEAR WITH FABRIC INSERT	
• ABRASION, TABER	ASTM DJ389
• ABRASION, PICO	ASTM D2228
• COMPRESSIBILITY	
• DISPERSION RATING AS OBSERVED UNDER A 60 POWER MICROSCOPE & DARK FIELD MICROSCOPY	
• PUNCTURE RESISTANCE	
• PROPERTIES ON CURED MATERIAL RUN AT 212°F, 250°F AND 300°F:	
• TENSILE AND ELONGATION	ASTM D412
• TEAR STRENGTH, DIE C	ASTM D624
• TROUSER TEAR WITH FABRIC INSERT	
• COMPRESSIBILITY	
• PUNCTURE RESISTANCE	
• FLEX FATIGUE TESTS:	
• DEMATTIA AND ROSS CUT GROWTH UNAGED AND AFTER AGING 70 HOURS @ 212°F	ASTM D813
• GOODRICH FLEX AT 122°F	ASTM D623, METHOD A USING A .175 IN. STROKE AND 141.6 PSI FOR DETERMINING HEAT BUILD UP AND USING A 0.30 INCH STROKE WITH 14..6 OR 265.4 PSI PRESSURE FOR BLOW-OUT TEST

TABLE 1

PROPERTIES STUDIED (Continued)

EFFECT ON SBR PROPERTIES	PROCESSING & COMPOUNDING VARIATIONS	EFFECT ON NATURAL RUBBER PROPERTIES
REDUCED TENSILE, TEAR, DEMATTIA AND GOODRICH FLEX FATIGUE; IMPROVED ABRASION	1. INCREASED BATCH SIZE	IMPROVED PICO ABRASION AND GOODRICH BLOW OUT
NO SIGNIFICANT CHANGE	2. DECREASED BATCH SIZE	NO SIGNIFICANT CHANGE
NO SIGNIFICANT CHANGE	3. NO MASTICATION	NO SIGNIFICANT CHANGE
NO SIGNIFICANT CHANGE	4. INCREASED MASTICATION	NO SIGNIFICANT CHANGE
NO SIGNIFICANT CHANGE	5. REDUCED MIX TIME	NO SIGNIFICANT CHANGE
IMPROVED TABER ABRASION; DEMATTIA FLEX FATIGUE	6. INCREASED MIX TIME	REDUCED TENSILE STRENGTH; SOME IMPROVEMENT IN GOODRICH BLOW OUT
IMPROVED TABER ABRASION	7. MIX TEMPERATURE, > 200°F	SLIGHT IMPROVEMENT IN GOODRICH BLOW OUT
NO SIGNIFICANT CHANGE	8. TREATED OR PREDISPERSED ZINC OXIDE	IMPROVED ABRASION AND SLIGHT IMPROVEMENT IN GOODRICH BLOW OUT
NO SIGNIFICANT CHANGE	9. SPIDER SULFUR	IMPROVED TABER ABRASION AND SLIGHT IMPROVEMENT IN BLOW OUT
NO SIGNIFICANT CHANGE	10. PREDISPERSED CURING INGREDIENTS	IMPROVED GOODRICH BLOW OUT
NO SIGNIFICANT CHANGE	11. REDUCED ACCELERATOR	IMPROVED TABER ABRASION AND DEMATTIA FLEX AFTER AGING
SLIGHTLY REDUCED BLOW OUT	12. REDUCED SULFUR	IMPROVED ABRASION, DEMATTIA FLEX AND SLIGHT IMPROVEMENT IN BLOW OUT
REDUCED TENSILE, ELONGATION, TEAR AND DEMATTIA AT ROOM TEMPERATURE; IMPROVED BLOW OUT	13. INCREASED SULFUR	REDUCED ABRASION, TEAR STRENGTH, AND DEMATTIA AT ELEVATED TEMPERATURE; IMPROVED DEMATTIA AT ROOM TEMPERATURE AND BLOW OUT

TABLE 1

PROPERTIES STUDIED (Continued)

EFFECT ON SBR PROPERTIES	PROCESSING & COMPOUNDING VARIATIONS	EFFECT ON NATURAL RUBBER PROPERTIES
SLIGHT IMPROVEMENT IN BLOW OUT	14. CHANGE IN BLACK	LOWER TEAR & TABER ABRASION; IMPROVED DEMATTIA FLEX AND BLOW OUT
IMPROVED BLOW OUT	15. CHANGED POLYMERS	NO SIGNIFICANT CHANGES EXCEPT LOWER TEAR FOR SYNTHETIC NATURAL
REDUCED ABRASION & DEMATTIA; IMPROVED GOODRICH FLEX PROPERTIES	16. HIGH SPEED MIXING WITH 220°F DUMP	REDUCED DEMATTIA; IMPROVED BLOW OUT
REDUCED ABRASION & DEMATTIA; IMPROVED GOODRICH FLEX PROPERTIES	17. SUBSTITUTION OF VISTENAMER 8012	REDUCED DEMATTIA; IMPROVED BLOW OUT
REDUCED TABER ABRASION & DEMATTIA UNAGED; IMPROVED DEMATTIA AFTER AGING	18. INCREASED CURE TEMPERATURE	REDUCED DEMATTIA; IMPROVED BLOW OUT
REDUCED TABER ABRASION & DEMATTIA UNAGED; IMPROVED DEMATTIA AFTER AGING & BLOW OUT	19. REDUCED CURE TEMPERATURE	IMPROVED PICO ABRASION, TEAR & BLOW OUT
REDUCED DEMATTIA UNAGED; IMPROVED DEMATTIA AFTER AGING & BLOW OUT	20. REDUCED CURE TIME	IMPROVED ABRASION & BLOW OUT; REDUCED DEMATTIA AFTER AGING
REDUCED DEMATTIA UNAGED; IMPROVED DEMATTIA AFTER AGING	21. INCREASED CURE TIME	NO SIGNIFICANT CHANGE
REDUCED TENSILE & DEMATTIA; IMPROVED TABER ABRASION & BLOW OUT	22. REDUCED CURE PRESSURE	REDUCED TENSILE & DEMATTIA AFTER AGING; IMPROVED BLOW OUT AND TEAR STRENGTH

TABLE 2

EFFECT OF POLY-ISOPRENE POLYMER ON PROPERTIES

PROPERTIES	NAT-1 NATURAL RSS-1	NAT-10 NATURAL SMR-CV	NAT-20 NATURAL SMR-GP	NAT-50 NATURAL SMR-5	NAT-60 NATURAL SMR-WF	NAT-70 NATURAL SMR-L	NAT-21 NATURAL PALE CREPE # 1	NAT-27 SYNTHETIC AMERIPOL SN-606	NAT-85 GUAYULE N-351 TEXAS A&M
ORIGINAL PROPERTIES									
TENSILE STRENGTH, PSI	3,870	3,353	3,480	3,897	4,083	4,063	3,209	3,550	3,433
20.3% MODULUS, PSI	712	721	742	887	1,000	1,020	737	571	1,150
ELONGATION, %	503	493	503	527	533	517	453	560	443
HARDNESS, IRHD, PTS.	71	71	70	68	68	67	68	65	75
REBOUND, %	44	44	45	44	42	41	48	46	41
TABER ABRASION, GR./1000	.3517	.4364	.4396	.0340	.0402	.0283	.3989	.4198	.3566
TEAR STRENGTH, ASTM DIE C									
UNAGED, LB/IN	595	570	591	563	621	484	632	457	452
AT 250° F, LB/IN	296	293	323	353	290	288	328	288	190
FLEX FATIGUE TESTS									
DEMATTIA, CRACK GROWTH									
UNAGED, MIL/MIN	18.5	14.3	16.9	12.3	19.3	17.7	14.1	17.2	21.3
20 HRS. @ 250°F, MIL/MIN	127.	271.	99.0	317.	196.	264.	467.	227.	36.7
GOODRICH FLEX									
TEMPERATURE RISE, °C	24.	25.3	21.6	17.7	18.0	18.3	20.6	22.8	17.7
BLOW OUT TIME, MIN	29	21	31	58	52	63	44	36	120
HEAT RESISTANCE AT 250°F									
F/F_0 = 70%, MIN	110	60	70	100	120	90	72	125	153

important finding was the use of ten parts of trans-polyoctenamer (a German polymer to aid processing) which produced a marked increase in modulus.

Tear strength values were about twice as high in value when compared to SBR, with the best retention after aging exhibited by SMR-GP. The resistance to crack growth dropped dramatically after heat aging at 250 F, in some instances more than 97 percent. The results after aging were spread over a wide range, making a valid assessment very difficult.

To determine the effect of different carbon blacks on natural rubber, 10 compounds were evaluated. Table 3 shows the physical properties for all ten different carbon blacks which include small particle sizes to large particle sizes, as well as high and low structures. Included in the study were also some specialty, conductive, and limited production carbon blacks. A more detailed explanation in the classification of these fillers can be found under ASTM method D-1765. The formulation used was natural rubber-100, zinc oxide-4, stearic acid-2, carbon black-45, TMQ antioxidant-0.5, PPD antioxidant-0.5, DOPPD antiozonant-3, sulfur-2.5, and accelerator-0.8 parts by weight.

The reinforcement level is consistent with the lower particle size, high providing higher tensile strength. The heat buildup was relatively low for all types of carbon blacks, the one with larger particle size performing the best. Also, the more reinforcing types (small particle size, i.e., N-121, N-110) exhibited better crack growth resistance than the ones with larger particle size (i.e., N-351).

Vulcanization is an irreversible process by which rubber is changed from a plastic material to an elastic one by means of heat and pressure. The process consists of the formation of a molecular network by chemically tying together the independent chain molecules forming cross-links. These cross-links may be chains of sulfur atoms, carbon-carbon bonds, polyvalent organic radicals or polyvalent metal ions. Sulfur is the oldest vulcanization agent for rubber, however, the efficiency of sulfur curing varies inversely with the average number of sulfur atoms per cross-link. The use of accelerators produces vulcanizates more resistant to heat, chemical attack, and retention of properties upon aging. Since retention of properties after heat aging is a very important consideration for the application on hand, we studied the effect of various curing systems on the physical properties of natural rubber compounds.

TABLE 3

EFFECT OF TYPE OF CARBON BLACK ON PROPERTIES

PROPERTIES	NAT-1 SAF N-110	NAT-19 SAF-HS N-121	NAT-57 N-110 + XE2	NAT-16 ISAF N-220	NAT-18 ISAF-HS N-234	NAT-41 GPF-HS N-299	NAT-44 HAF N-330	NAT-42 HAF-LS N-326	NAT-43 HAF-HS N-351	NAT-36 XCF N-472
ORIGINAL PROPERTIES										
TENSILE STRENGTH, PSI	3,870	4,397	4,017	3,476	3,811	3,717	3,513	3,800	3,713	3,253
200% MODULUS, PSI	712	1,063	870	881	865	1,197	1,093	897	1,207	880
ELONGATION, %	503	517	510	440	493	453	430	507	447	490
HARDNESS, IRHD, PTS.	71	65	69	70	71	70	65	66	66	67
REBOUND, %	44	47	42	47	47	48	55	51	52	48
TABER ABRASION, GR./1000	.3517	.2527	.0410	.4722	.5540	.2707	.3525	.4096	.2974	.3261
TEAR STRENGTH, ASTM DIE C										
UNAGED, LB/IN	595	544	609	496	512	478	477	454	555	504
AT 250° F, LB/IN	296	254	274	252	289	289	242	243	250	288
FLEX FATIGUE TESTS										
DEMATTIA, CRACK GROWTH										
UNAGED, MIL/MIN	18.5	24.3	14.3	16.9	18.2	18.3	19.3	14.8	18.5	15.3
20 HRS. @ 250°F, MIL/MIN	127.	1281.	1000.	75.	97.	102	79.	129	111	102.
GOODRICH FLEX										
TEMPERATURE RISE, °C	24.	15.7	18.5	20.3	22.2	20.8	14.	16.8	17.8	19.2
BLOW OUT TIME, MIN	29	61.	61.	> 120	> 120	65.	> 120	> 120	> 120	68.
HEAT RESISTANCE AT 250°F										
F/F_0 = 70%, MIN	110	123	173	135	133	168	218	177	228	140

NOTE: COMPOUNDS CONTAINED 45 PARTS OF BLACK

Various curing systems were investigated to modify and improve heat resistance properties (Table 4). Some of the accelerated cure systems used were: a) Sulfur, b) Sulfenamides, c) Thiurams, d) Dithiocarbamates, e) Thiazoles, and f) Urethanes.

The chemistry of these accelerated vulcanization systems is a very complex one and the selection of an ideal system is a very difficult task. Different types of accelerators give vulcanization characteristics which differ in resistance to scorch and the rate of vulcanization after cross-link formation starts. In Table 5 the curing systems are compared and properties of the cured samples are shown in Table 6.

TABLE 4

EFFECT OF CURING SYSTEMS ON PROPERTIES

	NAT-1	NAT-22	NAT-25	NAT-37	NAT-48	NAT-64	NAT-65	NAT-68	NAT-69
PROPERTIES									
FLEX FATIGUE PROPERTY									
DEMATTIA FLEX									
UNAGED									
GROWTH RATE, MIL/MIN	18.5	6.8	18.2	7	23.4	18.4	21	8.3	14.8
70 HRS. @ 212°F									
GROWTH RATE, MIL/MIN	24.2	8.8	25.5	7.3	27.1	12.5	28.3	5.7	48.1
20 HRS. @ 250°F									
GROWTH RATE, MIL/MIN	127	8	53	52.	217	12.	27.	7.	27
CRACK INITIATION									
CYCLE x 1000	71.5	41.5	33.5	26.5	22.5	21	21	58	52.4
GOODRICH FLEX @ 50°C									
TEMPERATURE RISE, C	24	31.5	23.7		18.3	23	23.8	21	18.2
PERMANENT SET, %	3.2	3.7	1.8		1.4	8.3	8	4.8	4.3
BLOW OUT TIME									
@ 141.6 PSI, MIN.	28	120	>120	>120	>120	>120	>120	>120	>120
@ 286.4 PSI, MIN.	12	8.5	13.1	6.3	22.4	8	8.9	6.5	12.3
COMPRESSIBILITY									
UNAGED									
10%, PSI	139	141	118	88	152	185	247	86	100
20%, PSI	282	273	218	145	312	257	373	152	198
40%, PSI	718	583	638	376	926	257	373	152	198
70 HOURS @ 250°F									
10%, PSI	104	97	98	98	131	98	135	35	73
20%, PSI	183	157	155	158	211	186	232	86	153
40%, PSI	428	378	438	387	447	372	538	183	382
HEAT RESISTANCE									
F/FO = 70, MIN.	118	282	678	578	158	883	543	383	337

TABLE 5

COMPARISON OF VARIOUS CURING SYSTEMS

	NAT 1	NAT 22	NAT 25	NAT 37	NAT 48	NAT 54	NAT 55	NAT 58	NAT 59
SULFUR	2.5	.4	.75	-	4.0	.4	.95	-	1.3
SANTOCURE	8					-	.18	-	-
BUTYL TAUDS			.625		-	-	-	-	-
OCTOATE Z			1.5		-	-	-	-	-
AMYL LEDATE			1.0	-	-	-	-	-	-
AMAX			1.875	-	-	-	-	-	-
NOVOR 924		4.2			-	-	-	-	-
TMTM MONEX		1.5			-	1.5	1.92	-	-
SANTOCURE NS		.08				1.08		-	-
METHAZATE					1.0				
NOVOR 950					-	4.2	7.32	-	
VULKACIT J						-		2.7	
SANTOCURE IPS									3.2
SANTOGARD PVI						-		-	8.2
ETHYL CADMATE				1.5	-	-	-	-	-
MORFAX				1.5		-		-	-

TABLE 6

EFFECT OF CURING SYSTEMS ON PROPERTIES

	NAT-1	NAT-22	NAT-25	NAT-37	NAT-48	NAT-54	NAT-56	NAT-58	NAT-59
PROPERTIES									
ORIGINAL PROPERTIES									
TENSILE STRENGTH, PSI	3878	3289	3837	3388	3443	3398	3057	3787	4257
200% MODULUS, PSI	712	543	748	447	1278	587	889	583	948
ELONGATION, %	583	533	537	623	440	583	478	587	533
HARDNESS, IRHD	71	77	85	58	71	75	84	58	88
BASHORE REBOUND, %	44	44	46	41	48	43	44	44	47
SPECIFIC GRAVITY	1.108	1.11	1.1094	1.108	1.1239	1.071	1.0745	1.0879	1.1048
CURE, MIN/F	2[illegible]/300	20/300	20/300	15/300	15/280	40/300	35/300	35/300	30/300
ABRASION									
TABER, G/1000 CYCLES	.3617	.2529	.1655	.836	.3533	.8718	.1918	.1218	.1428
TEAR STRENGTH									
ASTM DIE C, LB/IN									
UNAGED	595	704	479	479	361	540	335	552	614
10 MIN. @ 250°F	296	288	270	B	226	>2248	224	>2038	333
4 HOURS @ 250°F	246	253	184	B	182	258	214	>2008	218
4 HOURS @ 300°F	186	144	138	B	>199	181	188	850	91
MOONEY VISCOMETER									
ML 3+4 (212)	49.2	63.9	47.3	35.6	37.5	28.8	29.1	34	38.4
T_s @ 250, MIN.	11.8	18.1	10	7.3	3	6.4	4.9	44.8	38.8

ELASTOMERS REINFORCED WITH FIBRILLATED KEVLAR FIBER

J. A. CROSSMAN, D. C. EDWARDS, J. WALKER
Polysar (Reprinted article)

Elastomers Research and Development

Elastomers Reinforced with Fibrillated KEVLAR Fiber

Research Objectives (Elastomers reinforced with KEVLAR)

- Explore feasibility of developing a process to disperse short fibrillated KEVLAR fibers in elastomers.
- Explore mechanisms and properties of reinforcing polymers with short fibers to significantly improve their tear strength and toughness. For tire and non-tire applications for a wide variety of elastomers.

Needs

- A novel, effective, efficient process to disperse fibers in elastomers during their manufacture since such fibers cannot be dispersed during conventional mixing and compounding.
- To significantly enhance reinforcement of elastomers for tough tire and non-tire applications.
- Fast, easy mixing to ensure good dispersion in compounds.

Results

- A process has been developed to obtain excellent dispersion of fibrillated KEVLAR fibers in a variety of elastomers.
- Elastomers reinforced with fibrillated KEVLAR fibers during the manufacturing process can be compounded using conventional rubber mixing procedures.
- Vulcanizates exhibit high modulus, hardness, and tear strength.
- Patents pending.

For Further Information Contact:
Polysar Limited
Elastomers Research & Development Division
South Vidal Street, Sarnia, Ontario, N7T 7M2
Tel. (519) 337 8751

Project Status

Research

- Semi commercial pilot plant for producing KEVLAR reinforced elastomers XC-940 (SBR), and XC-945 (NBR).
- Bench scale unit for producing other polymers reinforced with KEVLAR.

Potential Applications

Tires

Tread

- Mining, off the road, logging, heavy duty
- Improved cut and tear resistance
- " (15 to 25 phr XC-940)

Under Tread

- High modulus cut and penetration resistance
- (25 to 50 phr XC-940)

Bead Apex

- High hardness, modulus, and bending stiffness
- (25 to 100 phr XC-940)

Chafer Strips

- High modulus
- (15 to 50 phr XC-940)

Non Tire

Track Pads

- Cut and tear resistance

Hydraulic Hose

- High green strength (reduced necking down of spiral wire), high modulus

Timing Belts

- High modulus, reduced compressibility.

Packing Cup

- Improved dimensional stability.

Gaskets

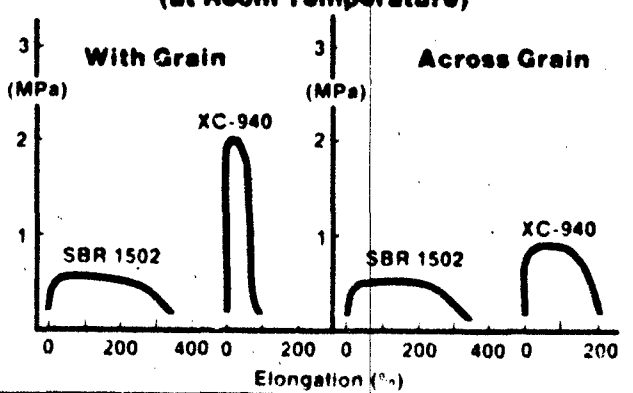
- Improved tear strength

'O' Ring

- Improved resistance to extrusion

Green Strength — SBR 1502 vs XC-940

(at Room Temperature)



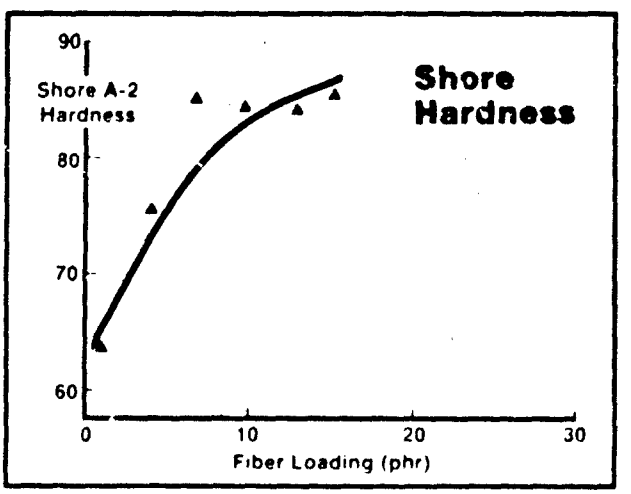
Reinforced Elastomers

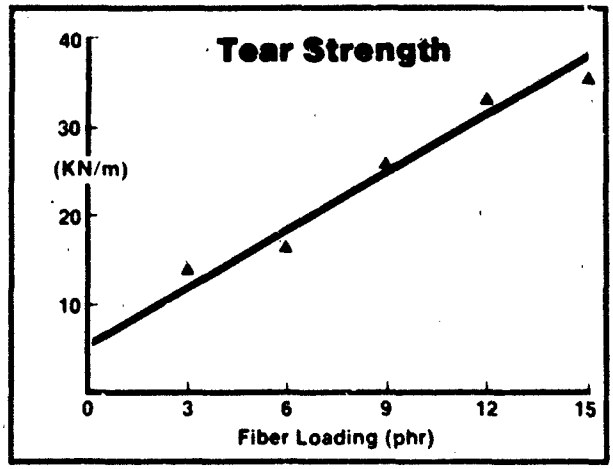
— Uncured Properties

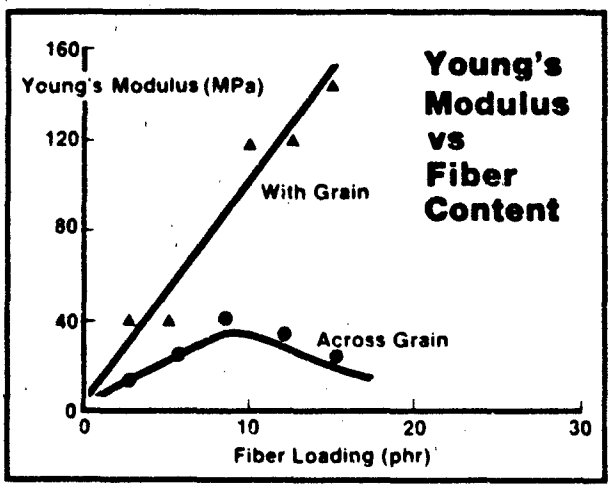
- Higher green strength
- Improved dimensional stability
- Higher viscosity

— Cured properties

- Increased hardness
- Very high Young's modulus
- Improved cut resistance
- Higher bending stiffness
- Better penetration resistance
- Good tear resistance




Tear Strength
40
30
(KN/m)
20
10
0
3
6
9
12
15
Fiber Loading (phr)


160
Young's Modulus (MPa)
120
80
40
0
With Grain
Across Grain
Young's Modulus vs Fiber Content
0
10
20
30
Fiber Loading (phr)

Physical Properties of KEVLAR Reinforced SBR

Fiber Loading (phr)			0	3	6	9	12	15
Tensile strength	(MPa)	(W)	30.5	23.7	18.8	20.1	23.5	23.1
		(A)	25.0	19.6	16.2	14.2	12.5	11.9
100% Modulus	(MPa)	(W)	2.55	10.5	16.7	—	—	—
		(A)	2.48	4.31	8.15	11.1	11.8	9.96
300% Modulus	(MPa)	(W)	17.4	20.1	—	—	—	—
		(A)	16.9	16.3	—	—	—	—
Ultimate elong. (%)		(A)	430	350	260	30	20	20
		(W)	360	350	260	190	110	140
Young's modulus	(MPa)	(W)	5.8	39.5	38.5	120	124	144
		(A)	6.9	10.9	22.5	32.0	24.8	19.8
Shore A-2 hardness			65	75	85.5	84	85	87

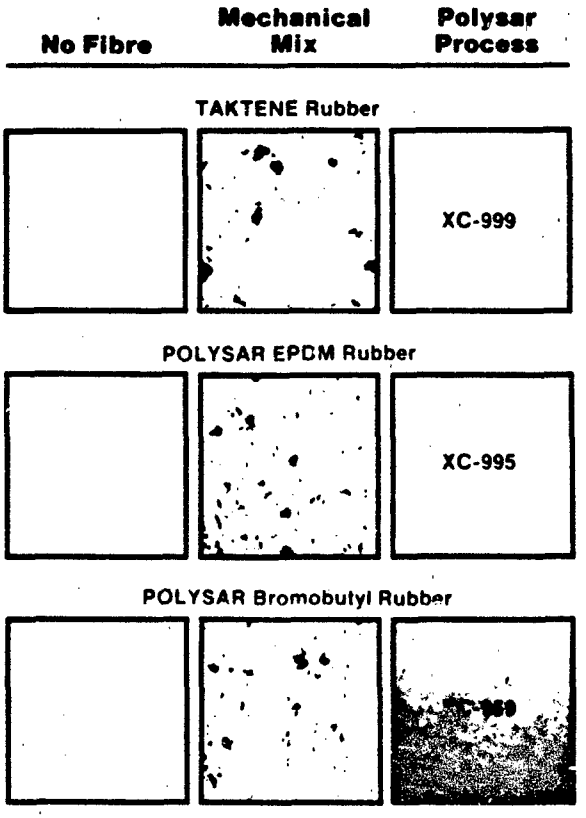
Compound Formulation

Krylene 1502	100
KEVLAR fiber	Variable
Vulcan 6 (N220 black)	50
Sundex 8125	3
NBS ZnO	3
NBS Stearic acid	1.5
Santoflex 13	.5
Santoflex 77	.5
DPG	.3
Santocure NS	1.2
NBS Sulfur	2

Press Cure. 10 min at 150 C

Process Capabilities — Dispersion Characteristics (with 10 phr fiber)

Solution Polymers



POLYSAR Process vs Banbury Mixing (Mechanical Addition)

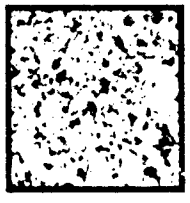
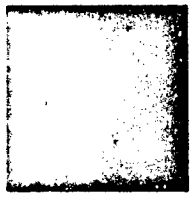
Banbury Mix

Dispersion after 30 minutes
Mixing in Model B Banbury

POLYSAR Process

Dispersion after 5 minutes
Mixing in Model B Banbury

Emulsion Polymers

No Fibre	Mechanical Mix	Polysar Process
KRYLENE Rubber		
		XC-940
KRYNAC Rubber		
		

High-strength, light weight Du Pont KEVLAR aramid fiber has been used for years in:

- Tires
- Mechanical rubber goods
- Advanced: fiber-reinforced composite parts for aircraft, boats and automobiles
- Bullet-resistant apparel
- Large ropes and cables
- Brakes and clutch facings
- Gasket Sheeting
- Cut- and heat-resistant protective apparel

Now chopped KEVLAR fiber and pulp are being used to reinforce molded elastomeric products, too.

Small amounts of KEVLAR added to an elastomer can achieve:

- Increased heat resistance
- Improved strength at high temperatures
- Excellent tear strength
- Improved creep resistance
- Good wear resistance
- Improved modulus

KEVLAR can solve design problems in a variety of applications. Evaluations are underway in O-rings, gaskets, reinforced hoses, tank treads, and other applications demanding excellent strength at high temperatures.



KEVLAR Pulp | KEVLAR Pulp Fibrillated | Chopped Fiber | Sample

POLYSAR

POLYSAR, KRYFLEX, KRYLENE, KRYMIX, KRYNAC, KRYNOL, TARTENE, TRANS-PIP and SS 250 are registered trade marks of Polysar Limited, Sarnia, Ontario, Canada.

Information given herein is furnished in good faith, without warranty, representation, inducement or a license of any kind. Polysar does not assume any legal responsibility for use of or reliance upon same. No warranty or representation is given that Polysar products described will be suitable in purchasers' formulations or processes for any particular end use. No representation is given as to freedom from patent infringement. Materials not manufactured or supplied by Polysar may present hazards in handling and use. Reference should be made to the manufacturer or supplier for all information relating to such materials.

08-85
PRINTED IN CANADA

TACOM TRACK RUBBER PROGRAM

G. C. SZAKACS, M. KING, AND J. PATT
U. S. Army Tank Automotive Command, Track & Suspension Group:
AMSTA-RTT, Warren, Michigan 48397-5000

The track and suspension rubber requirements for Army tanks and other tracked vehicles are summarized, with an emphasis on the Abrams M-1 Main Battle Tank. Comparisons are given for various vehicles to illustrate the severe demands placed on the M-1 (T-156) track in terms of relative loading, speed, and other factors. TACOM is sponsoring a wide variety of efforts designed to improve track rubber performance. The program includes fundamental material characterization, material prototype development, mathematical modeling studies, and alternate engineering design considerations.

WORKSHOP PANEL DISCUSSION ON TRACK RUBBER--PRESENT REQUIREMENTS AND FUTURE PROSPECTS

CHAIRMAN: ROBERT E. SINGLER--U. S. Army Materials and Mechanics Research Center
PANEL MEMBERS: A. ALESI--AMMRC; D. LESUER--Lawrence Livermore Labs; J. MCGRATH--Virginia Polytechnic Institute and State University; A. MEDALIA--Retired, Cabot Corporation; J. PATT--U. S. Army Tank Automotive Command; G. SZAKACS--U. S. Army Tank Automotive Command; P. TOUCHET--U. S. Army Belvoir R&D Center

INTRODUCTION

Since improved track rubber performance is a critical Army readiness requirement, an open panel discussion was held to focus on this need. The panel convened on the last day in order to take advantage of all that was discussed during the week. Approximately 40 of the conference attendees were present at this session.

The M-1 and M-60 fighting vehicles are both main battle tanks in the heavy weight class. The combat weight (in round numbers) of the M-1 and M-60 tanks is 60 tons and 54 tons, respectively. There have been several versions of the M-60 since it was introduced in 1959.

Although the M-60 is still in use, the M-1 tank was developed to meet the threat of the larger number of tanks in use by the Warsaw Pact countries. The M-1 tank is the heaviest, fastest, hardest hitting, best protected tank the Army has ever produced. It is the first really new type of tank the U.S. has built since the 1950s. The M-1 was introduced in 1980. The M-1 series of tanks are expected to be the Army's main battle tank into the 21st century.

The format for the panel was for the chairman to make some opening remarks, to be followed by discussions from individual panel members. The panel had been given a list of questions from which they could choose to address the problem (Table 1). After the panel discussion, the audience was invited to participate with their opinions or by asking questions of the panel members. The audience had also been provided the list of questions in Table 1.

TABLE 1

WORKSHOP PANEL DISCUSSION QUESTIONS REGARDING TRACK RUBBER--
PRESENT REQUIREMENTS AND FUTURE PROSPECTS

1. Can the traditional approach (new rubber formulations and compounding procedures) still lead to significant improvements in track rubber?

2. New Materials--Are there any we should try? Can new polymer structures be designed which would lead to rubbers able to meet the performance requirements for track pads? Will reinforcements be useful?

3. The chunking of track pads on cross country courses and the abrasion of pads on paved roads are two track pad failure mechanisms. Heat build-up is also a problem. Past experience has shown that the improvement of the resistance to one, resulted in a decrease of resistance to the other and vice versa. This seems to be true for filled elastomers and polyurethanes. Do we have to accept this as unavoidable?

4. Computer Modelling Studies--What do they tell us? How can we use them?

5. How realistic is it to try to simulate field performance in the laboratory?

6. Where are we lacking fundamental knowledge?

7. It is more than just a materials problem. What can be expected from design?

8. How do we define elastomer fracture criteria and what properties affect fracture?

9. Modelling--Are the computer codes we are using useful or do we need more development in this area?

DISCUSSION

Chairman: Opening remarks included pictures of new and worn M-1 track blocks. The worn M-1 track blocks served to illustrate the severe failure modes: chunking and tearing of

the rubber, and blowouts caused by heat build-up. Separation of the rubber from the metal parts and abrasion could be seen as well. The wearing of a single track block is generally the result of several processes, although in some cases, a specific wear process such as tearing or heat build-up would predominate.

The revised specification, MIL-T-11891D, was also discussed, focussing on the reference compounds which provide a basis for comparison and qualifications of the vendors proprietary materials. The reference compounds are listed in Table 2. There is also an accelerated heat build-up test on M-1 (T-156) track blocks in the specification that is used to screen out materials with poor hysteresis characteristics. This is a dynamic compression (30 Hz) test with a static load of 1900 lbs. and a dynamic load of 2300 lbs. Good materials will last about 30 minutes before blowout occurs. Temperatures can be as high as 600°F.

TABLE 2

MIL-T-11891D TRACK BLOCKS AND PADS RUBBER COMPOUNDS

Materials	Parts Per Hundred Rubber-PHR	
	Ground Side	Wheel Side
Styrene-Butadiene SBR-1500	35	60
Polybutadiene Taktene-220	30	40
Natural Rubber SMR-20	35	0
N220 Carbon Black	65	65
Zinc Oxide	3	3
Stearic Acid	1.50	1.50
Sunolite 100--Hydrocarbon Wax	1.50	1.50
Santoflex 13--Antidegradant	3	3
Flectol Flakes--Antidegradant	2	2
Sundex 790--High Aromatic Oil	4	4
Sulfur	1.3	1.3
Dibs Sulfenamide Accelerator	3.2	3.2
Santogard PVI	0.2	0.2
	184.70	184.70

Geza Szakacs, Acting Chief, Track & Suspension Group, gave an overview of the TACOM track program, focussing on the M-1 track. From a military standpoint, the track is operationally successful for the M-1 to perform its mission. The problem is primarily one of logistics and supply costs: track repair and replacement costs are currently running over $100 million per year and are expected to be over $200 million per year by 1990 with full implementation of the M-1 tank by the Army. Thus, improvements must be made to keep costs at an acceptable level.

About 11 percent of the gross vehicle weight is normally allotted to the track. The M-1 tank uses an integrally molded pad design (designated T-156) which is a lighter track, accounting for only 7 percent of the gross vehicle weight. On this basis alone, the materials used, both rubber and metal, must be more durable than before. Besides investigating new materials, alternate designs are being evaluated, such as the German Diehls track and the replaceable pad (T-158) track. These alternate designs are heavier tracks. Testing to date on alternate designs has been inconclusive.

TACOM is also pursuing the development of three common track designs for three weight classes of vehicles. A common track for a weight class (heavy, medium, light) could simplify logistics and reduce maintenance costs.

In the future, track requirements will be more severe. Top cruising speed for the M-1 is 45 mph; future tanks are projected at 60-75 mph. Computer modeling studies are being conducted at Waterways Experimental Station and Battelle Laboratories.

Dr. Donald LeSuer, Lawrence Livermore Laboratories (LLL), narrated a movie that was taken by LLL more than 5 years ago at Yuma Proving Grounds, which showed an M-60 pad undergoing deformations in contact with a road surface. This movie was part of a TACOM sponsored program, and it still provides one of the best examples of the types of deformation that the rubber must endure in service. Pads filmed were both at ambient temperatures and preheated to 100°C prior to service.

Anthony Alesi, Composites Development Division, AMTL, commented on two of the listed questions. Are the service conditions under which tracked combat vehicles operate too severe for conventional rubber materials to withstand? Little improvement in mileage has been achieved from material changes in the past 5 years or so of determined and extensive effort. Although a better understanding of the phenomena involved has been obtained, we have not been able to use it to improve

service life. Can reinforcement with fibers make up what has been lacking in rubber? Such reinforcement could serve as crack or tear arrestors and perhaps reduce or eliminate chunking. Also, they could provide stiffness which properly oriented would reduce heat generation by hysteresis, and, by reducing deformation, diminish abrasion wear. Reinforcing fibers will, if not properly chosen and incorporated, perhaps reduce service life. This will be the case if the bond between rubber and fiber is not made or is broken when the rubber undergoes large deformations. The very large difference in moduli of fibers and rubbers will produce large stresses at the fiber surface. An appropriate fiber content for optimum content resistance to abrasion wear is unknown.

We also noted that cross country operation is regarded as a more severe use than operating on paved roads and seems to be true for tanks. However, the M-2 Bradley Fighting Vehicle is achieving in field tests service on the order of 3000 miles in cross country operation but only 350 miles on paved road. Jack Patt indicated that compared to the tank track shoes, the BVF pad was thinner.

Paul Touchet, Ft. Belvoir, summarized compounding studies conducted at Ft. Belvoir during the past 2 years. The emphasis has been NR and NR-SBR-BR blends. They have also been accumulating data on commercial samples.

Ft. Belvoir has a data base on materials being considered for track applications. However, it is often difficult to get prototypes made and tested. We do not have enough field data to compare with laboratory data, and this we must have if we are to effectively address the problem. We do not have sufficient means of predicting field performance in the laboratory.

Dr. Avrom Medalia, Cabot Corporation (retired), stressed the need for laboratory simulation of field performance. He proposed new instrument designs for testing heat build-up and abrasion in track pads.

Dr. James McGrath, Virginia Polytechnic Institute, discussed the use of new synthetic materials as an approach to the problem. As much as 25 percent improvement might be available in off-the-shelf commercial materials. Materials such as low nitrile rubber or various thermoplastic elastomers should be examined.

Dr. Jacob Patt, TACOM, stressed the need for laboratory models to simulate field performance. He mentioned that Michigan Technological University is designing an instrument to

better simulate heat build-up in the laboratory. Laboratory simulation is becoming even more important as the costs for track testing increase: The M-60 costs around $600,000 as compared to the M-1 of more than $1,000,000. Thus, we need to derive much information from our laboratory work as possible in order to circumvent the time and costs involved in field testing.

Open Panel Discussion: There was general agreement among the participants that the relationship between the Army and the major track rubber suppliers has not been conducive to solving the problem. As an example, although invited to Sagamore, they chose not to attend the conference.

The feeling expressed by some of the participants was that the major suppliers are not doing all they can to correct the problem. The materials they are supplying the government have not changed appreciably in years. They are resistant to changes in the specifications, such as implementation of standard quality control procedures in the compounding and manufacturing of track rubber components.

Improvement in track rubber performance using short fiber reinforcement was mentioned during the panel discussion. Three posters in this area were given earlier in the week, which described the general principles as well as providing some commercial examples such as off-the-road tires. It was mentioned that the Army is evaluating cellulose and aramid fiber reinforced rubber compounds.

One other problem area mentioned was that of making prototypes and having them tested. We have had difficulty in getting experimental rubber compounds custom mixed and processed into desired shapes for manufacturing. The Army does not have in-house capabilities available for large scale custom mixing and processing (normally extrusion) necessary for manufacturing at Red River Army Depot. Large quantities (500 lbs.) of rubber are necessary to manufacture the quantities of track shoes required for field testing. Large custom mixes and processing by Army standards are small compared to most commercial requirements, and it has been difficult to get industry to participate at these stages. However, the situation may be changing for the better as government contacts with industry increase.

SUMMARY

The panel forum stimulated considerable discussion among the conference attendees. It raised a number of questions,

many of which were left unanswered, but it provided an effective forum for exchange of ideas. The meeting ended on a positive note--the prospects for more cooperation among those working in the area along with some fresh insights from those having to date only a brief exposure to the problems. The stage is set for measurable progress in this area, provided we meet the challenge.

BANQUET PRESENTATION

ERNEST H. ZIELASKO[1], ROBERT E. GLEASON[2]
(1) Publisher, Rubber & Plastics News, (2) Midwest Sales Manager, Rubber & Plastics News.

I'm delighted Dr. Davidsohn and Dr. Singler invited me to be your banquet speaker at this Thirty-Second Sagamore Army Materials Research Conference. I'm delighted because, in a sense, it's a homecoming for me.*

It was 4 decades ago this year that I left the U. S. Army to return to civilian life after 5 years of service. I remember clearly that the decision to leave was not easy. Although I entered the Army as a draftee in June 1941, kicking and screaming at having my college education so rudely interrupted, I found after a few years that I liked being a soldier. Army discipline has given me a sense of orderliness and purpose that had been missing in my life.

So when it came time after World War II for me to decide whether to stay in or to be separated, I debated and debated, and finally chose to leave--but only because I felt I should complete my college education. If I had already been a college graduate, I may well have decided to make the Army my career.

I think I made the right decision. With all the changes that have taken place in the U. S. Army in the past 40 years--technologically and otherwise--I have a hunch I wouldn't have been able to keep up and soon would have been branded a has-been.

I don't have to tell you that's the way it is with change. You either keep up with the changes--whether they're good or bad--or, before you know it, you no longer belong.

During my 38 years in the rubber industry, I kept up for 2 decades or so, first as an employee with one of the major rubber companies in Akron and then as a reporter of the industry scene for trade publications.

But since the early '70s I'm no so sure I've been staying on top of things. Maybe that's because I'm in the twilight of my career or maybe it's because some of the recent changes in the rubber industry have upset the status quo. In other words, maybe in my old age I have come to resent change. I hope that's not the case.

* The banquet presentation was given by Robert Gleason acting on behalf of Ernest Zielasko, who was unable to attend the conference.

Until the 1970s or so, the rubber industry operated as it had for decades. It was dedicated to producing rubber products that were useful to society, industry, and business.

Those were the days when a compounder could tell if a stock met specifications by biting a hunk of it. Executives operated out of non-air conditioned offices located strategically near production lines where the air was thick with carbon black. Wives of those executives would yell at them at night because their white shirts were filthy from their having spent all day in the plant supervising things.

I remember how John L. Collyer, chairman and CEO of B. F. Goodrich during the early years I was with that company, would religiously devote one morning or afternoon each week to walking through the plant, chatting with workers here and there. It was his way of getting a feel for things. Workers loved him for it.

In those days, most employees--from executives to secretaries to line workers--were fiercely proud of the companies they worked for. "I work at The Goodyear," they would say. Or at The Firestone, The General, or The Goodrich. It was never Firestone Tire & Rubber Co. or any of the formal names on their paychecks. And all the while they were ready to defend their company verbally and, if necessary, with fisticuffs.

Workers were proud of what they did. Tire engineers worked long and hard to come up with high quality casings. And tire builders were proud to construct the tires the engineers developed.

But the elites of the industry in the '40s, '50s, and '60s were not the chief executives or the marketing vice presidents. They were the rubber chemists who knew how to discipline rubber. Through intensive research, trial and error, and sometimes shear luck, they used a dash of this chemical and a dash of another to fashion rubber that could be processed through machinery into thousands of essential products. They were recognized within their companies for what they were: The foundation upon which the industry was built.

I don't quite know how to put my finger on it, but the men and women in the industry 15 to 30 years ago carried on an intangible love affair with rubber itself and with the companies that employed them.

I remember how chests swelled at Goodrich in 1947 when Frank Herzegh developed the tubeless tire and in 1954 when Sam Horne duplicated natural rubber in the laboratory.

Later employees at Firestone were equally proud when it was learned that Fred Stavely's research team had actually developed polyisoprene a year earlier than Sam Horne. But they were disappointed that Firestone's management waited until 1955 to make the announcement.

I guess what I'm really trying to say is that back then rubber was paramount and the rubber manufacturers dedicated most of their resources to making useful products from it. In short, the rubber companies were primarily in the rubber business. Period.

Things began to change in the late 1970s with the oil crisis, longer-wearing radial tires, and the 55-miles-an-hour speed limit. Coupled with periodic recessions and the growing invasion of Japanese automobiles and its debilitating impact on production of cars in Detroit, they combined to bring the steady and impressive growth of tire sales to a screeching halt. Instead of annual growth rates of 4 to 6 percent, the industry, with a few exceptions, faced flat yearly growth rates.

Meanwhile, to keep pace with the growing demand for radial tires, and the threat from Michelin of France, the radial pioneer which had started building tire plants in the United States, the domestic companies were forced to build modern new radial plants of their own.

Then, as radials began to penetrate the market, they started to take market share from bias-ply tires, which had dominated the marketplace for decades. One by one tire plants that produced bias tires were closed. From 1973 until now, the tire comanies have shuttered some 29 plants. The slow death of bias tires was widely forecast at the time. But, like the inner tube, which is still around despite the acceptance of the tubeless tire, the bias tire continues to sell. At last count, it still claimed 25 percent of the auto tire replacement market.

In the early 1980s another outside factor arrived on the scene in the form of the strong dollar. This sharply curtailed U.S. exports and brought an influx of imported tires into the United States from Europe and Asia. It also contributed substantially to the rubber industry's whopping trade balance deficit of $3.2 billion as of the end of 1984.

As a result of the various forces, the number of tire and inner tube establishments fell to 160 in 1982 from 200 in 1977. Production of auto tires dropped to about 175 million annually between 1980 and 1982 from about 230 million yearly in the late 1970s. Employment in tire plants decreased to 71,000 in 1982 from 114,000 in 1977.

The years 1983 and 1984, however, were exceptions. Tire sales in both years grew, thanks to higher levels of auto production in Detroit and an increase in the number of car miles driven as fuel prices declined. Last year domestic shipments of car tires rose 4.4 percent to 214 million units, following an 8.5 percent increase in 1983.

This year it's a different story. In the first 4 months, that is, through April, auto tire shipments are 2 percent below last year and truck tires aren't much better.

This is in line with what economists are predicting for the balance of the decade. Through 1989 they see car tire shipments rising only 1 percent annually and truck tires 1.5 percent.

With that kind of flat growth facing them in the future, tire company managements are in a sweat. Because sales were quite good in 1983 and '84, they went ahead with expansions. In fact, there were 12 separate instances of companies increasing their radial capacities in 1984.

These moves have now led to overcapacity in the industry. While the tiremakers had their plants operating at 90 percent capacity and above in 1984, now they're announcing cutbacks, including layoffs, because of bulging inventories, slumping demand and aggressive penetration of imports.

So, to sum it up, here's how things stand at the moment. In the tire segment, which is the dominating force because it consumes 70 to 75 percent of the raw rubber used in the industry as a whole, sales and shipments have flattened. Forecasts call for the situation to remain pretty much the same through 1989.

In the non-tire area, the segment in which the nation's 2,000 smaller rubber product producers find their market niches, the picture is not much better.

Annual growth rates through 1989 for molded and extruded goods, for example, are forecast at only 1 percent. The brightest spot--I use that adjective loosely--is in industrial

rubber goods, principally hose and belting. The annual growth rate there through 1989 is about 2.5 percent.

From the gloomy growth picture I've painted for the rest of this decade, one might wonder why anyone would want to be in the rubber industry. Therefore, I think I need to put it into its proper perspective by pointing out that the factory F.O.B. value of U.S. shipments of all rubber products in 1984 totals $25 billion. Compare that in dollar terms with two of today's growth industries: home computers and home video. In 1983 sales of video recorders, video cameras, and blank tapes were only $4 billion and sales of home computers only $3 billion, peanuts in comparison.

In other words, while rubber at the moment may be a mature industry with dim growth prospects, it still offers well-managed companies excellent opportunities to make a good profit while providing employment for more than 200,000 people.

Nevertheless, the major rubber companies are finding the rubber business a little traumatic now for the reasons outlined before. Some are--and have been for the last decade--looking elsewhere for places to put their financial resources. And in the process they're changing their historic role in rubber drastically.

Not too many years ago, all of the five major rubber companies--Goodyear, Firestone, Goodrich, Uniroyal, and GenCorp--were everything to everybody in tires. No market would surface that they didn't try to satisfy with a line of tires.

All that has changed in the last 10 years. With the exception of Goodyear and--to a lesser degree--GenCorp, all have abandoned efforts to serve all markets. Instead, they've entered an era of niche-picking. A few examples:

In 1977 Goodrich decided that its salvation lay in the commodity chemical business of polyvinyl chloride. It invested sufficient funds to make it the world's largest producer of PVC. It also decided to pull its auto tires out of the original equipment business, which provides only a marginal profit, and concentrate on more profitable niches in the replacement tire field, such as high performance tires. The purpose was to use the Tire Group as a "cash cow" for its chemical and PVC businesses.

As has been widely publicized, the PVC business didn't take off as Goodrich had hoped. As a result, the company last

month announced a restructuring that, incidentally, has brought it considerable criticism from the business press.

It announced that by 1987 it will sell 25 percent of its assets totaling more than $500 million and take a write off of $365 million in its second quarter. It also said it planned to reduce the fixed and working assets in its Tire Group by 25 percent, although it did not reveal how it will do it.

What this means is that Goodrich will become more of a chemical concern and less of a maker of tires and industrial rubber products. Some industry observers even say the restructuring sets the stage for Goodrich to eventually leave the tire business, although Goodrich denies that's the case.

Uniroyal, whose CEO, Joe Flannery, did a magnificent job saving it from financial disaster in 1980, partially by closing two tire plants and reducing its tire sizes and types, now has major problems again.

To ward off a takeover bid, it is becoming a private company through a leveraged buyout in cooperation with a New York investment firm.

The big headache here is that the new private firm will lose controlling interest to institutional investors if it fails to pay $750 million in debts--largely an unfunded pension liability--within 30 months.

One way to solve the problem would be for the new private Uniroyal to sell one or more of its chemical or tire operations. Since Uniroyal is heavily into chemicals, analysts are saying it will dispose of its tire unit. The decision, if it's to be made at all, won't come until the leveraged buyout is complete. In any case, finding a buyer might not be easy. On the other hand, the new private company might not sell any of its units.

Firestone, meanwhile, has changed its corporate strategy under the new management that took over following the Firestone 500 tire recall disaster in the late '70s.

Throughout its history, Firestone's corporate strategy has always been based on two assumptions:

--That Firestone was first and foremost a tire manufacturer competing worldwide in every segment of the tire industry.

--That it would always be more dependent on its capabilities as a tire manufacturer than on its capabilities as a tire marketer.

While the new management admitted these assumptions had served Firestone well throughout its history, it believed the competitive environment had changed so radically that new thinking was required.

The direction it chose was to become more of a tire and automotive service marketer than a tire manufacturer. It based the decision on research that showed gas station and car dealership closings between 1977 and 1982 had resulted in a 30 percent drop in automotive service bays. The new management saw it as a niche Firestone was in a position to fill.

The company moved quickly. In 1983 it bought 300 J.C. Penney autoservice outlets and expanded its own outlets to 1,500 centers, which stress computer diagnosis of engine troubles.

To raise the required funds, Firestone sold a bevy of businesses, including plastics, beverage containers, energy absorbing bumpers, foam products, occupant restraints, and others.

It also sold its famous Firestone Country Club in Akron in 1981. John Nevin, Firestone chairman, told the National Tire Dealers & Retreaders Association in a speech in California last fall, that none of the other transactions generated as much controversy as the decision to sell the country club. He said there are many people at Firestone who still believe that--I'm quoting him here--"if that damn Nevin were a golfer instead of a tennis player--we would still own the country club."

He also told the tire dealers that Firestone bought eight corporate memberships in the new club and assigned them to senior Firestone executives. He added that while he doesn't have one of the memberships because he doesn't play golf, he has lunch at the club once a week during gold season because, he said, "It's the only opportunity I have, between Easter Sunday and Halloween, to see and talk to Firestone sales executives."

Now to get serious again. Firestone also sold its huge Nashville truck tire plant to Bridgestone, the Japanese tiremaker, because it found development of truck tires too costly. Now Bridgestone is making steel-belted radial truck tires there

for Firestone while Firestone produces its own light truck tires at its domestic plants.

Firestone also closed or sold nine tire plants in the United States and Canada and all or part of its equity in tire affiliates in seven foreign countries.

While all of these selling transactions were going on, strong rumors surfaced that Firestone was preparing to quit the tire business. Nevin forcefully squelched that rumor in his California speech to tire dealers with this statement:

"During the five-year 1980-84 period, Firestone investments in its tire-related businesses exceeded $900 million. That is not, I would suggest, a level of capital investment that would be authorized by a management planning to withdraw from the tire business."

I think we can conclude that, in the future, Firestone, which still has eight tire plants in North America, will be known as a tire and automotive service company.

Today, among the majors, we have only two U.S. tire companies--Goodyear and GenCorp--still producing a complete line of tires for all segments of the market. Those two have remained committed to meeting all market needs for tires and most other rubber products. They seem to have prospered as a result.

Other smaller tiremakers--Armstrong, Cooper, Mohawk, etc.--also have pretty much stuck with what they know best.

Michelin, the French tire manufacturer which revolutionized tiremaking by developing the steel-belted radial tire, did well here in the states after it established tire plants in the U.S. southeast. But they're still not making money, partially because it had to borrow heavily to build its U.S. plants and partially because American producers are now building radials of equal quality.

Michelin, along with its radial tire, brought with it to America its penchant for secrecy. No one, to my knowledge, has ever been given a tour of a Michelin factory. That's how jealously the company guards its secrets.

It's been reported that General DeGaulle once requested a tour of Michelin's headquarters factory in Clermont-Ferrand,

France. "Mais, Oui," a Michelin official responded, and promptly drove the General around the outside of the factory in a car. He never got inside the front door.

In America, however, Michelin has finally made its peace with the press. It imported a public relations manager, who does a commendable job of getting answers to questions and setting up interviews.

Even Francois Michelin, who leads the company with the simple title of manager, has made himself available to the press. He has spoken in Akron to the Tire Society and freely answered questions at the press conference that followed.

Francois is a fascinating man. Tall and gaunt, he reminds me of a quiet, old shoe type of guy who rarely speaks unless he really has something to say. When he responds at press conferences, he does so with a mischievious grin. He usually pauses, as if in deep thought, before he replies--and often he answers with a question of his own. A reporter recently asked him which he felt was more important: product development or manufacturing processes?

His answer, after a thoughtful pause, was: "Which of your legs do you think is most important?"

Well, there you have it--The U.S. Rubber Industry, Then and Now. Things have changed. You might even say parts of it have been dismantled.

While most of the industry is still dedicated to producing quality rubber products useful to society, industry, business and government, I doubt if any of today's compounders bite a hunk of rubber stock to determine if it meets specifications. Computers handle that task now.

I also doubt that executives go home with filthy shirts these days. They operate out of air conditioned offices and, if they get out into the plant, their shirts remain clean because ways have been found to keep carbon black dust down.

I really can't say whether employees are as proud of their companies as they used to be. That's a judgmental call. But I do know that in Akron they don't refer to their companies as "The Goodyear or The Firestone" anymore.

Are the workers as proud of what they do for their employers as they used to be? Probably they are, but I don't

know about tire builders. There are so few around Akron now that practically no auto tires are made in the Rubber Capital of the World.

Chemists are no longer the elite, either. They work in teams now, and individual stars don't seem to emerge, unless you put computers in that classification. What stars there are are accountants, lawyers and MBAs.

But I do know this: Rubber fills a need. It's a commodity the modern world can't do without. It's as indispensable as steel and wood and brick and mortar.

The late Ralph Wolf, who was probably the world's most prolific writer about rubber, put it this way in an article in Rubber World magazine in 1964:

"Civilization as we know it today is wholly dependent upon rubber. It is a material of myriad uses, totally unlike anything the world had previously known. It enters in a thousand ways into the fabric of our daily lives.

It is a servant that follows us, literally, from the cradle to the grave. We are ushered into the world by the rubber-covered hands of a doctor in surroundings made sterile and quiet by this ubiquitous substance, and we exit in a rubber-gasketed coffin hauled by a rubber-lined hearse."

Thank you.

PARTICIPANTS AND STAFF

1. Iqbal Ahmad
   U.S. Army European Research Office (USA RDSG-UK)
   223-231 Old Marylebone Rd., London NWI 5th
   LONDON, UK

2. Anthony L. Alesi
   AMTL
   Watertown, MA 02172-0001

3. Jeffrey T. Books
   Ethyl Corporation
   8000 G.S.R.I. Avenue
   Baton Rouge, LA 70808

4. James R. Brennick
   U.S. Army Natick R&D Center
   Kansas Street
   Natick, MA 01760

5. Forrest C. Burns
   AMTL
   Watertown, MA

6. Louis G. Carreiro
   AMTL
   Watertown, MA

7. Anthony J. Castro
   AKZO Chemie America
   2035 9th Avenue
   San Francisco, CA 94116

8. Joseph R. Crisci
   David W. Taylor Naval Ship R&D Center
   CODE 2801
   Annapolis, MD 21402

9. Andrew Crowson
   U.S. Army Research Office
   P.O. Box 12211
   Research Triangle Park, NC 27709

10. Wenzel E. Davidsohn
    AMTL
    Watertown, MA

11. Carolyn Deardoff
    FMC Corporation
    1105 Coleman Avenue
    Box 1201
    San Jose, CA 95108

12. George C. Derringer
    Battelle Columbus Division
    505 King Avenue
    Colulmbus, OH 43201

13. Richard Desper
    AMTL
    Watertown, MA

14. James A. Donovan
University of Massachusetts
Mechanical Engineering Department
Amherst, MA 01003

15. David A. Dunn
AMTL
Watertown, MA

16. David W. Dwight
Virginia Polytechnic Institute & State University
Department of Materials Engineering
Blacksburg, VA 24061

17. Richard Farris
University of Massachusetts
Polymer Science and Engineering
Amherst, MA 01003

18. Dominick Finocchio
Polaroid Corporation
Commercial Chemicals
238 South Main Street
Assonet, MA 02702

19. Richard Fischer
Gates Corporation
900 South Broadway
Denver, CO 80217

20. Andrew P. Foldi
C&C Consultants
2833 West Oakland Drive
Wilmington, DE 19808

21. Alan N. Gent
University of Akron
Institute of Polymer Science
Akron, OH 44325

22. Robert Gleason
Rubber and Plastics News,
Crain Communications
34 N. Hawkins Avenue
Akron, OH 44313

23. Alfred Goldberg
Lawrence Livermore National Laboratory
L342, Eng. Sci. Div.,
P.O. Box 808
Livermore, CA 94550

24. Patricia Gordon
AMTL
Watertown, MA

25. Kathleen E. Harrington
AMTL
Watertown, MA

26. Walter R. Hertler
E.I. DuPont de Nemours & Co.--Central R&D Dept.
Experimental Station--328
Wilmington, DE 19898

27. Morris Hoffman
U.S. Army Tank Automotive Command
ATTN: AMSTA-GBP
Warren, MI 48397-5000

28. James M. Hoover
Virginia Polytechnic Institute & State Univ.
Dept. of Chemistry
Blacksburg, VA 24061

29. Arthur R. Johnson
AMTL
Watertown, MA

30. Karen Kaloostian
AMTL
Watertown, MA

31. Peter J. Kane
AMTL
Watertown, MA

32. Harry S. Katz
Utility Research Corporation
Box 107
Montclair, NJ 07042

33. Michael King
U.S. Army Tank Automotive Command
ATTN: AMSTA-RTT
Warren, MI 48397-5000

34. Abram O. King
AMTL
Watertown, MA

35. Jack L. Koenig
Case Western Reserve University
Dept. of Macromolecular Science
205 Olin Bldg.
Cleveland, OH 44106

36. Richard Komoroski*
BF Goodrich Company

37. Roy Laible
U.S. Army Natick R&D Center
Kansas Street
Natick, MA 01760-5019

38. Robert F. Landel
Jet Propulsion Laboratory
4800 Oak Grove Drive
Pasadena, CA 91109

39. H.R. Nick Lawrence
FMC Corporation
532 Shadow Glen
San Jose, CA 95129

40. Bin Lee
Virginia Polytechnic Institute & State Univ.
Dept. of Chemistry
Blacksburg, VA 24061

41. Lidia Lee
AMTL
Watertown, MA

42. Donald Lesuer
Lawrence Livermore National Laboratory
Eng. Sciences Div.
P.O. Box 808, L-342
Livermore, CA 94550

43. Robert W. Lewis
Director, Science & Technology
U.S. Army Natick R&D Center
Natick, MA 01760-5019

44. Sin-Shong Lin
AMTL
Watertown, MA

45. Domenic P. Macaione
AMTL
Watertown, MA

46. Eugene E. Magat
U.S. Army Research Office
P.O. Box 12211
Research Triangle Park, NC 27709

47. J. E. Mark
University of Cincinnati
Department of Chemistry
Cincinnati, OH 45221

48. James W. McCauley
AMTL
Watertown, MA

*Present address: Dept. of Radiology, Univ. of Arkansas, Little Rock, AR 72205.

49. James E. McGrath
Virginia Polytechnic
Institute & State Univ.
404 Davidson Hall
Blacksburg, VA 24061

50. Emily McHugh
AMTL
Watertown, MA

51. E. L. McInnis
Polaroid Corporation
Commercial Chemicals
Lab.
238 S. Main Street
Assonnet, MA 02702

52. Donald McIntyre
Institute of Polymer
Science
University of Akron
Akron, OH 44325

53. Gregory B. McKenna
National Bureau of
Standards
Polymer Division
Gaithersburg, MD 20899

54. Joey Mead
AMTL
Watertown, MA

55. Steven P. Medaglia
AMTL
Watertown, MA

56. Avrom I. Medalia
Consultant
30 Dorr Road
Newton, MA 02158

57. Caryn Mee
AMTL
Watertown, MA

58. Warren B. Mueller
Ethyl Corporation
Ethyl Tower, 451 Florida
Baton Rouge, LA 70801

59. Jacob Patt
U.S. Army Tank
Automotive Command
ATTN: AMSTA-RTT
Warren, MI 48397-5000

60. Joan Purvis
SynerCom
1989 W. Fifth Avenue
Suite 5
Columbus, OH 43212

61. Gumersindo Rodriguez
Belvoir Research &
Development Center
ATTN: STRBE-VU, Mat'ls,
Fuels & Lubricants
Lab.
Ft. Belvoir,
VA 22060-5606

62. Douglas Rose
U.S. Army Tank
Automotive Command
ATTN: AMSTA-ZSA
Warren, MI 48397-5000

63. Julia A. Rosen
AMTL
Watertown, MA

64. David Roylance
Massachusetts Institute
of Technology
Room 6-202
Cambridge, MA 02139

65. Robert E. Sacher
AMTL
Watertown, MA

66. Rudy J. School
Rubber and Plastics News
34 North Hawkins Avenue
Suite 10
Akron, OH 44313

67. Michael Sennett
AMTL
Watertown, MA

68. Marshall L. Sherman
Ship Materials
Engineering Dept.
David Taylor Naval Ship
R&D Center
Annapolis, MD

69. C. F. Shih
Brown University
Division of Engineering
Box D
Providence, RI 02912

70. Glen R. Simula
Michigan Technological
University
Keweenaw Research Center
Houghton, MI 49931

71. Robert E. Singler
AMTL
Watertown, MA

72. Anil K. Sircar
University of Dayton
Research Institute
300 College Park,
KL-162
Dayton, OH 45469

73. James M. Sloan
AMTL
Watertown, MA

74. C. W. Spencer
Virginia Polytechnic
Institute & State
Univ.
201 Holden
Blacksburg, VA 24060

75. Geza C. Szakacs
U.S. Army Tank
Automotive Command
ATTN: AMSTA-RTT
Bldg. 215 (Track &
Suspension)
Warren, MI 48397-5000

76. Frank B. Testroet
Rock Island Arsenal
Engineering Directorate
ATTN: SMCRI-ENM-T
Rock Island, IL 61299

77. Andrew J. Tinker
The Malaysian Rubber
Producers' Research
Assoc.
Tun Abdul Razak Lab.
Brickendonbury, Hertford
ENGLAND SG13 8NL

78. Paul Touchet
Belvoir Research &
Development Center
ATTN: STRBE-VU
Ft. Belvoir, VA 22060

79. Larry Waksman
AMTL
Watertown, MA

80. John Walker
Polysar-Elastomers
Research & Development
Div.
S. Vidal Street
Sarnia, Ontario,
CANADA N7T TM2

81. Lloyd A. Walker
Monsanto Polymer
Products Company
260 Springside Drive
Akron, OH 44313

82. Richard Wheaton
U.S. Dept. of
Agriculture
Office of Critical
Materials
Room 223, West Auditors
Building
Washington, DC 20251

83. Anthony F. Wilde
AMTL
Watertown, MA

84. Eugene Wilusz
Army Natick R&D
Center
Kansas Street
Natick, MA 01760

85. Brian A. Zentner
AMTL
Watertown, MA

86. Walter X. Zukas
AMTL
Watertown, MA

INDEX

Note: The following index of key words is page numbered according to the first page of the paper or poster presentation.

A

Abrasion, 485
Abrasion resistance, 369, 427, 535
Allophanate, 369
Analysis
  compositional, 317
  curve fit, 307
  dynamic mechanical, 1, 119, 369
  electrothermal, 73
  finite element, 211, 451
  regression, 129
  thermal, 1, 73, 317, 473
  thermogravimetric, 73
  thermomechanical, 369
Antioxidants, 73, 155
Aramid fibers, 427, 547
Aramid pulp, 427
Armstrong, 565
Aryloxy-polyphosphazene, 421
Auger Spectroscopy, 281, 473
Axial probe penetration, 451
Axisymmetric deformation, 451

B

Bias tires, 565
Bimodal networks, 141
Blending, 155
Blow-out, 557
Boron trichloride, 297
Bridgestone, 565
Butadiene rubber, 55, 307
Butanediol, 369

C

Carbon-13 NMR, 31, 55
Carbon black, 73, 169, 175, 345, 535
Carboxyl-terminated butadiene-acrylonitrile copolymer, 55
Catalyst, 1, 369
Catalyzed polymerization, 297
Cavitation, 169, 197
Cellulose fibers, 485
Chain extender, 483
CHDI, see cyclohexane diisocyanate
Chemical agent screening studies, 379
Chipping, 485
Chunking, 485, 557
Clean sheet formulation, 129
Cohesive strength, 155
Compositional analysis, 317
Compound
  model, 1
  reference, 535, 557
  track rubber, 525
Compounding, 535
Compression fatigue, 251, 273, 369
Compression probe, 451
Compressive loading, 427
Computer modeling, 211
Constitutive equation, 197
Cooper, 565
Copolymer(s)
  carboxyl-terminated butadiene-acrylonitrile, 55
  graft, 155
  segmented, 405
  vinyl chloride-vinylidene chloride, 55
Covulcanization, 155
Crack initiation, 175
Craze formation, 197
Crazing, 155
Creep behavior, 525
Cross-country service, 229, 473
Crosslink density determinations, 55, 229, 251, 473
Crosslinker, 369
Crystallinity, 73, 483

CTBN, see carboxyl-terminated butadiene-acrylonitrile copolymer
Cure studies, 317
Curve fit analysis, 307
Cut resistance, 547
Cyclic loading, 197, 525
Cyclohexane diisocyanate, 369, 483
Cylinder model, 451

D

Dark field microscopy, 345
Degradation, 73
Degradation mechanism, 229
Desirability
  function, 129
  optimization, 129
Desorption, 405
4,4'-diaminodiphenylmethane, 1
Dibutyl tin dilaurate, 369
3,3'-dichloro-4,4'diaminodiphenylmethane, 483
Die swell, 155
Differential scanning calorimetry, 1, 251, 317, 369
Diffusion, 379, 405
Dilatometry, 197
Dispersion, 73, 281, 345, 427, 547
DMA, see dynamic mechanical analysis
DSC, see differential scanning calorimetry
Dynamic mechanical analysis, 1, 119, 317, 369
Dynamic mechanical properties, 273

E

Elastomers
  identification of, 73, 317
  nonhysteretic, 175
  phosphazene, 119, 421
Elastomer blend, 73, 353
Electrothermal analysis, 73
Equation(s)
  constitutive, 197
  Flory-Rehner, 31
  prediction, 129
  Valanis-Landel, 451
ESCA, 229
Estane, 1
EYPEL polymers, see phosphazene elastomers

F

FAB, see fast atom bombardment
Failure
  envelope, 525
  hysteresis, 369
  mechanisms, 251
  modes, 211, 473
  processes, 169
Fast atom bombardment, see mass spectrometry
Fatigue, 525
Fatigue testing, 485
Fiber(s)
  cellulose, 485
  fibrillated, 547
  Kevlar, 427, 547
  Santoweb, 485
Fiber
  orientation, 427
  reinforcement, 415, 485, 555
Fibrillated fiber, 547
Fickian diffusion, 405
Field testing track rubber, 229, 473, 485
Filler affect, 1
Filler particle sizes, 141
Finite element analysis, 211, 451
Fire resistance, 421
Firestone, 565
Flex fatigue, 535
Flory-Rehner Equation, 31
Fluid resistance, 119

Fluoroelastomer
  phosphazene, 119
Foam insulation, 421
Fracture mechanics, 175, 191

G

Gas chromatography, 353
Gen Corp, 565

German Diehls track, 557
Glass transition
methods for measurement, 73
Goodrich, 565
Goodrich Flexometer, 485, 535
Goodyear, 565
Graft copolymer, 155
Gravel service, 229
Guayule rubber, 269, 535

H

Hard segment, 1, 483
Hardness, 369
HDPE, see polyethylene
Heat aging
changes in physical properties, 535
Heat build-up, 251, 273, 427, 485, 557
Heat-generation rate, 211
Hose reinforcement, 485
Hydrolysis resistance, 483
Hysteresis, 273, 369

I

Immersion testing, 379
Impact strength, 155
Inclusion, 169
Incremental vapor sorption, 405
Infrared - ATR, 369
Infrared spectroscopy, 1, 307
Injection molding, 483
Interfacial adhesion, 155

J

J-integral, 175

K

Kevlar fiber, 427, 547

M

M-1 tank, 557
M-2 Bradley Fighting Vehicle, 557
M-60 Tank, 557
m-phenylene bismaleimide, 155
Magic angle spinning, see nuclear magnetic resonance
Mass spectrometry, 332, 353
MDI, see methylene bis(4-phenyl isocyanate)
Mechanical
model, 211
properties, 525
testing, 535
Mechanism(s)
crosslinking, 31
cure, 31
degradation, 229
failure, 251
reaction, 297
vulcanization, 31
wear, 229
Methylene bis(4-cyclohexyl isocyanate), 369
Methylene bis(4-phenyl isocyanate), 1, 369
Michelin, 565
Microscopy, 345, 473
Microstructure, 281
Military specification, 557
Mixing, 345
MOCA, see 3,3'-dichloro-4,4'diaminodiphenylmethane
Model
cyclinder, 451
mechanical, 211
thermal, 211
model compound, 1
model networks, 141
Modeling
computer, 211
Mohawk, 565
Monte Carlo simulations, 141
Multi-property optimization, 129

N

Natural rubber, 55, 155, 307, 473, 535
Natural rubber curing studies, 31
NBR, see nitrile butadiene rubber
Networks
bimodal, 141
model, 141
Newton-Raphson method, 451
Nitrile-butadiene rubber, 547
Non-elastic, 175

Nonhysteretic elastomers, 197
Nuclear magnetic resonance
attached proton test, 55
copolymers, 55
CPMAS, 55
crosslinking, 55
crosslinking mechanism, 31
cross polarization, 55
DEPT, 55
dipolar decoupling, 55
magic angle spinning, 31, 55

O

Optimization of properties, 129

P

p-phenylene diisocyanate, 483
Paved surface tests, 229, 473
PDMS, see poly(dimethylsiloxane)
Penetration resistance, 427
Phase
mixing, 1
separation, 197
Phenol formaldehyde resin, 155
Phenyl isocyanate, 1
Phosphazene
polymerization, 297
elastomers, 119, 421
Plasticizer, 73
PNF, see phosphazene elastomer
Poisson's ratio, 197
Poly(dichlorophosphazene), 297
Poly(dimethylsiloxane), 141
Poly(tetramethylene oxide), 1, 369
Polybutadiene rubber, 55, 307
Polyethylene, 155
cis-1,4-polyisoprene, 155
Polymerization
catalyzed, 297
solution, 297
Polyoctenamer, 535
Polyphosphazene, 119, 297, 421
Polypropylene, 155
Polyurea, 1
Polyurethane, 1, 251, 369, 405, 415, 483
Poly(urethaneurea), 1
Post cure, 369
PPDI, see p-phenylene diisocyanate
Precipitated silica, 141
Prediction equations, 129
Prepolymer, 1
Properties
dynamic mechanical, 1, 119, 369
mechanical, 525
PTMO, see poly(tetramethylene oxide)
Pyrolysis, 307, 353

R

Radial tires, 565
Raman spectroscopy, 297
Reaction mechanism, 297
Reference compound, 535, 557
Regression analysis, 129
Reinforcement, see also carbon black
fiber, 415, 427, 485, 547, 557
hose, 485
silica, 141
Resistance
abrasion, 369, 427, 535
cut, 547
fire, 421
fluid, 119
hydrolysis, 483
penetration, 427
sour crude, 119
tear, 427
Reversion, 31
Rheometry, 317
Rotational isomeric state theory, 141
Rubber
characterization, 333, 353
components, 281
guayule, 535
inhomogeneity, 229
natural, see natural rubber
polybutadiene, 307
styrene-butadiene, 55,

229, 307, 345
synthetic natural, 565
blends, 307

S

SAM, see scanning Auger microscopy
Santoweb Fibers, 485
SBR, see styrene-butadiene rubber
Scanning Auger image, 281
Scanning Auger microscopy, 281
Scanning electron microscopy, 155
Screening designs, 129
Secondary electron detector (SED), 281
Segmented copolymers, 405
SEM, see scanning electron microscopy
Short fibers, 427, 485
SMR, see standard Malaysian rubber
Soft segment, 1
Solubility parameter, 155, 379
Solution polymerization, 297
Sorption, 379, 405
Sour crude resistance, 119
Spectral editing, 55
Spectroscopy
Auger, 281, 473
infrared, 1, 307
Raman, 297
Standard Malaysian rubber, 535
curing studies, 31
Stannous chloride dihydrate, 155
Statistical experimental design, 129
Statistical process control, 473
Stearic acid, 31
Studies
chemical agent screening, 379
natural rubber curing, 31
track design, 211
Styrene-butadiene rubber, 55, 229, 307, 345, 473, 485, 535, 547
Substituent effects, 55
Sulfenamide accelerator, 31
Sulfur, 55, 155
Swelling, 31, 141
Swelling measurements, 229, 251, 473
Synthesis, 1, 369
Synthetic natural rubber, 565

T

Tan delta, 273
Tear, 169
resistance, 427
strength, 369, 535, 547
testing, 485
Tearing energy, 175
Temperature(s)
dependence, 119
track pad, 211
use, 119
Testing
fatigue, 485
field, 485
immersion, 379
mechanical, 535
tear, 485
Tetraethylorthosilicate, 141
Tetramethylthiuram disulfide, 31, 55, 155
TGA, see thermogravimetric analysis
Thermal analysis, see also specific method, 1, 73, 317, 473
Thermal model, 211
Thermogravimetric analyses, 1, 73, 317
Thermomechanical analysis, 1, 317, 369
Thermomechanical degradation, 251
Tires, 73, 369
TMA, see thermomechanical analysis
TMTD, see tetramethylthiuram disulfide
Track
design studies, 211
German Diehls, 557
pad prototype evaluation, 415
pad temperatures, 211

pads, 307, 369, 473
rubber, 229, 317
rubber compounds, 525
T-142, 211
T-156, 211, 557
T-157, 473, 557
Track block
T-156, 557
T-158, 557
Triblend, 55, 525, 557
Trimethylol propane, 369
Tubeless tire, 565

U

Ultimate properties, 141

V

Vacuole formation, 197
Valanis-Landel Equation, 451
Vibration damping, 119
Vinyl chloride-vinylidene chloride copolymers, 55
Vulcanization, 55, 73, 535
Vulcanization mechanism, 31

W

Wear mechanism, 229
Weight gain, 379
Wire and cable jacketing, 421

Z

Zinc accelerator complex, 31
Zinc oxide, 31
Zinc stearate, 155